Author:
Oldroyd, Nicola L

Title:
Catalytic and Stoichiometric Studies of the Polymerisation of Phosphine-boranes and Depolymerisation of Polyaminoboranes

Catalytic and Stoichiometric Studies of the Polymerisation of Phosphine-boranes and Depolymerisation of Polyaminoboranes

Nicola Louise Oldroyd

A dissertation submitted to the University of Bristol in accordance with the requirements for award of the degree of Doctor of Philosophy in the Faculty of Science

School of Chemistry

February 2020

Word Count 43,358

Abstract

This thesis describes new catalytic and stoichiometric routes towards polyphosphinoboranes and explores the carbene initiated depolymerisation of polyaminoboranes.

Chapter 1 gives a general introduction to the synthesis and properties of polyaminoboranes and polyphosphinoboranes, along with the properties and applications of nitrogen heterocyclic carbenes and cyclic (alkyl)(amino)carbenes.

Chapter 2 describes the metal-free dehydropolymerisation of phosphine-boranes using cyclic (alkyl)(amino)carbenes as hydrogen acceptors. The synthesis of both P-mono and P-disubstituted polyphosphinoboranes are described along with a discussion of the dehydrogenation mechanism supported by DFT studies.

Chapter 3 describes the use of $Ni(COD)_2$ as a precatalyst for the dehydropolymerisation of $PPhH_2{\cdot}BH_3$. The optimisation of polymerisation conditions is described along with investigations into the substate scope. Preliminary investigations into the polymerisation mechanism are discussed.

Chapter 4 describes a detailed study into the carbene-mediated depolymerisation of poly(N-methylaminoborane) $[MeHN–BH_2]_n$. The reactivity of selected N-heterocyclic carbenes and cyclic (alkyl)(amino)carbenes towards $[MeHN–BH_2]_n$, $[MeHN–BH_2]_3$ and $MeNH_2{\cdot}BH_3$ is discussed and depolymerisation mechanisms proposed.

Chapter 5 is split into two sections. The first focusses on expanding the substrate scope of the cyclic (alkyl)(amino)carbene mediated dehydropolymerisation of phosphine-boranes described in Chapter 2 and the second explores the reactivity of the adduct $IDipp–BH_2NMeH$, both thermally and upon the addition of Lewis acids.

Chapter 6 describes ongoing and potential future work based upon the results presented in Chapters 2–5.

Declaration

I declare that the work in this dissertation was carried out in accordance with the requirements of the University's *Regulations and Code of Practice for Research Degree Programmes* and that it has not been submitted for any other academic award. Except where indicated by specific reference in the text, the work is the candidate's own work. Work done in collaboration with, or with the assistance of, others, is indicated as such. Any views expressed in the dissertation are those of the author.

Nicola Oldroyd

2nd February 2020

Acknowledgements

I would like to take this opportunity to highlight a number of people that I have engaged with during my PhD. Firstly, I would like to acknowledge my supervisor, Prof. Ian Manners, for the opportunity to join his research group, and providing me with inspiration, numerous invaluable discussions and unwavering support. I would like to thank Deborah O'Hanlon Manners for all of her work in ensuring the smooth running of the group, and in particular the logistics involved with moving to Canada.

During my PhD I had the opportunity to work at both the University of Bristol and the University of Victoria. I would like to thank every member of the Manners' group whom I have been lucky enough to work with both in the UK and Canada. I have been fortunate to meet a diverse group of talented individuals who have provided me with support, memories and friendships. There are too many people to mention individually, however I would like to highlight Dr. Saurabh Chitnis whose enthusiasm, never ending ideas and mentoring ensured that my PhD got off to the best possible start.

Outside of the lab I am grateful for all the people I met and opportunities I gained through being involved with multiple running groups. In particular I would like to thank everyone from Clover Point parkrun, an immensely supportive community who quickly welcomed me to Victoria. I am especially grateful for Ed and Mona adopting me as an 'extra bonus daughter' and making Canada feel like home-away-from-home. Additionally, I am grateful for Joe, Molly and Cat who were always there for me after the inevitable bad day in the lab and have provided me with what I am sure will be lifelong friendships.

I would like to thank my family for their endless encouragement, not just during my PhD, but at every stage up until this point. Last but not least I would like to thank Aggy for his invaluable support – even when I moved almost 5000 miles away!

Table of Contents

Chapter 1 Introduction 1
1.1 Research objectives 1
1.2 Formation of main group element-element bonds 1
1.2.1 Synthesis of E-E and E-E' bonds 1
1.2.2 Extension to polymers 2
1.3 Polyaminoboranes 4
1.3.1 Synthesis and structure of amine-boranes and aminoboranes 4
1.3.2 Synthesis of polyaminoboranes 5
1.3.2.1 Metal-catalysed dehydropolymerisation of amine-boranes 6
1.3.2.2 Metal-free routes to polyaminoboranes 7
1.3.3 Substrate scope of polyaminoboranes 8
1.3.4 Properties and applications of polyaminoboranes 9
1.4 Polyphosphinoboranes 10
1.4.1 Synthesis and structure of phosphine-boranes and phosphinoboranes 10
1.4.2 Synthesis of P-monosubstituted polyphosphinoboranes 11
1.4.2.1 Thermolysis of phosphine-boranes 11
1.4.2.2 Metal-catalysed dehydropolymerisation of phosphine-boranes 11
1.4.2.3 Metal-free routes to polyphosphinoboranes 12
1.4.3 Substrate scope of polyphosphinoboranes 13
1.4.3.1 P-monosubstituted polyphosphinoboranes 13
1.4.3.2 P-disubstituted polyphosphinoboranes 14
1.4.4 Properties and applications of polyphosphinoboranes 15
1.5 Mechanistic insights into the synthesis of polyaminoboranes and polyphosphinoboranes 15
1.5.1 Mechanisms of transition-metal mediated amine-borane dehydropolymerisation 16
1.5.2 Mechanisms of transition-metal mediated phosphine-borane dehydropolymerisation 20
1.5.3 Mechanism of metal-free synthesis of polyaminoboranes and polyphosphinoboranes 24
1.6 Carbenes 25
1.6.1 Nitrogen heterocyclic carbenes (NHCs) 26
1.6.1.1 Reactivity and applications of NHCs 27
1.6.2 Cyclic (alkyl)(amino)carbenes CAACs 28
1.6.2.1 Reactivity and applications of CAACs 29
1.7 Thesis summary and acknowledgement of collaborators 31

1.8 References 32

Chapter 2 Metal-free dehydropolymerisation of phosphine-boranes using cyclic (alkyl)(amino)carbenes as hydrogen acceptors 44

2.1 Abstract 44

2.2 Introduction 44

2.3 Results and Discussion 47

2.3.1 Reactivity of IDipp with $PhPH_2{\cdot}BH_3$ and $Ph_2PH{\cdot}BH_3$ 47

2.3.2 Reactivity of $CAAC^{Me}$ with $PhPH_2{\cdot}BH_3$ 48

2.3.3 Mechanistic studies into the dehydrogenation 50

2.3.3.1 Kinetic studies 51

2.3.3.2 DFT calculations 51

2.3.3.3 Dehydrogenation mechanisms considered and subsequently discounted 55

2.3.4 Substrate Scope 58

2.3.4.1 Polymerisation attempts of $Ph_2PH{\cdot}BH_3$ and $PhEtPH{\cdot}BH_3$ using $CAAC^{Me}$ and $CAAC^{Cy}$ 58

2.3.4.2 Adduct formation with bulkier P-disubstituted phosphine-boranes 61

2.3.5 Mechanism of polymerisation from phosphinoborane monomers 62

2.4 Conclusions 65

2.5 Supporting Information 66

2.5.1 General procedures, reagents and equipment 66

2.5.2 Synthesis of IDipp phosphidoborane salts 68

2.5.2.1 Synthesis of 2.1a 68

2.5.2.2 Synthesis of 2.1b 70

2.5.3 Polymerisation attempts of $PhPH_2{\cdot}BH_3$ using $CAAC^{Me}$ 71

2.5.3.1 Synthesis of 2.3a 71

2.5.3.2 General procedure for dehydropolymerisation of $PhPH_2{\cdot}BH_3$ using $CAAC^{Me}$ 74

2.5.3.3 More detailed procedure for run 4 78

2.5.3.4 Synthesis of $(CAAC^{Me})H_2$ 80

2.5.4 Mechanistic studies 82

2.5.4.1 Kinetics measurements to probe reaction mechanism 82

2.5.4.2 DFT calculations 85

2.5.4.3 Reaction of $CAAC^{Me}$ with H_2 at ca. 4 atm 91

2.5.5 Polymerisation attempts of P-disubstituted phosphine-boranes using $CAAC^{Me}$ and $CAAC^{Cy}$ 91

2.5.5.1 Synthesis of 2.3b 91

2.5.5.2 Dehydropolymerisation of $Ph_2PH{\cdot}BH_3$ 93

2.5.5.3 Synthesis of 2.3c 99

2.5.5.4 Dehydropolymerisation of rac-$PhEtPH{\cdot}BH_3$ 101

2.5.6 Synthesis of CAAC^{Me}-phosphinoborane adducts 106
2.5.6.1 Synthesis of 2.4a 106
2.5.6.2 Synthesis of 2.4b 109
2.5.6.3 Reaction of $Ph_2PH{\cdot}BH_3$ with two equivalents of CAAC^{Me} 111
2.5.7 Supplementary Tables 112
2.5.7.1 X-ray crystallography 112
2.5.8 Supplementary Data 114
2.5.8.1 Cartesian coordinates and SCF energies of the calculated structures 114
2.6 References 136
Chapter 3 Ni(COD)$_2$-catalysed dehydropolymerisation of phosphine-boranes 141
3.1 Abstract 141
3.2 Introduction 141
3.3 Results and Discussion 143
3.3.1 Polymerisation of $PhPH_2{\cdot}BH_3$ using Ni(COD)$_2$ 143
3.3.1.1 Optimisation of polymerisation conditions in THF 143
3.3.1.2 Influence of solvent on the polymerisation 146
3.3.1.3 Influence of air on the polymerisation 148
3.3.1.4 Polymerisation under scaled up and optimised conditions 149
3.3.2 Investigation into the polymerisation mechanism 151
3.3.2.1 Molar mass dependence on conversion 151
3.3.2.2 Effect of additional monomer 151
3.3.2.3 Effect of reacting oligomeric material with Ni(COD)$_2$ 152
3.3.2.4 Evidence for a homogeneous vs heterogeneous mechanism 152
3.3.2.5 Postulated polymerisation mechanism 153
3.3.3 Expansion of the substrate scope 154
3.4 Conclusions 156
3.5 Supporting Information 156
3.5.1 General procedures, reagents and equipment 156
3.5.2 General procedure for Ni(COD)$_2$-catalysed dehydropolymerisation of $PhPH_2{\cdot}BH_3$ 157
3.5.2.1 Concentration dependence 158
3.5.2.2 Catalyst loading dependence 159
3.5.2.3 Temperature dependence 161
3.5.2.4 Control reaction with no catalyst 162
3.5.2.5 Solvent dependence 164
3.5.3 Carrying out polymerisation in air 167
3.5.4 Scaled up optimised conditions 167

3.5.5 Isolation of $[PhHP–BH_2]_3$ (3.1) 170
3.5.6 Reaction of $[PhHP–BH_2]_3$ with $Ni(COD)_2$ 172
3.5.7 Polymer growth kinetics 172
3.5.8 Addition of more monomer after 100% conversion 174
3.5.9 Reaction of oligomeric material with $Ni(COD)_2$ 175
3.5.10 Homogenous vs heterogenous tests 175
3.5.10.1 PPh_3 poisoning 175
3.5.10.2 Hg poisoning 176
3.5.10.3 Filtration 177
3.5.10.4 UV-Vis 177
3.5.10.5 Reaction of $PPhH_2{\cdot}BH_3$ with nickel nanoparticles 178
3.5.10.6 Addition of $Me_2NH{\cdot}BH_3$ to the crude reaction of the $Ni(COD)_2$-catalysed dehydropolymerisation of $PhPH_2{\cdot}BH_3$ 178
3.5.11 Substrate scope 178
3.5.11.1 *n*-$HexPH_2{\cdot}BH_3$ 178
3.5.11.2 $Ph_2PH{\cdot}BH_3$ 181
3.5.11.3 $PhEtPH{\cdot}BH_3$ 183
3.5.12 Supplementary tables 184
3.5.12.1 X-ray crystallography 184
3.6 References 185

Chapter 4 Stoichiometric and catalytic carbene-mediated depolymerisation of poly(N-methylaminoborane) $[MeHN–BH_2]_n$ 192

4.1 Abstract 192
4.2 Introduction 193
4.3 Results 195
4.3.1 Stoichiometric reactions between polyaminoborane $[MeHN–BH_2]_n$ and carbenes 195
4.3.2 Substoichiometric reactions between polyaminoborane $[MeHN–BH_2]_n$ and carbenes 197
4.3.3 Further reactivity studies with poly(N-methylaminoborane) $[MeHN–BH_2]_n$ and cyclic borazane $[MeHN–BH_2]_3$ 199
4.3.3.1 Solution stability of poly(N-methylaminoborane) $[MeHN–BH_2]_n$ 199
4.3.3.2 Reaction between cyclic borazane $[MeHN–BH_2]_3$ and carbenes 200
4.3.3.3 Attempted detection of $MeHN{=}BH_2$ at low temperature 200
4.3.3.4 Carbene-mediated depolymerisation of $[MeHN–BH_2]_n$ in the presence of cyclohexene 201
4.3.3.5 Solution stability of $[MeHN–BH_2]_n$ in the presence of cyclohexene 201
4.3.3.6 Reactivity of IDipp–BH_2NMeH (4.1) with excess cyclohexene 201
4.3.4 Reactivity of $MeNH_2{\cdot}BH_3$ with carbenes 202
4.4 Discussion 206

4.4.1 Depolymerisation of [MeHN–BH_2]$_n$ mediated by NHCs and weaker donors 207
4.4.2 Depolymerisation of [MeHN–BH_2]$_n$ mediated by CAAC^{Me} 209
4.5 Conclusions 211
4.6 Supporting Information 212
4.6.1 General procedures, reagents and equipment 212
4.6.2 Synthesis of poly(N-methylaminoborane) 213
4.6.3 Stoichiometric reactions between [MeHN–BH_2]$_n$ and IDipp, I*t*Bu and CAAC^{Me} 214
4.6.3.1 Synthesis of IDipp–BH_2NMeH (4.1) 214
4.6.3.2 Reaction of [MeHN–BH_2]$_n$ with I*t*Bu 214
4.6.3.3 Reaction of [MeHN–BH_2]$_n$ with CAAC^{Me} 215
4.6.3.2 Effect on the addition order of carbene to [MeHN–BH_2]$_n$ and vice versa 216
4.6.4 Substoichiometric reactions between [MeHN–BH_2]$_n$ and IDipp, I*t*Bu and CAAC^{Me} 217
4.6.4.1 Reaction of [MeHN–BH_2]$_n$ with substoichiometric IDipp 217
4.6.4.2 Reaction of [MeHN–BH_2]$_n$ with substoichiometric ItBu 218
4.6.4.3 Reaction of [MeHN–BH_2]$_n$ with substoichiometric CAAC^{Me} 219
4.6.5 Control reactions 220
4.6.5.1 Solution stability of [MeHN–BH_2]$_n$ in THF 220
4.6.5.2 Reactions of [MeHN–BH_2]$_3$ with IDipp, I*t*Bu and CAAC^{Me} 220
4.6.5.3 Attempted observation of MeHN=BH_2 at low temperature 220
4.6.5.3.1 Reaction of [MeHN–BH_2]$_n$ with stoichiometric IDipp 221
4.6.5.3.2 Reaction of [MeHN–BH_2]$_n$ with stoichiometric CAAC^{Me} 221
4.6.5.3.3 Reaction of [MeHN–BH_2]$_n$ with 10 mol% IDipp 222
4.6.5.4 Cyclohexene trapping reactions 223
4.6.5.4.1 Depolymerisation of [MeHN–BH_2]$_n$ with stoichiometric IDipp in the presence of cyclohexene 223
4.6.5.4.2 Depolymerisation of [MeHN–BH_2]$_n$ with substoichiometric IDipp in the presence of cyclohexene 223
4.6.5.4.3 Control reaction of [MeHN–BH_2]$_n$ with cyclohexene 223
4.6.5.4.4 Reaction of IDipp–BH_2NMeH with cyclohexene 224
4.6.6 Reactions of $MeNH_2$·BH_3 with IDipp, I*t*Bu and CAAC^{Me} 224
4.6.6.1 $MeNH_2$·BH_3 with one equivalent of IDipp 224
4.6.6.2 $MeNH_2$·BH_3 with one equivalent of I*t*Bu 224
4.6.6.3 $MeNH_2$·BH_3 with two equivalents of I*t*Bu 226
4.6.6.4 $MeNH_2$·BH_3 with two equivalents of CAAC^{Me} 227
4.6.6.5 Synthesis of the *cis*- and *trans*-(CAAC^{Me}H)HB=NMe(CAAC^{Me}H) (4.3) 228
4.6.7 Reaction of [MeHN–BH_2]$_n$ with stoichiometric $NMeH_2$ 233

4.6.8 Supplementary tables 233
4.6.5.2 X-ray crystallography 233
4.6.9 Supplementary data 234
4.6.5.2 Cartesian coordinates and SCF energies of the calculated structures 234
4.7 References 239
Chapter 5 Extension of the substrate scope of the CAAC-mediated dehydropolymerisation of phosphine-boranes and studies of the reactivity of IDipp–BH_2NMeH 243
5.1 Introductory comments 243
5.2 Abstract 243
5.3 Extension of the substrate scope of the CAAC-mediated dehydropolymerisation of phosphine-boranes 244
5.3.1 Introduction 244
5.3.2 Results and discussion 246
5.3.2.1 Polymerisation of *rac*-Ph(Me)PH·BH_3 using CAAC^{Me} 246
5.3.2.2 Polymerisation of Et_2PH·BH_3 using CAAC^{Me} 247
5.3.2.3 Polymerisation of *n*Hex_2PH·BH_3 using CAAC^{Me} 251
5.3.2.4 Attempted synthesis of the copolymers $[Ph_2P–BH_2]_n$-*r*-$[PhHP–BH_2]_m$ mediated by CAAC^{Me} 251
5.3.3 Conclusions 253
5.4 Studies of the reactivity of IDipp–BH_2NMeH 254
5.4.1 Introduction 254
5.4.2 Results and discussion 256
5.4.2.1 Thermal reactivity of IDipp–BH_2NMeH 256
5.4.2.2 Attempts to regenerate $[MeHN–BH_2]_n$ from IDipp–BH_2NMeH by addition of Lewis acids 259
5.4.3 Conclusions 261
5.5 Supporting information 262
5.5.1 General procedures, reagents and equipment 262
5.5.2 Polymerisation of *rac*-Ph(Me)PH·BH_3 using CAAC^{Me} 264
5.5.3 Polymerisation of Et_2PH·BH_3 using CAAC^{Me} 267
5.5.3.1 Synthesis of $PEt_2H·BH_3$ 267
5.5.3.2 Synthesis of CAAC^{Me}(H)Et_2PBH_3 (5.1) 267
5.5.3.3 Synthesis of $[Et_2P–BH_2]_n$ 270
5.5.3.4 Thermal analysis of $[Et_2P–BH_2]_n$ 272
5.5.4 Polymerisation of *n*Hex_2PH·BH_3 using CAAC^{Me} 274
5.5.4.1 Synthesis of *n*$Hex_2P·BH_3$ 274
5.5.4.2 Synthesis of $[nHex_2P–BH_2]_n$ 275

5.5.5 Attempted synthesis of copolymers $[Ph_2P–BH_2]_n$-r-$[PhHP–BH_2]_m$ using $CAAC^{Me}$ 276
5.5.6 Thermolysis of Dipp–BH_2NMeH 278
5.5.6.1 Synthesis of ring expansion product (5.2) 278
5.5.6.2 Synthesis of IDipp–BH_2NMeBHNMeH (5.3) 279
5.5.7 Addition of Lewis acids to IDipp–BH_2NMeH 280
5.5.7.1 Attempted regeneration of $[MeHN–BH_2]_n$ from IDipp–BH_2NMeH with $Ph_2N=BCl_2$ 280
5.5.7.2 Attempted regeneration of $[MeHN–BH_2]_n$ from IDipp–BH_2NMeH with BCl_3 282
5.5.7.3 Attempted regeneration of $[MeHN–BH_2]_n$ from IDipp–BH_2NMeH with $B(C_6F_5)_3$ 284
5.5.8 Supplementary Tables 285
5.5.8.1 X-ray crystallography 285
5.6 References 286
Chapter 6 Outlook 288
6.1 Investigating other metal-free routes for the dehydropolymerisation of phosphine-boranes 288
6.2 Material properties and applications of P-disubstituted polyphosphinoboranes 289
6.3 Detailed mechanistic studies into the dehydropolymerisation of phosphine-boranes using $Ni(COD)_2$ precatalyst 290
6.4 Reactivity of the cyclic trimer $[PhHP–BH_2]_3$ 290
6.5 Reactivity of ammonia-borane with CAACs 292
6.6 Thermolysis of IDipp–BH_2NMeH adduct 292
6.7 References 293

List of Figures

Figure 1.1 Representative synthesis of polysilanes using the Wurtz reaction. 2

Figure 1.2 a Homo-dehydrocoupling; and **b** hetero-dehydrocoupling to form main group element-element bonds. 2

Figure 1.3 Formation of a B–B bond using Pt-based catalyst. 2

Figure 1.4 Common syntheses of inorganic polymers via **a** catalytic dehydropolymerisation; and **b** ring-opening polymerisation. 3

Figure 1.5 Examples of main group polymers. 3

Figure 1.6 Polyaminoboranes and polyphosphinoboranes are isoelectronic with polyolefins. 4

Figure 1.7 Structure of amine-boranes (left) and aminoboranes (right). 5

Figure 1.8 Substrate scope of polyaminoboranes. M_w (Da) given for first reported examples.[79–81,94–96] 8

Figure 1.9 Structural extremes of phosphinoboranes.[111] 11

Figure 1.10 Summary of P-monosubstituted polyphosphinoboranes.[117,119–121,123,125–128] 13

Figure 1.11 Typical dehydrocoupling pathway for ammonia-borane and primary amine-boranes. 16

Figure 1.12 Metal-catalysed dehydrogenation of amine-boranes: **a** inner sphere B–H/N–H activation; **b** ligand assisted cooperative mechanism; or **c** hydride abstraction/boronium co-catalysis.[30] 17

Figure 1.13 Mechanistic proposal for the dehydropolymerisation of $MeNH_2{\cdot}BH_3$ using $[Rh(Xantphos)\{H_2BNMe_3(CH_2)_2tBu\}][BAr^F{}_4]$ catalyst.[145] 18

Figure 1.14 Mechanistic proposal for the dehydropolymerisation of $NH_3{\cdot}BH_3$ using $[IrH_2(H_2)_2(PCy_3)_2][BAr^F{}_4]$ catalyst.[146] 19

Figure 1.15 Mechanistic proposal for the polymerisation of $H_2N{=}BH_2$ using IrH_2POCOP catalyst. A separate metal-centre is responsible for the dehydrogenation of $NH_3{\cdot}BH_3$. 20

Figure 1.16 Mechanistic proposal for the dehydrocoupling of $Ph_2PH{\cdot}BH_3$ and $CyPH_2{\cdot}BH_3$ using $[Rh(dppp)(\eta^6\text{-}C_6H_5F)][BAr^F{}_4]$ catalyst.[154] 22

Figure 1.17 a Mechanistic proposal for the synthesis of the active species in the reaction between $PhPH_2{\cdot}BH_3$ and $[RhCp^*(PMe_3)Me(ClCH_2Cl)][BAr^F{}_4]$; and **b** proposed reversible chain-transfer polymerisation. 23

Figure 1.18 Mechanistic proposal for the dehydrocoupling of $PhPH_2{\cdot}BH_3$ using $[CpFe(CO)_2(OTf)]$ catalyst.[118] 24

Figure 1.19 Head-to-tail polymerisation of aminoboranes and phosphinoboranes. 25

Figure 1.20 a Molecular orbital diagram of linear and bent carbenes; and **b** illustrative representation of the occupation of the orbitals in triplet and singlet carbenes.[160] 25

Figure 1.21 a The 'push-pull' effect demonstrated in a diamido-substituted carbene; and **b** the first isolated NHC.[165] 26
Figure 1.22 Relative HOMO and LUMO energies of NHC (left) vs CAAC (right). 28
Figure 1.23 Small molecule and E–H bond activation by CAACs.[200–205] 30
Figure 2.1 Thermal ellipsoid plot of **2.1b**. Ellipsoids are shown at the 30% probability level. Second molecule of **2.1b** and THF solvent molecules from the asymmetric unit, along with H atoms other than those bound to C1 and B1 have been omitted for clarity. 48
Figure 2.2 Simplified schematic reaction profile calculated for the reaction of *N*-phenyl CAAC (**A**) with $PhPH_2{\cdot}BH_3$ (**B**) at the PBE0/6-31+G(d,p)/IEFPCM(THF) level of theory; Gibbs free energies for the second diastereomer are given in round brackets. **C-1$_{pair}$, C-2$_{pair}$ and C-3$_{pair}$,** which differ in the orientation of the ions, have been simplified to **C$_{pair}$.** (For a comprehensive depiction of the reaction profile see Figure S2.30). 54
Figure 2.3 ^{31}P NMR of products of the dehydropolymerisation of $Ph_2PH{\cdot}BH_3$ using **a** CAAC^{Me} in THF; **b** CAAC^{Me} in toluene; and **c** CAAC^{Cy} in toluene before and after precipitation into hexanes (*denotes excess $Ph_2PH{\cdot}BH_3$, ~denotes CAAC^{Me}(H)PPH_2, ^denotes CAAC^{Cy}(H)PPH_2, #denotes Ph_2PH). 60
Figure 2.4 Thermal ellipsoid plot of **2.3c**. H atoms other than those bound to C9 and B1 have been omitted for clarity. Ellipsoids are shown at the 30% probability level. 60
Figure 2.5 a Thermal ellipsoid plot of **2.4a**; and **b** thermal ellipsoid plot of **2.4b**. For both **4a** and **4b** ellipsoids are shown at the 30% probability level, and H atoms other than those at the B1 centre have been omitted for clarity. 62
Figure 2.6 a Proposed addition head-to-tail polymerisation sequence; and **b** chain-end capping resulting in linear polymers. 63
Figure 3.1 $^{31}P\{^1H\}$ NMR spectra (122 MHz, 25 °C) of the reaction mixtures for runs 1, 10 and 13 (Table 3.1) (#oligomeric material removed by precipitaion, ~trace $PPhH_2$). 147
Figure 3.2 GPC chromatograms of isolated $[PhHP–BH_2]_n$ from for runs 1, 10 and 13 (Table 3.1) (*below calibration region). 148
Figure 3.3 GPC chromatogram of both the precipitate and supernatant of run 15 (Table 3.1). 149
Figure 3.4 Thermal ellipsoid plot of $[PhHP–BH_2]_3$ (**3.1**). Ellipsoids are shown at the 30% probability level. H atoms other than those bound to B and P atoms have been omitted for clarity..... 150
Figure 3.5 Plot of conversion vs M_n and M_w (1 mol% cat., 1 M, 70 °C, THF). No data below ca. 70% conversion as not possible to integrate the GPC trace..... 151
Figure 4.1 Carbenes explored in this work. 194
Figure 4.2 Thermal ellipsoid plot of IDipp–BH_2NMeH (**4.1**). Ellipsoids are shown at the 30% probability level. H atoms other than those on B1 and N1 have been omitted for clarity. 196

Figure 4.3 Thermal ellipsoid plot of *trans*-**4.3**. Ellipsoids are shown at the 30% probability level. H atoms other than those on C1, C22 and B1 have been omitted for clarity. 206
Figure 4.4 Proposed mechanism for the spontaneous depolymerisation of $[MeHN–BH_2]_n$ in THF. .. 207
Figure 4.5 Proposed mechanism for depolymerisation of $[MeHN–BH_2]_n$ mediated by NHCs and weak donors. 208
Figure 4.6 Proposed mechanism for depolymerisation of $[MeHN–BH_2]_n$ mediated by $CAAC^{Me}$. 210
Figure 5.1 GPC trace of the products of the reaction between $Ph_2PH·BH_3$ and $CAAC^{Me}$ after work up to exemplify the minor high molar mass component. $(CAAC^{Me})H_2$ is removed through precipitation of the reaction mixture into cold (-40 °C) hexanes.[1] 245
Figure 5.2 Thermal ellipsoid plot of $CAAC^{Me}(H)Et_2PBH_3$ (**5.1**). Ellipsoids are shown at the 30% probability level. H atoms other than those on C5 and B1 have been omitted for clarity. 248
Figure 5.3 ^{31}P NMR spectra (122 MHz, 25 °C, $CDCl_3$) of the isolated material from the copolymerisations of $PhPH_2·BH_3$ with $Ph_2PH·BH_3$. 252
Figure 5.4 ESI(+)-MS spectrum in positive mode in THF:IPA (1:9) of the isolated material from the polymerisations of **a** $PhPH_2·BH_3$; **b** $PhPH_2·BH_3$ with $Ph_2PH·BH_3$ (50:50); and **c** $Ph_2PH·BH_3$. 253
Figure 5.5 Representative ^1H NMR spectrum (C_6D_6, 500 MHz, 298 K) of the reaction mixture of the thermolysis of IDipp–BH_2NMeH (run 1). 256
Figure 5.6 Thermal ellipsoid plot of IDipp–BH_2NMeBHNMeH (**5.3**). Ellipsoids are shown at the 30% probability level. H atoms other than those on B1, H2A and N4 have been omitted for clarity. 257
Figure 5.7 Illustration of the donor-acceptor stabilised iminoborane. 257
Figure 6.1 Main group FLP systems which have been successful for catalytic dehydrogenation of amine-boranes.[1,2] 289
Figure 6.2 a and **b** Trapped iminoboranes reported by Rivard *et al*; and **c** proposed trapped iminoborane. 293

Figure S2.1 ^1H NMR spectrum (400 MHz, 298 K THF-d_8) of **2.1a**. Iminium C-H proton is very broad. The iminium C-H proton resonance is 8.07. (*denotes residual partially protiated THF). 69
Figure S2.2 $^{11}B\{^1H\}$ (left) and ^{11}B (right) NMR spectra (96 MHz, 295 K, THF-d_8) of **2.1a** (*denotes trace μ-$(PhPH)B_2H_5$). 69
Figure S2.3 $^{31}P\{^1H\}$ (top) and ^{31}P (bottom) NMR spectra (122 MHz, 296 K, THF-d_8) of **2.1a** (*denotes trace $PhPH_2$). 69
Figure S2.4 ^1H NMR spectrum (400 MHz, 295 K, THF-d_8) of **2.1b** (*denotes residual partially protiated THF, ~denotes THF). 70
Figure S2.5 $^{11}B\{^1H\}$ (left) and ^{11}B (right) NMR spectra (96 MHz, 295 K, THF-d_8) of **2.1b**. 71

Figure S2.6 $^{31}P\{^{1}H\}$ (left) and ^{31}P (right) NMR spectra (122 MHz, 296 K, THF-d_8) of **2.1b**..... 71
Figure S2.7 ^{1}H NMR spectrum (400 MHz, 298 K, THF-d_8) of **2.3a** (*denotes $(CAAC^{Me})H_2$, #denotes residual partially protiated THF). Doublet of quartets of doublets splitting pattern of P–H proton is expanded. 73
Figure S2.8 $^{11}B\{^{1}H\}$ (left) and ^{11}B (right) NMR spectra (96 MHz, 295 K, THF-d_8) of **2.3a** (*denotes trace $(CAAC^{Me})\cdot BH_3$ adduct).[38] 74
Figure S2.9 $^{31}P\{^{1}H\}$ (left) and ^{31}P (right) NMR spectra (122 MHz, 296 K, THF-d_8) of **2.3a**. 74
Figure S2.10 ESI(+)-MS spectrum of $[PhHP–BH_2]_n$ product from run 1 of Table S2.1 in DCM..... 75
Figure S2.11 ESI(+)-MS spectrum of $[PhHP–BH_2]_n$ product from run 2 of Table S2.1 in DCM..... 75
Figure S2.12 ESI(-)-MS spectrum of $[PhHP–BH_2]_n$ product from run 3 of Table S2.1 in DCM. 76
Figure S2.13 ESI(+)-MS spectrum of $[PhHP–BH_2]_n$ product from run 5 of Table S2.1 in DCM..... 76
Figure S2.14 ESI(+)-MS spectrum of $[PhHP–BH_2]_n$ product from run 6 of Table S2.1 in DCM..... 77
Figure S2.15 ESI(+)-MS spectrum of $[PhHP–BH_2]_n$ product from run 7 of Table S2.1 in DCM..... 77
Figure S2.16 GPC chromatogram of precipitated $[PhHP–BH_2]_n$ products from for runs 1-7 from Table S2.1. 2 mg mL^{-1} in THF with 0.1 w/w% nBu$_4$NBr in the THF eluent (*oligomeric material, ~system peak). 78
Figure S2.17 $^{31}P\{^{1}H\}$ NMR spectra (122 MHz, 298 K, THF-d_8) of the crude reaction mixture between $PhPH_2\cdot BH_3$ and $CAAC^{Me}$ for run 4 (*denotes material which may be a mixture of linear and cyclic oligomers[54])..... 78
Figure S2.18 ^{1}H NMR spectrum (400 MHz, 298 K, THF-d_8) of isolated $[PhHP–BH_2]_n$ from run 4 (*denotes partially protiated THF, #denotes THF, ~denotes hexanes)..... 79
Figure S2.19 $^{11}B\{^{1}H\}$ (left) and ^{11}B (right) NMR spectra (96 MHz, 295 K, THF-d_8) of isolated $[PhHP–BH_2]_n$ from run 4. 79
Figure S2.20 $^{31}P\{^{1}H\}$ (left) and ^{31}P (right) NMR spectra (122 MHz, 298 K, THF-d_8) of isolated $[PhHP–BH_2]_n$ from run 4. 79
Figure S2.21 ESI(-)-MS (left) and ESI(+)-MS (right) spectra of $[PhHP–BH_2]_n$ product from run 4 in Table S2.1. The predominant species are linear systems with a BH_3 end group $(BH_3\text{-}[PhHP–BH_2]_n\text{-}H)^-$ or a $PPhH_2$ end group $(H\text{-}[PhHP–BH_2]_n\text{-}PPhH)^+$ respectively..... 79
Figure S2.22 GPC chromatogram of precipitated $[PhHP–BH_2]_n$ product from run 4 of Table S2.1. 2 mg mL^{-1} in THF with 0.1 w/w% nBu$_4$NBr in the THF eluent. 80
Figure S2.23 Photograph of isolated $[PhHP–BH_2]_n$. 80
Figure S2.24 ^{1}H NMR spectrum (400 MHz, 298 K, C_6D_6) of $(CAAC^{Me})H_2$ (*denotes residual partially protiated benzene). 81
Figure S2.25 ^{13}C NMR spectrum (101 MHz, 298 K, C_6D_6) of $(CAAC^{Me})H_2$ (*denotes benzene). 81

Figure S2.26 Thermal ellipsoid plot of (CAAC^{Me})H_2. Ellipsoids are shown at the 30% probability level. H atoms other than those at the C1 centre have been omitted for clarity. 81
Figure S2.27 Plot of ln[**2.3a**] with reaction time for runs 8 – 15 from Table S2.2 (y = ln[**2.3a**], x = time (s)). 83
Figure S2.28 Plot of ln[**2.3a**] with reaction time for runs 11 ([**2.3a**] = 0.5 M, blue circles), 13 ([**2.3a**] = 0.3 M, orange diamonds) and 14 ([**2.3a**] = 0.7 M, grey triangles) from Table S2.2. The calculation of equivalent half-lives for different initial concentration of **2.3a** using Supplementary Equations 1 and 2 indicates unimolecular first order kinetics. 84
Figure S2.29 Eyring plot using data from runs 8 -12 from Table S2.2 used to calculate values for $\Delta H^{\ddagger}$ and $\Delta S^{\ddagger}$ using Supplementary Equations 3-6 ($\Delta H^{\ddagger}$ = 21.5 kcal mol^{-1}, $\Delta S^{\ddagger}$ = -9.5 K^{-1} mol^{-1}). (y = ln[**2.3a**], x = time (s)). 84
Figure S2.30 Schematic Gibbs energy profile for the P–H activation of $PhPH_2{\cdot}BH_3$ (**A**) with CAAC (**B**) and subsequent reaction steps; standard Gibbs free energies are given in kcal mol^{-1} relative to those of **A** and **B** in THF; Gibbs free energies for toluene as solvent are given in square brackets. 86
Figure S2.31 Schematic Gibbs energy profiles for substitution at boron (left) and B–H activation from CAAC (**B**) and $PhPH_2{\cdot}BH_3$ (**A**) (right); standard Gibbs free energies are given in kcal mol^{-1} relative to those of **A** and **B** in THF; Gibbs free energies for toluene as solvent are given in square brackets. 87
Figure S2.32 Schemes depicting the intermolecular hydride abstraction pathway: a) intermolecular hydride abstraction from **F** (**F'**) by the [CAAC(H)]$^+$ (**D**) iminium ion leading to a phosphinoborenium ion **M** (**M'**) and CAAC(H_2) (**G**) and b) subsequent conversion of **M** (**M'**) to **D** and phosphinoborane [PhHP–BH_2] (**H**); standard Gibbs free energies are given in THF. 90
Figure S2.33 $^{11}B\{^1H\}$ (left) and ^{11}B (right) NMR spectra (96 MHz, 295 K, THF) of **2.3b**. 92
Figure S2.34 $^{31}P\{^1H\}$ (left) and ^{31}P (right) NMR spectra (122 MHz, 295 K, THF) of **2.3b**. 92
Figure S2.35 ESI(+)-MS spectrum in positive mode of unseparated $[Ph_2P–BH_2]_n$ and $Ph_2PH{\cdot}BH_2$–$PPh_2{\cdot}BH_3$ (m/z = 398.2) formed from $Ph_2PH{\cdot}BH_3$ and CAAC^{Me} in THF. The species highlighted in yellow is a linear system with a PPh_2H end group (H-$[Ph_2P–BH_2]_n$-$PPh_2H)^+$ and the species highlighted in blue is a linear system with a CAAC^{Me} end group (H-$[Ph_2P–BH_2]_n$-CAAC$^{Me})^+$. 94
Figure S2.36 ESI(+)-MS spectrum in positive mode of $[Ph_2P–BH_2]_n$ formed from $Ph_2PH{\cdot}BH_3$ and CAAC^{Me} in toluene. The species highlighted in yellow is a linear system with a PPh_2H end group (H-$[Ph_2P–BH_2]_n$-$PPh_2H)^+$ and the species highlighted in blue is a linear system with a CAAC^{Me} end group (H-$[Ph_2P–BH_2]_n$-CAAC$^{Me})^+$. 95
Figure S2.37 GPC chromatogram of $[Ph_2P–BH_2]_n$ formed from $Ph_2PH{\cdot}BH_3$ and CAAC^{Me} in toluene. 2 mg mL^{-1} in THF with 0.1 w/w% $n$$Bu_4NBr$ in the THF eluent. The highest molar mass peak accounts for ca. 10% of the precipitated material. The bimodal distribution can be explained by the competition between chain termination and propagation. Most of the material undergoes early termination,

potentially by addition of a free CAAC^{Me} unit as evidenced in the ESI-MS, whereas a small percentage of the material undergoes significant further polymerisation to give high molar mass material..... 95
Figure S2.38 GPC chromatograms of the separation attempts of the $[Ph_2P–BH_2]_n$ formed from $Ph_2PH·BH_3$ and CAAC^{Cy} in toluene. 2 mg mL^{-1} in THF with 0.1 w/w% nBu$_4$NBr in the THF eluent. The GPC chromatograms have been normalised to the low molar mass material. Although the stepwise precipitation of material does show an increase in the percentage of high molar mass material for the earlier fraction there is still not a significant amount. For Fraction A M_n = 59,600 and $Đ$ = 1.08, however, since the standard used for the calibration of the GPC instrument is polystyrene $[PhCHCH_2]_n$, the intrinsic values shown here may not be accurate especially as the presence of a second phenyl group will most likely reduce the amount of coiling of the polymer chains in solution. 97
Figure S2.39 ^{1}H NMR spectrum (400 MHz, 298 K, $CDCl_3$) of $[Ph_2P–BH_2]_n$ formed from $Ph_2PH·BH_3$ and CAAC^{Cy} in toluene (Fraction A) (*denotes partially protiated $CDCl_3$, ~denotes trace DCM, $^{\#}$denotes trace THF, ^denotes trace hexanes). 97
Figure S2.40 ^{11}B{^{1}H} (left) and ^{11}B (right) NMR spectra (96 MHz, 295 K, $CDCl_3$) of $[Ph_2P–BH_2]_n$ formed from $Ph_2PH·BH_3$ and CAAC^{Cy} in toluene. (Fraction A). 98
Figure S2.41 ^{31}P{^{1}H} (left) and ^{31}P (right) NMR spectra (122 MHz, 295 K, $CDCl_3$) of $[Ph_2P–BH_2]_n$ formed from $Ph_2PH·BH_3$ and CAAC^{Cy} in toluene. (Fraction A). The observation of two peaks can be explained by the presence of both oligomeric and polymeric material, as is observed in the GPC chromatogram. 98
Figure S2.42 ESI(+)-MS spectrum in positive mode of $[Ph_2P–BH_2]_n$ formed from $Ph_2PH·BH_3$ and CAAC^{Cy} in toluene (Fraction A). The species highlighted in blue is a linear system with a CAAC^{Cy} end group (H-$[Ph_2P–BH_2]_n$-CAAC^{Cy})$^+$ and the species highlighted in yellow is a linear system with an unidentified end group (m/z of end group = 178.3). 98
Figure S2.43 Photograph of $[Ph_2P–BH_2]_n$ (Fraction A). 99
Figure S2.44 ^{1}H NMR spectrum (400 MHz, 298 K, $CDCl_3$) of **2.3c'** (*denotes residual partially protiated $CDCl_3$). 100
Figure S2.45 ^{13}C NMR spectrum (101 MHz, 298 K, $CDCl_3$) of **3c'** (*denotes $CDCl_3$). 100
Figure S2.46 ^{11}B{^{1}H} (left) and ^{11}B (right) NMR spectra (96 MHz, 295 K, THF) of **2.3c**. 101
Figure S2.47 ^{31}P{^{1}H} (left) and ^{31}P (right) NMR spectra (122 MHz, 295 K THF) of **2.3c**. 101
Figure S2.48 ESI(+)-MS spectrum of **2.3c** in DCM showing the [**2.3c**+H]$^+$ peak (sample injection performed under ambient conditions in air). 101
Figure S2.49 ^{31}P{^{1}H} NMR spectra (122 MHz, 295 K, toluene) of dehydropolymerisation of *rac*-PhEtPH·BH_3 using CAAC^{Me} over time **a** 10 min at 22 °C; **b** 1 h at 100 °C; and **c** 20 h at 100 °C ($^{\#}$denotes trace CAAC^{Me}(H)(PhEtP), ~denotes trace PhEtPH). 102

Figure S2.50 ESI(+)-MS spectrum in positive mode in DCM of $[PhEtP–BH_2]_n$ formed from *rac*-$PhEtPH·BH_3$ and $CAAC^{Me}$ in toluene. The predominant species is a linear system with a $CAAC^{Me}$ end group (H-$[PhEtP–BH_2]_n$-$CAAC^{Me}$)$^+$. 103
Figure S2.51 ^1H NMR spectrum (400 MHz, 298 K, $CDCl_3$) of $[PhEtP–BH_2]_n$ formed from $PhEtPH·BH_3$ and $CAAC^{Cy}$ in toluene (* denotes residual partially protiated $CDCl_3$, ~ denotes trace DCM, # denotes trace $(CAAC^{Me})H_2$, ^denotes trace hexanes). 104
Figure S2.52 $^{11}B\{^1H\}$ (left) and ^{11}B (right) NMR spectra (96 MHz, 298 K, $CDCl_3$) of $[PhEtP–BH_2]_n$ formed from $PhEtPH·BH_3$ and $CAAC^{Cy}$ in toluene. 104
Figure S2.53 $^{31}P\{^1H\}$ (left) and ^{31}P (right) NMR spectra (122 MHz, 295 K, $CDCl_3$) of $[PhEtP–BH_2]_n$ formed from $PhEtPH·BH_3$ and $CAAC^{Cy}$ in toluene. 104
Figure S2.54 ESI(+)-MS spectrum in positive mode in DCM of $[PhEtP–BH_2]_n$ formed from $PhEtPH·BH_3$ and $CAAC^{Cy}$ in toluene The predominant species is a linear system with a $CAAC^{Cy}$ end group (H-$[PhEtP–BH_2]_n$-$CAAC^{Cy}$)$^+$. 105
Figure S2.55 GPC chromatogram of $[PhEtP–BH_2]_n$ formed from $PhEtPH·BH_3$ and $CAAC^{Cy}$ in toluene. 2 mg mL^{-1} in THF with 0.1 w/w% $n$$Bu_4NBr$ in the THF eluent. The highest molar mass peak accounts for ca. 18% of the precipitated material. The bimodal distribution can be explained by the competition between chain termination and propagation. Most of the material undergoes early termination, potentially by a free $CAAC^{Cy}$ unit as evidenced in the ESI-MS, whereas a small percentage of the material undergoes significant further polymerisation to give high molar mass material. 105
Figure S2.56 Photograph of isolated $[PhEtP–BH_2]_n$. 106
Figure S2.57 ^1H NMR spectrum (400 MHz, 298 K, C_6D_6) of **2.4a** (*denotes residual partially protiated benzene). 107
Figure S2.58 $^{11}B\{^1H\}$ (left) and ^{11}B (right) NMR spectra (128 MHz, 298 K, C_6D_6) of **2.4a**. 107
Figure S2.59 $^{31}P\{^1H\}$ (left) and ^{31}P (right) NMR spectra (162 MHz, 298 K, C_6D_6) of **2.4a**. 108
Figure S2.60 $^{13}C\{^1H\}$ NMR spectrum (101 MHz, 298 K, C_6D_6) of **2.4a** (*denotes benzene). 108
Figure S2.61 ESI(+)-MS spectrum of H[**2.4a**]$^+$ cation in DCM (sample injection performed under ambient conditions in air). 108
Figure S2.62 1H NMR spectrum (400 MHz, 298 K, C_6D_6) of **2.4b** (*denotes residual partially protiated C_6D_6). 110
Figure S2.63 $^{11}B\{^1H\}$ (left) and ^{11}B (right) NMR spectra (128 MHz, 298 K, C_6D_6) of **2.4b**. 110
Figure S2.64 31P{1H} (left) and 31P (right) NMR spectra (128 MHz, 298 K, C_6D_6) of **2.4b**..... 110
Figure S 2.65 $^{13}C\{^1H\}$ NMR spectrum (101 MHz, 298 K, C_6D_6) of **2.4b** (*denotes benzene). 111
Figure S2.66 ESI(+)-MS spectrum of H[**2.4b**]$^+$ cation in DCM (sample injection performed under ambient conditions in air). 111

Figure S2.67 ESI(+)-MS spectrum in DCM of the products from the reaction of $Ph_2PH{\cdot}BH_3$ with two equiv. of $CAAC^{Me}$ (sample injection performed under ambient conditions in air). 112
Figure S3.1 $^{11}B\{^1H\}$ NMR spectra (96 MHz, 298 K, THF) of the reaction mixture for runs 1-3 (Table S3.1) (*unreacted $PhPH_2{\cdot}BH_3$, #unidentified impurity). 158
Figure S3.2 $^{31}P\{^1H\}$ NMR spectra (122 MHz, 298 K, THF) of the reaction mixture for runs 1-3 (Table S3.1) (*$PPhH_2$, #oligomeric material). 158
Figure S3.3 GPC chromatogram of isolated $[PhHP–BH_2]_n$ from for runs 1-3 (Table S3.1). 2 mg mL^{-1} in THF with 0.1 w/w% nBu$_4$NBr in the THF eluent (*below calibration region). 159
Figure S3.4 Plot of conversion vs time for runs 1, 4, 5 and 9 (Table S3.1). Conversion determined using relative integrals of ^{11}B NMR spectra. 159
Figure S3.5 $^{11}B\{^1H\}$ NMR spectra (96 MHz, 298 K, THF) of the reaction mixture for runs 1, 4 and 5 (Table S3.1) (*unreacted $PhPH_2{\cdot}BH_3$, #unidentified impurity). 160
Figure S3.6 $^{31}P\{^1H\}$ NMR spectra (122 MHz, 298 K, THF) of the reaction mixture for runs 1, 4 and 5 (Table S3.1) (*$PPhH_2$, #oligomeric material). 160
Figure S3.7 GPC chromatogram of isolated $[PhHP–BH_2]_n$ from for runs 1, 4 and 5 (Table S3.1). 2 mg mL^{-1} in THF with 0.1 w/w% nBu$_4$NBr in the THF eluent (*below calibration region). 160
Figure S3.8 Plot of conversion vs time for runs 1, 6 and 7 (Table S3.1). Conversion determined using relative integrals of ^{11}B NMR spectra. 161
Figure S3.9 GPC chromatogram of isolated $[PhHP–BH_2]_n$ from for runs 1, 6 and 7 (Table S3.1). 2 mg mL^{-1} in THF with 0.1 w/w% nBu$_4$NBr in the THF eluent (*below calibration region). 161
Figure S3.10 Plot of conversion vs time for run 9 (Table S3.1). Conversion determined using relative integrals of ^{11}B NMR spectra. 162
Figure S3.11 $^{11}B\{^1H\}$ NMR spectra (96 MHz, 298 K, THF) of the reaction mixture for runs 1, 8 and 9 (Table S3.1) (*unreacted $PhPH_2{\cdot}BH_3$, #unidentified impurity). 162
Figure S3.12 $^{31}P\{^1H\}$ NMR spectra (122 MHz, 298 K, THF) of the reaction mixture for runs 1, 8 and 9 (Table S3.1) (*$PPhH_2$, #oligomeric material). 163
Figure S3.13 ^1H NMR spectrum (500 MHz, 298 K, $CDCl_3$) of $[PhHP–BH_2]_n$ (run 9) (^denotes residual partially protiated $CDCl_3$). 163
Figure S3.14 ^{31}P NMR spectrum (96 MHz, 298 K, $CDCl_3$) of $[PhHP–BH_2]_n$ (run 9). 163
Figure S3.15 GPC chromatogram of isolated $[PhHP–BH_2]_n$ from for run 9 (Table S3.1). 2 mg mL^{-1} in THF with 0.1 w/w% nBu$_4$NBr in the THF eluent. 164
Figure S3.16 $^{31}P\{^1H\}$ NMR spectra (122 MHz, 298 K, 1,4-dioxane) of the reaction mixture for runs 10, 11 and 12 (Table S3.1). Run 1 included for a comparison with THF (*$PPhH_2$, #oligomeric material).. 164
Figure S3.17 GPC chromatogram of isolated $[PhHP–BH_2]_n$ from for runs 1, 10, 11 and 12 (Table S3.1). 2 mg mL^{-1} in THF with 0.1 w/w% nBu$_4$NBr in the THF eluent (*below calibration region). 165

Figure S3.18 $^{31}P\{^{1}H\}$ NMR spectra (122 MHz, 298 K, 2-*methyl*-THF) of the reaction mixture for run 13 (Table **S3.1**). Run 1 included for a comparison with THF (*$PPhH_2$, #oligomeric material). 165
Figure S3.19 ^{1}H NMR spectrum (500 MHz, 298 K, $CDCl_3$) of $[PhHP–BH_2]_n$ (run 13) (^denotes residual partially protiated $CDCl_3$, * hexanes). 166
Figure S3.20 ^{31}P NMR spectrum (96 MHz, 298 K, $CDCl_3$) of $[PhHP–BH_2]_n$ (run 13). (*shoulder to $[PhHP–BH_2]_n$ potentially due to chain branching). 166
Figure S3.21 GPC chromatogram of isolated $[PhHP–BH_2]_n$ from for runs 1 and 13 (Table S3.1). 2 mg mL^{-1} in THF with 0.1 w/w% $n$$Bu_4NBr$ in the THF eluent (*below calibration region). 166
Figure S3.22 $^{31}P\{^{1}H\}$ NMR spectrum (122 MHz, 298 K, THF) of the reaction mixture for run 14 (Table 3.1) (*$PPhH_2$, #oligomeric material, ~unidentified impurity, presumably from some decomposition occurring in air). 167
Figure S3.23 GPC chromatogram of isolated $[PhHP–BH_2]_n$ from for runs 1 and 14 (Table 3.1). 2 mg mL^{-1} in THF with 0.1 w/w% $n$$Bu_4NBr$ in the THF eluent (*below calibration region). 167
Figure S3.24 $^{11}B\{^{1}H\}$ NMR spectra (96 MHz, 298 K, THF) of the **a** polymerisation reaction mixture; **b** supernatant; and **c** precipitate for run 15 (Table 3.1) (#unidentified impurity). 168
Figure S3.25 $^{31}P\{^{1}H\}$ NMR spectra (96 MHz, 298 K, THF) of the **a** polymerisation reaction mixture; **b** supernatant; and **c** precipitate for run 15 (Table 3.1) (*$PPhH_2$, #oligomeric material, ~$P(O)PhH_2$). 168
Figure S3.26 ^{1}H NMR spectrum (500 MHz, 298 K, $CDCl_3$) of $[PhHP–BH_2]_n$ (run 15) (^denotes residual partially protiated $CDCl_3$, * hexanes). 169
Figure S3.27 ^{31}P NMR spectrum (96 MHz, 298 K, $CDCl_3$) of $[PhHP–BH_2]_n$ (run 15). 169
Figure S3.28 ESI(+)-MS spectrum of isolated $[PhHP–BH_2]_n$ (*m/z* = 122) from run 15 (Table 3.1) The species highlighted in yellow is a linear system with a $PPhH_2$ end group $(H\text{-}[PhHP–BH_2]_n\text{-}PPhH_2)^+$ and the species highlighted in blue has an unidentified end group. 169
Figure S3.29 ^{1}H NMR spectrum (500 MHz, 298 K, $CDCl_3$) of **3.1** (^denotes residual partially protiated $CDCl_3$, ~THF, #hexanes, *HMDSO). 170
Figure S3.30 $^{11}B\{^{1}H\}$ (left) and ^{11}B (right) NMR spectra (96 MHz, 298 K, $CDCl_3$) of **3.1**. 170
Figure S3.31 $^{31}P\{^{1}H\}$ (left) and ^{31}P (right) NMR spectra (122 MHz, 298 K, $CDCl_3$) of **3.1**. 171
Figure S3.32 ^{13}C NMR spectra (101 MHz, 298 K, $CDCl_3$) of **3.1**. 171
Figure S3.33 ESI(+)-MS spectrum of **3.1**. 171
Figure S3.34 Plot of conversion vs time for polymerisation of $PhPH_2{\cdot}BH_3$ using $Ni(COD)_2$. 172
Figure S3.35 $^{11}B\{^{1}H\}$ NMR spectra (96 MHz, 298 K, $CDCl_3$) over time of reaction mixture for polymerisation of $PPhH_2{\cdot}BH_3$ using $Ni(COD)_2$ (*$PhPH_2{\cdot}BH_3$, #unidentified impurity). 172
Figure S3.36 $^{31}P\{^{1}H\}$ NMR (122 MHz, 298 K, $CDCl_3$) over time of reaction mixture for polymerisation of $PhPH_2{\cdot}BH_3$ using $Ni(COD)_2$ (~$PhPH_2{\cdot}BH_3$, #oligomeric material, *$PPhH_2$). 173

Figure S3.37 Colour over time of reaction mixture for polymerisation of $PhPH_2{\cdot}BH_3$ using $Ni(COD)_2$. 173
Figure S3.38 GPC chromatograms of the reaction mixture for polymerisation of $PhPH_2{\cdot}BH_3$ using $Ni(COD)_2$ over time. 2 mg mL^{-1} in THF with 0.1 w/w% nBu$_4$NBr in the THF eluent. 173
Figure S3.39 GPC chromatograms of $[PhHP–BH_2]_n$ before and after addition of extra $PhPH_2{\cdot}BH_3$ after 100% conversion. 2 mg mL^{-1} in THF with 0.1 w/w% nBu$_4$NBr in the THF eluent (*below calibration region). 174
Figure S3.40 Plot of conversion vs time for first and second equiv. of $PhPH_2{\cdot}BH_3$. Conversion determined using relative integrals of ^{11}B NMR spectra. 175
Figure S3.41 Plot of conversion vs time for PPh_3 poisoning experiment and control reaction. Conversion determined using relative integrals of ^{11}B NMR spectra. 176
Figure S3.42 Plot of conversion vs time for Hg poisoning experiment and control reaction. Conversion determined using relative integrals of ^{11}B NMR spectra. 176
Figure S3.43 Plot of conversion vs time for filtration experiments and a control with no filtration. Conversion determined using relative integrals of ^{11}B NMR spectra. 177
Figure S3.44 UV-Vis spectrum of a catalysis solution (1 mol% cat. 4 M, THF) 100x diluted. 177
Figure S3.45 ^{11}B NMR spectrum (96 MHz, 298 K, THF) of the reaction mixture for the attempted dehydrogenation of $MeNH_2{\cdot}BH_2$ after 20h at 70 °C (*peaks present from the $[PhHP–BH_2]_n$ reaction mixture prior to addition of $MeNH_2{\cdot}BH_2$). 178
Figure S3.46 GPC chromatogram of isolated $[n$HexHP–$BH_2]_n$ from polymerisation of nHexPH$_2{\cdot}$BH$_3$ with 1 mol% $Ni(COD)_2$ (Table S3.2). Not possible to integrate high molar mass material. 2 mg mL^{-1} in THF with 0.1 w/w% nBu$_4$NBr in the THF eluent (*below calibration region). 179
Figure S3.47 GPC chromatogram of isolated $[n$HexHP–$BH_2]_n$ from polymerisation of nHexPH$_2{\cdot}$BH$_3$ with 2.5 mol% $Ni(COD)_2$ (Table S3.2). 2 mg mL^{-1} in THF with 0.1 w/w% nBu$_4$NBr in the THF eluent (*below calibration region). 179
Figure S3.48 ^{1}H NMR spectrum (300 MHz, 298 K, $CDCl_3$) of isolated $[n$HexHP–$BH_2]_n$ from polymerisation of nHexPH$_2$BH$_3$ with 2.5 mol% $Ni(COD)_2$ (Table S3.2) (*denotes residual partially protiated $CDCl_3$). 180
Figure S3.49 ^{11}B{^{1}H} (left) and ^{11}B (right) NMR spectra (96 MHz, 298 K, $CDCl_3$) of isolated $[n$HexHP–$BH_2]_n$ from polymerisation of nHexPH$_2$BH$_3$ with 2.5 mol% $Ni(COD)_2$ (Table S3.2). 180
Figure S3.50 ^{31}P{^{1}H} (left) and ^{31}P (right) NMR spectra (122 MHz, 298 K, $CDCl_3$) of $[n$HexHP–$BH_2]_n$ from polymerisation of nHexPH$_2$BH$_3$ with 2.5 mol% $Ni(COD)_2$ (Table S3.2). 180
Figure S 3.51 ESI(+)-MS spectrum of isolated $[n$HexPHBH$_2]_n$ from polymerisation of nHexPH$_2{\cdot}$BH$_3$ with 2.5 mol% $Ni(COD)_2$. 181

Figure S3.52 $^{11}B\{^{1}H\}$ (left) and ^{11}B (right) NMR spectra (96 MHz, 298 K, $CDCl_3$) of the precipitated material from the reaction of $Ph_2PH{\cdot}BH_3$ with 1 mol% $Ni(COD)_2$. Species identified based on literature values.[64] 181
Figure S3.53 $^{31}P\{^{1}H\}$ (left) and ^{31}P (right) NMR spectra (122 MHz, 298 K, $CDCl_3$) of the precipitated material from the reaction of $Ph_2PH{\cdot}BH_3$ with 1 mol% $Ni(COD)_2$. Species identified based on literature values.[64] 182
Figure S3.54 ESI(-)-MS spectrum of the precipitated material from the reaction of $Ph_2PH{\cdot}BH_3$ with 1 mol% $Ni(COD)_2$. No evidence of any higher molar mass material. 182
Figure S3.55 GPC chromatogram of the precipitated material from the reaction of $Ph_2PH{\cdot}BH_3$ with 1 mol% $Ni(COD)_2$. 2 mg mL^{-1} in THF with 0.1 w/w% nBu$_4$NBr in the THF eluent (*below calibration region). 183
Figure S3.56 $^{11}B\{^{1}H\}$ (left) and ^{11}B (right) NMR spectra (96 MHz, 298 K, $CDCl_3$) of the precipitated material from the reaction of $PhEtPH{\cdot}BH_3$ with 1 mol% $Ni(COD)_2$ 183
Figure S3.57 $^{31}P\{^{1}H\}$ (left) and ^{31}P (right) NMR spectra (122 MHz, 298 K, $CDCl_3$) of the precipitated material from the reaction of $PhEtPH{\cdot}BH_3$ with 1 mol% $Ni(COD)_2$. 183
Figure S3.58 ESI(+)-MS (left) and ESI(-)-MS (right) spectra of the precipitated material from the reaction of $PhEtPH{\cdot}BH_3$ with 1 mol% $Ni(COD)_2$. 184
Figure S3.59 GPC chromatogram of the precipitated material from the reaction of $PhEtPH{\cdot}BH_3$ with 1 mol% $Ni(COD)_2$. 2 mg mL^{-1} in THF with 0.1 w/w% nBu$_4$NBr in the THF eluent (*below calibration region). 184
Figure S4.1 ^{11}B NMR spectra ($CDCl_3$, 96 MHz, 296 K) of $[MeHN–BH_2]_n$. 213
Figure S4.2 GPC chromatogram of $[MeHN–BH_2]_n$. 2 mg mL^{-1} in THF with 0.1 w/w% nBu$_4$NBr in the THF eluent. 213
Figure S4.3 ^{11}B NMR spectra (THF, 96 MHz, 296 K) of the reaction mixture of $[MeHN–BH_2]_n$ and ItBu after **a** 30 min; **b** 20 h; and **c** 48 h. 214
Figure S4.4 EI mass spectrum (+) of the reaction solution of ItBu and $[MeHN–BH_2]_n$. 215
Figure S4.5 a $^{11}B\{^{1}H\}$; and **b** ^{11}B NMR spectra (THF, 96 MHz, 295 K) of the reaction mixture of $[MeHN–BH_2]_n$ and CAAC^{Me}. 216
Figure S4.6 $^{11}B\{^{1}H\}$ NMR spectra (THF, 116 MHz, 298 K) of the reaction mixture of $[MeHN–BH_2]_n$ and IDipp after 10 min. **a** IDipp added to $[MeHN–BH_2]_n$; and **b** $[MeHN–BH_2]_n$ added to IDipp (*traces of $[BF_4]^-$ from the imidazolium salt) 216
Figure S4.7 Stacked ^{11}B NMR (THF, 116 MHz, 298 K) for the reaction of $[MeHN–BH_2]_n$ and **a** 0 mol%; **b** 5 mol%; **c** 10 mol%; **d** 25 mol%; **e** 50 mol% and **f** 100 mol% of IDipp 217
Figure S4.8 GPC chromatogram of the reaction of $[MeHN–BH_2]_n$ and 5 mol% of IDipp. 2 mg mL^{-1} in THF with 0.1 w/w% nBu$_4$NBr in the THF eluent. 218

Figure S4.9 a $^{11}B\{^{1}H\}$; and **b** ^{11}B NMR spectra (THF, 116 MHz, 298 K) of the reaction mixture of $[MeHN–BH_2]_n$ and 10 mol% ItBu after 48 h. 218
Figure S4.10 Stacked ^{11}B NMR NMR spectra (THF, 116 MHz, 298 K) for the reaction of $[MeHN–BH_2]_n$ and **a** 0 mol%; **b** 5 mol%; **c** 10 mol%; **d** 25 mol%; **e** 50 mol%; **f** 75 mol%; **g** 90 mol%; and **h** 100 mol% of $CAAC^{Me}$. 219
Figure S4.11 GPC chromatograms (high molar mass region) of reaction of $[MeHN–BH_2]_n$ with 0 mol%, 5 mol%, 10 mol%, 25 mol%, 50 mol%, 75 mol% and 90 mol% of $CAAC^{Me}$. Normalised to the polymer peak. 2 mg mL^{-1} in THF with 0.1 w/w% nBu$_4$NBr in the THF eluent..... 220
Figure S4.12 Stacked ^{11}B NMR NMR spectra (THF, 116 MHz) for the stoichiometric reaction of $[MeHN–BH_2]_n$ and Dipp from -80 °C to 20 °C. 221
Figure S4.13 Stacked ^{11}B NMR NMR spectra (THF, 116 MHz) for the stoichiometric reaction of $[MeHN–BH_2]_n$ and $CAAC^{Me}$ from -80 °C to 20 °C. 222
Figure S4.14 $^{11}B\{^{1}H\}$ NMR spectra (THF, 116 MHz, 298 K) of the reaction of $[MeHN–BH_2]_n$ with excess cyclohexene after **a** 0 days; **b** 1 days; **c** 3 days; **d** 8 days; **e** 14 days; and **f** 30 days..... 223
Figure S4.15 GPC chromatograms of reaction of $[MeHN–BH_2]_n$ with cyclohexene after 0 days and 30 days. 2 mg mL^{-1} in THF with 0.1 w/w% nBu$_4$NBr in the THF eluent. 224
Figure S4.16 a $^{11}B\{^{1}H\}$ and **b** ^{11}B NMR spectra (THF, 116 MHz, 298 K) of the reaction mixture of $MeNH_2{\cdot}BH_3$ and one equiv. of ItBu after 2 h (*traces of $[BH_4]^-$ from the imidazolium salt). 225
Figure S4.17 EI(+) mass spectrum of the reaction solution of I*t*Bu and $MeNH_2{\cdot}BH_3$..... 225
Figure S4.18 a $^{11}B\{^{1}H\}$; and **b** ^{11}B NMR spectra (THF, 116 MHz, 298 K) of the reaction mixture of $MeNH_2{\cdot}BH_3$ and two equiv. of ItBu after 48 h (*traces of $[BH_4]^-$ from carbene salt, #unidentified product). 226
Figure S4.19 EI (+) mass spectrum of the reaction solution of 2 equiv. of I*t*Bu and $MeNH_2{\cdot}BH_3$..... 227
Figure S4.20 $^{11}B\{^{1}H\}$ NMR spectra (THF, 116 MHz, 298 K) of the reaction mixture of $MeNH_2{\cdot}BH_3$ and two equiv. of $CAAC^{Me}$ after 15 min (#unidentified product). 228
Figure S4.21 ^{1}H NMR spectra (C_6D_6, 300 MHz, 298 K) of the reaction of $MeNH_2{\cdot}BH_3$ and two equiv. of $CAAC^{Me}$ after CAAC–BH_3 was removed by recrystallisation from hexanes. The septets corresponding to the (C*H*$(CH_3)_2$) groups in $(CAAC^{Me})H_2$ and each of the isomers have been highlighted along with the carbene C–H protons and the NMe_3 groups in the isomers. 228
Figure S4.22 ^{1}H NMR spectra (C_6D_6, 500 MHz, 298 K) of *trans*-**4.3**. 230
Figure S4.23 ^{13}C NMR spectra (C_6D_6, 91 MHz, 298 K) of *trans*-**4.3**. 231
Figure S4.24 ^{11}B NMR (C_6D_6, 116 MHz, 298 K) of *trans*-**4.3**. 231
Figure S4.25 ^{1}H NMR spectra (C_6D_6, 500 MHz, 298 K) of *cis*-**4.3**.Trace quantities of *trans*-**4.3**.and $(CAAC^{Me})H_2$ remain as the small quantity of material isolated prevents further purification..... 231
Figure S4.26 ^{13}C NMR spectra (C_6D_6, 91 MHz, 298 K) of *cis*-**4.3** 232

Figure S4.27 ^{11}B NMR (C_6D_6, 116 MHz, 298 K) of *cis*-**4.3** 232
Figure S4.28 EI mass spectrum (+) of *trans*-**4.3** 232
Figure S4.29 ^{11}B NMR spectra (THF, 96 MHz, 296 K) of the reaction mixture of $[MeHN–BH_2]_n$ and $MeNH_2$ after 24 h (*unidentified product). 233
Figure S5.1 $^{31}P\{^1H\}$ (left) and ^{31}P (right) NMR spectra (122 MHz, 298 K, toluene) of the reaction mixture of $PhMePH·BH_3$ and $CAAC^{Me}$ prior to heating showing formation of $CAAC^{Me}(H)PhMePBH_3$... 265
Figure S5.2 ^1H NMR spectrum (300 MHz, 298 K, $CDCl_3$) of isolated $[PhMeP–BH_2]_n$ formed from $PhMePH·BH_3$ and $CAAC^{Me}$ (*denotes residual partially protiated $CDCl_3$, ~denotes trace hexanes, $^{\#}$unidentified impurity)..... 265
Figure S5.3 $^{11}B\{^1H\}$ (left) and ^{11}B (right) NMR spectra (96 MHz, 298 K, $CDCl_3$) of isolated $[PhEtP–BH_2]_n$ formed from $PhMePH·BH_3$ and $CAAC^{Me}$. 265
Figure S5.4 $^{31}P\{^1H\}$ (left) and ^{31}P (right) NMR spectra (122 MHz, 298 K, $CDCl_3$) of isolated $[PhEtP–BH_2]_n$ formed from $PhMePH·BH_3$ and $CAAC^{Me}$ (*denotes unidentified impurities). 265
Figure S5.5 ESI(+)-MS spectrum in positive mode in THF:IPA (1:9) of isolated $[PhMeP–BH_2]_n$ formed from $PhMePH·BH_3$ and $CAAC^{Me}$. The predominant species, highlighted in yellow, is a linear system with a $CAAC^{Me}$ end group $(H\text{-}[PhMeP–BH_2]_n\text{-}CAAC^{Me})^+$..... 266
Figure S5.6 GPC chromatogram of isolated $[PhMeP–BH_2]_n$ formed from $PhMePH·BH_3$ and $CAAC^{Me}$. 2 mg mL^{-1} in THF with 0.1 w/w% nBu$_4$NBr in the THF eluent. The highest molar mass peak accounts for ca. 18% of the precipitated material. 266
Figure S5.7 ^1H NMR spectrum ($CDCl_3$, 500 MHz, 298 K) of **5.1**. 268
Figure S5.8 ^1H NMR spectrum ($CDCl_3$, 126 MHz, 298 K) of **5.1**. 268
Figure S5.9 $^{11}B\{^1H\}$ (left) and ^{11}B (right) NMR spectra ($CDCl_3$, 96 MHz, 295 K) of **5.1**. 269
Figure S5.10 $^{31}P\{^1H\}$ (left) and ^{31}P (right) NMR spectra ($CDCl_3$, 122 MHz, 298 K) of **5.1**. 269
Figure S 5.11 ESI(+)-MS spectrum of **5.1** in DCM (sample injection performed under ambient conditions in air). 269
Figure S5.12 ^1H NMR (CP-MAS) of $[Et_2P–BH_2]_n$ (*postulated to be residual *o*-xylene trapped within the polymer chains). 270
Figure S5.13 ^{13}C NMR (CP-MAS) of $[Et_2P–BH_2]_n$. 270
Figure S5.14 a ^{11}B NMR (*o*-xylene, 96 MHz, 298 K) and **b** ^{11}B NMR (CP-MAS) of $[Et_2P–BH_2]_n$ (*denotes possible end group). 271
Figure S5.15 a ^{31}P NMR (*o*-xylene, 122 MHz, 298 K) and **b** ^{31}P NMR (CP-MAS) of $[Et_2P–BH_2]_n$ (*denotes possible end group). 271
Figure S5.16 ESI(+)-MS spectrum in positive mode in THF:IPA (1:9) of isolated $[Et_2P–BH_2]_n$ formed from $Et_2PH·BH_3$ and $CAAC^{Me}$ 272
Figure S5.17 TGA thermogram of $[Et_2P–BH_2]_n$ (heating rate: 5 °C min^{-1})..... 272

Figure S5.18 DSC thermogram for $[Et_2P–BH_2]_n$ synthesised in *o*-xylene (heating rate: 10 °C min^{-1} and first cycle excluded). 273
Figure S5.19 DSC thermogram for $[Et_2P–BH_2]_n$ synthesised in mesitylene (heating rate: 10 °C min^{-1} and first cycle excluded). 273
Figure S5.20 Powder XRD spectrum of $[Et_2P–BH_2]_n$ synthesised in *o*-xylene. 274
Figure S5.21 ^{1}H NMR spectrum (300 MHz, 298 K, $CDCl_3$) of the crude reaction of $CAAC^{Me}$ and nHex$_2$PH·BH$_3$ (~denotes residual partially protiated $CDCl_3$, *denotes $(CAAC^{Me})H_2$). 275
Figure S5.22 $^{11}B\{^{1}H\}$ (left) and ^{11}B (right) NMR spectra (96 MHz, 298 K, $CDCl_3$) of the crude reaction of $CAAC^{Me}$ and nHex$_2$PH·BH$_3$. 275
Figure S5.23 $^{31}P\{^{1}H\}$ (left) and ^{31}P (right) NMR spectra (122 MHz, 298 K, $CDCl_3$) of the crude reaction of $CAAC^{Me}$ and nHex$_2$PH·BH$_3$. The observation of two peaks is explained by the presence of oligomeric and polymeric material. 275
Figure S5.24 ESI(+)-MS spectrum in positive mode in THF:IPA (1:9) of the material from the crude reaction of $CAAC^{Me}$ and nHex$_2$PH·BH$_3$. The predominant species, highlighted in yellow, is a linear system with a $CAAC^{Me}$ end group $(H\text{-}[n\text{Hex}_2P–BH_2]_n\text{-}CAAC^{Me})^+$. 276
Figure S5.25 GPC chromatogram of the material from the crude reaction of $CAAC^{Me}$ and nHex$_2$PH·BH$_3$. 2 mg mL^{-1} in THF with 0.1 w/w% nBu$_4$NBr in the THF eluent (*oligomeric material and $(CAAC^{Me})H_2$). 276
Figure S5.26 $^{31}P\{^{1}H\}$ NMR spectra (122 MHz, 298 K, $CDCl_3$) of the isolated material from the copolymerisations of PhPH$_2$·BH$_3$ with Ph$_2$PH·BH$_3$ (*unreacted Ph$_2$PH·BH$_3$). 277
Figure S5.27 ESI(+)-MS spectrum in positive mode in THF:IPA (1:9) of the isolated material from the copolymerisations of PhPH$_2$·BH$_3$ with Ph$_2$PH·BH$_3$ 277
Figure S5.28 GPC chromatograms of the isolated material from the copolymerisations of PhPH$_2$·BH$_3$ with Ph$_2$PH·BH$_3$**.** 2 mg mL^{-1} in THF with 0.1 w/w% nBu$_4$NBr in the THF eluent. 278
Figure S5.29 ^{1}H NMR spectra (C_6D_6, 500 MHz, 298 K) of **5.3** (*denotes residual partially protiated C_6D_6). 279
Figure S5.30 ^{13}C NMR spectra (C_6D_6, 91 MHz, 298 K) of **5.3**. 279
Figure S5.31 $^{11}B\{^{1}H\}$ (left) and ^{11}B (right) NMR spectra (THF, 116 MHz, 298 K) of **5.3** (*unidentified impurity). 280
Figure S5.32 EI (+) mass spectrum of **5.3**. 280
Figure S5.33 $^{11}B\{^{1}H\}$ (left) and ^{11}B (right) NMR spectra (96 MHz, 293 K, toluene) of the reaction solution of Ph$_2$N=BCl$_2$ and IDipp–BH$_2$NMeH (*unassigned products). 281
Figure S5.34 GPC chromatogram of the products of the reaction between Ph$_2$N=BCl$_2$ and IDipp–BH$_2$NMeH. 2 mg mL^{-1} in THF with 0.1 w/w% nBu$_4$NBr in the THF eluent. 281

Figure S5.35 ESI(+)-MS spectrum the products of the reaction between $Ph_2N{=}BCl_2$ and IDipp–BH_2NMeH. in DCM:IPA (1:9). 282
Figure S5.36 $^{11}B\{^1H\}$ (left) and ^{11}B (right) NMR spectra (96 MHz, 293 K, toluene) of the reaction solution of $Ph_2N{=}BCl_2$ and IDipp–BH_2NMeH (*unassigned products). 283
Figure S5.37 GPC chromatogram of the products of the reaction between BCl_3 and IDipp–BH_2NMeH. 2 mg mL^{-1} in THF with 0.1 w/w% nBu$_4$NBr in the THF eluent. 283
Figure S5.38 ESI-MS ESI(+)-MS spectrum the products of the reaction between BCl_3 and IDipp–BH_2NMeH in DCM:IPA (1:9). 284
Figure S5.39 $^{11}B\{^1H\}$ (left) and ^{11}B (right) NMR spectra (96 MHz, 293 K, toluene) of the reaction solution of $Ph_2N{=}BCl_2$ and IDipp–BH_2NMeH (*unassigned products). 284

List of Schemes

Scheme 1.1 Syntheses of amine-boranes. 4

Scheme 1.2 Dehydropolymerisation of amine-boranes. 5

Scheme 1.3 Metal-catalysed dehydrocoupling of **a** secondary and **b** primary amine-borane adducts with $[Rh(COD)(\mu\text{-}Cl)]_2$ at 25 or 45 °C for 48-60 h.[48] 6

Scheme 1.4 Metal-catalysed dehydropolymerisation of $MeNH_2{\cdot}BH_3$ using IrH_2(POCOP).[71] 7

Scheme 1.5 Metal-free syntheses of polyaminoboranes.[91,92] 7

Scheme 1.6 Synthesis of phosphine-boranes. 10

Scheme 1.7 Metal-catalysed dehydropolymerisation of phosphine-boranes. 12

Scheme 1.8 $B(C_6F_5)_3$ catalysed dehydropolymerisation of $PPhH_2{\cdot}BH_3$.[122] 12

Scheme 1.9 Synthesis of $[t\text{BuHP–BH}_2]_n$ from $t\text{BuPHBH}_2{\cdot}NMe_3$.[123] 12

Scheme 1.10 Attempted polymerisations of $Ph_2PH{\cdot}BH_3$.[117,123] 14

Scheme 1.11 Synthesis of P-disubstituted polyphosphinoboranes via the hydrophosphination of $[PhHP–BH_2]_n$.[129] 14

Scheme 1.12 Synthesis of NHCs by deprotonation of imidazolium salts.[166] 27

Scheme 1.13 a NHC dehydrogenation of an amine-borane; and **b** NHC facilitating the dehydrocoupling of phosphines. 28

Scheme 1.14 Synthesis of CAACs through the hydroamination route.[194] 29

Scheme 1.15 Synthesis of $(CAAC)_2Be$.[196] 29

Scheme 1.16 Synthesis of a CAAC coordinated biradical.[191] 30

Scheme 2.1 a and **b** Current methods of synthesising polyphosphinoboranes; and **c** proposed CAAC-mediated dehydrogenation. 46

Scheme 2.2 a Synthesis of **2.1a** and **2.1b** by deprotonation of the phosphine-borane using IDipp; and **b** synthesis of **2.1a** and **2.1b** using salt metathesis route. 47

Scheme 2.3 a Synthesis of **2.3a** through oxidative-addition of $PhPH_2{\cdot}BH_3$; **b** synthesis of **2.3a** through stepwise reaction of $PhPH_2$ then $BH_3{\cdot}THF$; and **c** synthesis of **2.3a** through salt metathesis route. 49

Scheme 2.4 P–H activation followed by σ-bond metathesis. 55

Scheme 2.5 P–H activation followed by elimination of dihydrogen. 55

Scheme 2.6 Concerted hydrogen transfer. 56

Scheme 2.7 B–H activation followed by σ-bond metathesis. 56

Scheme 2.8 Homolytic cleavage of P–C bond. 57

Scheme 2.9 Intermolecular hydride abstraction. 57

Scheme 2.10 $CAAC^{Me}$-mediated dehydrocoupling of $Ph_2PH{\cdot}BH_3$. 58

Scheme 2.11 CAAC^{Cy}-mediated dehydrocoupling of $Ph_2PH{\cdot}BH_3$. 59
Scheme 2.12 **a** CAAC^{Me}-mediated dehydrocoupling of *rac*-Ph(Et)PH·BH_3; and **b** CAAC^{Cy}-mediated dehydrocoupling of *rac*-Ph(Et)PH·BH_3. 61
Scheme 2.13 Synthesis of **2.4a** and **2.4b**. 61
Scheme 3.1 Current methods of synthesising polyphosphinoboranes. 143
Scheme 3.2 Reactions between **a** *n*Hex$PH_2{\cdot}BH_3$; **b** $Ph_2PH{\cdot}BH_3$; and **c** PhEtPH·BH_3 and catalytic $Ni(COD)_2$. 154
Scheme 4.1 Depolymerisation of **a** polyaminoboranes; and **b** polyphosphinoboranes using NHCs. Spectroscopic yields are shown. 194
Scheme 4.2 Products of the stoichiometric reactions between $[MeHN–BH_2]_n$ and **a** IDipp[24]; **b** I*t*Bu; and **c** CAAC^{Me}. The carbene is added to a polymer solution unless otherwise stated. Spectroscopic yields of the boron containing species are given in brackets. 197
Scheme 4.3 Products of the reactions between poly(N-methylaminoborane) $[MeHN–BH_2]_n$ and substoichiometric amounts of **a** IDipp; **b** I*t*Bu; and **c** CAAC^{Me}. The carbene is added to a polymer solution in each reaction (x = mol% of carbene). 199
Scheme 4.4 Reaction of $[MeHN–BH_2]_3$ with **a** IDipp; **b** I*t*Bu; and **c** CAAC^{Me}. 200
Scheme 4.5 Reaction of **4.1** with excess cyclohexene in THF. 202
Scheme 4.6 Reaction of $MeNH_2{\cdot}BH_3$ with **a** 1 equiv.;[42] and **b** 2 equiv.[24] of IDipp. 202
Scheme 4.7 Products of the reaction of $MeNH_2{\cdot}BH_3$ with **a** 1 equiv.; and **b** 2 equiv. of I*t*Bu. 204
Scheme 4.8 Reaction of $MeNH_2{\cdot}BH_3$ with **a** 2 equiv.; and **b** 3 equiv. of CAAC^{Me}. 205
Scheme 5.1 Reaction of $Ph_2PH{\cdot}BH_3$ with CAAC^{Me} 244
Scheme 5.2 Previously reported copolymerisations of amine-boranes[2,3] 245
Scheme 5.3 CAAC^{Me} mediated dehydropolymerisation of *rac*-Ph(Me)PH·BH_3. 246
Scheme 5.4 Synthesis of **5.1** through **a** direct P–H activation of $Et_2PH{\cdot}BH_3$; and **b** a stepwise approach. 247
Scheme 5.5 CAAC-mediated dehydropolymerisation of $Et_2PH{\cdot}BH_3$. 249
Scheme 5.6 CAAC-mediated dehydropolymerisation of *n*Hex$_2$PH·BH_3. 251
Scheme 5.7 Copolymerisation of $PhPH_2{\cdot}BH_3$ with $Ph_2PH{\cdot}BH_3$ using CAAC^{Me} 252
Scheme 5.8 Syntheses of IDipp–BH_2NMeH.[6] 254
Scheme 5.9 Thermal ring expansion reaction of IDipp–BH_2NHDipp.[7] 254
Scheme 5.10 Previously reported displacement of aminoboranes by Lewis acids.[6,8] 255
Scheme 5.11 Proposed recycling route of polyaminoboranes using Lewis acids to abstract the NHC from the adduct. 255
Scheme 5.12 Proposed routes to **a** [(HCNDipp)$_2$$CH_2$BNMeH]; and **b** IDipp–$BH_2$NMeBHNMeH. 258
Scheme 5.13 Postulated route for the formation of [IDippH]Cl. 260
Scheme 5.14 Reaction of IDipp–BH_2NMeH with $Ph_2N{=}BCl_2$ or BCl_3. 261
Scheme 5.15 Reaction of IDipp–BH_2NMeH with $B(C_6F_5)_3$. 261

List of Tables

Table 2.1 Influence of temperature, solvent and concentration on the formation of polyphenylphosphinoborane, $[PhHP–BH_2]_n$, in a closed system 50
Table 3.1 $Ni(COD)_2$-catalysed dehydropolymerisation of $PhPH_2·BH_3$. 144
Table 5.1 T_g values for a series of analogous polyolefins and polyphosphinoboranes. 250
Table 5.2 Ratio of **5.2** and **5.3** formed under different conditions 259

Table S2.1 Influence of temperature, solvent and concentration on the formation of polyphenylphosphinoborane, $[PhHP–BH_2]_n$ in a closed system. 74
Table S2.2 Conditions for kinetics experiments. 82
Table S2.3 Optimised minimum structures and transition states with their imaginary frequencies in THF; standard Gibbs free energies are given below the structures in kcal mol^{-1} relative to the sum of the Gibbs free energies of **A** and **B** in THF; Gibbs free energies and imaginary frequencies for toluene as solvent are given in square brackets. 88
Table S2.4 Calculated isodesmic reaction between $[CAAC(H)]^+$ and $(NHC)H_2$; Gibbs free energies are given below the structures in kcal mol^{-1} in the gas phase. 90
Table S2.5 Optimised minimum structures of M and M'. 90
Table S2.6 Selected crystallographic data for **2.1b,** $(CAAC^{Me})H_2$ and **2.3c**. 113
Table S2.7 Selected crystallographic data for **2.4a** and **2.4b**. 114
Table S3.1 Conditions for optimisation of and exploration of polymerisation conditions. 158
Table S3.2 Conditions for polymerisation of *n*$HexPH_2BH_3$. 179
Table S3 Selected crystallographic data for **3.1**. 185
Table S4.1 Relative amounts of IDipp used in the substoichiometric reactions with $[MeHN–BH_2]_n$. 217
Table S4.2 Relative amounts of $CAAC^{Me}$ used in the substoichiometric reactions with $[MeHN–BH_2]_n$, conversion into borazine and M_n, M_w and PDI values of resulting material. 219
Table S4.3 Selected crystallographic data for **4.2** and *trans*-**4.3**. 234
Table S5.1 Copolymerisation of $PhPH_2·BH_3$ with $Ph_2PH·BH_3$. 277
Table S5.2 Selected crystallographic data for **5.1** and **5.3**. 285

List of Abbreviations

Ad	Adamantyl
Ar	Aryl
BAr^F	$B(C_6H_3(m\text{-}CF_3)_2)$
br	Broad
ca.	Circa
CAAC	Cyclic (alkyl)(amino)carbene
Cat.	Catalyst
$CHCl_3$	Chloromethane
COD	1,5-Cyclooctadiene
Cp	$\eta^5\text{-}C_5H_5$
Cp*	$\eta^5\text{-}C_5Me_5$
CP-MAS	Cross Polarization Magic Angle Spinning
Cy	Cyclohexyl
d	Doublet
δ	Chemical shift
Đ	Polydispersity Index
DCM	Dichloromethane
DFT	Density Functional Theory
Dipp	2,6-diisopropylphenyl
DMAP	4-dimethylaminopyridine
DMPAP	2,2-dimethoxy-2-phenylacetophenone
DMSO	Dimethylsulfoxide
DP	Degree of Polymerisation
dppp	$Ph_2P(CH_2)_3PPh_2$
dq	Doublet of quartets
DSC	Differential Scanning Calorimetry
DTBP	2,6-di-*t*-butylpyridine
E	Main Group Element
EA	Elemental Analysis
EI-MS	Electron Ionisation Mass Spectrometry
ESI-MS	Electrospray Ionisation Mass Spectrometry
ESD	Estimated standard deviation
Et	Ethyl
Et_2O	Diethyl ether
FLP	Frustrated Lewis Pairs
GPC	Gel Permeation Chromatography
HMDSO	Hexamethyldisiloxane
*i*Pr	Isopropyl
k	Rate constant
m	Multiplet
m	Meta
m/z	Mass to charge ratio
Me	Methyl
Mes	1,3,5-trimethylbenzene
M_n	Number Average Molecular Weight
M_w	Weight Average Molecular Weights

*n*Bu	Butyl
NHC	N-Heterocyclic Carbene
*n*Hex	Hexyl
NMR	Nuclear Magnetic Spectroscopy
*n*Pr	Propyl
o	Ortho
p	Para
PDI	Polydispersity Index
Ph	Phenyl
POCOP	η^3-1,3-$(OP^tBu_2)_2C_6H_3$
ppm	Parts per million
q	Quartet
ROP	Ring-Opening Polymerisation
rpm	Revolutions per minute
s	Singlet
sept	Septet
SMe_2	Dimethylsulfide
t	Triplet
*t*Bu	*Tertiary*-butyl
TEM	Transition Electron Microscopy
TEMPO	2,2,6,6- tetramethylpiperidin-1-yl)oxyl
Tf	Triflate
T_g	Glass transition temperature
TGA	Thermogravimetric Analysis
THF	Tetrahydrofuran
Tol	Toluene
TS	Transition State
UV-vis	Ultraviolet-Visible
wt.	Weight
Xantphos	4,5-Bis(diphenylphosphino)-9,9-dimethylxanthene
XRD	X-ray Diffraction

Chapter 1
Introduction

1.1 Research objectives

The research described in this thesis encompasses two main themes. The first is the investigation of new synthetic routes for the dehydropolymerisation of phosphine-boranes, one of which is metal-free and the other transition-metal catalysed. The second is an exploration of the carbene induced depolymerisation of polyaminoboranes.

This chapter aims to introduce the chemistry associated with polyaminoboranes, polyphosphinoboranes and stable carbenes; however, it is a not a comprehensive review. Within each subsequent chapter further background material will be discussed in greater detail as is considered necessary.

1.2 Formation of main group element-element bonds

The formation of C–C bonds is a well-developed area of synthetic organic chemistry with breakthroughs in olefin polymerisation,[1] olefin metathesis[2–4] and palladium-catalysed cross couplings[5,6] being awarded Noble Prizes in 1963, 2005 and 2010, respectively.[7] Significant developments have also been made in the formation of C–E bonds (E = *p*-block element), for example hydroboration, hydrosilylation and hydrophosphination reactions.[8,9] In contrast, routes to form E–E' bonds (E and E' = *p*-block elements) are considerably less established. This is in part due to the covalent bonds in both substrates and products containing heavier *p*-block elements being inherently weaker than in the lighter congeners.[10]

1.2.1 Synthesis of E-E and E-E' bonds

Salt elimination and reductive coupling routes traditionally provided access to main group element-element bonds, an example of which is the synthesis of polysilanes from organochlorosilanes and stoichiometric amounts of an alkali metal using the Wurtz reaction (Figure 1.1).[11] However, these routes are often element-specific, require harsh conditions, result in unwanted by-products and have a narrow substrate scope.[12]

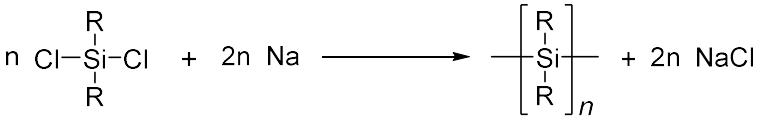

Figure 1.1 Representative synthesis of polysilanes using the Wurtz reaction.

A more recently developed and convenient synthetic pathway for the formation of main group element-element bonds is the catalytic dehydrocoupling of E–H bonds. This can be either homocoupling between two of the same element to form E–E bonds or heterocoupling between two different elements to form E–E' bonds (Figure 1.2).

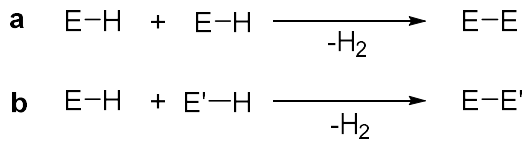

Figure 1.2 a Homo-dehydrocoupling; and **b** hetero-dehydrocoupling to form main group element-element bonds.

In 1984 Sneddon *et al.* reported the first example of catalytic E–E bond formation through the dehydrocoupling of two polyhedral boron cages using $PtBr_2$ as a catalyst (Figure 1.3).[13]

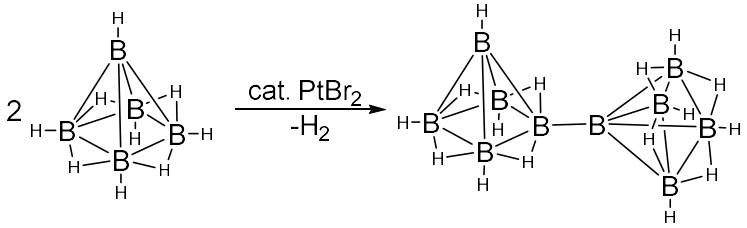

Figure 1.3 Formation of a B–B bond using Pt-based catalyst.

There have been many subsequent examples of transition-metal catalysed dehydrocoupling reactions to form a broad range of E–E and E–E' bonds under mild conditions.[10,12,14] Additionally there has been a recent evolution in main group catalysts capable of carrying out the dehydrocoupling process.[15–19]

1.2.2 Extension to polymers

Polymers are diverse and increasingly popular materials which can display a wide range of applications (e.g. house insulation, packaging, car parts, bulletproof vests, medical implants and drug delivery systems) and over 300 million tonnes of polymers are produced annually.[20] Although there are a multitude of organic polymers with carbon backbones the synthesis of inorganic polymers is less developed, largely due to the challenging preparation of suitable precursors and polymerisation methodologies.[21] The development of catalytic dehydrocoupling (Figure 1.4a) and ring-opening polymerisation (ROP) of cyclic monomers

(Figure 1.4b) has allowed for the development of a growing number of inorganic polymers comprising main group elements in the backbone.

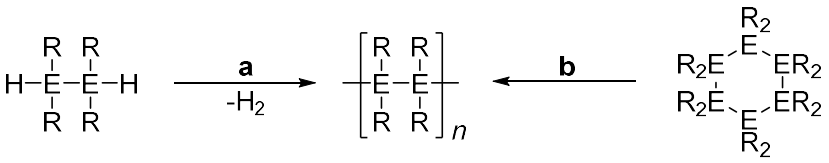

Figure 1.4 Common syntheses of inorganic polymers via **a** catalytic dehydropolymerisation; and **b** ring-opening polymerisation.

The area of main group polymer synthesis is of high interest due to the materials formed displaying unique properties which differ significantly from organic carbon-based polymers. Numerous classes of main group polymer have been reported, of which a selection are discussed below (Figure 1.5).

Two of the earliest examples of main group polymers are polysiloxanes and polyphosphazenes. Polysiloxanes $[R_2SiO]_n$ are a well-developed class of chemically stable inorganic polymer with numerous commercial applications such as thermally stable elastomers, adhesive coatings, surgical implants and sealants.[22] Polyphosphazenes $[R_2PN]_n$ have a backbone of alternating phosphorus and nitrogen atoms separated by alternating single and double bonds and have displayed potential as elastomers and hydrogels.[23] Polysilanes $[R_2Si]_n$ have a backbone comprised entirely of silicon atoms and display interesting electrical and optical properties as a result of strong delocalisation of σ electrons along the main chain.[24] The heavier group 14 analogues, polygermanes[25] and polystannanes,[26] have also been reported. Our group recently reported a new class of inorganic polymer, polyphosphonates $[RPO_2]_n$, through the ROP of cyclic phosphonates.[27]

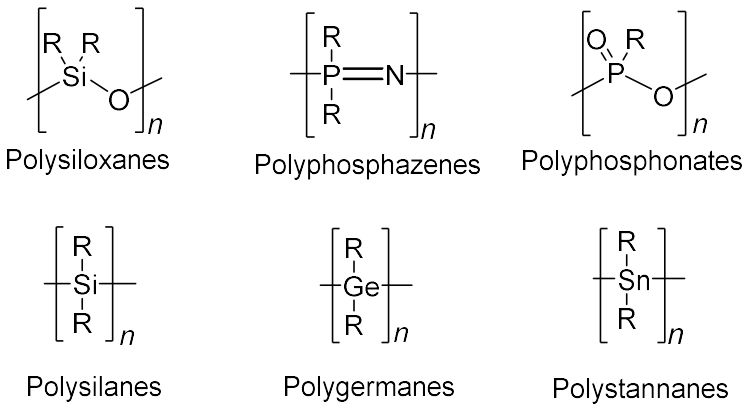

Figure 1.5 Examples of main group polymers.

The work described in this thesis focusses on polyaminoboranes $[R_2N–BH_2]_n$ and polyphosphinoboranes $[R_2P–BH_2]_n$, classes of main group polymer consisting of alternating B–N

or B–P units in the backbone, respectively (Figure 1.6). These polymers are isoelectronic with polyolefins, but these materials display markedly different properties. The synthetic routes towards polyaminoboranes and polyphosphinoboranes, along with their properties, will be discussed in further detail in the next two sections.

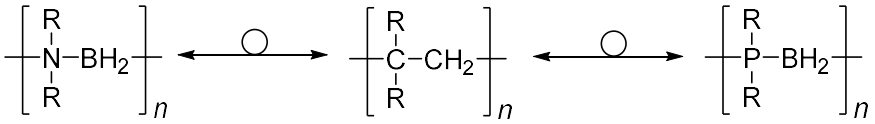

Figure 1.6 Polyaminoboranes and polyphosphinoboranes are isoelectronic with polyolefins.

1.3 Polyaminoboranes

Polyaminoboranes have a backbone of alternating σ-bonded boron and nitrogen atoms. Although initially reported in the course of investigations into using ammonia-borane, $NH_3{\cdot}BH_3$, as a hydrogen source, polyaminoboranes have more recently been reported to display their own useful applications such a ceramic precursors to boron nitride and piezoelectric materials.[28–30] Most syntheses of polyaminoboranes involve the dehydropolymerisation of amine-boranes.[31]

1.3.1 Synthesis and structure of amine-boranes and aminoboranes

Amine-boranes are adducts between an amine (Lewis base) and a borane (Lewis acid) through a dative bond. Gay-Lussac *et al*. reported the first amine-borane, $NH_3{\cdot}BF_3$, in 1809.[32] This was followed by the synthesis of $NH_3{\cdot}BH_3$, prepared by Shore and Parry in 1955.[33] There is now an extensive library of amine-borane species with functionalisation at both the nitrogen and boron atoms.[34,35]

A number of synthetic routes for amine-boranes have been developed. The most frequently used is the direct reaction of the amine with $BH_3{\cdot}L$ where the labile donor (L = THF or SMe_2) is displaced and a stronger bond is formed between boron and the amine N-donor (Scheme 1.1a). This route has several disadvantages such as requiring a large volume of solvent, poor long-term stability and, low concentrations available of $BH_3{\cdot}THF$, and the flammability and malodour associated with $BH_3{\cdot}SMe_2$. A second popular route is a salt metathesis reaction between ammonium salts and borohydrides (Scheme 1.1b).[34]

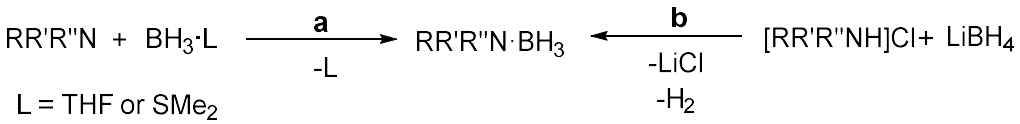

Scheme 1.1 Syntheses of amine-boranes.

The electronegativity difference between boron and nitrogen (χ_B = 2.04, χ_N = 3.04)[36] induces overall polarity into the molecules and results in the hydrogens on nitrogen and boron displaying protic and hydridic character, respectively.[37] The removal of one equivalent of dihydrogen from an amine-borane gives aminoboranes, RR'N=BH_2, species with a formal double bond and planar geometries around both the nitrogen and boron atoms (Figure 1.7). Large nitrogen substituents are required to give stable aminoboranes.[38]

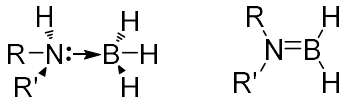

Figure 1.7 Structure of amine-boranes (left) and aminoboranes (right).

As already alluded to, extensive research into the dehydrogenation of ammonia-borane has been reported as its high gravimetric hydrogen content (19.6 wt.%) made it an attractive candidate for hydrogen storage with numerous reviews on this topic.[39–42] Nevertheless there are challenges, the key one being the thermochemical and kinetic challenges of regeneration of the spent material into ammonia-borane.[28] The work reported in this thesis is concentrated on the dehydrogenation product, polyaminoboranes, and thus the synthesis, substrate scope and application of the polymers will be the focus of the next sections.

1.3.2 Synthesis of polyaminoboranes

The synthesis of well-defined polyaminoboranes from amine-boranes is challenging as both the dehydrogenation and subsequent polymerisation steps must be controlled (Scheme **1.2**).[30] The control of dehydrogenation is especially important for $NH_3{\cdot}BH_3$ and primary amine-boranes, $RNH_2{\cdot}BH_3$, as intractable, presumably cross-linked material, is formed when more than one equivalent of dihydrogen is released.[29]

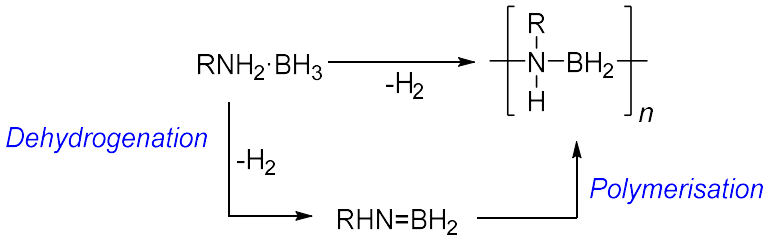

Scheme 1.2 Dehydropolymerisation of amine-boranes.

Attempts to synthesise the simplest polyaminoborane, $[H_2N–BH_2]_n$, using the thermal decomposition of either $NH_3{\cdot}BH_3$[43] or $[H_2N–BH_2]_3$[44] led to insoluble, poorly characterised materials. Thermal dehydrogenation of primary and secondary amine-boranes affords

mixtures of small cyclic species, or aminoborane monomers, rather than polymeric material, if the substituents display a large degree of steric bulk.[30,45–47]

1.3.2.1 Metal-catalysed dehydropolymerisation of amine-boranes

The dehydrocoupling of amine-boranes at ambient temperature, with the goal of synthesising linear, soluble polyaminoboranes has been a focus of recent work.

In 2001 Manners *et al*. reported a rhodium precatalyst, $[Rh(COD)(\mu\text{-}Cl)]_2$ (COD = 1,5-cyclooctadiene), which was able to catalytically dehydrocouple amine-boranes under mild conditions.[48] With $Me_2NH{\cdot}BH_3$ quantitative conversion to the cyclic dimer $[Me_2N–BH_2]_2$ is achieved (Scheme 1.3a). The rhodium precatalyst is also active for the dehydrocoupling of the primary amine-borane $MeNH_2{\cdot}BH_3$, with two equivalents of hydrogen being released to give (N-methyl)borazine $[MeNBH]_3$ as the product (Scheme 1.3b). Under the same conditions $NH_3{\cdot}BH_3$ forms a mixture of borazine and insoluble oligomers and/or polymers. The active catalyst has been shown to be heterogeneous in nature.[49]

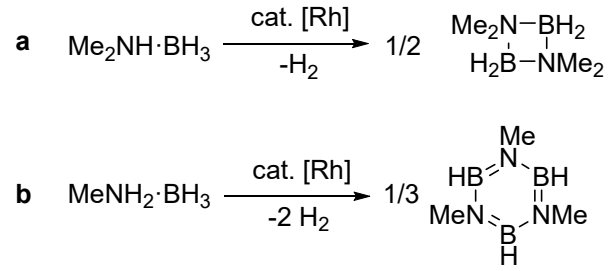

Scheme 1.3 Metal-catalysed dehydrocoupling of **a** secondary and **b** primary amine-borane adducts with $[Rh(COD)(\mu\text{-}Cl)]_2$ at 25 or 45 °C for 48-60 h.[48]

Since this initial report a substantial amount of work has been performed in this area and a large library of transition-metal precatalysts have been reported for the dehydrocoupling of amine-boranes using a wide range of metals including titanium,[50,51] manganese,[52] iron,[53–55] cobalt,[56–58] nickel,[59,60] rhodium,[61–66] ruthenium,[67–69] rhenium[70] and iridium.[71,72] Additionally, a number of main group species have been reported to facilitate the dehydrocoupling of amine-boranes.[73–77]

The first efficient homogeneous dehydropolymerisation of ammonia-borane was achieved using an iridium precatalyst, IrH_2(POCOP) (POCOP = $[\eta^3\text{-}1,3\text{-}(OP^tBu_2)_2C_6H_3]$), by Goldberg *et al*. in 2006 to give an insoluble, poorly characterised, product assigned as the cyclic pentamer $[H_2N–BH_2]_5$ through the release of one equivalent of hydrogen per monomer.[71] In 2008 Manners *et al.* used the same iridium catalyst with $MeNH_2{\cdot}BH_3$ to synthesise high molar mass

poly(N-methylaminoborane) ([MeHN–BH_2]$_n$) (M_w = 160,000 Da, $Đ$ = 2.9) (Scheme 1.4).[78,79] Since 2008, a variety of other precatalysts capable of catalysing the formation of high molar mass polyaminoboranes have been reported based on titanium,[80,81] iron,[82–84] cobalt,[85] zirconium,[86] ruthenium,[69] rhodium[87–89] and iridium.[90]

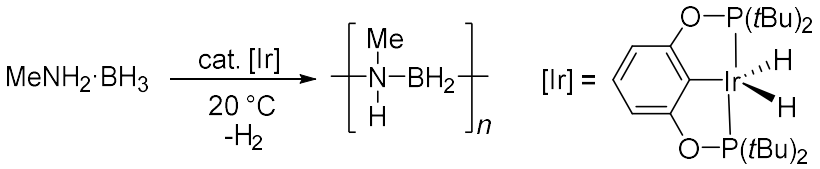

Scheme 1.4 Metal-catalysed dehydropolymerisation of $MeNH_2{\cdot}BH_3$ using IrH_2(POCOP).[71]

1.3.2.2 Metal-free routes to polyaminoboranes

In 1970 Kwon and McGee reported the synthesis of [H_2N–BH_2]$_n$ by subjecting borazine vapour to a radio frequency discharge followed by immediate quenching at -196 °C.[43] $H_2N{=}BH_2$ was reported to form and spontaneously polymerise between -196 °C and -155 °C, but only the infrared spectrum of the presumed polymeric product was reported.

In 2014 Manners *et al.* reported an ambient temperature, metal-free route to low molar mass (< 5000 Da) [MeHN–BH_2]$_n$. The amine-borane $MeNH_2{\cdot}BH_3$ was treated with $[H(OEt_2)_2][B(C_6F_5)_4]$ in Et_2O and spontaneous dihydrogen elimination gave the amine-boronium cation salt $[(MeH_2N{\cdot}BH_2)(Et_2O)][B(C_6F_5)_4]$. Deprotonation with 2,6-di-*t*-butylpyridine (DTBP) yielded the aminoborane monomer, $MeHN{=}BH_2$, which was detected using low temperature ^{11}B NMR spectroscopy at -10 °C, and undergoes a head-to-tail polymerisation (Scheme 1.5a).[91]

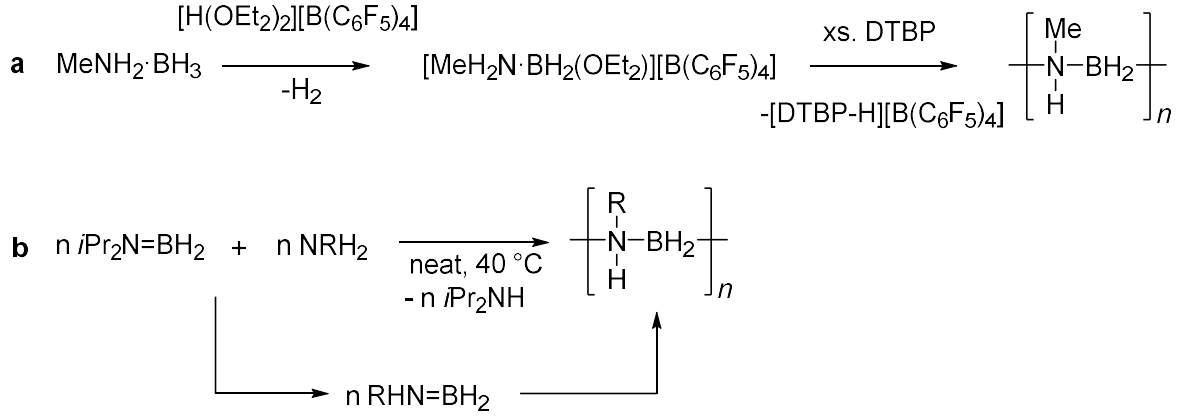

Scheme 1.5 Metal-free syntheses of polyaminoboranes.[91,92]

Alcaraz *et al.* have recently reported a metal-free synthesis using $iPr_2N{=}BH_2$ as a BH_2 transfer reagent. The reaction of $iPr_2N{=}BH_2$ with primary amines, NRH_2 (R = Me, Et, *n*Pr, *n*Bu, allyl), at -40 °C under solvent-free conditions forms $RHN{=}BH_2$ *in situ,* which immediately polymerises

to yield what have been assigned as very high molar mass polyaminoboranes (M_w = ca. 200,000 – 500,000 Da; $Đ$ = 1.2 – 10.2) (Scheme 1.5b).[92]

1.3.3 Substrate scope of polyaminoboranes

A number of N-alkyl-substituted polyaminoboranes been reported using either catalytic routes or the Alcaraz stoichiometric BH_2 transfer route (Figure 1.8). N-aryl-substituted polyaminoboranes have not been reported as the monomers ($RNH_2{\cdot}BH_3$ R = Ph, *p*-$C_6H_4CF_3$ and *p*-C_6H_4OMe) undergo spontaneous dehydrocoupling to a multitude of non-polymeric products.[93]

Reports of B-substituted polyaminoboranes, $[H_2N–BHR]_n$, are much more limited with only two reported examples (R = Ph or *p*-$C_6H_4CF_3$).[94] In each case a significant quantity of borazine is formed and the phenyl derivative is particularly thermally unstable. Attempts to synthesise $[H_2N–BMeH]_n$ through the dehydrogenation $H_3N{\cdot}BH_2Me$ were unsuccessful as upon heating a sample thermal redistribution of the methyl and hydrogen substituents on boron occurred to give $H_3N{\cdot}BH_{3-x}Me_x$ (x = 0 – 3) and attempted metal-catalysed dehydropolymerisation yielded borazine $[HNBMe]_3$ and bis(amino)borane, $MeB(NH_2)_2$.[35]

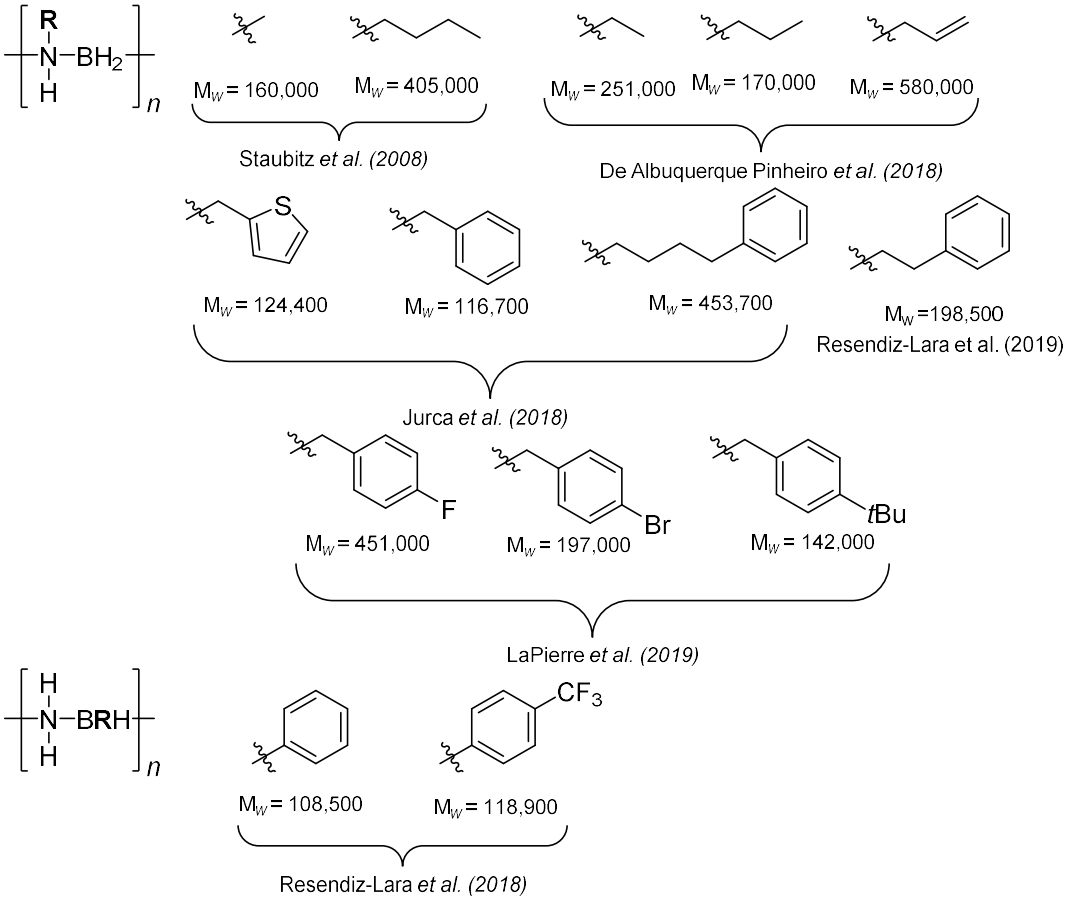

Figure 1.8 Substrate scope of polyaminoboranes. M_w (Da) given for first reported examples.[79–81,94–96]

Thus far all examples of polyaminoboranes have been either N-mono or B-monosubstituted. There are no reported examples of any isolated disubstituted polymers. The dehydrogenation of disubstituted amine-boranes yields either monomeric aminoboranes (e.g. iPr$_2$N=BH$_2$) or small cyclic species (e.g. [Me$_2$N–BH$_2$]$_2$).[30]

1.3.4 Properties and applications of polyaminoboranes

Polyaminoboranes display very different properties to their polyolefin analogues. For example, poly(N-methylaminoborane) is soluble in a range of polar solvents (e.g. THF, DCM, $CHCl_3$), whereas polypropylene, the isoelectronic C–C backbone species, is only soluble in non-polar xylenes at elevated temperatures. This is explained by a combination of the alternating B–N backbone and the substituents inducing polarity. Thermal decomposition of [MeHN–BH$_2$]$_n$ occurs at a temperature significantly lower than polypropylene (160 vs 400 °C). This has been attributed to the formally dative N→B bonds between the monomers weakening and releasing B–N fragments at relatively low temperatures. It may also be related to the polarity as the presence of hydridic B–H and protic N–H hydrogens may allow for release of dihydrogen from the polymer and initiate fragmentation into species such as borazine [MeNBH]$_3$.[29,97]

There are several reported potential applications of polyaminoboranes. One of which is as preceramic polymers for boron nitride, a material which in its hexagonal crystal morph (h-BN) is the B–N analogue of graphite.[79,98,99] As the BN layers are bonded by weak van der Waals forces the layers are able to slide over each other giving h-BN lubricant properties. h-BN displays many additional useful characteristics such as high temperature resistance, thermal shock resistance, high thermal conductivity, poor wettability, chemical inertness and non-toxicity.[100,101] Preceramic polymers are attractive as they can be moulded into the desired shape prior to heating to give the final ceramic material.[29]

Polyaminoboranes have also been considered as hydrogen storage materials due to the potential to release a further equivalent of hydrogen, as mentioned above.[41] However, as one equivalent has already been lost in the dehydropolymerisation process, they are a less attractive hydrogen source than the parent amine-boranes. Another potential application of polyaminoboranes is as piezoelectric materials. [H$_2$N–BH$_2$]$_n$ and [H$_2$N–BF$_2$]$_n$ have been investigated computationally by Nakhmanson *et al.* and reported to display a 50% and 100% improvement in spontaneous polarisability when compared to polyvinylidene fluoride,

$[H_2CCF_2]_n$, resulting in enhanced piezoelectric responses.[102] Polyaminoboranes have also been reported as precursors for aluminium borate nanowires.[103]

The high boron content in polyaminoboranes gives them potential as a delivery agents for boron neutron capture therapy, in which a high concentration of ^{10}B nuclei are irradiated to yield high energy α particles which destroy tumour cells.[104]

1.4 Polyphosphinoboranes

Polyphosphinoboranes can be compared to polyaminoboranes, but with the nitrogen atoms in the main chain replaced with phosphorus atoms. They are also isoelectronic with polyolefins. Initial interest in polyphosphinoboranes was shown in the 1950s and 1960s as it was predicted that they would exhibit useful properties such as high temperature stability and flame retardancy.[105] The most common synthetic routes involve the dehydrogenation of phosphine-borane monomers.

1.4.1 Synthesis and structure of phosphine-boranes and phosphinoboranes

As with amine-boranes, phosphine-boranes are Lewis base (phosphine) - Lewis acid (borane) adducts. The first phosphine-borane derivative, $PH_3{\cdot}BCl_3$, was reported in 1890 by Besson.[106] It was not until 1966 that the simplest phosphine-borane, $PH_3{\cdot}BH_3$, was reported[107] having previously been synthesised and incorrectly reported as diborane diphosphine, $B_2H_6{\cdot}2(PH_3)$, in 1940.[108] There is now a library of primary, secondary and tertiary P-functionalised phosphine-boranes.

There are two main synthetic routes for the synthesis of phosphine-boranes. The first is direct addition of a phosphine to $BH_3{\cdot}L$ (L = THF or SMe_2) where displacement of the weaker Lewis base by the phosphine occurs (Scheme 1.6a)[109] and the second is through the reduction of chlorophosphines with two equivalents of $LiBH_4$ (Scheme 1.6b).[110]

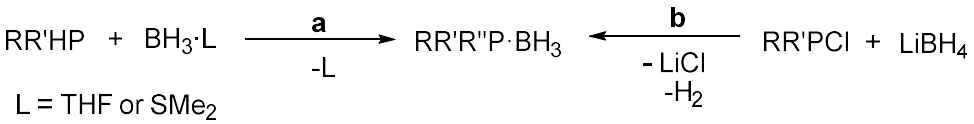

Scheme 1.6 Synthesis of phosphine-boranes.

Analogous to amine-boranes the dehydrogenation of phosphine-boranes, $R_2PH{\cdot}BH_3$, would give phosphinoboranes $[R_2P{-}BH_2]$. The P–H and B–H bonds display little polarity (χ_P = 2.19, χ_B = 2.04, χ_H= 2.20)[36] which reduces the favourability of dehydrogenation of phosphine-boranes as opposed to amine-boranes. Tertiary phosphines have a high energy barrier to pyramidal

inversion, a process which involves a hybridisation change of the phosphorus from sp^3 to sp^2.[38] This results in phosphinoboranes showing a lower propensity to have planar, rather than pyramidal, geometry at the phosphorus centre with the two structural extremes shown in Figure 1.9.[111]

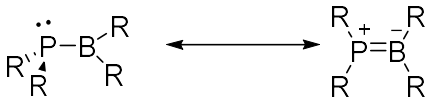

Figure 1.9 Structural extremes of phosphinoboranes.[111]

1.4.2 Synthesis of P-monosubstituted polyphosphinoboranes

1.4.2.1 Thermolysis of phosphine-boranes

The synthesis of polyphosphinoboranes was first reported in the 1950s by thermal (175 – 200 °C) dehydrocoupling of $Me_2PH{\cdot}BH_3$ and $MePH_2{\cdot}BH_3$ in the presence of amines to yield $[RMeP–BH_2]_n$ (R = H or Me); however, only low yields of low molecular weight, poorly soluble material, lacking convincing structure characterisation were reported.[112–114] The thermolysis of $PhPH_2{\cdot}BH_3$ (100 - 150 °C) was reported in 1964 to give a benzene-soluble, low molar mass (M_n = ca. 2000), poorly characterised, polymer with a claimed average composition of $[PhHP–BH_2]_x$.[115]

1.4.2.2 Metal-catalysed dehydropolymerisation of phosphine-boranes

It was not until the late 1990s that a rhodium precatalyst, $[Rh(\mu\text{-}Cl)(1,5\text{-}cod)]_2$ (COD = 1,5-cyclooctadiene), was used in the melt phase (90 – 130 °C) to dehydrocouple $PhPH_2{\cdot}BH_3$, giving the first definitively characterised high molecular weight polyphosphinoborane $[PhHP–BH_2]_n$ (M_w = 31,000 Da).[116,117] The air- and moisture-stable polymer displayed a large degree of chain branching and cross linking resulting from the high temperature melt phase polymerisation conditions.

In 2015 an iron precatalyst, $[CpFe(CO)_2OTf]$ (Cp = $[\eta^5\text{-}C_5H_5]^-$, OTf = $[SO_3CF_3]^-$), was used to synthesise $[PhHP–BH_2]_n$ (M_n = 59,000 Da) from $PPhH_2{\cdot}BH_3$ in solution (toluene) rather than the melt phase.[118] This route had the advantages of using an earth abundant first-row transition-metal, rather than a precious metal catalyst, and operating at a lower temperature (100 °C), to yield material with relatively low polydispersity ($Đ$ = 1.6). Additionally, it was possible to control the molar mass of the polymer by altering the catalyst loading, and a chain-growth mechanism was proposed.

Since the significant breakthrough by Manners *et al.* in 2015 a series of other metal catalysts based on iron, iridium and rhodium have been reported to be effective in the solution phase dehydropolymerisation of phosphine-boranes.[119–121]

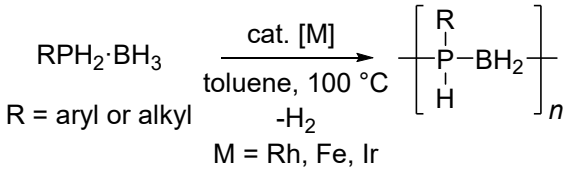

Scheme 1.7 Metal-catalysed dehydropolymerisation of phosphine-boranes.

1.4.2.3 Metal-free routes to polyphosphinoboranes

As alluded to above the thermal dehydrocoupling of phosphine-boranes was not successful for the synthesis of convincingly characterised high molar mass polyphosphinoboranes. Despite this there have been a few reports on alternative metal-free syntheses.

In 2003 Gaumont *et al.* reported dehydropolymerisation of $PPhH_2{\cdot}BH_3$ using the strong Lewis acid tris(pentafluorophenyl)borane ($B(C_6F_5)_3$) as a catalyst. ^{31}P NMR analysis suggested the presence of oligomeric or cyclic structures and GPC analysis showed formation of only low molar mass material (M_n = 830 - 3900 Da) and there have been no follow up studies reported.[122]

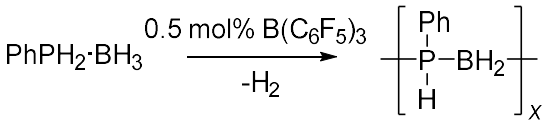

Scheme 1.8 $B(C_6F_5)_3$ catalysed dehydropolymerisation of $PPhH_2{\cdot}BH_3$.[122]

The first metal-free route to high molar mass polyphosphinoboranes was reported in 2015.[123] This stemmed from a collaboration between our group and the Scheer group which reported a Lewis base stabilised monomeric phosphinoborane, $RR'PBH_2{\cdot}NMe_3$.[124] The thermally-induced elimination of NMe_3 yielded monomeric [RR'P–BH_2] which underwent a head-to-tail polymerisation. High molar mass [*t*BuHP–BH_2]$_n$ (M_n = 27,800 – 35,000) was synthesised through this method from *t*BuPHB$H_2{\cdot}NMe_3$.

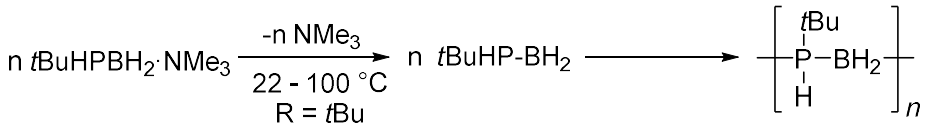

Scheme 1.9 Synthesis of [*t*BuHP–BH_2]$_n$ from *t*BuPHB$H_2{\cdot}NMe_3$.[123]

1.4.3 Substrate scope of polyphosphinoboranes

1.4.3.1 P-monosubstituted polyphosphinoboranes

The above-mentioned metal-catalysed and metal-free routes have enabled access to a range of aryl and alkyl P-monosubstituted polyphosphinoboranes, including the synthesis of metal containing polymers.

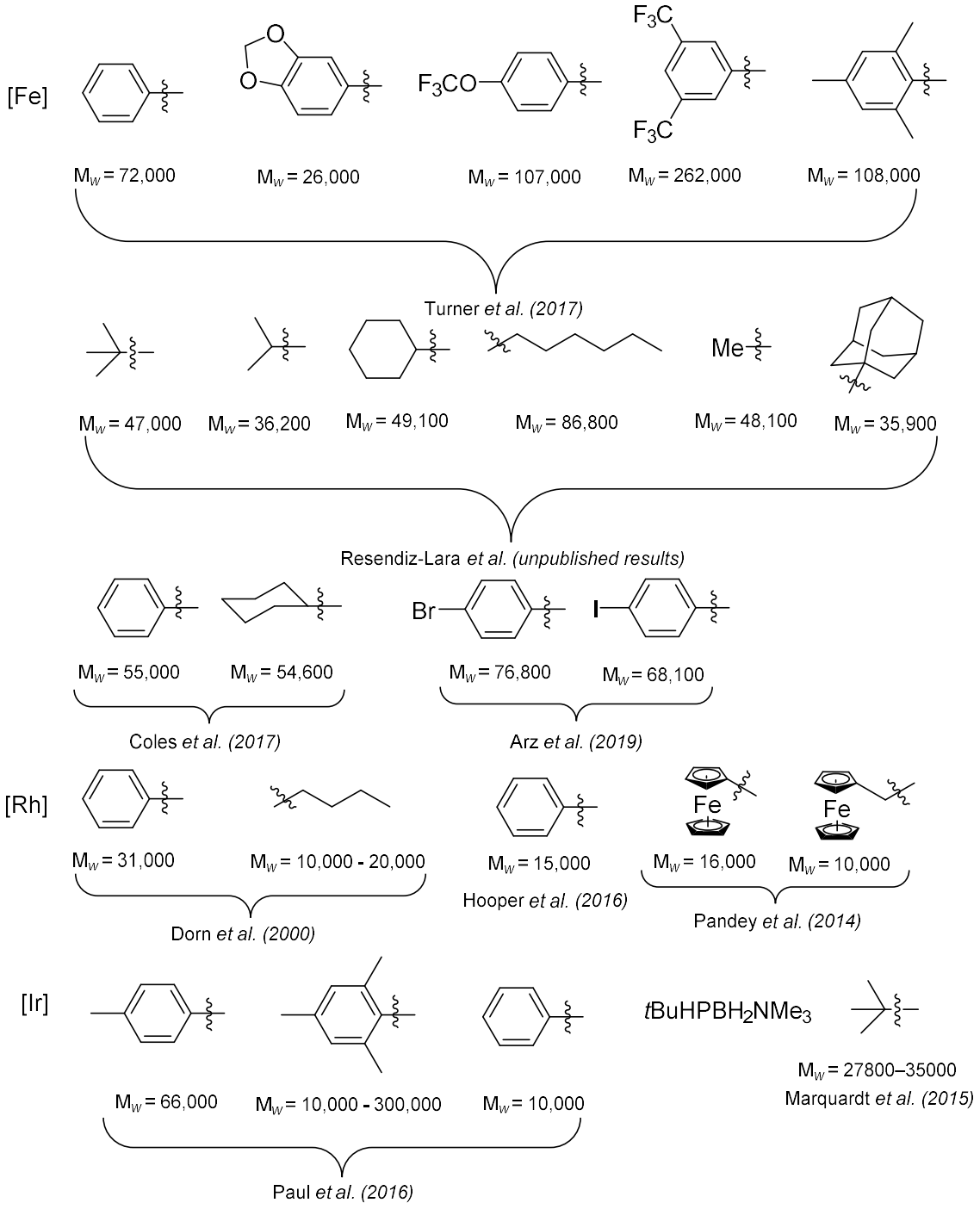

Figure 1.10 Summary of P-monosubstituted polyphosphinoboranes.[117,119–121,123,125–128]

1.4.3.2 P-disubstituted polyphosphinoboranes

Although there have been significant developments in the synthesis of P-monosubstituted polyphosphinoboranes the synthesis of the P-disubstituted polymers is much more elusive. The absence of a P–H in the P-disubstituted polymers $[RR'P–BH_2]_n$ make them an attractive synthetic target as it is anticipated that they will be less reactive than the P-monosubstituted derivatives and therefore more amenable to applications.

The use of metal catalysts for the attempted dehydropolymerisation of P-disubstituted monomers has so far only resulted in the synthesis of small cyclic species or short oligomers. This is exemplified by $Ph_2PH{\cdot}BH_3$ producing either the linear dimer $PPh_2H{\cdot}BH_2–PPh_2{\cdot}BH_3$ or the cyclic trimer and tetramer $[Ph_2P–BH_2]_x$ (x = 3 or 4) when reacted with $[Rh(\mu\text{-Cl})(1,5\text{-cod})]_2$ (Scheme 1.10a)[117] or $[Ph_2P–BH_2]_x$ (x ≤ 6) through the thermolysis of $Ph_2PHBH_3{\cdot}NMe_3$ (Scheme 1.10b).[123]

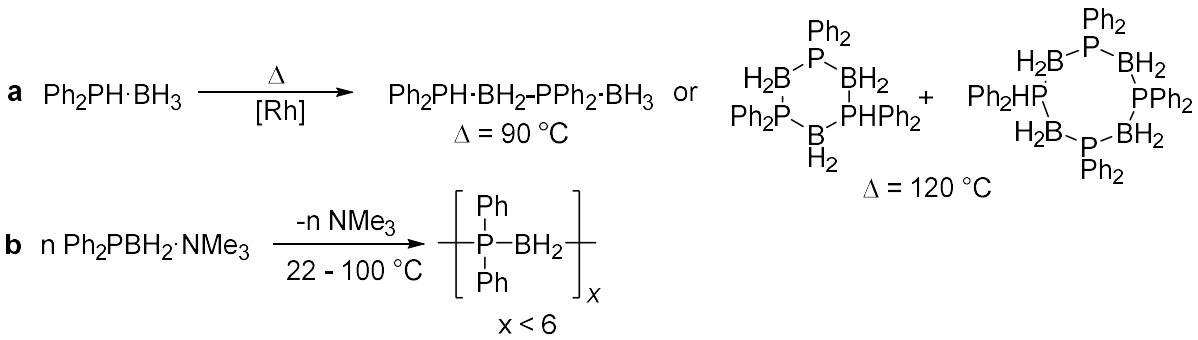

Scheme 1.10 Attempted polymerisations of $Ph_2PH{\cdot}BH_3$.[117,123]

A recent development in our group was the report of a post-polymerisation modification route which involves the insertion of olefins into the P–H bonds of $[PhHP–BH_2]_n$ using a hydrophosphination reaction under benchtop conditions to give $[PhRP–BH_2]_n$ (R = alkyl) (Scheme 1.11).[129] This method has allowed access to fully P-disubstituted polymers and random copolymers, the properties of which can be altered by varying the degree of hydrophosphination and identity of alkene used. There is, however, the drawback that a molar mass decline is observed, especially at high degrees of insertion.

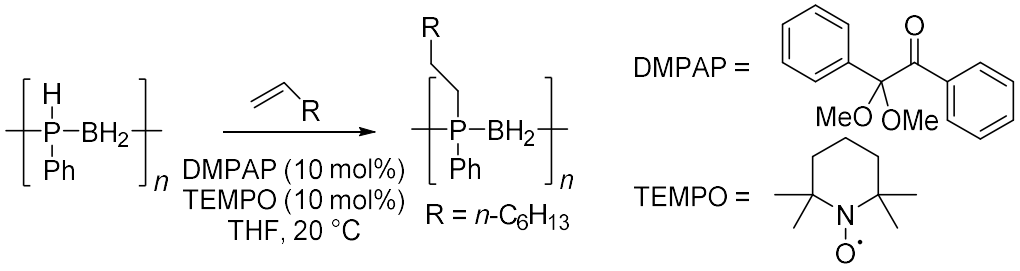

Scheme 1.11 Synthesis of P-disubstituted polyphosphinoboranes via the hydrophosphination of $[PhHP–BH_2]_n$.[129]

1.4.4 Properties and applications of polyphosphinoboranes

The air- and moisture-stability of polyphosphinoboranes makes them attractive candidates to be developed as materials with real-life applications. Polyphosphinoboranes are generally soft, malleable materials with glass transition temperatures (T_g) dependant on the phosphorus substituents.[29] The T_g values of polyphosphinoboranes are generally lower than that of the analogous organic polymer (e.g. T_g = 38 °C for $[PhHP–BH_2]_n$ vs 107 °C for $[PhHC\text{-}CH_2]_n$).[125,130] It is anticipated that this is a result of the relatively longer B–P than C–C bond (1.90 – 2.00 vs 1.54 Å).

Polyphosphinoboranes have displayed potential as electron beam resists for lithography, and in producing hydrophobic polymer-coated surfaces with the water droplet contact angle being tuneable by varying the substituent at phosphorus.[118,125,131] The polymers have been suggested to be useful as ceramic precursors to boron phosphide as, depending on the substituents, they can display high ceramic yields.[132]

Cross linking of P-monosubstituted polyphosphinoboranes, through the loss of dihydrogen, has been shown to give solvent swellable-gels. The degree of cross-linking is reported to be affected by both the polymerisation conditions and the phosphorus substituents.[125] Recently post-polymerisation hydrophosphination of 1,5-hexadiene with $[PhHP–BH_2]_n$ has allowed the controlled synthesis of a cross-linked polyphosphinoborane which displays reversible organogel behaviour.[129]

Additionally, it has been suggested that polyphosphinoboranes may be useful as flame retardants with high thermal stability[133–135] or as non-linear optical materials;[136] these applications are still under investigation.[137]

1.5 Mechanistic insights into the synthesis of polyaminoboranes and polyphosphinoboranes

Developing an understanding of the mechanisms of the formation of polyaminoboranes and polyphosphinoboranes should allow for the design of better catalysts and improved synthetic methods for the polymerisation to be developed. As the majority of reported synthetic routes to polyaminoboranes and polyphosphinoboranes use a transition-metal catalyst to induce dehydropolymerisation of amine-borane or phosphine-borane monomers this will be the focus of the following sections. In addition, recent developments and studies of the mechanism of metal-free polymerisations will also be discussed.

1.5.1 Mechanisms of transition-metal mediated amine-borane dehydropolymerisation

For ammonia-borane, $NH_3{\cdot}BH_3$, and primary amine-boranes the dehydropolymerisation to yield linear polyaminoboranes is challenging. This is due to the favourable formation of cyclic species, such as borazane, and the potential for further dehydrogenation to give the thermodynamically favoured borazine product (Figure 1.11).[31]

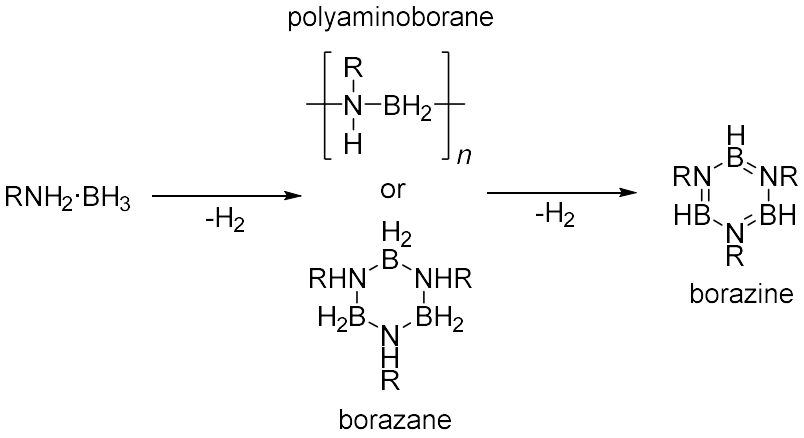

Figure 1.11 Typical dehydrocoupling pathway for ammonia-borane and primary amine-boranes.

Several catalysts have been developed which are able to both dehydrogenate the amine borane monomer and control the B–N coupling steps to produce well-defined polymers (Section 1.3.2.1), but only a small number of examples have been studied in detail.

The initial dehydrogenation of amine-boranes is the first step that must be studied in the dehydropolymerisation and a number of techniques can be used. Measuring the volume or pressure of the H_2 gas released as a function of time can provide kinetic information along with information on the number of equivalents of dihydrogen released. Using deuterated amine-boranes allows for the calculation of kinetic isotope effects which can be supported by computational studies.[138] The disubstituted amine-borane $Me_2NH{\cdot}BH_3$ is commonly used as a model system for this step as it forms the easily identified cyclic dimer $[H_2B–NMe_2]_2$ as the almost exclusive product.

Metal-catalysed dehydrogenation of amine-boranes has been reported to proceed via one of three routes: (a) inner sphere B–H/N–H activation; (b) ligand-assisted cooperative mechanism; or (c) hydride abstraction/boronium co-catalysis (Figure 1.12). Each case involves the formation of a σ-amine-borane complex with a 3-centre 2-electron M–H–B interaction.[30] The study of aminoborane monomers is challenging due to their instability with respect to oligomerisation events. Nevertheless, there are examples of aminoboranes interacting with

metal centres[72,139–141] and it is possible, under certain conditions, to use cyclohexene as a trapping reagent which undergoes hydroboration to yield RHN=BCy_2 (R = H, Me). There is, however, a dependence on the relative rates of hydroboration vs polymerisation.[142]

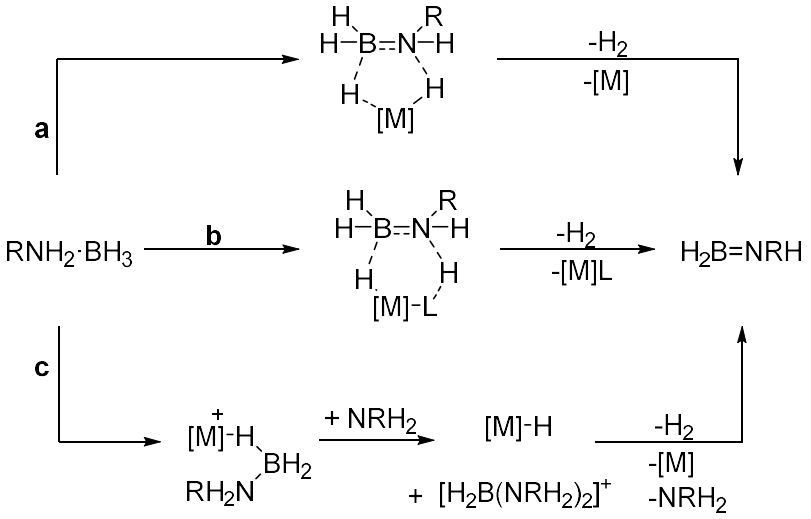

Figure 1.12 Metal-catalysed dehydrogenation of amine-boranes: **a** inner sphere B–H/N–H activation; **b** ligand assisted cooperative mechanism; or **c** hydride abstraction/boronium co-catalysis.[30]

Following dehydrogenation of the amine-borane a polymerisation step must occur. A chain-growth process can be identified by high molar mass material forming at low conversion with gradual monomer consumption. In contrast in step-growth polymerisations high molar mass material is only detected at high conversions. A decrease in molar mass of the material formed at a greater catalyst loading is indicative of a chain-growth mechanism as there is an increase in the number of active sites per monomer.[143]

Several mechanisms for the B–N coupling of aminoborane monomers have been reported. The first is a coordination/ dehydrogenation/ insertion chain-growth mechanism.[53,69] This process is analogous to the chain-growth mechanism for single-site olefin polymerisation.[144] The rhodium system [Rh(Xantphos){$H_2BNMe_3(CH_2)_2tBu$}][BAr^F_4] is suggested to proceed via this mechanism.[145] The observation of an induction period suggested that an active species is formed from the precatalyst and this is proposed to be a Rh-amidoborane. Subsequently $MeNH_2·BH_3$ coordinates to, and is dehydrogenated by, the active Rh centre to yield $MeHN=BH_2$ which inserts into the polymer chain at the metal centre (Figure 1.13). A chain-growth process was proposed based on high molar mass material forming at low conversion and an increase in catalyst loading resulting in lower molar mass material. It is suggested that hydrogen acts a chain transfer agent as carrying out the polymerisation under hydrogen resulted in only low molar mass material being formed. Using THF, rather than

fluorobenzene, as the solvent allowed for the synthesis of higher molar mass material and this is attributed to THF reducing the probability of chain transfer events.

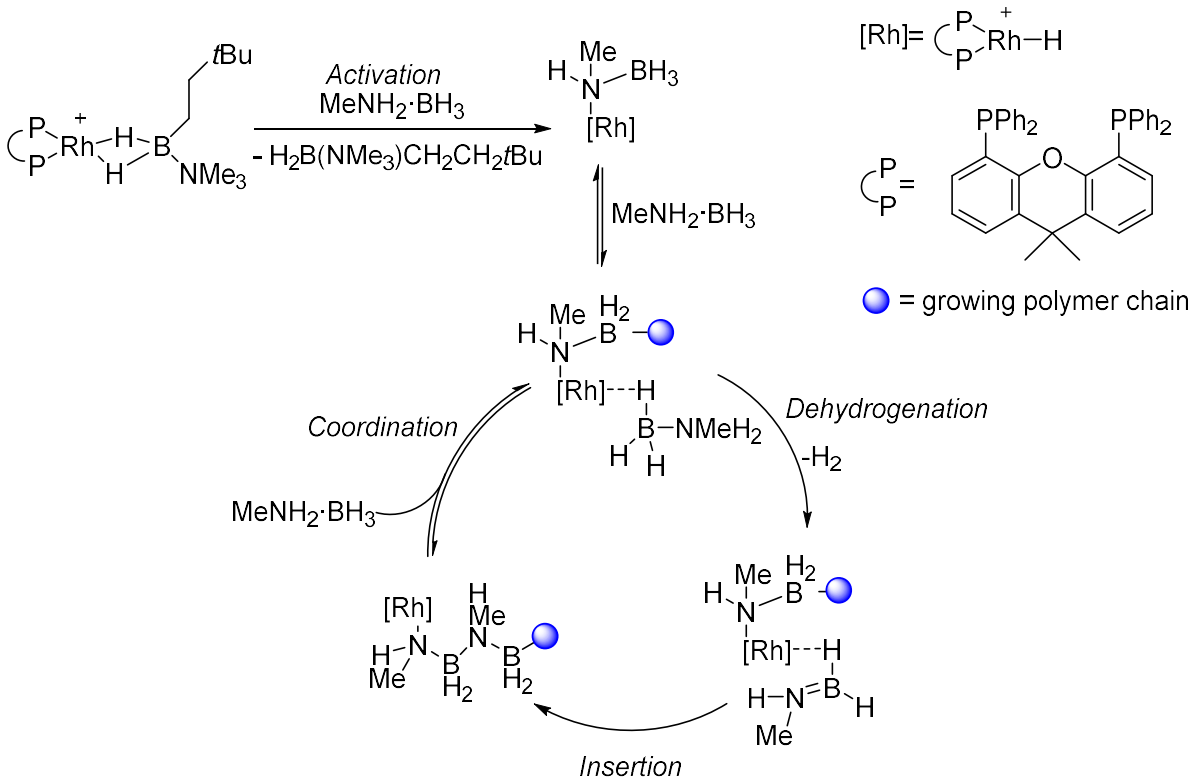

Figure 1.13 Mechanistic proposal for the dehydropolymerisation of $MeNH_2{\cdot}BH_3$ using $[Rh(Xantphos)\{H_2BNMe_3(CH_2)_2tBu\}][BAr^F{}_4]$ catalyst.[145]

The second polymerisation mechanism is a dehydrogenation/ insertion via sigma-bound complexes which undergo reversible chain-transfer. This mechanism has been proposed for the dehydropolymerisation of $NH_3{\cdot}BH_3$ using $[IrH_2(H_2)_2(PCy_3)_2][BAr^F{}_4]$ ($BAr^F{}_4$ = $[B(3,5\text{-}(CF_3)_2C_6H_3)_4]$) (Figure 1.14).[146] The reaction of $[IrH_2(H_2)_2(PCy_3)_2][BAr^F{}_4]$ with 10 equiv. of $NH_3{\cdot}BH_3$ resulted in metal-bound oligomers $[Ir(PCy_3)_2(H)_2\{\eta^2\text{-}H_3B{\cdot}(H_2N\text{–}BH_2)_n{\cdot}NH_3\}][BAr^F{}_4]$ (n = 1– 4) which were detected using ESI-MS. The solid state structures of $[Ir(PCy_3)_2(H)_2\{\eta^2\text{-}H_3B{\cdot}(H_2N\text{–}BH_2)_n{\cdot}NH_3\}][BAr^F{}_4]$ (n = 0 and 2) were obtained and confirmed the η^2 binding mode of the amine-borane. The addition of extra equivalents of $NH_3{\cdot}BH_3$ to $[Ir(PCy_3)_2(H)_2\{\eta^2\text{-}H_3B\ NH_3\}][BAr^F{}_4]$ resulted in a mixture of $[Ir(PCy_3)_2(H)_2\{\eta^2\text{-}H_3B{\cdot}(H_2N\text{–}BH_2)_n{\cdot}NH_3\}][BAr^F{}_4]$ (n = 1 - 3) together with free $H_3B{\cdot}(NH_2\text{–}BH_2)_n{\cdot}NH_3$. This suggested that the sigma bound oligomeric units are weakly bound and can be displaced by additional amine-borane to undergo reversible chain-transfer. Computational studies provided evidence that the polymerisation is an on-metal process as the initial dehydrogenation of $NH_3{\cdot}BH_3$ is higher in energy than both the dehydrogenation of a second amine-borane and metal-promoted B–N bond formation.[146] When the bulkier amine-boranes

$MeNH_2{\cdot}BH_3$ and $Me_2NH{\cdot}BH_3$ were reacted with $[IrH_2(H_2)_2(PCy_3)_2][BAr^F{}_4]$, the species $[Ir(PCy_3)_2(H)_2\{\eta^2\text{-}H_3B{\cdot}(MeHN{-}BH_2)_n{\cdot}NMeH_2\}][BAr^F{}_4]$ (n = 0 and 1) and $[Ir(PCy_3)_2(H)_2\{\eta\text{-}(Me_2N\text{-}BH_2)\}][BAr^F{}_4]$ were detected with no higher oligomers.[72,147] This suggested that steric factors play an important role in the B–N coupling.

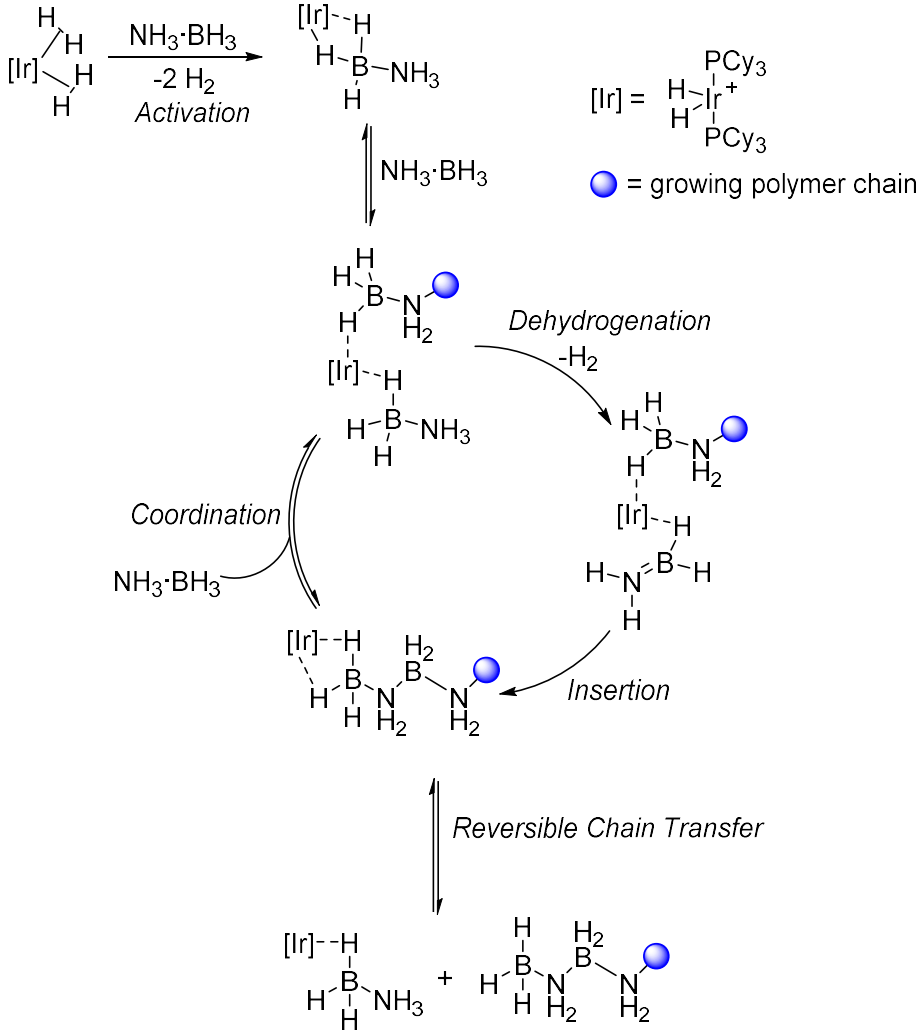

Figure 1.14 Mechanistic proposal for the dehydropolymerisation of $NH_3{\cdot}BH_3$ using $[IrH_2(H_2)_2(PCy_3)_2][BAr^F{}_4]$ catalyst.[146]

A third polymerisation mechanism has been proposed in which separate metal-centres are responsible for the dehydrogenation and polymerisation steps. Although the polymerisation is still metal-mediated, systems proceeding via this mechanism show no clear correlation between molecular weight and catalyst loading due to the dual role of the metal-centres. A combination of experimental studies by Manners *et al*. and computational studies by Paul *et al.* suggest that the polymerisation of $NH_3{\cdot}BH_3$ using IrH_2POCOP (POCOP = $[\eta^3\text{-}1,3\text{-}(OP^tBu_2)_2C_6H_3]$), proceeds by this mechanism.[78,148] It is proposed that the metal centre acts to dehydrogenate the amine-borane $NH_3{\cdot}BH_3$ prior to binding to an aminoborane monomer through an

η^2 coordination mode.[149] The complex [Ir(POCOP)$(H)_2(H_2N–BH_2)$] acts as a chain initiator species in which the terminal amine undertakes nucleophilic attack on a free aminoborane unit resulting in fast head-to-tail B–N bond formation (Figure 1.15). The addition steps were calculated to be strongly exergonic resulting in a low energy oligomerisation pathway. A similar mechanism with nucleophilic chain-growth has been reported for the {Rh-(Xantphos-R)} (R = *i*Pr) catalysed dehydropolymerisation of $MeNH_2{\cdot}BH_3$.[150]

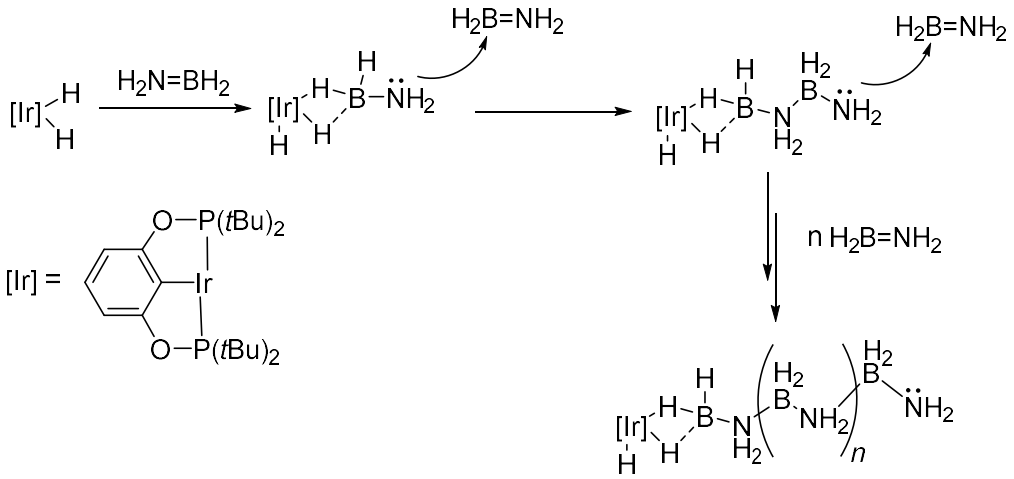

Figure 1.15 Mechanistic proposal for the polymerisation of $H_2N{=}BH_2$ using IrH_2POCOP catalyst. A separate metal-centre is responsible for the dehydrogenation of $NH_3{\cdot}BH_3$.

In 2018 our group reported a titanium catalyst, formed from the *in situ* reaction of $TiCl_2Cp^*_2$ ($Cp^* = [\eta^5\text{-}C_5Me_5]^-$) with two equivalents of *n*BuLi, which dehydropolymerises $MeNH_2{\cdot}BH_3$ via a step-growth, rather than chain-growth, polymerisation. The evidence for the step-growth mechanism is the observation of high molar mass material only at high conversions, a higher degree of polymerisation with higher catalyst loading, and the observation that treating isolated low molar mass material with catalyst afforded high molar mass polymer.[80] Following this, a well-defined Ti(III) complex, Cp^*_2TiMe, has been reported as the first isolable early-metal catalyst for the dehydropolymerisation of primary amine-boranes. Preliminary mechanistic studies using $Me_2NH{\cdot}BH_3$ as a model system suggest a bond metathesis/β-hydride elimination, redox neutral mechanism with a Ti(III)-H resting state.[81]

1.5.2 Mechanisms of transition-metal mediated phosphine-borane dehydropolymerisation

There have been significantly fewer studies reported on the mechanism of the dehydropolymerisation of phosphine-boranes as opposed to amine-boranes.[31] The polymerisation of phosphine-boranes using $[Rh(\mu\text{-}Cl)(1,5\text{-cod})]_2$ (COD = 1,5-cyclooctadiene) is probably a homogeneous catalytic process that has been proposed to proceed via

step-growth mechanism. This assertion is based on studies of the dehydrocoupling of the adduct $Ph_2PH{\cdot}BH_3$ and the dehydropolymerisation of $RPH_2{\cdot}BH_3$ (R = Ph, *i*Bu, p-*n*BuC_6H_4 and p-dodecylC_6H_4), where high molar masses were achieved only at high conversion.[49,132,151] For the dehydrocoupling of $Ph_2PH{\cdot}BH_3$ no suppression of activity was observed upon either the addition of excess mercury, a known poison for heterogeneous catalysts through the formation of an amalgam or adsorption on the catalyst surface, or the addition of 0.5 equivalents of PPh_3. A heterogeneous system can be poisoned by <1 equivalent of ligand (per metal atom) as only a fraction of the metal atoms are on the surface. Additionally no reduction in the rate of dehydrocoupling was observed after filtration of the reaction mixture through a 0.5 μm filter, no induction period was observed and there was no evidence of a black metallic precipitate forming.[152] These experimental results suggest the dehydrocoupling proceeds through a homogeneous catalytic process. The necessity of carrying out the polymerisation of the primary phosphine-boranes in the melt-phase makes the observation of intermediates challenging; however, a step-growth mechanism was proposed based on the observation that high conversions of monomer (>99%) were required to produce high molar mass polymers and this was challenging to achieve due to increased viscosity in the melt phase.[132]

In 2012 Weller *et al.* reported the first detailed mechanistic study of a rhodium catalysed reaction in which the catalyst $[Rh(COD)_2][BAr^F_4]$ (BAr^F_4 = $[B(3,5\text{-}(CF_3)_2C_6H_3)_4]^-$) was used to dehydrocouple the secondary phosphine-borane, *t*$Bu_2PH{\cdot}BH_3$, under melt conditions to give the linear dimer *t*$Bu_2PH{\cdot}BH_2$–P*t*$Bu_2{\cdot}BH_3$ as the major product. Upon dissolving in 1,2-$F_2C_6H_4$ the cations $[Rh(tBu_2PH)_2(\eta^6\text{-}F_2C_6H_4)]^+$ and $[Rh(tBu_2PH)_2(\eta^2\text{-}H_3BtBu_2PBH_2tBu_2PH)]^+$ were observed using ESI-MS. Substitution of the COD ligands by *in situ* generated *t*Bu_2PH occurred, presumably from the cleavage of the P–B bond of the phosphine-borane at the Rh centre. Independently synthesised $[Rh(tBu_2PH)_2(\eta^6\text{-}F_2C_6H_4)]^+$ was found to catalyse the dehydrocoupling at the same rate as the precatalyst and was predicted to form through the reaction of $[Rh(tBu_2PH)_2]^+$ with solvent. $[Rh(tBu_2PH)_2]^+$ has been identified as the active species.[153]

Further mechanistic studies using the more stable precatalyst with a chelating phosphine ligand, $[Rh(dppp)(\eta^6\text{-}C_6H_5F)][BAr^F_4]$ (dppp = $Ph_2P(CH_2)_3PPh_2$), were carried out.[154] Reaction of $[Rh(dppp)(\eta^6\text{-}C_6H_5F)][BAr^F_4]$ with two equivalents of $Ph_2PH{\cdot}BH_3$ formed the Rh(III) complex

[Rh(dppp)H(σ,η-PPh_2BH_3)(η^1-$H_3B{\cdot}PPh_2H$)][BAr^F_4] in which one phosphine-borane undergoes a P–H activation and forms a B–H agostic interaction with the metal, and the other is a B–H σ-bound ligand. Over a short period of time B–P dehydrocoupling occurred to give a Rh^{III} diboraphosphine complex. When substrates with more electron withdrawing aryl groups are used the dehydrocoupling occurs more rapidly and vice versa when more electron donating aryl groups are used.[155] [Rh(dppp)(η^6-C_6H_5F)][BAr^F_4] was also reacted with the primary phosphine-borane $CyPH_2{\cdot}BH_3$ and intermediates analogous to those with $Ph_2PH{\cdot}BH_3$ were observed. The isolation of diastereomers of [Rh(dppp)(H)(σ,η^2-$PCyH{\cdot}BH_2$–$PCyH{\cdot}BH_3$)][BAr^F_4] in a 6:1 ratio suggests that diastereoselectivity is imparted by the metal.

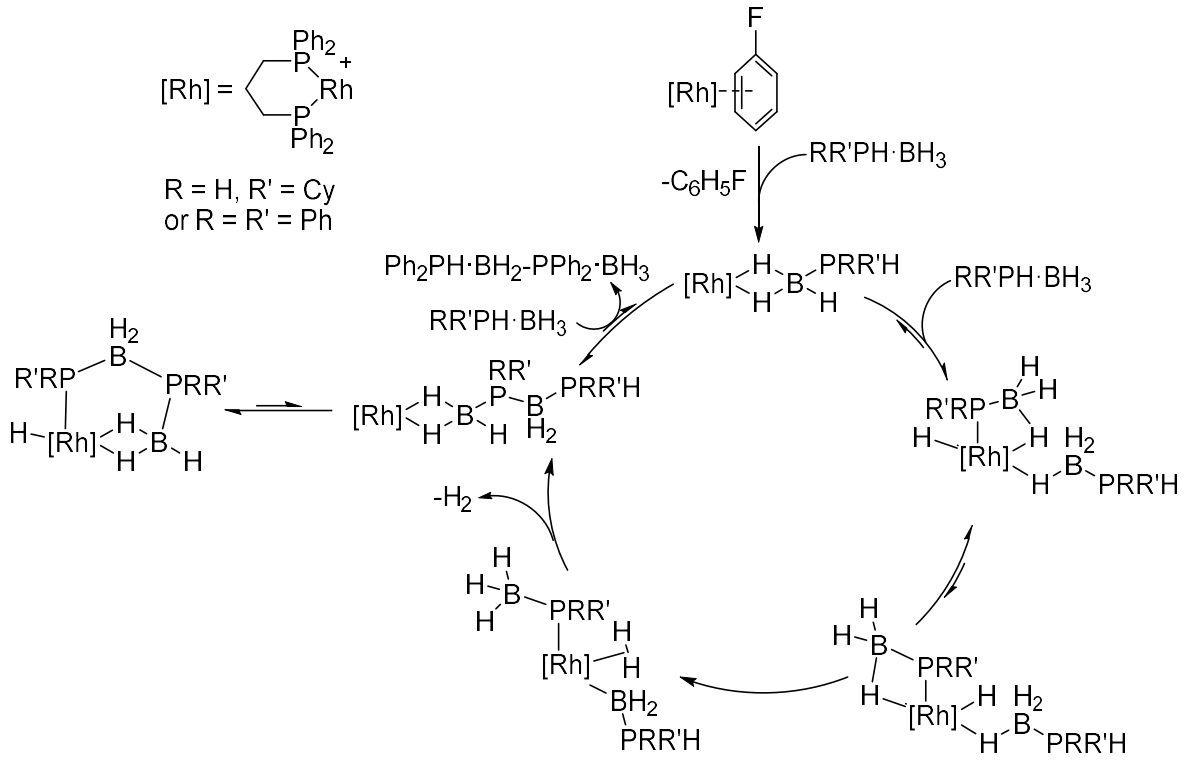

Figure 1.16 Mechanistic proposal for the dehydrocoupling of $Ph_2PH{\cdot}BH_3$ and $CyPH_2{\cdot}BH_3$ using [Rh(dppp)(η^6-C_6H_5F)][BAr^F_4] catalyst.[154]

[RhCp*(PMe_3)Me($ClCH_2Cl$)][BAr^F_4] has proven to be an effective catalyst for the dehydropolymerisation of $PhPH_2{\cdot}BH_3$ in solution and was the focus of a mechanistic study by Weller *et al.* in 2016.[120] The combination of using secondary phosphine-boranes as model systems and computational studies showed that B–H activation precedes P–H activation to give a phosphidoborane complex [RhCp*(PMe_3)($PhHPBH_2$)] as the active species. A step-growth mechanism via a reversible chain transfer was predicted (Figure 1.17). Evidence for this was rapid consumption of $PhPH_2{\cdot}BH_3$ with a significant quantity of the linear dimer $PhPH_2{\cdot}BH_2$–$PPhH{\cdot}BH_3$ being observed at short reaction time.

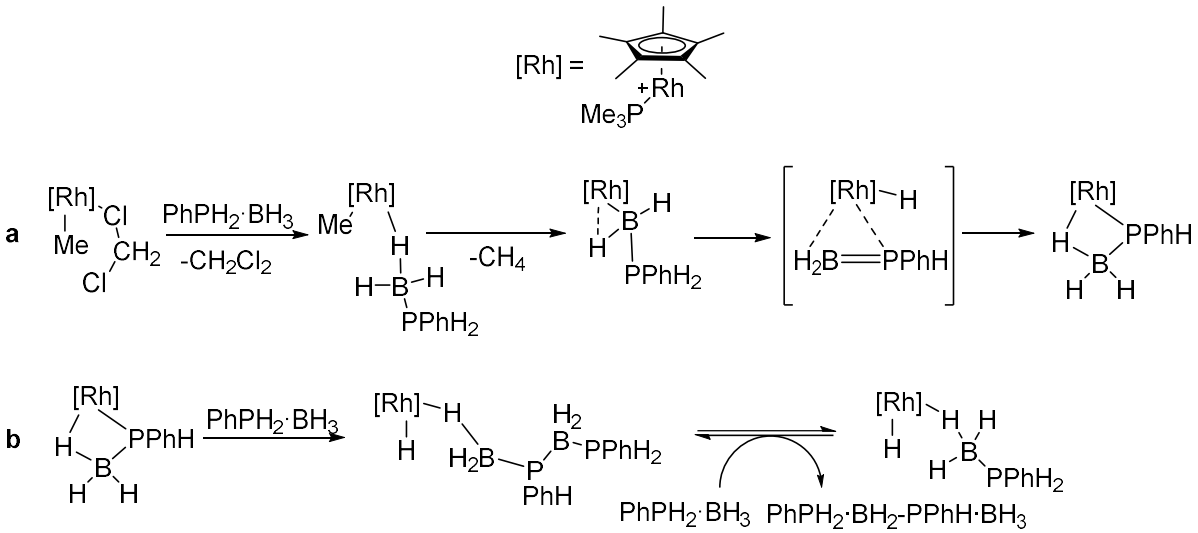

Figure 1.17 a Mechanistic proposal for the synthesis of the active species in the reaction between $PhPH_2{\cdot}BH_3$ and [RhCp*(PMe_3)Me($ClCH_2Cl$)][BAr^F_4]; and **b** proposed reversible chain-transfer polymerisation.

The iron precatalyst [$CpFe(CO)_2(OTf)$], reported by Manners *et al.* in 2015, and capable of solution based dehydropolymerisation of phosphine-boranes has also been the subject of mechanistic studies.[118] The system was determined to be homogenous using the PMe_3 poisoning experiment and the observation that no conversion of phosphine-borane occurred upon the addition of previously generated Fe nanoparticles. A chain-growth polymerisation mechanism was suggested as high molar mass polymer is detected at low conversion and there is an inverse relationship between catalyst loading and molar mass. The phosphidoborane complex [$CpFe(CO)_2(PPhHBH_3)$] was formed by a stoichiometric reaction between [$CpFe(CO)_2(OTf)$] and $PhPH_2{\cdot}BH_3$ and was shown to be equally active for the dehydropolymerisation. This observation suggests that the active catalyst is formed via ligand displacement and P–H activation. This was followed by release of CO to give a B–H agostic phosphidoborane complex [$CpFe(CO)(\kappa^2\text{-P,H-}PPhHBH_3)$]. After formation of the phosphidoborane complex a second monomer coordinates to the Fe centre followed by activation of a B–H bond and formation of a B–P bond by insertion into the [Fe]–P bond. P–H activation was proposed to occur to produce H_2 and form a new Fe–P bond, prior to elimination of dihydrogen from the metal centre which opens up a site for coordination of another monomer (Figure 1.18).

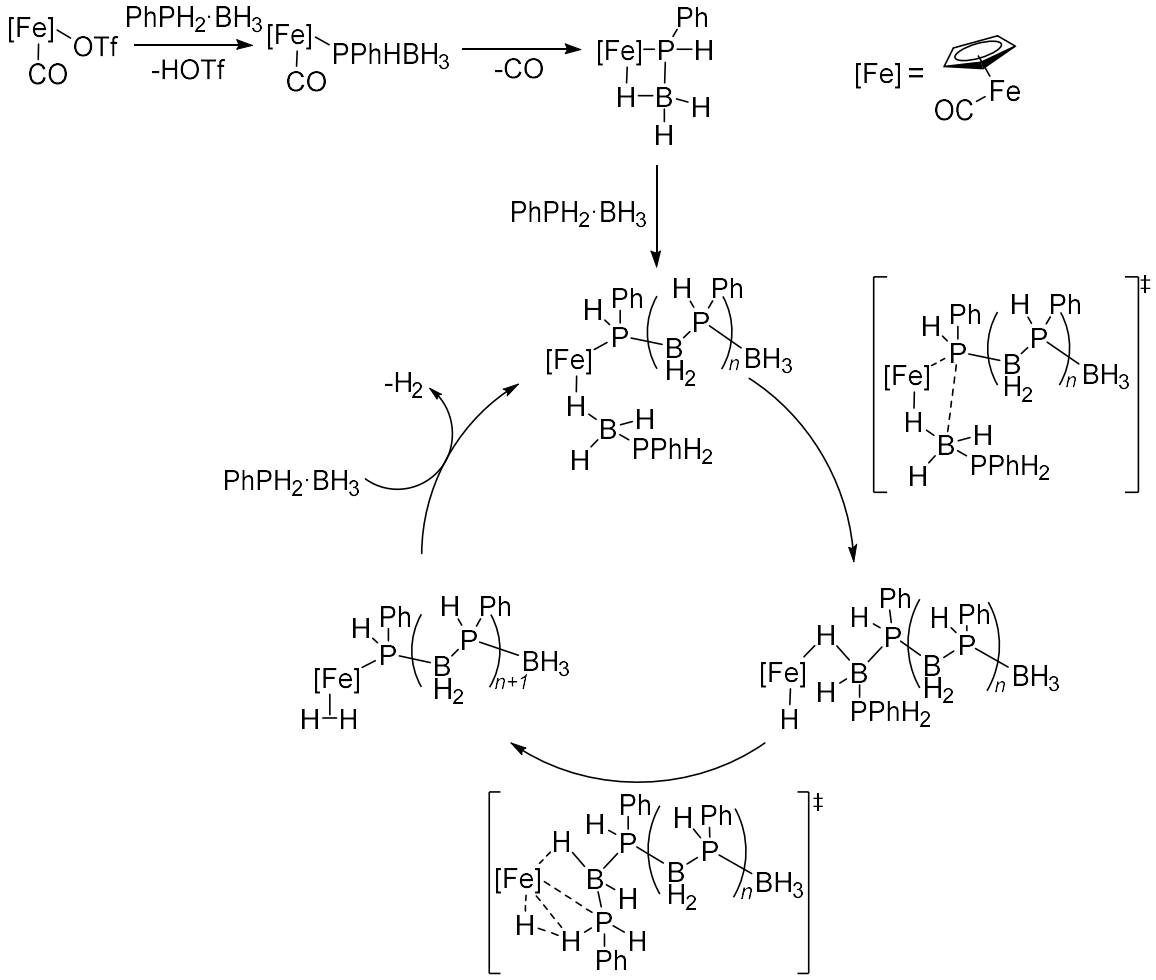

Figure 1.18 Mechanistic proposal for the dehydrocoupling of $PhPH_2{\cdot}BH_3$ using $[CpFe(CO)_2(OTf)]$ catalyst.[118]

1.5.3 Mechanism of metal-free synthesis of polyaminoboranes and polyphosphinoboranes

Recent work has reported that it is possible to synthesise high molar mass polyaminoboranes and polyphosphinoboranes using metal-free routes, indicating that it is not necessary to have a metal catalyst to mediate the polymerisation process.

A collaboration between our group and the Scheer group reported the synthesis of $[t\text{BuHP–BH}_2]_n$ through the thermolysis of $t\text{BuPHBH}_2{\cdot}\text{NMe}_3$ (Section 1.4.2.3) which released the phosphinoborane monomer $t\text{BuHP=BH}_2$.[123] Alcaraz *et al*. reported the synthesis of $[\text{RHN–BH}_2]_n$ (R = Me, Et, *n*Pr, *n*Bu, allyl) using $i\text{Pr}_2\text{N=BH}_2$ as a BH_2 transfer agent with primary amines to form the aminoborane monomers RHN=BH_2 (Section 1.3.2.2).[92] In each case it is predicted that the monomers released undergo a spontaneous head-to-tail polymerisation, however, full mechanistic details, including potential termination steps, have not been reported.

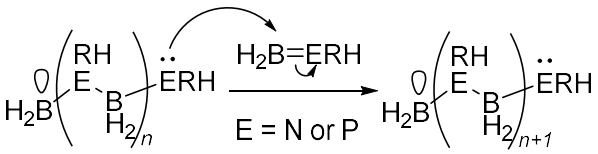

Figure 1.19 Head-to-tail polymerisation of aminoboranes and phosphinoboranes.

1.6 Carbenes

Carbenes, :CR_2, are neutral species with six valence electrons, four of which are involved in the C–R bonds. Such species are typically highly reactive, due to coordinative unsaturation, resulting in their widespread use in bond activation and catalysis.[156] Carbenes have been the focus of much research, particularly in organometallic chemistry, and in 2005 the Nobel Prize in Chemistry was awarded to Grubbs and Schrock for their work on olefin metathesis with "Schrock-type" carbene (metal-alkylidene) complexes.[157]

Carbenes can adopt either a linear or bent structure. The linear structure can be viewed as sp-hybridised at carbon with two degenerate, non-bonding orbitals, p_x and p_y. The bent structure, by contrast, is sp^2-hybridised, resulting in the p_x orbital (now known as σ) gaining s-character, and thus being stabilised; the energy of the p_y orbital (now known as p_π) remains unchanged (Figure 1.20). The relative pπ and σ orbital energies, along with the pairing energy, determine whether carbenes adopt singlet or triplet ground states. On the basis of Hund's rule the triplet state is more stable for linear systems;[158] however, as the energy gap between the orbitals increases the singlet state becomes more energetically favourable. Hoffman calculated that if $\Delta E > 46$ kcal mol^{-1} the carbene will be a singlet and if $\Delta E < 35$ kcal mol^{-1} the carbene will be in the triplet state (where $\Delta E = E_{triplet} - E_{singlet}$).[159]

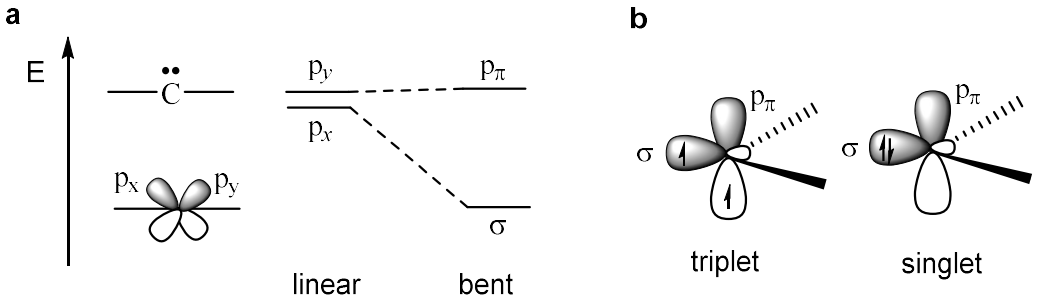

Figure 1.20 a Molecular orbital diagram of linear and bent carbenes; and **b** illustrative representation of the occupation of the orbitals in triplet and singlet carbenes.[160]

Both the steric and electronic properties of a carbene can be varied. Electron withdrawing substituents lower the energy of the σ orbital via inductive effects resulting in an increased HOMO/LUMO gap, which promotes singlet character. π-Donating substituents raise the

energy of the p_π orbital through mesomeric effects but do not affect the σ orbital, again raising the HOMO/LUMO gap. In addition, through incorporation of the carbene into a cyclic system, the HOMO takes on more s-character, as a result of the decreased R–C–R bond angle, lowering its energy and thereby promoting a singlet ground state.

Following the report by Bertrand *et al.* of the first bottleable carbene, [bis(diisopropylamino)phosphino](trimethylsilyl)carbene[161] numerous examples of different types of carbene have been isolated.[162,163] The carbenes utilised in this thesis are nitrogen heterocyclic carbenes (NHCs) and cyclic (alkyl)(amino)carbenes (CAACs), thus these will be focussed on in this introduction.

1.6.1 Nitrogen heterocyclic carbenes (NHCs)

Wanzlick recognised in the 1960s that the stability of carbenes could be enhanced through the use of amino substituents which exhibit both σ-withdrawing and π-donating properties - the so-called 'push-pull' effect (Figure 1.21a). By additionally employing a cyclic backbone, the preparation of 1,3-diphenylimidazolidin-2-ylidene was targeted; however, instead of the free carbene, the dimerisation product, a tetra(amino) olefin was formed.[164] It was not until 1991 that Arduengo reported the first isolable NHC, 1,3-di-1-adamantyl-imidazol-2-ylidene. This carbene was incorporated into an unsaturated nitrogen heterocycle (Figure 1.21b).[165] Bulky adamantyl substituents provide kinetic stability and reduce the propensity for dimerisation.

Figure 1.21 a The 'push-pull' effect demonstrated in a diamido-substituted carbene; and **b** the first isolated NHC.[165]

An NHC is a singlet diamino carbene in which the nitrogen lone pair donates into the empty p_π orbital, increasing the energy of the LUMO. The energy of the carbene lone pair (HOMO σ orbital) is lowered through the inductive effect of the two electronegative nitrogen atoms. The free NHC is usually synthesised through deprotonation of the corresponding imidazolium salt with a strong base in a non-protic solvent (Scheme 1.12).[166]

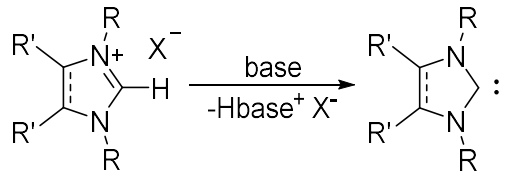

Scheme 1.12 Synthesis of NHCs by deprotonation of imidazolium salts.[166]

1.6.1.1 Reactivity and applications of NHCs

NHCs exhibit ambiphilic behaviour due to the simultaneous presence of a filled σ orbital and empty p_π orbital on the carbenic carbon, enabling Lewis basic and Lewis acidic character on the same atom. Variation of the nitrogen substituent allows alteration of the steric influences of the NHC[166] and changing the backbone, for example changing the degree of saturation or altering the substituents, allows the electronic donation properties of the carbene to be adjusted.[167] The synthesis of a huge library of NHCs has allowed the chemistry of these species to be explored and they have displayed uses in a broad range of applications.[156]

NHCs are versatile, widely used ligands in modern organometallic chemistry.[166] The strong σ-bonding and comparatively weak π-accepting properties can be compared to those of phosphines. There are, however, a number of differences between the ligands. In general, NHCs are more electron-donating than phosphines and thus form stronger and shorter metal-ligand bonds than phosphines. Additionally, NHCs are generally more sterically demanding as the nitrogen substituents are orientated towards the metal centre and it is synthetically easier to vary their steric and electronic properties.[168]

NHCs are versatile, widely used ancillary ligands in homogeneous transition-metal catalysis of organic transformations such as cross-coupling,[169,170] olefin metathesis[171,172] and asymmetric catalysis[173] to name a few.[174] They also display uses in materials chemistry[175] for example as coordination polymers,[176] photoactive materials,[177] liquid crystals[178] and metal-organic frameworks.[179] There have been a number of reports of the medicinal application of NHC-transition metal complexes, in particular Ag(I)-NHCs have shown promise as antibacterial and anticancer agents.[180]

NHCs also coordinate strongly to a range of *p*-block elements[181] and a number of applications of these adducts have been reported including stabilisation of low oxidation states[182] and radical species[183] and as frustrated Lewis pairs.[184] The ability of NHCs to coordinate to carbon-electrophiles gives rise to another major application class as organocatalysts,[185,186] including as initiators for ring-opening polymerisations.[187,188]

There are also examples of NHCs acting as hydrogen acceptors (Scheme 1.13a)[189] and an NHC has been reported to facilitate the reductive P–P coupling of both primary and secondary phosphines (Scheme 1.13b).[190]

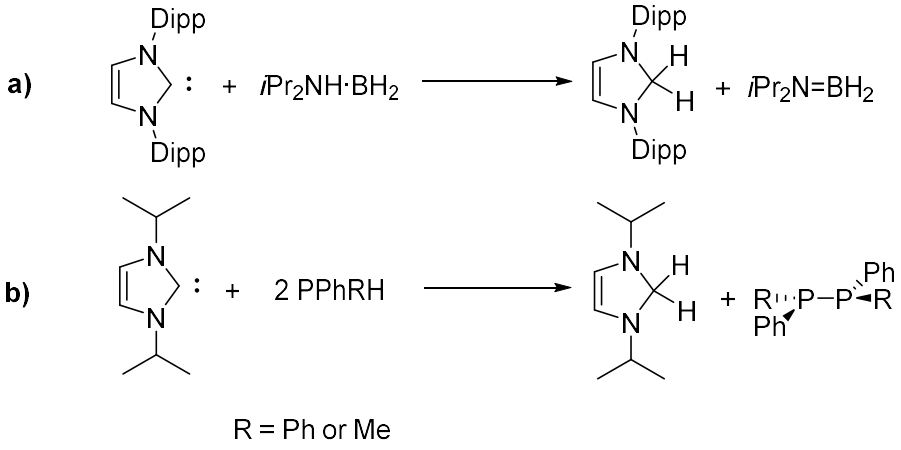

Scheme 1.13 a NHC dehydrogenation of an amine-borane; and **b** NHC facilitating the dehydrocoupling of phosphines.

1.6.2 Cyclic (alkyl)(amino)carbenes CAACs

In 2005 Bertrand *et al*. pioneered the synthesis of CAACs.[191] These are a new family of carbenes displaying a similar structure to NHCs, but with one of the σ-withdrawing and π-donating amino substituents being replaced by a σ-donating, but not π-donating, alkyl group. This substitution increases both the π-electrophilicity and σ-nucleophilicity relative to NHCs (Figure 1.22) and the resulting electronic structure is reflected in NMR data.[162] The carbenic carbon of the free carbene has very low-field shift (^{13}C > 300 ppm) and CAAC-phosphinidene adducts have a very distinctive low-field ^{31}P shift.[192] The presence of a quaternary carbon at an α position to the carbene results in a very different steric environment compared to a related NHC.

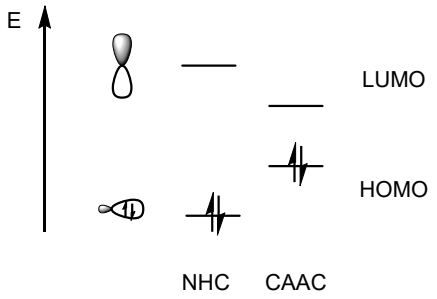

Figure 1.22 Relative HOMO and LUMO energies of NHC (left) vs CAAC (right).

The sp^3 carbon centre adjacent to the nitrogen in a CAAC precursor salt must be quaternary to avoid competing deprotonation; however, the substituents R^1 and R^2 (Scheme 1.14) are very much unrestricted. 2,6-Diisopropylphenyl (Dipp) has been shown to be a more useful

nitrogen substituent in CAACs than mesityl (Mes) as when the latter is used there is competing deprotonation of the methyl substituents of the Mes group.[193] The most economical synthesis is via the hydroimination route (Scheme 1.14) where the salt can be synthesised in up to 80% yield, and the final deprotonation step to form the carbene is quantitative.[194]

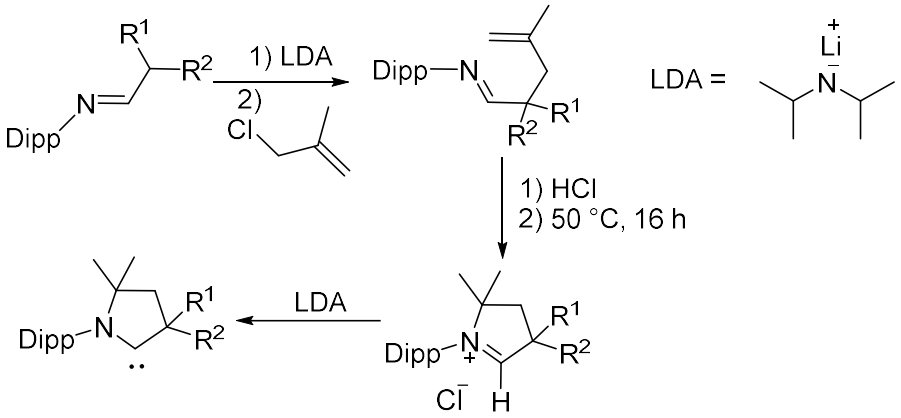

Scheme 1.14 Synthesis of CAACs through the hydroamination route.[194]

1.6.2.1 Reactivity and applications of CAACs

Many uses of CAACs in chemistry have been reported and extensively reviewed[162,193] including: (1) as ligands for the stabilisation of low-valent transition-metal compounds,[195] (2) in the stabilisation of unusual diamagnetic and paramagnetic main group species[151] and (3) in small molecule activation. In contrast to NHCs, CAACs have not yet found a use in organocatalysis as their strong basicity results in them displaying poor leaving group properties.[193]

Their strong π-accepting properties has allowed the synthesis of low valent metal compounds that have not been accessible using NHCs. An example of which is the isolation of $(CAAC)_2Be$ as the first example of a neutral zero-valent s-block metal compound (Scheme 1.15).[196]

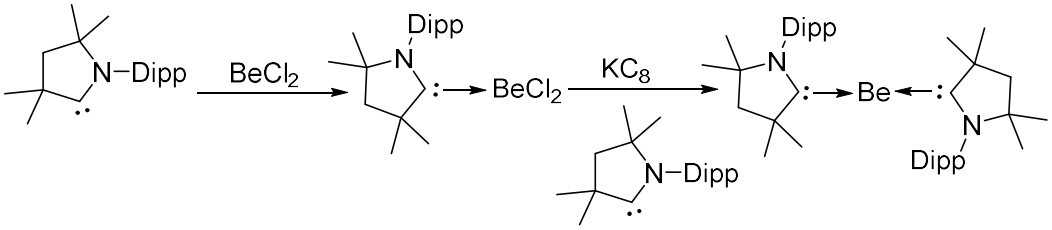

Scheme 1.15 Synthesis of $(CAAC)_2Be$.[196]

CAACs have been shown to be superior to NHCs in the stabilisation of radical species. This is attributed to both their stronger σ-donating and π-accepting properties combined with the presence of the quaternary carbon adjacent to the carbene centre increasing the steric profile.[162,197] An example of this is that the NHC stabilised dichlorosilylene $[(NHC)SiCl_2]$ exists

in a non-radical monomeric form, whereas $SiCl_2$ stabilised by two CAACs [$(CAAC\cdot)_2SiCl_2$] exists as a biradical species (Scheme 1.16).[198,199]

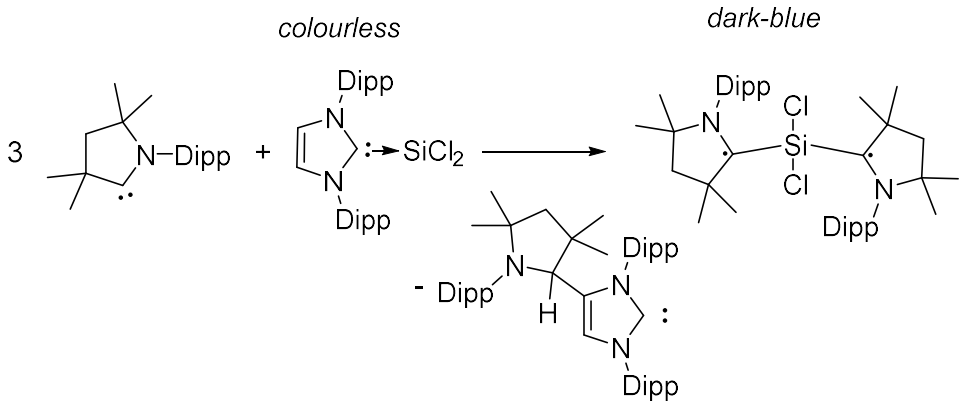

Scheme 1.16 Synthesis of a CAAC coordinated biradical.[191]

The most relevant property to the work discussed in this thesis, is the ability to activate small molecules, e.g. CO,[200] H_2,[201] and P_4[202] and E–H bonds (E = N, Si, B, P, C, O),[201,203–205] at the carbene centre under mild conditions (Figure 1.23). This is possible due to the ambiphilicity of the carbene centre and demonstrates that oxidative addition can occur; however, a catalytic system involving only a CAAC has yet to be realised since the high strength of the C–H bonds resulting from substrate activation prevents reductive-elimination or insertions following oxidative-addition.[193]

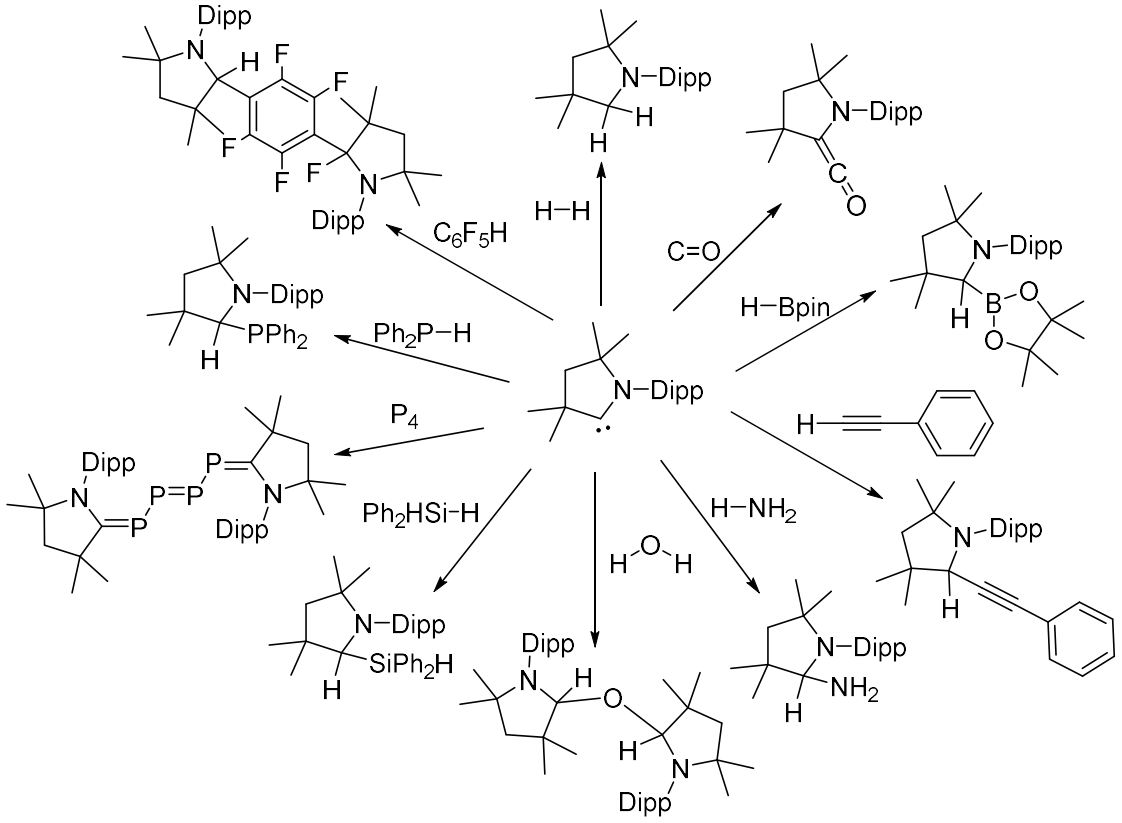

Figure 1.23 Small molecule and E–H bond activation by CAACs.[200–205]

Notably in 2017 Radius and Marder used NMR studies to report the first example of reversible oxidative-addition of organoboronate esters at the CAAC carbene centre, opening up avenues for CAACs to be used in a catalytic manner.[206]

1.7 Thesis summary and acknowledgement of collaborators

The work described in this PhD thesis is a compilation of research projects which focus on new synthetic routes towards polyphosphinoboranes and explores the carbene initiated depolymerisation of polyaminoboranes. This thesis comprises four results chapters along with an outlook chapter which highlights the impact of this work and discusses future potential research directions. The chapters are organised as follows:

- **Chapter 2** describes the metal-free dehydropolymerisation of phosphine-boranes using cyclic (alkyl)(amino)carbenes as hydrogen acceptors.
- **Chapter 3** details the use of $Ni(COD)_2$ as a catalyst for the dehydropolymerisation of phosphine-boranes.
- **Chapter 4** explores the carbene-mediated depolymerisation of poly(N-methylaminoborane) $[MeHN–BH_2]_n$.
- **Chapter 5** discusses attempts of expanding the substrate scope of the work discussed in Chapter 2 and explores the reactivity of the adduct IDipp–BH_2NMeH.

In accordance with the system implemented by Prof. Ian Manners, each chapter of this thesis has been written in the form of a self-contained manuscript that may be published in peer-reviewed scientific literature. The majority of the work in this thesis was carried out by the author; however, in the spirit of collaboration the work has benefitted from contributions of colleagues from within the Manners' group and external collaborators. These contributions are outlined below:

Chapter 2 has been reproduced almost without modification from *Nature Communications,* ***2019*** *,10*, 1370. Initial work was carried out under the lab direction of Dr. Saurabh S. Chitnis. Dr. Vincent T. Annibale was responsible for the synthesis of **2.4a** and **2.4b**. Dr. Marius I. Arz performed the DFT calculations. X-ray crystallography was performed by Dr. Vincent T. Annibale and Dr. Hazel A. Sparkes.

Chapter 3 contains as of yet unpublished results. X-ray crystallography was performed by Dr. Brian O. Patrick and Dr. Etienne A. LaPierre. Air sensitive mass spectrometry was performed by Dr. Tyler Trefz.

Chapter 4 contains as of yet unpublished results. Low temperature NMR was carried out by Chris Arthur. Dr. Hazel A. Sparkes and Dr. Vincent T. Annibale performed X-ray crystallography.

Chapter 5 contains as of yet unpublished results. Dr. Hazel A. Sparkes and Dr. Etienne A. LaPierre performed X-ray crystallography. Air-sensitive mass spectrometry was performed by Dr. Tyler Trefz. Solid state NMR was performed by Dr. Eric Ye and powder XRD was performed by Anita Lam.

1.8 References

(1) Natta, G.; Pino, P.; Mazzanti, G.; Giannini, U. A Crystallizable Organometallic Complex Containing Titanium and Aluminum. *J. Am. Chem. Soc.* **1957**, *79*, 2975–2976.

(2) Chauvin, Y. Olefin Metathesis: The Early Days (Nobel Lecture). *Angew. Chem. Int. Ed.* **2006**, *45*, 3741–3747.

(3) Schrock, R. R. Multiple Metal-Carbon Bonds for Catalytic Metathesis Reactions (Nobel Lecture). *Angew. Chem. Int. Ed.* **2006**, *45*, 3748–3759.

(4) Grubbs, R. H. Olefin-Metathesis Catalysts for the Preparation of Molecules and Materials (Nobel Lecture). *Angew. Chem. Int. Ed.* **2006**, *45*, 3760–3765.

(5) Beletskaya, I. P.; Cheprakov, A. V. The Heck Reaction as a Sharpening Stone of Palladium Catalysis. *Chem. Rev.* **2000**, *100*, 3009–3066.

(6) Miyaura, N.; Suzuki, A. Palladium-Catalyzed Cross-Coupling Reactions of Organoboron Compounds. *Chem. Rev.* **1995**, *95*, 2457–2483.

(7) https://www.nobelprize.org/prizes/lists/all-nobel-prizes-in-chemistry.

(8) Obligacion, J. V.; Chirik, P. J. Earth-Abundant Transition Metal Catalysts for Alkene Hydrosilylation and Hydroboration. *Nat. Rev. Chem.* **2018**, *2*, 15–34.

(9) Nakajima, Y.; Shimada, S. Hydrosilylation Reaction of Olefins: Recent Advances and Perspectives. *RSC Adv.* **2015**, *5*, 20603–20616.

(10) Leitao, E. M.; Jurca, T.; Manners, I. Catalysis in Service of Main Group Chemistry Offers a Versatile Approach to p-Block Molecules and Materials. *Nat. Chem.* **2013**, *5*, 817–829.

(11) Jones, R. G.; Holder, S. J. High-Yield Controlled Syntheses of Polysilanes by the Wurtz-Type Reductive Coupling Reaction. *Polym. Int.* **2006**, *5*, 711–718.

(12) Clark, T. J.; Lee, K.; Manners, I. Transition-Metal-Catalyzed Dehydrocoupling: A Convenient Route to Bonds between Main-Group Elements. *Chem. Eur. J.* **2006**, *12*, 8634–8648.

(13) Corcoran, E. W.; Sneddon, L. G. Transition-Metal-Promoted Reactions of Boron Hydrides. 6. Platinum(II) Bromide Catalyzed Borane and Carborane Dehydrodimerization Reactions: A New Synthetic Route to Boron-Boron Linked Multicage Boranes and Carboranes. *J. Am. Chem. Soc.* **1984**, *106*, 7793–7800.

(14) Waterman, R. Mechanisms of Metal-Catalyzed Dehydrocoupling Reactions. *Chem. Soc. Rev.* **2013**, *42*, 5629–5641.

(15) Less, R. J.; Melen, R. L.; Wright, D. S. Catalytic versus Stoichiometric Dehydrocoupling Using Main Group Metals. *RSC Adv.* **2012**, *2*, 2191–2199.

(16) Melen, R. L. Dehydrocoupling Routes to Element-Element Bonds Catalysed by Main Group Compounds. *Chem. Soc. Rev.* **2016**, *45*, 775–788.

(17) Hill, M. S.; Liptrot, D. J.; Weetman, C. Alkaline Earths as Main Group Reagents in Molecular Catalysis. *Chem. Soc. Rev.* **2016**, *45*, 972–988.

(18) Weetman, C.; Inoue, S. The Road Travelled: After Main-Group Elements as Transition Metals. *ChemCatChem* **2018**, *10*, 4213–4228.

(19) Melen, R. L. Frontiers in Molecular p-Block Chemistry: From Structure to Reactivity. *Science* **2019**, *484*, 479–484.

(20) Walsh, D. J.; Hyatt, M. G.; Miller, S. A.; Guironnet, D. Recent Trends in Catalytic Polymerizations. *ACS Catal.* **2019**, *9*, 11153–11188.

(21) Manners, I. Polymer Science with Transition Metals and Main Group Elements: Towards Functional, Supramolecular Inorganic Polymeric Materials. *J. Polym. Sci. Part A Polym. Chem.* **2002**, *40*, 179–191.

(22) Shit, S. C.; Shah, P. A Review on Silicone Rubber. *Natl. Acad. Sci. Lett.* **2013**, *36*, 355–365.

(23) Rothemund, S.; Teasdale, I. Preparation of Polyphosphazenes: A Tutorial Review. *Chem. Soc. Rev.* **2016**, *45*, 5200–5215.

(24) Miller, R. D.; Michl, J. Polysilane High Polymers. *Chem. Rev.* **1989**, *89*, 1359–1410.

(25) Choi, N.; Tanaka, M. Zirconocene-Catalyzed Dehydrogenative Coupling of Phenylgermane and Properties of the Resulting Partially Network Polyphenylgermanes. *J. Organomet. Chem.* **1998**, *564*, 81–84.

(26) Imori, T.; Lu, V.; Cai, H.; Tilley, T. D. Metal-Catalyzed Dehydropolymerization of Secondary Stannanes to High Molecular Weight Polystannanes. *J. Am. Chem. Soc.* **1995**, *117*, 9931–9940.

(27) Arz, M. I.; Annibale, V. T.; Kelly, N. L.; Hanna, J. V; Manners, I. Ring-Opening Polymerization of Cyclic Phosphonates: Access to Inorganic Polymers with a P(V)–O Main Chain. **2018**, *141*, 6–11.

(28) Staubitz, A.; Robertson, A. P. M.; Manners, I. Ammonia-Borane and Related Compounds as Dihydrogen Sources. *Chem. Rev.* **2010**, *110*, 4079–4124.

(29) Staubitz, A.; Hoffmann, J.; Gliese, P. *Group 13-Group 15 Element Bonds Replacing Carbon-Carbon Bonds in Main Group Polyolefin Analogs. In Smart Inorganic Polymers: Synthesis, Properties, and Emerging Applications in Materials and Life Sciences*; Hey-Hawkins, E., Hissler, M., Eds.; Wiley-VCH, 2019; 17–39.

(30) Colebatch, A. L.; Weller, A. S. Amine-Borane Dehydropolymerization: Challenges and Opportunities. *Chem. Eur. J.* **2019**, *25*, 1379–1390.

(31) Han, D.; Anke, F.; Trose, M.; Beweries, T. Recent Advances in Transition Metal Catalysed Dehydropolymerisation of Amine Boranes and Phosphine Boranes. *Coord. Chem. Rev.* **2019**, *380*, 260–286.

(32) Gay-Lussac, J. L.; Thenard, J. A. NH_3BF_3. *Mem. Phys. Chim. Soc. D'Arcueil* **1809**, *69*, 207–234.

(33) Shore, S. G.; Parry, R. W. The Crystalline Compound Ammonia-Borane, NH_3BH_3. *J. Am. Chem. Soc.* **1955**, *77*, 6084–6085.

(34) Staubitz, A.; Robertson, A. P. M.; Sloan, M. E.; Manners, I. Amine- and Phosphine-Borane Adducts: New Interest in Old Molecules. *Chem. Rev.* **2010**, *110*, 4023–4078.

(35) Stubbs, N. E.; Schäfer, A.; Robertson, A. P. M. M.; Leitao, E. M.; Jurca, T.; Sparkes, H. A.; Woodall, C. H.; Haddow, M. F.; Manners, I. B-Methylated Amine-Boranes: Substituent Redistribution, Catalytic Dehydrogenation, and Facile Metal-Free Hydrogen Transfer Reactions. *Inorg. Chem.* **2015**, *54*, 10878–10889.

(36) Atkins, P.; Overton, T.; Rourke, J.; Weller, M.; Armstrong, F. *Inorganic Chemistry*, Vol 6.; Oxford University Press: New York, U.S.A., 2014.

(37) Liu, Z.; Marder, T. B. B-N versus C-C: How Similar Are They? *Angew. Chem. Int. Ed.* **2008**, *47*, 242–244.

(38) Power, P. P. π-Bonding and the Lone Pair Effect in Multiple Bonds Between Heavier Main Group Elements. **1999**, *99*, 3643–3503.

(39) Stephens, F. H.; Pons, V.; Baker, R. T. Ammonia–Borane: The Hydrogen Source Par Excellence? **2007**, 2613–2626.

(40) Marder, T. B. Will We Soon Be Fueling Our Automobiles with Ammonia-Borane? *Angew. Chem. Int. Ed.* **2007**, *46*, 8116–8118.

(41) Hamilton, C. W.; Baker, R. T.; Manners, I. B–N Compounds for Chemical Hydrogen Storage. *Chem. Soc. Rev.* **2009**, *38*, 279–293.

(42) Bhunya, S.; Malakar, T.; Ganguly, G.; Paul, A. Combining Protons and Hydrides by Homogeneous Catalysis for Controlling the Release of Hydrogen from Ammonia−Borane: Present Status and Challenges. *ACS Catal.* **2016**, *6*, 7907–7934.

(43) Mcgee, H. A.; Kwon, C. T. Cryochemical Preparation of Monomeric Aminoborane. *Inorg. Chem.* **1970**, *9*, 2458–2461.

(44) Baumann, J.; Baitalow, F.; Wolf, G. Thermal Decomposition of Polymeric Aminoborane $(H_2BNH_2)_x$ under Hydrogen Release. *Thermochim. Acta* **2005**, *430*, 9–14.

(45) Chopard, P. A.; Hudson, R. F.; Geneva, C. Some Adducts of Phosphines and Amines with Borane. *J. Inorg. Nucl. Chem.* **1963**, *25*, 801–805.

(46) Beachley, O. Intermediates in the Formation of N-Methylaminoborane Trimer. *Inorg. Chem.* **1965**, 870–874.

(47) Ryschkewitsch, G. E.; Wiggins, J. W. Hydrogen Elimination in Dimethylamine-Borane. *Inorg. Chem.* **1969**, *9*, 314–317.

(48) Jaska, C. A.; Temple, K.; Lough, A. J.; Manners, I. Rhodium-Catalyzed Formation of Boron–Nitrogen Bonds: A Mild Route to Cyclic Aminoboranes and Borazines. *Chem. Commun.* **2001**, 962–963.

(49) Jaska, C. A.; Manners, I. Heterogeneous or Homogeneous Catalysis? Mechanistic Studies of the Rhodium-Catalyzed Dehydrocoupling of Amine-Borane and Phosphine-Borane Adducts. *J. Am. Chem. Soc.* **2004**, *126*, 9776–9785.

(50) Sloan, M. E.; Staubitz, A.; Clark, T. J.; Russell, C. A.; Lloyd-Jones, G. C.; Manners, I. Homogeneous Catalytic Dehydrocoupling/Dehydrogenation of Amine-Borane Adducts by Early Transition Metal, Group 4 Metallocene Complexes. *J. Am. Chem. Soc.* **2010**, *132*, 3831–3841.

(51) Helten, H.; Dutta, B.; Vance, J. R.; Sloan, M. E.; Haddow, M. F.; Sproules, S.; Collison, D.; Whittell, G. R.; Guy, C. L. J.; Manners, I. Paramagnetic Titanium(III) and Zirconium(III) Metallocene Complexes as Precatalysts for the Dehydrocoupling/Dehydrogenation of Amine-Boranes. *Angew. Chem. Int. Ed.* **2013**, *52*, 437–440.

(52) Sharpe, H. R.; Geer, A. M.; Blundell, T. J.; Hastings, F. R.; Fay, M. W,; Rance, G. A.; Lewis, W.; Blake, A. J.; Kays, D. L. Dehydrocoupling of Dimethylamine–borane Promoted by Manganese(II) m-Terphenyl Complexes. *Catal. Sci. Technol.* **2018**, 8, 229

(53) Baker, R. T.; Gordon, J. C.; Hamilton, C. W.; Henson, N. J.; Lin, P. H.; Maguire, S.; Murugesu, M.; Scott, B. L.; Smythe, N. C. Iron Complex-Catalyzed Ammonia-Borane Dehydrogenation. A Potential Route Toward B-N-Containing Polymer Motifs Using Earth-Abundant Metal Catalysts. *J. Am. Chem. Soc.* **2012**, *134*, 5598–5609.

(54) Bhattacharya, P.; Krause, J. A.; Guan, H. Mechanistic Studies of Ammonia Borane Dehydrogenation Catalyzed by Iron Pincer Complexes. *J. Am. Chem. Soc.* **2014**, *136*, 11153–11161.

(55) Luo, W.; Campbell, P. G.; Zakharov, L. N.; Liu, S. Y. A Single-Component Liquid-Phase Hydrogen Storage Material. *J. Am. Chem. Soc.* **2011**, *133*, 19326–19329.

(56) Maier, T. M.; Sandl, S.; Shenderovich, I. G.; Jacobi von Wangelin, A.; Weigand, J. J.; Wolf, R. Amine-Borane Dehydrogenation and Transfer Hydrogenation Catalyzed by α-Diimine Cobaltates. *Chem. Eur. J.* **2019**, *25*, 238–245.

(57) Todisco, S.; Luconi, L.; Giambastiani, G.; Rossin, A.; Peruzzini, M.; Golub, I. E.; Filippov, O. A.; Belkova, N. V.; Shubina, E. S. Ammonia Borane Dehydrogenation Catalyzed by (κ^4-EP_3)Co(H) [EP_3 = $E(CH_2CH_2PPh_2)_3$; E = N, P] and H_2 Evolution from Their Interaction with NH Acids. *Inorg. Chem.* **2017**, *56*, 4296–4307.

(58) Pagano, J. K.; Stelmach, J. P. W.; Waterman, R. Cobalt-Catalyzed Ammonia Borane Dehydrocoupling and Transfer Hydrogenation under Aerobic Conditions. *Dalton Trans.* **2015**, *44*, 12074–12077.

(59) Keaton, R. J.; Blacquiere, J. M.; Baker, R. T. Base Metal Catalyzed Dehydrogenation of Ammonia-Borane for Chemical Hydrogen Storage. *J. Am. Chem. Soc.* **2007**, *129*, 1844–1845.

(60) Vogt, M.; de Bruin, B.; Berke, H.; Trincado, M.; Grützmacher, H. Amino Olefin Nickel(I) and Nickel(0) Complexes as Dehydrogenation Catalysts for Amine Boranes. *Chem. Sci.* **2011**, *2*, 723–727.

(61) Jaska, C. A.; Temple, K.; Lough, A. J.; Manners, I. Transition Metal-Catalyzed Formation of Boron-Nitrogen Bonds: Catalytic Dehydrocoupling of Amine-Borane Adducts to Form Aminoboranes and Borazines. *J. Am. Chem. Soc.* **2003**, *125*, 9424–9434.

(62) Douglas, T. M.; Chaplin, A. B.; Weller, A. S. Amine-Borane σ-Complexes of Rhodium. Relevance to the Catalytic Dehydrogenation of Amine-Boranes. *J. Am. Chem. Soc.* **2008**, *130*, 14432–14433.

(63) Dallanegra, R.; Chaplin, A. B.; Tsim, J.; Weller, A. S. Amino-Borane Oligomers Bound to a Rh(I) Metal Fragment. *Chem. Commun.* **2010**, *46*, 3092–3094.

(64) Sewell, L. J.; Lloyd-Jones, G. C.; Weller, A. S. Development of a Generic Mechanism for the Dehydrocoupling of Amine-Boranes: A Stoichiometric, Catalytic, and Kinetic Study of $H_3B{\cdot}NMe_2H$ Using the $[Rh(PCy_3)_2]^+$ Fragment. *J. Am. Chem. Soc.* **2012**, *134*, 3598–3610.

(65) Zahmakiran, M.; Özkar, S. Dimethylammonium Hexanoate Stabilized Rhodium(0) Nanoclusters Identified as True Heterogeneous Catalysts with the Highest Observed Activity in the Dehydrogenation of Dimethylamine-Borane. *Inorg. Chem.* **2009**, *48*, 8955–8964.

(66) Chen, Y.; Fulton, J. L.; Linehan, J. C.; Autrey, T. In Situ XAFS and NMR Study of Rhodium-Catalyzed Dehydrogenation of Dimethylamine Borane. *J. Am. Chem. Soc.* **2005**, *127*, 3254–3255.

(67) Friedrich, A.; Drees, M.; Schneider, S. Ruthenium-Catalyzed Dimethylamineborane Dehydrogenation: Stepwise Metal-Centered Dehydrocyclization. *Chem. Eur. J.* **2009**, *15*, 10339–10342.

(68) Käß, M.; Friedrich, A.; Drees, M.; Schneider, S. Ruthenium Complexes with Cooperative PNP Ligands: Bifunctional Catalysts for the Dehydrogenation of Ammonia-Borane. *Angew. Chem. Int. Ed.* **2009**, *48*, 905–907.

(69) Marziale, A. N.; Friedrich, A.; Klopsch, I.; Drees, M.; Celinski, V. R.; Schmedt auf der Günne, J.; Schneider, S. The Mechanism of Borane-Amine Dehydrocoupling with Bifunctional Ruthenium Catalysts. *J. Am. Chem. Soc.* **2013**, *135*, 13342–13355.

(70) Jiang, Y.; Berke, H. Dehydrocoupling of Dimethylamine-Borane Catalysed by Rhenium Complexes and Its Application in Olefin Transfer-Hydrogenations. *Chem. Commun.* **2007**, *34*, 3571.

(71) Denney, M. C.; Pons, V.; Hebden, T. J.; Heinekey, D. M.; Goldberg, K. I. Efficient Catalysis of Ammonia Borane Dehydrogenation. *J. Am. Chem. Soc.* **2006**, *128*, 12048–12049.

(72) Stevens, C. J.; Dallanegra, R.; Chaplin, A. B.; Weller, A. S.; MacGregor, S. A.; Ward, B.; McKay, D.; Alcaraz, G.; Sabo-Etienne, S. $[Ir(PCy_3)_2(H)_2(H_2B\text{-}NMe_2)]^+$ as a Latent Source of Aminoborane: Probing the Role of Metal in the Dehydrocoupling of $H_3B\text{-}NMe_2H$ and Retrodimerisation of $[H_2BNMe_2]_2$. *Chem. Eur. J.* **2011**, *17* (10), 3011–3020.

(73) Harder, S.; Spielmann, J. Unprecedented Reactivity of an Aluminium Hydride Complex with $ArNH_2BH_3$: Nucleophilic Substitution versus Deprotonation. *Chem. Commun.* **2011**, *47*, 11945–11947.

(74) Erickson, K. A.; Wright, D. S.; Waterman, R. Dehydrocoupling of Amine Boranes via Tin(IV) and Tin(II) Catalysts. *J. Organomet. Chem.* **2014**, *751*, 541–545.

(75) Bellham, P.; Hill, M. S.; Kociok-Köhn, G. Stoichiometric and Catalytic Reactivity of Tert-Butylamine-Borane with Calcium Silylamides. *Organometallics* **2014**, *33*, 5716–5721.

(76) Stephens, F. H.; Baker, R. T.; Matus, M. H.; Grant, D. J.; Dixon, D. A. Acid Initiation of Ammonia-Borane Dehydrogenation for Hydrogen Storage. *Angew. Chem. Int. Ed.* **2007**, *46*, 746–749.

(77) Boom, D. H. A.; di Boed, E. J. J.; Nicolas, E.; Nieger, M.; W., E. A.; Jupp, A. R.; Slootweg, J. C. Catalytic Dehydrogenation of Amine-Boranes Using Geminal Phosphino-Boranes. *Z. Anorg. Allg. Chem*. 10.1002/zaac.201900313

(78) Staubitz, A.; Sloan, M. E.; Robertson, A. P. M.; Friedrich, A.; Schneider, S.; Gates, P. J.; Manners, I.; Schmedt auf der Günne, J. Catalytic Dehydrocoupling/Dehydrogenation of N-Methylamine-Borane and Ammonia-Borane: Synthesis and Characterization of High Molecular Weight Polyaminoboranes. *J. Am. Chem. Soc.* **2010**, *132*, 13332–13345.

(79) Staubitz, A.; Soto, A. P.; Manners, I. Iridium-Catalyzed Dehydrocoupling of Primary Amine-Borane Adducts: A Route to High Molecular Weight Polyaminoboranes, Boron-Nitrogen Analogues of Polyolefins. *Angew. Chem. Int. Ed.* **2008**, *47*, 6212–6215.

(80) Jurca, T.; Dellermann, T.; Stubbs, N. E.; Resendiz-Lara, D. A.; Whittell, G. R.; Manners, I. Step-Growth Titanium-Catalysed Dehydropolymerisation of Amine-Boranes. *Chem. Sci.* **2018**, *9*, 3360–3366.

(81) Lapierre, E. A.; Patrick, B. O.; Manners, I. Trivalent Titanocene Alkyls and Hydrides as Well-Defined, Highly Active, and Broad Scope Pre-Catalysts for Dehydropolymerization of Amine-Boranes. *J. Am. Chem. Soc.* **2019**, *141*, 20009–200015.

(82) Vance, J. R.; Robertson, A. P. M.; Lee, K.; Manners, I. Photoactivated, Iron-Catalyzed Dehydrocoupling of Amine-Borane Adducts: Formation of Boron-Nitrogen Oligomers and Polymers. *Chem. Eur. J.* **2011**, *17*, 4099–4103.

(83) Anke, F.; Han, D.; Klahn, M.; Spannenberg, A.; Beweries, T. Formation of High-Molecular Weight Polyaminoborane by Fe Hydride Catalysed Dehydrocoupling of Methylamine Borane. *Dalton Trans.* **2017**, *46*, 6843–6847.

(84) Coles, N. T.; Webster, R. L. Iron Catalyzed Dehydrocoupling of Amine- and Phosphine-Boranes. *Isr. J. Chem* **2017**, *57*, 1070–1081.

(85) Boyd, T. M.; Andrea, K. A.; Baston, K.; Johnson, A.; Ryan, D. E.; Weller, A. S. A Simple Cobalt–Based Catalyst System for the Controlled Dehydropolymerisation of $H_3B{\cdot}NMeH_2$ on the Gram-Scale. *Chem. Commun.* **2019**, *56*, 482–485.

(86) Trose, M.; Reiß, M.; Reiß, F.; Anke, F.; Spannenberg, A.; Boye, S.; Lederer, A.; Arndt, P.; Beweries, T. Dehydropolymerisation of Methylamine Borane Using a Dinuclear 1,3-Allenediyl Bridged Zirconocene Complex. *Dalton Trans.* **2018**, *47*, 12858–12862.

(87) Dallanegra, R.; Robertson, A. P. M. M.; Chaplin, A. B.; Manners, I.; Weller, A. S. Tuning the $[L_2Rh{\cdots}H_3B{\cdot}NR_3]^+$ interaction Using Phosphine Bite Angle. Demonstration by the Catalytic Formation of Polyaminoboranes. *Chem. Commun.* **2011**, *47*, 3763–3765.

(88) Adams, G. M.; Ryan, D. E.; Beattie, N. A.; Mckay, A. I.; Lloyd-Jones, G. C.; Weller, A. S. Dehydropolymerization of $H_3B{\cdot}NMeH_2$ Using a $[Rh(DPEphos]^+$ Catalyst: The Promoting Effect of $NMeH_2$. *ACS Catal.* **2019**, *9*, 3657–3666.

(89) Adams, G. M.; Colebatch, A. L.; Skornia, J. T.; Mckay, A. I.; Johnson, H. C.; Jones, G. C. L.; Macgregor, S. A.; Beattie, N. A.; Weller, A. S. Dehydropolymerization of $H_3B{\cdot}NMeH_2$ To Form Polyaminoboranes Using [Rh(Xantphos-Alkyl)] Catalysts. *J. Am. Chem. Soc.* **2018**, *140*, 1481–1495.

(90) Johnson, H. C.; Robertson, A. P. M.; Chaplin, A. B.; Sewell, L. J.; Thompson, A. L.; Haddow, M. F.; Manners, I.; Weller, A. S. Catching the First Oligomerization Event in the Catalytic Formation of Polyaminoboranes: $H_3BNMeHBH_2NMeH_2$ Bound to Iridium. *J. Am. Chem. Soc.* **2011**, *133*, 11076–11079.

(91) Metters, O. J.; Chapman, A. M.; Robertson, A. P. M.; Woodall, C. H.; Gates, P. J.; Wass, D. F.; Manners, I. Generation of Aminoborane Monomers $RR'N{=}BH_2$ from Amine-Boronium Cations $[RR'NH{\cdot}BH_2L]^+$: Metal Catalyst-Free Formation of Polyaminoboranes at Ambient Temperature. *Chem. Commun.* **2014**, *50*, 12146–12149.

(92) De Albuquerque Pinheiro, C. A.; Roiland, C.; Jehan, P.; Alcaraz, G.; Jéhan, P.; Alcaraz, G. Solventless and Metal-Free Synthesis of High Molecular Mass Polyaminoboranes from Diisopropylaminoborane and Primary Amines. *Angew. Chem. Int. Ed.* **2017**, *57*, 1519–1522.

(93) Helten, H.; Robertson, A. P. M. M.; Staubitz, A.; Vance, J. R.; Haddow, M. F.; Manners, I. "Spontaneous" Ambient Temperature Dehydrocoupling of Aromatic Amine-Boranes. *Chem. Eur. J.* **2012**, *18*, 4665–4680.

(94) Resendiz-Lara, D. A.; Stubbs, N. E.; Arz, M. I.; Pridmore, N. E.; Sparkes, H. A.; Manners, I. Boron-Nitrogen Main Chain Analogues of Polystyrene: Poly(B-Aryl)Aminoboranes via Catalytic Dehydrocoupling. *Chem. Commun.* **2017**, *53*, 11701–11704.

(95) De Albuquerque Pinheiro, C. A.; Roiland, C.; Jehan, P.; Alcaraz, G. Solventless and Metal-Free Synthesis of High-Molecular-Mass Polyaminoboranes from Diisopropylaminoborane and Primary Amines. *Angew. Chem. Int. Ed.* **2018**, *57*, 1519–1522.

(96) Resendiz-Lara, D. A.; Whittell, G. R.; Leitao, E. M.; Manners, I. Catalytic Synthesis, Characterization, and Properties of Polyaminoborane Homopolymers and Random Copolymers. *Macromolecules* **2019**, *52*, 7052–7064.

(97) Wideman, T.; Sneddon, L. G. Dipentylamine-Modified Polyborazylene: A New, Melt-Spinnable Polymeric Precursor to Boron Nitride Ceramic Fibers. *Chem. Mater.* **1996**, *8*, 3–5.

(98) Kim, D.; Moon, K.; Kho, J.; Economy, J.; Babonneau, F. Synthesis and Characterization of Poly-(Aminoborane) as a New Boron Nitride Precursor. *Polym. Adv. Technol.* **1999**, *10*, 702–712.

(99) Wang, X.; Hooper, T. N.; Kumar, A.; Priest, I. K.; Sheng, Y.; Samuels, T. O. M.; Wang, S.; Robertson, A. W.; Pacios, M.; Bhaskaran, H.; et al. Oligomeric Aminoborane Precursors for the Chemical Vapour Deposition Growth of Few-Layer Hexagonal Boron Nitride. *Cryst. Eng. Comm.* **2017**, *19*, 285–294.

(100) Eichler, J.; Lesniak, C. Boron Nitride (BN) and BN Composites for High-Temperature Applications. *J. Eur. Ceram. Soc* **2008**, *28*, 1105–1109.

(101) Bernard, S.; Miele, P. Polymer-Derived Boron Nitride: A Review on the Chemistry, Shaping and Ceramic Conversion of Borazine Derivatives. *Materials* **2014**, *7*, 7436–7459.

(102) Nakhmanson, S. M.; Nardelli, M. B.; Bernholc, J. Ab Initio Studies of Polarization and Piezoelectricity in Vinylidene Fluoride and BN-Based Polymers. *Phys. Rev. Lett.* **2004**, *92*, 1–4.

(103) Du, V. A.; Jurca, T.; Whittell, G. R.; Manners, I. Aluminum Borate Nanowires from the Pyrolysis of Polyaminoborane Precursors. *Dalton Trans.* **2016**, *45*, 1055–1062.

(104) Barth, R. F.; Coderre, J. A.; Vicente, M. G. H.; Blue, T. E. Boron Neutron Capture Therapy of Cancer: Current Status and Future Prospects. *Clin. Cancer. Res.* **2005**, *11*, 3987–4003.

(105) Parshall, G. W. *The Chemistry of Boron and Its Compounds*; Wiley: New York, 1967.

(106) Besson, A. C. R. *Acad. Sci. Paris* **1890**, *110*, 516.

(107) Rudolph, R. W.; Parry, R. W.; Farran, C. F. The Structure of Phosphine Borane. *Inorg. Chem.* **1966**, *5*, 723–726.

(108) Gamble, E. L.; Gilmont, P. Preparation and Properties of Diborane Diphosphine. *J. Am. Chem. Soc.* **1940**, *62*, 717–721.

(109) Hurtado, M.; Yanez, M.; Herrero, R.; Guerrero, A.; Juan, Z. D.; Jose-Luis, M. A.; Khater, B.; Guillemin, J. C. The Ever-Surprising Chemistry of Boron: Enhanced Acidity of Phosphine-Boranes. *Chem. Eur. J.* **2009**, *15*, 4622–4629.

(110) Burg, A. B.; Slota, P. J. New Approaches to the Phosphinoborine Polymers. *J. Am. Chem. Soc.* **1960**, *82*, 2145–2148.

(111) Bailey, J. A.; Pringle, P. G. Monomeric Phosphinoboranes. *Coord. Chem. Rev.* **2015**, *297–298*, 77–90.

(112) Burg, A. B.; Wagner, R. I. Chemistry of P-B Bonding: The Phosphinoborines and Their Polymers. *J. Am. Chem. Soc.* **1953**, *75*, 3872–3877.

(113) Burg, A. Phosphinoborine Polymer Rings and Chains from Tetramethylbiphosphine. *J. Inorg. Nucl. Chem.* **1959**, *2*, 258.

(114) Wagner, R. I.; Caserio, F. F. Linear Phosphinoborane Polymers. *J. Inorg. Nucl. Chem.* **1959**, *11*, 259.

(115) Korshak, V. V.; Zamyatina, V. A.; Solomatina, A. I. Izv. *Akad. Nauk. SSSR, Ser. Khim* **1964**, *8*, 1541.

(116) Dorn, H.; Singh, R. A.; Massey, J. A.; Lough, A. J.; Manners, I. Rhodium-Catalyzed Formation of Phosphorus-Boron Bonds: Synthesis of the First High Molecular Weight Poly(Phosphinoborane). *Angew. Chem. Int. Ed.* **1999**, *38*, 3321–3323.

(117) Dorn, H.; Singh, R. A.; Massey, J. A.; Nelson, J. M.; Jaska, C. A.; Lough, A. J.; Manners, I. Transition Metal-Catalyzed Formation of Phosphorus-Boron Bonds: A New Route to Phosphinoborane Rings, Chains, and Macromolecules. *J. Am. Chem. Soc.* **2000**, *122*, 6669–6678.

(118) Schäfer, A.; Jurca, T.; Turner, J.; Vance, J. R.; Lee, K.; Du, V. A.; Haddow, M. F.; Whittell, G. R.; Manners, I. Iron-Catalyzed Dehydropolymerization: A Convenient Route to Poly(Phosphinoboranes) with Molecular-Weight Control. *Angew. Chem. Int. Ed.* **2015**, *54*, 4836–4841.

(119) Paul, U. S. D.; Braunschweig, H.; Radius, U. Iridium-Catalysed Dehydrocoupling of Aryl Phosphine-Borane Adducts: Synthesis and Characterisation of High Molecular Weight Poly(Phosphinoboranes). *Chem. Commun.* **2016**, *52*, 8573–8576.

(120) Hooper, T. N.; Weller, A. S.; Beattie, N. A.; Macgregor, S. A. Dehydrocoupling of Phosphine-Boranes Using the $[RhCp^*Me(PMe_3)(CH_2Cl_2)][BAr^F{}_4]$ Precatalyst: Stoichiometric and Catalytic Studies. *Chem. Sci.* **2016**, *7*, 2414–2426.

(121) Coles, N. T.; Mahon, M. F.; Webster, R. L. Phosphine- and Amine-Borane Dehydrocoupling Using a Three-Coordinate Iron(II) β-Diketiminate Precatalyst. *Organometallics* **2017**, *36*, 2262–2268.

(122) Denis, J.-M.; Forintos, H.; Szelke, H.; Toupet, L.; Pham, T.-N.; Madec, P.-J.; Gaumont, A.-C. $B(C_6F_5)_3$-Catalyzed Formation of B–P Bonds by Dehydrocoupling of Phosphine–Boranes. *Chem. Commun.* **2003**, 54–55.

(123) Marquardt, C.; Jurca, T.; Schwan, K. C.; Stauber, A.; Virovets, A. V.; Whittell, G. R.; Manners, I.; Scheer, M. Metal-Free Addition/Head-to-Tail Polymerization of Transient Phosphinoboranes, $RPH\text{-}BH_2$: A Route to Poly(Alkylphosphinoboranes). *Angew. Chem. Int. Ed.* **2015**, *54*, 13782–13786.

(124) Schwan, K.; Scheer, M.; Timoskin, A.; Zabel, M. Lewis Base Stabilized Phosphanylborane. *Chem. Eur. J.* **2006**, *12*, 4900–4908.

(125) Turner, J. R.; Resendiz-lara, D. A.; Jurca, T.; Schäfer, A.; Vance, J. R.; Beckett, L.; Whittell, G. R.; Musgrave, R. A.; Sparkes, H. A.; Manners, I. Synthesis, Characterization, and Properties of Poly(Aryl)Phosphinoboranes Formed via Iron-Catalyzed Dehydropolymerization. *Macromol. Chem. Phys.* **2017**, *218*, 1700120.

(126) Resendiz-Lara, D. A.; Annibale, V. T.; Knights, A. W.; Chitnis, S. S.; Manners, I. High Molar Mass Poly(Alkylphosphinoboranes) via Iron-Catalyzed Dehydropolymerization. *Manuscript in Preparation*.

(127) Pandey, S.; Lönnecke, P.; Hey-Hawkins, E. Phosphorus-Boron-Based Polymers Obtained by Dehydrocoupling of Ferrocenylphosphine-Borane Adducts. *Eur. J. Inorg. Chem.* **2014**, 2456–2465.

(128) Arz, M. I.; Knights, A. W.; Manners, I. Synthesis and Post-Polymerization Functionalization of Halogen-Substituted Polyphosphinoboranes to Access Alkyne-Functionalized Derivatives. *Macromol. Rapid Commun.* **2019**, 1900468.

(129) Knights, A. W.; Chitnis, S. S.; Manners, I. Photolytic, Radical-Mediated Hydrophosphination: A Convenient Post-Polymerisation Modification Route to P-Di(Organosubstituted) Polyphosphinoboranes $[RR'PBH_2]_n$. *Chem. Sci.* **2019**, *10*, 7281–7289.

(130) Rieger, J. The Glass Transition Temperature of Polystyrene Results of a Round Robin Test. *J. Therm. Anal.* **1996**, *46*, 965–972.

(131) Clark, T. J.; Rodezno, J. M. J. M.; Clendenning, S. B.; Aouba, S.; Brodersen, P. M.; Lough, A. J.; Ruda, H. E.; Manners, I. Rhodium-Catalyzed Dehydrocoupling of Fluorinated Phosphine–Borane Adducts: Synthesis, Characterization, and Properties of Cyclic and Polymeric Phosphinoboranes with Electron-Withdrawing Substituents at Phosphorus. *Chem. Eur. J.* **2005**, *5*, 4526–4534.

(132) Dorn, H.; Rodezno, J. M.; Brunnhöfer, B.; Rivard, E.; Massey, J. A.; Manners, I. Synthesis, Characterization, and Properties of the Polyphosphinoboranes $[RPH\text{-}BH_2]_n$ (R = Ph, iBu, p-$nBuC_6H_4$, p-$DodecylC_6H_4$): Inorganic Polymers with a Phosphorus-Boron Backbone. *Macromolecules* **2003**, *36*, 291–297.

(133) Mayer-Gall, T.; Knittel, D.; Gutmann, J. S.; Opwis, K. Permanent Flame Retardant Finishing of Textiles by Allyl- Functionalized Polyphosphazenes. *ACS Appl. Mater, Interfaces* **2015**, *7*, 9349–9363.

(134) Priegert, A. M.; Siu, P. W.; Hu, T. Q.; Gates, D. P. Flammability Properties of Paper Coated with Poly(Methylenephosphine), an Organophosphorus Polymer. *Fire Mater.* **2015**, *39*, 647–657.

(135) Joseph, P.; Tretsiakova-Mcnally, S. Reactive Modifications of Some Chain- and Step-Growth Polymers with Phosphorus- Containing Compounds: Effects on Flame Retardance—a Review. *Polym. Adv. Technol.* **2011**, *22*, 395–406.

(136) Jacquemin, D. Theoretical Study of Dehydrogenation Effects upon the First Hyperpolarizability of Polyphosphinoborane. *J. Phys. Chem. A* **2004**, *108*, 500–506.

(137) Knights, A. W.; Manners, I. Unpublished Results.

(138) Colebatch, A. L.; Hawkey Gilder, B. W.; Whitell, G. R.; Oldroyd, N. L.; Manners, I.; Weller, A. S. A General, Rhodium-Catalyzed, Synthesis of Deuterated Boranes and N-Methyl Polyaminoboranes. *Chem. Eur. J.* **2018**, *24*, 5450–5455.

(139) Kumar, A.; Beattie, N. A.; Pike, S. D.; Macgregor, S. A.; Weller, A. S. The Simplest Amino-Borane $H_2B{=}NH_2$ Trapped on a Rhodium Dimer: Pre-Catalysts for Amine-Borane Dehydropolymerization. *Angew. Chem. Int. Ed.* **2016**, *55*, 6651–6656.

(140) Drover, M. W.; Bowes, E. G.; Schafer, L. L.; Love, J. A.; Weller, A. S. Phosphoramidate-Supported $Cp^*Ir(III)$ Aminoborane $H_2B{=}NR_2$ Complexes: Synthesis, Structure, and Solution Dynamics. *Chem. Eur. J.* **2016**, *22*, 6793–6797.

(141) Addy, D. A.; Bates, J. I.; Kelly, M. J.; Riddlestone, I. M.; Aldridge, S. Aminoborane σ Complexes: Significance of Hydride Co-Ligands in Dynamic Processes and Dehydrogenative Borylene Formation. *Organometallics* **2013**, *32*, 1583–1586.

(142) Pons, V.; Baker, R. T.; Szymczak, N. K.; Heldebrant, D. J.; Linehan, J. C.; Matus, M. H.; Grant, D. J.; Dixon, D. A. Coordination of Aminoborane, NH_2BH_2, Dictates Selectivity and Extent of H_2 Release in Metal-Catalysed Ammonia Borane Dehydrogenation. *Chem. Commun.* **2008**, 6597–6599.

(143) Ravve, A. *Principles of Polymer Chemistry*; Springer: New York, 2012.

(144) Hartwig, J. F. *Organotransition Metal Chemistry: From Bonding to Catalysis*; University Science Books: Sausalito, California, 2012.

(145) Johnson, H. C.; Leitao, E. M.; Whittell, G. R.; Manners, I.; Lloyd-Jones, G. C.; Weller, A. S. Mechanistic Studies of the Dehydrocoupling and Dehydropolymerization of Amine-Boranes Using a $[Rh(Xantphos)]^+$ Catalyst. *J. Am. Chem. Soc.* **2014**, *136*, 9078–9093.

(146) Kumar, A.; Johnson, H. C.; Hooper, T. N.; Weller, A. S.; Algarra, A. G.; Macgregor, S. A. Multiple Metal-Bound Oligomers from Ir-Catalysed Dehydropolymerisation of $H_3B{\cdot}NH_3$ as Probed by Experiment and Computation. *Chem. Sci.* **2014**, *5*, 2546–2553.

(147) Johnson, H. C.; Robertson, A. P. M.; Chaplin, A. B.; Sewell, L. J.; Thompson, A. L.; Haddow, M. F.; Manners, I.; Weller, A. S. Catching the First Oligomerization Event in the Catalytic Formation of Polyaminoboranes: $H_3B{\cdot}NMeHBH_2{\cdot}NMeH_2$ Bound to Iridium. *J. Am. Chem. Soc.* **2011**, *133*, 11076–11079.

(148) Bhunya, S.; Malakar, T.; Paul, A. Unfolding the Crucial Role of a Nucleophile in Ziegler-Natta Type Ir Catalyzed Polyaminoborane Formation. *Chem. Commun.* **2014**, *50*, 5919–5922.

(149) Paul, A.; Musgrave, C. B. Catalyzed Dehydrogenation of Ammonia-Borane by Iridium Dihydrogen Pincer Complex Differs from Ethane Dehydrogenation. *Angew. Chem. Int. Ed.* **2007**, *46*, 8153–8156.

(150) Adams, G. M.; Colebatch, A. L.; Skornia, J. T.; McKay, A. I.; Johnson, H. C.; Lloyd-Jones, G. C.; Macgregor, S. A.; Beattie, N. A.; Weller, A. S. Dehydropolymerization of $H_3B{\cdot}NMeH_2$ To Form Polyaminoboranes Using [Rh(Xantphos-Alkyl)] Catalysts. *J. Am. Chem. Soc.* **2018**, *140*, 1481–1495.

(151) Jaska, C. A.; Manners, I. Catalytic Dehydrocoupling of Amine-Borane and Phosphine-Borane Adducts: The Mechanism Is Heterogeneous in One Case and Homogeneous in the Other. *J. Am. Chem. Soc.* **2004**, *126*, 1334–1335.

(152) Widegren, J. A.; Finke, R. G. A Review of the Problem of Distinguishing True Homogeneous Catalysis from Soluble or Other Metal-Particle Heterogeneous Catalysis under Reducing Conditions. *J. Mol. Catal. A Chem.* **2003**, *198*, 317–341.

(153) Huertos, M. A.; Weller, A. S. Intermediates in the Rh-Catalysed Dehydrocoupling of Phosphine-Borane. *Chem. Commun.* **2012**, *48*, 7185–7187.

(154) Huertos, M. A.; Weller, A. S. Revealing the P–B Coupling Event in the Rhodium Catalysed Dehydrocoupling of Phosphine–Boranes $H_3B{\cdot}PR_2H$ (R =tBu, Ph). *Chem. Sci.* **2013**, *4*, 1881–1888.

(155) Hooper, T. N.; Huertos, M. A.; Jurca, T.; Pike, S. D.; Weller, A. S.; Manners, I. Effect of the Phosphine Steric and Electronic Profile on the Rh-Promoted Dehydrocoupling of Phosphine-Boranes. *Inorg. Chem.* **2014**, *53*, 3716–3729.

(156) Hopkinson, M. N.; Richter, C.; Schedler, M.; Glorius, F. An Overview of N-Heterocyclic Carbenes. *Nature* **2014**, *510*, 485–496.

(157) Casey, C. P. 2005 Nobel Prize in Chemistry. Development of the Olefin Metathesis Method in Organic Synthesis. *J. Chem. Educ.* **2006**, *83*, 192.

(158) Engel, T.; Reid, P. *Physical Chemistry*; Pearson: New York, 2006.

(159) Gleiter, R.; Hoffmann, R. On Stabilizing a Singlet Methylene. *Org. Biol. Chem.* **1968**, *90*, 5457–5460.

(160) Bourissou, D.; Guerret, O.; Gabbaï, F. P.; Bertrand, G. Stable Carbenes. *Chem. Rev.* **2000**, *100*, 39–91.

(161) Igau, A.; Grützmacher, H.; Baceiredo, A.; Bertrand, G. Analogous α,α'-Bis-Carbenoid Triply Bonded Species: Synthesis of a Stable λ^3-Phosphinocarbene- λ^5-Phosphaacetylene. *J. Am. Chem. Soc.* **1988**, *110*, 6463–6466.

(162) Melaimi, M.; Jazzar, R.; Soleilhavoup, M.; Bertrand, G. Cyclic (Alkyl)(Amino)Carbenes (CAACs): Recent Developments. *Angew. Chem. Int. Ed.* **2017**, *56*, 10046–10068.

(163) Hahn, F. E. Introduction: Carbene Chemistry. *Chem. Rev.* **2018**, *118* , 9455–9456.

(164) Wanzlick, H.-W. Aspects of Nucleophilic Carbene Chemistry. *Angew. Chem. Int. Ed.* **1962**, *1*, 75–80.

(165) Kline, M.; Harlow, R. L.; Arduengo, A. J. A Stable Crystalline Carbene. *J. Am. Chem. Soc.* **1991**, *113*, 361–363.

(166) Hahn, F. E. E.; Jahnke, M. C. C. Heterocyclic Carbenes: Synthesis and Coordination Chemistry. *Angew. Chem. Int. Ed.* **2008**, *47*, 3122–3172.

(167) Nelson, D. J.; Nolan, S. P. Quantifying and Understanding the Electronic Properties of N-Heterocyclic Carbenes. *Chem. Soc. Rev.* **2013**, *42*, 6723–6753.

(168) Crabtree, R. H. NHC Ligands versus Cyclopentadienyls and Phosphines as Spectator Ligands in Organometallic Catalysis. *J. Organomet. Chem.* **2005**, *690*, 5451–5457.

(169) Han, F.; Xu, Y.; Zhu, R.; Liu, G.; Chen, C.; Wang, J. Highly Active NHC–Pd(II) Complexes for Cross Coupling of Aryl Chlorides and Arylboronic Acids: An Investigation of the Effect of Remote Bulky Groups. *New J. Chem.* **2018**, *42*, 7422–7427.

(170) Kuntze-Fechner, M. W.; Kerpen, C.; Schmidt, D.; Häring, M.; Radius, U. NHC Nickel Catalyzed Hiyama- and Negishi-Type Cross-Coupling of Aryl Fluorides and Investigations on the Stability of Nickel(II) Fluoroaryl Alkyl Complexes. *Eur. J. Inorg. Chem.* **2019**, 1767–1775.

(171) Paradiso, V.; Costabile, C.; Grisi, F. Ruthenium-Based Olefin Metathesis Catalysts with Monodentate Unsymmetrical NHC Ligands. *Beilstein J. Org. Chem.* **2018**, *14*, 3122–3149.

(172) Vougioukalakis, G. C.; Grubbs, R. H. Ruthenium-Based Heterocyclic Carbene-Coordinated Olefin Metathesis. *Chem. Rev.* **2010**, *110*, 1746–1787.

(173) Wang, F.; Liu, L.; Wang, W.; Li, S.; Shi, M. Chiral NHC–metal-Based Asymmetric Catalysis. *Coord. Chem. Rev.* **2012**, *256*, 804–853.

(174) Díez-González, S.; Marion, N.; Nolan, S. P. N-Heterocyclic Carbenes in Late Transition Metal Catalysis. *Chem. Rev.* **2009**, *109*, 3612–3676.

(175) Mercs, L.; Albrecht, M. Beyond Catalysis: N-Heterocyclic Carbene Complexes as Components for Medicinal, Luminescent, and Functional Materials Applications. *Chem. Soc. Rev.* **2010**, *39*, 1903–1912.

(176) Boydston, A. J.; Williams, K. A.; Bielawski, C. W. A Modular Approach to Main-Chain Organometallic Polymers. *J. Am. Chem. Soc.* **2005**, *127*, 12496–12497.

(177) Visbal, R.; Gimeno, M. C. N-Heterocyclic Carbene Metal Complexes: Photoluminescence and Applications. *Chem. Soc. Rev.* **2014**, *43*, 3551–3574.

(178) Kuroda, Y.; Nakamura, S.; Srinivas, K.; Sathyanarayana, A.; Prabusankar, G.; Hisano, K.; Tsutsumi, O. Thermochemically Stable Liquid-Crystalline Gold(I) Complexes Showing Enhanced Room Temperature Phosphorescence. *Crystals* **2019**, *9*, 1–13.

(179) Oisaki, K.; Li, Q.; Furukawa, H.; Czaja, A. U.; Yaghi, O. M. A Metal-Organic Framework with Covalently Bound Organometallic Complexes. *J. Am. Chem. Soc.* **2010**, *132*, 9262–9264.

(180) Johnson, N. A.; Southerland, M. R.; Youngs, W. J. Recent Developments in the Medicinal Applications of Silver-NHC Complexes and Imidazolium Salts. *Molecules* **2017**, *22*, 1–20.

(181) Kuhn, N.; Al-sheikh, A. 2,3-Dihydroimidazol-2-Ylidenes and Their Main Group Element Chemistry. *Coord. Chem. Rev.* **2005**, *249*, 829–857.

(182) Martin, D.; Soleilhavoup, M.; Bertrand, G. Stable Singlet Carbenes as Mimics for Transition Metal Centers. *Chem. Sci.* **2011**, *2*, 389–399.

(183) Martin, C. D.; Soleilhavoup, M.; Bertrand, G. Carbene-Stabilized Main Group Radicals and Radical Ions. *Chem. Sci.* **2013**, *4*, 3020–3030.

(184) Kolychev, E. L.; Theuergarten, E.; Tamm, M. N-Heterocyclic Carbenes in FLP Chemistry. *Top. Curr. Chem.* **2013**, *334*, 121–155.

(185) Enders, D.; Niemeier, O.; Henseler, A. Organocatalysis by N-Heterocyclic Carbenes. *Chem. Rev.* **2007**, *107*, 5606–5655.

(186) Li, J.-L.; Liu, Y.-Q.; Zou, W.-L.; Zeng, R.; Zhang, X.; Liu, Y.; Han, B.; He, Y.; LEng, H.-J.; Li, Q.-Z. Radical Acylfluoroalkylation of Olefins through N-Heterocyclic Carbene Organocatalysis. *Angew. Chem. Int. Ed.* **2020**, *59*, 1862-1870..

(187) Fevre, M.; Pinaud, J.; Gnanou, Y.; Vignolle, J.; Taton, D. N-Heterocyclic Carbenes (NHCs) as Organocatalysts and Structural Components in Metal-Free Polymer Synthesis. *Chem. Soc. Rev.* **2013**, *42*, 2142–2172.

(188) Lohmeijer, B. G. G.; Dubois, G.; Leibfarth, F.; Pratt, R. C.; Nederberg, F.; Nelson, A.; Waymouth, R. M.; Wade, C.; Hedrick, J. L. Organocatalytic Living Ring-Opening Polymerization of Cyclic Carbosiloxanes. *Org. Lett.* **2006**, *8*, 4683–4686.

(189) Sabourin, K. J.; Malcolm, A. C.; Mcdonald, R.; Ferguson, M. J.; Rivard, E. Metal-Free Dehydrogenation of Amine–boranes by an N-Heterocyclic Carbene. *Dalton Trans.* **2013**, *42*, 4625–4632.

(190) Schneider, H.; Schmidt, D.; Radius, U. The Reductive P-P Coupling of Primary and Secondary Phosphines Mediated by N-Heterocyclic Carbenes. *Chem. Commun.* **2015**, *51*, 10138–10141.

(191) Lavallo, V.; Canac, Y.; Präsang, C.; Donnadieu, B.; Bertrand, G. Stable Cyclic (Alkyl)(Amino)Carbenes as Rigid or Flexible, Bulky, Electron-Rich Ligands for Transition-Metal Catalysts: A Quaternary Carbon Atom Makes the Difference. *Angew. Chem. Int. Ed.* **2005**, *44*, 5705–5709.

(192) Back, O.; Henry-Ellinger, M.; Martin, C. D.; Martin, D.; Bertrand, G. ^{31}P NMR Chemical Shifts of Carbene-Phosphinidene Adducts as an Indicator of the π-Accepting Properties of Carbenes. *Angew. Chem. Int. Ed.* **2013**, *52*, 2939–2943.

(193) Bertrand, G.; Soleilhavoup, M. Cyclic (Alkyl)(Amino) Carbenes (CAACs): Stable Carbenes on the Rise. *Acc. Chem. Res.* **2015**, *48*, 256–266.

(194) Jazzar, R.; Dewhurst, R. D.; Bourg, J. B.; Donnadieu, B.; Canac, Y.; Bertrand, G. Intramolecular "Hydroiminiumation" of Alkenes: Application to the Synthesis of Conjugate Acids of Cyclic Alkyl Amino Carbenes (CAACs). *Angew. Chem. Int. Ed.* **2007**, *46*, 2899–2902.

(195) Roy, S.; Mondal, K. C.; Roesky, H. W. Cyclic Alkyl(Amino) Carbene Stabilized Complexes with Low Coordinate Metals of Enduring Nature. *Acc. Chem. Res.* **2016**, *49*, 357–369.

(196) Arrowsmith, M.; Braunschweig, H.; Celik, M. A.; Dellermann, T.; Dewhurst, R. D.; Ewing, W. C.; Hammond, K.; Kramer, T.; Krummenacher, I.; Mies, J.; et al. Neutral Zero-Valent s-Block Complexes with Strong Multiple Bonding. *Nat. Chem.* **2016**, *8*, 890–894.

(197) Kundu, S.; Sinhababu, S.; Chandrasekhar, V.; Roesky, H. W.; Kundu, S.; Sinhababu, S.; Chandrasekhar, V. Stable Cyclic (Alkyl)(Amino)Carbene (CAAC) Radicals with Main Group Substituents. *Chem. Sci.* **2019**, *10*, 4727–4741.

(198) Ghadwal, R. S.; Roesky, H. W.; Merkel, S.; Henn, J.; Stalke, D. Lewis Base Stabilized Dichlorosilylene. *Angew. Chem. Int. Ed.* **2009**, *48*, 5683–5686.

(199) Mondal, K. C.; Roesky, H. W.; Schwarzer, M. C.; Frenking, G.; Tkach, I.; Wolf, H.; Kratzert, D.; Herbst-Irmer, R.; Niepötter, B.; Stalke, D. Conversion of a Singlet Silylene to a Stable Biradical. *Angew. Chem. Int. Ed.* **2013**, *52*, 1801–1805.

(200) Lavallo, V.; Canac, Y.; Donnadieu, B.; Schoeller, W. W.; Bertrand, G. CO Fixation to Stable Acyclic and Cyclic Alkyl Amino Carbenes: Stable Amino Ketenes with a Small HOMO-LUMO Gap. *Angew. Chem. Int. Ed.* **2006**, *45*, 3488–3491.

(201) Frey, G. D.; Lavallo, V.; Donnadieu, B.; Schoeller, W. W.; Bertrand, G. Facile Splitting of Hydrogen and Ammonia by Nucleophilic Activation at a Single Carbon Center. *Science* **2007**, *316*, 439–441.

(202) Masuda, J. D.; Schoeller, W. W.; Donnadieu, B.; Bertrand, G. Carbene Activation of P_4 and Subsequent Derivatization. *Angew. Chem. Int. Ed.* **2007**, *46*, 7052–7055.

(203) Frey, G. D.; Masuda, J. D.; Donnadieu, B.; Bertrand, G. Activation of Si-H, B-H, and P-H Bonds at a Single Nonmetal Center. *Angew. Chem. Int. Ed.* **2010**, *49*, 9444–9447.

(204) Turner, Z. R. Chemically Non-Innocent Cyclic (Alkyl)(Amino) Carbenes: Ligand Rearrangement, C-H and C-F Bond Activation. *Chem. Eur. J.* **2016**, *22*, 11461–11468.

(205) Li, Y.; Mondal, K. C.; Roesky, H. W.; Zhu, H.; Stollberg, P.; Herbst-Irmer, R.; Stalke, D.; Andrada, D. M.; Chandra Mondal, K.; Roesky, H. W.; et al. Acyclic Germylones: Congeners of Allenes with a Central Germanium Atom. *J. Am. Chem. Soc.* **2013**, *135*, 12422–12428.

(206) Chemistry, M.; Eichhorn, A. F.; Fuchs, S.; Flock, M.; Marder, T. B.; Radius, U. Reversible Oxidative Addition at Carbon. *Angew. Chem. Int. Ed.* **2017**, *56*, 10209 –10213.

Chapter 2
Metal-free dehydropolymerisation of phosphine-boranes using cyclic (alkyl)(amino)carbenes as hydrogen acceptors

2.1 Abstract

The divalent carbene carbon centre in cyclic (alkyl)(amino)carbenes (CAACs) is known to exhibit transition-metal like insertion into E–H σ-bonds (E = H, N, Si, B, P, C, O) with formation of new, strong C–E and C–H bonds. Although subsequent transformations of the products represent an attractive strategy for metal-free synthesis, few examples have been reported. Herein we describe the dehydrogenation of phosphine-boranes, RR'PH·BH_3, using a CAAC, which behaves as a stoichiometric hydrogen acceptor to release monomeric phosphinoboranes, [RR'P–BH_2], under mild conditions. The latter species are transient intermediates that either polymerise to the corresponding polyphosphinoboranes, [RR'P–BH_2]$_n$ (R = Ph; R' = H, Ph or Et), or are trapped in the form of CAAC-phosphinoborane adducts, CAAC·H_2BPRR' (R = R' = *t*Bu; R = R' = Mes). In contrast to previously established methods such as transition-metal catalysed dehydrocoupling, which only yield P-monosubstituted polymers, [RHP–BH_2]$_n$, the CAAC-mediated route also provides access to P-disubstituted polymers, [RR'P–BH_2]$_n$ (R = Ph; R' = Ph or Et).

2.2 Introduction

Polymers that feature *p*-block elements other than carbon in the main chain are interesting materials due to their potential uses as elastomers, etch-resists in lithography, polyelectrolytes, ceramic precursors and in optoelectronics.[1–4] Earlier syntheses of inorganic polymers were achieved by the use of polycondensation and ring-opening methods.[1,2,5] Access to stable yet reactive, polymerisable, multiply bonded *p*-block monomers required for addition polymerisation remains a major challenge in the synthesis of inorganic polymers.[6–8] More recently metal-catalysed coupling routes have been developed for accessing a broad range of inorganic macromolecules and materials.[2,9–14] In this context catalytic

dehydrocoupling between main group substrates has been shown to be a versatile method for the general formation of E–E' bonds, which can be also used to access polymers via catalytic dehydropolymerisation.[15–20]

Polyphosphinoboranes attracted initial interest in the 1950s as a result of their potential as flame-retardant materials with high thermal stability.[21–23] Attempts to dehydrocouple phosphine-borane adducts under thermal conditions yielded either low molecular weight or poorly soluble materials which lacked convincing structural characterisation by modern standards.[2,24,25] Since 1999 a rhodium-catalysed dehydrocoupling approach to prepare soluble, high molar mass (P-monosubstituted)polyphosphinoboranes has been available.[26–28] Examples of iron and iridium-catalysed dehydrocouplings have also been reported as routes to high molar mass poly(arylphosphinoboranes) (Scheme 2.1a).[29,30] Notably, these transition metal-catalysed protocols all require forcing conditions (≥ 100 °C, ≥ 20 h) and their scope is currently limited to the dehydrocoupling of primary arylphosphine-boranes, $RPH_2{\cdot}BH_3$ (R = aryl). More recently, from our collaboration with Scheer and co-workers a metal-free synthesis of polyphosphinoboranes through the thermolysis of amine-stabilised phosphinoboranes, $RR'PBH_2{\cdot}NMe_3$ was reported to proceed under milder conditions 22 - 40 °C.[31,32] This route successfully produced high molecular weight poly(*tert*-butylphosphinoborane), $[t\text{BuHP–BH}_2]_n$, presumably via the monomeric phosphinoborane [*t*BuHP–BH_2], but the precursors are challenging to prepare and attempts to access the P-disubstituted poly(diphenylphosphinoborane), $[Ph_2P–BH_2]_n$, by the thermolysis of $Ph_2PBH_2{\cdot}NMe_3$, yielded only very low molecular weight oligomers $[Ph_2P–BH_2]_x$ ($x \leq 6$) (Scheme 2.1b). The development of convenient and efficient dehydrocoupling of secondary phosphine-borane adducts to give the corresponding polymers therefore remains an open challenge. Herein we demonstrate the successful use of the carbene centres of cyclic (alkyl)(amino)carbenes (CAACs) to mediate this process.

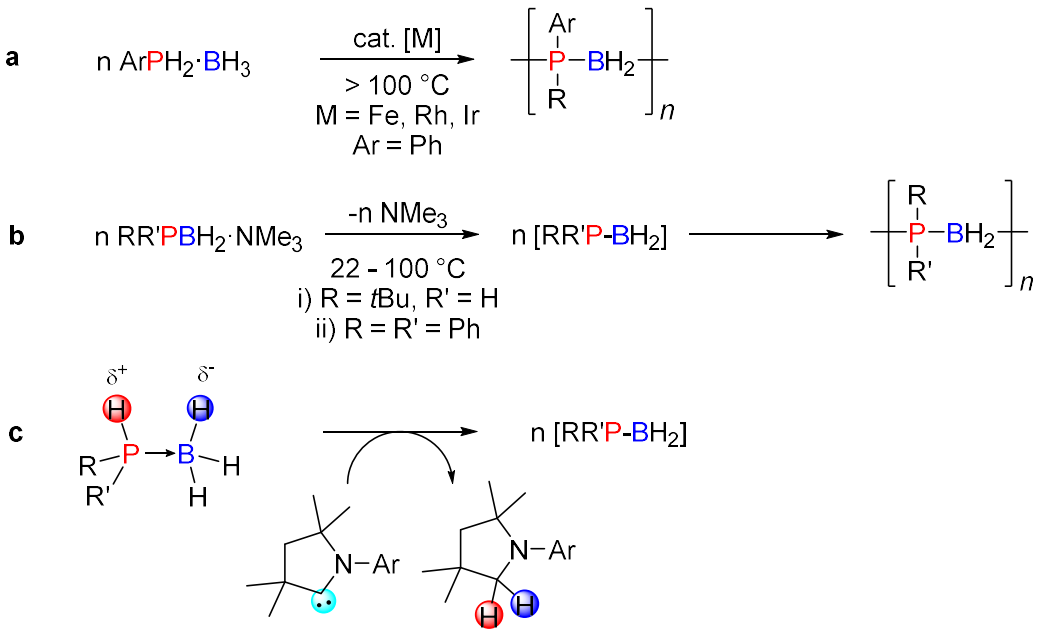

Scheme 2.1 a and **b** Current methods of synthesising polyphosphinoboranes; and **c** proposed CAAC-mediated dehydrogenation.

Cyclic (alkyl)(amino)carbenes (CAACs) are analogues of N-heterocyclic carbenes (NHCs) with one of the electronegative amino substituents replaced by a strong σ-donating alkyl group, which simultaneously increases the nucleophilicity and electrophilicity at the divalent carbene carbon centre.[33–36] The resulting small HOMO–LUMO gap of CAACs has allowed E–H (E = H, N, Si, B, P, C, O) bond activation by formal oxidative-addition to the carbene carbon centre for a variety of small molecules under mild conditions, with this process giving products featuring a H–C(sp^3)–E moiety;[37–42] however, the strength of the resulting C(sp^3)–H and C(sp^3)–E σ–bonds disfavours further reactivity of the H–C(sp^3)–E products, limiting the ability of CAACs to mimic transition metal centres in synthetic utility.

We envisioned that a CAAC-mediated dehydrogenation of primary and secondary phosphine-boranes, species that contain both protic P–H and hydridic B–H bonds, may be possible (Scheme 2.1c). Dehydrogenation of phosphine-boranes using this strategy leads to reactive phosphinoborane monomers which, given appropriate substituents at the phosphorus and boron centres, gives soluble oligomeric and polymeric material.

2.3 Results and Discussion

2.3.1 Reactivity of IDipp with $PhPH_2{\cdot}BH_3$ and $Ph_2PH{\cdot}BH_3$

The synthesis of monomeric aminoborane-NHC adducts (NHC-BH_2NHR) has been reported both through the use of an NHC for ambient temperature dehydrogenation of amine-boranes ($RNH_2{\cdot}BH_3$ R = H, Me)[43] and NHC-induced depolymerisation of poly(N-methylaminoborane).[44] More recently analogous species featuring the use of NHCs to stabilise phosphinoborane monomers have been isolated using NHC-induced thermal depolymerisation of polyphosphinoboranes.[45] Consequently, prior to investigating the reactivity of phosphine-boranes with CAACs, we explored the dehydrogenation potential of NHCs.

Upon addition of one equivalent of IDipp (IDipp = 1,3-bis(2,6-diisopropylphenyl)-1,3-dihydro-2*H*-imidazol-2-ylidene) to a solution of $PhPH_2{\cdot}BH_3$ in THF a homogeneous solution was formed after 10 min and analysis of the reaction mixture by ^{31}P and ^{11}B NMR spectroscopy showed complete conversion to a new species (δ_P = -84.2 ppm (br), δ_B = -33.4 ppm (dq) in THF) (Figure S2.2 and Figure S2.3). The similarity of these spectral features to those observed for $Li[PhPHBH_3]$ (δ_P = -93.8 ppm (d), δ_B = -34.6 ppm (dq) in THF),[46] an analogous compound with a different cation, is consistent with deprotonation of $PhPH_2{\cdot}BH_3$ by IDipp to yield the salt $[IDippH][PhPHBH_3]$ (**2.1a**) (Scheme 2.2a). The formation of this salt was further confirmed by an independent synthesis via a metathesis reaction in THF between [IDippH]Cl and $Li[PhHPBH_3]$. This showed ^{11}B and ^{31}P NMR spectral features that matched those assigned to **2.1a** along with precipitation of LiCl (Scheme 2.2b). The ^{13}C NMR spectrum of **2.1a** showed no $^1J_{CP}$ couplings involving the iminium carbon atom, which, together with the downfield chemical shift in the ^1H NMR spectrum of the imidazolium proton (δ_H = 10.0 ppm) (Figure S2.1), supports an ionic formulation for this species in solution. When $Ph_2PH{\cdot}BH_3$ was reacted with IDipp the analogous salt $[IDippH][Ph_2PBH_3]$ (**2.1b**) was formed and subsequently characterised using X-ray crystallography (Figure 2.1).

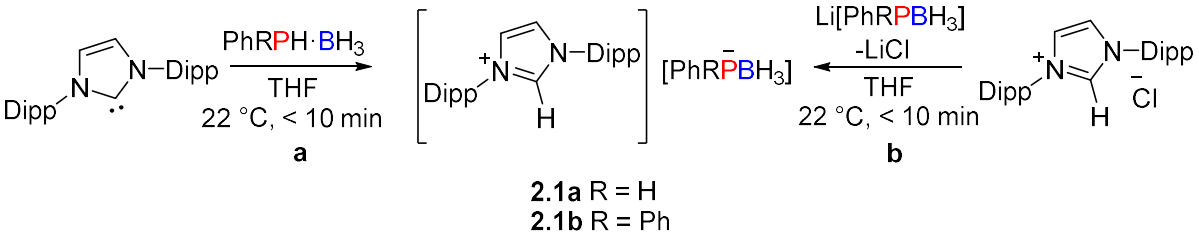

Scheme 2.2 a Synthesis of **2.1a** and **2.1b** by deprotonation of the phosphine-borane using IDipp; and **b** synthesis of **2.1a** and **2.1b** using salt metathesis route.

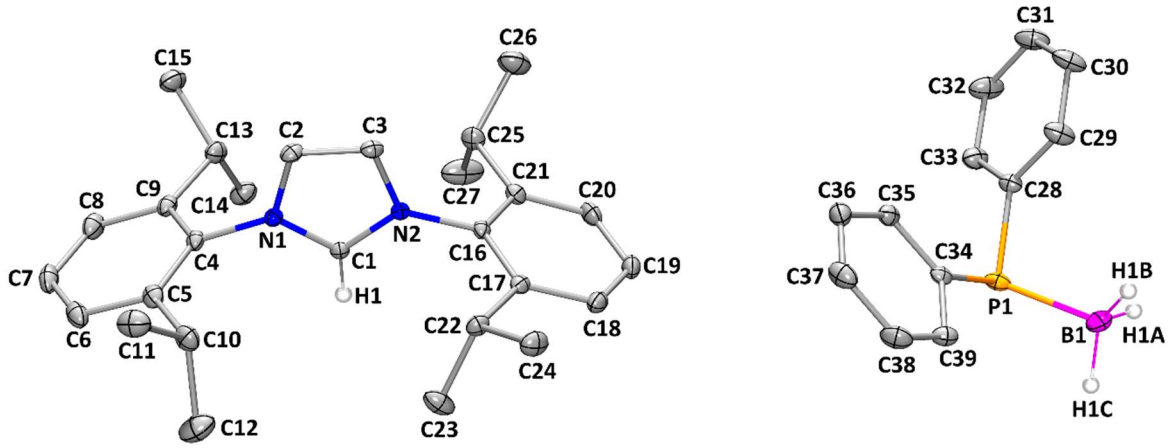

Figure 2.1 Thermal ellipsoid plot of **2.1b**. Ellipsoids are shown at the 30% probability level. Second molecule of **2.1b** and THF solvent molecules from the asymmetric unit, along with H atoms other than those bound to C1 and B1 have been omitted for clarity.

2.3.2 Reactivity of CAAC^{Me} with PhPH$_2$·BH$_3$

Next, we attempted the analogous reaction with a CAAC as the smaller HOMO-LUMO separation of CAACs renders them potentially better candidates for E–H bond activations. The P–H activation of PhPH$_2$·BH$_3$ by one equiv. of CAAC^{Me} (Scheme 2.3a) occurred readily at 22 °C in THF to give **2.3a,** which exists as two diastereomers (**2.3a'** and **2.3a''**). The identity of **2.3a** was initially established based on a distinctive doublet of quartet of doublets coupling pattern observed in the ^{1}H NMR spectrum for the P–H protons (Figure S2.7). This assignment was further corroborated by an independent synthesis via a stepwise procedure involving oxidative-addition of PhPH$_2$ to the carbene centre in CAAC^{Me} to yield **2.2a** (as a mixture of diastereomers each with indistinguishable enantiomers by NMR spectroscopy), followed by addition of BH$_3$·THF to give **2.3a** (Scheme 2.3b). The two diastereomers of **2.3a** were also formed immediately upon combining Li[PhPHBH$_3$] and [CAAC^{Me}H]Cl through elimination of LiCl (Scheme 2.3c). In contrast to the results obtained in the reaction of [IDippH]Cl and Li[PhPHBH$_3$] above (Scheme 2.2b), the lower steric hindrance and greater π-acidity[36] of the cation [CAAC^{Me}H]$^{+}$ leads to the formation of a molecular species with a distinct P–C bond, rather than the corresponding iminium salt [CAAC^{Me}H][PhPHBH$_3$]. The molecular formulation of **2.3a** is supported by the observation of both $^{1}J_{CP}$ ($^{1}J_{CP}$ = 41.0 Hz (**2.3a'**), $^{1}J_{CP}$ = 38.3 Hz (**2.3a''**)) and $^{2}J_{HP}$ ($^{2}J_{HP}$ = 4.2 Hz (**2.3a'**), $^{2}J_{HP}$ = 5.8 Hz (**2.3a''**)) coupling constants in the ^{13}C and ^{1}H NMR spectra.

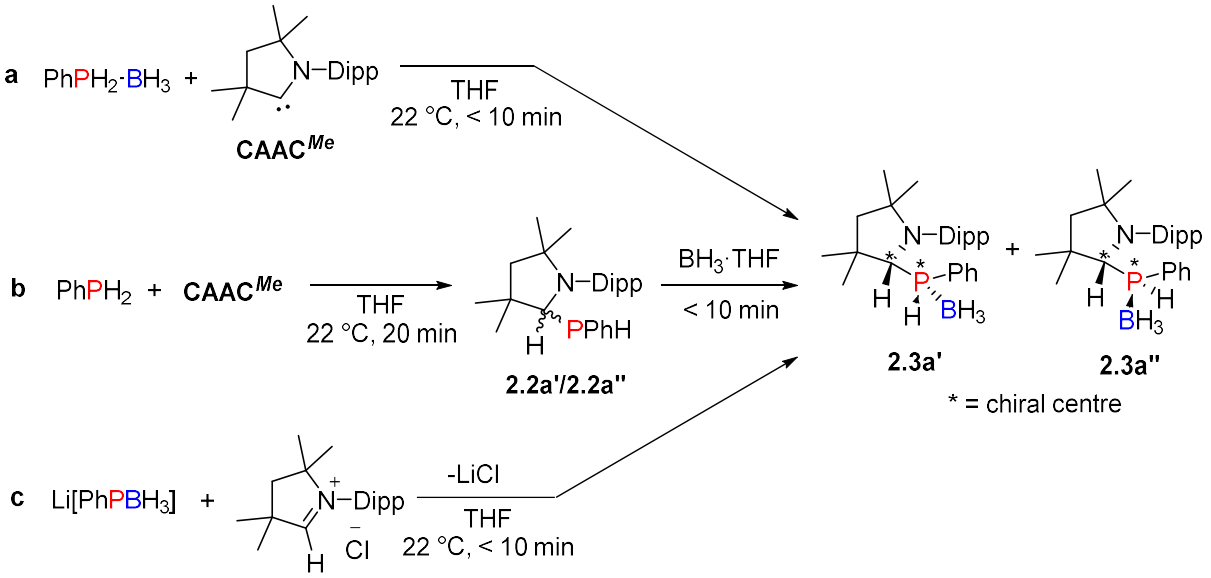

Scheme 2.3 a Synthesis of **2.3a** through oxidative-addition of $PhPH_2{\cdot}BH_3$; **b** synthesis of **2.3a** through stepwise reaction of $PhPH_2$ then $BH_3{\cdot}THF$; and **c** synthesis of **2.3a** through salt metathesis route.

Attempts to crystallographically characterise **2.3a** were unsuccessful as solutions in THF (0.10 M) spontaneously decomposed to a mixture of poly(phenylphosphinoborane) $[PhHP–BH_2]_n$ and $(CAAC^{Me})H_2$ as shown by ^{1}H, ^{11}B and ^{31}P NMR spectroscopy. Although only sensitive to low molar mass fractions,[47] ESI-MS confirmed the formation of $[PhHP–BH_2]_n$ (up to n = 22) by identifying repeat units of $\Delta(m/z)$ = 122 (molecular weight of $PhHP–BH_2$ = 122.1). Isolation of pure $[PhHP–BH_2]_n$ was achieved through precipitation of the reaction mixture into cold (−40 °C) hexanes to remove the hydrogenated carbene, $(CAAC^{Me})H_2$, which was also characterised by X-ray crystallography (Figure S2.26). In the present case, the eliminated phosphinoborane monomer $[PhHP–BH_2]$ polymerises, presumably due to the small size of the substituents at P and B.

The influence of temperature, solvent and concentration upon the molar mass of the poly(phenylphosphinoborane) obtained was systematically investigated with a view of optimising the polymerisation conditions (Table 2.1) In each case ESI-MS and GPC analyses were carried out. ESI-MS clearly confirmed the presence of the $[PhHP–BH_2]$ monomeric repeat unit in each case and allowed us to detect the presence of either BH_3 or $PPhH_2$ end groups (Figure S2.21); however, due to only the low molar mass fraction being detected by the method, it is not possible to draw links between the reaction conditions and the degree of polymerisation using this data.[47] In contrast GPC analysis permitted optimisation of the polymerisation conditions as this technique reveals the complete molar mass distribution. Increasing the temperature (run 1 vs 3, and 5 vs 6) reduced the reaction time, but has no

significant effect on the molar mass of the polymer obtained. Using a non-polar solvent (toluene) rather than THF (runs 3 vs 5) also had no significant effect on the polymer molar mass. It was found that at higher concentrations (run 2 vs 3 vs 4) a larger quantity of polymeric relative to oligomeric material was formed (Figure S2.16). This observation is consistent with head-to-tail polymerisation of transiently generated phenylphosphinoborane, [PhHP–BH_2]. The reaction was also attempted under solvent-free, melt conditions at 110 °C (run 7) and, although high molar mass material was formed, the molar mass was no greater than that obtained using a concentrated solution at 60 °C. Due to concerns about the homogeneity of the reaction as a result of poor mixing, subsequent studies were performed in concentrated solutions rather than in the melt phase.

Table 2.1 Influence of temperature, solvent and concentration on the formation of polyphenylphosphinoborane, [PhHP–BH_2]$_n$, in a closed system

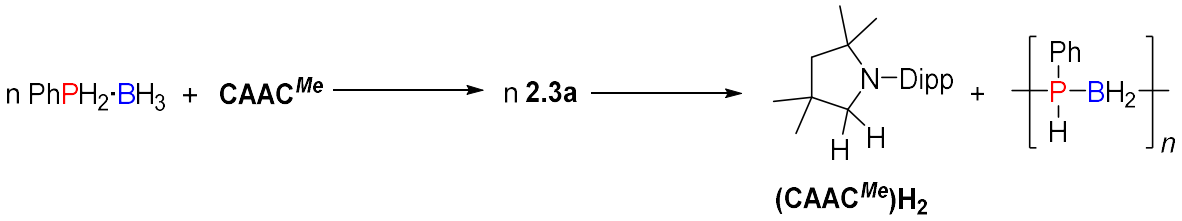

Run	Temp. (°C)	Solvent	Conc. (M)	Time (h)[a]	DP[b]	M_n (Da)[c]	PDI[c]
1	22	THF	0.50	120	205	25,000	1.55
2	60	THF	0.10	3	[d]	[d]	[d]
3	60	THF	0.50	3	410	50,100	1.27
4	60	THF	1.26	3	686	83,800	1.13
5	60	toluene	0.50	3	290	35,400	1.28
6	110	toluene	0.50	0.5	230	28,000	1.52
7	110	none	n/a	3	302	36,800	1.39

[a]Time taken for full conversion by ^{31}P NMR spectroscopy [b]degree of polymerisation measured by GPC [c]measured using GPC analysis [d]no high molecular weight material recovered after precipitation.

2.3.3 Mechanistic studies into the dehydrogenation

A series of experimental and density functional theory (DFT) studies have been undertaken to probe the mechanism of the dehydrogenation of $PhPH_2{\cdot}BH_3$ with CAAC^{Me}. Several mechanisms for the generation of monomeric [PhHP–BH_2] were considered and subsequently discounted (Section 2.3.3.3), based on experimental and computational evidence before the final mechanism discussed below was proposed and supported. Attempts to trap the released monomer with either cyclohexene[48] or 1,3-cyclohexadiene[49] proved unsuccessful.

2.3.3.1 Kinetic studies

Kinetic studies were conducted to assess the proposed mechanisms. A plot of ln[**2.3a**] versus reaction time showed equivalent half-lives of 1.5 h (Figure S2.27) for several initial concentrations between 0.3 M and 0.7 M at 50 °C, indicating a first-order process in **2.3a**. Monitoring the reaction at several temperatures between 22 °C and 60 °C allowed the enthalpy and entropy of activation to be calculated as 21.5 kcal mol^{-1} and -9.5 cal K^{-1} mol^{-1}, respectively, consistent with a substantial energy barrier involving a relatively ordered transition state (Figure S2.29).

2.3.3.2 DFT calculations

DFT calculations were carried out at the PBE0/6-31+G(d,p)/IEFPCM(THF) level of theory[50–52] with an *N*-phenyl model system for the CAAC^{Me} (**B**) to further elucidate the dehydrogenation mechanism. Schematic illustrations of the calculated reaction pathways are depicted in Figure S2.30 and Figure S2.31 and the calculated structures and their energy eigenvalues are summarised in Table S2.3. A simplified schematic of the proposed pathway is shown in Figure 2.2.

Four initial reaction steps were considered: a) P–H activation, b) B–H activation, c) substitution at boron, and d) concerted P–H/B–H activation. Whereas pathways a), b) and c) could be modelled by the calculations, attempts to locate a concerted transition state (TS) leading to (CAAC)H_2 and [PhHP–BH_2] in one step (pathway d) were unsuccessful. The P–H activation step, which first involves deprotonation of the P–H bond by the CAAC, requires a significantly low activation barrier (**TS1**: 4.9 kcal mol^{-1}; **TS1'**: 7.6 kcal mol^{-1}) (Figure S2.30) when compared to B–H activation (**TS2**: 34.2 kcal mol^{-1}) (Figure S2.31b) and nucleophilic substitution at boron (**TS3**: 26.2 kcal mol^{-1}) (Figure S2.31a) (ΔG^0 values in THF are given). We therefore inferred that neither initial B–H activation nor nucleophilic substitution plays a role in product formation and focused on further pathways from the P–H proton transfer.

Two transition states (**TS1** and **TS1'**) were calculated for the deprotonation of $PhPH_2{\cdot}BH_3$ (**A**), which differ in the spatial orientation of the CAAC (**B**) with respect to the phosphine-borane bearing a prochiral phosphorus atom. The structures of the formed ion pairs **C-1$_{pair}$** and **C-1'$_{pair}$** were derived by reverse intrinsic reaction coordinate (IRC) calculations and subsequent optimisation of the obtained structures. Note that the spatial orientation of $[CAAC(H)]^+$ and $[PhPH(BH_3)]^-$ in **C-1'$_{pair}$** differs from the orientation in **TS1'** and is similar to that found for

C-1$_{pair}$, indicating that the relative orientation present in **C-1$_{pair}$** is favoured (see Table S2.3). In addition, attempts to structurally optimise **C-1'$_{pair}$** with toluene as solvent furnished only the P–H activation product **F'**.

Subsequent nucleophilic attack at the iminium carbon of the $[CAAC(H)]^+$ cation by the phosphorus centre of the $[PhPH(BH_3)]^-$ anion leads via **TS4** to the S_P,*S* (**F**) diastereomer of the P–H activation product, or via **TS4',** to the other R_P,*S* (**F'**) diastereomer, the latter being slightly higher in energy. Attempts to obtain structures for the contact ion pairs **C-2$_{pair}$** and **C-2'$_{pair}$** by reverse IRC calculations from **TS4** or **TS4'** and subsequent optimisation of the respective structures were unsuccessful and furnished back the P–H activation products **F** or **F'**, respectively. This is characteristic of a very flat progression of the potential energy hypersurface and suggests, in agreement with the experimentally found rapid formation of **2.3a**, that the formation of **F** and **F'** occurs with a very small activation barrier. **F** and **F'** are kinetic products of the reaction. Significantly, this step is reversible via P–C dissociation. A slightly higher activation barrier was found for the dissociation of the S_P,*S* diastereomer **F** via **TS4** (ΔG^0 = 18.7 kcal mol^{-1}, ΔH^0 = 20.2 kcal mol^{-1}) compared to the dissociation of the R_P,*S* diastereomer **F'** via **TS4'** (ΔG^0 = 16.6 kcal mol^{-1}, ΔH^0 = 19.2 kcal mol^{-1}), which is in agreement with the experimentally observed faster conversion of one diastereomer of **2.3a** and in agreement with the experimentally derived enthalpy of activation for the overall reaction (ΔH^0 = 21.5 kcal mol^{-1}). According to the calculations, the dissociation of the P–H activation products **F** or **F'** via the transition states **TS4** or **TS4'** requires the highest activation energy in the overall mechanism, which is in agreement with the first-order rate law found for **2.3a** by the kinetic measurements.

The reversible P–C dissociation opens up a second reaction pathway from the contact ion pair (**C$_{pair}$**) leading to $(CAAC)H_2$ (**G**) and $[PhHP–BH_2]$ (**H**) via B–H hydride abstraction from the $[PhPH(BH_3)]^-$ anion by the π-acidic $[CAAC(H)]^+$ cation with a low activation barrier of 5.3 kcal mol^{-1} (via **TS5**). The structure of the contact ion pair **C-3$_{pair}$** was derived from a reverse IRC calculation from **TS5** and subsequent optimisation of the obtained structure. Importantly, the dissociation of **F** or **F'** followed by B–H hydride transfer to give $[PhHP–BH_2]$ (**H**) and $(CAAC)H_2$ (**G**) requires a change in the spatial orientation of the $[CAAC(H)]^+$ (**D**) cation with respect to the $[PhPH(BH_3)]^-$ (**E**) anion, as evidenced from the different orientation found in **C-3$_{pair}$**. A comparison of the energy differences of separated $[CAAC(H)]^+$ (**D**) and $[PhPH(BH_3)]^-$ (**E**) ions and the optimised ion pairs **C-1$_{pair}$**, **C-1'$_{pair}$** or **C-3$_{pair}$** reveals maximum

energy differences of 2.1 kcal mol^{-1} in THF and 20.9 kcal mol^{-1} in toluene. This implies a considerably better stabilisation of the [CAAC(H)]$^+$ (**D**) and [PhPH(BH_3)]$^-$ (**E**) ions in THF and suggests a lower activation barrier for the change in the spatial orientation to access **C-3$_{pair}$** in THF than in toluene, providing a rationale for the experimentally observed more rapid conversion of **2.3a** into [PhHP–BH_2]$_n$ and (CAAC^{Me})H_2 in THF compared to toluene.

The six-membered heterocycle *all-cis*-(PhPHBH_2)$_3$ (**L**), containing all phenyl substituents in equatorial positions, was calculated to model the thermodynamic driving force for the polymerisation of [PhHP–BH_2] (**H**) to [PhHP–BH_2]$_n$. The calculations show that the formation of the heterocycle is favoured by 25.6 kcal mol^{-1} with respect to the [PhPH-BH_2] (**H**) monomer and the overall formation of *all-cis*-[PhHP–BH_2]$_3$ and (CAAC)H_2 (**G**) from $PhPH_2$·BH_3 (**A**) and CAAC (**B**) is favoured by 52.7 kcal mol^{-1}.

Thus, the formation of [PhHP–BH_2]$_n$ from **2.3a** can be rationalised by the formation of transient [CAAC(H)]$^+$ and [PhPH(BH_3)]$^-$ ions via consecutive P–C bond scission and B–H hydride abstraction leading to (CAAC^{Me})H_2 and [PhHP–BH_2], the latter undergoing polymerisation to thermodynamically favoured [PhHP–BH_2]$_n$. A further discussion of the proposed polymerisation mechanism is detailed in Section 2.3.5.

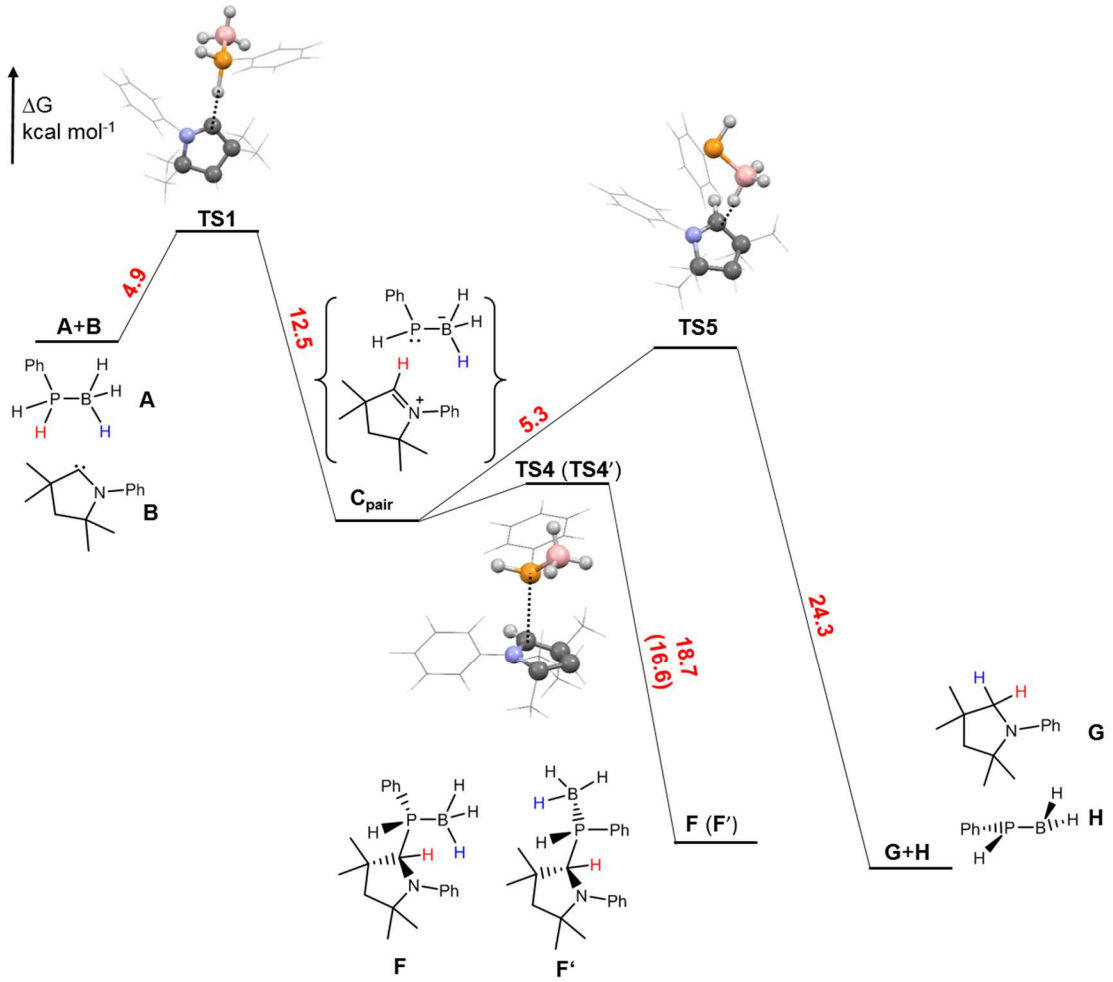

Figure 2.2 Simplified schematic reaction profile calculated for the reaction of *N*-phenyl CAAC (**A**) with $PhPH_2{\cdot}BH_3$ (**B**) at the PBE0/6-31+G(d,p)/IEFPCM(THF) level of theory; Gibbs free energies for the second diastereomer are given in round brackets. **C-1$_{pair}$**, **C-2$_{pair}$** and **C-3$_{pair}$**, which differ in the orientation of the ions, have been simplified to **C$_{pair}$** (For a comprehensive depiction of the reaction profile see Figure S2.30).

The fact that the reaction between $PhPH_2{\cdot}BH_3$ and IDipp stops at the $[IDipp(H)]^+$ and $[PhPH(BH_3)]^-$ ions (Scheme 2.2) can be traced back to the greater π-acidity of the $[CAAC(H)]^+$ compared to the analogous $[NHC(H)]^+$ cation, as suggested by the high exergonicity of the isodesmic reaction $[CAAC(H)]^+ + (NHC)H_2 \rightarrow [NHC(H)]^+ + (CAAC)H_2$ ($\Delta G^0 = -66.8$ kcal mol^{-1}; *N*-phenyl model systems) (Table S2.4).

2.3.3.3 Dehydrogenation mechanisms considered and subsequently discounted

For completeness this section describes other proposed mechanisms along with explanations of why they were discounted.

P–H activation followed by σ-bond metathesis

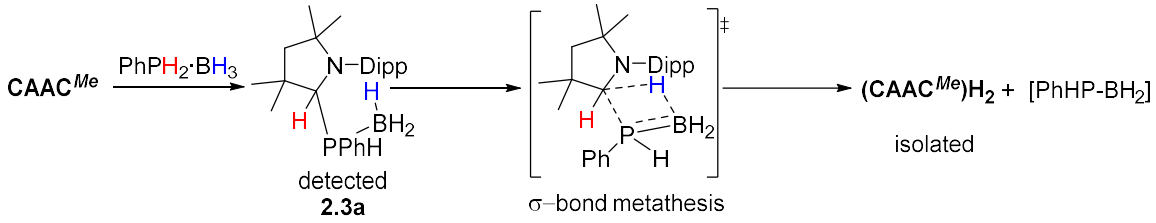

Scheme 2.4 P–H activation followed by σ-bond metathesis.

P–H activation to give **2.3a** followed by a σ-bond metathesis step, where simultaneous B–H and C–P bond cleavage occurs, releasing the reactive monomer, [PhHP–BH_2]. A similar hydride transfer mechanism has been reported previously for the conversion of an N-heterocyclic phosphinophosphine-borane to a mixture of N-heterocyclic phosphine and cyclic phosphinoboranes.[53] This mechanism was ruled out using DFT as no concerted transition state leading to (CAAC^{Me})H_2 and [PhHP–BH_2] could be located.

P–H activation followed by H_2 elimination

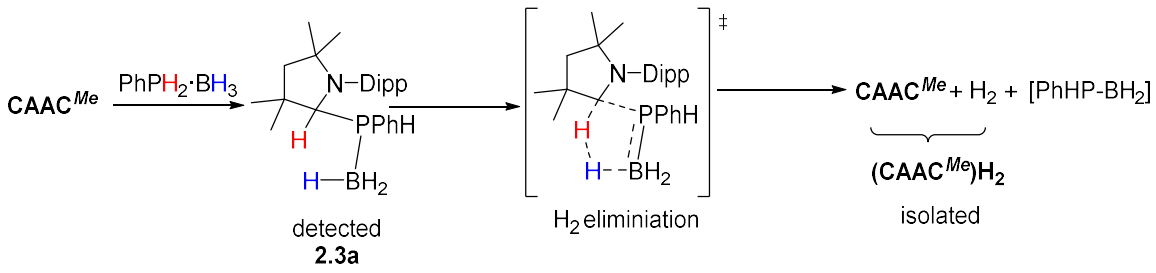

Scheme 2.5 P–H activation followed by elimination of dihydrogen.

P–H activation to give **2.3a** followed by the formation of a five-centre transition state where the B–H hydride and C–H proton combine to eliminate H_2 together with [PhHP–BH_2] and CAAC^{Me} which subsequently reacts with H_2 to give (CAAC^{Me})H_2. We were able to experimentally rule out this mechanistic proposal based on control experiments that showed CAAC^{Me} does not react with H_2 (0.2 M, 4 atm of H_2, C_6D_6, 60 °C, 24 h).

Concerted hydrogen transfer

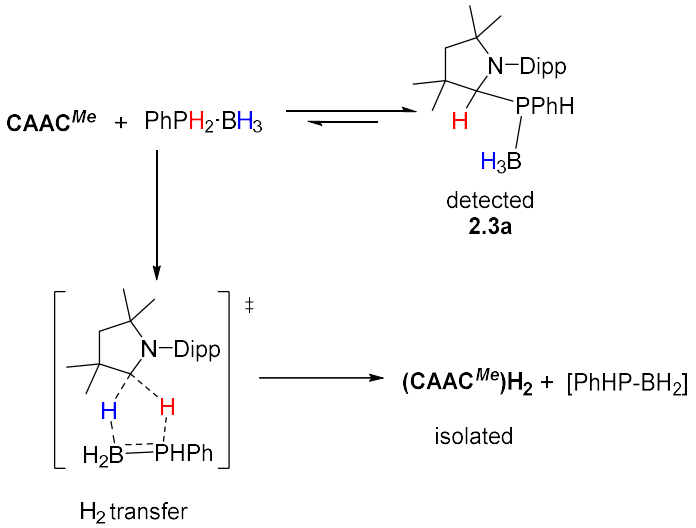

Scheme 2.6 Concerted hydrogen transfer.

The P–H activation to give **2.3a** is reversible and there is an irreversible concerted hydrogen transfer from $PhPH_2{\cdot}BH_3$ to $CAAC^{Me}$ to give $(CAAC^{Me})H_2$ and $[PhHP–BH_2]$. This mechanism was ruled out using DFT as no concerted transition state (TS) leading to $(CAAC^{Me})H_2$ and $[PhHP–BH_2]$ in one step could be located.

B–H activation followed by σ-bond metathesis

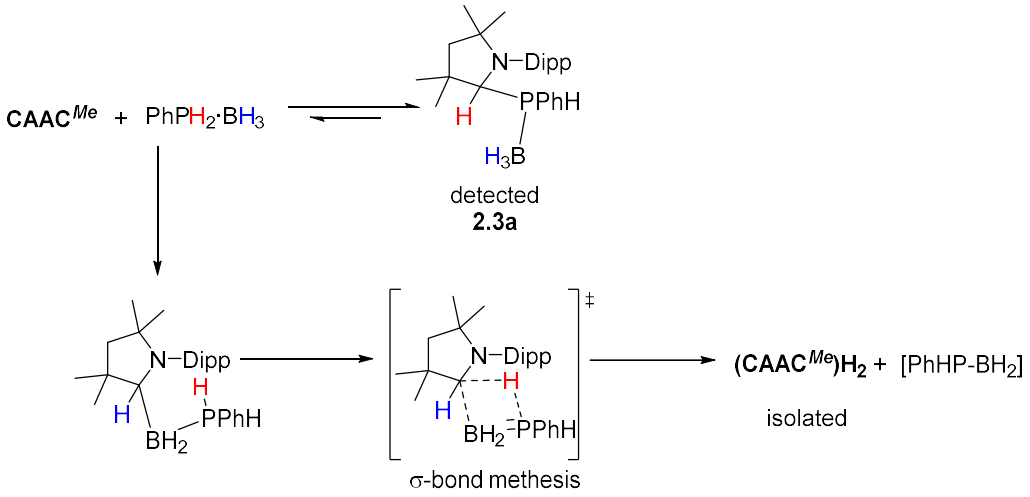

Scheme 2.7 B–H activation followed by σ-bond metathesis.

The P–H activation to give **2.3a** is reversible and the products are achieved via a B–H activation compound and undergo a σ-bond metathesis step where simultaneous P–H and C–B bond cleavage occurs. This mechanism was ruled out using DFT as the TS for the B–H activation step has a significantly higher energy barrier than for the P–H activation step (34.2 kcal mol^{-1} vs 4.9 kcal mol^{-1}) (Figure S2.31).

Homolytic cleavage of P–C bond

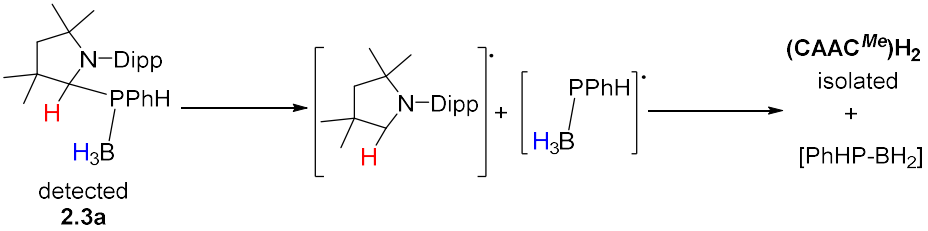

Scheme 2.8 Homolytic cleavage of P–C bond.

After **2.3a** is formed homolytic cleavage of the P–C bond occurs to give a $[CAAC^{Me}(H)]^{\bullet}$ and a $[PhPH(BH_3)]^{\bullet}$ radical. The mechanism was ruled out using DFT as the heterolytic cleavage of the P–C bond of the P–H activation product **F** (**F'**) to separated $[CAAC(H)]^{+}$ (**D**) and $[PhPH(BH_3)]^{-}$ (**E**) ions is energetically favoured compared to the homolysis to the $[CAAC(H)]^{\bullet}$ and $[PhPH(BH_3)]^{\bullet}$ radicals. This is evident from a comparison of the computed ΔG^0 and ΔH^0 values in THF, which strongly disfavour the involvement of radicals during the formation of monomeric $[PhHP–BH_2]$ (**H**).

(1) Heterolysis of **F** (**F'**): ΔH^0 = 35.3 (34.3), ΔG^0 = 20.7 (19.5) kcal mol^{-1}

(2) Homolysis of **F** (**F'**): ΔH^0 = 55.8 (54.8), ΔG^0 = 40.1 (38.9) kcal mol^{-1}

Intermolecular hydride abstraction with an iminium ion leading to a borenium ion

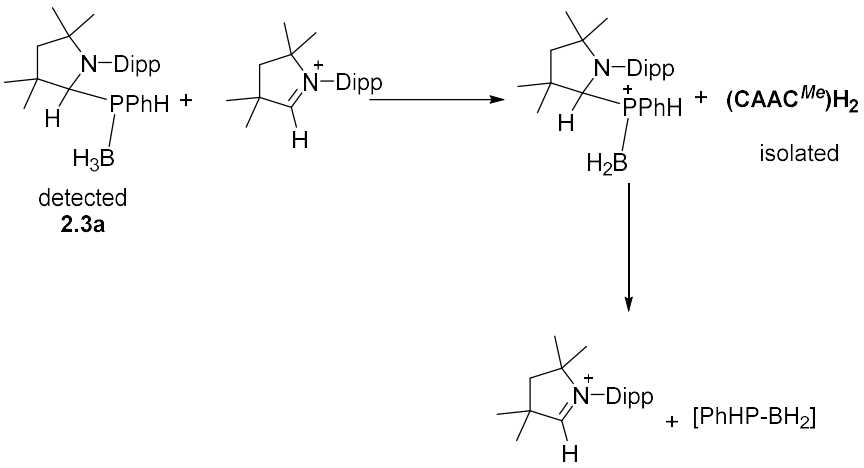

Scheme 2.9 Intermolecular hydride abstraction.

We considered an intermolecular hydride abstraction from **2.3a**, using the $[CAAC(H)]^{+}$ iminium ion, to give $(CAAC^{Me})H_2$ and a phosphinoborenium ion, which is subsequently converted to $[CAAC(H)]^{+}$ and $[PhHP–BH_2]$ via P–C bond cleavage. The intermolecular hydride abstraction pathway requires the presence of an iminium ion which is formed by P–C bond dissociation of **2.3a** as discussed above. According to DFT studies the intermolecular hydride abstraction step is energetically unlikely as the barrier for hydride abstraction from $[PhHP–BH_3]^{-}$ via **TS5**

(5.3 kcal mol^{-1}) (Figure S2.30) is considerably lower than the energy associated with the hydride abstraction from **2.3a** to give the phosphinoborenium intermediate (> 18 kcal mol^{-1}) (Figure S2.32). Experimentally it was also found that the addition of [CAAC^{Me}H]Cl did not accelerate the reaction rate.

2.3.4 Substrate Scope

2.3.4.1 Polymerisation attempts of $Ph_2PH{\cdot}BH_3$ and $PhEtPH{\cdot}BH_3$ using CAAC^{Me} and CAAC^{Cy}

Given the success with $PhPH_2{\cdot}BH_3$ the scope of the CAAC^{Me}-mediated dehydropolymerisation was extended with the aim of targeting hitherto inaccessible high molar mass P-disubstituted polyphosphinoboranes. CAAC^{Me}(H)Ph_2PBH_3 (**2.3b**) was synthesised from $Ph_2PH{\cdot}BH_3$ and CAAC^{Me} in THF (Scheme 2.10). Formation of **2.3b** was also detected immediately upon combining Li[Ph_2PBH_3] and [CAAC^{Me}H]Cl, and through the stepwise addition of Ph_2PH followed by $BH_3{\cdot}$THF to a solution of CAAC^{Me}.

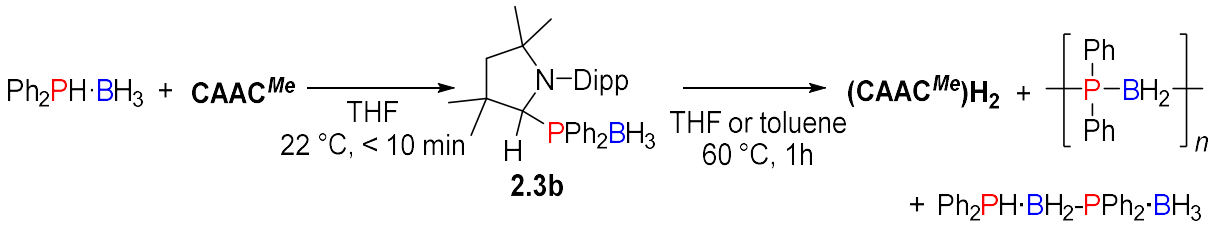

Scheme 2.10 CAAC^{Me}-mediated dehydrocoupling of $Ph_2PH{\cdot}BH_3$.

Heating a concentrated solution of **2.3b** (2.5 M, 60 °C and, 1 h, THF or toluene) effected complete conversion to (CAAC^{Me})H_2, the linear dimer $Ph_2PH{\cdot}BH_2$–$PPh_2{\cdot}BH_3$, cyclic oligomers $[Ph_2P–BH_2]_x$ (x = 3, 4), and the polymer $[Ph_2P–BH_2]_n$ as observed by ^{1}H and ^{31}P NMR spectroscopy (Scheme 2.10 and Figure 2.3a).[54] Removal of (CAAC^{Me})H_2 and cyclic oligomers was achieved by precipitation into hexanes, but attempts to separate $Ph_2PH{\cdot}BH_2$–$PPh_2{\cdot}BH_3$ and $[Ph_2P–BH_2]_n$ proved unsuccessful. Nevertheless, ESI-MS analysis of the product after precipitation confirmed the presence of the repeat unit Δ(*m*/z) = 198 (molecular weight of $Ph_2P–BH_2$ = 198.1, maximum value of n = 10) (Figure S2.35). GPC analysis, however, showed only a very small amount of high molar mass material. Interestingly when toluene, rather than THF, is used as the solvent a much smaller quantity of linear dimer is formed (Figure 2.3b). Under these conditions GPC analysis on the precipitated material showed a majority of low molar mass material (M_n = ca. 1,300 Da; *Đ*= 1.31) and a small amount (ca. 10%) of high molar mass material (M_n = 54,300 Da; *Đ* = 1.12) (Figure S2.37).

With the aim of increasing the yield and amount of high molar mass material we investigated the use of the more reactive CAAC^{Cy}, exemplified by its ability to activate dihydrogen under mild conditions.[37] The initially formed P–H activation compound is consumed within 1 h at 22°C (Scheme 2.11). Despite this GPC analysis again showed only a small amount (ca. 12%) of high molar mass material (M_n = 59,600 Da; $Đ$ = 1.08) with the majority being low molar mass material (M_n = ca. 1,100 Da; $Đ$ = 1.28) (Figure S2.38).

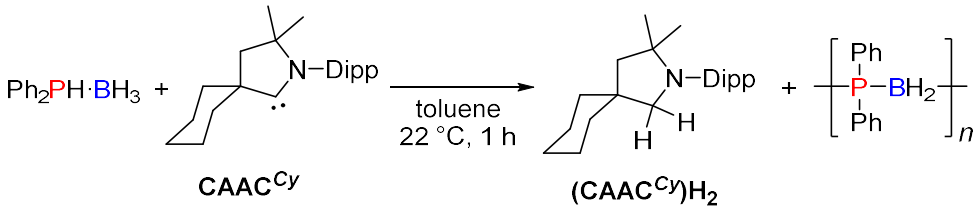

Scheme 2.11 CAAC^{Cy}-mediated dehydrocoupling of $Ph_2PH{\cdot}BH_3$.

It is postulated that three polymer architectures are formed in the head-to-tail polymerisation step of [$Ph_2P–BH_2$]: small cyclic oligomers, short chain linear oligomers and long chain linear polymers. In an attempt to explain the differences in the products formed under the different conditions (THF vs toluene, CAAC^{Me} vs CAAC^{Cy}) we compared the ^{31}P NMR spectra of the crude material and after precipitation into hexanes (Figure 2.3). For CAAC^{Me} in THF $Ph_2PH{\cdot}BH_2–PPh_2{\cdot}BH_3$ (δ_P = -3.3 ppm, -18.2 ppm [$CDCl_3$]) is detected both before and after precipitation along with a broad peak (δ_P = -15.6 ppm [$CDCl_3$]). When CAAC^{Me} is used in toluene a much smaller quantity of $Ph_2PH{\cdot}BH_2–PPh_2{\cdot}BH_3$ is observed; however, in the crude material there are two obvious broad peaks (δ_P = -15.7 ppm and -18.3 ppm [toluene]). The peak at -18.3 ppm is removed by precipitation. It is this coupled with the similarity in the shift to [$Ph_2P–BH_2$]$_{3\text{ or }4}$[54] which leads us to identify the product as small cyclic species. When using the more reactive CAAC^{Cy} only a very small amount of small cyclics are formed (δ_P = -18.3 [toluene]), postulated to be due to the greater reactivity of CAAC^{Cy} leading to a higher concentration of monomer in solution thereby favouring oligomerisation over small cyclic oligomers. This is also evidenced by the higher yield after precipitation when using CAAC^{Cy} as opposed to CAAC^{Me}. The bimodal appearance of the broad peak observed after precipitation can be explained by the presence of both oligomeric and polymeric products, as evidenced by the GPC chromatograms.

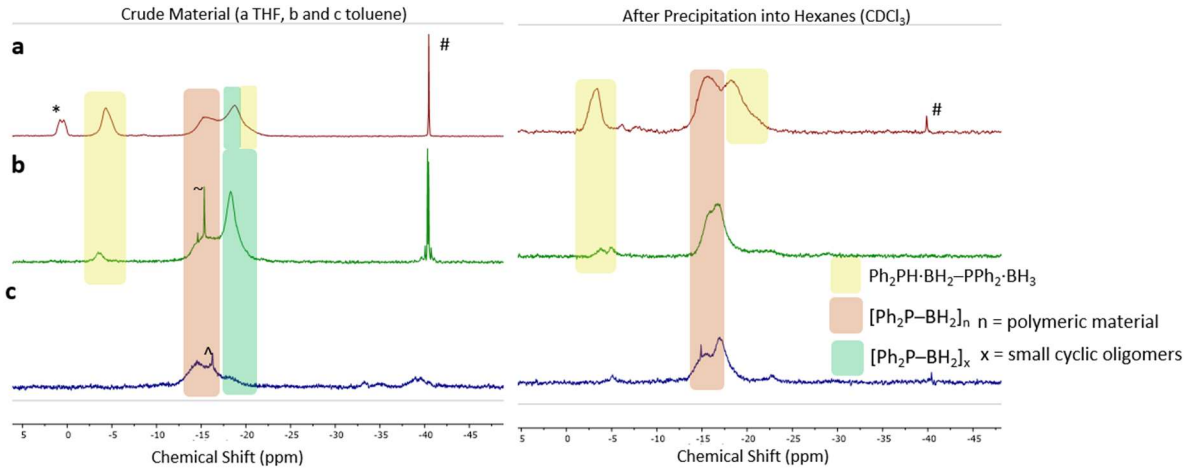

Figure 2.3 ^{31}P NMR of products of the dehydropolymerisation of $Ph_2PH{\cdot}BH_3$ using **a** $CAAC^{Me}$ in THF; **b** $CAAC^{Me}$ in toluene; and **c** $CAAC^{Cy}$ in toluene before and after precipitation into hexanes (*denotes excess $Ph_2PH{\cdot}BH_3$, ~denotes $CAAC^{Me}(H)PPH_2$, ^denotes $CAAC^{Cy}(H)PPH_2$, #denotes Ph_2PH).

In an attempt to further extend the scope of the dehydropolymerisation to other P-disubstituted phosphine-boranes the reactivity of *rac*-$Ph(Et)PH{\cdot}BH_3$ with $CAAC^{Me}$ and $CAAC^{Cy}$ was investigated. $CAAC^{Me}(H)PhEtPBH_3$ (**2.3c**) was formed through direct reaction of $CAAC^{Me}$ with *rac*-$Ph(Et)PH{\cdot}BH_3$ (Scheme 2.12a). Unlike with the mono- and di-phenyl derivatives, **2.3c** is stable at 22 °C which allowed the structure to be confirmed by X-ray diffraction (Figure 2.4).

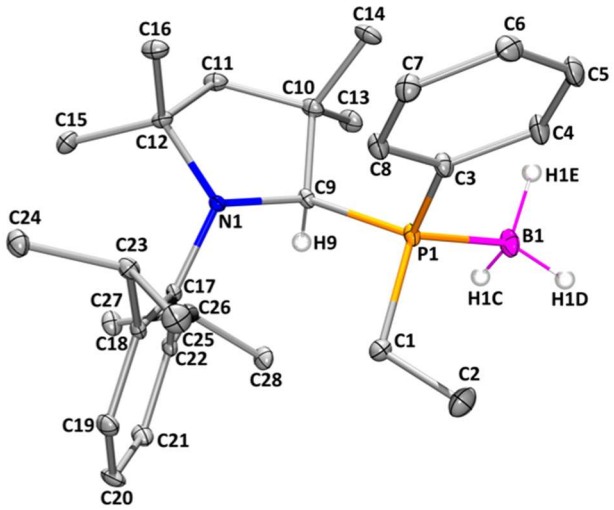

Figure 2.4 Thermal ellipsoid plot of **2.3c**. H atoms other than those bound to C9 and B1 have been omitted for clarity. Ellipsoids are shown at the 30% probability level.

Upon heating isolated **2.3c** to 100 °C the targeted dehydropolymerisation occurred to give $[PhEtP{-}BH_2]_n$ and $(CAAC^{Me})H_2$ (Scheme 2.12). Pure $[PhEtP{-}BH_2]_n$ was obtained in 23% yield as a fine white powder following precipitation. ESI-MS analysis of the precipitated sample confirmed the presence of the repeat unit of $[PhEtP{-}BH_2]_n$ ($\Delta(m/z)$ = 150, molar mass of

PhEtP–BH_2 = 150.1) and n = 33 (Figure S2.50); however, there was no convincing high molar mass material observed using GPC. In the analogous reaction using CAAC^{Cy} (Scheme 2.12b) the yield was also low (19%), but a GPC peak corresponding to high molar mass material (M_n = 62,600 Da, $Đ$ = 1.19, n = ca. 400) was observed (Figure S2.55). Again this was only a small amount (ca. 18%) compared to the low molar mass fraction (M_n = ca. 1,900 Da; $Đ$ = 1.47, n = ca. 13).

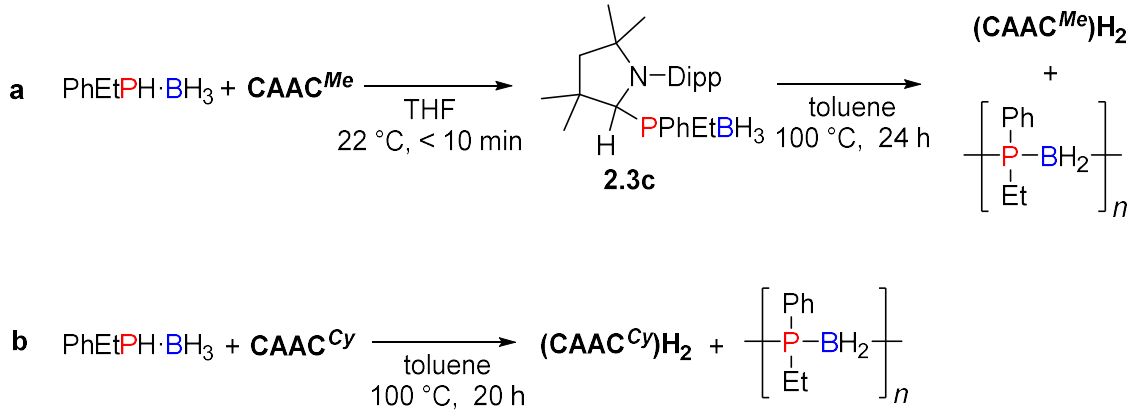

Scheme 2.12 a CAAC^{Me}-mediated dehydrocoupling of *rac*-Ph(Et)PH·BH_3; and **b** CAAC^{Cy}-mediated dehydrocoupling of *rac*-Ph(Et)PH·BH_3.

2.3.4.2 Adduct formation with bulkier P-disubstituted phosphine-boranes

When the reactivity of CAAC^{Me} with bulkier P-disubstituted phosphine-borane substrates (R = R' = *t*Bu or R = R' = Mes) was explored an enlightening divergence in reactivity was noted. For full conversion of these substrates two equiv. of CAAC^{Me} are required. *In situ* ^{1}H NMR spectroscopy reveals that an equimolar mixture of (CAAC^{Me})H_2 and the new species **2.4a**/**2.4b** are formed (Scheme 2.13).

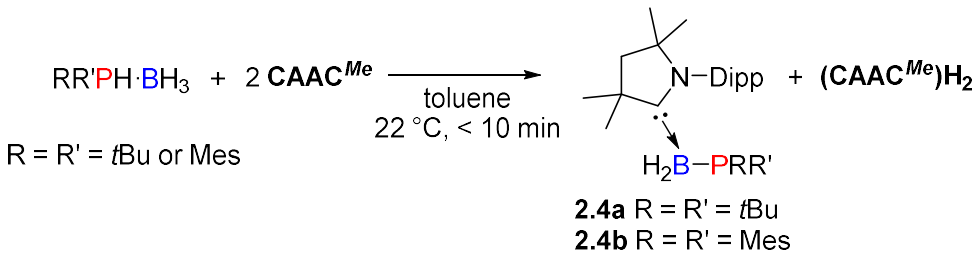

Scheme 2.13 Synthesis of **2.4a** and **2.4b**.

The structures of **2.4a** and **2.4b** were confirmed by X-ray crystallography revealing that in both compounds the CAAC^{Me} C-donor was bound to the boron of the phosphinoborane moiety (Figure 2.5a and b). Interestingly, species **2.4a** and **2.4b** are analogous to the previously mentioned NHC-phosphinoborane adducts that have been recently reported.[45]

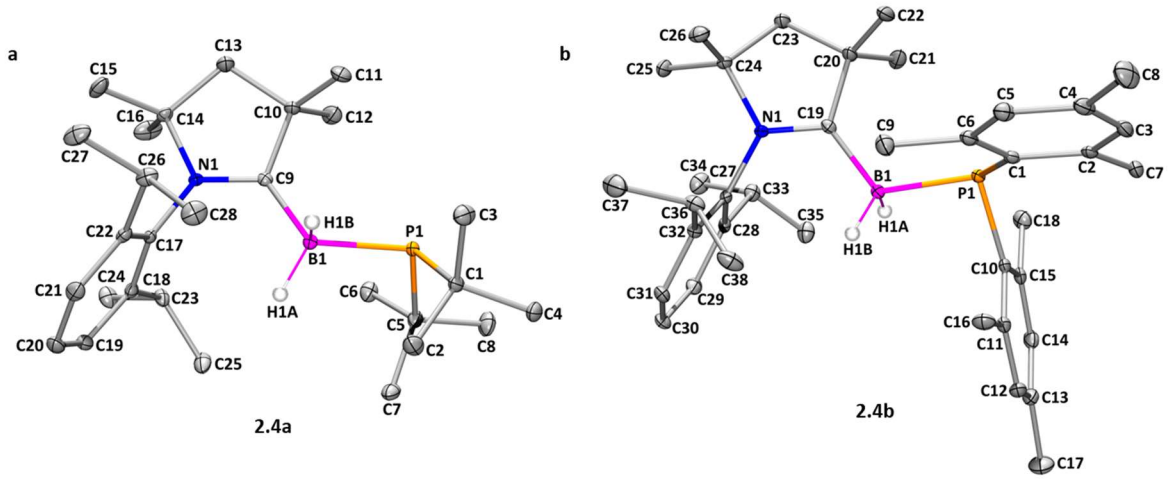

Figure 2.5 a Thermal ellipsoid plot of **2.4a**; and **b** thermal ellipsoid plot of **2.4b**. For both **4a** and **4b** ellipsoids are shown at the 30% probability level, and H atoms other than those at the B1 centre have been omitted for clarity.

The reactivity with the bulky, P-disubstituted phosphine-boranes contrasts with that observed with $PhPH_2{\cdot}BH_3$, $Ph_2PH{\cdot}BH_3$ and $PhEtPH{\cdot}BH_3$ as an initial P–H oxidative addition product analogous to compounds **2.3a-c** is not observed. The monomeric phosphinoborane generated upon dehydrogenation does not undergo head-to-tail polymerisation, instead it is trapped by a second equivalent of carbene. The absence of an observable P–H activation compound can be explained by the greater steric bulk around the phosphorus centre. The trapping provides further evidence for the release of monomeric phosphinoboranes in the proposed polymerisation mechanism. It is noteworthy that when $Ph_2PH{\cdot}BH_3$ is reacted with two equiv. of CAAC^{Me} clean conversion to the species equivalent to **2.4a** and **2.4b** is not observed; however, peaks for the short chain oligomers $CAAC(BH_2PPh_2)_x$ (x = 1 - 4) have been identified using ESI-MS (Figure S2.67).

2.3.5 Mechanism of polymerisation from phosphinoborane monomers

Studies on the mechanism of polymerisation of phosphinoborane monomers, [RR'P–BH_2], generated from the reaction of a CAAC with a phosphine-borane substrate, are complicated due to several key factors:

1) The monomers generated *in situ* are highly reactive and readily polymerise and thus have not been isolated in their pure monomeric form.

2) A number of different polymer architectures are obtained from the polymerisation reaction including cyclic and linear oligomers, and linear polymers.

3) There is not a single well-defined initiator-derived end-group, and there are limitations in determining the identity of the various end-groups present in samples of the polymers based on the experimental techniques available.

Here we propose a polymerisation mechanism which involves several non-mutually exclusive pathways which likely occur in parallel, and discuss our experimental observations and limitations.

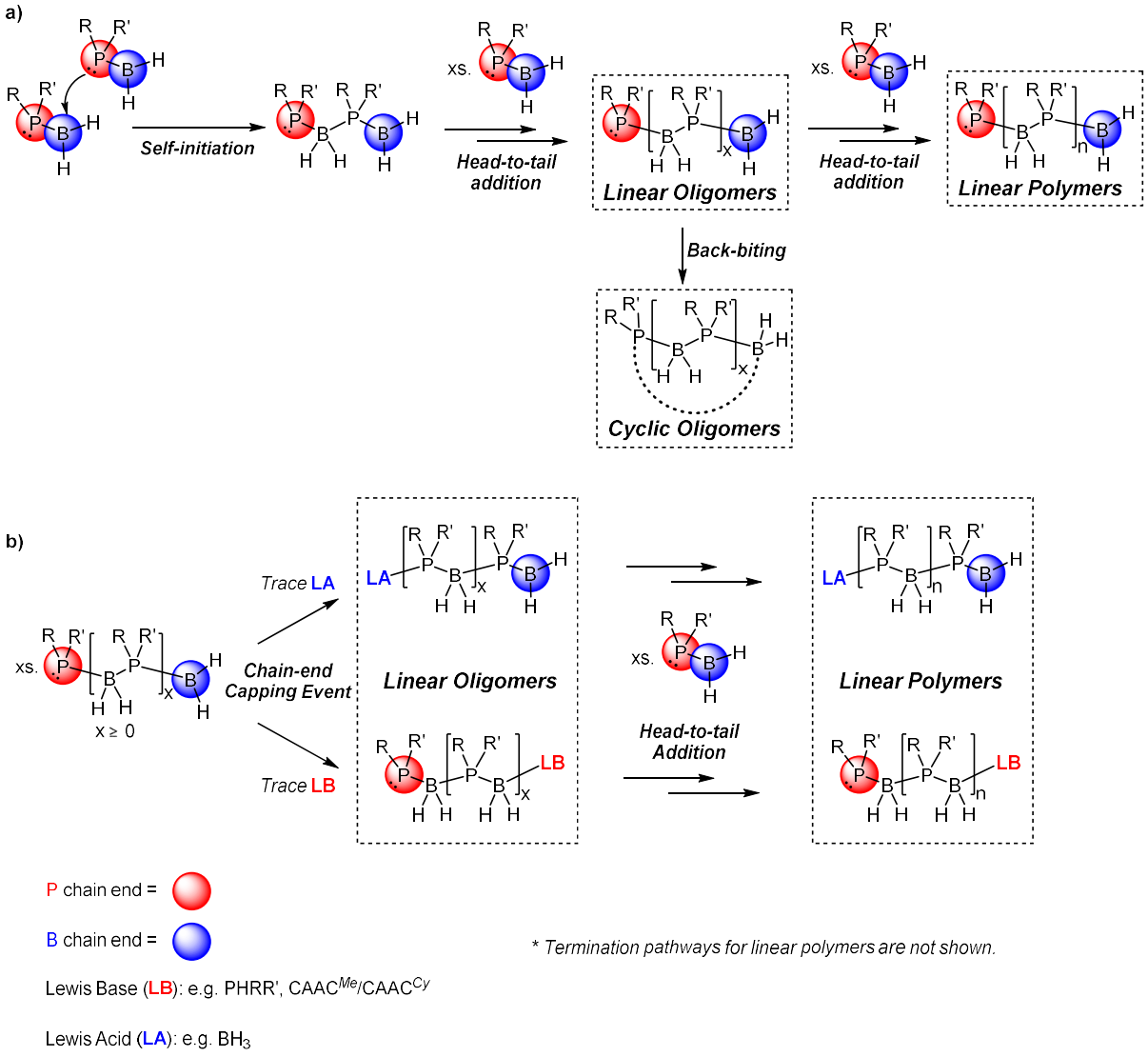

Figure 2.6 a Proposed addition head-to-tail polymerisation sequence; and **b** chain-end capping resulting in linear polymers.

We propose that the ambipolar phosphinoborane monomer can self-initiate and spontaneously undergo an addition head-to-tail polymerisation sequence, see pathway (Figure 2.6a). This mechanism is reminiscent of the metal-free thermolysis of amine-stabilised phosphinoboranes reported by Scheer and Manners.[31] Given the polar structure of the monomers and the fact that B–B and P–P linkages are not observable in polymer samples by

either ^{11}B or ^{31}P NMR spectroscopy it is likely that head-to-head and tail-to-tail propagation are not major pathways. It is possible to obtain both cyclic oligomers and linear polymers via a self-initiated route. Cyclic oligomers likely form through back-biting of the phosphorus chain end with the boron chain end. Linear polymers are obtained when the rate of linear chain propagation is greater than the rate of back-biting; these rates are often competitive and highly dependent on the nature of the substituents and the degree of substitution on the phosphinoborane monomer. For example, polymerisation of [PhHP–BH_2] favours mostly linear polymer, while for the P-disubstituted [Ph_2P–BH_2] a significant quantity of cyclic oligomers are obtained as determined by NMR spectroscopy in the crude polymeric material (Figure 2.3). The milder conditions required to generate the phosphinoborane using CAAC likely do not facilitate branching or cross-linking that could inhibit high molar mass material being formed as opposed to when the monomer is thermally generated from the phosphine-borane under more harsh thermal conditions.[54]

In addition, in concert with the proposed self-initiated pathway (Figure 2.6a), trace Lewis acids or bases present in the reaction mixture could engage in chain-end capping of polymer chain or monomer at any point during the polymerisation. These chain-end capping reactions may favour linear propagation by preventing the back-biting reaction (Figure 2.6b). Traces of free phosphine and borane can be generated thermally from dissociation of the phosphine-borane adduct, and traces of free CAAC can also be present in the reaction mixture. It is noteworthy that the electronic effect of the neutral Lewis acid or base capping group on the reactive P or B chain-end diminishes as the polymer chain lengthens, this is in contrast to radical or ionic chain polymerisations. In well-defined chain polymerisations the radical or charged reactive site consistently migrates to the end of polymer chain with each monomer addition, leading to solely unidirectional chain growth. The reactivity of the P or B chain-end towards the successive addition of further monomer or oligomers is expected to be approximately equivalent for both Lewis acid or base capped polymer chains with a high degree of polymerisation and for completely uncapped (oligo)polymer chains capable of bidirectional growth.

Some experimental evidence for chain termination involving chain-end capping with Lewis acids and bases are the detection of phosphine- and borane-based end groups for [PhHP–BH_2]$_n$ (Figure S2.21), and CAAC-based end groups for [Ph_2P–BH_2]$_n$ and [PhEtP–BH_2]$_n$ (Figure S2.35,

Figure S2.36, Figure S2.42, Figure S2.50 and Figure S2.54) using ESI-MS. The reaction of 2 equiv. of CAAC^{Me} with $PhPH_2{\cdot}BH_3$ at an initial concentration of 1.26 M in THF at 60 °C for 3h (see Table S2.1 run 4, for analogous conditions with one equiv. of CAAC^{Me}) resulted in primarily oligomeric material below the calibration limit of the GPC (M_n < ca. 2,300 Da) and only trace quantities of higher mass polymer. The excess of CAAC^{Me} likely results in a significant degree of chain-end capping reactions leading to reduced molecular masses for the resulting material.

The polymerisation mechanism may involve a combination of both chain-growth and step-growth processes. Another possibility during the polymerisation reaction that may be occurring to an extent in either of the pathways shown above is the head-to-tail addition of oligomers which possess reactive B and/or P chain ends onto existing polymer chains with reactive termini.[55]

It should be noted that there are some experimental limitations of ESI-MS as a technique, in particular for the identification of cyclic species and polymer end-groups. The lack of evidence for cyclic species in the ESI-MS data could be a feature of the ionisation method rather than the sample. ESI-MS only detects charged species and the ionisation of cyclic species is inherently difficult given the lack of available lone pairs or vacant orbitals. In comparison, depending on the end-groups, linear species can readily be ionised and are expected to be over-represented in the ESI-MS spectra. ESI-MS is also only detecting the oligomeric fraction of the material that is present (below ca. 3,000 Da) and it is possible that the bulk of the high molar mass material could have different end groups. In addition, the ionisation conditions within the ESI-MS instrument may be altering the end groups actually present in the polymer sample.

2.4 Conclusions

In summary, we have shown that cyclic alkyl(amino)carbenes can be used as stoichiometric reagents to effect P–H/B–H dehydrogenative coupling of primary and secondary phosphine-boranes. These results illustrate the complementarity between organic and transition metal ambiphiles in the context of main group redox transformations, and hint at a potentially broad utility for CAACs in accessing new inorganic polymers and materials. The carbene centre in CAAC^{Me} inserts into the P–H bond of phosphine-boranes, $RR'PH{\cdot}BH_3$ (R = Ph; R' = H, Ph or Et), to give derivatives of CAAC^{Me}(H)PRR'BH_3 (**2.3a-c**) which undergo thermolysis to give the hydrogenated carbene (CAAC^{Me})H_2 and polymers $[RR'P–BH_2]_n$. Most remarkable is that in the

case of $Ph_2PH{\cdot}BH_3$ with $CAAC^{Cy}$ the dehydropolymerisation proceeds within 1 h at 22 °C. In contrast, with respect to the reactivity of sterically encumbered P-disubstituted phosphine-boranes (R = R' = *t*Bu or Mes) with $CAAC^{Me}$ it is noteworthy that polymers are not generated post H_2-transfer. Instead the transient phosphinoboranes were trapped by a second equivalent of carbene to yield $CAAC^{Me}$-phosphinoborane adducts, **2.4a** and **2.4b**. The novel dehydropolymerisation using CAACs has been used to prepare samples of P-disubstituted polyphosphinoboranes, $[Ph_2P–BH_2]_n$ and $[PhEtP–BH_2]_n$, which cannot be accessed via previous transition-metal catalysed or stoichiometric routes, and contain high molar mass fractions. The development of catalytic rather than stoichiometric reactions involving main group species is a rapidly developing field.[56,57] The reactions of phosphine-boranes with species that undergo E–H bond activation e.g. stannylenes[58] and frustrated Lewis pairs that reversibly bind H_2[59,60] are under current investigation. Future studies will target the generation of a well-defined propagating site which should allow access to predominantly linear polymers, molar mass control, and potentially block copolymers. A more atom-economic catalytic synthesis would also allow a more facile scale up and thereby the properties of the new materials to be investigated in detail.

2.5 Supporting Information

2.5.1 General procedures, reagents and equipment

All manipulations were carried out either under an atmosphere of nitrogen gas using standard vacuum line and Schlenk techniques, or under an atmosphere of argon within an M. Braun glovebox MB150G-B maintained at < 0.1 ppm of H_2O and < 0.1 ppm of O_2. All solvents were dried via a Grubbs design solvent purification system,[61] except tetrahydrofuran (THF) which was vacuum distilled from sodium metal/benzophenone ketyl.

Deuterated solvents (benzene-d_6, chloroform-*d* and tetrahydrofuran-d_8) were purchased from Sigma Aldrich and dried by storing over activated molecular sieves (4Å). NMR spectra were recorded using Oxford Jeol Eclipse 300 MHz, Bruker 400 MHz, Bruker 500 MHz and Varian 400 MHz NMR spectrometers. ^{1}H NMR spectra were calibrated using the residual protio signal of the solvent: (δ (ppm) ^{1}H($CDCl_3$) = 7.24; ^{1}H (C_6D_6) = 7.16; and ^{1}H $(CD_2)_4O$ = 3.58, 1.72). ^{13}C NMR spectra were calibrated using the solvent signals (δ = ^{13}C(C_6D_6) = 128.0). ^{11}B and ^{31}P NMR spectra were calibrated against external standards (^{11}B: $BF_3{\cdot}OEt_2$ (δ ^{11}B = 0.0); ^{31}P: 85% H_3PO_4 (aq) (δ ^{31}P = 0.0)). All chemical shifts are given in ppm (parts per million).

IDipp,[62] [IDippH]Cl,[62] CAAC^{Me},[34] [CAAC^{Me}H]Cl,[34] CAAC^{Cy},[34] $PhPH_2{\cdot}BH_3$,[63] $Mes_2PH{\cdot}BH_3$,[64] *rac*-PhEtPHBH_3,[65] and $Ph_2PH{\cdot}BH_3$[66] were prepared according to literature procedures. $BH_3{\cdot}THF$ (1 M in THF) was purchased from Acros Organics and trap-to-trap vacuum transferred prior to use. $PPhH_2$ (ca. 10% weight in hexanes), Ph_2PH, tBu$_2$PH·BH_3, and *n*BuLi (1.6 M in hexanes) were purchased from Sigma Aldrich and used as received.

GPC was performed on a Malvern RI max Gel Permeation Chromatograph, equipped with an automatic sampler, a pump, an injector, and inline degasser. The columns (T5000) were contained within an oven (35 °C) and consisted of styrene/divinyl benzene gels. Sample elution was detected by means of a differential refractometer. THF (Fisher), containing 0.1 wt% [*n*Bu$_4$N]Br, was used as the eluent at a flow rate of 1 mL min^{-1}. Samples were dissolved in THF (2 mg mL^{-1}) and filtered with a Ministart SRP15 filter poly(tetrafluoroethylene) membrane of 450 nm pore size before analysis. The calibration was conducted using monodisperse polystyrene standards obtained from Aldrich. The lowest and highest molecular weight standards used were 2,300 Da and 994,000 Da respectively. Data for low molar mass components (i.e. M_n < 2,300 Da) is estimated.

The ESI-MS spectra were obtained using a Waters Synapt G2S instrument equipped with a nanospray ionisation module (Advion TriVersa Nanomate). Solutions (40 µL) of approximately 1 mg mL^{-1} were loaded under ambient conditions in air into the sample tray, and aliquots of 3 µL were introduced into the spectrometer using a spray voltage of 1.5 kV. Positive and negative ion spectra were recorded at a rate of 1 scan second^{-1} and summed to obtain the final spectra. Elemental analyses (C, H, N) were performed externally by Elemental Microanalysis Ltd. in Devon, UK.

2.5.2 Synthesis of IDipp phosphidoborane salts

2.5.2.1 Synthesis of 2.1a

Method A

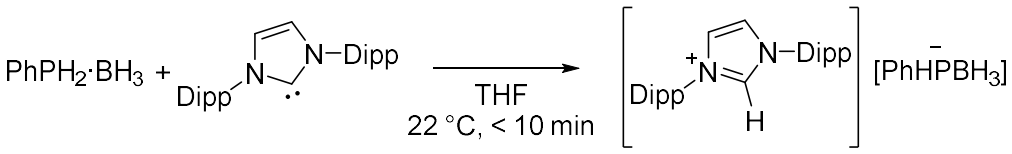

2.1a

$PhPH_2{\cdot}BH_3$ (16 mg, 0.13 mmol) was dissolved in THF-d_8 (0.5 mL) in a quartz J. Young NMR tube and IDipp (50 mg, 0.13 mmol) added. Immediately a white precipitate was detected prior to the solution becoming homogeneous. The initial precipitate observed is attributed to the fast formation of the poorly soluble salt which is dissolved upon stirring. Crystals of **2.1a** were grown from a layered THF/hexane solution at -40 °C; however, the crystals were not of high enough quality to give a publishable data set, only a preliminary structure which confirmed the connectivity could be obtained. Yield = 38 mg (58%).

Method B

Independent synthesis of **2.1a** through salt metathesis

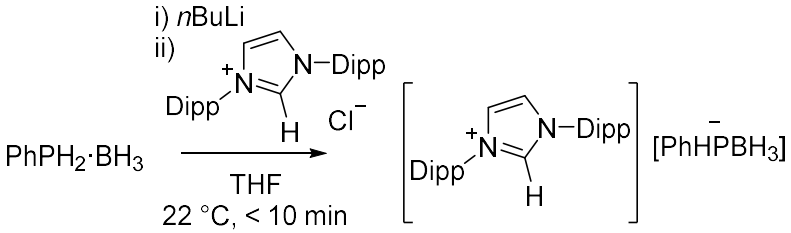

2.1a

An *n*BuLi solution (630 µL of a 1.6 M in hexanes solution, 1.00 mmol) was added to a solution of $PhPH_2{\cdot}BH_3$ (124 mg, 1.00 mmol) in THF (1 mL) and allowed to stir for 10 min at 22 °C before being added to a solution of [IDippH]Cl (435 mg, 1.00 mmol) in THF (1 mL). Immediate conversion to the product was observed and the identity confirmed using ^{1}H, ^{11}B and ^{31}P NMR spectroscopy. No attempts to isolate the product obtained through this route were made.

^{1}H NMR (400 MHz, 298 K, THF-d_8): δ = 0.61 (m, 3H, B*H*), 1.20 (d, $^{3}J_{HH}$ = 6.9 Hz, 12H, CH(CH_3)$_2$), 1.24 (d, $^{3}J_{HH}$ = 6.9 Hz, 12H, CH(CH_3)$_2$), 2.53 (sept, $^{3}J_{HH}$ = 6.9 Hz, 4H, C*H*(CH$_3$)$_2$), 6.33-7.14 (m, ArH (Ph)), 7.39 (d, $^{3}J_{HH}$ = 7.7 Hz, Ar^{m} (Dipp), 4H), 7.57 (t, $^{3}J_{HH}$ = 7.7 Hz, Ar^{p} (Dipp)), 8.07 (s, 2H, NC*HCH*N), 10.05 (s, H, NC*H*). P–H proton cannot be detected in ^{1}H NMR spectrum.

^{11}B NMR (96 MHz, 295 K, THF-d_8): δ = -33.4 (qd, $^{1}J_{BH}$ = 91.4 Hz, $^{1}J_{BH}$ = 26.6 Hz).

^{31}P NMR (122 MHz, 296 K, THF-d_8): δ = -84.2 (m, br).

Elemental analysis for $C_{33}H_{46}BN_2P$ (calcd/expt): C (77.33/76.58), H (9.05/9.22), N (5.47/5.44).

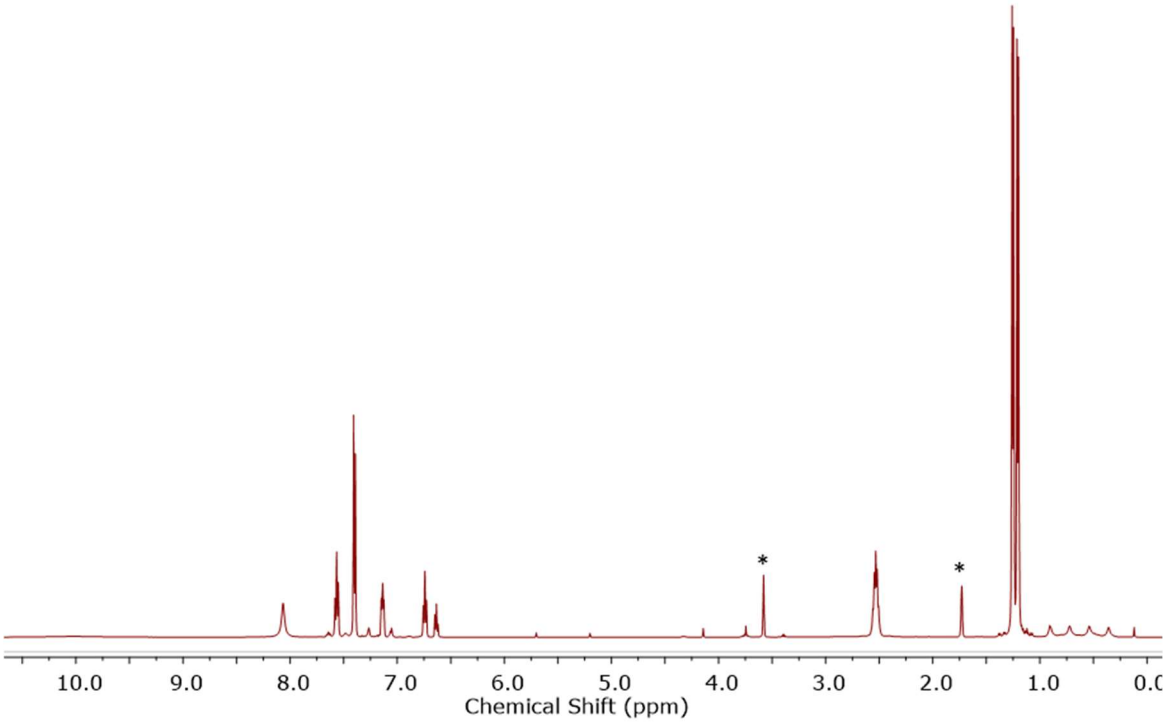

Figure S2.1 ^{1}H NMR spectrum (400 MHz, 298 K THF-d_8) of **2.1a**. Iminium C-H proton is very broad. The iminium C-H proton resonance is 8.07. (*denotes residual partially protiated THF).

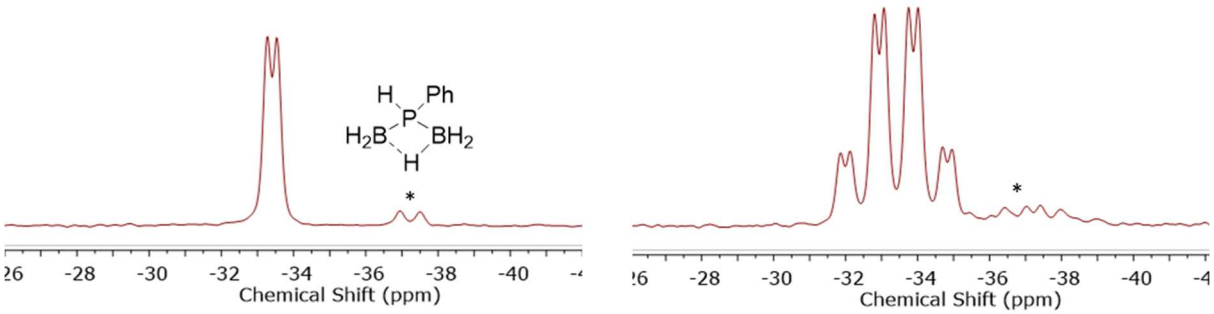

Figure S2.2 $^{11}B\{^{1}H\}$ (left) and ^{11}B (right) NMR spectra (96 MHz, 295 K, THF-d_8) of **2.1a** (*denotes trace μ-$(PhPH)B_2H_5$).

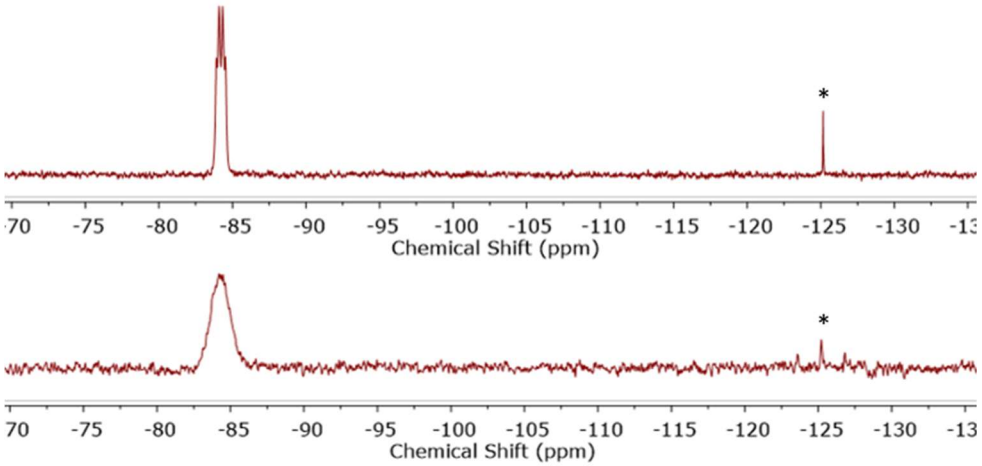

Figure S2.3 $^{31}P\{^{1}H\}$ (top) and ^{31}P (bottom) NMR spectra (122 MHz, 296 K, THF-d_8) of **2.1a** (*denotes trace $PhPH_2$).

2.5.2.2 Synthesis of 2.1b

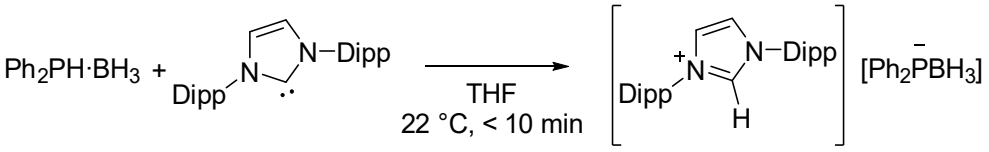

2.1b

$Ph_2PH{\cdot}BH_3$ (24 mg, 0.13 mmol) and IDipp (50 mg, 0.13 mmol) were dissolved in THF-d_8 (0.5 mL) in a quartz J. Young NMR tube and immediately a white precipitate was detected prior to the solution becoming homogeneous. The solvent was removed *in vacuo* to give a white solid which was washed with hexanes to give the product. Singe crystals of **2.1b** suitable for X-ray diffraction were grown from a layered THF/hexane solution at -40 °C. Yield prior to crystallisation = 40 mg (53%).

^{1}H NMR (400 MHz, 298 K, THF-d_8): δ = 0.98 (m, 3H, B*H*), 1.18 (d, $^3J_{HH}$ = 6.9 Hz, 12H, CH(CH_3)$_2$), 1.21 (d, $^3J_{HH}$ = 6.9 Hz, 12H, CH(CH_3)$_2$), 2.73 (sept, $^3J_{HH}$ = 6.9 Hz, 4H, C*H*(CH$_3$)$_2$), 7.25 – 7.33, 7.39-7.47, 7.55-7.62 (m, aromatic and NC*HCH*N backbone). C–H proton cannot be detected in ^{1}H NMR spectrum.

^{11}B NMR (96 MHz, 295 K, THF-d_8): δ = -34.4 (m).

^{31}P NMR (122 MHz, 296 K, THF-d_8): δ = -21.6 (br).

Elemental analysis for $C_{39}H_{50}BN_2P$ (calcd/expt): C(79.58/79.04), H (8.56/8.74), N(4.76/4.72).

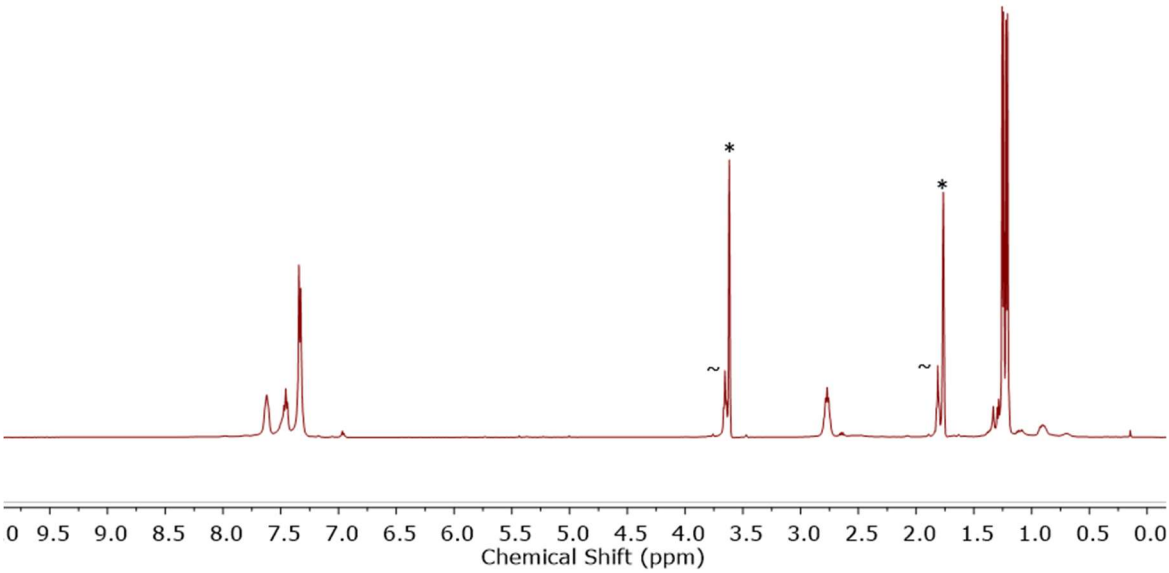

Figure S2.4 ^{1}H NMR spectrum (400 MHz, 295 K, THF-d_8) of **2.1b** (*denotes residual partially protiated THF, ~denotes THF).

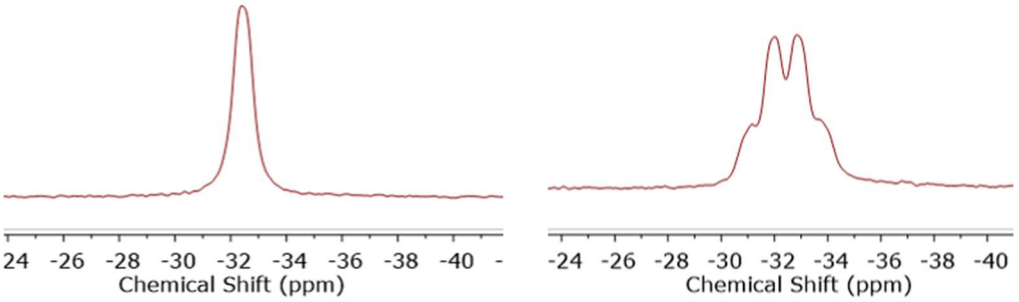

Figure S2.5 $^{11}B\{^{1}H\}$ (left) and ^{11}B (right) NMR spectra (96 MHz, 295 K, THF-d_8) of **2.1b**.

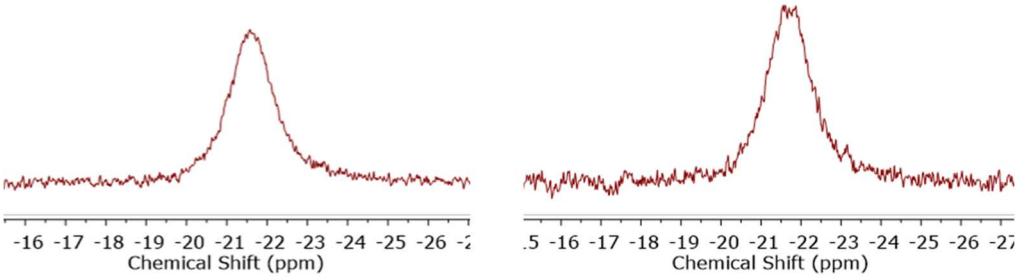

Figure S2.6 $^{31}P\{^{1}H\}$ (left) and ^{31}P (right) NMR spectra (122 MHz, 296 K, THF-d_8) of **2.1b**.

2.5.3 Polymerisation attempts of $PhPH_2{\cdot}BH_3$ using CAAC^{Me}

2.5.3.1 Synthesis of 2.3a

Method A

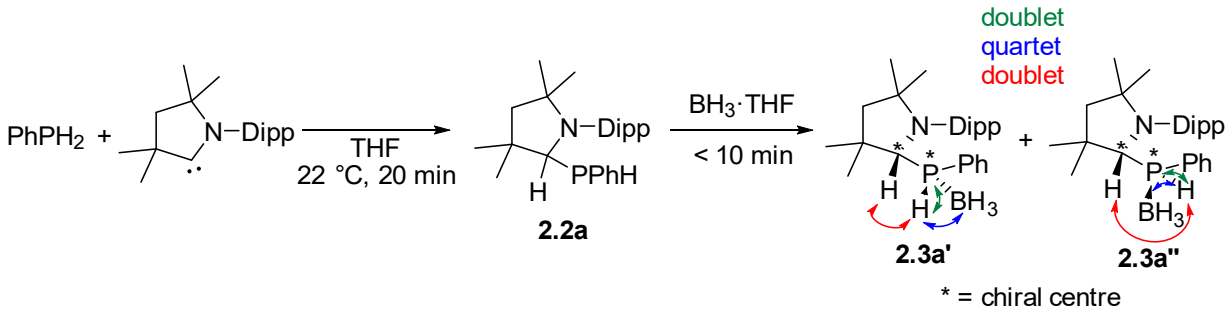

$PhPH_2{\cdot}BH_3$ (74 mg, 0.60 mmol) and CAAC^{Me} (171 mg, 0.599 mmol) were dissolved in THF (0.5 mL) in a quartz J. Young NMR tube. P–H activation occurred instantly at 22 °C to give two diastereomers. This was immediately followed by a degree of formation of $[PhHP–BH_2]_n$ and $(CAAC^{Me})H_2$, hence isolation of these compounds has not been achieved and there are traces of $(CAAC^{Me})H_2$ visible in the ^{1}H NMR spectrum. The initial ratio of diastereomers observed after 10 min in solution was 1:12.4.

Method B

2.3a can also be synthesised through a stepwise procedure

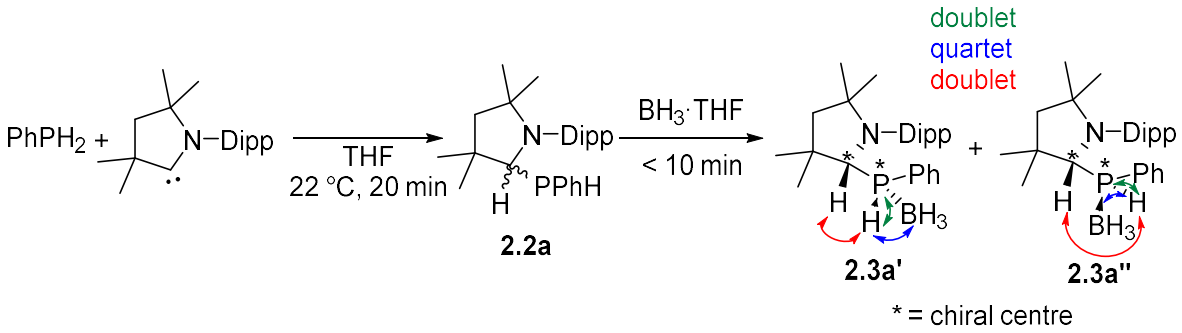

$PPhH_2$ (used as a ca. 10% weight solution in hexanes, 4.24 g of hexanes solution, 3.90 mmol) was added to a solution of $CAAC^{Me}$ (1.00 g, 3.50 mmol) in THF (10 mL) and stirred for 20 min at 22 °C. The volatiles were removed *in vacuo* to leave a pale yellow powder. NMR spectroscopic data for $CAAC^{Me}$(H)(PPhH) obtained was directly comparable to those described in the literature for $CAAC^{Cy}$(H)(PPhH).[38] The powder was redissolved in THF (5 mL) and BH_3·THF (3.50 mL of a 1M in THF solution, 3.50 mmol) was added. Volatiles were immediately removed *in vacuo*; however, as with method A above it was not possible to isolate the product as a degree of formation of $[PhHP–BH_2]_n$ and $(CAAC^{Me})H_2$ immediately occurs.

Method C

2.3a was also independently synthesised through a salt metathesis reaction

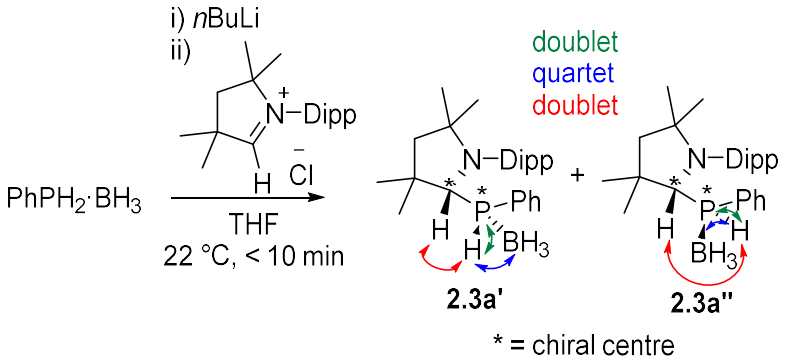

*n*BuLi (56 µL of a 1.6 M in hexanes solution, 0.081 mmol) was added to a solution of $PhPH_2$·BH_3 (10 mg, 0.081 mmol) in THF (0.5 mL) in a quartz J. Young NMR tube and at 22 °C and after 10 min $[CAAC^{Me}H]Cl$ (30 mg, 0.093 mmol) was added. Immediate conversion to the product was observed and the identity confirmed using ^{1}H, ^{11}B and ^{31}P NMR spectroscopy; however as above it was not possible to isolate the product as the formation of $[PhHP–BH_2]_n$ and $(CAAC^{Me})H_2$ immediately occurs.

^{1}H NMR (400 MHz, 298 K, THF-d_8): δ = 7.70-7.38 (m, 5H, Ar), 7.26-7.20 (m, 3H, Ar^{Dipp}), 4.84 (dqd, $^{1}J_{PH}$ = 364 Hz, $^{3}J_{HH}$ = 7.2 Hz and $^{3}J_{HH}$ = 2.5 Hz, 1H, P*H*), 4.42 (dd, $^{2}J_{HP}$ = 4.2 Hz, $^{3}J_{HH}$ = 2.5 Hz, 1H, NC*H*), 4.11 (sept, $^{3}J_{HH}$ = 6.6 Hz, 1H, C*H*(CH$_3$)$_2$), δ = 3.08 (sept, $^{3}J_{HH}$ = 6.6 Hz, 1H, C*H*(CH$_3$)$_2$), 2.05 (ABq, 1H, C*H*$_2$), 1.64 (s, 3H, NC(CH$_3$)$_2$), 1.58 (s, 3H, NC(CH$_3$)$_2$), 1.37 (d, $^{3}J_{HH}$ = 6.6 Hz, 3H, CH(C*H*$_3$)$_2$), 1.29 (d, $^{3}J_{HH}$ = 6.6 Hz, 3H, CH(C*H*$_3$)$_2$), 1.24 (d, $^{3}J_{HH}$ = 6.6 Hz, 3H, CH(C*H*$_3$)$_2$), 1.20 (d, $^{3}J_{HH}$ = 6.6 Hz, 3H, CH(C*H*$_3$)$_2$), 0.95 (s, 3H, C(CH$_3$)$_2$), 0.84 (s, 3H, C(CH$_3$)$_2$). Data given only for the major diastereomer, **2.3a'**.

^{11}B NMR (96 MHz, 295 K, THF-d_8): δ = -40.1 (m, br).

No detection of separate peaks for the different isomers, postulated to be due to broad peaks overlapping.

^{31}P NMR (122 MHz, 296 K, THF-d_8): δ = -4.1 (d, $^{1}J_{PH}$ = 364 Hz) (**2.3a''**), -12.4 (d, $^{1}J_{PH}$ = 364 Hz) (**2.3a'**).

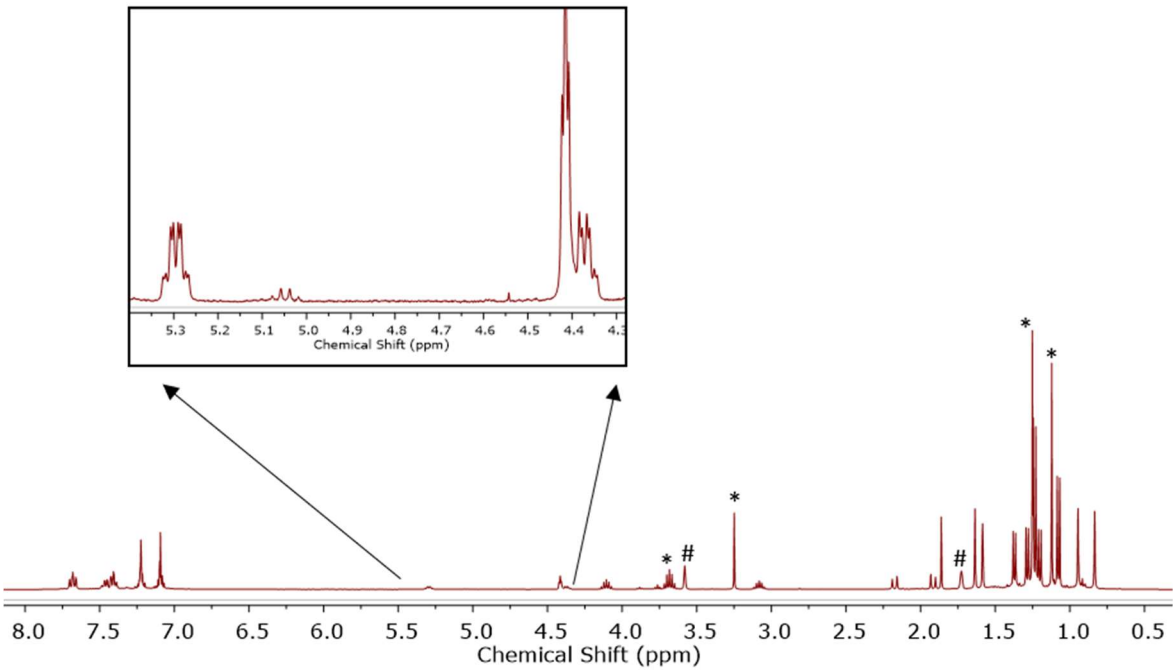

Figure S2.7 ^{1}H NMR spectrum (400 MHz, 298 K, THF-d_8) of **2.3a** (*denotes (CAAC^{Me})H$_2$, $^{\#}$denotes residual partially protiated THF). Doublet of quartets of doublets splitting pattern of P–H proton is expanded.

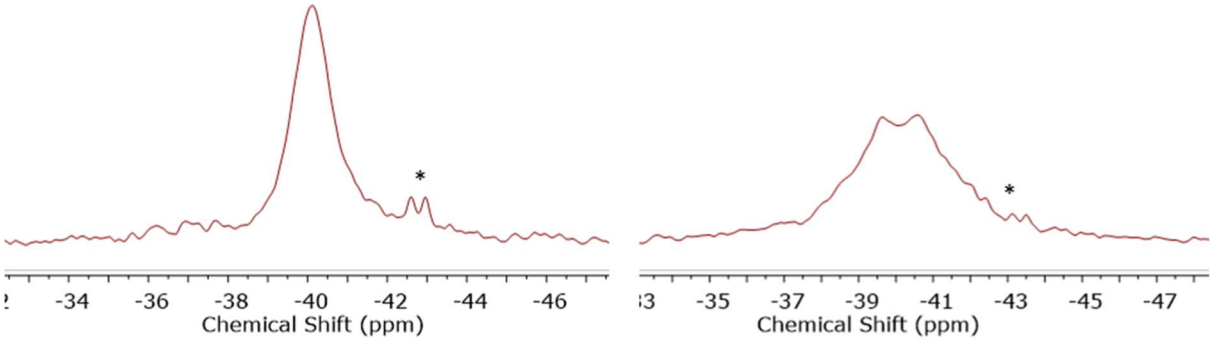

Figure S2.8 $^{11}B\{^{1}H\}$ (left) and ^{11}B (right) NMR spectra (96 MHz, 295 K, THF-d_8) of **2.3a** (*denotes trace (CAAC^{Me})·BH_3 adduct).[38]

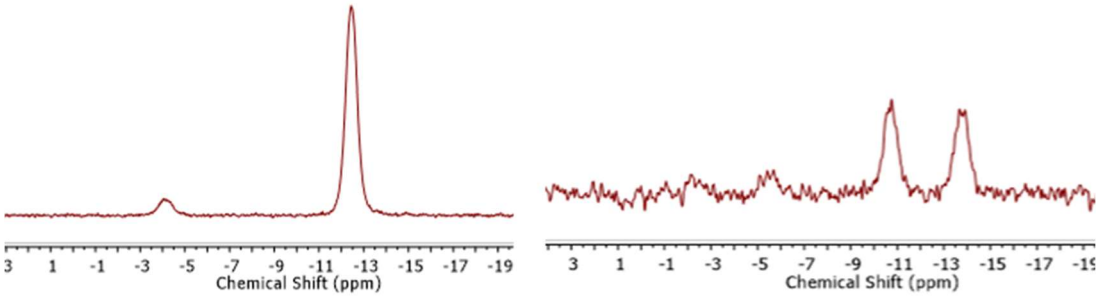

Figure S2.9 $^{31}P\{^{1}H\}$ (left) and ^{31}P (right) NMR spectra (122 MHz, 296 K, THF-d_8) of **2.3a**.

2.5.3.2 General procedure for dehydropolymerisation of $PhPH_2$·BH_3 using CAAC^{Me}

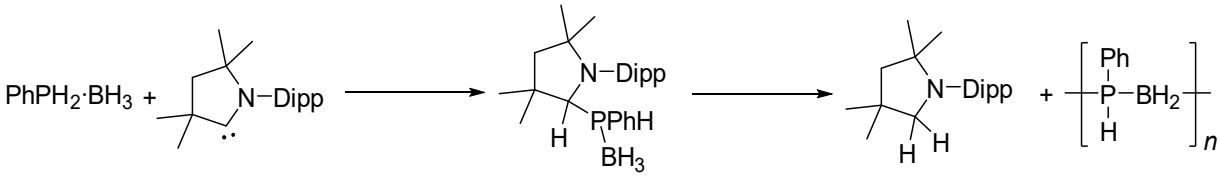

$PhPH_2$·BH_3 and CAAC^{Me} were dissolved in THF or toluene in the quantities shown in Table S2.1 and the reaction performed under the conditions shown in either a J. Young NMR tube or a J. Young Schlenk tube. Mass spectrometry and GPC analysis were carried out after precipitation of the reaction mixture into cold (−40 °C), stirring hexanes. More detailed information on run 4 is shown below.

Table S2.1 Influence of temperature, solvent and concentration on the formation of polyphenylphosphinoborane, $[PhHP–BH_2]_n$ in a closed system.

Run	Temp. (°C)	Solvent	Volume (mL)	CAAC^{Me} (mg)	$PhPH_2$·BH_3 (mg)	Time (h)[a]	DP[b]	M_n (Da)[c]	PDI[c]
1	22	THF	0.5	71	31	120	205	25,000	1.55
2	60	THF	0.5	14	6	3	[d]	[d]	[d]
3	60	THF	0.5	71	31	3	410	50,100	1.27
4	60	THF	1.0	360	156	3	686	83,800	1.13
5	60	toluene	0.5	71	31	3	290	35,400	1.28
6	110	toluene	0.5	71	31	0.5	230	28,000	1.52
7	110	none	n/a	142	62	3	302	36,800	1.39

[a]Time taken for full conversion by ^{31}P NMR spectroscopy [b]degree of polymerisation measured by GPC [c]measured using GPC analysis [d]no high molecular weight material recovered after precipitation.

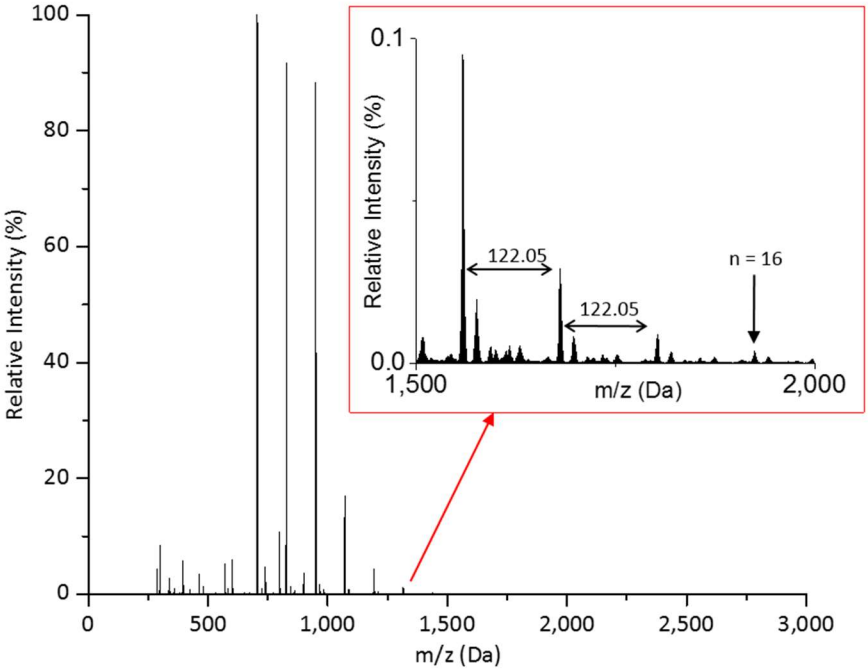

Figure S2.10 ESI(+)-MS spectrum of $[PhHP–BH_2]_n$ product from run 1 of Table S2.1 in DCM.

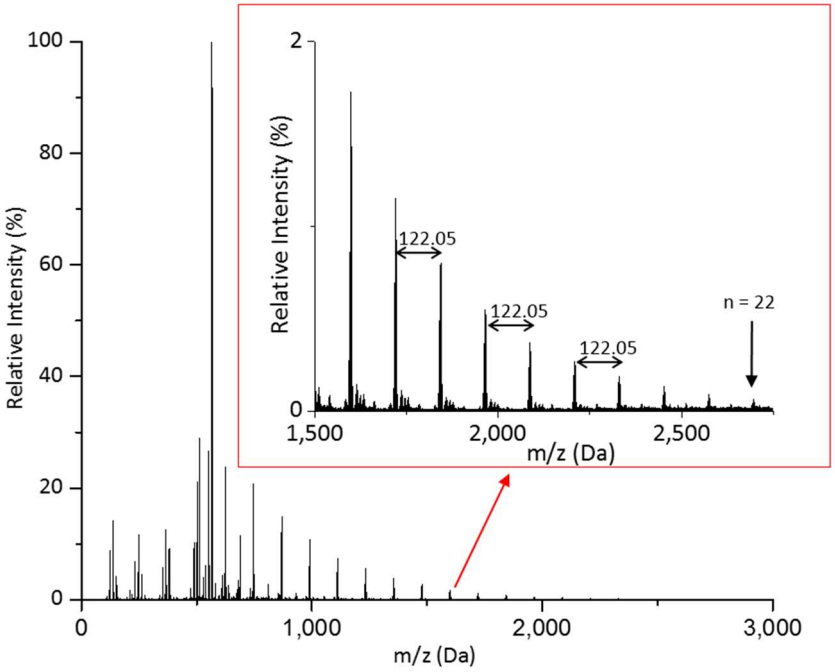

Figure S2.11 ESI(+)-MS spectrum of $[PhHP–BH_2]_n$ product from run 2 of Table S2.1 in DCM.

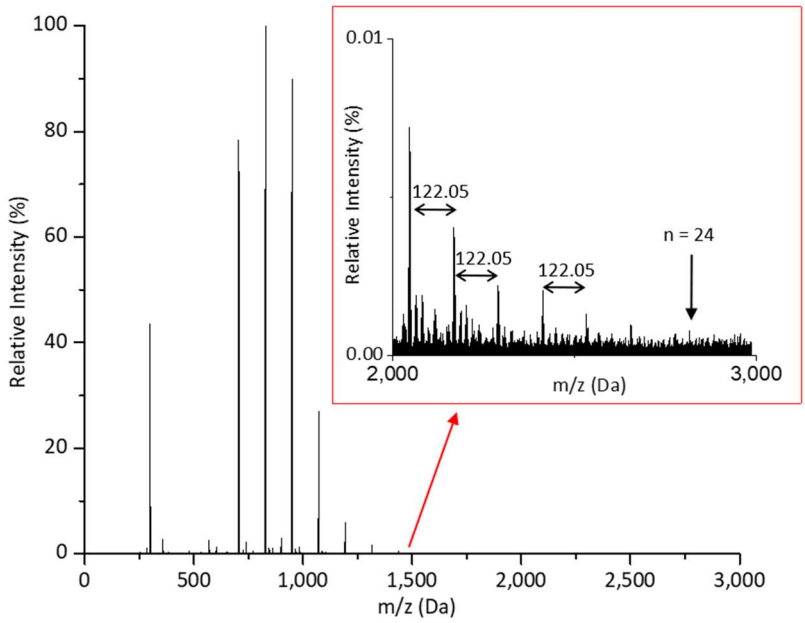

Figure S2.12 ESI(-)-MS spectrum of $[PhHP–BH_2]_n$ product from run 3 of Table S2.1 in DCM.

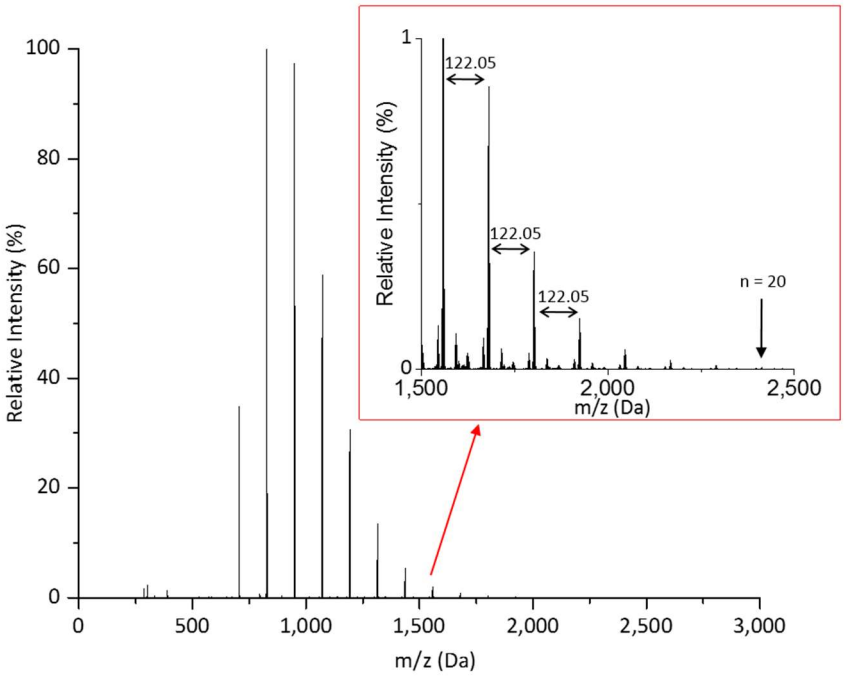

Figure S2.13 ESI(+)-MS spectrum of $[PhHP–BH_2]_n$ product from run 5 of Table S2.1 in DCM.

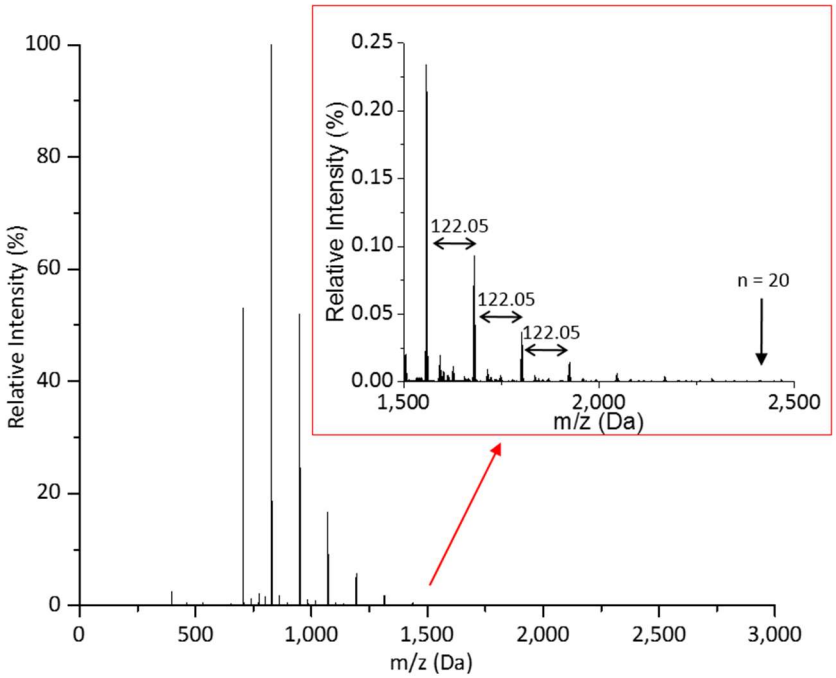

Figure S2.14 ESI(+)-MS spectrum of $[PhHP–BH_2]_n$ product from run 6 of Table S2.1 in DCM.

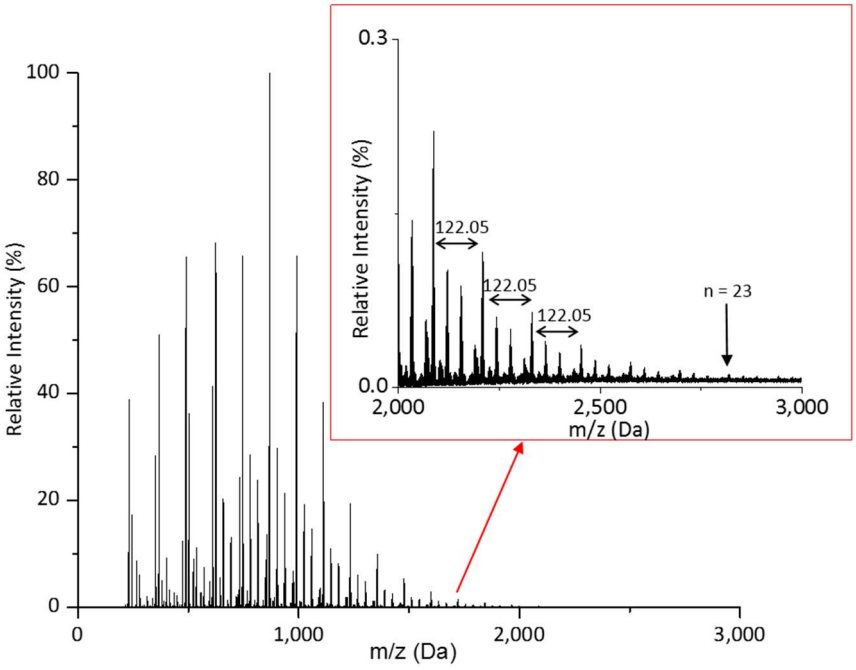

Figure S2.15 ESI(+)-MS spectrum of $[PhHP–BH_2]_n$ product from run 7 of Table S2.1 in DCM.

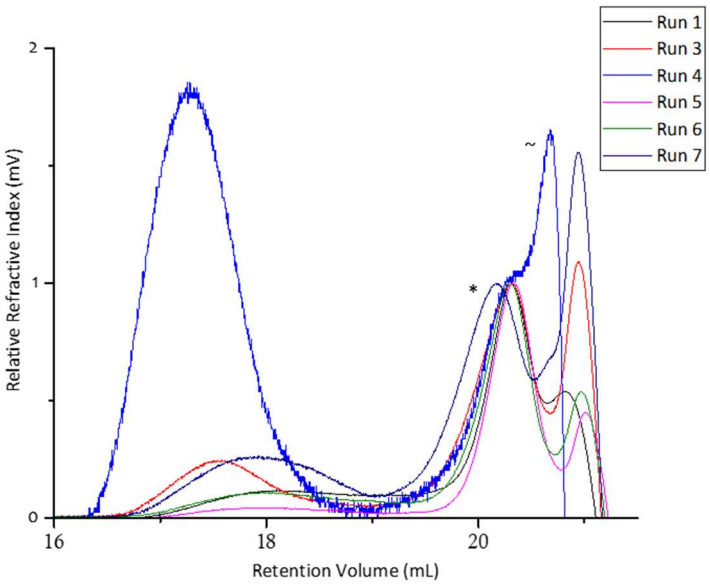

Figure S2.16 GPC chromatogram of precipitated $[PhHP–BH_2]_n$ products from for runs 1-7 from Table S2.1. 2 mg mL^{-1} in THF with 0.1 w/w% nBu$_4$NBr in the THF eluent (*oligomeric material, ~system peak).

2.5.3.3 More detailed procedure for run 4

$PhPH_2{\cdot}BH_3$ (156 mg, 1.26 mmol) and CAAC^{Me} (360 mg, 1.26 mmol) were dissolved in THF (1 mL) in a J. Young Schlenk tube, sealed, and the reaction mixture was stirred at 60 °C for 3 h. The reaction mixture was added dropwise into 20 mL of rapidly stirred cold hexanes at -40 °C yielding a precipitate and the supernatant was decanted. The precipitation was repeated twice more prior to drying *in vacuo* to leave a white powder of the $[PhHP–BH_2]_n$ polymer product. Yield (precipitated material) = 42 mg (27%). GPC (2 mg mL^{-1}): M_n = 83,800 Da; $Đ$ = 1.17.

^{1}H NMR (400 MHz, 298 K, THF-d_8): δ = 7.38-7.03 (m, 5H, Ar), 4.32 (d, $^1J_{PH}$ = 370 Hz, 1H, PH), 1.86-1.20 (m, 2H, BH).

^{11}B NMR (96 MHz, 295 K, THF-d_8): δ = -34.6 (m, br).

^{31}P NMR (122 MHz, 298 K, THF-d_8): δ = -48.4 (d, $^1J_{PH}$ = 348 Hz).

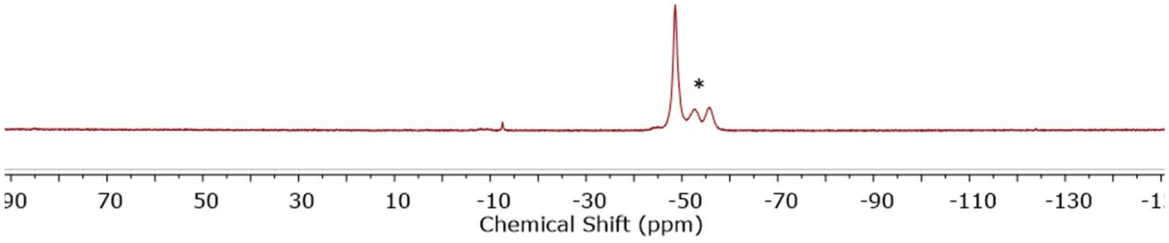

Figure S2.17 ^{31}P{^{1}H} NMR spectra (122 MHz, 298 K, THF-d_8) of the crude reaction mixture between $PhPH_2{\cdot}BH_3$ and CAAC^{Me} for run 4 (*denotes material which may be a mixture of linear and cyclic oligomers[54]).

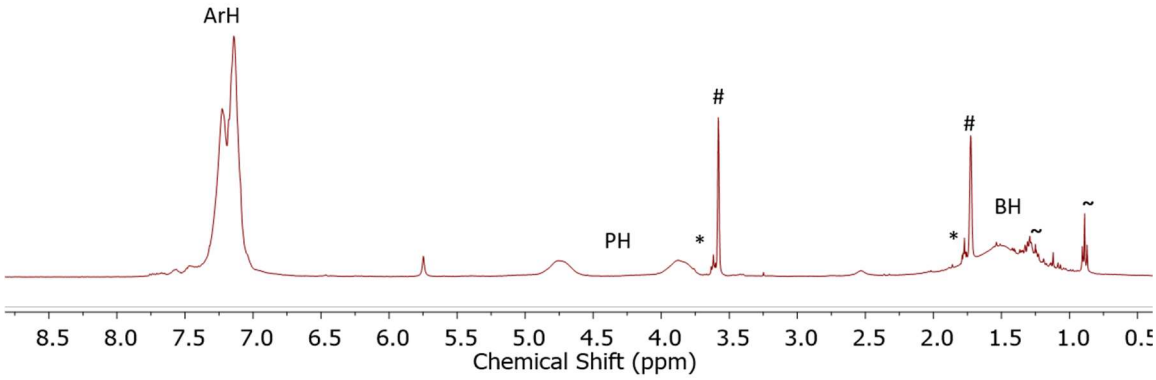

Figure S2.18 ^{1}H NMR spectrum (400 MHz, 298 K, THF-d_8) of isolated [PhHP–BH_2]$_n$ from run 4 (*denotes partially protiated THF, #denotes THF, ~denotes hexanes).

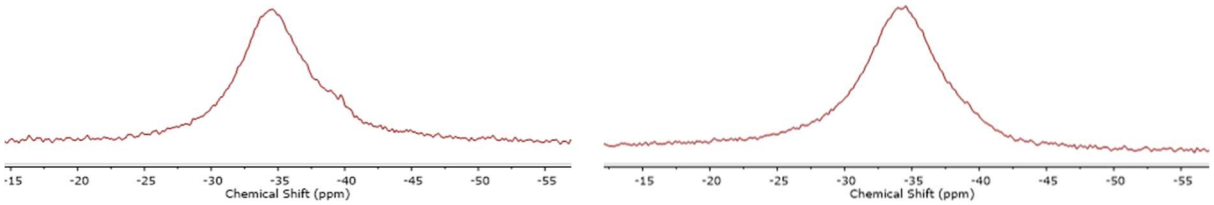

Figure S2.19 ^{11}B{^{1}H} (left) and ^{11}B (right) NMR spectra (96 MHz, 295 K, THF-d_8) of isolated [PhHP–BH_2]$_n$ from run 4.

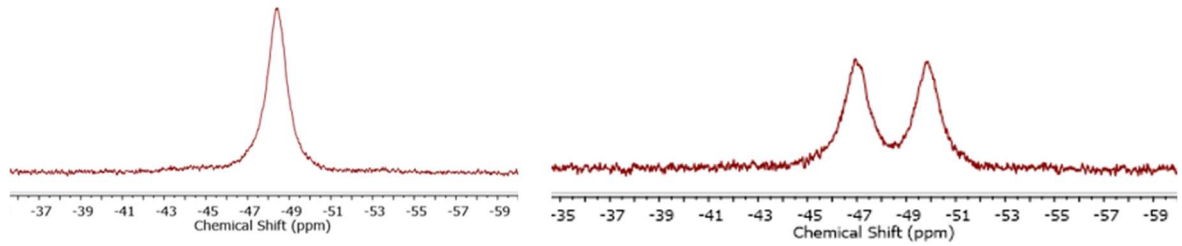

Figure S2.20 ^{31}P{^{1}H} (left) and ^{31}P (right) NMR spectra (122 MHz, 298 K, THF-d_8) of isolated [PhHP–BH_2]$_n$ from run 4.

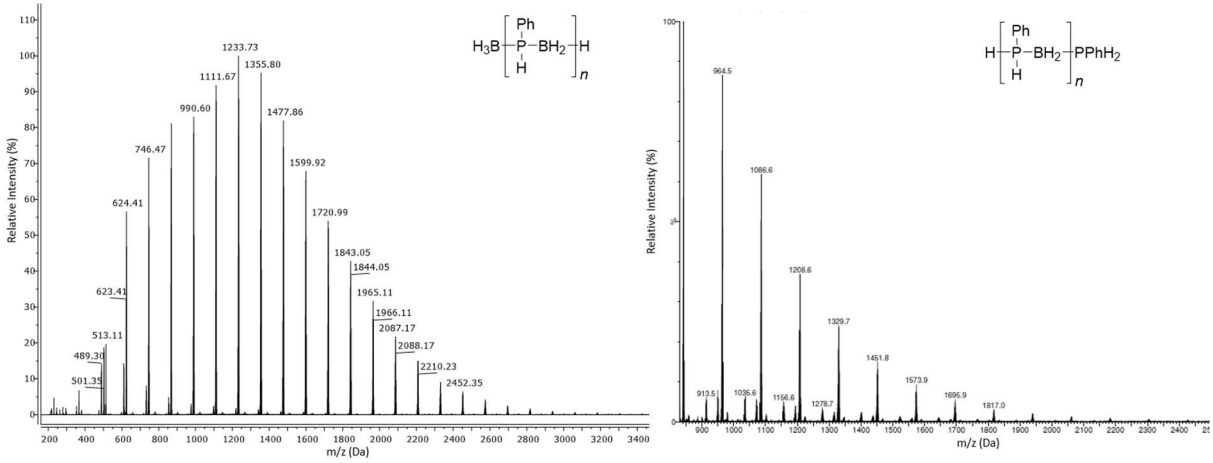

Figure S2.21 ESI(-)-MS (left) and ESI(+)-MS (right) spectra of [PhHP–BH_2]$_n$ product from run 4 in Table S2.1. The predominant species are linear systems with a BH_3 end group (BH_3-[PhHP–BH_2]$_n$-H)$^-$ or a $PPhH_2$ end group (H-[PhHP–BH_2]$_n$-PPhH)$^+$ respectively.

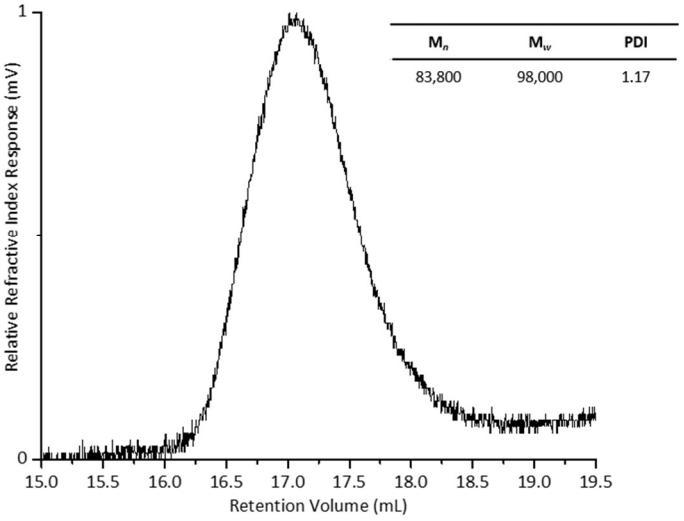

Figure S2.22 GPC chromatogram of precipitated $[PhHP–BH_2]_n$ product from run 4 of Table S2.1. 2 mg mL^{-1} in THF with 0.1 w/w% nBu$_4$NBr in the THF eluent.

Figure S2.23 Photograph of isolated $[PhHP–BH_2]_n$.

2.5.3.4 Synthesis of (CAAC^{Me})H$_2$

(CAAC^{Me})H$_2$ was obtained by removing the solvent *in vacuo* from the filtrate post precipitation of the polymer in run 4. Single crystals suitable for X-ray diffraction were obtained through sublimation (22 °C, 5 x 10^{-2} Pa).

^{1}H NMR (400 MHz, 298 K, C_6D_6): δ = 7.24 (m, 1H, Ar^p), 7.32 (d, 2H, Ar^m), 3.72 (sept, $^3J_{HH}$ = 6.7 Hz, 2H, C*H*(CH$_3$)$_2$), 3.34 (s, 2H, NC*H*$_2$), 1.97 (s, 2H, NC(CH$_3$)$_2$C*H*$_2$),BH 1.38 (d, $^3J_{HH}$ = 6.7 Hz, 6H, CH(C*H*$_3$)$_2$), 1.37 (s, 6H, NC(C*H*$_3$)$_2$), 1.25 (s, 6H, C(C*H*$_3$)$_2$), 1.23 (d, $^3J_{HH}$ = 6.7 Hz, 6H, CH(C*H*$_3$)$_2$).

^{13}C NMR (101 MHz, 298 K, C_6D_6): δ = 152.4 (Ar^i), 139.1 (Ar^o), 126.5 (Ar^m), 123.9 (Ar^p), 67.7 (N*C*H$_2$), δ = 63.3 (N*C*(CH$_3$)$_2$), 56.8 (NC(CH$_3$)$_2$(*C*H$_2$), 37.3 (NC(*C*H$_3$)$_2$), 30.4 (N(CH$_2$)C(*C*H$_3$)$_2$), 29.0 (*C*H(CH$_3$)$_2$), 28.4 (NC(*C*H$_3$)$_2$), 26.7 (CH(*C*H$_3$)$_2$), 23.2 (CH(*C*H$_3$)$_2$).

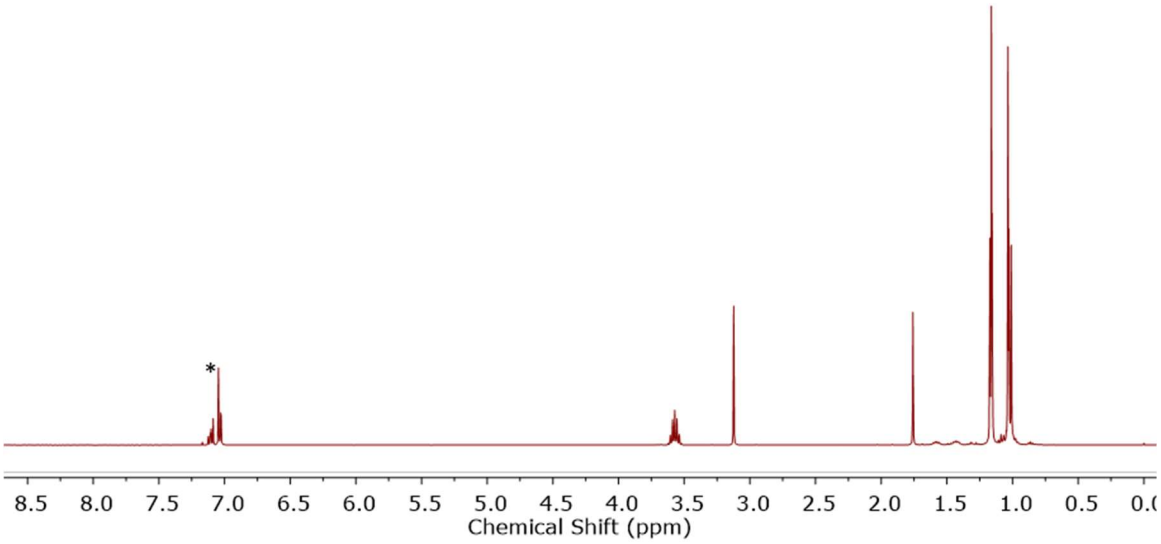

Figure S2.24 ^{1}H NMR spectrum (400 MHz, 298 K, C_6D_6) of (CAAC^{Me})H_2 (*denotes residual partially protiated benzene).

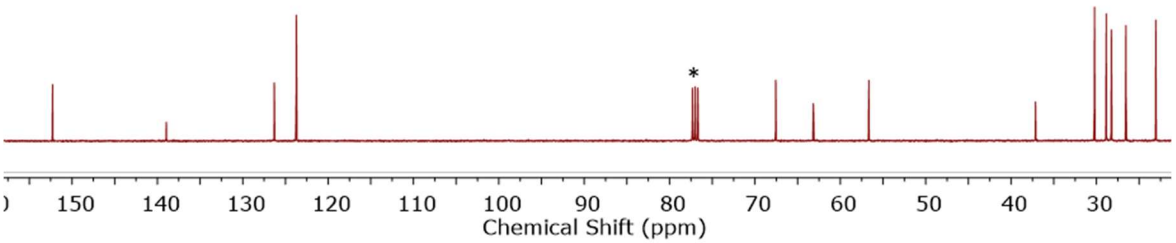

Figure S2.25 ^{13}C NMR spectrum (101 MHz, 298 K, C_6D_6) of (CAAC^{Me})H_2 (*denotes benzene).

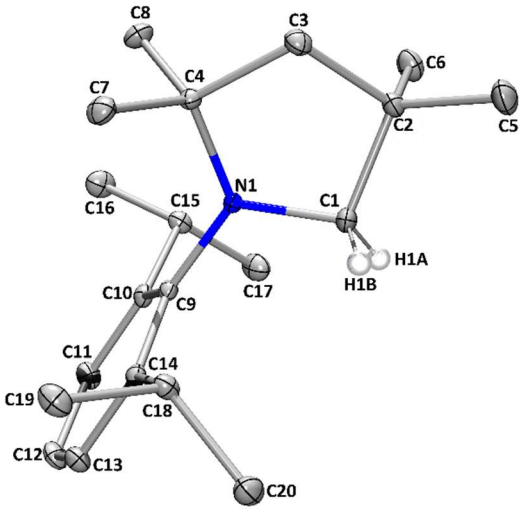

Figure S2.26 Thermal ellipsoid plot of (CAAC^{Me})H_2. Ellipsoids are shown at the 30% probability level. H atoms other than those at the C1 centre have been omitted for clarity.

2.5.4 Mechanistic studies

2.5.4.1 Kinetics measurements to probe reaction mechanism

$PhPH_2{\cdot}BH_3$ and $CAAC^{Me}$ in the quantities shown in Table S2.2 were dissolved in THF (0.5 mL) in a quartz J. Young NMR tube containing a capillary of neat PCl_3 as an internal standard. The peak corresponding to **2.3a''** (δ_P = -12.4 ppm) was integrated relative to the capillary over at least two half lives in each case. The kinetic studies were all performed solely on the **2.3a''** diastereomer as **2.3a'** is consumed much more rapidly.

Table S2.2 Conditions for kinetics experiments.

Run	Conc. (M)	$CAAC^{Me}$ (mg)	$PhPH_2{\cdot}BH_3$ (mg)	Temp. (°C)	k	$T^{1/2}$ (h)
8	0.50	71	31	22	7.87×10^{-6}	24.5
9	0.50	71	31	30	1.64×10^{-5}	11.7
10	0.50	71	31	40	5.56×10^{-5}	3.5
11	0.50	71	31	50	1.42×10^{-4}	1.4
12	0.50	71	31	60	4.33×10^{-4}	0.5
13	0.30	43	19	50	1.39×10^{-4}	1.4
14	0.70	100	43	50	1.24×10^{-4}	1.6
15[a]	0.50	71	31	50	8.00×10^{-5}	2.4

[a]Toluene used as solvent

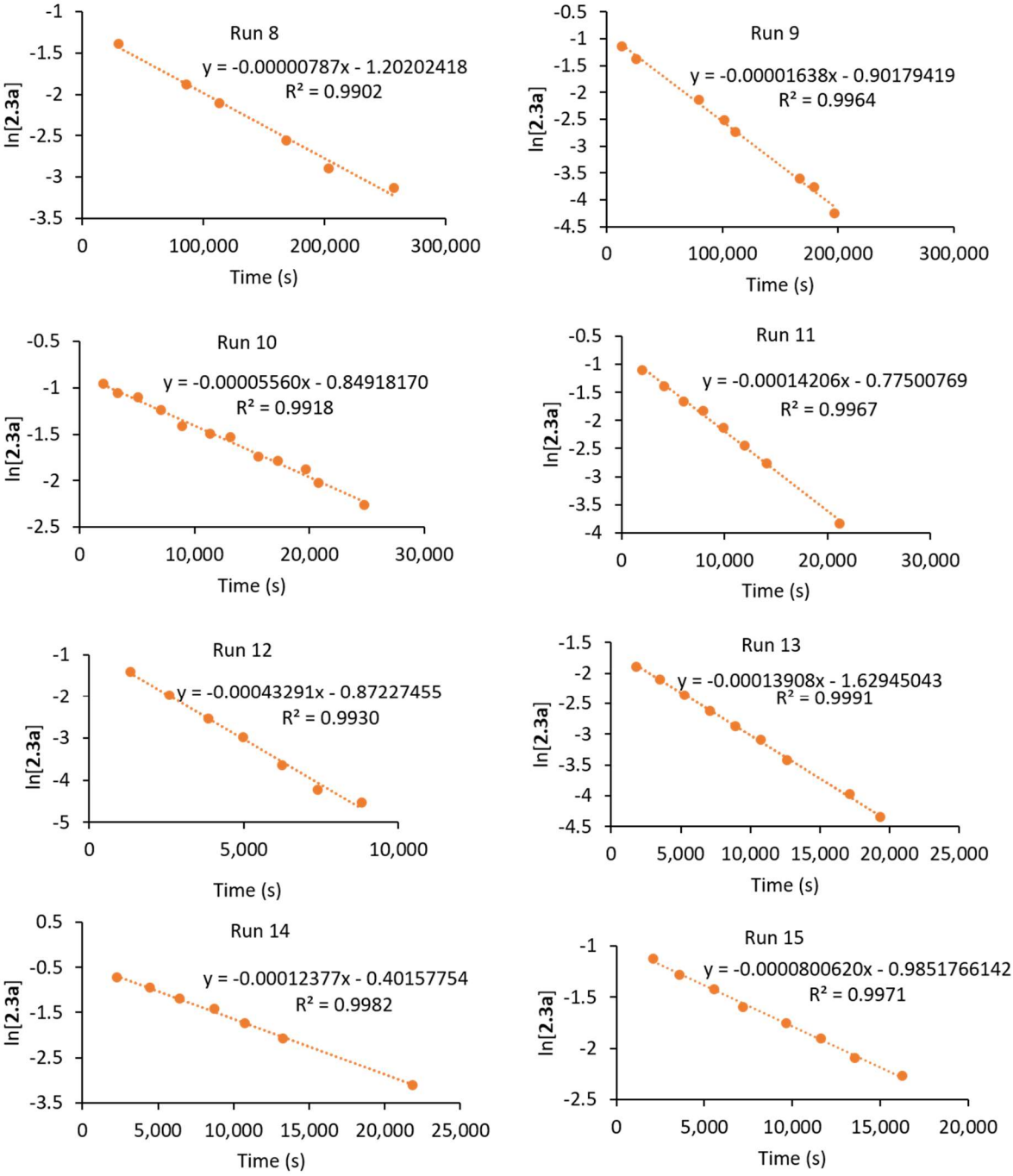

Figure S2.27 Plot of ln[**2.3a**] with reaction time for runs 8 – 15 from Table S2.2 (*y* = ln[**2.3a**], *x* = time (s)).

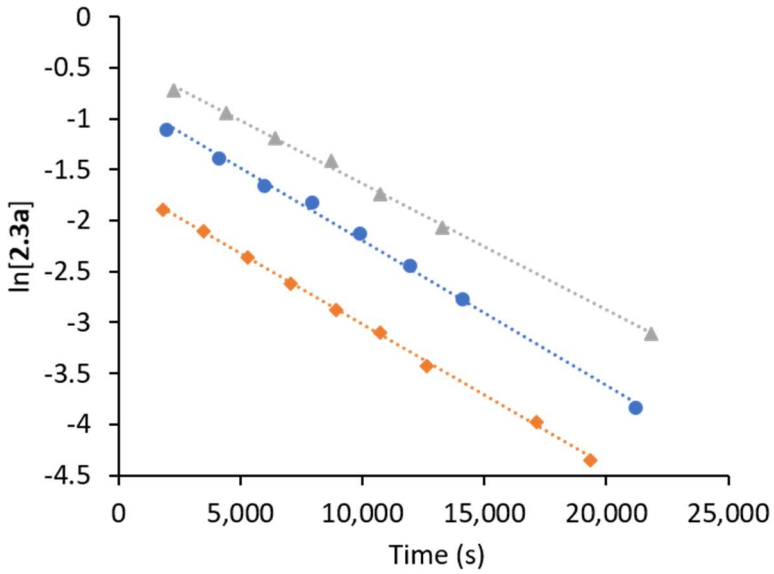

Figure S2.28 Plot of ln[**2.3a**] with reaction time for runs 11 ([**2.3a**] = 0.5 M, blue circles), 13 ([**2.3a**] = 0.3 M, orange diamonds) and 14 ([**2.3a**] = 0.7 M, grey triangles) from Table S2.2. The calculation of equivalent half-lives for different initial concentration of **2.3a** using Supplementary Equations 1 and 2 indicates unimolecular first order kinetics.

$$\ln[\mathrm{A}] = -kt + \ln[\mathrm{A}]_0 \quad (1)$$

$$t\left(\frac{1}{2}\right) = \frac{\ln(2)}{k} \quad (2)$$

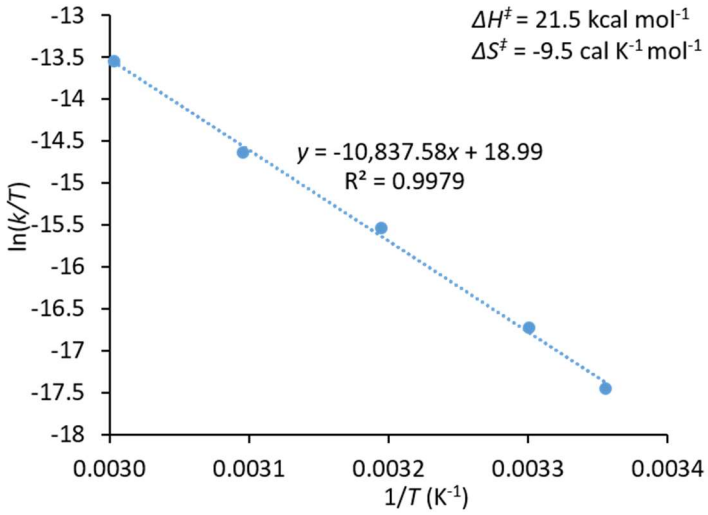

Figure S2.29 Eyring plot using data from runs 8 -12 from Table S2.2 used to calculate values for $\Delta H^{\ddagger}$ and $\Delta S^{\ddagger}$ using Supplementary Equations 3-6 ($\Delta H^{\ddagger}$ = 21.5 kcal mol^{-1}, $\Delta S^{\ddagger}$ = -9.5 K^{-1} mol^{-1}). (y = ln[**2.3a**], x = time (s)).

$$k = \frac{k_B T}{h} e^{\frac{-\Delta H^{\ddagger}}{RT}} e^{\frac{\Delta S^{\ddagger}}{R}} \quad (3)$$

$$\ln\left(\frac{k}{T}\right) = \frac{-\Delta H^{\ddagger}}{RT} + \ln\left(\frac{k_B}{h}\right) + \frac{\Delta S^{\ddagger}}{R} \quad (4)$$

$$\text{Gradient} = \frac{-\Delta H^{\ddagger}}{R} (5)$$

$$\text{Intercept} = \ln\left(\frac{k_B}{h}\right) + \frac{\Delta S^{\ddagger}}{R} (6)$$

2.5.4.2 DFT calculations

Density functional theory (DFT) calculations were carried out with the Gaussian 09 program package[50] using the hybrid exchange-correlation function PBE0[51,67] in combination with the split-valence double-ζ basis set 6-31+G(d,p).[52,68–72] All *N*-heterocyclic compounds were calculated using *N*-phenyl model systems. Optimisations were carried out with tight convergence criteria and pruned (99,590) grids[73] were used for numerical integrations. Solvents [THF (ε = 7.4257) and toluene (ε = 2.3741)] were accounted for during the optimisations with the polarisable continuum model (PCM) using the integral equation formalism variant (IEFPCM).[74–77] Initial guesses for transition states were obtained by relaxed potential energy surface scans along major reaction coordinates. All stationary points were identified as minima or transition states by analytical vibrational frequency calculations. Transition states were confirmed to interconnect precursors and products by reverse and forward internal reaction coordinate (IRC) scans.[78,79] Standard Gibbs free energies are reported with thermal and zero-point energy corrections.

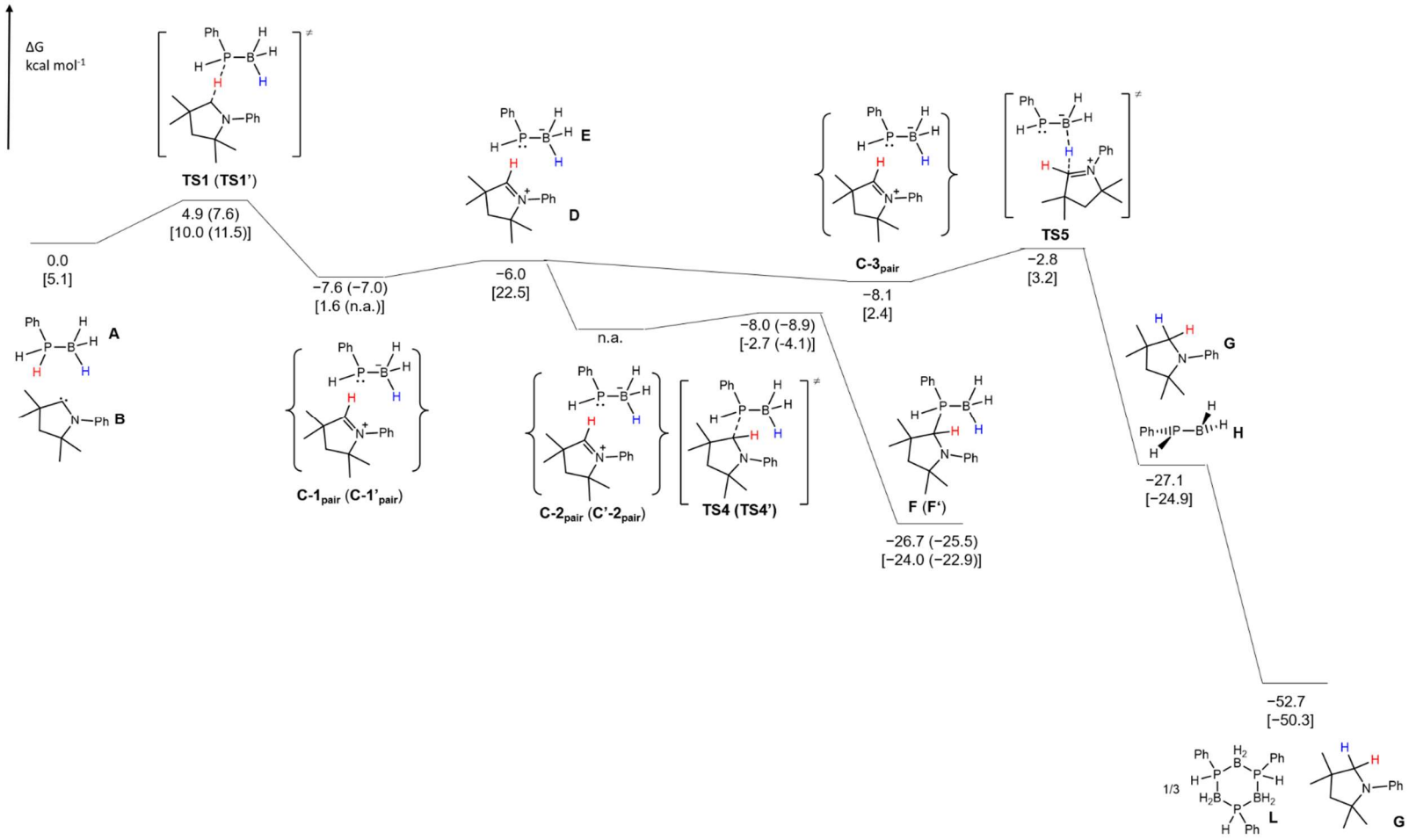

Figure S2.30 Schematic Gibbs energy profile for the P–H activation of $PhPH_2{\cdot}BH_3$ (**A**) with CAAC (**B**) and subsequent reaction steps; standard Gibbs free energies are given in kcal mol^{-1} relative to those of **A** and **B** in THF; Gibbs free energies for toluene as solvent are given in square brackets.

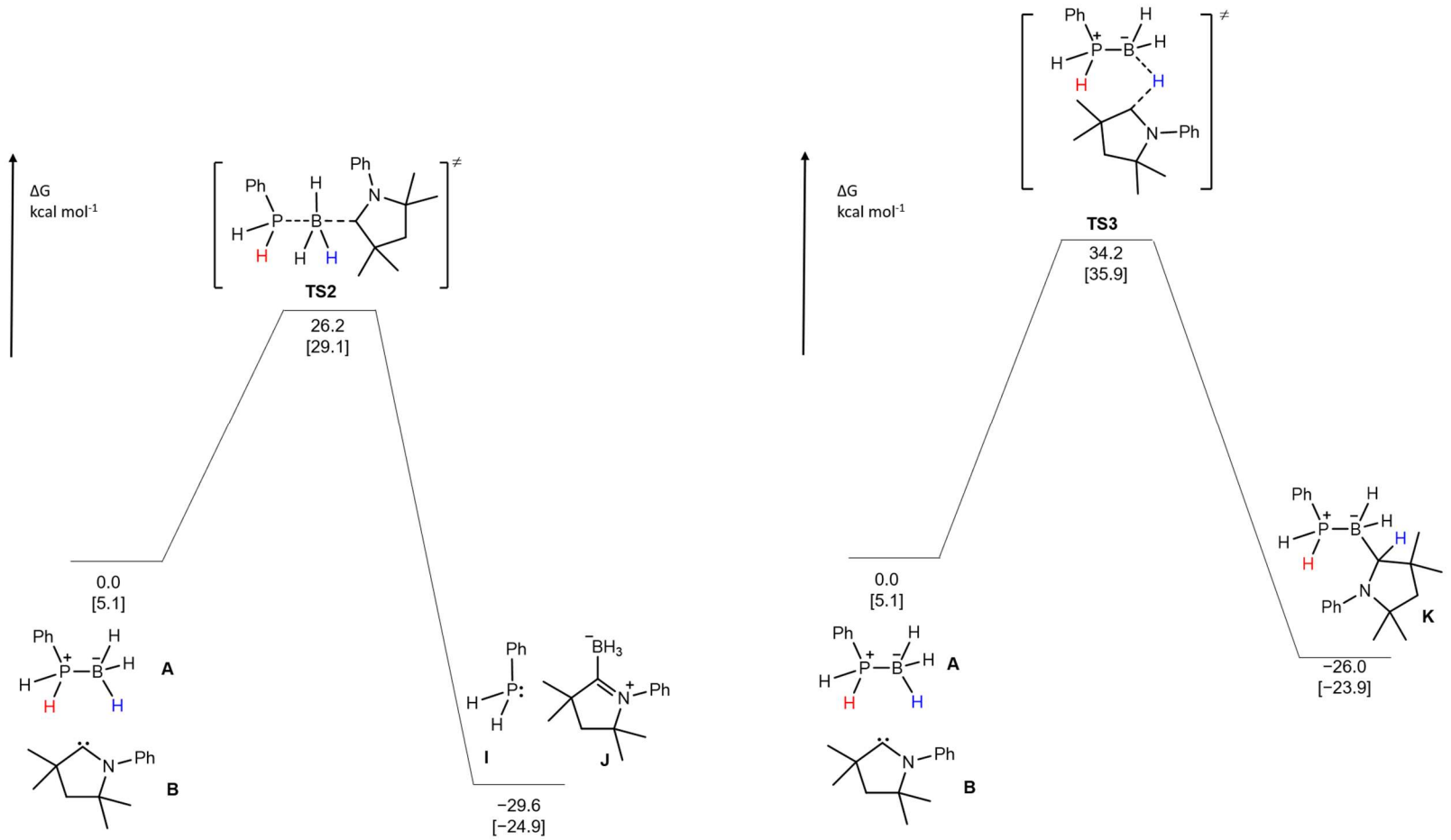

Figure S2.31 Schematic Gibbs energy profiles for substitution at boron (left) and B–H activation from CAAC (**B**) and $PhPH_2 \cdot BH_3$ (**A**) (right); standard Gibbs free energies are given in kcal mol^{-1} relative to those of **A** and **B** in THF; Gibbs free energies for toluene as solvent are given in square brackets.

Table S2.3 Optimised minimum structures and transition states with their imaginary frequencies in THF; standard Gibbs free energies are given below the structures in kcal mol^{-1} relative to the sum of the Gibbs free energies of **A** and **B** in THF; Gibbs free energies and imaginary frequencies for toluene as solvent are given in square brackets.

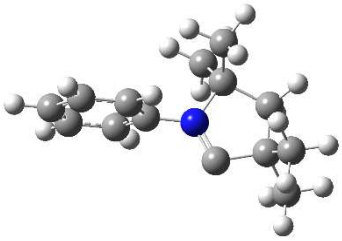	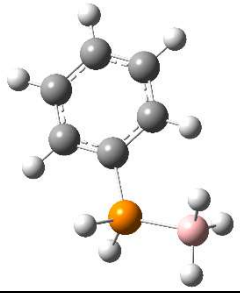	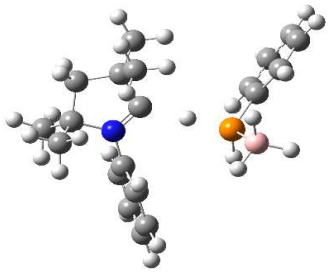
A	**B**	**TS1**, −426 [−677] cm^{-1}
0.0 [5.1]		4.9 [10.0]
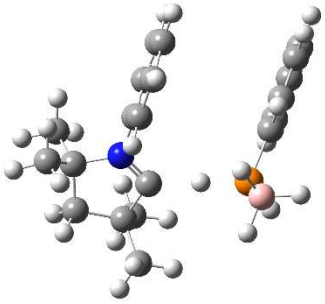	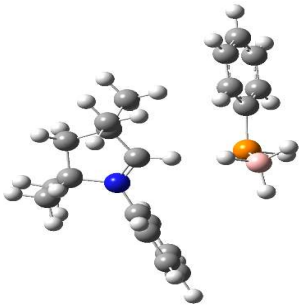	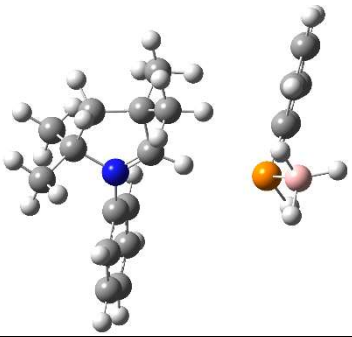
TS1', −446 [−695] cm^{-1}	**C-1$_{pair}$**	**C-1'$_{pair}$**
7.6 [11.5]	−7.6 [1.6]	−7.0 [n.a.][a]
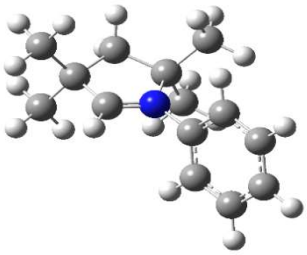	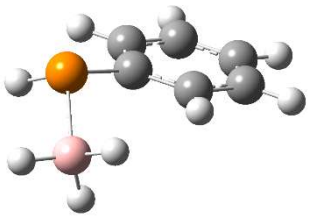	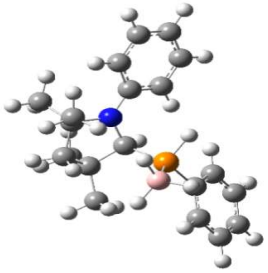
D	**E**	**F**
−6.0 [22.5]		−26.7 [−24.0]
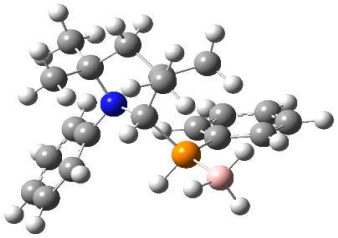	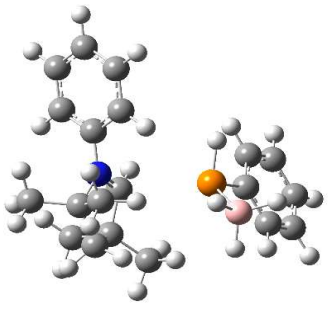	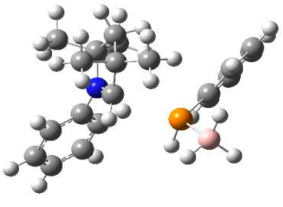
F'	**TS4**, −91.3 [−96.5] cm^{-1}	**TS4'**, −122.5 [−120.2] cm^{-1}
−25.5 [−22.9]	−8.0 [−2.7]	−8.9 [−4.1]

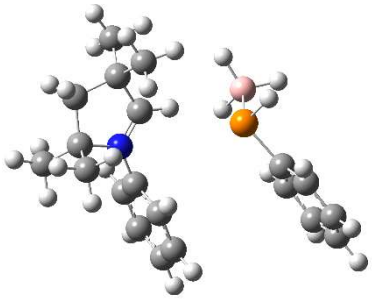	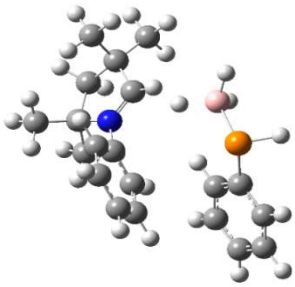	
C-3$_{pair}$	**TS5**, −181 [−70] cm^{-1}	
−8.1 [2.4]	−2.8 [3.2]	
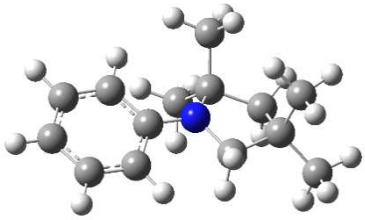	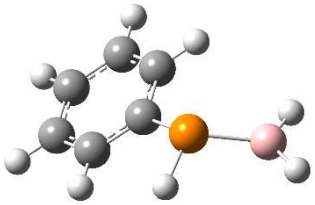	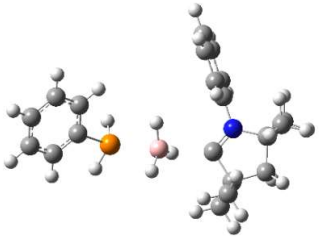
G	**H**	**TS2**, −404 [−390] cm^{-1}
−27.1 [−24.9]		26.2 [29.1]
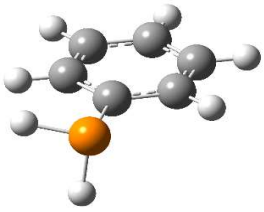	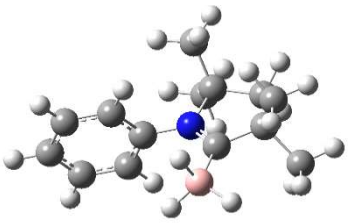	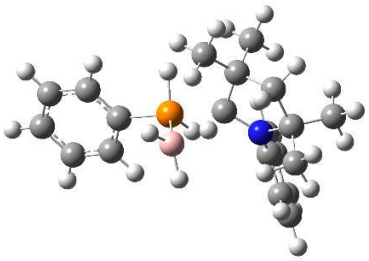
I	**J**	**TS3**, −219 [−194] cm^{-1}
−29.6 [−24.9]		34.2 [35.9]
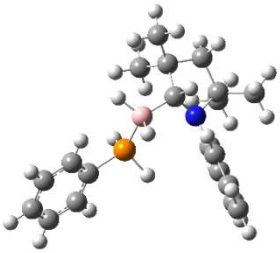	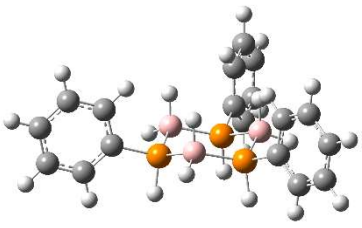	
K	**L**	
−26.0 [−23.9]	−52.7 [−50.3][b]	

[a] Structural optimisation of **C-1'$_{pair}$** in toluene was unsuccessful, [b]the Gibbs free energies for the formation of **L** were calculated using the formula $\Delta G^0 = [1/3 \cdot \Delta G^0(\mathbf{L}) + \Delta G^0(\mathbf{G})] - [\Delta G^0(\mathbf{A})_{THF} - \Delta G^0(\mathbf{B})_{THF}]$.

Table S2.4 Calculated isodesmic reaction between $[CAAC(H)]^+$ and $(NHC)H_2$; Gibbs free energies are given below the structures in kcal mol^{-1} in the gas phase.

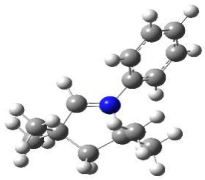	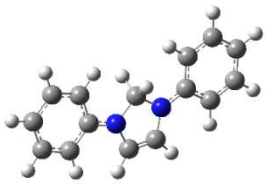	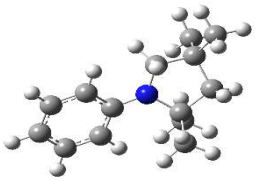	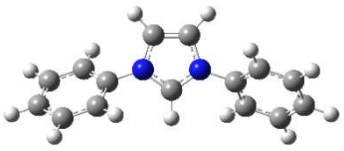
$[CAAC(H)]^+$	$NHC\text{-}H_2$	$CAAC\text{-}H_2$	$[NHC(H)]^+$
0.0		−66.8	

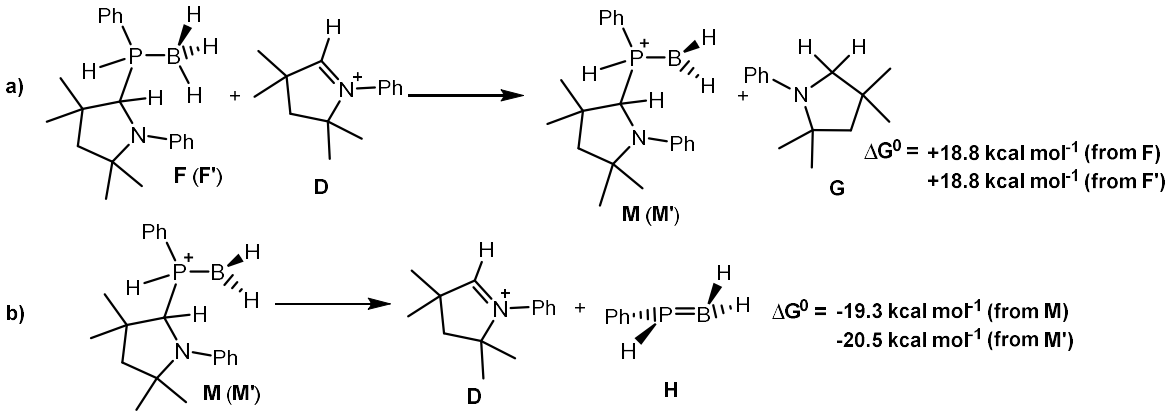

Figure S2.32 Schemes depicting the intermolecular hydride abstraction pathway: a) intermolecular hydride abstraction from **F** (**F'**) by the $[CAAC(H)]^+$ (**D**) iminium ion leading to a phosphinoborenium ion **M** (**M'**) and $CAAC(H_2)$ (**G**) and b) subsequent conversion of **M** (**M'**) to **D** and phosphinoborane $[PhHP–BH_2]$ (**H**); standard Gibbs free energies are given in THF.

Table S2.5 Optimised minimum structures of **M** and **M**'.

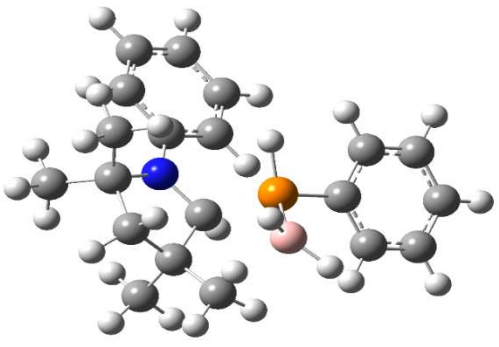	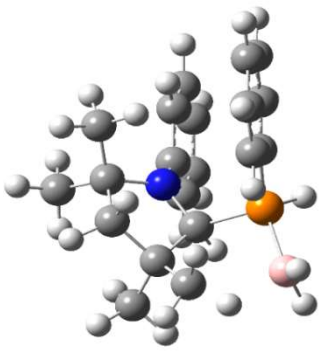
M	**M'**

2.5.4.3 Reaction of CAAC^{Me} with H_2 at ca. 4 atm

CAAC^{Me} (86 mg, 0.30 mmol) was dissolved in C_6D_6 (1.50 mL) in a vial and 0.50 mL of this solution was transferred to a J. Young NMR tube. The solution was degassed through freeze-pump-thaw cycles prior to adding H_2 (1 atm) whilst chilling at -196 °C using liquid nitrogen. Upon thawing no dihydrogen activation was observed using ^{1}H NMR spectroscopy either at 22 °C or upon heating to 60 °C for 24 h.

2.5.5 Polymerisation attempts of P-disubstituted phosphine-boranes using CAAC^{Me} and CAAC^{Cy}

2.5.5.1 Synthesis of 2.3b

Method A

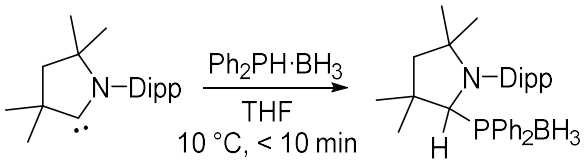

2.3b

$Ph_2PH{\cdot}BH_3$ (500 mg, 2.50 mmol) and CAAC^{Me} (714 mg, 2.50 mmol) were dissolved in THF (2 mL) in a J. Young Schlenk tube and immediately at 22 °C a white precipitate was observed. After ten min the solution became homogeneous. Similar to the case of compound **2.3a**, isolation of compound **2.3b** has not been achieved due to significant polymerisation occurring immediately at 22 °C.

It is proposed that the initial precipitate is due to initial deprotonation of the phosphine-borane to form ionic [CAAC^{Me}H][Ph_2PBH_3], as is observed in the reaction between $PhRPH{\cdot}BH_3$ (R = H or Ph) and IDipp, prior to the formation of the neutral molecular species by cation-anion recombination.

Method B

2.3b can also be synthesised through a stepwise procedure

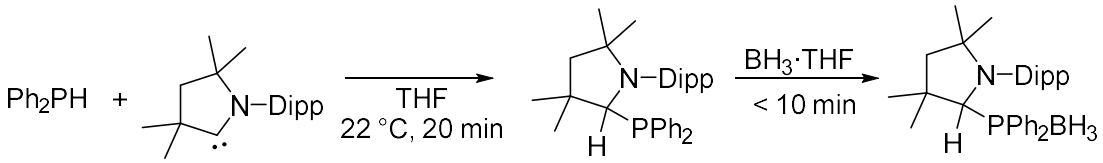

2.2b **2.3b**

Ph_2PH (250 mg, 1.34 mmol) was added to a solution of CAAC^{Me} (383 mg, 1.34 mmol) in THF (1 mL) in a J. Young Schlenk tube, the vessel was sealed and stirred for 20 min at 22 °C. $BH_3{\cdot}THF$ (1.34 mL of a 1M in THF solution, 1.34 mmol) was added and the reaction mixture was stirred for 10 min before ^{11}B and ^{31}P NMR spectra were recorded.

Method C

3b was also independently synthesised through a salt metathesis reaction

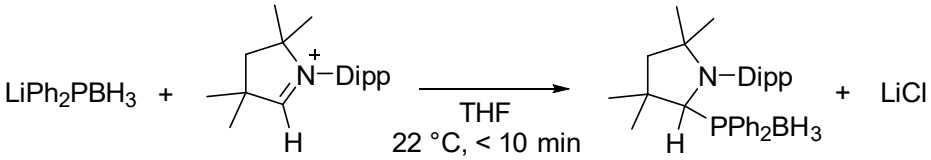

2.3b

$LiPh_2PBH_3$ (15 mg, 0.073 mmol) and [CAAC^{Me}H]Cl (23 mg, 0.07 mmol) were dissolved in THF (0.5 mL) in a quartz J. Young NMR tube. Immediate conversion to the products was observed and the identity confirmed using ^{11}B and ^{31}P NMR spectroscopy. No purification of the product formed from this method was carried out.

^{11}B NMR (96 MHz, 295 K, THF): δ = -39.1 (br).

^{31}P NMR (122 MHz, 295 K, THF): δ = 10.9 (br).

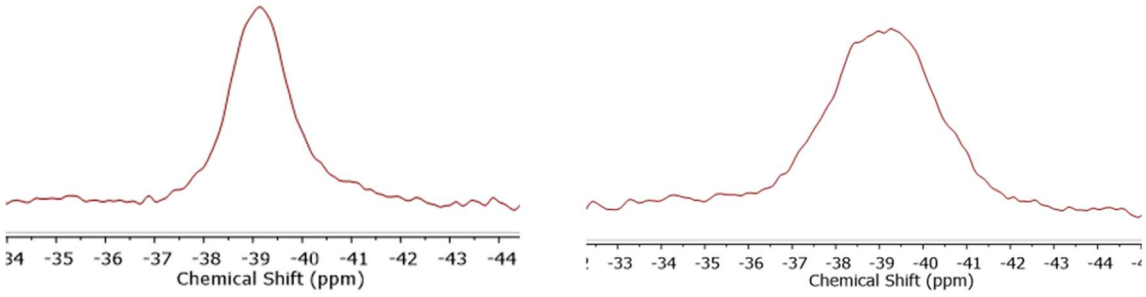

Figure S2.33 ^{11}B{^{1}H} (left) and ^{11}B (right) NMR spectra (96 MHz, 295 K, THF) of **2.3b**.

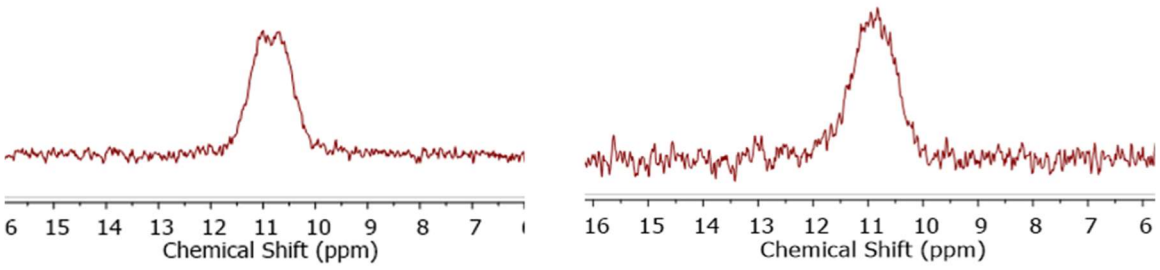

Figure S2.34 ^{31}P{^{1}H} (left) and ^{31}P (right) NMR spectra (122 MHz, 295 K, THF) of **2.3b**.

2.5.5.2 Dehydropolymerisation of $Ph_2PH{\cdot}BH_3$

Method A

CAAC^{Me} in THF

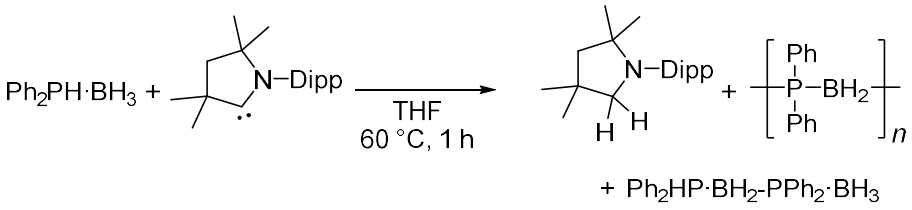

$Ph_2PH{\cdot}BH_3$ (500 mg, 2.50 mmol), CAAC^{Me} (714 mg, 2.50 mmol) and THF (1 mL) were added to a J. Young Schlenk and heated as a closed system at 60 °C for 1 h. ^{31}P NMR spectroscopy of the crude reaction mixture showed the formation of $Ph_2PH{\cdot}BH_2{-}PPh_2{\cdot}BH_3$ (~ 25%) and $[Ph_2P{-}BH_2]_n$ (Figure 2.3). The simultaneous formation of cyclic oligomers of the form $[Ph_2P{-}BH_2]_x$ cannot be unambiguously ruled out as the phosphorus and boron chemical shifts coincide with those of the internal atoms of the linear dimer. The reaction mixture was added dropwise into 20 mL of rapidly stirred cold hexanes at -40 °C yielding a precipitate and the supernatant was decanted. The precipitation was repeated twice more prior to drying *in vacuo* to leave a white powder which by ^{11}B and ^{31}P NMR analysis was determined to be a mixture of $Ph_2PH{\cdot}BH_2{-}Ph_2P{\cdot}BH_3$ (~35%) and $[Ph_2P{-}BH_2]_n$ (Figure 2.3). Attempts to separate the product further by precipitation into acetonitrile, or through washing with diethyl ether were unsuccessful. GPC analysis showed only a very small amount of high molar mass material which it was not possible to analyse. Yield (precipitated material) = 260 mg (52%).

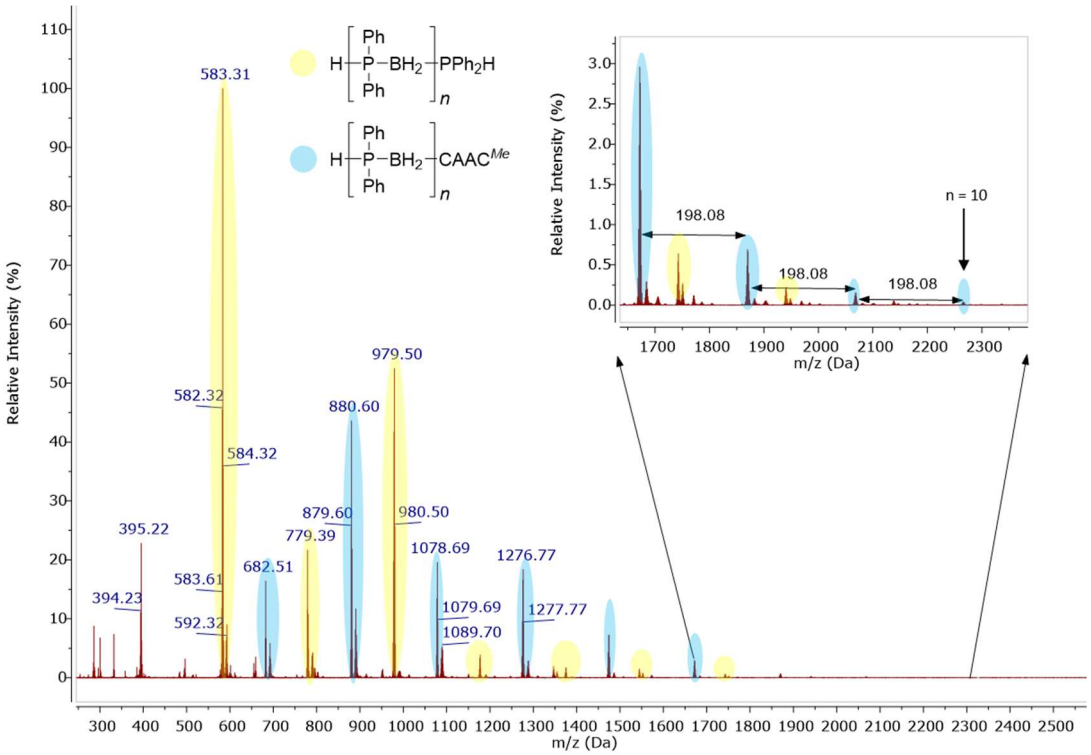

Figure S2.35 ESI(+)-MS spectrum in positive mode of unseparated $[Ph_2P–BH_2]_n$ and $Ph_2PH{\cdot}BH_2–PPh_2{\cdot}BH_3$ (m/z = 398.2) formed from $Ph_2PH{\cdot}BH_3$ and CAAC^{Me} in THF. The species highlighted in yellow is a linear system with a PPh_2H end group $(H\text{-}[Ph_2P–BH_2]_n\text{-}PPh_2H)^+$ and the species highlighted in blue is a linear system with a CAAC^{Me} end group $(H\text{-}[Ph_2P–BH_2]_n\text{-CAAC}^{Me})^+$.

<u>Method B</u>

CAAC^{Me} in toluene

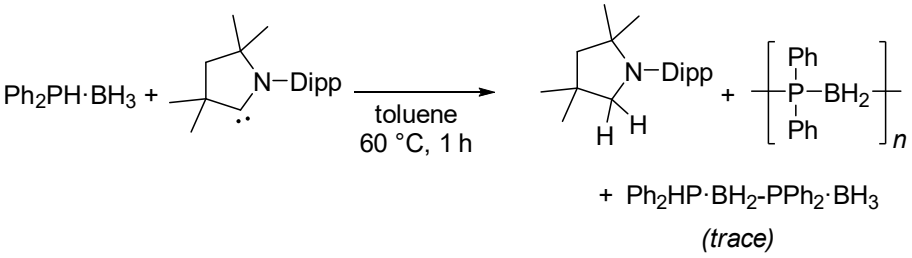

$Ph_2PH{\cdot}BH_3$ (200 mg, 1.00 mmol), CAAC^{Me} (285 mg, 1.00 mmol) and toluene (400 µL) were added to a J. Young NMR tube and heated in a closed system at 60 °C for 1 h. ^{31}P NMR spectroscopy of the crude reaction mixture showed the formation of $Ph_2PH{\cdot}BH_2–PPh_2{\cdot}BH_3$ (~ 8%) and $[Ph_2P–BH_2]_n$ (Figure 2.3). The reaction mixture was added dropwise into 20 mL of rapidly stirred cold hexanes at -40 °C yielding a precipitate and the supernatant was decanted. The precipitation was repeated twice more prior to drying in vacuo to leave a white powder. GPC analysis showed a bimodal distribution with a small amount (ca. 10%) of high molar mass material (Figure S2.37). Yield (precipitated material) = 26 mg (25%).

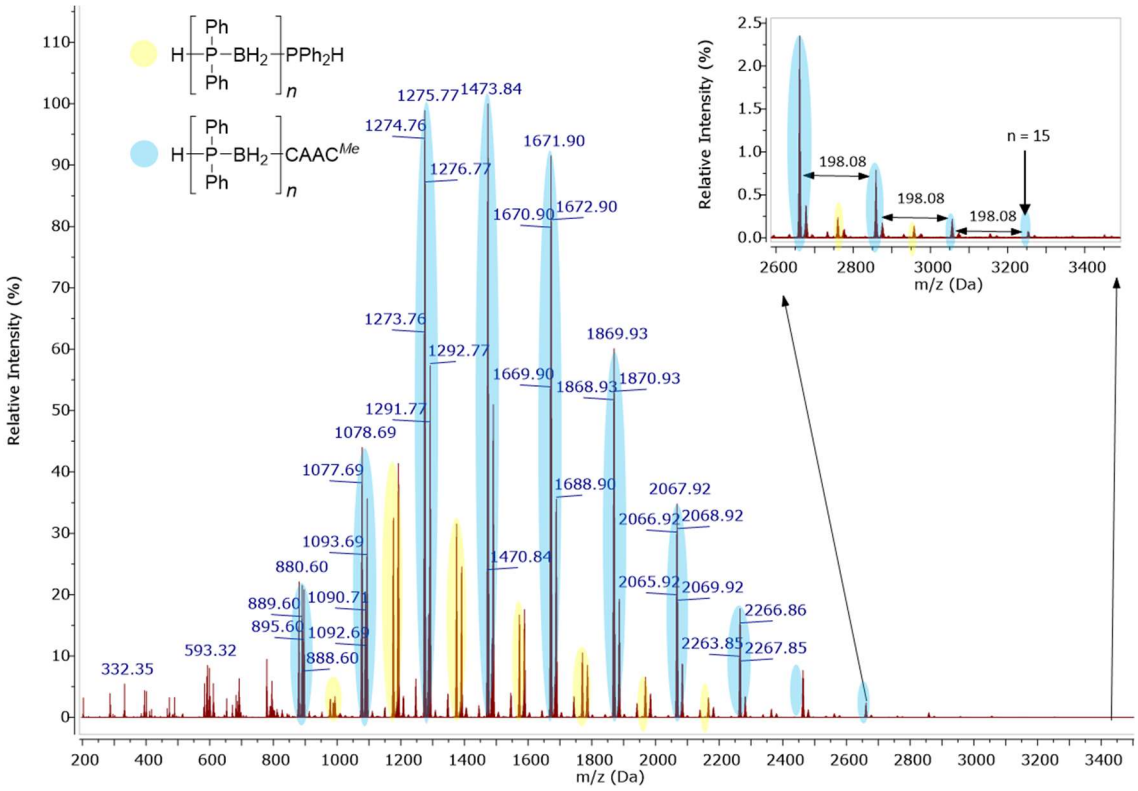

Figure S2.36 ESI(+)-MS spectrum in positive mode of $[Ph_2P–BH_2]_n$ formed from $Ph_2PH·BH_3$ and CAAC^{Me} in toluene. The species highlighted in yellow is a linear system with a PPh_2H end group $(H-[Ph_2P–BH_2]_n-PPh_2H)^+$ and the species highlighted in blue is a linear system with a CAAC^{Me} end group $(H-[Ph_2P–BH_2]_n-CAAC^{Me})^+$.

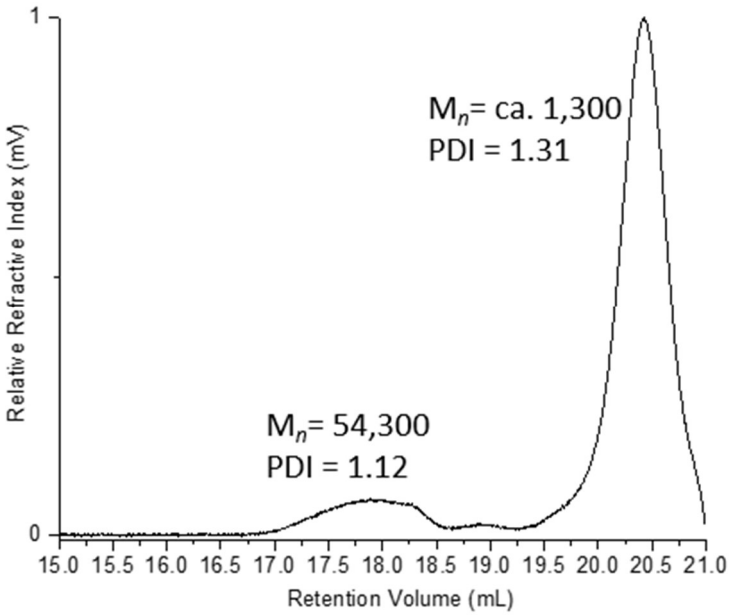

Figure S2.37 GPC chromatogram of $[Ph_2P–BH_2]_n$ formed from $Ph_2PH·BH_3$ and CAAC^{Me} in toluene. 2 mg mL^{-1} in THF with 0.1 w/w% nBu$_4$NBr in the THF eluent. The highest molar mass peak accounts for ca. 10% of the precipitated material. The bimodal distribution can be explained by the competition between chain termination and propagation. Most of the material undergoes early termination, potentially by addition of a free CAAC^{Me} unit as evidenced in the ESI-MS, whereas a small percentage of the material undergoes significant further polymerisation to give high molar mass material.

Method C

CAAC^{Cy} in toluene

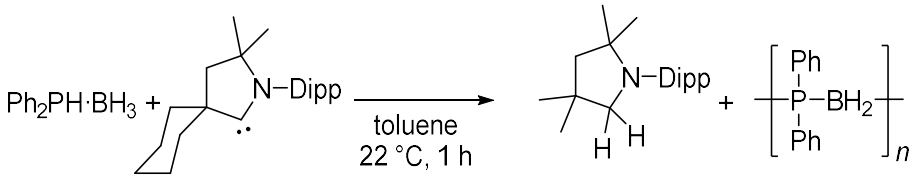

$Ph_2PH{\cdot}BH_3$ (200 mg, 1.00 mmol), CAAC^{Cy} (325mg, 1.00 mmol) and toluene (400 µL) were added to a J. Young NMR tube. After 1 h at 22 °C ^{31}P NMR spectroscopy of the crude reaction mixture showed the complete consumption of $Ph_2PH{\cdot}BH_3$ and formation of $[Ph_2P–BH_2]_n$ (Figure 2.3). The reaction mixture was added dropwise into 20 mL of rapidly stirred cold hexanes at -40 °C yielding a precipitate and the supernatant was decanted. The precipitation was repeated twice more prior to drying in vacuo to leave an off-white powder. GPC analysis showed a bimodal distribution with a small amount (ca. 12%) of high molar mass material (Figure S2.38). Yield (precipitated material) = 95 mg (48%).

An attempt to further separate the high molar mass component observed in the GPC chromatogram from lower mass oligomers was made. The material was dissolved in THF (5 mL) and a small quantity of hexanes (5 mL) added until some material precipitated. The supernatant was removed to leave fraction A. The process was repeated, adding further 5 mL portions of hexanes to the supernatant each time, to give three further fractions of product. The results of this separation attempt are reported below and show that isolation of the pure high molar mass fraction was unsuccessful, although some fractionation was possible.

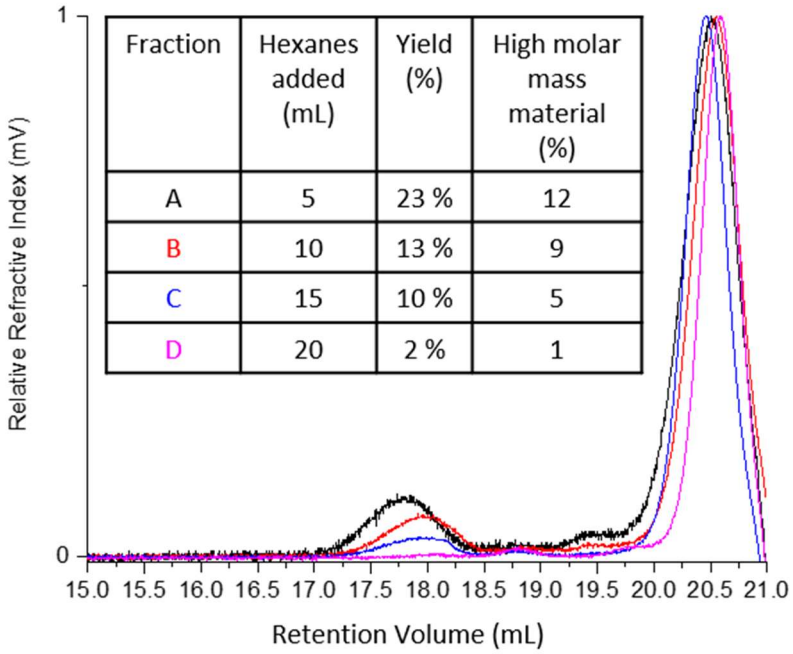

Fraction	Hexanes added (mL)	Yield (%)	High molar mass material (%)
A	5	23 %	12
B	10	13 %	9
C	15	10 %	5
D	20	2 %	1

Figure S2.38 GPC chromatograms of the separation attempts of the $[Ph_2P–BH_2]_n$ formed from $Ph_2PH{\cdot}BH_3$ and $CAAC^{Cy}$ in toluene. 2 mg mL^{-1} in THF with 0.1 w/w% nBu$_4$NBr in the THF eluent. The GPC chromatograms have been normalised to the low molar mass material. Although the stepwise precipitation of material does show an increase in the percentage of high molar mass material for the earlier fraction there is still not a significant amount. For Fraction A M_n = 59,600 and $Đ$ = 1.08; however, since the standard used for the calibration of the GPC instrument is polystyrene $[PhCHCH_2]_n$, the intrinsic values shown here may not be accurate especially as the presence of a second phenyl group will most likely reduce the amount of coiling of the polymer chains in solution.

NMR data is given for Fraction A

^{1}H NMR (400 MHz, 298 K, $CDCl_3$): δ = 7.50- 6.50 (m, br, Ar), 2.85 – 0.25 (m, br, BH_2).

^{11}B NMR (96 MHz, 295 K, $CDCl_3$): δ = -30.4 (br).

^{31}P NMR (122 MHz, 295 K, $CDCl_3$): δ = -15.2, -16.6 (br).

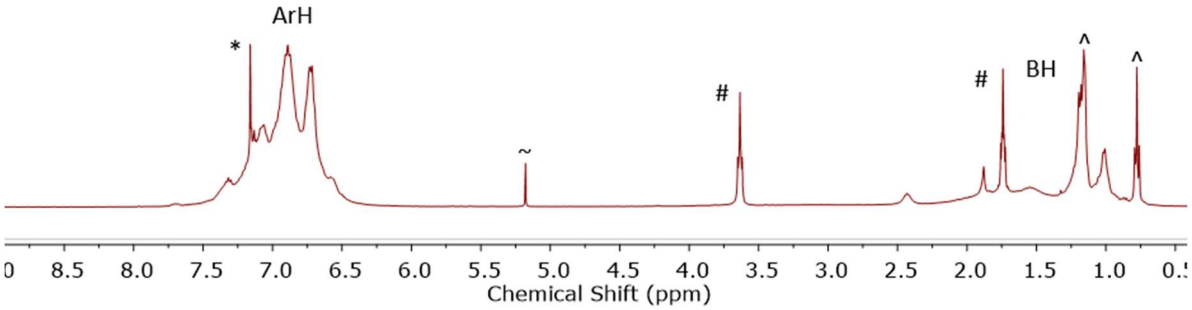

Figure S2.39 ^{1}H NMR spectrum (400 MHz, 298 K, $CDCl_3$) of $[Ph_2P–BH_2]_n$ formed from $Ph_2PH{\cdot}BH_3$ and $CAAC^{Cy}$ in toluene (Fraction A) (*denotes partially protiated $CDCl_3$, ~denotes trace DCM, $^{\#}$denotes trace THF, ^denotes trace hexanes).

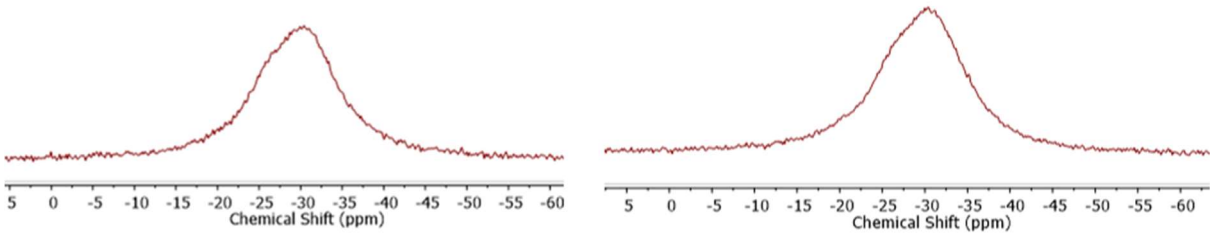

Figure S2.40 $^{11}B\{^{1}H\}$ (left) and ^{11}B (right) NMR spectra (96 MHz, 295 K, $CDCl_3$) of $[Ph_2P–BH_2]_n$ formed from $Ph_2PH{\cdot}BH_3$ and $CAAC^{Cy}$ in toluene. (Fraction A).

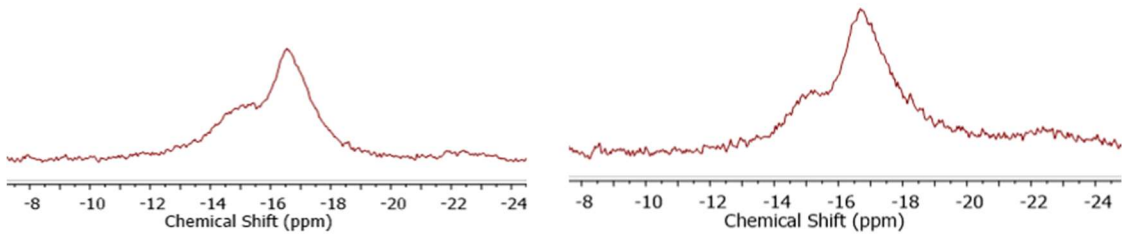

Figure S2.41 $^{31}P\{^{1}H\}$ (left) and ^{31}P (right) NMR spectra (122 MHz, 295 K, $CDCl_3$) of $[Ph_2P–BH_2]_n$ formed from $Ph_2PH{\cdot}BH_3$ and $CAAC^{Cy}$ in toluene. (Fraction A). The observation of two peaks can be explained by the presence of both oligomeric and polymeric material, as is observed in the GPC chromatogram.

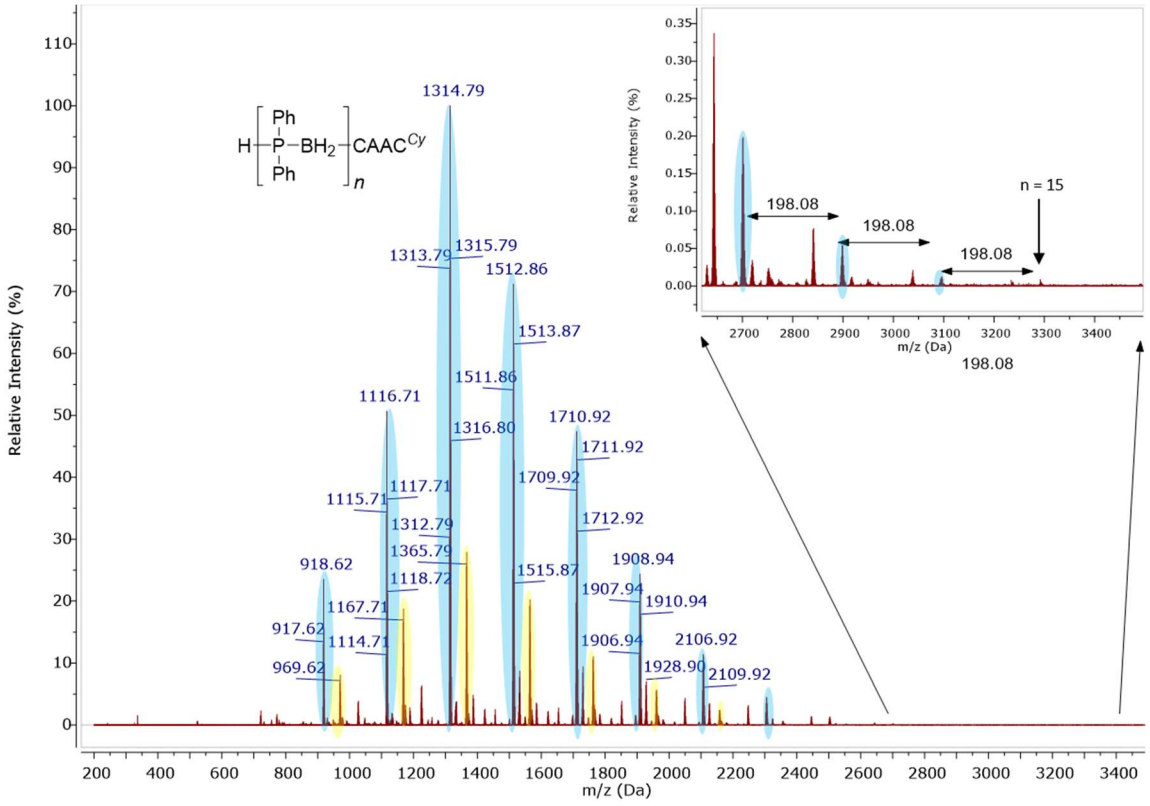

Figure S2.42 ESI(+)-MS spectrum in positive mode of $[Ph_2P–BH_2]_n$ formed from $Ph_2PH{\cdot}BH_3$ and $CAAC^{Cy}$ in toluene (Fraction A). The species highlighted in blue is a linear system with a $CAAC^{Cy}$ end group $(H\text{-}[Ph_2P–BH_2]_n\text{-}CAAC^{Cy})^+$ and the species highlighted in yellow is a linear system with an unidentified end group (m/z of end group = 178.3).

Figure S2.43 Photograph of $[Ph_2P–BH_2]_n$ (Fraction A).

2.5.5.3 Synthesis of 2.3c

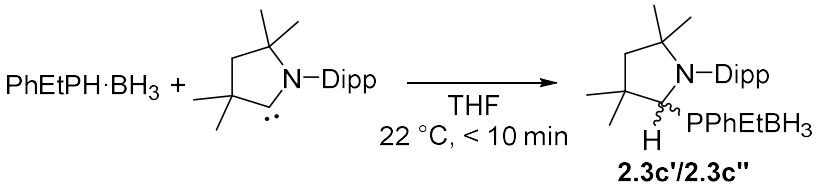

rac-PhEtPH·BH_3 (50 mg, 0.33 mmol) and CAAC^{Me} (94 mg, 0.33 mmol) were dissolved in THF (2 mL) in a J. Young Schlenk tube. Immediate conversion to the product (as two diastereomers **2.3c'** and **2.3c''**) was observed through ^{31}P NMR spectroscopy. The initial ratio of diastereomers observed after 10 min in solution was 1:1.14. Single rystals of **2.3c** suitable for X-ray diffraction of one diastereomer were obtained from layering a THF solution with hexane at -40 °C. Yield = 54 mg (38%).

^{1}H NMR (500 MHz, 295 K, $CDCl_3$): δ = 8.07-7.98 (m, 2H, Ar^{p}), 7.50-7.38 (m, 3H, Ar^{o,m}), 7.20-7.05 (m, 3H, Ar^{Dipp}), 4.51 (d, $^{2}J_{PH}$ = 6.9 Hz, 1H, NC*H*), 4.10 (sept, $^{3}J_{HH}$ = 6.8 Hz, 1H, C*H*(CH_3)$_2$), 3.07 (sept, $^{3}J_{HH}$ = 6.8 Hz, 1H, C*H*(CH_3)$_2$), 2.02, 1.99 (d, $^{2}J_{HH}$ = 213 Hz), 1.48 (d, $^{3}J_{HH}$ = 6.8 Hz, 6H, CH(C*H*$_3$)$_2$), 1.47 (s, 3H, C(CH_3)$_2$), 1.43 (s, 3H, NC(CH_3)$_2$), 1.36 (dm, 2H, PCH_2), 1.33 (d br, 3H, CH(C*H*$_3$)$_2$), 1.28 (d, $^{3}J_{HH}$ = 6.8 Hz, 6H, CH(C*H*$_3$)$_2$), 1.24 (d, $^{3}J_{HH}$ = 6.8 Hz, 6H, CH(C*H*$_3$)$_2$), 1.15 (s br, 3H, C(CH_3)$_2$), 0.91 (s, 3H, NC(CH_3)$_2$), 0.54 (m, 3H, , PCH_2C*H*_3). Unable to assign BH_3 as broad and overlapping other signals.

^{13}C (101 MHz, 298 K, $CDCl_3$): δ = 149.0 (Ar^{Dipp-o}), 146.7 (Ar^{Dipp-o}), 145.4 (Ar^{Dipp-i}), 133.7 (Ar^{m}), 130.8, (Ar^{p}), 127.9 (Ar^{i}), 126.5 (Ar^{Dipp-p}), 126.0 (Ar^{Dipp-m}), 124.4 (Ar^{Dipp-m}), 77.0 (N*C*H), 64.4 (NC(CH_3)$_2$*C*H_2), 43.4 (NCHP*C*(CH_3)$_2$), 32.2 (C(*C*H_3)$_2$), 32.2 (NC(*C*H_3)$_2$), 29.5 (C(*C*H_3)$_2$), 29.0 (NC(*C*H_3)$_2$), 28.6 (*C*H(CH_3)$_2$), 27.6 (*C*H(CH_3)$_2$), 26.7 (CH(*C*H_3)$_2$), 25.4 (CH(*C*H_3)$_2$), 24.5 (CH(*C*H_3)$_2$), 24.4 (CH(*C*H_3)$_2$), 17.2(PCH_2), 6.3 (PCH_2*C*H_3). Data only given for crystallised diastereomer **2.3c'**.

^{11}B NMR (96 MHz, 295 K, $CDCl_3$): δ = -41.0 (br), -42.5 (br) (two diastereomers).

^{31}P NMR (122 MHz, 295 K, toluene): δ = 25.2 (br, **2.3c'**), 21.3 (br **2.3c''**) (two diastereomers).

Elemental analysis for $C_{28}H_{45}BNP$ (calcd/expt): C (76.88/76.38), H (10.37/10.60), N (3.20/3.05).

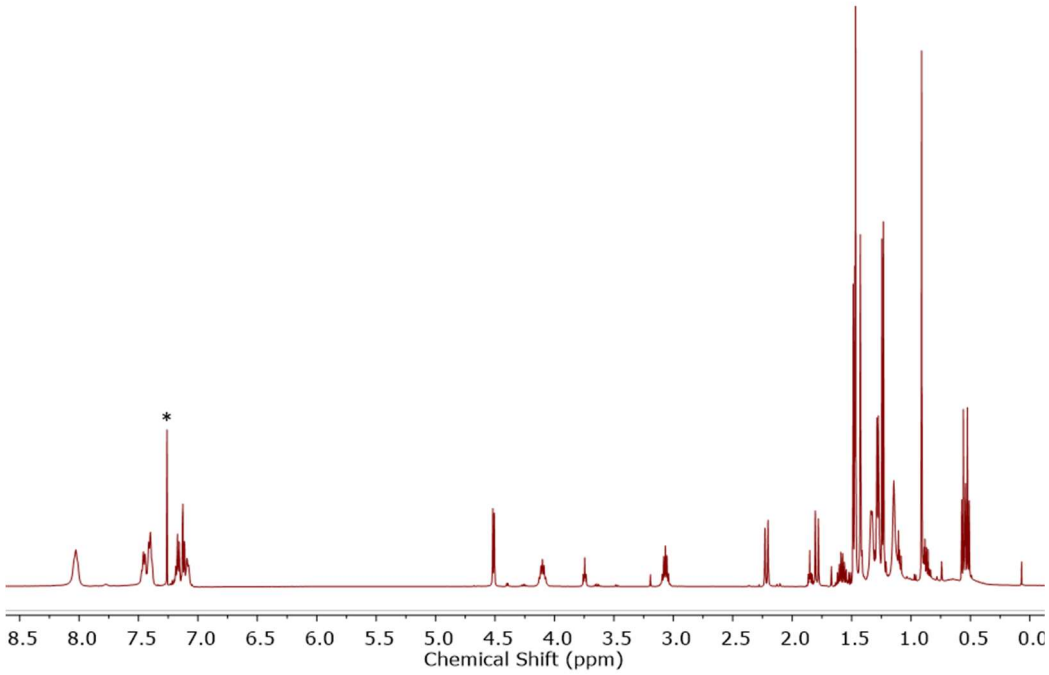

Figure S2.44 ^{1}H NMR spectrum (400 MHz, 298 K, $CDCl_3$) of **2.3c'** (*denotes residual partially protiated $CDCl_3$).

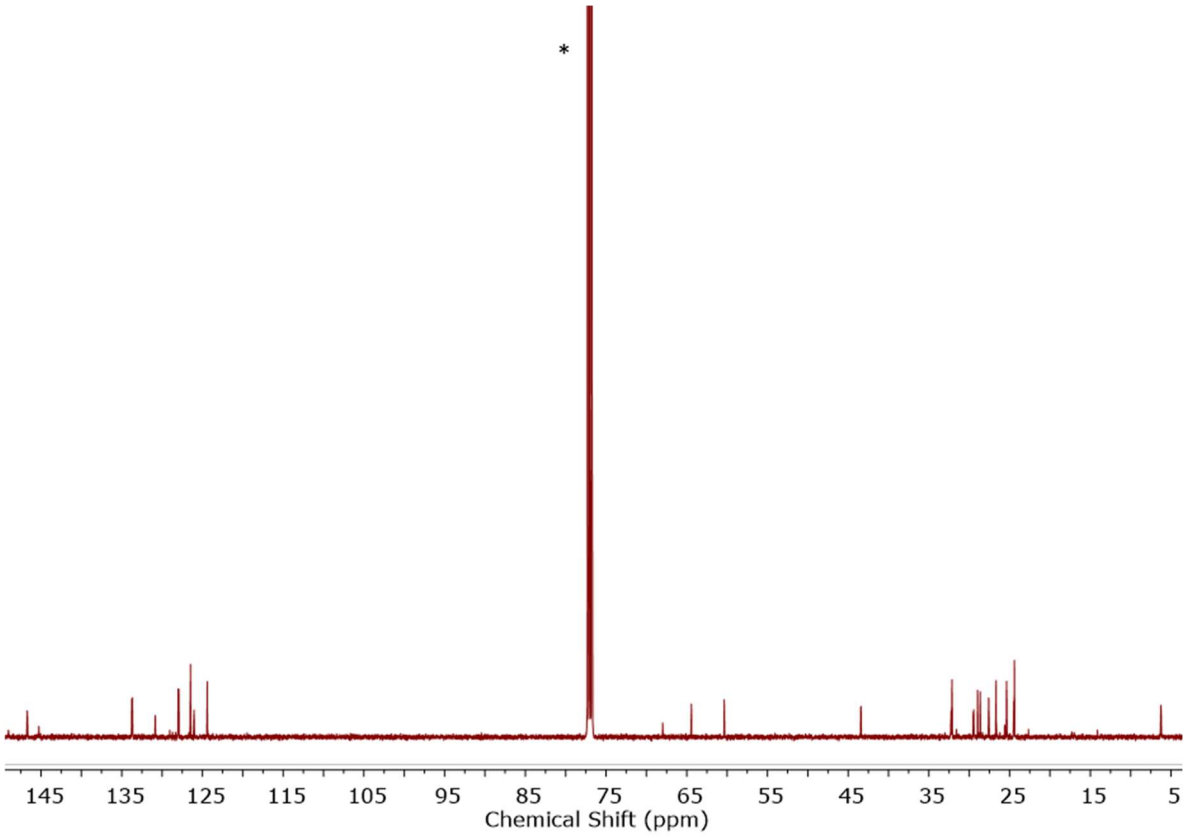

Figure S2.45 ^{13}C NMR spectrum (101 MHz, 298 K, $CDCl_3$) of **3c'** (*denotes $CDCl_3$).

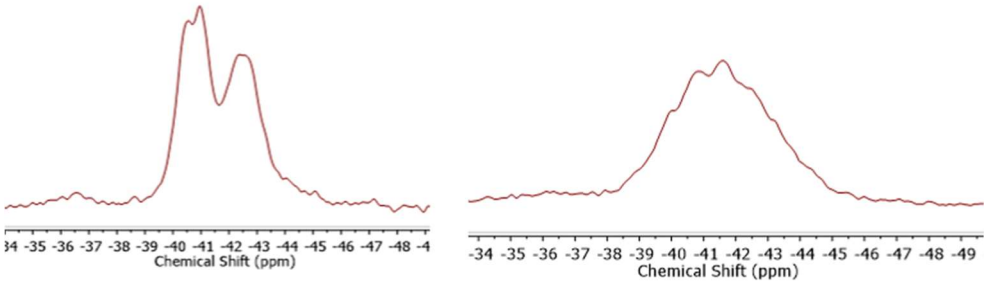

Figure S2.46 $^{11}B\{^{1}H\}$ (left) and ^{11}B (right) NMR spectra (96 MHz, 295 K, THF) of **2.3c**.

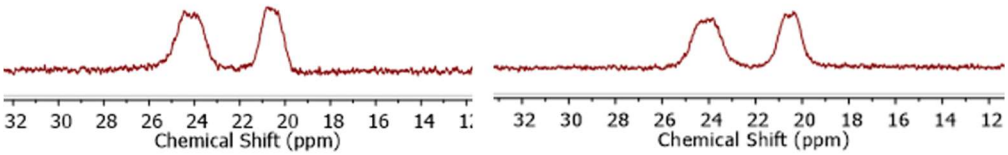

Figure S2.47 $^{31}P\{^{1}H\}$ (left) and ^{31}P (right) NMR spectra (122 MHz, 295 K THF) of **2.3c**.

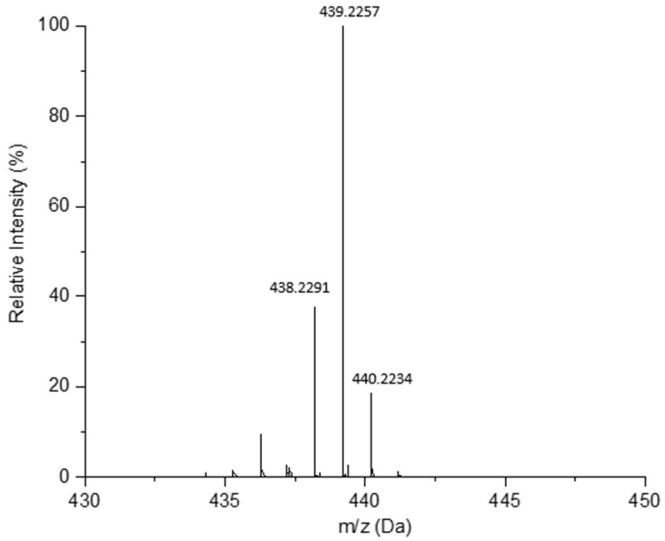

Figure S2.48 ESI(+)-MS spectrum of **2.3c** in DCM showing the [**2.3c**+H]$^{+}$ peak (sample injection performed under ambient conditions in air).

2.5.5.4 Dehydropolymerisation of rac-PhEtPH·BH_3

Method A

CAAC^{Me}-mediated

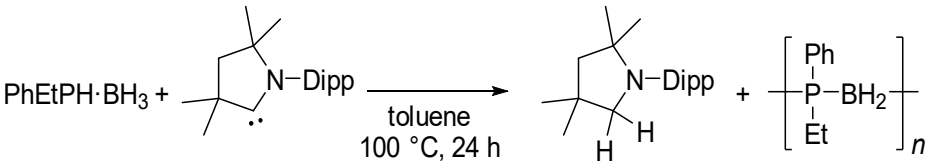

rac-PhEtPH·BH_3 (300 mg, 1.97 mmol) and CAAC^{Me} (564 mg, 1.97 mmol) were dissolved in toluene (1 mL) in a sealed J. Young Schlenk tube and heated at 100 °C for 24 h (60°C requires ca. two weeks for full conversion). The reaction mixture was added dropwise into 20 mL of rapidly stirred cold hexanes at -40 °C yielding a precipitate and the supernatant was decanted. The precipitation was repeated twice more prior to drying in vacuo to leave a white powder. GPC analysis showed no convincing high molecular weight material. Yield (precipitated material) = 67 mg (23%). The low yield is attributed to the loss of low molar mass material during purification.

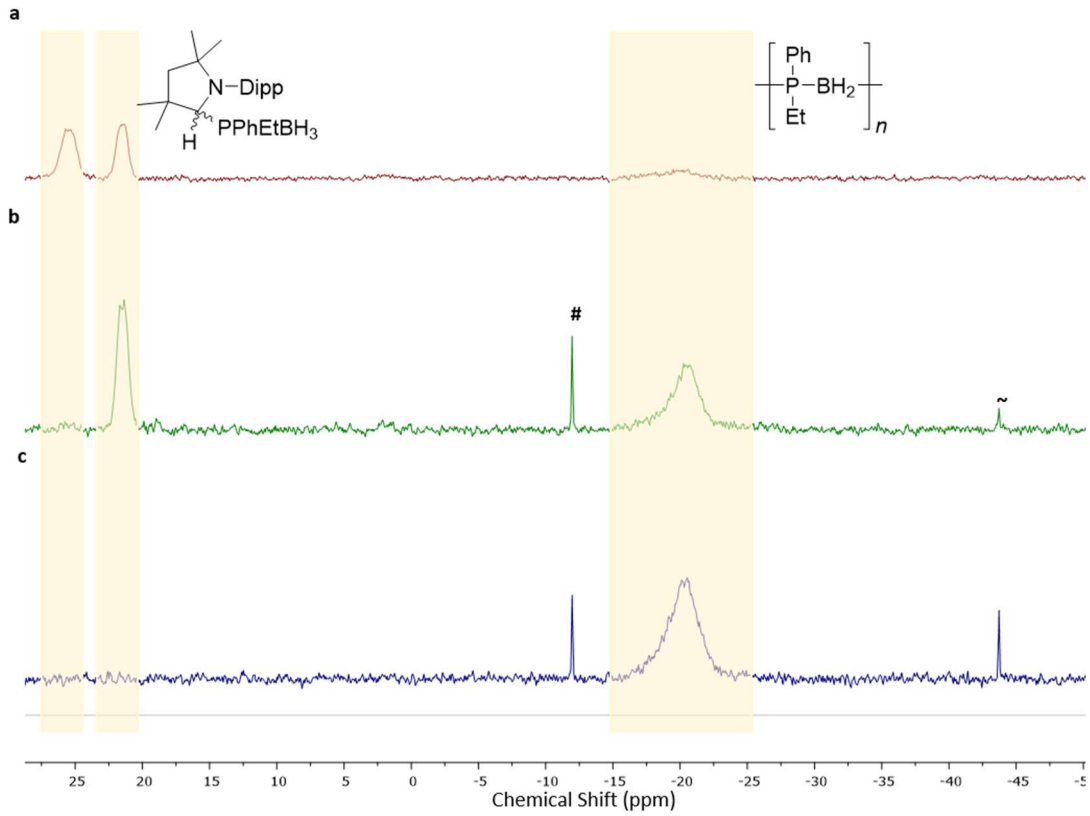

Figure S2.49 $^{31}P\{^1H\}$ NMR spectra (122 MHz, 295 K, toluene) of dehydropolymerisation of *rac*-PhEtPH·BH_3 using CAAC^{Me} over time **a** 10 min at 22 °C; **b** 1 h at 100 °C; and **c** 20 h at 100 °C (#denotes trace CAAC^{Me}(H)(PhEtP), ~denotes trace PhEtPH).

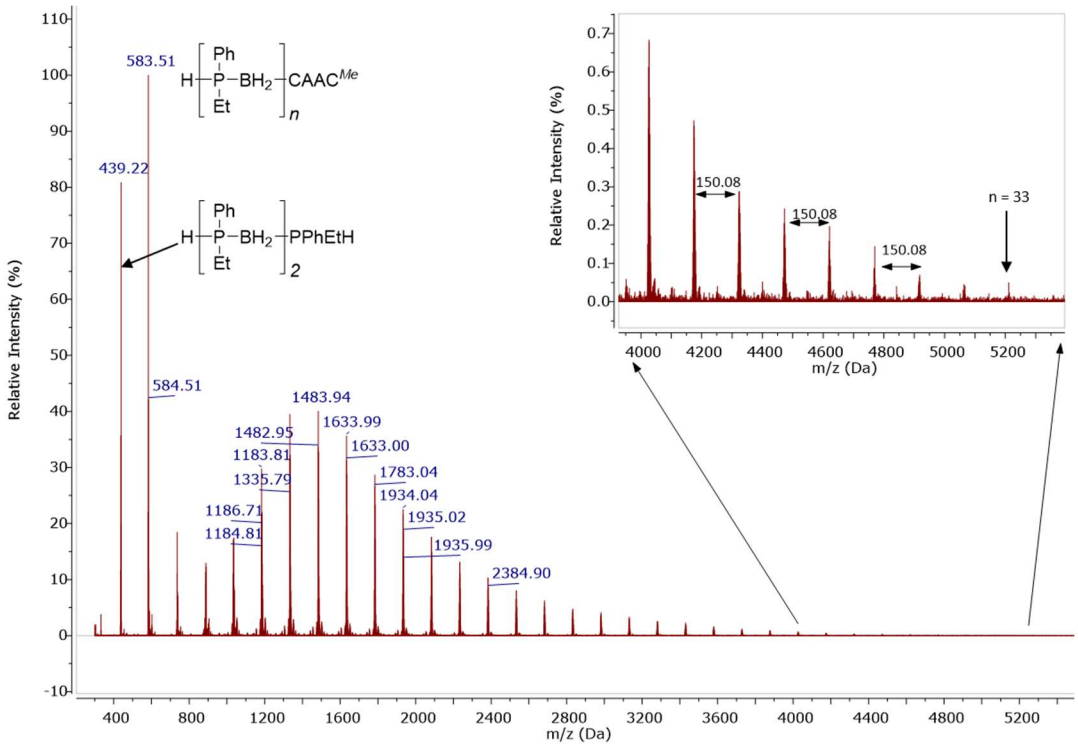

Figure S2.50 ESI(+)-MS spectrum in positive mode in DCM of $[PhEtP–BH_2]_n$ formed from *rac*-PhEtPH·BH_3 and $CAAC^{Me}$ in toluene. The predominant species is a linear system with a $CAAC^{Me}$ end group (H-$[PhEtP–BH_2]_n$-$CAAC^{Me}$)$^+$.

Method B

$CAAC^{Cy}$-mediated

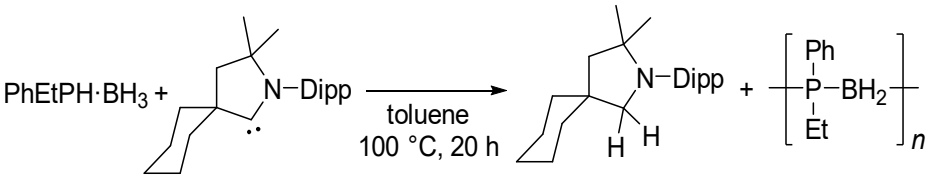

rac-PhEtPH·BH_3 (52 mg, 0.34 mmol) and $CAAC^{Cy}$ (111 mg, 0.340 mmol) were dissolved in toluene (100 µL) in a J. Young NMR tube and heated at 100 °C for20 h. The reaction mixture was added dropwise into 20 mL of rapidly stirred cold hexanes at -40 °C yielding a precipitate and the supernatant was decanted. The precipitation was repeated twice more prior to drying in vacuo to leave a white powder. GPC analysis showed a bimodal distribution with 18% corresponding to high molar mass material. Yield (precipitated material) = 10 mg (19%).

^{1}H NMR (400 MHz, 298 K, $CDCl_3$): δ = 7.82- 6.84 (m, br, Ar), 1.91 – 0.60 (m, br, BH_2, CH_2, CH_3).

^{11}B NMR (96 MHz, 298 K, $CDCl_3$): δ = -33.0 (br).

^{31}P NMR (122 MHz, 295 K, $CDCl_3$): δ = -21.76 (br).

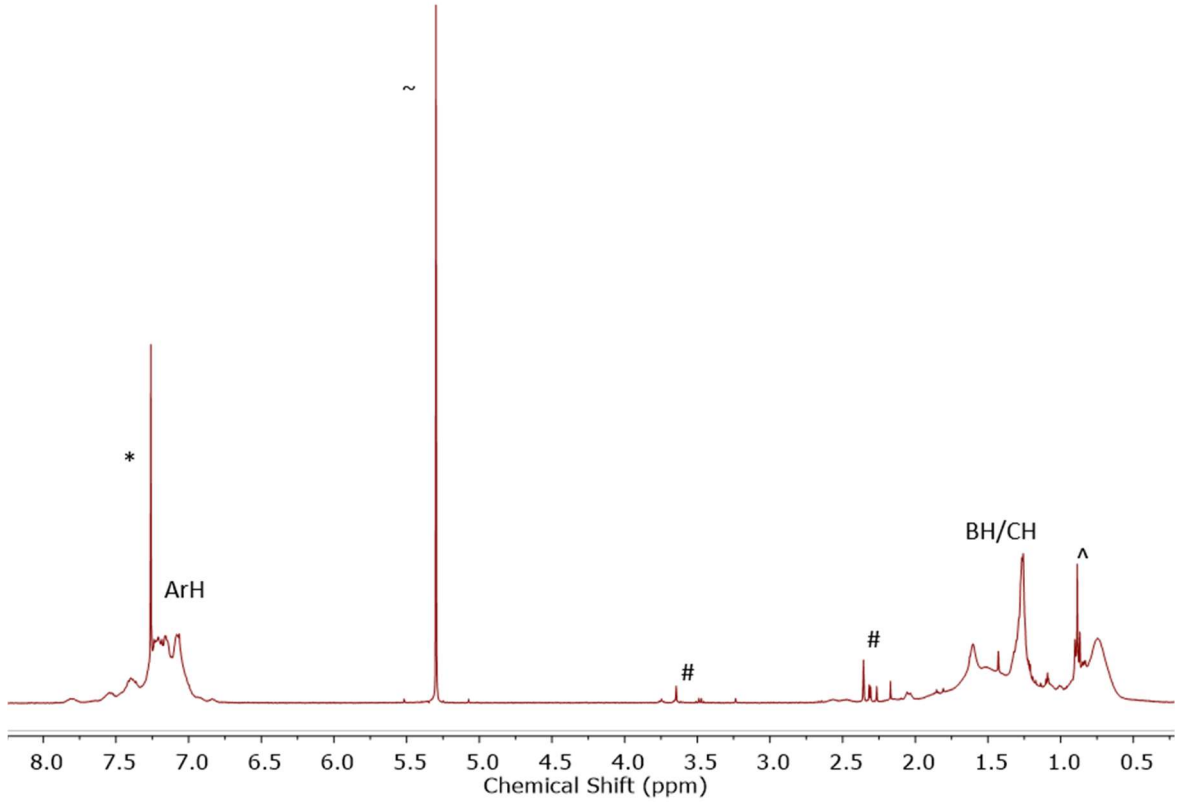

Figure S2.51 ^{1}H NMR spectrum (400 MHz, 298 K, $CDCl_3$) of $[PhEtP–BH_2]_n$ formed from $PhEtPH{\cdot}BH_3$ and $CAAC^{Cy}$ in toluene (* denotes residual partially protiated $CDCl_3$, ~ denotes trace DCM, # denotes trace $(CAAC^{Me})H_2$, ^denotes trace hexanes).

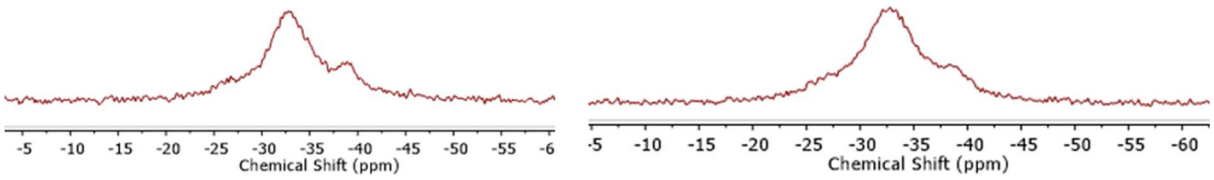

Figure S2.52 $^{11}B\{^{1}H\}$ (left) and ^{11}B (right) NMR spectra (96 MHz, 298 K, $CDCl_3$) of $[PhEtP–BH_2]_n$ formed from $PhEtPH{\cdot}BH_3$ and $CAAC^{Cy}$ in toluene.

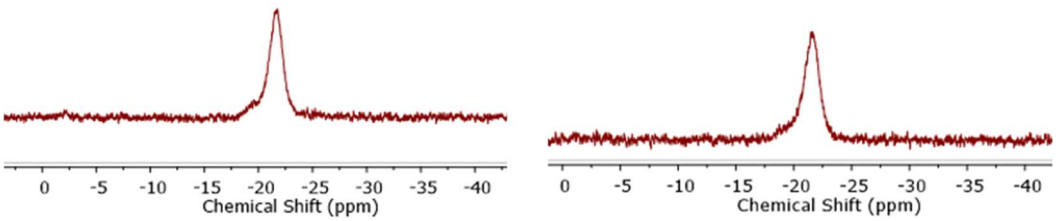

Figure S2.53 $^{31}P\{^{1}H\}$ (left) and ^{31}P (right) NMR spectra (122 MHz, 295 K, $CDCl_3$) of $[PhEtP–BH_2]_n$ formed from $PhEtPH{\cdot}BH_3$ and $CAAC^{Cy}$ in toluene.

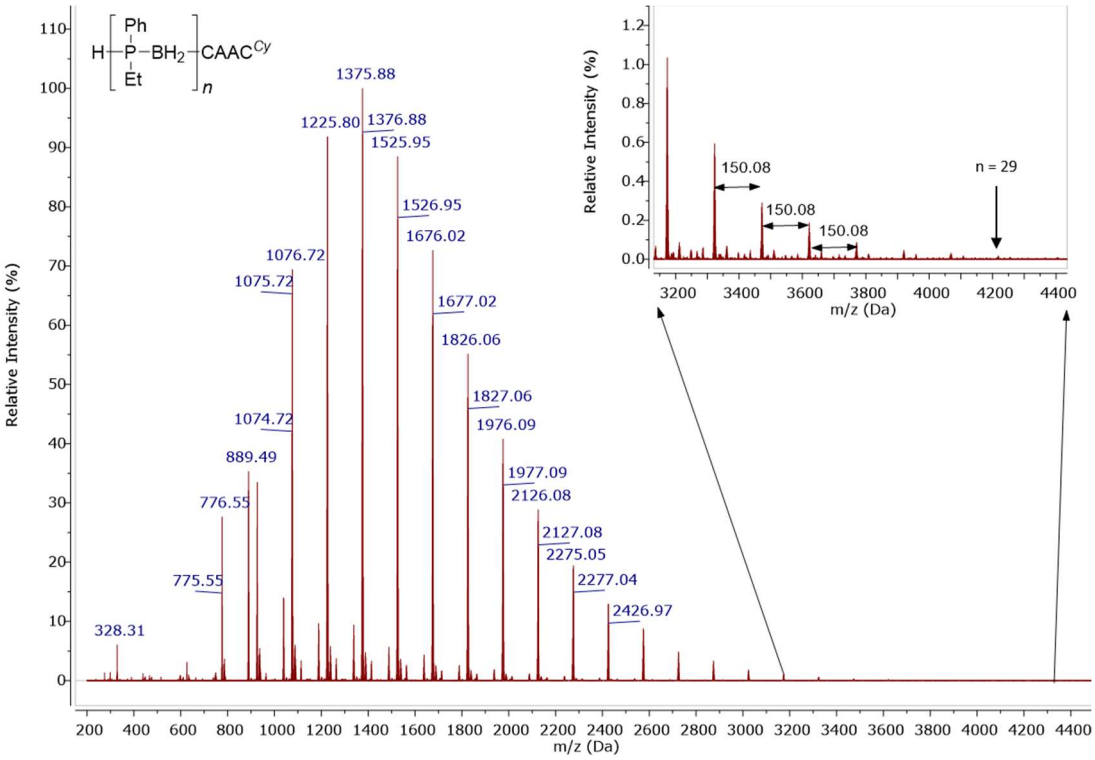

Figure S2.54 ESI(+)-MS spectrum in positive mode in DCM of $[PhEtP–BH_2]_n$ formed from $PhEtPH{\cdot}BH_3$ and $CAAC^{Cy}$ in toluene The predominant species is a linear system with a $CAAC^{Cy}$ end group $(H\text{-}[PhEtP–BH_2]_n\text{-}CAAC^{Cy})^+$.

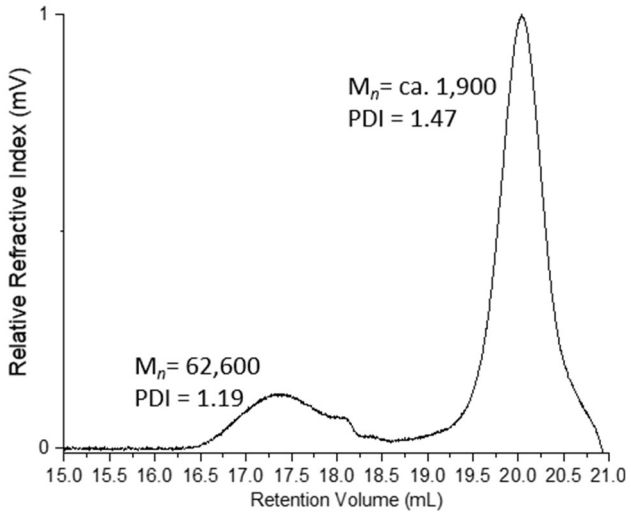

Figure S2.55 GPC chromatogram of $[PhEtP–BH_2]_n$ formed from $PhEtPH{\cdot}BH_3$ and $CAAC^{Cy}$ in toluene. 2 mg mL^{-1} in THF with 0.1 w/w% nBu$_4$NBr in the THF eluent. The highest molar mass peak accounts for ca. 18% of the precipitated material. The bimodal distribution can be explained by the competition between chain termination and propagation. Most of the material undergoes early termination, potentially by a free $CAAC^{Cy}$ unit as evidenced in the ESI-MS, whereas a small percentage of the material undergoes significant further polymerisation to give high molar mass material.

Figure S2.56 Photograph of isolated $[PhEtP–BH_2]_n$.

2.5.6 Synthesis of CAAC^{Me}-phosphinoborane adducts

2.5.6.1 Synthesis of 2.4a

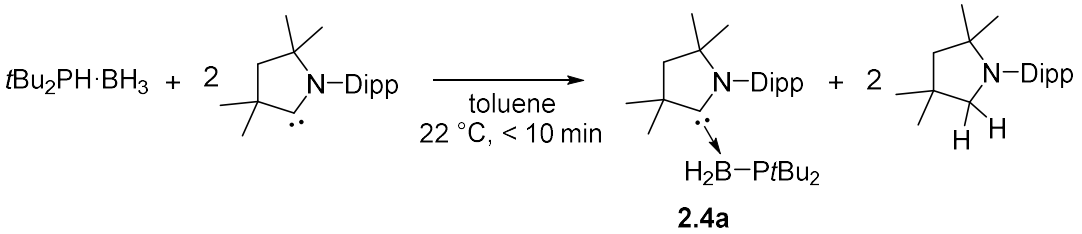

2.4a

5 mL of a colourless toluene solution of CAAC^{Me} (142 mg, 0.497 mmol) was added to a vial charged with colourless solid tBu$_2$PH·BH$_3$ (40 mg, 0.25 mmol) at 22 °C, instantly a bright yellow solution resulted. After 20 min at 22 °C the solvent and volatiles were removed *in vacuo* resulting in a bright yellow microcrystalline solid which was washed with 2 mL of cold *n*-pentane three times to remove the soluble (CAAC^{Me})H$_2$ byproduct. The bright yellow crystalline product **2.4a** was dried *in vacuo*. Yield = 57 mg (51%). Single crystals of **2.4a** suitable for X-ray diffraction were obtained from slow evaporation of an *n*-pentane solution at 22 °C.

^{1}H NMR (400 MHz, 298 K, C_6D_6) δ = 7.11–7.07 (m, 1H, Dipp *p*-C*H*), 7.02 (s, 1H, Dipp *m*-C*H*), 7.00 (d, $^4J_{HH}$ = 1.2 Hz, 1H, Dipp *m*-C*H*), 2.64 (sept, $^3J_{HH}$ = 6.6 Hz, 2H, C*H*(CH$_3$)$_2$), 1.84 (d, *J* = 2.0 Hz, 6H, DippNC(C*H*$_3$)$_2$CH$_2$), 1.50 (s, 2H, Me$_2$CC*H*$_2$CMe$_2$), 1.47 (d, $^3J_{HP}$ = 10.0 Hz, 18H, P(C(C*H*$_3$)$_3$)$_2$), 1.41 (d, $^3J_{HH}$ = 6.5 Hz, 6H, -CH(C*H*$_3$)$_2$), 1.14 (d, $^3J_{HH}$ = 6.6 Hz, 6H, -CH(C*H*$_3$)$_2$), 0.83 (s, 6H, CC(C*H*$_3$)$_2$CH$_2$).

N.B. The B*H*$_2$ resonances could not be observed in the ^{1}H NMR spectrum.

^{11}B NMR (128 MHz, 298 K, C_6D_6) δ = -24.62 (td, $^1J_{BH}$ = 89.2, $^1J_{BP}$ = 42.1 Hz).

^{11}B{^{1}H} NMR (128 MHz, 298 K, C_6D_6) δ = -24.62 (d, $^1J_{BP}$ = 42.1 Hz).

^{31}P NMR (162 MHz, 298 K C_6D_6) δ = 13.23 (br m).

$^{31}P\{^{1}H\}$ NMR (162 MHz, 298 K, C_6D_6) δ = 13.23 (m, $^{1}J_{BP}$ = 41.4 Hz).

$^{13}C\{^{1}H\}$ NMR (101 MHz, 298 K, C_6D_6) δ = 145.48 (Dipp *o*-*C*), 133.95 (Dipp *i*-*C*), 129.22 (Dipp *p*-*C*H), 125.13 (Dipp *m*-*C*H), 75.40 (*C*(carbene)), 53.63 (m, $Me_2CCH_2CMe_2$), 53.53 ($Me_2CCH_2CMe_2$), 32.45 (d, $^{2}J_{CP}$ = 12.1 Hz, $P(C(CH_3)_3)_2$), 31.64 (d, $^{1}J_{CP}$ = 21.7 Hz, $P(C(CH_3)_3)_2$), 30.47 (d, *J* = 16.7 Hz, $DippNC(CH_3)_2CH_2$), 29.15 ($CH(CH_3)_2$), 29.13 ($CC(CH_3)_2CH_2$), 27.60 ($CH(CH_3)_2$), 24.40 ($-CH(CH_3)_2$).

Elemental analysis for $C_{28}H_{51}BNP$ (calcd/expt): C (75.83/75.89), H (11.59/11.65), N (3.16/3.32).

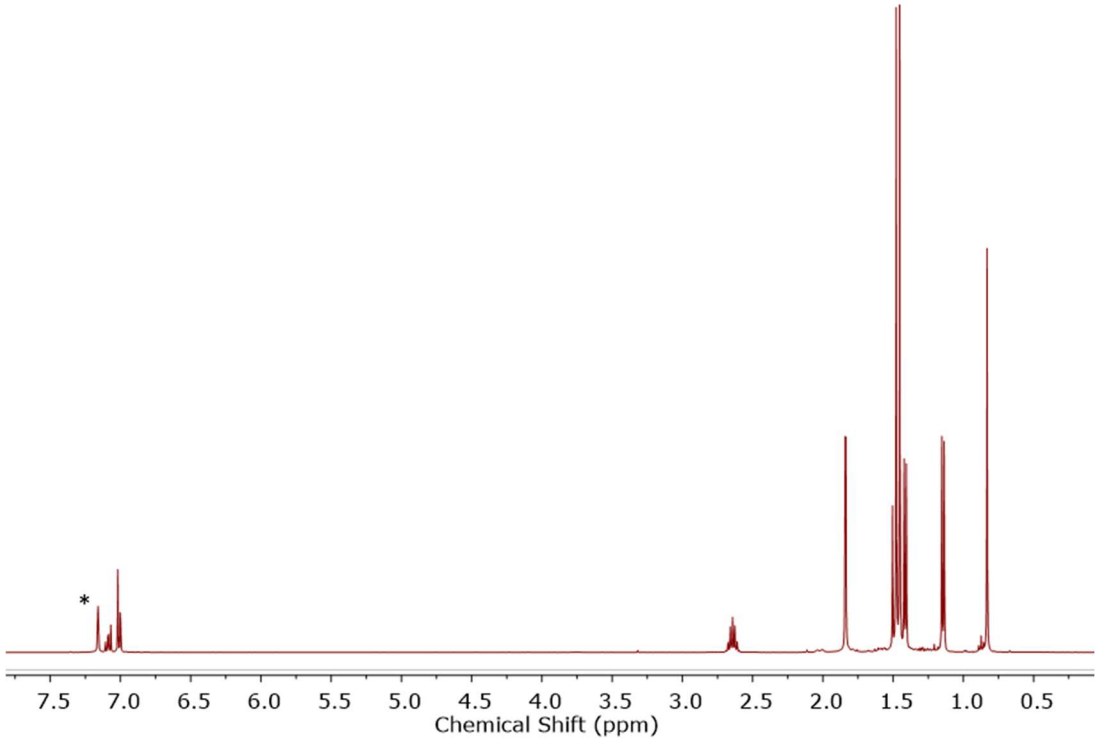

Figure S2.57 ^{1}H NMR spectrum (400 MHz, 298 K, C_6D_6) of **2.4a** (*denotes residual partially protiated benzene).

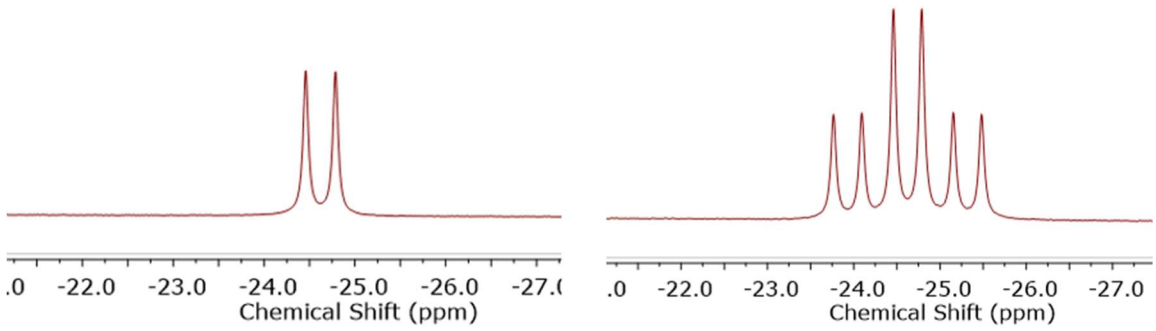

Figure S2.58 $^{11}B\{^{1}H\}$ (left) and ^{11}B (right) NMR spectra (128 MHz, 298 K, C_6D_6) of **2.4a**.

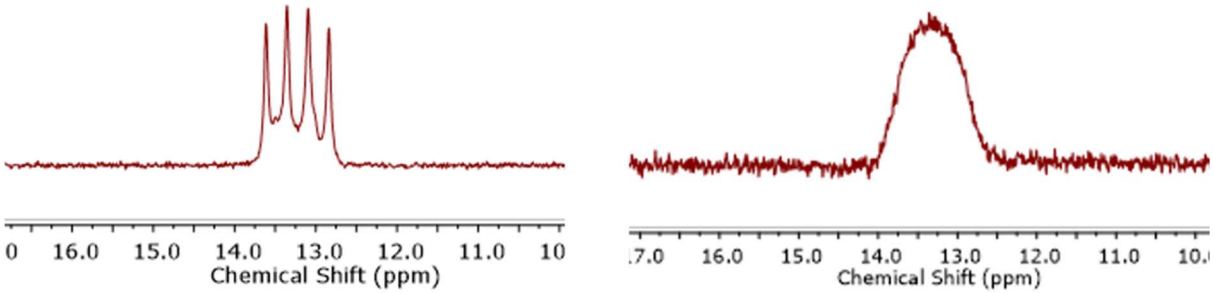

Figure S2.59 $^{31}P\{^{1}H\}$ (left) and ^{31}P (right) NMR spectra (162 MHz, 298 K, C_6D_6) of **2.4a**.

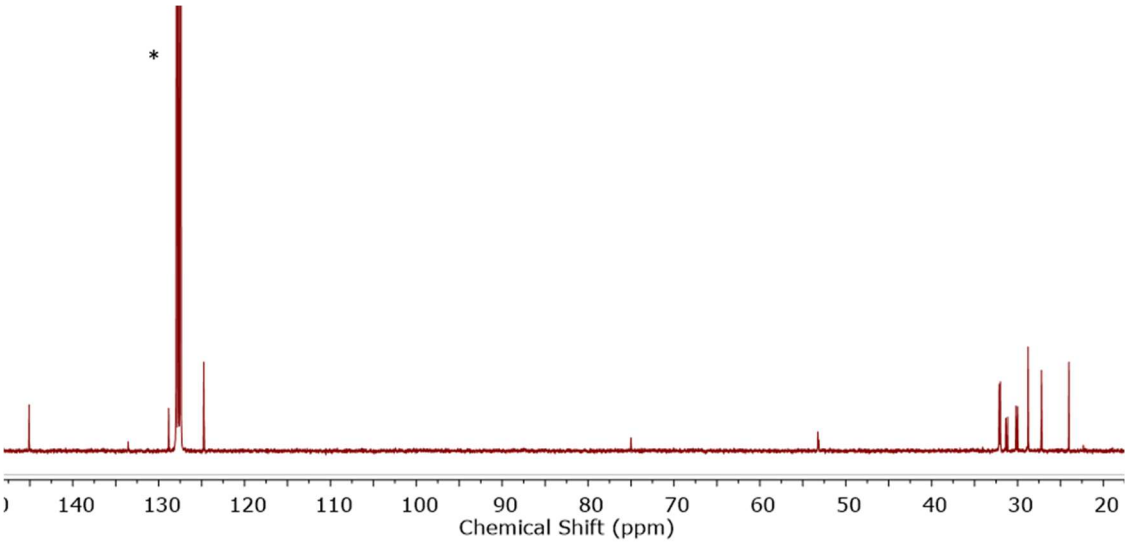

Figure S2.60 $^{13}C\{^{1}H\}$ NMR spectrum (101 MHz, 298 K, C_6D_6) of **2.4a** (*denotes benzene).

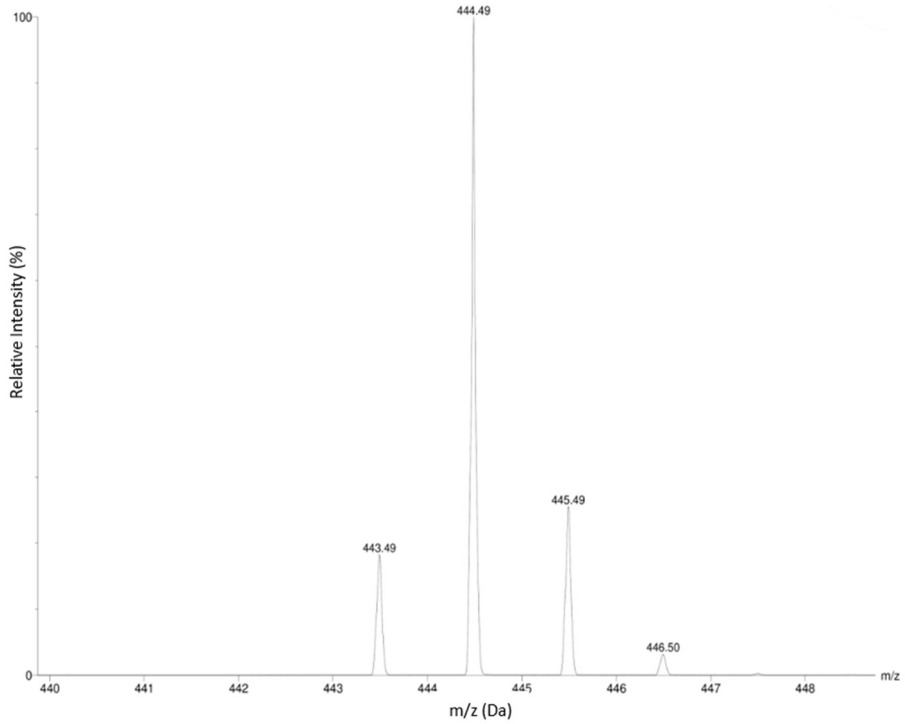

Figure S2.61 ESI(+)-MS spectrum of H[**2.4a**]$^{+}$ cation in DCM (sample injection performed under ambient conditions in air).

2.5.6.2 Synthesis of 2.4b

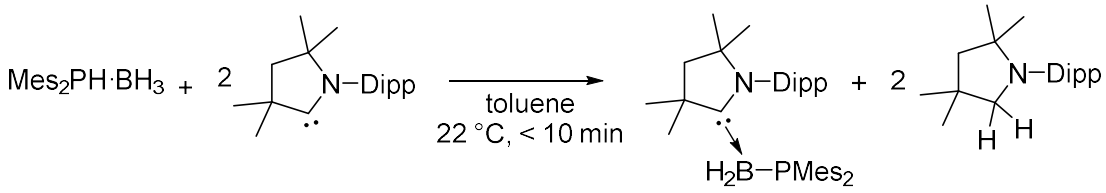

2.4b

5 mL of a colourless toluene solution of CAAC^{Me} (142 mg, 0.497 mmol) was added to a vial charged with colourless solid $Mes_2PH{\cdot}BH_3$ (70 mg, 0.25 mmol) at 22 °C, instantly a yellow solution resulted. After 20 min at 22 °C the solvent and volatiles were removed *in vacuo* resulting in yellow microcrystalline solids which were washed with 2 mL of *n*-pentane three times to remove the soluble (CAAC^{Me})H_2 byproduct. The yellow crystalline product **2.4b** was dried *in vacuo*. Yield = 74 mg (52%). Single crystals of **2.4b** suitable for X-ray diffraction were obtained from diffusion of *n*-pentane into a toluene solution of the compound at -40 °C.

^{1}H NMR (400 MHz, 298 K, C_6D_6) δ = 7.03 – 6.99 (m, 1H, Dipp *p*-C*H*), 6.92 (s, 1H, Dipp *m*-C*H*), 6.90 (m, 1H, Dipp *m*-C*H*), 6.82 (d, $^4J_{HH}$ = 1.8 Hz, 4H, Mes *m*-C*H*), 2.64 (s, 12H, Mes 2,6-(CH_3)), 2.63 (sept, $^3J_{HH}$ = 6.6 Hz, 2H, C*H*(CH_3)$_2$), 2.17 (s, 6H, Mes 4-(CH_3)), 1.79 (d, $^4J_{HH}$ = 1.8 Hz, 6H, DippNC(CH_3)$_2$CH_2), 1.47 (s, 2H, Me_2CCH_2CMe_2), 1.26 (d, $^3J_{HH}$ = 6.5 Hz, 6H, -CH(CH_3)$_2$), 1.11 (d, $^3J_{HH}$ = 6.6 Hz, 6H, -CH(CH_3)$_2$), 0.82 (s, 6H, CC(CH_3)$_2$CH_2).

N.B. The BH_2 resonances could not be observed in the ^{1}H NMR spectrum.

^{11}B NMR (128 MHz, 298 K, C_6D_6) δ = -21.60 (br m).

^{11}B{^{1}H} NMR (128 MHz, 298 K, C_6D_6) δ = -21.60 (br m).

^{31}P NMR (162 MHz, 298 K, C_6D_6) δ = -59.30 (br m).

^{31}P{^{1}H} NMR (162 MHz, 298 K, C_6D_6) δ = -59.30 (br m).

^{13}C{^{1}H} NMR (101 MHz, 298 K, C_6D_6) δ = 145.26 (Dipp *o*-*C*), 142.37 (d, J_{CP} = 11.8 Hz, Mes *i*-*C*), 140.45 (d, J_{CP} = 17.8 Hz, Mes *o*-*C*), 134.47 (Mes *p*-*C*), 133.31 (Dipp *i*-*C*), 129.45 (Dipp *p*-*C*H), 129.39 (d, *J* = 2.9 Hz, Mes *m*-*C*H), 125.30 (s, Dipp *m*-*C*H), 76.45 (s, *C(*carbene)), 54.09 (Me_2*C*CH_2CMe_2), 52.49 (m, Me_2C*C*H_2CMe_2), 29.53 (d, *J* = 17.0 Hz, DippNC(*C*H_3)$_2$CH_2), 29.27 (CH(*C*H_3)$_2$), 29.16 (CC(*C*H_3)$_2$CH_2), 27.05 (CH(*C*H_3)$_2$), 24.47 (CH(*C*H_3)$_2$), 23.97 (d, $^3J_{CP}$ = 12.2 Hz, Mes 2,6-(*C*H_3)), 21.05 (Mes 4-(*C*H_3)).

Elemental analysis for $C_{38}H_{55}BNP$ (calcd/expt): C (80.40/80.41), H (9.77/9.71), N (2.47/2.44).

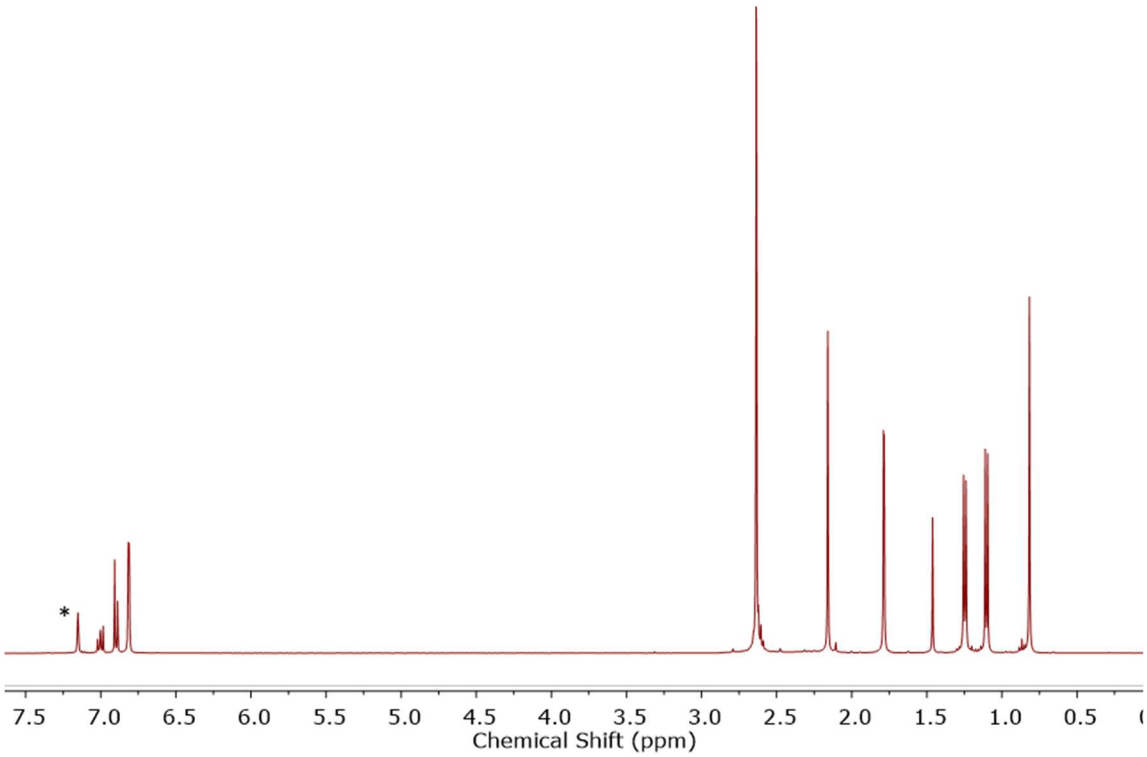

Figure S2.62 1H NMR spectrum (400 MHz, 298 K, C_6D_6) of **2.4b** (*denotes residual partially protiated C_6D_6).

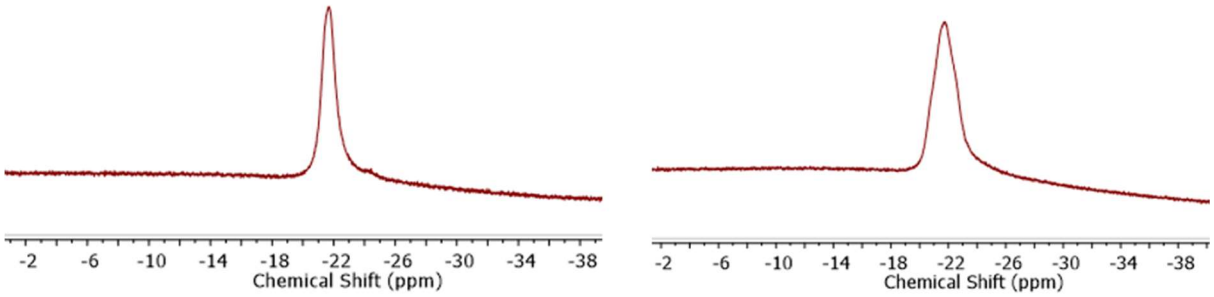

Figure S2.63 $^{11}B\{^1H\}$ (left) and ^{11}B (right) NMR spectra (128 MHz, 298 K, C_6D_6) of **2.4b**.

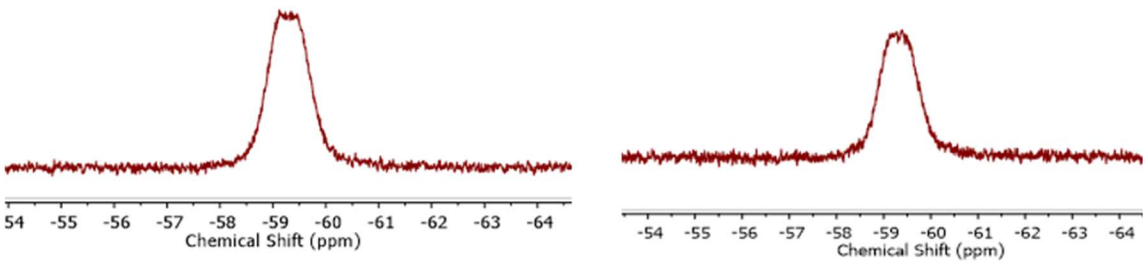

Figure S2.64 31P{1H} (left) and 31P (right) NMR spectra (128 MHz, 298 K, C_6D_6) of **2.4b**.

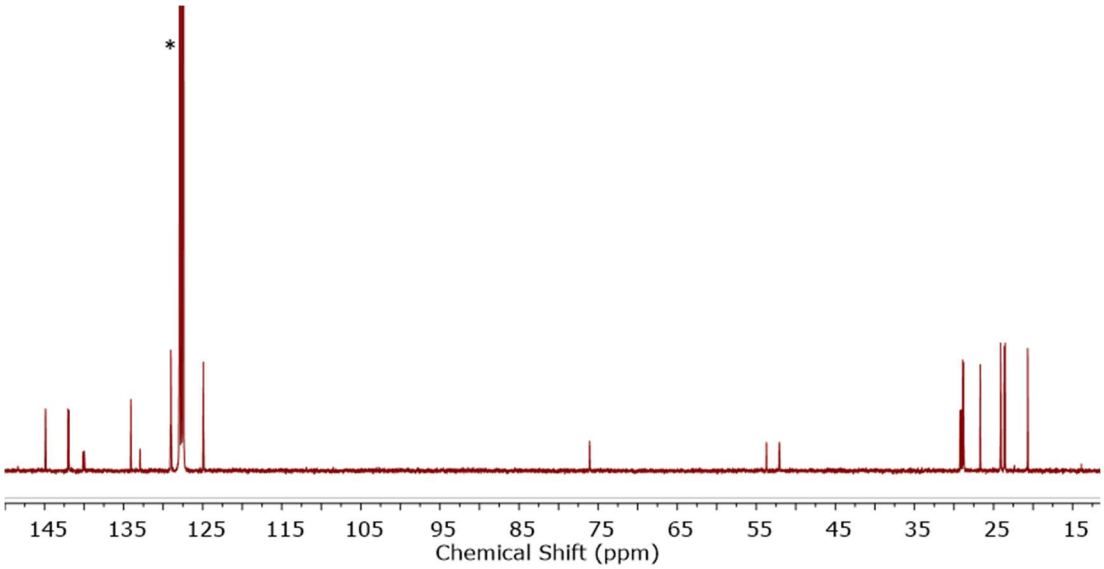

Figure S 2.65 $^{13}C\{^{1}H\}$ NMR spectrum (101 MHz, 298 K, C_6D_6) of **2.4b** (*denotes benzene).

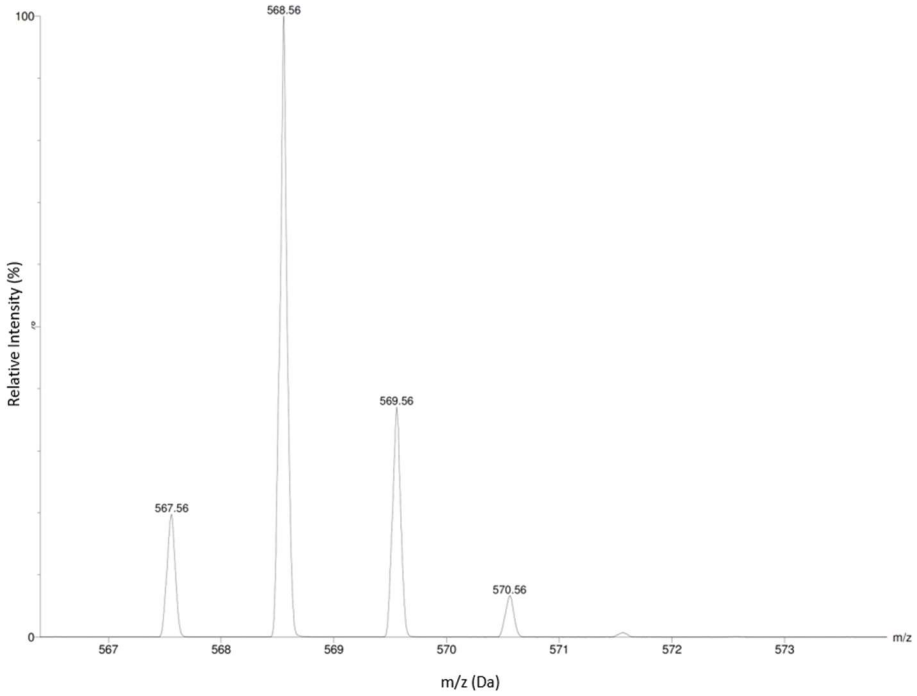

Figure S2.66 ESI(+)-MS spectrum of H[**2.4b**]$^{+}$ cation in DCM (sample injection performed under ambient conditions in air).

2.5.6.3 Reaction of $Ph_2PH{\cdot}BH_3$ with two equivalents of CAAC^{Me}

CAAC^{Me} (57 mg, 0.20 mmol) was added to solution of $Ph_2PH{\cdot}BH_3$ (20 mg, 0.10 mmol) in thf-d_8 (0.5 mL) and heated to 60 °C for 2 h. ^{31}P and ^{11}B NMR spectra showed a number of unidentified peaks; however, ESI-MS showed the presence of short chain oligomers CAAC$(BH_2PPh_2)_x$ (x = 1 - 4).

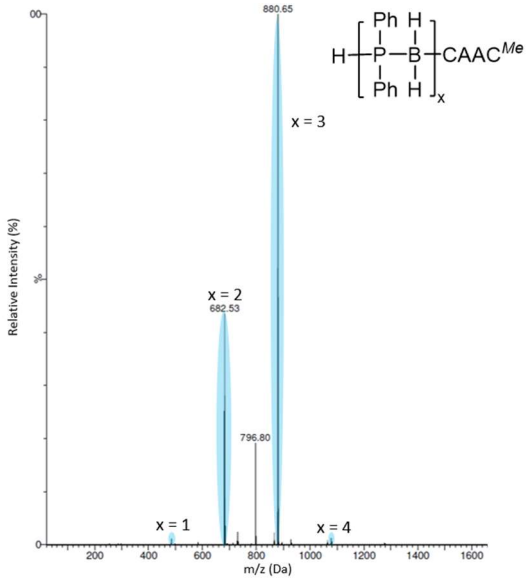

Figure S2.67 ESI(+)-MS spectrum in DCM of the products from the reaction of $Ph_2PH{\cdot}BH_3$ with two equiv. of $CAAC^{Me}$ (sample injection performed under ambient conditions in air).

2.5.7 Supplementary Tables

2.5.7.1 X-ray crystallography

X-ray diffraction experiments on **2.1b**, **2.3c**, **2.4a**, **2.4b** and $(CAAC^{Me})H_2$ were carried out at 100(2) K on a Bruker APEX II CCD diffractometer using Mo-K_α radiation (λ = 0.71073 Å). Intensities were integrated in SAINT[80] and absorption corrections based on equivalent reflections were applied using SADABS[81]. The structures were solved using SHELXT[82] and refined against all F^2 in SHELXL[83] using Olex2.[84] All the non-hydrogen atoms were refined anisotropically. While all of the hydrogen atoms were located geometrically and refined using a riding model, apart from the B-H protons in **2.1b**, **2.3c**, **2.4a** and **2.4b** which were located in the difference map and refined freely. In **2.3c** H9 and H26 were also located in the difference map with isotropic displacement parameters Uiso(H) = 1.2Ueq(C). Disordered portions of a THF solvent molecule in the structure of **2.1b**·(THF) were successfully modelled over two positions and refined with the sum of the occupancies set to 1. Residual electron density from a disordered solvent molecule in the lattice of **2.4b** was removed using a solvent mask in Olex2, and the contributions were excluded from the formula.

Crystallographic data for compounds **2.1b**, **2.3c**, **2.4a**, **2.4b** and $(CAAC^{Me})H_2$ have been deposited with the Cambridge Crystallographic Data Centre as supplementary publication CCDC 1867656-1867660. Copies of the data can be obtained free of charge on application to CCDC, 12 Union Road, Cambridge CB2 1EZ, UK [fax(+44) 1223 336033, e-mail: deposit@ccdc.cam.ac.uk.

Table S2.6 Selected crystallographic data for **2.1b,** (CAAC^{Me})H$_2$ and **2.3c**.

Compound	**2.1b**·(THF)	(CAAC^{Me})H$_2$	**2.3c**
Empirical formula	$C_{43}H_{58}BN_2OP$	$C_{20}H_{33}N$	$C_{28}H_{45}BNP$
Formula weight	1321.38	287.47	437.43
Temperature/K	100(2)	100(2)	100(2)
Crystal system	triclinic	orthorhombic	monoclinic
Space group	*P*$\bar{1}$	*Pbcn*	*Cc*
a/Å	12.6945(5)	12.3826(4)	9.0629(4)
b/Å	16.3421(7)	12.3164(3)	19.2145(8)
c/Å	19.2329(8)	23.6194(6)	15.3373(7)
α/°	81.437(2)	90	90
β/°	87.371(2)	90	103.835(3)
γ/°	86.212(2)	90	90
Volume/Å^3	3934.2(3)	3602.17(17)	2593.3(2)
Z	4	8	4
ρ_{calc} g/cm^3	1.115	1.060	1.12
μ/mm^{-1}	0.104	0.060	0.121
F(000)	1432.0	1280.0	960
Crystal size/mm^3	0.48 × 0.35 × 0.3	0.35 × 0.18 × 0.10	0.60 × 0.39 × 0.21
2θ range for data collection/°	2.142 to 55.214	4.664 to 55.176	4.24 to 55.848
Reflections collected	70384	32539	23735
Independent reflections	18210	4173	5919
Goodness-of-fit on F^2	1.018	1.033	1.037
Final R indexes [I>=2σ (I)]	R_1 = 0.0431, wR_2 = 0.0959	R_1 = 0.0473, wR_2 = 0.1128	R_1 = 0.0347, wR_2 = 0.0835
Final R indexes [all data]	R_1 = 0.0626, wR_2 = 0.1045	R_1 = 0.0694, wR_2 = 0.1251	R_1 = 0.0392, wR_2 = 0.0856
Largest diff. peak/hole / e Å^{-3}	0.32/-0.27	0.34/-0.23	0.38/-0.19
Flack Parameter	-	-	-0.01(3)

Table S2.7 Selected crystallographic data for **2.4a** and **2.4b**.

Compound	**2.4a**	**2.4b**
Empirical formula	$C_{28}H_{51}BNP$	$C_{38}H_{55}BNP$
Formula weight	443.47	567.61
Temperature/K	100(2)	100(2)
Crystal system	monoclinic	triclinic
Space group	$P2_1/n$	$P\bar{1}$
a/Å	9.3737(4)	11.4350(17)
b/Å	21.3623(8)	12.2983(18)
c/Å	14.3960(5)	14.056(2)
α/°	90	70.215(7)
β/°	97.875(2)	79.929(8)
γ/°	90	89.278(7)
Volume/Å^3	2855.52(19)	1829.1(5)
Z	4	2
ρ_{calc} g/cm^3	1.032	1.031
μ/mm^{-1}	0.111	0.099
F(000)	984.0	620.0
Crystal size/mm^3	0.48 × 0.45 × 0.4	0.5 × 0.2 × 0.15
2θ range for data collection/°	3.434 to 55.062	3.524 to 55.174
Reflections collected	27008	32259
Independent reflections	6569	8380
Goodness-of-fit on F^2	1.032	1.028
Final R indexes [I>=2σ (I)]	R_1 = 0.0388, wR_2 = 0.0969	R_1 = 0.0445, wR_2 = 0.1033
Final R indexes [all data]	R_1 = 0.0463, wR_2 = 0.1013	R_1 = 0.0672, wR_2 = 0.1121
Largest diff. peak/hole / e Å^{-3}	0.56/-0.24	0.31/-0.32

2.5.8 Supplementary Data

2.5.8.1 Cartesian coordinates and SCF energies of the calculated structures

A (THF); E_H = −598.95586866

C	0.97144300	-1.16398200	-0.30930900
C	2.39826300	-0.65581200	-0.18809700
C	2.29748500	0.88740000	-0.10623100
H	2.96533500	1.31146200	0.65033600
H	2.57391600	1.33033900	-1.06958900
C	0.82783600	1.20935800	0.20338800
C	2.99723300	-1.26869300	1.08739600
H	2.98693400	-2.36191200	1.03292100
H	2.44304700	-0.97107900	1.98351300
H	4.03571200	-0.93815500	1.20580500
C	3.22055000	-1.11021700	-1.39617800
H	4.24651100	-0.73025000	-1.32183600
H	2.78871400	-0.73947000	-2.33223000
H	3.26015800	-2.20289300	-1.45021300
C	0.58789500	1.57219900	1.66898200
H	1.08581700	2.52045100	1.89539200
H	0.98732100	0.80768100	2.34168600
H	-0.47923700	1.69633400	1.87855600
C	0.26573700	2.29997800	-0.70262000
H	-0.79361400	2.48917400	-0.50335700
H	0.38358300	2.03616600	-1.75825000
H	0.81211600	3.23156900	-0.52282200
C	-1.23743100	-0.26486700	-0.08382400
C	-3.27192600	-0.78786100	1.10169500
H	-3.77316100	-1.09252000	2.01591500
C	-4.01080100	-0.54767300	-0.05615200
H	-5.09098200	-0.66076800	-0.04640600
C	-3.35763100	-0.17146500	-1.22936800
H	-3.92610900	0.00569800	-2.13782500
N	0.19262100	-0.13181000	-0.09974700

C	-1.88544900	-0.64697700	1.09020600
H	-1.30046500	-0.84777200	1.98262300
C	-1.97159700	-0.02823000	-1.24538200
H	-1.45499600	0.25142100	-2.15837900

A (toluene); E_H = −598.95166567

C	0.97215500	-1.16692100	-0.30540100
C	2.39808900	-0.65565400	-0.18369900
C	2.29890800	0.88847500	-0.10510500
H	2.96303100	1.31347000	0.65464000
H	2.58186600	1.33015300	-1.06736300
C	0.82768500	1.21146400	0.19583200
C	2.99473000	-1.26623300	1.09367000
H	2.97641600	-2.35916900	1.04241300
H	2.44132800	-0.96335500	1.98867400
H	4.03510500	-0.94098500	1.21203400
C	3.22058000	-1.11491700	-1.38959000
H	4.24875900	-0.74037700	-1.31527100
H	2.79100900	-0.74474200	-2.32690700
H	3.25173400	-2.20758600	-1.44202700
C	0.58048700	1.57943500	1.65919200
H	1.07168400	2.53129400	1.88612000
H	0.98156100	0.81888300	2.33552900
H	-0.48837000	1.69709400	1.86410500
C	0.27110300	2.30106300	-0.71519800
H	-0.78992700	2.48934300	-0.52413100
H	0.39621100	2.03561000	-1.76968600
H	0.81509000	3.23407600	-0.53436600
C	-1.23534500	-0.26513100	-0.08565200
C	-3.26362900	-0.80922100	1.10113200
H	-3.75970100	-1.13206500	2.01197200
C	-4.00902200	-0.54711400	-0.04733000
H	-5.08917600	-0.66031200	-0.03368900
C	-3.36213900	-0.15131500	-1.21705500
H	-3.93545200	0.03997500	-2.11964300
N	0.19430000	-0.13097600	-0.10469500
C	-1.87762600	-0.66913300	1.08385800
H	-1.28598100	-0.89084800	1.96681000
C	-1.97641800	-0.00893200	-1.23829500
H	-1.46421600	0.28147600	-2.15027900

B (THF); E_H = −600.40015047

P	-1.82986200	-0.58525300	-0.01679800
H	-1.98888100	-1.52290400	-1.05598800
C	-0.04703000	-0.23223000	-0.01675900
C	0.89853400	-1.26507400	0.00901400
C	0.37661900	1.09956400	-0.04232400
C	2.25709300	-0.96300800	0.01016500
H	0.57748200	-2.30340900	0.02740500
C	1.73934400	1.39672100	-0.04111700
H	-0.35698900	1.90041200	-0.06367600
C	2.67792600	0.36784800	-0.01462000
H	2.98798500	-1.76608600	0.03009200
H	2.06447600	2.43270200	-0.06123500
H	3.73898400	0.60026400	-0.01381200
B	-3.02529200	0.92644500	-0.09935700
H	-4.13611100	0.43604000	-0.08992900
H	-2.76397200	1.49692700	-1.13874100
H	-2.01151400	-1.42225400	1.10192100
H	-2.78873100	1.58949600	0.88982600

B (toluene); E_H = −600.39658784

P	-1.83256300	-0.58057900	-0.01902000
H	-1.98521700	-1.52098300	-1.05855600
C	-0.04806100	-0.23309000	-0.01753500
C	0.89816700	-1.26487100	0.01081100
C	0.37487100	1.09862900	-0.04506000
C	2.25638100	-0.96286600	0.01252300
H	0.57752800	-2.30353600	0.03079400
C	1.73733000	1.39593600	-0.04326400
H	-0.36065800	1.89774100	-0.06844100
C	2.67627300	0.36796600	-0.01428200
H	2.98779700	-1.76548000	0.03444900
H	2.06202900	2.43202600	-0.06490000
H	3.73724600	0.60092000	-0.01302600
B	-3.02659000	0.93048400	-0.09704500
H	-4.13540300	0.43829300	-0.08845800
H	-2.75871900	1.49775500	-1.13566700
H	-2.00761100	-1.42691400	1.09542400
H	-2.78273800	1.58477000	0.89531600

TS1 (THF); E_H = −1199.35971457

P	-1.65668100	1.27758200	0.88668400
C	-3.13280200	0.88525100	-0.10955600
C	-3.14161500	1.07727700	-1.49877300
C	-4.25972800	0.32356800	0.50365100
C	-4.25532200	0.71966800	-2.25534600
H	-2.27651700	1.51434200	-1.99206600
C	-5.37133800	-0.03950800	-0.25638400
H	-4.26807900	0.18028500	1.58078800
C	-5.37286600	0.15803200	-1.63625700
H	-4.25109400	0.88101900	-3.32996000
H	-6.24018000	-0.47080300	0.23341600
H	-6.24122000	-0.12006100	-2.22695000
B	-2.02020800	1.54405000	2.78050100
H	-0.95154700	1.88224300	3.26124100
H	-2.37578400	0.45999100	3.21289600
H	-1.20693600	2.46109100	0.25768300
H	-2.87874800	2.39921000	2.90067800
C	0.55497700	-0.97472900	0.10898000
C	0.48248900	-2.47945000	0.18757500
C	1.91071300	-2.96633000	-0.16411100

H	2.25066200	-3.76564600	0.50113100
H	1.92741000	-3.36144100	-1.18548900
C	2.83251400	-1.73786700	-0.07288300
C	0.07149300	-2.84745300	1.62336700
H	-0.90473900	-2.41989600	1.87223300
H	0.79577600	-2.48862700	2.36116300
H	0.00377000	-3.93697100	1.71596400
C	-0.56820700	-3.00936300	-0.79247200
H	-0.60335300	-4.10372100	-0.74745800
H	-0.33409300	-2.71948200	-1.82221500
H	-1.56230700	-2.62313100	-0.54617400
C	3.65836400	-1.69515900	1.21186800
H	4.37827100	-2.51929800	1.20540400
H	3.02762900	-1.79922000	2.09939700
H	4.22041900	-0.75949100	1.29189000
C	3.74039000	-1.59493600	-1.28872500
H	4.35598100	-0.69204900	-1.23276500
H	3.16063900	-1.57167100	-2.21658200
H	4.41363200	-2.45683700	-1.33139800
C	2.19555800	0.75348100	-0.06989500
C	2.71646500	2.79575900	1.09572700
H	2.83476200	3.34059900	2.02757000
C	2.91147700	3.44095400	-0.12457900
H	3.18758100	4.49103100	-0.14629000
C	2.74182200	2.73903200	-1.31757200
H	2.88186500	3.24031200	-2.27074800
N	1.80059300	-0.62923000	-0.03628900
C	2.35885600	1.44922100	1.12685400
H	2.19035500	0.94125200	2.07160000
C	2.38311100	1.39278300	-1.29428900
H	2.23455200	0.84344300	-2.21870400
H	-0.59427400	0.19069600	0.47702100

TS1 (toluene); E_H = −1199.35332280

P	-1.56755600	1.28690000	0.72589600
C	-3.16378400	0.74906500	0.02598300
C	-3.40469900	0.80812700	-1.35443500
C	-4.14643400	0.20600500	0.86249500
C	-4.60532900	0.34187700	-1.88384900
H	-2.65147700	1.22610200	-2.01848500
C	-5.34531500	-0.26688000	0.32944000
H	-3.97166200	0.16719400	1.93424100
C	-5.57844700	-0.19952300	-1.04277400
H	-4.78212000	0.40114500	-2.95452000
H	-6.10152700	-0.68112500	0.99086700
H	-6.51508200	-0.56309700	-1.45636000
B	-1.56504700	1.45065600	2.66609200
H	-0.46546500	1.89824300	2.94291400
H	-1.70209700	0.31409400	3.08748600
H	-1.37597700	2.52415300	0.06687100
H	-2.47036500	2.18980600	3.00168100
C	0.56622500	-0.80075100	-0.36618200
C	0.37316200	-2.29198700	-0.24211000
C	1.80857400	-2.87154300	-0.16746800
H	1.90120700	-3.64566000	0.60028200
H	2.07554100	-3.32898300	-1.12644800
C	2.75013500	-1.68913600	0.11926600
C	-0.43775600	-2.55882500	1.03767100
H	-1.42436700	-2.08894800	0.98249000
H	0.06492600	-2.17826200	1.93200600
H	-0.58054900	-3.63816900	1.15988000
C	-0.40268900	-2.82216700	-1.45181200
H	-0.52203400	-3.90872800	-1.37297900
H	0.12215700	-2.60510500	-2.38825000
H	-1.39778000	-2.36985900	-1.50491100
C	3.19053700	-1.60983600	1.58038500
H	3.82763200	-2.46865100	1.81371400
H	2.33339200	-1.62543500	2.25955500
H	3.76943200	-0.70115600	1.77215600
C	3.96513500	-1.66795500	-0.80066800
H	4.59717800	-0.79365500	-0.61799800
H	3.66614300	-1.67294000	-1.85350800
H	4.56831800	-2.56245200	-0.61594100
C	2.30985800	0.82547400	-0.18372700
C	2.67802800	2.90534900	0.97058600
H	2.60089500	3.50250700	1.87417900
C	3.20833500	3.45682900	-0.19408300
H	3.55551900	4.48584900	-0.19909600
C	3.28049500	2.69049100	-1.35680200
H	3.68096500	3.12013000	-2.27033400
N	1.82627200	-0.52930800	-0.18354700
C	2.22909500	1.58614500	0.98129500
H	1.79295500	1.15919300	1.87916800
C	2.82961100	1.37270000	-1.35569600
H	2.86558900	0.77351000	-2.26028600
H	-0.50526600	0.29839700	0.03702300

TS1' (THF); E_H = −1199.35943684

C	-2.68196600	-1.73467600	-0.37096400
C	-1.43511800	-0.94720500	-0.05118900
C	-3.22138600	0.66795100	-0.10063100
C	-3.84826700	-0.73524400	-0.16924800
H	-4.59042400	-0.79812500	-0.97064000
H	-4.36412900	-0.95220000	0.77213400
C	-2.79194900	-2.94747300	0.55810400
H	-3.71364600	-3.49999500	0.34373800
H	-1.94547700	-3.62706100	0.41736500
H	-2.81515300	-2.64364600	1.60981900
C	-2.56554800	-2.21683700	-1.82644500
H	-1.68348100	-2.85162300	-1.95744500
H	-3.45271000	-2.80305000	-2.09022400
H	-2.48974000	-1.38108800	-2.52912600
C	-3.72839500	1.47959800	1.08575100
H	-3.23679200	2.45501500	1.15023700

H	-4.80242600	1.65229600	0.96472800
H	-3.57448700	0.94360100	2.02717400
C	-3.38349700	1.46414500	-1.39441100
H	-4.44397700	1.68461600	-1.55019800
H	-2.84727600	2.41680900	-1.34570300
H	-3.02048400	0.90292400	-2.26040900
N	-1.76241900	0.30379100	0.08730200
C	-0.77870100	1.32050300	0.34866200
C	-0.12093900	1.93327500	-0.71667500
C	-0.48087500	1.67175100	1.66399900
C	0.83485500	2.91419300	-0.46129700
H	-0.34843800	1.63221800	-1.73468400
C	0.47841300	2.65149000	1.91166000
H	-0.98585200	1.17107700	2.48417900
C	1.13261600	3.27713000	0.85144100
H	1.35273900	3.38736300	-1.29026500
H	0.71830600	2.91910400	2.93640700
H	1.88115200	4.03900200	1.04839100
H	2.99066500	-2.45903700	2.98456900
H	1.75051900	-0.86998100	3.20001100
H	1.00829100	-2.74041900	3.29714100
B	1.86712100	-2.02087300	2.81478700
C	2.70328800	-1.07566600	-0.09055700
C	2.78490500	-1.25341700	-1.47930800
C	3.53402000	-0.12994300	0.52184000
C	3.68214700	-0.50399500	-2.23666500
H	2.14873500	-1.98539600	-1.97157300
C	4.42801100	0.62321900	-0.23873200
H	3.48260600	0.01021100	1.59802500
C	4.50532400	0.43818700	-1.61807800
H	3.74022700	-0.65707200	-3.31097700
H	5.06947400	1.35152600	0.25018600
H	5.20591300	1.02155500	-2.20912800
P	1.48619300	-1.99866700	0.90557500
H	1.59145200	-3.29010400	0.33797900
H	0.07706700	-1.50089300	0.40472800

TS1' (toluene); E_H = −1199.35272843

C	-2.63351900	-1.72423300	-0.55007300
C	-1.39619800	-0.86556600	-0.44555800
C	-3.22243700	0.55676000	0.21702000
C	-3.75745700	-0.88110400	0.10280500
H	-4.68745500	-0.91352000	-0.47308200
H	-3.97781300	-1.26999300	1.10269800
C	-2.42045100	-3.05984700	0.16912700
H	-3.33689200	-3.65880700	0.12393300
H	-1.61617000	-3.63428600	-0.30125800
H	-2.16161100	-2.91273300	1.22274200
C	-2.88953700	-1.98639300	-2.04359300
H	-2.04057300	-2.50592300	-2.49856400
H	-3.77952800	-2.61505300	-2.15873200
H	-3.05519900	-1.05832400	-2.59971400
C	-3.44371200	1.15411300	1.60214500
H	-3.01768800	2.15852000	1.68420300
H	-4.51975800	1.22940400	1.78861400
H	-3.00821500	0.52135500	2.38132400
C	-3.77372400	1.49462000	-0.85596600
H	-4.84576400	1.64211900	-0.69259000
H	-3.28976600	2.47520400	-0.81170000
H	-3.63510900	1.08283200	-1.85995900
N	-1.74981000	0.31899400	-0.03609900
C	-0.79365400	1.38441700	0.10195100
C	-0.43540900	2.13165700	-1.01881100
C	-0.21781400	1.64446800	1.34389500
C	0.49819300	3.15712900	-0.89109800
H	-0.87671900	1.89792200	-1.98300500
C	0.71848200	2.66921500	1.46218400
H	-0.47628600	1.03135900	2.20120400
C	1.07267900	3.42951400	0.34942600
H	0.78329000	3.73598000	-1.76461100
H	1.17941200	2.86231000	2.42626100
H	1.80598500	4.22480500	0.44563100
H	2.38643500	-2.47756800	3.03629000
H	1.21166600	-0.82462400	3.01743700
H	0.36820500	-2.65325400	2.93620700
B	1.34524100	-1.98054200	2.65250700
C	2.76876000	-1.05854800	-0.03371200
C	3.04978200	-1.16059600	-1.40357000
C	3.56902100	-0.23161700	0.76295000
C	4.11323500	-0.45626300	-1.96172500
H	2.43705000	-1.79815600	-2.03678300
C	4.62985100	0.47761200	0.20101800
H	3.36251600	-0.15538600	1.82694300
C	4.90542700	0.36686100	-1.16038900
H	4.32474400	-0.55023500	-3.02357300
H	5.24694400	1.11188100	0.83188400
H	5.73603300	0.91543100	-1.59604600
P	1.34944600	-1.93170700	0.70627000
H	1.49876600	-3.22308400	0.14605700
H	0.03760200	-1.37826100	-0.04116000

C-1$_{pair}$ (THF); E_H = −1199.38697716

P	-1.90102800	1.79534200	0.59116600
C	-3.23497300	0.70380000	-0.04729500
C	-3.63919500	0.74232200	-1.39347700
C	-3.81546100	-0.27266800	0.77863000
C	-4.58427500	-0.15190100	-1.89132900
H	-3.20864100	1.48703200	-2.06035600
C	-4.75323900	-1.17738100	0.27908700
H	-3.53813900	-0.30889000	1.82938500
C	-5.14416400	-1.12323100	-1.05832400
H	-4.88587600	-0.09056900	-2.93436600
H	-5.18893700	-1.92032600	0.94313700
H	-5.88020000	-1.82219500	-1.44617300

B	-2.28201400	2.16529600	2.49544300
H	-1.50954800	3.06278100	2.81453200
H	-2.00583100	1.14470700	3.11954600
H	-2.29519400	2.97272900	-0.10506900
H	-3.45015300	2.48891200	2.67077800
C	0.68238100	-0.67047100	-0.07430400
C	0.25490300	-2.09216300	-0.15041400
C	1.59116400	-2.81674900	-0.44097300
H	1.71510000	-3.70087900	0.18905200
H	1.61162200	-3.14865600	-1.48311000
C	2.73296400	-1.80565400	-0.19774200
C	-0.36175100	-2.47839400	1.20767900
H	-1.25071400	-1.87763300	1.42045800
H	0.34743100	-2.35499600	2.03099700
H	-0.66017800	-3.53047100	1.16674900
C	-0.78574200	-2.27842700	-1.26228100
H	-1.05266900	-3.33794800	-1.32500600
H	-0.39210600	-1.96734200	-2.23467700
H	-1.69460600	-1.70615000	-1.05212100
C	3.45744500	-2.01456800	1.12930500
H	3.99778100	-2.96422900	1.08700500
H	2.75950700	-2.05445100	1.97029800
H	4.18579800	-1.21962800	1.31356200
C	3.72345300	-1.75490200	-1.35257400
H	4.51296800	-1.01828300	-1.18030200
H	3.22285600	-1.53309600	-2.29969700
H	4.19542700	-2.73767100	-1.44114900
C	2.59099400	0.77688400	0.03820400
C	3.27996700	2.58686600	1.45544200
H	3.34429000	3.03658400	2.44115900
C	3.78699600	3.25448800	0.34222600
H	4.25268700	4.22810400	0.46027200
C	3.68746100	2.68030600	-0.92446300
H	4.06907600	3.20554600	-1.79440100
N	1.95693000	-0.50800100	-0.11060900
C	2.67716000	1.34002900	1.30922900
H	2.27137800	0.81430100	2.16775300
C	3.08765900	1.43389000	-1.08514600
H	2.99058200	0.98826900	-2.06948900
H	0.00614400	0.19394400	0.03709900

C-1$_{pair}$ (toluene); E_H = −1199.37560183

P	-1.22332800	1.08417700	0.27320000
C	-2.86718300	0.28225900	0.05404900
C	-3.56967900	0.39800000	-1.15784400
C	-3.42238600	-0.52804000	1.05537500
C	-4.78233500	-0.25671800	-1.35623200
H	-3.15896400	1.01492900	-1.95505700
C	-4.62882900	-1.20062300	0.85214400
H	-2.91190900	-0.60655400	2.01182300
C	-5.31653800	-1.06786300	-0.35241900
H	-5.31162500	-0.13769000	-2.29877900
H	-5.03969500	-1.81841500	1.64745100
H	-6.26058300	-1.58344800	-0.50743800
B	-0.80592100	1.11416700	2.20520200
H	0.04791800	1.98276900	2.33983000
H	-0.32282700	0.01470400	2.48455100
H	-1.62655400	2.41080000	-0.04270800
H	-1.78879700	1.34920900	2.89038500
C	1.18689500	-1.40629100	-0.28620000
C	0.66626500	-2.79801800	-0.21383500
C	1.94400300	-3.59973200	0.12754100
H	1.76051300	-4.33976900	0.91060300
H	2.29176800	-4.13713800	-0.76051100
C	3.02039300	-2.58738600	0.57045300
C	-0.40990800	-2.87464600	0.88424800
H	-1.26312700	-2.23335600	0.64787400
H	-0.02476100	-2.57310400	1.86153000
H	-0.76241500	-3.90902500	0.95062400
C	0.05320900	-3.19720900	-1.56318200
H	-0.28321200	-4.23738600	-1.50953700
H	0.78033800	-3.11510700	-2.37730700
H	-0.81226400	-2.57210700	-1.80146100
C	3.16054800	-2.46980300	2.08699300
H	3.56493100	-3.40709900	2.47963200
H	2.19793600	-2.27959000	2.56910600
H	3.84811100	-1.66323000	2.35783100
C	4.37078300	-2.86642700	-0.07368300
H	5.13181700	-2.14706700	0.23949700
H	4.30363000	-2.87186300	-1.16586500
H	4.69991900	-3.85967600	0.24608400
C	3.08943200	-0.01921400	0.16764400
C	3.25621000	2.14305400	1.18854700
H	2.88632700	2.87231200	1.90248600
C	4.33790100	2.44281800	0.36392000
H	4.82645300	3.40971800	0.43891900
C	4.78421900	1.50947400	-0.57159500
H	5.61282300	1.74866800	-1.23104900
N	2.41875600	-1.29047400	0.06924000
C	2.62261400	0.90593800	1.09763900
H	1.76007100	0.68202800	1.72190600
C	4.16012000	0.26988500	-0.67782800
H	4.48512800	-0.44643300	-1.42433300
H	0.58701100	-0.52101500	-0.55094900

C-1'$_{pair}$ (THF); E_H = −1199.38666950

C	-1.44521700	0.11390900	-1.63118400
C	-0.90034500	0.53345500	-0.31389600
C	-3.20040800	0.92176900	-0.05354500
C	-2.91993700	0.57140000	-1.53144100
H	-3.07268200	1.45860300	-2.15290400
H	-3.60736600	-0.20118500	-1.88435000
C	-1.28876400	-1.41558500	-1.74113200
H	-1.70482900	-1.73965600	-2.70009600

H	-0.23505100	-1.70858000	-1.70683000
H	-1.82050100	-1.94065100	-0.94231500
C	-0.67866500	0.79736900	-2.77038500
H	0.37765000	0.51235300	-2.76413900
H	-1.11404000	0.49112500	-3.72657600
H	-0.74250400	1.88714300	-2.69856400
C	-3.97674800	-0.16199800	0.68980400
H	-4.05815100	0.06672600	1.75634600
H	-4.98824000	-0.21350500	0.27748300
H	-3.51093400	-1.14461900	0.57457600
C	-3.87405700	2.27749200	0.10655900
H	-4.84798800	2.23616400	-0.38948100
H	-4.04423000	2.52730700	1.15737800
H	-3.28872800	3.07287500	-0.36392400
N	-1.79287100	0.96138100	0.50622300
C	-1.49686700	1.32253000	1.86848900
C	-1.44047200	2.66602200	2.23176600
C	-1.25374900	0.30776800	2.79137600
C	-1.13946600	2.99341200	3.55136700
H	-1.60725800	3.44247500	1.49307900
C	-0.95497400	0.64934200	4.10797000
H	-1.29246100	-0.73143700	2.47981300
C	-0.90096700	1.98896900	4.48845900
H	-1.08265000	4.03753700	3.84252000
H	-0.75931100	-0.13458600	4.83276500
H	-0.66438800	2.25143100	5.51505000
H	4.74220900	0.49817900	-1.61300800
H	2.92849400	0.94524800	-2.39105100
H	3.73455600	2.15338600	-1.01065000
B	3.64307200	0.99173600	-1.39403500
C	2.81841500	-1.76606000	-0.30597900
C	2.85448900	-2.71975400	0.72633200
C	2.80088100	-2.23875400	-1.62837500
C	2.87711000	-4.08504100	0.44983900
H	2.87105000	-2.38659700	1.76237100
C	2.81122900	-3.60598400	-1.90724100
H	2.79804400	-1.52259200	-2.44652900
C	2.85011000	-4.53816800	-0.87093100
H	2.91736300	-4.79912000	1.26907100
H	2.80188600	-3.94286000	-2.94127300
H	2.86690100	-5.60282800	-1.08758200
P	2.68225600	0.03304600	0.04292500
H	3.56194200	0.05815200	1.16152500
H	0.16076100	0.46931600	-0.01991900

D (THF); E_H = −599.45005436

C	1.20306100	-1.42254200	-0.33180200
C	0.66969600	-2.80629900	-0.24461700
C	1.92771900	-3.60053400	0.18205700
H	1.70581500	-4.29708600	0.99374600
H	2.29729300	-4.18609500	-0.66437600
C	3.00505900	-2.58120500	0.61402500
C	-0.44912700	-2.82773600	0.81446300
H	-1.28163500	-2.17984900	0.52498800
H	-0.08945300	-2.51525400	1.79867300
H	-0.82679200	-3.85117800	0.89756500
C	0.11023900	-3.25253300	-1.60156500
H	-0.23399200	-4.28767200	-1.51940100
H	0.87163400	-3.20715300	-2.38549600
H	-0.74071600	-2.63408700	-1.90189300
C	3.15016300	-2.45241600	2.12779400
H	3.55161800	-3.39072400	2.51979800
H	2.18874500	-2.26374200	2.61344700
H	3.84451400	-1.65086100	2.39499600
C	4.35297700	-2.84502400	-0.04148000
H	5.10147600	-2.10325100	0.24922000
H	4.27187300	-2.87136900	-1.13203200
H	4.70591700	-3.82469500	0.29327400
C	3.07722800	-0.01558500	0.17812700
C	3.37242400	2.08636100	1.29662800
H	3.11026000	2.77082700	2.09710200
C	4.34202800	2.43795500	0.35932000
H	4.83906000	3.40051100	0.42949100
C	4.67115300	1.55968300	-0.67241800
H	5.41783000	1.83731600	-1.40955600
N	2.40723800	-1.28792300	0.09176200
C	2.73168200	0.85271700	1.21130300
H	1.97602000	0.56596400	1.93612400
C	4.03996200	0.32234400	-0.77024700
H	4.27972900	-0.35947200	-1.57908600
H	0.65174200	-0.55766600	-0.69495400

D (toluene); E_H = −599.43047691

C	1.20458100	-1.42266800	-0.32825300
C	0.66911900	-2.80578100	-0.24246300
C	1.92929400	-3.60158900	0.17592200
H	1.70997100	-4.30377700	0.98361900
H	2.29661000	-4.18249900	-0.67493400
C	3.00744700	-2.58401300	0.61093700
C	-0.44526400	-2.83140000	0.82139200
H	-1.27940500	-2.18131500	0.54113000
H	-0.08145300	-2.52752800	1.80696200
H	-0.82611200	-3.85398600	0.90005200
C	0.10324700	-3.24579900	-1.59913000
H	-0.24174000	-4.28098600	-1.52180300
H	0.85985800	-3.19809200	-2.38782700
H	-0.74973400	-2.62716200	-1.89368500
C	3.14797100	-2.45263100	2.12507300
H	3.54727900	-3.38957800	2.52254100
H	2.18506200	-2.26206700	2.60737800
H	3.84163000	-1.65097600	2.39353700
C	4.35686500	-2.84956500	-0.04053100
H	5.10607500	-2.10915800	0.25140300
H	4.28009500	-2.87726200	-1.13152400

H	4.70885100	-3.82949500	0.29462100
C	3.08075600	-0.01579100	0.17583800
C	3.36253400	2.09078600	1.28888600
H	3.09359800	2.77794800	2.08469600
C	4.33842300	2.44048700	0.35774200
H	4.83271000	3.40429500	0.42795900
C	4.67795700	1.55920900	-0.66775600
H	5.42969900	1.83631000	-1.39983000
N	2.41129000	-1.28898200	0.08873000
C	2.72519700	0.85563000	1.20312600
H	1.96676700	0.56868100	1.92539900
C	4.05073100	0.32010900	-0.76591400
H	4.29917900	-0.36397300	-1.57041400
H	0.65335000	-0.55565400	-0.68790000

E (THF); E_H = −599.91947563

P	-1.39385600	0.91193500	0.75408000
C	-3.05943300	0.55339700	0.06430100
C	-3.39655800	0.84655500	-1.26892200
C	-4.02331800	-0.10746700	0.84456200
C	-4.63799600	0.49796000	-1.79740100
H	-2.67494100	1.35859500	-1.90258100
C	-5.26314100	-0.46531300	0.31593100
H	-3.79793500	-0.33280800	1.88402200
C	-5.58073600	-0.16466000	-1.00896600
H	-4.87096800	0.74624400	-2.83043200
H	-5.98840600	-0.97460800	0.94656800
H	-6.54864000	-0.43834100	-1.42032100
B	-1.67197300	1.59038800	2.59619600
H	-0.58985000	2.05787300	2.94105600
H	-1.94345400	0.62453700	3.30321300
H	-1.16884600	2.09622300	-0.00791800
H	-2.56080100	2.43573000	2.64179000

E (toluene); E_H = −599.89434458

P	-1.39572200	0.99952800	0.71798200
C	-3.05965600	0.60257000	0.04244100
C	-3.38820800	0.81714000	-1.30821200
C	-4.02988700	-0.01312900	0.85092500
C	-4.62539300	0.44087100	-1.82530100
H	-2.65840100	1.28904000	-1.96371400
C	-5.26450400	-0.40351300	0.33331700
H	-3.81058900	-0.16621200	1.90464800
C	-5.57371100	-0.17870100	-1.00819200
H	-4.85112400	0.63029700	-2.87281500
H	-5.99502300	-0.87520300	0.98745300
H	-6.53881200	-0.47618700	-1.41063200
B	-1.66316100	1.51780600	2.61381900
H	-0.60000600	2.01971400	2.96720600
H	-1.85712900	0.48318300	3.24680900
H	-1.26125700	2.24780000	0.03863400
H	-2.59826800	2.30123700	2.74081100

F (THF); E_H = −1199.42894789

C	0.11742900	-1.84851500	-0.99847200
C	-0.05712800	-0.43317100	-0.40967200
C	-2.10509900	-1.67414100	0.09544500
C	-0.92384600	-2.62563300	-0.18730100
H	-1.25849600	-3.53378000	-0.69870400
H	-0.47150600	-2.92975600	0.76412400
C	1.51202800	-2.45242200	-0.85287100
H	1.52127000	-3.45142700	-1.30249300
H	2.26616600	-1.85020300	-1.36979600
H	1.80871600	-2.56031400	0.19439400
C	-0.22086100	-1.77882600	-2.49566500
H	0.60262800	-1.30955900	-3.04527600
H	-0.36758400	-2.78513900	-2.90267800
H	-1.12375600	-1.19493900	-2.69168700
C	-2.61547700	-1.94331600	1.51903600
H	-3.55928300	-1.44386400	1.74820300
H	-2.78875000	-3.01958800	1.62858100
H	-1.87112200	-1.64301000	2.26021300
C	-3.24453100	-1.89899300	-0.90929500
H	-3.67117500	-2.89340200	-0.74227600
H	-4.05019600	-1.17061500	-0.79432300
H	-2.89384100	-1.85243900	-1.94180600
N	-1.46247500	-0.33686300	-0.07423400
P	1.00943800	0.02012200	1.09124600
H	0.40911900	1.25871600	1.39559900
B	1.12830400	-1.08315200	2.68176100
H	1.83902900	-0.41064100	3.40540100
H	0.00283700	-1.18355000	3.11701300
H	1.62810400	-2.14856100	2.38846300
C	2.62924000	0.53439000	0.43677200
C	2.74753800	1.62787800	-0.43111000
C	3.77730500	-0.17480700	0.80748600
C	3.99445900	1.99777200	-0.92932500
H	1.87164900	2.20737500	-0.71197300
C	5.02336600	0.19674900	0.30699700
H	3.69450300	-1.01406000	1.49222900
C	5.13320400	1.28041900	-0.56317700
H	4.07666500	2.84970500	-1.59800700
H	5.90911600	-0.35861600	0.60152400
H	6.10557900	1.57078900	-0.95063300
C	-2.11786200	0.88858600	-0.04670000
C	-1.49352300	2.06808900	-0.51239100
C	-3.43193100	1.02962600	0.45042200
C	-2.14755500	3.29681200	-0.49090500
H	-0.48788400	2.04395800	-0.91283600
C	-4.07620000	2.26137400	0.46149700
H	-3.96229100	0.17528200	0.84418600
C	-3.44741700	3.41382500	-0.00718100
H	-1.62198600	4.17207400	-0.86398700

H	-5.08832900	2.31402000	0.85438000
H	-3.95390000	4.37374400	0.00963800
H	0.22686000	0.30266500	-1.17092500

F (toluene); E_H = −1199.42469202

C	0.11604700	-1.85333900	-0.99712400
C	-0.05402900	-0.43819000	-0.40691200
C	-2.10535600	-1.67166300	0.09743400
C	-0.92620400	-2.62705100	-0.18355000
H	-1.26356700	-3.53549300	-0.69321600
H	-0.47365100	-2.92974200	0.76814900
C	1.50986200	-2.46000600	-0.85513500
H	1.51822400	-3.45725500	-1.30892800
H	2.26466000	-1.85670200	-1.37015500
H	1.80700400	-2.57202100	0.19134200
C	-0.22594800	-1.78143100	-2.49341600
H	0.59848300	-1.31652200	-3.04559900
H	-0.37834600	-2.78652900	-2.90174000
H	-1.12650400	-1.19288400	-2.68655800
C	-2.61394600	-1.93410700	1.52296600
H	-3.55640800	-1.43155600	1.75110700
H	-2.78911000	-3.00958100	1.63808100
H	-1.86852500	-1.63257800	2.26240900
C	-3.24670100	-1.89764100	-0.90515400
H	-3.68274800	-2.88637300	-0.72816500
H	-4.04532100	-1.16025100	-0.79893500
H	-2.89584900	-1.86464200	-1.93819500
N	-1.46052100	-0.33730500	-0.07903800
P	1.00689700	0.00440400	1.10136700
H	0.39881500	1.23753600	1.41406300
B	1.13994400	-1.11857800	2.67594500
H	1.84301300	-0.44417500	3.40364300
H	0.01638900	-1.23767400	3.10888200
H	1.65312500	-2.17167400	2.36328000
C	2.62087200	0.53509100	0.44337500
C	2.72942100	1.62691100	-0.42754100
C	3.77551600	-0.16177700	0.81585700
C	3.97209500	2.00685700	-0.92806200
H	1.84748500	2.19818300	-0.70716900
C	5.01748800	0.21936700	0.31279600
H	3.69907800	-0.99698800	1.50631100
C	5.11717100	1.30063000	-0.56099900
H	4.04661100	2.85818400	-1.59857600
H	5.90862400	-0.32623100	0.60948500
H	6.08671900	1.59866400	-0.94986900
C	-2.11144000	0.89083000	-0.05221700
C	-1.48282900	2.06690600	-0.51950600
C	-3.42451700	1.03753400	0.44425800
C	-2.13258900	3.29762700	-0.50131800
H	-0.47665700	2.03717400	-0.91851900
C	-4.06434200	2.27106800	0.45218700
H	-3.95609300	0.18568700	0.84168900
C	-3.43179000	3.41986100	-0.01895000
H	-1.60440400	4.17082400	-0.87557500
H	-5.07598300	2.32868100	0.84548500
H	-3.93489300	4.38146600	-0.00421400
H	0.23527200	0.29713900	-1.16686400

F' (THF); E_H = −1199.42684957

C	0.24568100	2.37301400	-0.16531900
C	-0.23417100	1.08534900	0.57985900
C	-1.78724400	1.35891100	-1.19265300
C	-0.71630100	2.43875100	-1.37595400
H	-1.16861600	3.43021900	-1.48093000
H	-0.15910200	2.23460900	-2.29662100
C	1.68646400	2.31225700	-0.68002500
H	1.88761300	3.20576900	-1.28177600
H	2.41470700	2.29631100	0.13738200
H	1.85163700	1.43780500	-1.31599600
C	0.10359700	3.58857100	0.75576100
H	0.73442200	3.48075300	1.64445700
H	0.41219900	4.49834000	0.22933900
H	-0.93118000	3.72743800	1.08682200
C	-2.23282200	0.79632000	-2.53741500
H	-3.02389900	0.04879300	-2.42553500
H	-2.63065700	1.60937300	-3.15402000
H	-1.38952400	0.34327100	-3.06799100
C	-3.00953500	1.90233100	-0.43971300
H	-3.48606900	2.69257000	-1.02880200
H	-3.74957000	1.11379800	-0.27012600
H	-2.74084500	2.33008100	0.53147600
N	-1.03784300	0.34427800	-0.38438100
P	1.07343200	0.06979500	1.44290600
C	-1.79436900	-0.77076000	0.08248000
C	-2.34164800	-0.84514400	1.37144500
C	-1.99799800	-1.85106500	-0.78770700
C	-3.06677200	-1.96548200	1.77419700
H	-2.21039000	-0.02651500	2.07276000
C	-2.73807900	-2.96187800	-0.39001000
H	-1.55966100	-1.81507000	-1.78029200
C	-3.27357000	-3.02737100	0.89578600
H	-3.47623100	-2.00200400	2.78003500
H	-2.88124100	-3.78586300	-1.08368900
H	-3.83918300	-3.89898600	1.21188600
H	0.28544600	-0.99937100	1.91028500
H	2.56154500	0.12613800	3.49481300
H	2.61594400	1.87495100	2.47392300
H	0.99421200	1.40149800	3.58758800
B	1.92172500	0.98485700	2.92005700
C	2.19748400	-0.76711700	0.28368100
C	1.73034200	-1.69687300	-0.65348600
C	3.56916600	-0.50294000	0.37095300
C	2.62684300	-2.33963300	-1.50423700
H	0.67034900	-1.92092700	-0.71695600

C	4.46217600	-1.14930600	-0.48082700
H	3.93600800	0.20682600	1.10720100
C	3.99175100	-2.06477400	-1.42140600
H	2.25844100	-3.05975400	-2.22933700
H	5.52536400	-0.93980800	-0.40651700
H	4.68868400	-2.56945700	-2.08456100
H	-0.82573200	1.42051200	1.45236100

F' (toluene); E_H = −1199.42294119

C	0.24731800	2.36638500	-0.16989200
C	-0.23299400	1.08030300	0.57765400
C	-1.78906700	1.35386000	-1.19227500
C	-0.71645300	2.43156600	-1.37914900
H	-1.16713900	3.42387900	-1.48536100
H	-0.16107700	2.22446900	-2.30033000
C	1.68754100	2.30360800	-0.68612400
H	1.88911900	3.19630300	-1.28918600
H	2.41594500	2.28852500	0.13094400
H	1.85176000	1.42793000	-1.32054700
C	0.10829500	3.58283000	0.75061800
H	0.73715900	3.47295600	1.64024500
H	0.42050900	4.49176800	0.22464700
H	-0.92661100	3.72558000	1.08016200
C	-2.23830900	0.79068700	-2.53574500
H	-3.03135400	0.04555700	-2.42182600
H	-2.63461400	1.60348300	-3.15381500
H	-1.39642000	0.33479500	-3.06618800
C	-3.00949800	1.90039400	-0.43817400
H	-3.48855700	2.68863000	-1.02808900
H	-3.74884300	1.11251300	-0.26278600
H	-2.73752300	2.33194700	0.53041900
N	-1.04056900	0.33973400	-0.38423100
P	1.07540900	0.06948500	1.44490300
C	-1.79739400	-0.77320400	0.08550000
C	-2.33733000	-0.84769200	1.37744800
C	-2.00883000	-1.85268700	-0.78368700
C	-3.06304700	-1.96606300	1.78337700
H	-2.19830100	-0.03022500	2.07869600
C	-2.74960900	-2.96144600	-0.38269400
H	-1.57525900	-1.81674300	-1.77838600
C	-3.27798300	-3.02637400	0.90563700
H	-3.46610500	-2.00264600	2.79177100
H	-2.89879800	-3.78484900	-1.07582600
H	-3.84383200	-3.89675500	1.22450900
H	0.28779000	-1.00237600	1.90810600
H	2.55661700	0.14021200	3.49773600
H	2.60643700	1.88323100	2.46404100
H	0.98280700	1.40970600	3.57680500
B	1.91668600	0.99409600	2.91828300
C	2.19949200	-0.76342600	0.28224400
C	1.73320200	-1.66398000	-0.68313200
C	3.57320000	-0.52328900	0.39785100
C	2.63338200	-2.30185200	-1.53316900
H	0.67069500	-1.86724600	-0.76871300
C	4.46966700	-1.16474900	-0.45382000
H	3.93699100	0.16295200	1.15764500
C	4.00071500	-2.05102600	-1.42204200
H	2.26614700	-2.99999700	-2.28018300
H	5.53472000	-0.97449000	-0.35718300
H	4.70052500	-2.55224300	-2.08493200
H	-0.82363500	1.41936000	1.44941100

TS4 (THF); E_H = −1199.39272398

C	0.19480000	2.22889700	-0.49459400
C	0.50814500	0.76616300	-0.62230500
C	2.27930100	1.57534600	0.70679800
C	1.15906100	2.63853200	0.63871200
H	1.57038100	3.63960300	0.48240500
H	0.61169600	2.64662700	1.58623900
C	-1.26088200	2.56797500	-0.19347700
H	-1.38590700	3.65594100	-0.19453200
H	-1.92925400	2.14971600	-0.95254900
H	-1.56523200	2.18277900	0.78261100
C	0.58289400	2.86199800	-1.84969100
H	-0.08021400	2.51175000	-2.64711900
H	0.48150500	3.94953100	-1.77635100
H	1.61319800	2.63429800	-2.13646400
C	2.49795600	1.08850700	2.13634900
H	3.28994300	0.33589800	2.19253400
H	2.80015700	1.93991500	2.75397500
H	1.57365700	0.67540300	2.55191200
C	3.59971100	2.03484200	0.09304700
H	4.01494100	2.84199400	0.70346400
H	4.32833700	1.21850800	0.07395500
H	3.46951500	2.40947800	-0.92569400
N	1.69476000	0.48309600	-0.13980700
P	-1.38800400	-0.60105200	1.08925000
H	-0.96106800	-1.95291100	1.00273600
B	-1.61621200	-0.16599700	2.99486200
H	-2.40069000	-0.94796900	3.51081300
H	-0.49669700	-0.24961600	3.48268500
H	-2.01699000	0.98849500	3.05020600
C	-3.00668800	-0.78765900	0.26397600
C	-3.19687700	-1.70834000	-0.78024800
C	-4.07954800	0.04804000	0.61216000
C	-4.41649100	-1.79388300	-1.44789300
H	-2.38356900	-2.37117200	-1.06848100
C	-5.29772200	-0.03269800	-0.06121600
H	-3.96087900	0.75685200	1.42782600
C	-5.47316400	-0.95310500	-1.09438400
H	-4.54301600	-2.52125500	-2.24589300
H	-6.11607600	0.62120800	0.22951900
H	-6.42450000	-1.01955000	-1.61490100
C	2.35063600	-0.76405300	-0.38461300

C	2.99322000	-0.96112500	-1.60709900
C	2.33036300	-1.77049300	0.58154900
C	3.62661400	-2.17510900	-1.86233200
H	2.99563400	-0.16525200	-2.34617800
C	2.96818600	-2.98081000	0.31756600
H	1.80982000	-1.61499400	1.52036400
C	3.61705000	-3.18369200	-0.89974600
H	4.12806300	-2.33022900	-2.81285200
H	2.95061100	-3.76820900	1.06495700
H	4.11174900	-4.12954500	-1.09961600
H	0.05100400	0.09986000	-1.34439600

TS4 (toluene); E_H = −1199.38447630

C	0.16860200	2.16500200	-0.55451800
C	0.52333700	0.70947200	-0.67117600
C	2.24114900	1.57263200	0.69798000
C	1.08499400	2.59465700	0.61097300
H	1.46310700	3.61280600	0.48032800
H	0.51000800	2.56611800	1.54158600
C	-1.30344100	2.46412900	-0.29376600
H	-1.46189500	3.54789100	-0.30982200
H	-1.94264600	2.01694100	-1.06141900
H	-1.61895500	2.08153500	0.67956300
C	0.58022200	2.81494600	-1.89391900
H	-0.05350900	2.45635600	-2.71162200
H	0.45502100	3.90021200	-1.82096500
H	1.62252100	2.60929100	-2.15373700
C	2.45494700	1.09353200	2.13114400
H	3.28959900	0.38922200	2.20203600
H	2.69192100	1.95761100	2.75981400
H	1.55019100	0.62135800	2.52584300
C	3.55552200	2.08382900	0.11055600
H	3.93501500	2.89768900	0.73565100
H	4.31156500	1.29254200	0.09482500
H	3.42996300	2.46541200	-0.90634300
N	1.71340900	0.46560500	-0.16312100
P	-1.37464200	-0.68368200	1.01727900
H	-1.00654700	-2.04972600	0.89681300
B	-1.47950400	-0.20350800	2.91852400
H	-2.30034900	-0.91305000	3.47377700
H	-0.34928500	-0.36997500	3.35453100
H	-1.78141700	0.98081800	2.95914000
C	-3.02613900	-0.77345600	0.24587200
C	-3.26981700	-1.58284800	-0.87573300
C	-4.07249800	0.02763900	0.72684000
C	-4.51773000	-1.59402300	-1.49324000
H	-2.47580300	-2.21800900	-1.26339200
C	-5.31898700	0.02253600	0.10271600
H	-3.90938900	0.64337600	1.60756900
C	-5.54826000	-0.78666000	-1.00918400
H	-4.68760600	-2.23672300	-2.35346600
H	-6.11828100	0.64587300	0.49554900
H	-6.52231700	-0.79474600	-1.49047300
C	2.39441200	-0.77448900	-0.36173000
C	3.09943400	-0.98096400	-1.54758500
C	2.33285400	-1.77070300	0.61359000
C	3.75645700	-2.19130600	-1.75576100
H	3.12905800	-0.19394100	-2.29587100
C	2.99488200	-2.97723000	0.39739600
H	1.76076900	-1.60808600	1.52106600
C	3.70733700	-3.18784800	-0.78222200
H	4.30698900	-2.35348600	-2.67760400
H	2.94561100	-3.75630100	1.15210500
H	4.22046900	-4.13105500	-0.94484000
H	0.11288300	0.03532200	-1.41351500

TS4' (THF); E_H = −1199.39414559

C	0.37141700	2.05115200	-1.41569000
C	0.86782800	0.64306500	-1.20941200
C	1.09063300	1.62733200	0.93154600
C	0.18611600	2.51143300	0.04415300
H	0.41801300	3.57243700	0.17329000
H	-0.85909900	2.36161300	0.33365900
C	-0.89672100	2.19651400	-2.24694800
H	-1.11946300	3.25950500	-2.38860700
H	-0.78051600	1.73792300	-3.23330700
H	-1.75113800	1.72693800	-1.75506700
C	1.51298600	2.80901100	-2.12830300
H	1.64747300	2.43472400	-3.14826100
H	1.25675300	3.87180400	-2.18768900
H	2.46797700	2.71893800	-1.60399900
C	0.33654300	1.12907900	2.16236600
H	0.97573900	0.52657400	2.81442900
H	-0.00075100	1.99613300	2.73940900
H	-0.54395200	0.54490300	1.87887600
C	2.38352200	2.31911000	1.36417200
H	2.14084000	3.14501700	2.03938400
H	3.03665400	1.62489200	1.90229100
H	2.93660300	2.72457700	0.51326500
N	1.42226100	0.51319300	-0.01138200
P	-1.26378100	-1.04664400	-1.40219800
C	2.29414900	-0.56827900	0.31338000
C	3.55295900	-0.62790700	-0.28895600
C	1.89261800	-1.56672600	1.20283200
C	4.41121900	-1.68521400	0.00204300
H	3.85585500	0.15671000	-0.97643000
C	2.75986600	-2.61758000	1.49477700
H	0.90463000	-1.53213400	1.64775800
C	4.01778800	-2.67911400	0.89730600
H	5.38926600	-1.72795300	-0.46781700
H	2.44436800	-3.39568500	2.18343200
H	4.68850700	-3.50208900	1.12558600
H	-0.60490600	-2.23717000	-1.00158800
H	-2.83575700	-2.38864300	-3.02391900

H	-2.82835400	-0.38906400	-3.36463600
H	-1.25461700	-1.50451800	-3.93793900
B	-2.15661000	-1.37873200	-3.12221200
C	-2.46617600	-0.93163400	-0.03642700
C	-2.30745600	-1.65007400	1.15983700
C	-3.57056000	-0.07066900	-0.14916400
C	-3.21451700	-1.50704100	2.20844700
H	-1.47518900	-2.34185000	1.26686200
C	-4.47564700	0.07342000	0.89984300
H	-3.73260700	0.47765700	-1.07393600
C	-4.30074600	-0.64090700	2.08578900
H	-3.07490800	-2.08026600	3.12139700
H	-5.32576000	0.74125900	0.78728500
H	-5.00903500	-0.53060500	2.90204500
H	1.23320100	0.02192600	-2.01995000

TS4' (toluene); E_H = −1199.38594867

C	0.35589600	2.02885400	-1.41157400
C	0.85227000	0.62021700	-1.20192400
C	1.09495800	1.61850000	0.93308500
C	0.17993800	2.49473700	0.04801500
H	0.40734200	3.55781000	0.17123600
H	-0.86247200	2.34058000	0.34519500
C	-0.91920900	2.16662100	-2.23331700
H	-1.13621200	3.22744400	-2.39983400
H	-0.82246800	1.67876900	-3.20745100
H	-1.77194200	1.71637100	-1.72099400
C	1.49079100	2.78678600	-2.13362700
H	1.61374900	2.41471700	-3.15601200
H	1.23890400	3.85102400	-2.18999900
H	2.45106200	2.69229600	-1.61887100
C	0.34959800	1.12191200	2.17058200
H	0.99517400	0.52264100	2.81972700
H	0.01227900	1.98819100	2.74912500
H	-0.53102500	0.53448800	1.89431500
C	2.38449600	2.32243500	1.35770200
H	2.14168100	3.14674800	2.03519100
H	3.04841500	1.63387100	1.89009700
H	2.92750100	2.73242500	0.50220400
N	1.42877500	0.50582800	-0.00613700
P	-1.27992100	-1.06830500	-1.39862700
C	2.30292400	-0.57171700	0.31789900
C	3.56296000	-0.62796700	-0.28241000
C	1.90416900	-1.57517600	1.20316200
C	4.42428300	-1.68299400	0.00639300
H	3.86260100	0.15908200	-0.96879700
C	2.77421700	-2.62376000	1.49416000
H	0.91386800	-1.54459300	1.64351800
C	4.03299700	-2.67997900	0.89876100
H	5.40268000	-1.72247600	-0.46315100
H	2.46003300	-3.40564900	2.17922700
H	4.70555800	-3.50195700	1.12519600
H	-0.62897600	-2.26387800	-1.00219600
H	-2.80276400	-2.32238100	-3.11151900
H	-2.78160400	-0.30601900	-3.35957000
H	-1.19167200	-1.39822900	-3.93651700
B	-2.12446800	-1.31170000	-3.15276400
C	-2.47652200	-0.93523800	-0.03322900
C	-2.30526600	-1.62397100	1.17847800
C	-3.59193700	-0.09181700	-0.16366200
C	-3.20943300	-1.46669800	2.22678300
H	-1.46723000	-2.30752000	1.29475400
C	-4.49335000	0.06729400	0.88581300
H	-3.76668600	0.42286400	-1.10520700
C	-4.30489300	-0.61503800	2.08798500
H	-3.06246800	-2.01894700	3.15150300
H	-5.35404900	0.71890400	0.75957400
H	-5.01208600	-0.49442600	2.90374400
H	1.22505300	0.00537000	-2.01441200

C-3$_{pair}$ (THF); E_H = −1199.38960487

C	-3.06548000	-1.59079100	0.17899400
C	-1.82375300	-0.91275600	0.64620900
C	-3.29523900	0.88862600	0.33296600
C	-4.08758500	-0.42810400	0.18456800
H	-4.69237300	-0.41808500	-0.72537700
H	-4.76946300	-0.53963800	1.03305200
C	-3.43551500	-2.71077700	1.16201200
H	-4.37905300	-3.16544300	0.84463300
H	-2.66509600	-3.48714700	1.17511600
H	-3.56617500	-2.32857700	2.17912000
C	-2.83746000	-2.18932600	-1.21980100
H	-2.03736900	-2.93396500	-1.19824000
H	-3.76226800	-2.67749600	-1.54344600
H	-2.57294800	-1.42303500	-1.95300800
C	-3.86081500	1.79741400	1.41587500
H	-3.26572100	2.70766100	1.53157600
H	-4.87454700	2.09087700	1.12821400
H	-3.91642800	1.28357100	2.38007200
C	-3.13717600	1.64492400	-0.98353500
H	-4.12475300	1.97781500	-1.31511400
H	-2.50847000	2.53139500	-0.86197500
H	-2.70842100	1.01152100	-1.76515000
N	-1.94417000	0.36372800	0.76175800
C	-0.88346000	1.22010000	1.22342200
C	-0.03204600	1.82019800	0.29898400
C	-0.73355500	1.42448400	2.59314400
C	0.98707400	2.64835900	0.76373500
H	-0.14731300	1.62112100	-0.76087200
C	0.29000500	2.25418300	3.04387800
H	-1.40445600	0.93612600	3.29310800
C	1.14619700	2.86832500	2.13091200
H	1.66362400	3.11194900	0.05259600
H	0.41848500	2.41557200	4.10964000

H	1.94509700	3.51222300	2.48615800
H	1.98244900	-3.58635600	0.61142900
H	0.89974100	-2.12724600	1.48784100
H	-0.03649900	-3.55167400	0.43838200
B	0.98946600	-2.88124000	0.51890300
C	2.67765100	-0.99150800	-1.22250700
C	3.26770200	-0.70402900	-2.46533100
C	3.37190800	-0.60597100	-0.06491700
C	4.50326000	-0.06564300	-2.54782100
H	2.75325400	-0.98786700	-3.38141100
C	4.60402600	0.04316800	-0.14574700
H	2.94520400	-0.83089300	0.90922800
C	5.17859300	0.31621700	-1.38676800
H	4.94110700	0.13446100	-3.52290200
H	5.12180000	0.32702200	0.76747800
H	6.14183500	0.81511500	-1.45021100
P	1.00996500	-1.74995200	-1.10245700
H	1.15869600	-2.67977200	-2.16951300
H	-0.89031100	-1.41531700	0.90768500

C-3$_{pair}$ (toluene); E_H = −1199.37491371

C	-3.23224900	-1.54318100	-0.12793100
C	-1.94754400	-0.81890900	-0.35864800
C	-3.15180800	0.68319900	0.98936900
C	-3.89422300	-0.66924100	0.96185100
H	-4.96237800	-0.53044900	0.77492500
H	-3.78875500	-1.16278500	1.93273200
C	-3.05153900	-2.99534900	0.31560300
H	-4.03905300	-3.42400500	0.51679200
H	-2.56112500	-3.58922900	-0.45855800
H	-2.44049200	-3.06434300	1.21800400
C	-3.99912400	-1.50800700	-1.46725600
H	-3.45223900	-2.04603800	-2.24717300
H	-4.96649500	-2.00079100	-1.32835800
H	-4.18199900	-0.48697000	-1.81471700
C	-2.70916300	1.07976800	2.39275000
H	-2.14268400	2.01533300	2.38694400
H	-3.59844700	1.22465600	3.01325900
H	-2.09641400	0.29770800	2.85040600
C	-3.93958700	1.81514800	0.33495200
H	-4.84204000	1.99618400	0.92591800
H	-3.36370500	2.74425200	0.31263600
H	-4.24747700	1.56336100	-0.68413600
N	-1.93220000	0.36112900	0.15982100
C	-0.84779900	1.29433100	-0.01247400
C	-0.95134800	2.29060000	-0.98092900
C	0.28560200	1.16794700	0.78385900
C	0.10221500	3.18648900	-1.14055300
H	-1.82976900	2.35060100	-1.61514300
C	1.33519400	2.06607300	0.60878700
H	0.35920900	0.35450200	1.49851800
C	1.24142100	3.07697900	-0.34471700
H	0.03669800	3.95990400	-1.89968900
H	2.23775700	1.95065200	1.20047700
H	2.06689600	3.76885500	-0.48213800
H	1.37396600	-3.48273600	0.88262700
H	-0.06131200	-2.06884600	0.93199300
H	-0.18315400	-3.55695000	-0.40432700
B	0.59198900	-2.83242500	0.20679000
C	2.96986400	-0.98366000	-0.46470300
C	3.88066900	-0.28851600	-1.27662400
C	3.21615300	-1.01434400	0.91494200
C	4.99914800	0.34026600	-0.73479500
H	3.70481200	-0.23668700	-2.34936200
C	4.32709200	-0.37156400	1.46430500
H	2.53626000	-1.56810300	1.55728800
C	5.22525800	0.30800900	0.64303800
H	5.69433500	0.86252600	-1.38804900
H	4.49848000	-0.41616600	2.53763500
H	6.09521300	0.80167400	1.06835700
P	1.45476200	-1.74350200	-1.19286300
H	2.11039900	-2.71972400	-1.99434900
H	-1.10644700	-1.15538200	-0.97028200

TS5 (THF); E_H = −1199.38381031

C	-2.98581100	-1.45739900	-0.12614600
C	-1.86528700	-0.66074300	-0.73666300
C	-2.39260000	0.55930600	1.20997300
C	-3.05774300	-0.83247900	1.28254700
H	-4.08705200	-0.76253900	1.64458800
H	-2.50142400	-1.46484400	1.98158000
C	-2.78967200	-2.96888700	-0.09356900
H	-3.66833900	-3.43070800	0.36841800
H	-2.68049700	-3.37390700	-1.10336200
H	-1.90028300	-3.24308700	0.47695600
C	-4.23483600	-1.13679900	-0.97702400
H	-4.12598300	-1.53172100	-1.99189300
H	-5.10489400	-1.61614800	-0.51758300
H	-4.43382300	-0.06414200	-1.04644100
C	-1.39078100	0.76647400	2.34141400
H	-0.91520200	1.74987600	2.28765900
H	-1.92366000	0.70342300	3.29511700
H	-0.61713500	-0.00684200	2.33327900
C	-3.39162600	1.71383300	1.17423900
H	-3.91589200	1.75852000	2.13311600
H	-2.88260400	2.67051800	1.02359600
H	-4.13659400	1.58745100	0.38453200
N	-1.68686900	0.47513700	-0.11478700
C	-0.91982400	1.55718000	-0.65976400
C	-1.49307900	2.35306200	-1.65165000
C	0.37598500	1.79883400	-0.20721600
C	-0.76027600	3.40659800	-2.19241700
H	-2.50320500	2.14652900	-1.99289800
C	1.09947900	2.85673300	-0.75291200

H	0.82594000	1.15451300	0.54030400
C	0.53391300	3.66131800	-1.74059500
H	-1.20238300	4.02656500	-2.96638700
H	2.11378500	3.04036600	-0.41206900
H	1.10469300	4.48223400	-2.16432800
H	0.75357400	-3.25328900	0.11091100
H	-0.40617800	-1.68578400	-0.31330500
H	-0.08815000	-3.05043200	-1.73193000
B	0.44370800	-2.48893000	-0.78865400
C	3.01902400	-0.97712100	-0.11136400
C	4.33582600	-0.54494900	-0.34396900
C	2.55984700	-0.98366600	1.21373100
C	5.16367600	-0.15214900	0.70496200
H	4.71712100	-0.51633200	-1.36296200
C	3.38055500	-0.57250100	2.26604200
H	1.55388200	-1.33911300	1.42321500
C	4.68760300	-0.15739000	2.01815000
H	6.18230800	0.16629900	0.49702000
H	2.99890300	-0.58961700	3.28428700
H	5.33020100	0.15589700	2.83646700
P	1.91243200	-1.40615400	-1.52268400
H	2.73992200	-2.42174000	-2.08318300
H	-1.51568600	-0.77087900	-1.75778400

TS5 (toluene); E_H = −1199.37440703

C	-3.10682300	-1.47115900	-0.17364000
C	-1.87165600	-0.72492700	-0.58083600
C	-2.77319000	0.63457900	1.11492900
C	-3.49651400	-0.72886600	1.12309000
H	-4.57947800	-0.60434300	1.20887800
H	-3.15969800	-1.31450200	1.98397500
C	-2.93871100	-2.97255400	0.03948400
H	-3.89977500	-3.39052000	0.35784700
H	-2.63041700	-3.47250000	-0.88156800
H	-2.18357800	-3.18472700	0.79830500
C	-4.12290100	-1.23621800	-1.31441700
H	-3.77969200	-1.69863600	-2.24497800
H	-5.07506100	-1.69937100	-1.03713000
H	-4.30219500	-0.17399800	-1.50418400
C	-2.02704200	0.89543900	2.41908400
H	-1.48981200	1.84780200	2.39409600
H	-2.75299200	0.93799500	3.23670400
H	-1.31700200	0.09172100	2.63481300
C	-3.68924600	1.80919000	0.78073100
H	-4.41733600	1.93052900	1.58797900
H	-3.12365800	2.74152600	0.69521600
H	-4.23903900	1.64631700	-0.15035000
N	-1.78669900	0.43402500	-0.00308700
C	-0.82667000	1.43760400	-0.37169100
C	-1.15456400	2.35533500	-1.36767600
C	0.41092300	1.46962700	0.26294400
C	-0.22409500	3.32719300	-1.72604400
H	-2.12114300	2.29974600	-1.85963500
C	1.33631800	2.44182000	-0.10723900
H	0.66238100	0.72375900	1.00893200
C	1.01829800	3.37186000	-1.09470300
H	-0.46805000	4.04257000	-2.50551800
H	2.31388100	2.45117700	0.36486000
H	1.74551000	4.12470400	-1.38389200
H	1.00316200	-3.28479600	0.59609900
H	-0.33171800	-1.82176500	0.31062800
H	-0.18321400	-3.27943700	-1.04922200
B	0.46138500	-2.60514600	-0.26020300
C	3.03551700	-0.91058700	-0.30822200
C	4.16465100	-0.30174400	-0.88075200
C	2.95745700	-0.95266300	1.09094500
C	5.18002400	0.22972600	-0.08950200
H	4.24441300	-0.24160800	-1.96446600
C	3.96346400	-0.40328700	1.88820000
H	2.10790200	-1.44679200	1.55614200
C	5.08115000	0.18891300	1.30299500
H	6.04880000	0.68418300	-0.55996500
H	3.87951900	-0.45368400	2.97154400
H	5.86936900	0.60891800	1.92225400
P	1.66746600	-1.52770400	-1.38209200
H	2.41391900	-2.54108900	-2.04708500
H	-1.23855100	-0.95326100	-1.43401600

G (THF); E_H = −600.21989081

C	2.38354500	-0.70239900	0.06430300
C	2.27801300	0.72523200	-0.48911000
H	3.02925500	1.39881200	-0.06337100
H	2.44515700	0.69583900	-1.57280500
C	0.84085500	1.23072500	-0.21250600
C	2.72424200	-0.73061200	1.55813500
H	2.83244400	-1.76513000	1.90382700
H	1.94311000	-0.26045300	2.16206900
H	3.66865100	-0.21007800	1.75287600
C	3.40502600	-1.53752400	-0.70373200
H	4.41623100	-1.14041400	-0.55994700
H	3.19158100	-1.53890300	-1.77846200
H	3.40472600	-2.57693600	-0.35545400
C	0.84411800	2.19621800	0.98229600
H	1.46538100	3.06560700	0.74114200
H	1.25922800	1.72058400	1.87398700
H	-0.15150400	2.56726300	1.23413200
C	0.30834100	1.94049300	-1.46395800
H	-0.68578400	2.37060800	-1.31981100
H	0.25997100	1.24324600	-2.30692300
H	0.98799000	2.75563700	-1.73488000
C	-1.26266300	-0.18704700	0.05400800
C	-3.53374600	0.68270300	0.30398300
H	-4.18066000	1.53489700	0.49772100
C	-4.08837200	-0.57750900	0.07803900

H	-5.16405200	-0.72437500	0.08933400
C	-3.22127200	-1.64048800	-0.16287700
H	-3.61743200	-2.63582700	-0.34910300
N	0.11212900	-0.03518300	0.07474200
C	-2.15785100	0.87992000	0.29664000
H	-1.78289300	1.87458800	0.49523900
C	-1.84115700	-1.45651300	-0.18181000
H	-1.21082700	-2.31283000	-0.39036100
C	0.95481800	-1.19582800	-0.16504600
H	0.83992200	-1.57769300	-1.19564000
H	0.69373200	-2.01145800	0.51997300

G (toluene); E_H = −600.21792944

C	2.38387800	-0.70258100	0.06552500
C	2.27784000	0.72404700	-0.49059100
H	3.02991500	1.39836100	-0.06706200
H	2.44416700	0.69289200	-1.57448700
C	0.84062300	1.22940500	-0.21304800
C	2.72410700	-0.72751200	1.55946800
H	2.83578600	-1.76095000	1.90727500
H	1.94021100	-0.25983400	2.16153100
H	3.66683000	-0.20404300	1.75488800
C	3.40511800	-1.53923100	-0.70103300
H	4.41683000	-1.14290600	-0.55849100
H	3.19209000	-1.54310400	-1.77587200
H	3.40510800	-2.57817200	-0.35130000
C	0.84708100	2.19916500	0.97854100
H	1.46905700	3.06742800	0.73453700
H	1.26135900	1.72548500	1.87158500
H	-0.14779600	2.57172400	1.23051900
C	0.30415500	1.93518300	-1.46510800
H	-0.69241000	2.35914300	-1.32022900
H	0.25596000	1.23625900	-2.30663000
H	0.97907800	2.75333600	-1.73927100
C	-1.26295700	-0.18687600	0.05711800
C	-3.53227600	0.68176000	0.31181700
H	-4.17929700	1.53216400	0.51254000
C	-4.08659400	-0.57574000	0.07450500
H	-5.16225900	-0.72216400	0.08333700
C	-3.22048000	-1.63684000	-0.17391400
H	-3.61717500	-2.63024100	-0.36862500
N	0.11373600	-0.03491200	0.08021300
C	-2.15661700	0.87790200	0.30814900
H	-1.78040300	1.86988400	0.51752900
C	-1.84062800	-1.45323200	-0.18962400
H	-1.21019900	-2.30785800	-0.40453300
C	0.95448300	-1.19494100	-0.16220900
H	0.83887500	-1.57709000	-1.19314700
H	0.69305900	-2.01073900	0.52274600

H (THF); E_H = −599.18608125

B	-3.01669900	0.68511100	0.65148500
H	-4.13489600	0.31547000	0.85675300
H	-2.66212000	1.79014200	0.93738500
P	-1.93934400	-0.37924800	-0.39003100
H	-2.16345300	-1.73771600	-0.09828200
C	-0.15302400	-0.14761100	-0.14545700
C	0.40552100	1.13375600	-0.24440600
C	0.68853400	-1.24256700	0.08742000
C	1.77739100	1.31624400	-0.08960300
H	-0.23127000	1.99270100	-0.44030900
C	2.06230600	-1.05535800	0.23226500
H	0.27377300	-2.24436000	0.16350000
C	2.61119300	0.22315400	0.14770400
H	2.19621700	2.31613200	-0.16134400
H	2.70282900	-1.91345200	0.41614800
H	3.68152700	0.36722100	0.26266100

H (toluene); E_H = −599.18466517

B	-3.01476400	0.68120900	0.65602500
H	-4.13158400	0.30917000	0.86402200
H	-2.66077100	1.78521200	0.94641900
P	-1.93943900	-0.37422500	-0.39731100
H	-2.16203900	-1.73413100	-0.10862500
C	-0.15348000	-0.14575200	-0.14867400
C	0.40677000	1.13431500	-0.24930800
C	0.68664200	-1.24033300	0.08858600
C	1.77804500	1.31580600	-0.09200100
H	-0.22922600	1.99302200	-0.44870900
C	2.05994900	-1.05450800	0.23564100
H	0.27047600	-2.24147200	0.16657000
C	2.61016100	0.22285300	0.14937000
H	2.19803300	2.31512100	-0.16511200
H	2.69931400	-1.91277100	0.42284100
H	3.68039800	0.36610400	0.26615800

TS2 (THF); E_H = −1199.32957625

P	-2.91289300	-0.76091200	-1.65460400
H	-3.54138400	-1.79524400	-2.39142000
C	-4.29765800	-0.29213600	-0.55703600
C	-5.36984200	-1.15976000	-0.31434200
C	-4.23889500	0.92522700	0.13586800
C	-6.36907300	-0.81135000	0.59352000
H	-5.43138100	-2.10988100	-0.83871800
C	-5.24333900	1.27456700	1.03546000
H	-3.40548400	1.60451300	-0.02589800
C	-6.31106000	0.40732100	1.26760800
H	-7.19668300	-1.49313300	0.76891900
H	-5.18896200	2.22495500	1.55913700
H	-7.09211400	0.67947800	1.97176500
B	-0.79560400	-0.94801500	-0.66487500
H	-0.90261000	0.16770000	-0.21893200

H	-0.23843400	-1.12021400	-1.72392600
H	-3.01944900	0.24591400	-2.64658500
H	-1.10593500	-1.89868800	0.00828500
C	1.55090700	-1.06537800	0.17873500
C	2.36518400	-2.34139400	0.28763000
C	3.82905100	-1.93901100	-0.01987000
H	4.54399000	-2.40450600	0.66613600
H	4.09626600	-2.25650800	-1.03398000
C	3.88684700	-0.40700900	0.07060900
C	2.19536000	-2.86066500	1.72481300
H	1.14246900	-3.07086800	1.93708000
H	2.55043500	-2.13732200	2.46605100
H	2.76701700	-3.78708900	1.85404300
C	1.84823500	-3.39943800	-0.68938600
H	2.44514800	-4.31532200	-0.60270500
H	1.91180700	-3.04744800	-1.72439600
H	0.80251200	-3.64094600	-0.47957500
C	4.50397600	0.09630700	1.37553600
H	5.56596300	-0.16782700	1.40292800
H	4.01788300	-0.35134000	2.24725900
H	4.42671300	1.18524300	1.45686300
C	4.60570400	0.21814800	-1.12046900
H	4.61035100	1.31116000	-1.06685800
H	4.14541900	-0.08732200	-2.06530300
H	5.64695300	-0.12054900	-1.12612800
C	1.97479100	1.28679200	0.02503500
C	1.20612800	3.25397800	1.19091600
H	0.93865800	3.74933500	2.11992800
C	1.11322000	3.93819500	-0.02069800
H	0.77542800	4.97038900	-0.03929000
C	1.44721000	3.29008800	-1.20927200
H	1.36528600	3.81322000	-2.15776400
N	2.40688700	-0.08205300	0.05743900
C	1.63723500	1.92925500	1.21543400
H	1.69970900	1.38220600	2.15135500
C	1.87946600	1.96521700	-1.18920800
H	2.12273600	1.45109800	-2.11353000

TS2 (toluene); E_H = −1199.32446882

P	-2.90425000	-0.80812600	-1.60385900
H	-3.52823500	-1.85335800	-2.33129800
C	-4.29979400	-0.33974700	-0.51518200
C	-5.55395300	-0.95803300	-0.59003400
C	-4.08065400	0.63504800	0.46733400
C	-6.57289600	-0.59827600	0.29012000
H	-5.73936800	-1.72168000	-1.34096000
C	-5.10449200	1.00154500	1.33816200
H	-3.10307100	1.10174500	0.55674500
C	-6.35230500	0.38570800	1.25249200
H	-7.54114100	-1.08648100	0.22084000
H	-4.92262600	1.76272300	2.09179600
H	-7.14791200	0.66735600	1.93652900
B	-0.79005900	-0.95844700	-0.62997900
H	-0.87731300	0.17600800	-0.22939600
H	-0.24422700	-1.17337500	-1.68769000
H	-3.02124700	0.17957200	-2.61636800
H	-1.09230000	-1.87815300	0.08718900
C	1.56283000	-1.05017800	0.19515700
C	2.38119200	-2.32081800	0.32472700
C	3.84368600	-1.92183400	0.00323200
H	4.56198500	-2.36858300	0.69854600
H	4.10965500	-2.26369700	-1.00340500
C	3.89673100	-0.38756300	0.05669000
C	2.21653300	-2.81085500	1.77247000
H	1.16278100	-3.00629300	1.99285000
H	2.58049300	-2.07518300	2.49733400
H	2.78179500	-3.73901800	1.91781100
C	1.85917100	-3.39754000	-0.62885100
H	2.45504200	-4.31280300	-0.52744300
H	1.91626700	-3.06546000	-1.67073500
H	0.81381100	-3.63125400	-0.40982400
C	4.52361600	0.14853800	1.34394500
H	5.58786700	-0.10739900	1.36872600
H	4.04802800	-0.28328500	2.22944300
H	4.43884200	1.23844300	1.40225300
C	4.60383900	0.21191400	-1.15475300
H	4.60186800	1.30596800	-1.12834800
H	4.13708300	-0.11892900	-2.08789600
H	5.64717300	-0.12077900	-1.16203700
C	1.97799200	1.29808100	-0.00910700
C	1.20630200	3.28358800	1.12225900
H	0.93983500	3.79524300	2.04276000
C	1.10506700	3.94415500	-0.10135300
H	0.76249900	4.97431200	-0.13807700
C	1.43391100	3.27424900	-1.27869600
H	1.34182900	3.77774900	-2.23685500
N	2.41627700	-0.06775900	0.04791600
C	1.64230500	1.96156900	1.16987300
H	1.70654600	1.43001300	2.11443900
C	1.87126900	1.95204600	-1.23531300
H	2.10587000	1.41831400	-2.15059500

I (THF); E_H = −573.78289764

P	2.32671600	-0.06427900	-0.09942100
H	2.56089700	1.31153600	-0.35758700
C	0.48715200	0.01188400	-0.03488200
C	-0.22797100	1.21660700	-0.04194800
C	-0.22604500	-1.19393600	-0.01278000
C	-1.62184700	1.21431800	-0.01797100
H	0.30482200	2.16362700	-0.06400900
C	-1.61975800	-1.19631200	0.02681200
H	0.31041400	-2.13989700	-0.02978700
C	-2.32116500	0.00838200	0.02206700
H	-2.16150200	2.15740400	-0.02638100

H	-2.15667500	-2.14056100	0.05054400
H	-3.40727400	0.00794100	0.04371800
H	2.58760400	0.05317200	1.29475000

I (toluene); E_H = −573.78144763

P	2.32797800	-0.09764700	-0.04140400
H	2.57458200	1.22383400	-0.50089200
C	0.48713300	-0.00323600	-0.01183700
C	-0.22128500	1.20551900	-0.00308300
C	-0.23271000	-1.20418900	-0.01933300
C	-1.61436300	1.21117100	0.00626000
H	0.31784700	2.14929000	-0.00244400
C	-1.62711700	-1.19958800	0.00293500
H	0.30067700	-2.15143100	-0.04766100
C	-2.32067200	0.00840900	0.01413400
H	-2.14918500	2.15705000	0.01009300
H	-2.16976300	-2.14083400	0.00159200
H	-3.40697500	0.01424000	0.02324400
H	2.56921900	0.23729800	1.32152100

J (THF); E_H = −625.62147152

C	0.98789900	-0.95459200	-0.15953200
C	2.40309300	-0.41719500	-0.10215700
C	2.22921100	1.11556000	-0.16455800
H	2.87113100	1.63133000	0.55519100
H	2.49952400	1.47792400	-1.16184300
C	0.74530500	1.41216300	0.10273500
C	3.04270900	-0.88760000	1.21468200
H	3.07724600	-1.97973100	1.25597300
H	2.48971000	-0.52967400	2.08861800
H	4.06621800	-0.50265000	1.27711300
C	3.23892500	-0.92731200	-1.28081600
H	4.22703900	-0.45489700	-1.25225900
H	2.77073900	-0.67690700	-2.23855600
H	3.36747200	-2.01095300	-1.23343100
C	0.48412100	1.89727400	1.52879900
H	0.96535000	2.86998300	1.66828500
H	0.89274700	1.20482800	2.27048800
H	-0.58617400	2.02139800	1.71858400
C	0.16311300	2.39955200	-0.90259900
H	-0.90063000	2.58266200	-0.72482800
H	0.29491000	2.04444500	-1.92915600
H	0.68982600	3.35360300	-0.80329700
C	-1.27924500	-0.13038000	-0.04264600
C	-3.29022600	-0.57486400	1.20318900
H	-3.78014500	-0.80354500	2.14500300
C	-4.04047000	-0.44575400	0.03532600
H	-5.11886700	-0.57093800	0.06539700
C	-3.40410800	-0.16364300	-1.17293000
H	-3.98310900	-0.07137100	-2.08701400
N	0.14478700	0.04584300	-0.07908600
C	-1.90633100	-0.41762800	1.16774300
H	-1.31240400	-0.53271500	2.06877700
C	-2.02105800	-0.00428500	-1.21543900
H	-1.51588100	0.20154600	-2.15375000
H	-0.41719600	-2.66507200	-0.87277000
H	1.52362300	-3.17485100	-0.56705200
H	0.31510000	-2.76418200	0.96934300
B	0.58481700	-2.49028800	-0.19967700

J (toluene); E_H = −625.61588641

C	0.98606600	-0.95713100	-0.15812600
C	2.40166500	-0.41828000	-0.10160600
C	2.22829500	1.11478300	-0.16673300
H	2.86878000	1.63216900	0.55363500
H	2.50130200	1.47614100	-1.16397500
C	0.74356800	1.41118100	0.09665100
C	3.04568400	-0.88677400	1.21325600
H	3.07648300	-1.97864700	1.25532500
H	2.49445400	-0.52886900	2.08849400
H	4.06995500	-0.50271200	1.27325800
C	3.23389100	-0.93151200	-1.28160500
H	4.22430200	-0.46314100	-1.25679600
H	2.76369600	-0.68221500	-2.23874600
H	3.35543400	-2.01569100	-1.23377500
C	0.47969200	1.89207400	1.52413200
H	0.95654600	2.86630100	1.66965000
H	0.88996300	1.19766800	2.26321900
H	-0.59148600	2.00993500	1.71336300
C	0.16678700	2.40576000	-0.90515500
H	-0.89779700	2.58811400	-0.73160600
H	0.30198800	2.05590200	-1.93322500
H	0.69338500	3.35946400	-0.79994000
C	-1.28092000	-0.12758600	-0.05429700
C	-3.28846700	-0.59567000	1.18826600
H	-3.77520800	-0.84682300	2.12600400
C	-4.04236700	-0.44181500	0.02618600
H	-5.12062300	-0.56820200	0.05688200
C	-3.40955800	-0.13771300	-1.17802200
H	-3.99101900	-0.03068100	-2.08896400
N	0.14306500	0.04784000	-0.09091200
C	-1.90507700	-0.43950100	1.15126300
H	-1.30675900	-0.58091100	2.04553500
C	-2.02671000	0.02050300	-1.22158100
H	-1.52347000	0.23797200	-2.15824600
H	-0.46141300	-2.67894800	-0.75568900
H	1.50677800	-3.17173700	-0.58736700
H	0.41900500	-2.73492100	1.02431700
B	0.58886300	-2.48924000	-0.17122300

TS3 (THF); E_H = −1199.32545457

P	-1.33936500	-0.45712100	0.00666400

H	-0.96476800	0.84545500	0.38645400
C	-3.19645300	-0.08669000	-0.00400800
C	-4.13017900	-1.07923000	0.31022800
C	-3.66598200	1.17492000	-0.38428800
C	-5.50011800	-0.82250600	0.24652600
H	-3.78681600	-2.06838300	0.61466200
C	-5.03379400	1.44127700	-0.45124400
H	-2.95559100	1.96526700	-0.62824100
C	-5.95361600	0.44047200	-0.13581600
H	-6.21343400	-1.60352100	0.49760800
H	-5.38312600	2.42794800	-0.74498300
H	-7.01972100	0.64493100	-0.18482700
B	-0.68074300	-1.03796000	-1.67442000
H	-0.43621200	-0.13215100	-2.42368100
H	-1.08940800	-2.08082700	-2.11149300
H	-1.44168900	-1.44111700	1.01137000
C	0.71225300	-0.97827500	-0.12658900
C	1.29105700	-2.26560300	0.48981600
C	2.71557500	-2.27067700	-0.10909000
H	3.44731100	-2.72637100	0.56752300
H	2.71154200	-2.86655200	-1.02988600
C	3.09480500	-0.80294300	-0.44382200
C	1.33458200	-2.08927800	2.01336500
H	0.32479100	-2.05447000	2.43701000
H	1.85186600	-1.16742000	2.29499600
H	1.86537400	-2.92917900	2.47622900
C	0.53948600	-3.54829300	0.14575300
H	1.06575700	-4.41199400	0.56705900
H	0.46738500	-3.69563100	-0.93672000
H	-0.47575600	-3.54961100	0.55681100
C	4.16249900	-0.25468900	0.50307200
H	5.09782400	-0.80655400	0.36445400
H	3.85717000	-0.35424000	1.54903900
H	4.36448300	0.80274500	0.30412200
C	3.59217000	-0.71014400	-1.89196000
H	3.95575500	0.29330600	-2.13299800
H	2.79349000	-0.97179000	-2.59450400
H	4.42263900	-1.40815500	-2.04881900
C	1.69790500	1.28550400	-0.00738500
C	1.07268900	3.12898600	1.45197000
H	0.66070300	3.47347100	2.39680900
C	1.51686500	4.05102800	0.50388400
H	1.44739700	5.11707000	0.70013000
C	2.04916000	3.58877100	-0.69881800
H	2.39023000	4.29574400	-1.45043100
N	1.79742600	-0.10118800	-0.24165700
C	1.17327500	1.76227700	1.20417700
H	0.85779300	1.04536300	1.95711300
C	2.12796400	2.22139800	-0.95874600
H	2.50919800	1.87549600	-1.91347800
H	0.58743000	-1.43146000	-1.31623700

TS3 (toluene); E_H = −1199.32265473

P	-1.32865200	-0.46467200	0.00803200
H	-0.94705000	0.83130400	0.40596900
C	-3.18184300	-0.07961300	0.00219200
C	-4.12435000	-1.07072000	0.29110500
C	-3.63920200	1.19424800	-0.34886500
C	-5.49139000	-0.80091100	0.23103000
H	-3.78980000	-2.07002800	0.57152400
C	-5.00406500	1.47388400	-0.41198900
H	-2.92086200	1.98317300	-0.57345700
C	-5.93284900	0.47433200	-0.12199400
H	-6.21203700	-1.58151300	0.46164200
H	-5.34426400	2.47006600	-0.68347100
H	-6.99704000	0.68908200	-0.16844100
B	-0.67356500	-1.03308500	-1.68016900
H	-0.42275000	-0.12385300	-2.42224200
H	-1.08362300	-2.07311500	-2.12103100
H	-1.44324200	-1.46388100	0.99817800
C	0.71548300	-0.99227700	-0.12062000
C	1.29428100	-2.28492300	0.48395700
C	2.72457100	-2.27660100	-0.10239400
H	3.45236700	-2.73918800	0.57409500
H	2.73060200	-2.85968600	-1.03140700
C	3.10026500	-0.80293300	-0.41291400
C	1.32356000	-2.12937300	2.01004000
H	0.30991200	-2.10748400	2.42525500
H	1.83136000	-1.20732200	2.30768900
H	1.85584600	-2.97138200	2.46752300
C	0.55023100	-3.56524700	0.11585300
H	1.07443100	-4.43368900	0.53016000
H	0.48695900	-3.69777600	-0.96898800
H	-0.46888000	-3.57443400	0.51707000
C	4.15434700	-0.25939500	0.55205000
H	5.09941200	-0.79391000	0.41040400
H	3.84290600	-0.38259900	1.59364900
H	4.34074700	0.80488300	0.37524900
C	3.61254700	-0.68499400	-1.85413300
H	3.97030000	0.32541600	-2.07445200
H	2.82344500	-0.94140400	-2.56936400
H	4.45070700	-1.37331500	-2.01347800
C	1.68656900	1.27982000	-0.00820400
C	1.09320800	3.14559300	1.43408600
H	0.71787800	3.50664100	2.38790700
C	1.47435100	4.05065600	0.44374900
H	1.39298200	5.11979500	0.61728900
C	1.95706400	3.56959500	-0.77189400
H	2.24588300	4.26447800	-1.55590700
N	1.79917600	-0.11237000	-0.21176100
C	1.20900900	1.77556600	1.21420200
H	0.93902200	1.06982300	1.99505500
C	2.05127200	2.19799600	-1.00194300
H	2.38976100	1.83314000	-1.96572000
H	0.59408500	-1.43038900	-1.31741000

K (THF); E_H = −1199.42547708

B	-0.44116600	-0.99160100	-1.06790700
H	-0.91711200	-2.09431500	-1.27026200
P	-1.39719700	-0.32610300	0.49437400
H	-1.22481300	-1.01821400	1.70959900
H	-1.05553900	0.97888600	0.89592500
C	-3.20564600	-0.24911800	0.30461000
C	-3.99544900	0.41455000	1.25219000
C	-3.81216100	-0.86414300	-0.79483300
C	-5.37836000	0.45845200	1.09995800
H	-3.53294000	0.89982400	2.10805700
C	-5.19815400	-0.81765100	-0.94295700
H	-3.20129200	-1.37363000	-1.53399500
C	-5.98077900	-0.15861100	0.00250400
H	-5.98576400	0.97582300	1.83687000
H	-5.66379200	-1.29606600	-1.79963000
H	-7.06004900	-0.12221200	-0.11508900
C	1.16975300	-1.02086500	-0.82508000
C	1.76365700	-2.33313700	-0.26858800
C	3.08635500	-0.39311400	0.54366300
C	3.17944500	-1.87283400	0.10439700
H	3.82127000	-1.94542800	-0.78237500
H	3.63315600	-2.49755300	0.88242000
N	1.69733900	-0.00679200	0.11366900
C	4.16178600	0.42768700	-0.17686300
H	4.14880600	1.47781700	0.13241600
H	5.15266500	0.01932300	0.05115700
H	4.02005400	0.38725500	-1.26248400
C	3.27957600	-0.25618500	2.05727400
H	4.24596000	-0.68565200	2.34468500
H	3.28406500	0.79003600	2.37538900
H	2.49431400	-0.78300900	2.60700500
C	1.79772900	-3.43134100	-1.32853500
H	2.30678500	-4.32375600	-0.94516700
H	0.78394700	-3.72347700	-1.62332900
H	2.33033700	-3.09893300	-2.22737900
C	1.01933600	-2.85790900	0.96267600
H	0.94529000	-2.09873300	1.74676400
H	0.00689200	-3.18250200	0.69919300
H	1.54777000	-3.72173100	1.38349700
H	-0.82936500	-0.21627900	-1.92343300
C	1.46103500	1.35329100	-0.16941600
C	1.14844700	1.81177700	-1.46015100
C	1.50610300	2.30810800	0.86488700
C	0.90392200	3.16272700	-1.70474300
H	1.09371700	1.10647800	-2.28127300
C	1.28040800	3.65776200	0.61324800
H	1.69476800	1.98024100	1.88135000
C	0.97494500	4.09893100	-0.67544900
H	0.66318700	3.48298200	-2.71554300
H	1.32363800	4.36682200	1.43623900
H	0.78620400	5.15083900	-0.86971500
H	1.64586600	-0.89553300	-1.82104700

K (toluene); E_H = −1199.42247017

B	-0.43782800	-0.99766200	-1.06521600
H	-0.91925000	-2.10041700	-1.25112600
P	-1.39283400	-0.31133800	0.48739300
H	-1.22650500	-0.98738800	1.71355800
H	-1.05416600	0.99865800	0.87687500
C	-3.20160200	-0.23923700	0.29576100
C	-3.99802100	0.40137800	1.25321700
C	-3.80105000	-0.83385400	-0.81826800
C	-5.38019600	0.44257500	1.09721300
H	-3.54048200	0.87203300	2.12007500
C	-5.18647300	-0.79008900	-0.97028700
H	-3.18380700	-1.32418100	-1.56504700
C	-5.97547400	-0.15444700	-0.01475900
H	-5.99272700	0.94229600	1.84208200
H	-5.64677500	-1.25247000	-1.83859000
H	-7.05448800	-0.12038500	-0.13574300
C	1.17211300	-1.02697500	-0.81930600
C	1.76362300	-2.33811000	-0.25820300
C	3.09434400	-0.39480200	0.53390000
C	3.18164900	-1.87973400	0.10969800
H	3.82376500	-1.96470300	-0.77571100
H	3.63237500	-2.49860700	0.89427200
N	1.69999700	-0.01328500	0.11934800
C	4.15810000	0.41997700	-0.21053900
H	4.14535400	1.47389300	0.08531200
H	5.15353600	0.01748200	0.00822800
H	4.00152400	0.36700400	-1.29351700
C	3.30823700	-0.24203700	2.04305400
H	4.27769400	-0.66985100	2.32258800
H	3.31893400	0.80758700	2.34957100
H	2.52926800	-0.76211600	2.60822100
C	1.79055400	-3.44243900	-1.31164300
H	2.29711200	-4.33489300	-0.92503600
H	0.77502600	-3.73148100	-1.60283200
H	2.32176500	-3.11713500	-2.21381700
C	1.02026900	-2.85099900	0.97863600
H	0.95286700	-2.08470100	1.75665900
H	0.00579000	-3.17274600	0.71958900
H	1.54496600	-3.71448500	1.40479500
H	-0.82566500	-0.23066400	-1.92718900
C	1.45748200	1.34743900	-0.15932700
C	1.14023600	1.80834000	-1.44740500
C	1.49791500	2.29767300	0.87891800
C	0.88639500	3.15829800	-1.68565300
H	1.08710400	1.10532800	-2.27054900
C	1.26357200	3.64671600	0.63313700
H	1.68958200	1.96541900	1.89346800
C	0.95316600	4.09041500	-0.65297900

H	0.64117300	3.48099200	-2.69448000
H	1.30418400	4.35315300	1.45851400
H	0.75765400	5.14181400	-0.84290900
H	1.64896700	-0.90405500	-1.81518000

L (THF); E_H = −1797.73253917

H	1.82976100	-0.58294700	1.02075700
H	2.86996200	-0.93159200	-0.68551600
H	-0.40730000	1.87969000	0.99785200
H	-0.62690900	2.93954800	-0.71797100
H	-1.42946300	-1.28175400	1.01276800
H	-2.22984800	-2.02515800	-0.69670100
P	0.38817300	-1.79623600	-0.72142700
H	0.43388000	-1.99459000	-2.11848200
P	1.36241400	1.22136000	-0.74001700
H	1.50806700	1.34072500	-2.13918000
P	-1.73534200	0.55617200	-0.75195300
H	-1.90233600	0.60432500	-2.15303000
B	-1.41665300	-1.28395500	-0.19885900
B	1.82242600	-0.59016300	-0.19090500
B	-0.39837700	1.86622400	-0.21370800
C	0.74429000	-3.47810200	-0.12142600
C	0.93120900	-4.53923000	-1.01370300
C	0.82737900	-3.71384300	1.25627300
C	1.19836700	-5.82055800	-0.53317500
H	0.86898900	-4.36975900	-2.08542500
C	1.09407400	-4.99511000	1.73219500
H	0.68464400	-2.89722400	1.95910300
C	1.28001200	-6.05052300	0.83892200
H	1.34244800	-6.63817900	-1.23374200
H	1.15692500	-5.16905600	2.80259600
H	1.48819600	-7.04910900	1.21227400
C	2.64175500	2.37934900	-0.15861000
C	3.46603800	3.05866800	-1.06201700
C	2.80584300	2.58968300	1.21594000
C	4.44211900	3.93829200	-0.59548300
H	3.34951100	2.90385200	-2.13143700
C	3.78209500	3.46878600	1.67784400
H	2.17102100	2.06805200	1.92736400
C	4.60165800	4.14471300	0.77350700
H	5.07724600	4.46161900	-1.30455600
H	3.90222700	3.62620900	2.74590900
H	5.36226600	4.83034400	1.13584000
C	-3.38208500	1.09219800	-0.18934200
C	-4.37700000	1.45007400	-1.10546300
C	-3.65592100	1.15036100	1.18257200
C	-5.63061000	1.86099200	-0.65418400
H	-4.17733400	1.40938100	-2.17302500
C	-4.90925300	1.56140300	1.62924700
H	-2.89128400	0.87409100	1.90381800
C	-5.89864000	1.91729100	0.71226600
H	-6.39689200	2.13662100	-1.37313700
H	-5.11319400	1.60322300	2.69537300
H	-6.87568000	2.23731800	1.06282800

L (toluene); E_H = −1797.72709301

H	1.83491100	-0.58351600	1.02244800
H	2.87193000	-0.92990000	-0.68619400
H	-0.41004100	1.88414700	0.99861400
H	-0.62760500	2.93939800	-0.72034800
H	-1.43277200	-1.28789900	1.01095700
H	-2.22766500	-2.02657600	-0.70312400
P	0.39023400	-1.79486700	-0.71668500
H	0.43761000	-1.99470200	-2.11475300
P	1.36178400	1.22146200	-0.73315200
H	1.50943800	1.34180800	-2.13331800
P	-1.73398200	0.55505600	-0.74712000
H	-1.90291600	0.60500600	-2.14919300
B	-1.41738700	-1.28699900	-0.20025900
B	1.82619500	-0.59006900	-0.18883900
B	-0.39946800	1.86866600	-0.21253800
C	0.74640700	-3.47794700	-0.12104200
C	0.91345500	-4.54166700	-1.01338700
C	0.84760400	-3.71187500	1.25520400
C	1.17887200	-5.82366000	-0.53491200
H	0.83683300	-4.37333300	-2.08442100
C	1.11233600	-4.99372200	1.72934500
H	0.72084500	-2.89236700	1.95752200
C	1.27849500	-6.05172500	0.83590200
H	1.30757300	-6.64349000	-1.23596000
H	1.18948900	-5.16616400	2.79907800
H	1.48540600	-7.05103900	1.20810900
C	2.64090100	2.38122200	-0.15577800
C	3.47214300	3.05098100	-1.05917700
C	2.79789300	2.60173400	1.21744900
C	4.44814500	3.93098100	-0.59447900
H	3.36087000	2.88804800	-2.12800800
C	3.77407700	3.48102100	1.67779500
H	2.15662300	2.08749700	1.92825500
C	4.60066800	4.14731800	0.77336000
H	5.08884500	4.44698800	-1.30396600
H	3.88862900	3.64641400	2.74528800
H	5.36138400	4.83340500	1.13471100
C	-3.38194500	1.09043000	-0.18860000
C	-4.37370500	1.45359400	-1.10526600
C	-3.65926400	1.14330400	1.18226900
C	-5.62760400	1.86453800	-0.65614300
H	-4.17083700	1.41695600	-2.17243000
C	-4.91271900	1.55448800	1.62706400
H	-2.89637700	0.86234100	1.90336100
C	-5.89898500	1.91570100	0.70943000
H	-6.39163100	2.14433600	-1.37595100
H	-5.11939500	1.59224700	2.69283300
H	-6.87641900	2.23590600	1.05882100

(CAAC-H)$^+$; E_H = −599.30723087

C	1.20024600	-1.42407400	-0.33522300
C	0.65313900	-2.80840400	-0.23603500
C	1.92812500	-3.62055400	0.15308900
H	1.71983600	-4.33846400	0.96092900
H	2.27801700	-4.19710000	-0.71862800
C	3.02887800	-2.60860900	0.58475200
C	-0.44377900	-2.82267300	0.86585300
H	-1.28488400	-2.15940800	0.60698200
H	-0.05058600	-2.52237700	1.84984300
H	-0.83774200	-3.84837200	0.95318900
C	0.04029700	-3.25186900	-1.58511800
H	-0.30660300	-4.29415100	-1.49672000
H	0.77616500	-3.20583400	-2.40385700
H	-0.82824400	-2.63066400	-1.85762300
C	3.18430000	-2.47532500	2.10834000
H	3.59509300	-3.41759600	2.50404300
H	2.22011300	-2.28860300	2.60725800
H	3.88301500	-1.66613000	2.37313400
C	4.38037600	-2.88808100	-0.07991900
H	5.14821000	-2.15770600	0.21813500
H	4.30100800	-2.90836500	-1.17872200
H	4.72349200	-3.88240200	0.24850900
C	3.09469400	-0.00568400	0.16777700
C	3.27417300	2.15331900	1.24361600
H	2.93506000	2.86587400	2.00029800
C	4.32942700	2.48477400	0.37991800
H	4.81466400	3.46111600	0.46159100
C	4.75962400	1.56885800	-0.59348000
H	5.57077100	1.83313900	-1.27720600
N	2.42897600	-1.28978800	0.06532100
C	2.64705600	0.90352700	1.14186900
H	1.83092500	0.62986400	1.81726100
C	4.14738200	0.31250700	-0.70608700
H	4.46454800	-0.39258200	-1.47776500
H	0.64666800	-0.54643400	-0.69034500

NHC-H_2; E_H = −688.72842455

C	2.43891100	0.11483900	0.04631300
C	4.02530000	-1.72473700	0.07770700
H	4.20670400	-2.79614900	0.08195200
C	5.09605600	-0.83584300	0.09731000
H	6.11834500	-1.19959100	0.11692200
C	4.82809800	0.53365200	0.09118400
H	5.64748300	1.24730800	0.10611300
N	1.13553400	0.56277000	0.02139800
C	2.71163200	-1.26596600	0.05249000
H	1.90124100	-1.98725700	0.03771000
C	3.52492800	1.01097600	0.06615100
H	3.35465300	2.08202300	0.06205500
N	-1.13551700	0.56278400	-0.02193200
C	-2.43890700	0.11487100	-0.04645000
C	-2.71166800	-1.26593100	-0.05142300
C	-3.52489800	1.01102200	-0.06706300
C	-4.02535000	-1.72468500	-0.07623200
H	-1.90129900	-1.98723300	-0.03601800
C	-4.82808100	0.53371500	-0.09167100
H	-3.35459100	2.08206700	-0.06390300
C	-5.09608000	-0.83577700	-0.09660200
H	-4.20678600	-2.79609500	-0.07954300
H	-5.64744600	1.24738300	-0.10721600
H	-6.11838100	-1.19951100	-0.11589100
C	-0.67109600	1.87856100	-0.01362100
H	-1.33869200	2.72362600	-0.02682900
C	0.67115200	1.87855300	0.01197000
H	1.33877200	2.72361000	0.02445800
C	-0.00000400	-0.34188600	0.00012800
H	-0.01713000	-0.99223500	0.89449200
H	0.01710200	-0.99301700	-0.89366700

CAAC-H_2; E_H = −600.21572526

C	2.38461200	-0.70290600	0.06790800
C	2.27777800	0.72256300	-0.49131000
H	3.03070300	1.39779900	-0.07031900
H	2.44323100	0.68952200	-1.57538500
C	0.84024900	1.22749900	-0.21268300
C	2.72553300	-0.72364000	1.56164300
H	2.83838900	-1.75578900	1.91296000
H	1.94055400	-0.25538700	2.16164000
H	3.66796400	-0.19927500	1.75643800
C	3.40478200	-1.54168600	-0.69751500
H	4.41714300	-1.14585700	-0.55803400
H	3.19071000	-1.54924500	-1.77215400
H	3.40561700	-2.57981400	-0.34533500
C	0.85109900	2.20595100	0.97197800
H	1.47556400	3.07097700	0.72232900
H	1.26342700	1.73681600	1.86831800
H	-0.14239900	2.58317400	1.22188000
C	0.29667400	1.92408500	-1.46678100
H	-0.70353200	2.33884200	-1.32071100
H	0.25001800	1.22077900	-2.30474600
H	0.96377800	2.74652100	-1.74764300
C	-1.26309900	-0.18675200	0.06363100
C	-3.53039400	0.68022700	0.32479700
H	-4.17753400	1.52768300	0.53661400
C	-4.08422800	-0.57270000	0.06748600
H	-5.15989700	-0.71826700	0.07111500
C	-3.21928200	-1.63075400	-0.19304200
H	-3.61663500	-2.62069200	-0.40263500
N	0.11632500	-0.03464300	0.09253300
C	-2.15488300	0.87452100	0.32837600
H	-1.77720900	1.86200000	0.55581300

C	-1.83958300	-1.44803800	-0.20232400
H	-1.20917000	-2.29998100	-0.42752500
C	0.95424600	-1.19356600	-0.15707300
H	0.83682500	-1.57334500	-1.18930900
H	0.69288100	-2.01145300	0.52571600

(NHC-H)$^+$; E_H = −687.94069071

C	-0.00000200	-0.23870400	0.00007700
C	2.44236300	0.07274200	-0.02728600
C	4.14104100	-1.31237200	-0.99389200
H	4.45472000	-2.03600500	-1.73939500
C	5.05373800	-0.82563200	-0.06007600
H	6.08031600	-1.17783100	-0.07321300
C	4.65450700	0.11437000	0.88877900
H	5.36450800	0.48921800	1.61898600
N	1.08549900	0.54030600	-0.00651500
C	2.82481300	-0.85885600	-0.98871900
H	2.11663400	-1.20483400	-1.73632300
C	3.33902100	0.56807000	0.91560800
H	3.01218500	1.27927900	1.66865800
H	-0.00001300	-1.31811600	0.00053000
N	-1.08548700	0.54033400	0.00602200
C	-2.44236000	0.07281700	0.02719200
C	-2.82482500	-0.85796800	0.98940600
C	-3.33901200	0.56737300	-0.91611300
C	-4.14106200	-1.31145300	0.99496500
H	-2.11665100	-1.20333300	1.73729800
C	-4.65450700	0.11372200	-0.88889800
H	-3.01216600	1.27794500	-1.66975900
C	-5.05375300	-0.82547600	0.06074500
H	-4.45475300	-2.03445500	1.74107500
H	-5.36450400	0.48797300	-1.61941600
H	-6.08033900	-1.17764400	0.07418100
C	-0.68040700	1.85839300	0.00375100
H	-1.39029700	2.67057900	0.02411700
C	0.68044700	1.85837500	-0.00535600
H	1.39035500	2.67052800	-0.02640600

(CAAC-H)$^\bullet$; E_H = −599.57034013

C	1.10628600	-1.35718400	-0.14143100
C	0.62864600	-2.77929000	-0.09873700
C	1.96204500	-3.55077400	0.02671900
H	1.90502700	-4.37888700	0.74066500
H	2.22754500	-3.97663400	-0.94785000
C	3.05435000	-2.54417800	0.43830100
C	-0.30876700	-3.03605100	1.09408800
H	-1.20443800	-2.40920900	1.02028400
H	0.17913700	-2.81170300	2.04692900
H	-0.63023800	-4.08505900	1.11243300
C	-0.11353400	-3.16147300	-1.38873200
H	-0.39584300	-4.22147700	-1.37681300
H	0.51296500	-2.98323600	-2.26907100
H	-1.03125600	-2.57231600	-1.49848600
C	3.20582600	-2.43513900	1.95924900
H	3.54087600	-3.39068800	2.37608600
H	2.25852900	-2.16296900	2.43321900
H	3.94791100	-1.67265200	2.21871800
C	4.39123700	-2.94638100	-0.17979300
H	5.22151000	-2.34010800	0.19191700
H	4.35775700	-2.88186300	-1.27196900
H	4.60151400	-3.98642600	0.09224600
C	3.11155700	-0.02217400	0.08458500
C	2.99925100	2.28569300	0.84883400
H	2.43785800	3.08071900	1.33301300
C	4.29693800	2.52128000	0.39715400
H	4.75411400	3.49933200	0.51475900
C	4.99500900	1.48217300	-0.22108900
H	5.99964800	1.65183900	-0.59949600
N	2.49172600	-1.27083800	-0.10303600
C	2.41269300	1.03179200	0.69982800
H	1.41095200	0.84845700	1.07665800
C	4.41147400	0.23039700	-0.38867900
H	4.95369600	-0.54124100	-0.92106900
H	0.56043700	-0.55200700	-0.62445500

[PhPH(BH$_3$)]$^\bullet$; E_H = −599.76342720

P	-1.66089000	1.17791100	0.83803600
C	-3.18492400	0.64963600	0.08717100
C	-3.45619600	0.90006900	-1.27235100
C	-4.11894000	-0.07154800	0.85653100
C	-4.64047300	0.44850400	-1.84093500
H	-2.74175500	1.45148300	-1.87754000
C	-5.30074800	-0.51771000	0.27815700
H	-3.91679300	-0.27027200	1.90520300
C	-5.56413000	-0.26017100	-1.06899900
H	-4.84644500	0.65047200	-2.88781800
H	-6.01996600	-1.06686200	0.87836600
H	-6.48861300	-0.61160200	-1.51756000
B	-1.53560100	1.60218800	2.72111000
H	-0.35848600	1.77998100	2.94165800
H	-2.02327300	0.67585000	3.32940300
H	-1.11820200	2.07004500	-0.10833900
H	-2.19541700	2.62826500	2.79308500

M; E_H = −1198.63269258

C	-0.12190200	-2.38136000	-0.78789900
C	-0.08043100	-0.86195300	-0.53893900
C	-2.29512600	-1.61041700	0.13589200
C	-1.31843100	-2.80470300	0.07280600
H	-1.80632500	-3.70110700	-0.31920400
H	-0.98016800	-3.04555300	1.08760700
C	1.15444800	-3.10237000	-0.38540800

H	1.10859900	-4.17267700	-0.61887400
H	2.06080000	-2.70788800	-0.84612700
H	1.23077700	-3.23147700	0.75262600
C	-0.33757500	-2.62965500	-2.28851000
H	0.56275200	-2.37706700	-2.85763300
H	-0.57510700	-3.68169200	-2.47038800
H	-1.15777000	-2.02016200	-2.67392600
C	-2.81018800	-1.47448000	1.57509100
H	-3.56422200	-0.69574000	1.69754700
H	-3.26784500	-2.42268800	1.87500400
H	-1.98975700	-1.26520700	2.26897300
C	-3.46105800	-1.82863400	-0.83841700
H	-4.03624200	-2.70085800	-0.51279100
H	-4.14519600	-0.98022900	-0.88125700
H	-3.10254200	-2.01909900	-1.85229600
N	-1.42498100	-0.47351200	-0.28604100
P	1.12957400	-0.45888900	0.91263300
H	0.34344700	0.16175100	1.89546200
B	1.86835100	-2.13487300	1.53680900
H	1.29302200	-2.62374700	2.46348300
H	3.03687200	-2.29538400	1.38817100
C	2.41539300	0.73390000	0.49401400
C	2.31394800	2.05768400	0.94159800
C	3.51043700	0.33462500	-0.28310400
C	3.30614200	2.97458800	0.60795600
H	1.46841200	2.37406600	1.54588500
C	4.49156500	1.26237700	-0.62015100
H	3.61203400	-0.69339900	-0.61955400
C	4.39061100	2.57978400	-0.17477500
H	3.23068400	3.99826400	0.96130800
H	5.33882100	0.95215900	-1.22369200
H	5.16150600	3.29910400	-0.43398500
C	-1.79503600	0.87169200	-0.34652000
C	-0.85460900	1.85316700	-0.72102500
C	-3.09712100	1.31718100	-0.04318100
C	-1.20235700	3.19987000	-0.79383700
H	0.16454000	1.58781300	-0.97466200
C	-3.43128700	2.66438600	-0.11999600
H	-3.86769900	0.62117500	0.25278500
C	-2.49250200	3.62415400	-0.49448100
H	-0.44336100	3.91845400	-1.09079500
H	-4.44833300	2.96139000	0.12050400
H	-2.76133500	4.67415300	-0.54995800
H	0.35729000	-0.33560400	-1.39521200
C	1.44903400	2.92081600	0.70082000
H	1.51605200	4.01292500	0.64645400
H	1.72270300	2.78418800	1.79759800
H	2.20280900	2.52718200	0.01816100
C	-0.97586400	3.33249300	1.10027900
H	-0.72452600	3.47832800	2.15627500
H	-0.97724100	4.31133700	0.61148300
H	-1.98987500	2.92942300	1.05181000
C	-0.78801200	0.24791800	-2.50779100
H	-1.51953900	-0.53271400	-2.73394600
H	-0.74025700	0.91083900	-3.37843500
H	0.19409100	-0.21418100	-2.37106200
C	-2.63995300	1.52823800	-1.44442300
H	-2.73647300	2.09175300	-2.37768000
H	-3.31719300	0.67045100	-1.50013100
H	-2.97013300	2.16830200	-0.62307300
N	-1.02599100	0.30569600	0.00183800
P	1.48218200	0.08776600	1.29566700
C	-1.95013700	-0.68230800	0.42755000
C	-2.73801200	-0.49382900	1.57231700
C	-2.09397000	-1.87322400	-0.29613000
C	-3.63953900	-1.47217800	1.98245800
H	-2.66477600	0.43009400	2.13937900
C	-3.01557100	-2.83919900	0.10379500
H	-1.47344300	-2.04819200	-1.16794100
C	-3.78820400	-2.64782200	1.24732500
H	-4.24123400	-1.30466700	2.87129400
H	-3.11476600	-3.75331000	-0.47477000
H	-4.49789900	-3.40621800	1.56387200
H	1.15195700	-0.92133000	2.21425200
H	3.64577500	1.67434000	1.77412600
H	2.19280500	1.70970700	3.26417800
B	2.54078000	1.45380100	2.15066200
C	2.21277400	-0.74268700	-0.12157800
C	1.68350900	-1.97557400	-0.52779600
C	3.27221900	-0.16398700	-0.83155000
C	2.21214100	-2.61886200	-1.64300400
H	0.86913800	-2.43731000	0.02360300
C	3.79093200	-0.81356300	-1.94792400
H	3.71006500	0.77690100	-0.51169000
C	3.26085100	-2.03741000	-2.35458600
H	1.80517800	-3.57624500	-1.95353100
H	4.61550800	-0.36605100	-2.49393500
H	3.67138900	-2.54292900	-3.22346300
H	-0.60874900	0.97033900	1.9549730

M'; E_H = −1198.62953343

C	0.03944000	2.40111900	0.42591000
C	-0.19275100	0.95976200	0.93890500
C	-1.19094800	1.06103600	-1.27443000
C	-0.20440700	2.23192900	-1.08390200
H	-0.58061300	3.15004000	-1.54403100
H	0.74018200	1.98431900	-1.58182400

2.6 References

(1) Jäkle, F. Advances in the Synthesis of Organoborane Polymers for Optical, Electronic, and Sensory Applications. *Chem. Rev.* **2010**, *110*, 3985–4022.

(2) Priegert, A. M.; Rawe, B. W.; Serin, S. C.; Gates, D. P. Polymers and the p-Block Elements. Chem. Soc. Rev. 2016, 45, 922–953.

(3) He, X.; Baumgartner, T. Conjugated Main-Group Polymers for Optoelectronics. *RSC Adv.* **2013**, *3*, 11334–11350.

(4) Jäkle, F.; Vidal, F. Functional Polymeric Materials Based on Main Group Elements. *Angew. Chem. Int. Ed.* **2018**, *58,* 5846 –5870.

(5) Fazen, P. J.; Remsen, E. E.; Beck, J. S.; Carroll, P. J.; McGhie, A. R.; Sneddon, L. G. Synthesis, Properties, and Ceramic Conversion Reactions of Polyborazylene. A High-Yield Polymeric Precursor to Boron Nitride. *Chem. Mater.* **1995**, *7*, 1942–1956.

(6) Chivers, T.; Manners, M. *Inorganic Rings and Polymers of the p-Block Elements;* Royal Society of Chemistry: Cambridge, 2009.

(7) Tsang, C. W.; Yam, M.; Gates, D. P. The Addition Polymerization of a P=C Bond: A Route to New Phosphine Polymers. *J. Am. Chem. Soc.* **2003**, *125*, 1480–1481.

(8) Pavelka, L. C.; Holder, S. J.; Baines, K. M. Addition Polymerization of 1,1-Dimesitylneopentylgermene: Synthesis of a Polygermene. *Chem. Commun.* **2008**, *20*, 2346–2348.

(9) He, G.; Kang, L.; Delgado, W. T.; Shynkaruk, O.; Ferguson, M. J.; McDonald, R.; Rivard, E. The Marriage of Metallacycle Transfer Chemistry with Suzuki−Miyaura Cross-Coupling To Give Main Group Element-Containing Conjugated Polymers. *J. Am. Chem. Soc.* **2013**, *135*, 5360–5363.

(10) Leitao, E. M.; Jurca, T.; Manners, I. Catalysis in Service of Main Group Chemistry Offers a Versatile Approach to p-Block Molecules and Materials. *Nat. Chem.* **2013**, *5*, 817–829.

(11) Linshoeft, J.; Baum, E. J.; Hussain, A.; Gates, P. J.; Näther, C.; Staubitz, A. Highly Tin-Selective Stille Coupling: Synthesis of a Polymer Containing a Stannole in the Main Chain. *Angew. Chem. Int. Ed.* **2014**, *53*, 12916–12920.

(12) McKeown, G. R.; Fang, Y.; Obhi, N. K.; Manion, J. G.; Perepichka, D. F.; Seferos, D. S. Synthesis of Macrocyclic Poly(3-Hexylthiophene) and Poly(3-Heptylselenophene) by Alkyne Homocoupling. *ACS Macro Lett.* **2016**, *5*, 1075–1079.

(13) Matsumura, Y.; Ishidoshiro, M.; Irie, Y.; Imoto, H.; Naka, K.; Tanaka, K.; Inagi, S.; Tomita, I. Arsole-Containing π-Conjugated Polymer by the Post-Element-Transformation Technique. *Angew. Chem. Int. Ed.* **2016**, *55*, 15040–15043.

(14) Adams, G. M.; Colebatch, A. L.; Skornia, J. T.; McKay, A. I.; Johnson, H. C.; Lloyd-Jones, G. C.; Macgregor, S. A.; Beattie, N. A.; Weller, A. S. Dehydropolymerization of $H_3B{\cdot}NMeH_2$ To Form Polyaminoboranes Using [Rh(Xantphos-Alkyl)] Catalysts. *J. Am. Chem. Soc.* **2018**, *140*, 1481–1495.

(15) Melen, R. L. Dehydrocoupling Routes to Element-Element Bonds Catalysed by Main Group Compounds. *Chem. Soc. Rev.* **2016**, *45*, 775–788.

(16) Johnson, H. C.; Hooper, T. N.; Weller, A. S. The Catalytic Dehydrocoupling of Amine–Boranes and Phosphine–Boranes. In *Synthesis and Application of Organoboron Compounds.*; Springer: Cambridge, 2015; pp 153–220.

(17) Colebatch, A. L.; Weller, A. S. Amine-Borane Dehydropolymerization: Challenges and Opportunities. *Chem. Eur. J.* **2019**, *25*, 1379–1390.

(18) Don Tilley, T. The Coordination Polymerization of Silanes to Polysilanes by a "σ-Bond Metathesis" Mechanism. Implications for Linear Chain Growth. *Acc. Chem. Res.* **1993**, *26*, 22–29.

(19) Imori, T.; Lu, V.; Cai, H.; Tilley, T. D. Metal-Catalyzed Dehydropolymerization of Secondary Stannanes to High Molecular Weight Polystannanes. *J. Am. Chem. Soc.* **1995**, *117*, 9931–9940.

(20) Choffat, F.; Käser, S.; Wolfer, P.; Schmid, D.; Mezzenga, R.; Smith, P.; Caseri, W. Synthesis and Characterization of Linear Poly(Dialkylstannane)s. *Macromolecules* **2007**, *40*, 7878–7889.

(21) Parshall, G. W. *The Chemistry of Boron and Its Compounds*; Wiley: New York, 1967.

(22) Mayer-Gall, T.; Knittel, D.; Gutmann, J. S.; Opwis, K. Permanent Flame Retardant Finishing of Textiles by Allyl- Functionalized Polyphosphazenes. *ACS Appl. Mater, Interfaces* **2015**, *7*, 9349–9363.

(23) Priegert, A. M.; Siu, P. W.; Hu, T. Q.; Gates, D. P. Flammability Properties of Paper Coated with Poly(Methylenephosphine), an Organophosphorus Polymer. *Fire Mater.* **2015**, *39*, 647–657.

(24) Burg, A. Phosphinoborine Polymer Rings and Chains from Tetramethylbiphosphine. *J. Inorg. Nucl. Chem.* **1959**, *2*, 258.

(25) Wagner, R. I.; Caserio, F. F. Linear Phosphinoborane Polymers. *J. Inorg. Nucl. Chem.* **1959**, *11*, 259.

(26) Dorn, H.; Singh, R. A.; Massey, J. A.; Lough, A. J.; Manners, I. Rhodium-Catalyzed Formation of Phosphorus-Boron Bonds: Synthesis of the First High Molecular Weight Poly(Phosphinoborane). *Angew. Chem. Int. Ed.* **1999**, *38*, 3321–3323.

(27) Pandey, S.; Lönnecke, P.; Hey-Hawkins, E. Phosphorus-Boron-Based Polymers Obtained by Dehydrocoupling of Ferrocenylphosphine-Borane Adducts. *Eur. J. Inorg. Chem.* **2014**, 2456–2465.

(28) Cavaye, H.; Clegg, F.; Gould, P. J.; Ladyman, M. K.; Temple, T.; Dossi, E. Primary Alkylphosphine-Borane Polymers: Synthesis, Low Glass Transition Temperature, and a Predictive Capability Thereof. *Macromolecules* **2017**, *50*, 9239–9248.

(29) Paul, U. S. D.; Braunschweig, H.; Radius, U. Iridium-Catalysed Dehydrocoupling of Aryl Phosphine-Borane Adducts: Synthesis and Characterisation of High Molecular Weight Poly(Phosphinoboranes). *Chem. Commun.* **2016**, *52*, 8573–8576.

(30) Schäfer, A.; Jurca, T.; Turner, J.; Vance, J. R.; Lee, K.; Du, V. A.; Haddow, M. F.; Whittell, G. R.; Manners, I. Iron-Catalyzed Dehydropolymerization: A Convenient Route to Poly(Phosphinoboranes) with Molecular-Weight Control. *Angew. Chem. Int. Ed.* **2015**, *54*, 4836–4841.

(31) Marquardt, C.; Jurca, T.; Schwan, K. C.; Stauber, A.; Virovets, A. V.; Whittell, G. R.; Manners, I.; Scheer, M. Metal-Free Addition/Head-to-Tail Polymerization of Transient Phosphinoboranes, RPH-BH_2: A Route to Poly(Alkylphosphinoboranes). *Angew. Chem. Int. Ed.* **2015**, *54*, 13782–13786.

(32) Stauber, A.; Jurca, T.; Marquardt, C.; Fleischmann, M.; Seidl, M.; Whittell, G. R.; Manners, I.; Scheer, M. A Convenient Route to Monoalkyl-Substituted Phosphanylboranes (HRP-BH_2-NMe_3): Prospective Precursors to Poly[(Alkylphosphino)-boranes]. *Eur. J. Inorg. Chem.* **2016**, 2684–2687.

(33) Lavallo, V.; Canac, Y.; Präsang, C.; Donnadieu, B.; Bertrand, G. Stable Cyclic (Alkyl)(Amino)Carbenes as Rigid or Flexible, Bulky, Electron-Rich Ligands for Transition-Metal Catalysts: A Quaternary Carbon Atom Makes the Difference. *Angew. Chem. Int. Ed.* **2005**, *44*, 5705–5709.

(34) Jazzar, R.; Dewhurst, R. D.; Bourg, J. B.; Donnadieu, B.; Canac, Y.; Bertrand, G. Intramolecular "Hydroiminiumation" of Alkenes: Application to the Synthesis of Conjugate Acids of Cyclic Alkyl Amino Carbenes (CAACs). *Angew. Chem. Int. Ed.* **2007**, *46*, 2899–2902.

(35) Bertrand, G.; Soleilhavoup, M. Cyclic (Alkyl)(Amino) Carbenes (CAACs): Stable Carbenes on the Rise. *Acc. Chem. Res.* **2015**, *48*, 256–266.

(36) Melaimi, M.; Jazzar, R.; Soleilhavoup, M.; Bertrand, G. Cyclic (Alkyl)(Amino) Carbenes (CAACs): Recent Developments Angewandte. *Angew. Chem. Int. Ed.* **2017**, *56*, 10046–10068.

(37) Frey, G. D.; Lavallo, V.; Donnadieu, B.; Schoeller, W. W.; Bertrand, G. Facile Splitting of Hydrogen and Ammonia by Nucleophilic Activation at a Single Carbon Center. *Science* **2007**, *316*, 439–441.

(38) Frey, G. D.; Masuda, J. D.; Donnadieu, B.; Bertrand, G. Activation of Si-H, B-H, and P-H Bonds at a Single Nonmetal Center. *Angew. Chem. Int. Ed.* **2010**, *49*, 9444–9447.

(39) Mohapatra, C.; Samuel, P. P.; Li, B.; Niepo, B.; Schu, C. J.; Herbst-irmer, R.; Stalke, D.; Maity, B.; Koley, D.; Roesky, H. W. Insertion of Cyclic Alkyl(Amino) Carbene into the Si−H Bonds of Hydrochlorosilanes. *Inorg. Chem.* **2016**, *55*, 1953–1955.

(40) Turner, Z. R. Chemically Non-Innocent Cyclic (Alkyl)(Amino) Carbenes: Ligand Rearrangement, C-H and C-F Bond Activation. *Chem. Eur. J.* **2016**, *22*, 11461–11468.

(41) Jin, L.; Melaimi, M.; Kostenko, A.; Karni, M.; Apeloig, Y.; Moore, C. E.; Rheingold, A. L.; Bertrand, G. Isolation of Cationic and Neutral (Allenylidene)(Carbene) and Bis(Allenylidene)Gold Complexes. *Chem. Sci.* **2016**, *7*, 150–154.

(42) Li, Y.; Mondal, K. C.; Roesky, H. W.; Zhu, H.; Stollberg, P.; Herbst-Irmer, R.; Stalke, D.; Andrada, D. M.; Chandra Mondal, K.; Roesky, H. W.; et al. Acyclic Germylones: Congeners of Allenes with a Central Germanium Atom. *J. Am. Chem. Soc.* **2013**, *135*, 12422–12428.

(43) Sabourin, K. J.; Malcolm, A. C.; Mcdonald, R.; Ferguson, M. J.; Rivard, E. Metal-Free Dehydrogenation of Amine–boranes by an N-Heterocyclic Carbene. *Dalt. Trans.* **2013**, *42*, 4625–4632.

(44) Stubbs, N. E.; Jurca, T.; Leitao, E. M.; Woodall, C. H.; Manners, I. Polyaminoborane Main Chain Scission Using N-Heterocyclic Carbenes; Formation of Donor-Stabilised Monomeric Aminoboranes. *Chem. Commun.* **2013**, *49*, 9098–9100.

(45) Marquardt, C.; Hegen, O.; Vogel, A.; Stauber, A.; Bodensteiner, M.; Stauber, A.; Bodensteiner, M.; Timoshkin, A. Y.; Scheer, M. Depolymerization of Poly(Phosphinoboranes): From Polymers to Lewis Base Stabilized Monomers. *Chem. Eur. J.* **2018**, *24*, 360–363.

(46) Jaska, C. A.; Lough, A. J.; Manners, I. Linear Hybrid Aminoborane/Phosphinoborane Chains: Synthesis, Proton-Hydride Interactions, and Thermolysis Behavior. *Inorg. Chem.* **2004**, *43*, 1090–1099.

(47) Staubitz, A.; Sloan, M. E.; Robertson, A. P. M.; Friedrich, A.; Schneider, S.; Gates, P. J.; Manners, I.; Schmedt auf der Günne, J. Catalytic Dehydrocoupling/Dehydrogenation of N-Methylamine-Borane and Ammonia-Borane: Synthesis and Characterization of High Molecular Weight Polyaminoboranes. *J. Am. Chem. Soc.* **2010**, *132*, 13332–13345.

(48) Metters, O. J.; Chapman, A. M.; Robertson, A. P. M.; Woodall, C. H.; Gates, P. J.; Wass, D. F.; Manners, I. Generation of Aminoborane Monomers RR'N=BH_2 from Amine-Boronium Cations [RR'NH-BH_2L]$^+$: Metal Catalyst-Free Formation of Polyaminoboranes at Ambient Temperature. *Chem. Commun.* **2014**, *50*, 12146–12149.

(49) Breunig, J. M.; Hübner, A.; Bolte, M.; Wagner, M.; Lerner, H. W. Reactivity of Phosphaboradibenzofulvene toward Hydrogen, Acetonitrile, Benzophenone, and 2,3-Dimethylbutadiene. *Organometallics* **2013**, *32*, 6792–6799.

(50) Frisch, M. J.; Trucks, G. W.; Schlegel, H. B.; Scuseria, G. E.; Robb, M. A.; Cheeseman, J. R.; Scalmani, G.; Barone, V.; Mennucci, B.; Petersson, G. A.; et al. *Gaussian 09, Revision D.01*; Gaussian: Wallingford CT, 2009.

(51) Adamo, C.; Barone, B. Toward Reliable Density Functional Methods without Adjustable Parameters: The PBE0 Model. *J. Chem. Phys.* **1999**, *110*, 6158–6170.

(52) Hehre, W. J.; Ditchfield, R.; Pople, J. A. Self-Consistent Molecular Orbital Methods. XII. Further Extensions of Gaussian-Type Basis Sets for Use in Molecular Orbital Studies of Organic Molecules. *J. Chem. Phys.* **1972**, *56*, 2257–2261.

(53) Burck, S.; Gudat, D.; Nieger, M.; Vinduš, D. Increasing the Lability of Polarised Phosphorus-Phosphorus Bonds. *Eur. J. Inorg. Chem.* **2008**, *2*, 704–707.

(54) Dorn, H.; Singh, R. A.; Massey, J. A.; Nelson, J. M.; Jaska, C. A.; Lough, A. J.; Manners, I. Transition Metal-Catalyzed Formation of Phosphorus-Boron Bonds: A New Route to Phosphinoborane Rings, Chains, and Macromolecules. *J. Am. Chem. Soc.* **2000**, *122*, 6669–6678.

(55) Hooper, T. N.; Weller, A. S.; Beattie, N. A.; Macgregor, S. A. Dehydrocoupling of Phosphine-Boranes Using the [RhCp*Me(PMe_3)(CH_2Cl_2)][BAr^F_4] Precatalyst: Stoichiometric and Catalytic Studies. *Chem. Sci.* **2016**, *7*, 2414–2426.

(56) Weetman, C.; Inoue, S. The Road Travelled: After Main-Group Elements as Transition Metals. *ChemCatChem* **2018**, *10*, 4213–4228.

(57) Hong, M.; Chen, J.; Chen, E. Y. Polymerization of Polar Monomers Mediated by Main-Group Lewis Acid − Base Pairs. *Chem. Rev.* **2018**, *118*, 10551–10616.

(58) Protchenko, A. V.; Bates, J. I.; Saleh, L. M. A.; Blake, M. P.; Schwarz, A. D.; Kolychev, E. L.; Thompson, A. L.; Jones, C.; Mountford, P.; Aldridge, S. Enabling and Probing Oxidative Addition and Reductive Elimination at a Group 14 Metal Center: Cleavage and Functionalization of E-H Bonds by a Bis(Boryl)Stannylene. *J. Am. Chem. Soc.* **2016**, *138*, 4555–4564.

(59) Mo, Z.; Rit, A.; Campos, J.; Kolychev, E. L.; Aldridge, S. Catalytic B-N Dehydrogenation Using Frustrated Lewis Pairs: Evidence for a Chain-Growth Coupling Mechanism. *J. Am. Chem. Soc.* **2016**, *138*, 3306–3309.

(60) Boudjelel, M.; Sosa Carrizo, E. D.; Mallet-Ladeira, S.; Massou, S.; Miqueu, K.; Bouhadir, G.; Bourissou, D. Catalytic Dehydrogenation of (Di)Amine-Boranes with a Geometrically Constrained Phosphine-Borane Lewis Pair. *ACS Catal.* **2018**, *8*, 4459–4464.

(61) Pangborn, A. B.; Giardello, M. A.; Grubbs, R. H.; Rosen, R. K.; Timmers, F. J. Safe and Convenient Procedure for Solvent Purification. *Organometallics* **1996**, *15*, 1518–1520.

(62) Jafarpour, L.; Stevens, E. D.; Nolan, S. P. A Sterically Demanding Nucleophilic Carbene: 1,3-Bis(2,6-Diisopropylphenyl)Imidazol-2-Ylidene). Thermochemistry and Catalytic Application in Olefin Metathesis. *J. Organomet. Chem.* **2000**, *606*, 49–54.

(63) Hurtado, M.; Yanez, M.; Herrero, R.; Guerrero, A.; Juan, Z. D.; Jose-Luis, M. A.; Khater, B.; Guillemin, J. C. The Ever-Surprising Chemistry of Boron: Enhanced Acidity of Phosphine-Boranes. *Chem. Eur. J.* **2009**, *15*, 4622–4629.

(64) Pelczar, E. M.; Nytko, E. A.; Zhura, M. A.; Smith, J. M.; Glueck, S.; Sommer, R.; Incar, C. D.; Rheingold, A. L. Synthesis and Structure of Platinum and Palladium Complexes of Dimesitylphosphine. *Polyhedron* **2002**, *21*, 2409–2419.

(65) Lebel, H.; Morin, S.; Paquet, V. Alkylation of Phosphine Boranes by Phase-Transfer Catalysis. *Org. Lett.* **2003**, *5*, 2347–2349.

(66) Nguyen, D. H.; Lauréano, H.; Jugé, S.; Kalck, P.; Daran, J. C.; Coppel, Y.; Urrutigoity, M.; Gouygou, M. First Dibenzophospholyl(Diphenylphosphino)Methane - Borane Hybrid P-(N_2-BH_3) Ligand: Synthesis and Rhodium(I) Complex. *Organometallics* **2009**, *28*, 6288–6292.

(67) Perdew, J. P.; Ernzerhof, M.; Burke, K. Rationale for Mixing Exact Exchange with Density Functional Approximations. *J. Chem. Phys.* **1996**, *105*, 9982–9985.

(68) Ditchfield, R.; Hehre, W. J.; Pople, J. A. Self-Consistent Molecular-Orbital Methods. IX. An Extended Gaussian-Type Basis for Molecular-Orbital Studies of Organic Molecules. *J. Chem. Phys.* **1971**, *54*, 724–728.

(69) Hariharan, P. C.; Pople, J. A. Accuracy of AH n Equilibrium Geometries by Single Determinant Molecular Orbital Theory. *Mol. Phys.* **1974**, *27*, 209–214.

(70) Hariharan, P. C.; Pople, J. A. The Influence of Polarization Functions on Molecular Orbital Hydrogenation Energies. *Theor. Chem. Acc.* **1973**, *28*, 213–222.

(71) Gordon, M. S. The Isomers of Silacyclopropane. *Chem. Phys. Lett.* **1980**, *76*, 163–168.

(72) Francl, M. M.; Pietro, W. J.; Hehre, W. J.; Binkley, J. S.; Gordon, M. S.; DeFrees, J. A.; Pople, J. A. Self-consistent Molecular Orbital Methods. XXIII. A Polarization-type Basis Set for Second-row Elements. *J. Chem. Phys.* **1982**, *77*, 3654–3665.

(73) Lebedev, V. I.; Skorokhodov, A. L. Quadrature Formulas of Orders 41, 47 and 53 for the Sphere. *Russ. Acad. Sci. Dokl. Math* **1992**, *45*, 587.

(74) Miertuš, S.; Scrocco, E.; Tomasi, J. Electrostatic Interaction of a Solute with a Continuum. A Direct Utilizaion of AB Initio Molecular Potentials for the Prevision of Solvent Effects. *Chem. Phys.* **1981**, *55*, 117–129.

(75) Pascual-Ahuir, J. L.; Silla, E. . T. GEPOL: An Improved Description of Molecular Surfaces. III. A New Algorithm for the Computation of a Solvent-Excluding Surface. *J. Comp. Chem.* **1994**, *15*, 1127–1138.

(76) Cancès, E.; Mennucci, B.; Tomasi, J. A New Integral Equation Formalism for the Polarizable Continuum Model: Theoretical Background and Applications to Isotropic and Anisotropic Dielectrics. *J. Chem. Phys.* **1997**, *107*, 3032–3041.

(77) Mennucci, B.; Cammi, R.; Tomasi, J. Excited States and Solvatochromic Shifts within a Nonequilibrium Solvation Approach: A New Formulation of the Integral Equation Formalism Method at the Self-Consistent Field, Configuration Interaction, and Multiconfiguration Self-Consistent Field Level. *J. Chem. Phys.* **1998**, *109*, 2798–2807.

(78) Fukui, K. The Path of Chemical Reactions - The IRC Approach. *Acc. Chem. Res.* **1981**, *14*, 363–368.

(79) Dykstra, C. E.; Frenking, G.; Sim, K. S.; Scuseria, G. *Theory and Applications of Computational Chemistry: The First 40 Years*; Elsevier, Amsterdam: Amsterdam, 2005.

(80) Bruker-AXS Apex II Software, Madison, WI, 2008.

(81) G. M. Sheldrick, SADABS V2012/1, University of Göttingen, Germany.

(82) Sheldrick, G. M. SHELXT - Integrated Space-Group and Crystal-Structure Determination. Acta Crystallogr. Sect. A Found. Crystallogr. 2015, 71, 3–8.

(83) Sheldrick, G. M. Crystal Structure Refinement with SHELXL. Acta Crystallogr. Sect. C Struct. Chem. 2015, 71, 3–8.

(84) Dolomanov, O. V.; Bourhis, L. J.; Gildea, R. J.; Howard, J. A. K.; Puschmann, H. OLEX2: A Complete Structure Solution, Refinement and Analysis Program. J. Appl. Crystallogr. 2009, 42, 339–341.

Chapter 3
$Ni(COD)_2$-catalysed dehydropolymerisation of phosphine-boranes

3.1 Abstract

$Ni(COD)_2$ (COD = 1,5-cyclooctadiene) was found to function as a precatalyst for the thermal dehydropolymerisation of $PhPH_2{\cdot}BH_3$, in THF at 70 °C over 72 h, to give high molar mass poly(phenylphosphinoborane), $[PhHP–BH_2]_n$, in ca. 50% isolated yield. Mechanistic studies point towards a homogenous active species facilitating a chain-growth polymerisation. $Ni(COD)_2$ is also active for the dehydropolymerisation of the P-alkyl substituted phosphine-borane *n*$HexPH_2{\cdot}BH_3$. The P-disubstituted phosphine-boranes $Ph_2PH{\cdot}BH_3$ and $PhEtPH{\cdot}BH_3$ undergo catalytic dehydrogenation under identical conditions to give the linear dimers, $PhRHP{\cdot}BH_2–PPhR{\cdot}BH_3$ (R = Ph or Et), as the major products. Additionally, the cyclic trimer $[PhHP–BH_2]_3$ (**3.1**) has been isolated, from the oligomeric material formed in catalytic dehydrogenation of $PhPH_2{\cdot}BH_3$ using $Ni(COD)_2$, and structurally characterised using X-ray crystallography.

3.2 Introduction

Polymers comprising *p*-block elements other than carbon in the backbone have been of increasing interest for over two decades as the inclusion of inorganic elements provides access to materials with unique chemical and physical properties.[1,2] Prominent examples are polyphosphazenes $[R_2PN]_n$,[3–15] polysiloxanes $[R_2SiO]_n$,[16–18] polysilanes $[SiR_2]_n$[19–22] and polystannanes $[SnR_2]_n$.[23–28] Polyaminoboranes $[RHN–BH_2]_n$[29–46] and polyphosphinoboranes $[RHP–BH_2]_n$[47] are classes of main group polymers with alternating group 13 (B) and group 15 (N/P) elements making them formally isoelectronic with polyalkenes.[48] They, however, display markedly different physical and chemical properties stemming from the bond polarity induced by the electronegativity differences.[49,50] Polyphosphinoboranes have potential uses in a broad range of applications such as ceramic precursors, elastomers, lithographic resists, optoelectronics and flame retardants with high thermal stability.[51–59]

The first reports of polyphosphinoboranes were made in the 1950s through the thermal (> 200 °C) dehydrocoupling of $Me_2PH{\cdot}BH_3$ and $MePH_2{\cdot}BH_3$ in the presence of amines; however, the composition of the low molar mass materials were not convincingly characterised by modern standards.[60–62] In 1999 our group reported the first example of a fully characterised polyphosphinoborane, $[PhHP–BH_2]_n$, an analogue of polystyrene, through the catalytic dehydrogenation of $PhPH_2{\cdot}BH_3$ using the Rh^I precatalyst $[\{(COD)Rh(\mu\text{-}Cl)\}_2]$ (COD = 1,5-cyclooctadiene).[63,64] The resulting material is polydisperse and is believed to possess a large degree of chain branching due to the reaction necessitating melt phase conditions at high temperature (130 °C, 3 h). Nevertheless a variety of alkyl and aryl P-monosubstituted polyphosphinoboranes, $[RHP–BH_2]_n$, have been synthesised using these catalysts.[51,52,65,66]

In 2015 we reported a much improved route towards the synthesis of $[PhHP–BH_2]_n$ using an Fe^{II} based precatalyst $[CpFe(CO)_2(OTf)]$ (Cp = η^5-C_5H_5, OTf = CF_3SO_3).[53] This route has the advantages of operating in the solution phase at a lower temperature (100 °C, toluene, 24 h), and using an earth-abundant metal, rather than a precious metal catalyst, to yield high molar mass material with relatively low dispersity values (M_n = 59,000; $Đ$ =1.6). Initial studies into the dehydropolymerisation showed an inverse dependence of molecular weight on catalyst loading and detection of high molar mass material at low conversions, which indicated a chain-growth process. The iron catalyst has been shown to be active for the dehydropolymerisation of a wide range of both aryl and alkyl phosphorus substituents.[67–69] An iridium pre-catalyst has also been shown to dehydropolymerise primary phosphine-boranes $RPH_2{\cdot}BH_3$ (R = Ph, *p*Tol, Mes) in solution (100 °C, toluene, 24 h) (Scheme 3.1a).[70]

In addition, there have been developments towards metal-free syntheses of high molar mass polyphosphinoboranes. In 2015 the thermolysis of Lewis-base stabilised phosphinoborane monomers was reported to give $[RHP–BH_2]_n$ (R = *t*Bu)[71,72] under relatively mild conditions (22 – 40 °C, toluene, 48 h) (Scheme 3.1b) and in 2019 we reported the dehydropolymerisation of phosphine-boranes using cyclic (alkyl)(amino)carbenes (CAACs) as hydrogen acceptors (22 – 100 °C, THF or toluene, 1 - 24 h) (Scheme 3.1c).[73] These metal-free routes have significant disadvantages of requiring synthetically challenging precursors or stoichiometric quantities of CAAC, respectively. The CAAC-mediated route does, however, have the

advantage of yielding P-disubstituted polymers, $[RR'P–BH_2]_n$ (R = Ph; R' = Ph or Et), a class of polymer which has not been accessible through a metal-catalysed route.

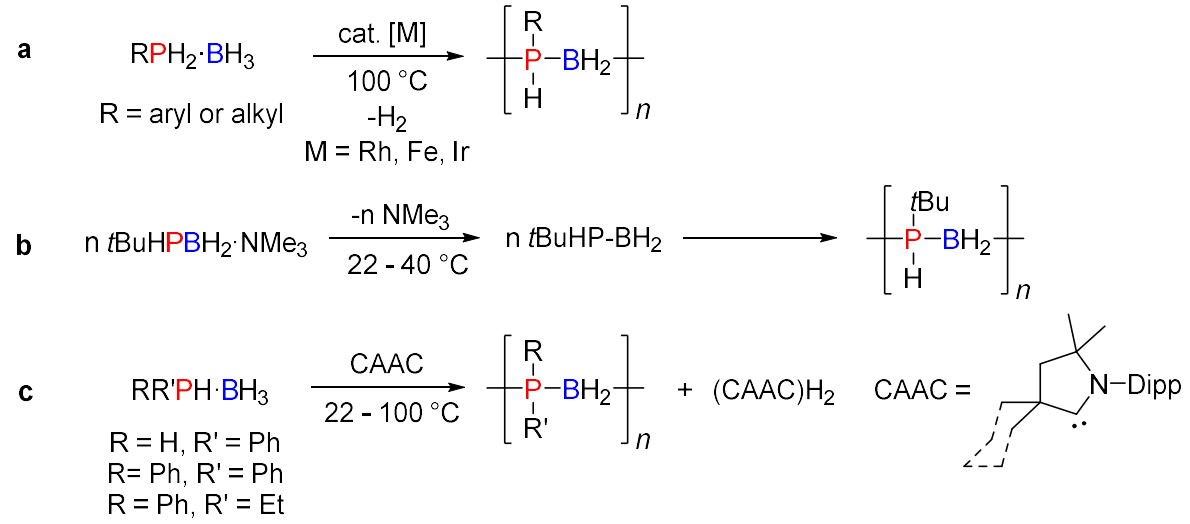

Scheme 3.1 Current methods of synthesising polyphosphinoboranes.

We are interested in further developing the methods for the synthesis of polyphosphinoboranes, with the goals of developing catalytic routes which produce high molar mass polymers under milder conditions, and allow convenient access to materials with a broad variety of phosphorus substituents. Nickel catalysis is a rapidly developing field, mentioned in over 40,000 articles, due to the relative abundance and low cost of nickel.[74] $Ni(COD)_2$ is a commercially available, ubiquitous source of Ni^0 used in a broad range of catalytic reactions,[75] prompting us to investigate its activity towards phosphine-boranes.

3.3 Results and Discussion

3.3.1 Polymerisation of $PhPH_2·BH_3$ using $Ni(COD)_2$

3.3.1.1 Optimisation of polymerisation conditions in THF

Preliminary experiments showed that poly(phenylphosphinoborane), $[PhHP–BH_2]_n$, could be synthesised through treatment of $PhPH_2·BH_3$ with catalytic (1 – 5 mol%) $Ni(COD)_2$ in THF at 70 °C. The initial reaction solution is a dark brown colour which becomes more orange upon heating (Figure S3.37). After 72 h, > 95% conversion of the monomer was observed using ^{11}B NMR spectroscopy and the $^{31}P\{^1H\}$ NMR spectra of the reaction mixture showed multiple broad peaks (δ_P = ca. -59 to -47 ppm). The higher field peaks, one of which has subsequently assigned as a 6-membered cyclic species, were no longer present in the $^{31}P\{^1H\}$ NMR spectrum of the product after precipitation into cold (-40 °C) hexanes (see section 3.3.1.4 for further discussion). The ^{11}B and ^{31}P NMR data of the precipitated material were in good agreement with previous reports of

the polymer [PhHP–BH_2]$_n$.[63] The ^{31}P NMR spectrum of the isolated material in $CDCl_3$ showed a doublet (δ_P = -49.8 ppm, $^1J_{PH}$ = 360 Hz) (Figure S3.27) and the ^{1}H NMR spectrum showed a doublet (δ_H = 4.26 ppm, $^1J_{PH}$ = 360 Hz) for the PH proton (Figure S3.26). The observation of clean $^1J_{PH}$ doublets by both ^{31}P and ^{1}H NMR indicated that the polymer had a well-defined, essentially linear main chain.[64] The ^{1}H NMR spectrum showed additional broad peaks for the BH (δ_H = 0.98 – 2.06 ppm) and phenyl (δ_H = 6.90 – 7.34 ppm) protons and the ^{11}B NMR spectrum showed a broad signal (δ_B = -33.9 ppm) (Figure S3.24c). Additionally, electrospray ionisation mass-spectroscopy (ESI-MS) was used to confirm the presence of the anticipated repeat unit (*m/z* of PhHP–BH_2 = 122) (Figure S3.28). Gel permeation chromatography (GPC) on the isolated polymers showed a bimodal distribution consisting of a higher molar mass polymeric fraction (M_n = 26,900 – 35,500 Da; $Đ$ = 1.63 – 2.11) and a lower molar mass fraction (M_n < ca. 1,200 Da) which could not be analysed in detail at it was located outside of the calibration range for the instrument. The lower molar mass fraction detected using GPC analysis had qualitatively identical ^{31}P chemical shift to that of the high molar mass fraction and is presumably higher in molar mass than the oligomers which were removed by precipitation. The polymerisation conditions in THF were optimised with the results shown in Table 3.1 (runs 1 – 7).

Table 3.1 Ni(COD)$_2$-catalysed dehydropolymerisation of $PhPH_2{\cdot}BH_3$.

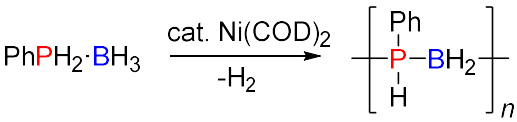

Run	Cat. (mol%)	Conc. (M)[a]	Solvent	Temp (°C)	Time (h)	Conversion (%)[b]	M_n (kDa)[c]	M_w (kDa)[c]	PDI[c]	Yield (%)[d]
1	1	1	THF	70	72	96	32.9	53.5	1.63	49
2	1	2	THF	70	72	100	26.9	56.9	2.11	55
3	1	4	THF	70	72	99	28.4	58.2	2.05	53
4	2.5	1	THF	70	72	98	35.5	43.8	1.72	41
5	5	1	THF	70	72	100	35.0	41.1	1.64	47
6	1	1	THF	50	195	74	17.8	25.2	1.59	33
7	1	1	THF	60	195	93	28.2	40.6	1.61	24
8	0	1	THF	70	72	20	23.1	31.3	1.36	2
9	0	1	THF	70	624	96	52.8	101.1	1.91	27
10	1	1	1,4-dioxane	70	110	92	16.7	29.0	1.74	37
11	1	1	1,4-dioxane	100	24	100	18.9	36.0	1.95	39
12	1	1	1,4-dioxane	100	72	100	24.2	41.2	1.70	49
13	1	1	2-*methyl*-THF	70	72	100	32.8	50.9	1.56	40
14[e]	1	1	THF	70	38	100	27.8	43.8	1.56	33
15[f]	1	4	THF	70	72	100	25.4	50.9	2.00	53

[a]Concentration of $PhPH_2{\cdot}BH_3$; [b]determined using ^{11}B NMR spectroscopy; [c]determined using GPC analysis; [d]combined isolated yield of high and low molar mass components in GPC; [e]reaction opened to air for 15 min. and then resealed; [f]larger scale reaction.

The $^{11}B\{^1H\}$ NMR spectra (Figure S3.1 and Figure S3.5) of the reaction mixtures upon altering the concentration (runs 1 - 3) or catalyst loading (runs 1, 4 and 5) were qualitatively identical; however, the corresponding $^{31}P\{^1H\}$ NMR spectra clearly showed a greater ratio of the polymeric material (which is isolated during work up) to the oligomeric material (which is removed during work-up), being formed at both higher concentrations and lower catalyst loadings (Figure S3.2 and Figure S3.6). GPC analysis of the isolated polymeric material showed a bimodal distribution for each set of conditions with the distribution being skewed towards the higher molar mass fraction at higher concentrations and lower catalyst loadings (Figure S3.3 and Figure S3.7). Analysis of the higher molar mass fraction showed that increasing the concentration results in a small increase in M_w of the material formed whereas increasing the catalyst loading leads to a decrease. The combination of the ^{31}P NMR spectra of the crude reaction mixture and the GPC data on the isolated material indicated that higher concentrations and lower catalyst loadings simultaneously favour polymerisation over termination or cyclisation events and promote the formation of larger relative quantities of the higher molar mass fraction of polymeric material.

The effect of temperature on the $Ni(COD)_2$-catalysed polymerisation in THF was explored (runs 1, 6 and 7). Below 50 °C there was no detectable dehydrogenation of $PhPH_2{\cdot}BH_3$ over 24 h, whereas at 50 °C and 60 °C monomer conversion was detected, although the reaction was significantly slower than at 70 °C (Figure S3.8). A comparison of the GPC data showed that higher molar mass material is formed as the temperature is increased from 50 °C to 70 °C.

$PPhH_2{\cdot}BH_3$ was heated at 70 °C in THF with no catalyst as a control reaction. After 72 h, the same time period used for the $Ni(COD)_2$-catalysed reactions, ca. 20% conversion was achieved. Precipitation into hexanes at this point gave a very low yield (ca. 2 %) of polymeric material (M_n = 23,100 Da; $Đ$ = 1.36) (run 8). This prompted us to repeat the same reaction, but with a prolonged reaction time. If the reaction mixture is heated for ca. 4 weeks, 95 % conversion of monomer is achieved (run 9) (Figure S3.10). Although this is considerably slower than the $Ni(COD)_2$-catalysed reactions the molar mass of the material isolated is significantly higher (M_n = 52,800; $Đ$ = 1.91) (Figure S3.15). The ^{11}B and ^{31}P NMR spectra of the reaction mixture prior to work-up showed the formation of the same species as in the analogous reaction in the presence of catalyst (run 1) (Figure S3.11 and Figure S3.12), but there is significantly greater formation of $PPhH_2$, presumably as a result of the longer reaction time

resulting in increased cleavage of the P–B bond of the starting material, $PPhH_2{\cdot}BH_3$. This dissociation explained the low isolated yield of $[PhHP–BH_2]_n$ (27%). The ^{31}P and ^{1}H NMR spectra of the isolated polymer both showed clean doublets for the $^{1}J_{PH}$ coupling. This is in contrast to the poorly resolved signals observed when neat $PPhH_2{\cdot}BH_3$ is heated (3 h at 90 °C and 3 h and 130 °C) where the resulting product is oligomeric.[64] This suggests that either using THF as a solvent and/or the use of the lower temperature promotes dehydrogenation to give a well-defined linear polymer.

From the optimisation studies it was determined that the best conditions for achieving high molar mass material in THF (both the amount as determined by the relative ratio of the peaks in the bimodal GPC chromatogram, and the size as determined by analysing the high molar mass peak in the GPC chromatogram) are to have a low catalyst loading and high monomer concentration.

3.3.1.2 Influence of solvent on the polymerisation

Although the optimised conditions in THF produced moderate yields of high molar mass material we wanted to explore different solvents to probe whether any further improvements to the polymerisation could be made. 1,4-Dioxane, a coordinating solvent which is significantly less polar than THF, and 2-*methyl*-THF, a solvent similar in polarity but less coordinating than THF, were investigated. When conditions analogous to run 1 were used (1 mol% cat., 1 M, 70 °C, 72 h) in 1,4-dioxane only 80% of monomer was consumed. Over 100 h of heating was required for the conversion to reach over 90% (run 10). Increasing the temperature to 100 °C, possible due to the higher boiling point of the solvent, allowed for full conversion within 24 h (run 11). Unlike when the polymerisation is carried out in THF at 70 °C, heating the reaction mixture beyond full conversion resulted in an increase in both the molar mass and yield of the isolated material, indicating polymerisation at 100 °C continues after consumption of the monomer (run 12). When the reaction was carried out in 2-*methyl*-THF using conditions analogous to run 1 (1 mol% cat., 1 M, 70 °C, 72 h) ^{11}B NMR spectroscopy indicated that 100% conversion of $PPhH_2{\cdot}BH_3$ was achieved (run 13). The relative rate of dehydropolymerisation was similar to when the reaction is carried out in THF as the conversions after 24 h and 48 h were comparable, 81 vs 90% and 88 vs 95% for 2-methyl-THF and THF, respectively.

A comparison of the $^{31}P\{^{1}H\}$ NMR spectra of the reaction mixtures of the polymerisations in THF, 1,4-dioxane and 2-*methyl*-THF (70 °C, 1 M) showed a greater proportion of oligomeric material is formed in 1,4-dioxane relative to the more polar solvents (Figure 3.1). GPC analysis on the isolated material showed a bimodal distribution for all solvents; however, the relative peak area was more skewed towards the lower molar mass fraction in 1,4-dioxane and 2-*methyl*-THF (Figure 3.2) . Additionally, for the reactions carried out in 1,4-dioxane there is a significant shoulder present on the high molar mass GPC peak (Figure S3.17). The ^{31}P NMR spectrum of the material isolated from the reaction in 2-*methyl*-THF showed a small shoulder upfield of the main polymer peak (Figure S3.20) and the doublet which corresponds to the PH proton in the ^{1}H NMR spectrum is slightly less well-defined than in the THF polymerisations (Figure S3.19). This is potentially due to chain branching occurring as a result of the longer reaction time, higher temperature, or less coordinating solvent used.

These results indicate that the combination of polarity and coordinating ability of the solvent are important, both for the formation of a greater quantity of polymeric material in the reaction mixture, and also for increasing the ratio of the higher molar mass fraction of the isolated material.

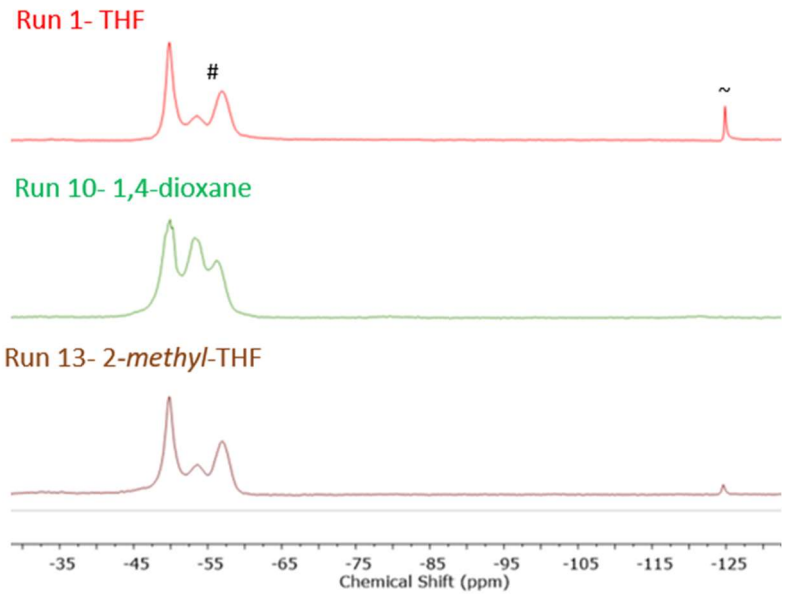

Figure 3.1 $^{31}P\{^{1}H\}$ NMR spectra (122 MHz, 25 °C) of the reaction mixtures for runs 1, 10 and 13 (Table 3.1) ($^{\#}$oligomeric material removed by precipitaion, $^{\sim}$trace $PPhH_2$).

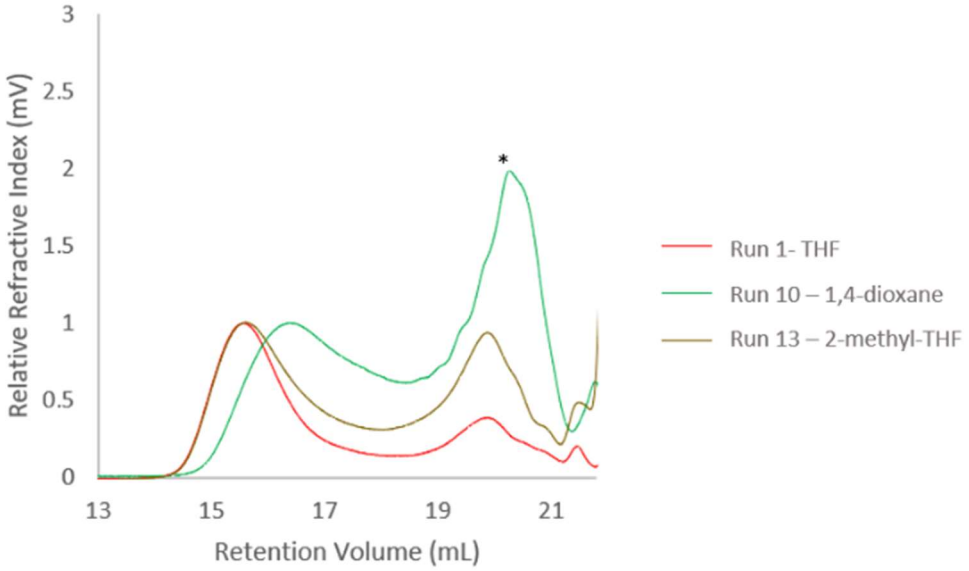

Figure 3.2 GPC chromatograms of isolated $[PhHP–BH_2]_n$ from for runs 1, 10 and 13 (Table 3.1) (*below calibration region).

3.3.1.3 Influence of air on the polymerisation

The effect of carrying out the polymerisation under ambient conditions, rather than an inert atmosphere, were probed (run 14). After setting up the reaction in THF under nitrogen it was opened to air for 15 min before the system was resealed and heated to 70 °C. Full consumption of $PhPH_2{\cdot}BH_3$ was observed after 38 h using ^{11}B NMR spectroscopy, almost twice as fast as under inert conditions. It is likely that rather than the catalysis occurring faster when exposed to air, the monomer is involved in a parallel side reaction alongside the dehydrogenation. Evidence for this comes in the form of additional peaks in the ^{31}P NMR spectrum (δ_P = -35 to 0 ppm) (Figure S3.22) and that the isolated yield was lower than the analogous reaction under an inert atmosphere (33% vs 49%). GPC analysis on the isolated material confirmed polymeric material was formed (M_n = 27,800; $Đ$ = 1.56) (Figure S3.23), albeit with a larger proportion of the lower molar mass fraction, and ^{11}B and ^{31}P NMR data matched that of $[PhHP–BH_2]_n$.

A control reaction that involved heating $PhPH_2{\cdot}BH_3$ in THF at 70 °C in the absence of precatalyst, after opening the reaction to air for 15 min prior to heating, showed an identical ^{31}P NMR spectrum to when $PhPH_2{\cdot}BH_3$ was heated under inert conditions (run 9). From this we conclude that the additional ^{31}P NMR signals observed when the catalysis is carried out under ambient conditions are from the formation of side products induced by the presence of $Ni(COD)_2$.

3.3.1.4 Polymerisation under scaled up and optimised conditions

To demonstrate the scalability of the dehydropolymerisation a larger scale reaction using the optimised conditions (1 mol% cat., 4 M, 70 °C, 72 h) was carried out (run 15). As with the smaller scale reactions three main peaks were observed in the ^{31}P NMR spectra of the reaction mixture (δ_P = -49.6 ppm, -52.9 ppm and -56.4 ppm) along with a major broad peak in the corresponding ^{11}B NMR spectra (δ_B = -36.4 ppm) (Figure S3.24 and Figure S3.25). The peak at δ_P = -49.6 ppm has previously been identified as polymeric [PhHP–BH_2]$_n$ and the peaks at δ_P = -52.9 ppm and δ_P = -56.4 ppm have been attributed to low molecular weight oligomers; however, no structural characterisation has been reported.[64] Precipitation into hexanes allowed for isolation of [PhHP–BH_2]$_n$ in a 53% yield. GPC analysis on the precipitate confirmed the presence of high molar mass material (M_n = 25,400 Da; $Đ$ = 2.00) with an almost monomodal distribution. GPC analysis was also carried out on the supernatant and the absence of any high molar mass peaks indicated no polymeric material was lost into the supernatant through the precipitation process (Figure 3.3). ESI-MS analysis confirmed the presence of the anticipated monomer repeat unit [PhHP–BH_2] (*m/z* = 122) and showed two main distributions, one of which was identified as a linear system with a $PPhH_2$ end group (Figure S3.28).

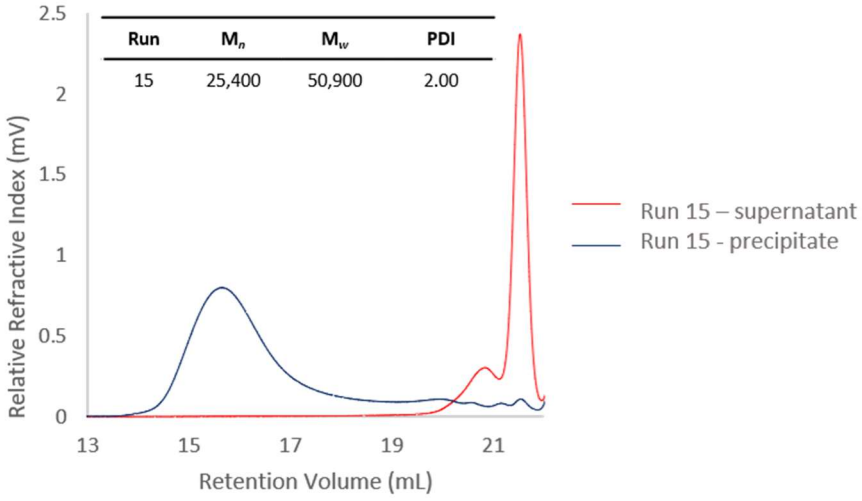

Figure 3.3 GPC chromatogram of both the precipitate and supernatant of run 15 (Table 3.1).

We were interested in attempting to isolate and characterise the oligomeric material which was removed through precipitation. Our strategy for this was to carry out the reaction using conditions which disfavour the formation of polymeric material (1,4-dioxane and low concentration) and focus on isolating material from the supernatant. Yellow crystals were

grown from a concentrated THF solution of the material retrieved from the supernatant layered with hexamethyldisiloxane (HMDSO) at 22 °C. The structure of the 6-membered ring $[PhHP–BH_2]_3$ (**3.1**) was conclusively determined using X-ray crystallography (Figure 3.4). The ring adopts the cis,cis,trans-chair conformation with P–B bond lengths ranging from 1.932(2) Å to 1.944(3) Å, with an average distance of 1.938(3) Å. The B–P–B and P–B–P bond angles are in the range 115.6(1) – 117.1(1)° (av. 116.4(1)°) and 108.0(1) – 111.1(1)° (av. 109.3(1)°), respectively. The structure can be compared to the previously reported P-disubstituted 6-membered ring, $[Ph_2P–BH_2]_3$.[76] This species also adopts the chair conformation in the solid state and has an average P–B bond length (1.948(4) Å) that is within three ESDs of the monosubstituted ring. The P-disubstituted ring has a wider average P–B–P angle (112.6(2)°) and a narrower average B–P–B angle (114.3(2)°) than $[PhHP–BH_2]_3$.

The ^{31}P and ^{11}B NMR spectra of **3.1** in $CDCl_3$ showed a broad doublet at δ_P = -52.5 ppm ($^2J_{PH}$ = 353 Hz) and a broad signal at δ_B = -35.8 ppm, respectively, and the ESI mass spectrum showed a peak with *m/z* = 365.1 which corresponds to the $[M – H]^+$ ion. The ^{31}P NMR signal corresponds to the most downfield oligomeric material observed in the ^{31}P NMR spectrum of the polymerisation reaction mixture (Figure S3.25) and work is ongoing to isolate and structurally characterise other oligomeric materials formed as a side product of the polymerisation (δ_P = -56.4 ppm).

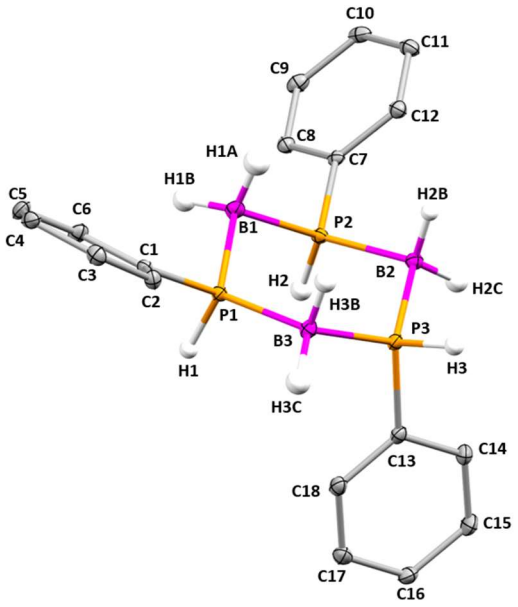

Figure 3.4 Thermal ellipsoid plot of $[PhHP–BH_2]_3$ (**3.1**). Ellipsoids are shown at the 30% probability level. H atoms other than those bound to B and P atoms have been omitted for clarity.

The reaction of isolated **3.1** with $Ni(COD)_2$ has been probed to investigate whether further dehydrogenation or dehydrocoupling occurs. No reaction was observed with 30 mol% $Ni(COD)_2$ (THF, 70 °C, 72 h).

3.3.2 Investigation into the polymerisation mechanism

3.3.2.1 Molar mass dependence on conversion

Polymer growth kinetics of the $Ni(COD)_2$-catalysed dehydropolymerisation of $PPhH_2{\cdot}BH_3$ were measured (1 mol% cat., 1 M, 70 °C, THF). It was determined that within 24 h, ca. 90% of the starting monomer is consumed with continued conversion until 48 h, beyond which there is negligible further conversion (Figure S3.34). GPC analysis was carried out on regular aliquots of the reaction mixture (from 22 – 100% conversion) and showed negligible high molar mass material until ca. 70% conversion of the monomer, and a steady increase in M_n from 70 - 100% conversion (25,100 Da to 31,000 Da) with a more significant increase in M_w (31,000 Da to 52,000 Da) indicative of a broadening of the molar mass distribution (Figure S3.38 and Figure 3.5). Heating the reaction mixture beyond 100% conversion resulted in no significant increase in molar mass under the conditions used (70 °C, THF) (Figure S3.38).

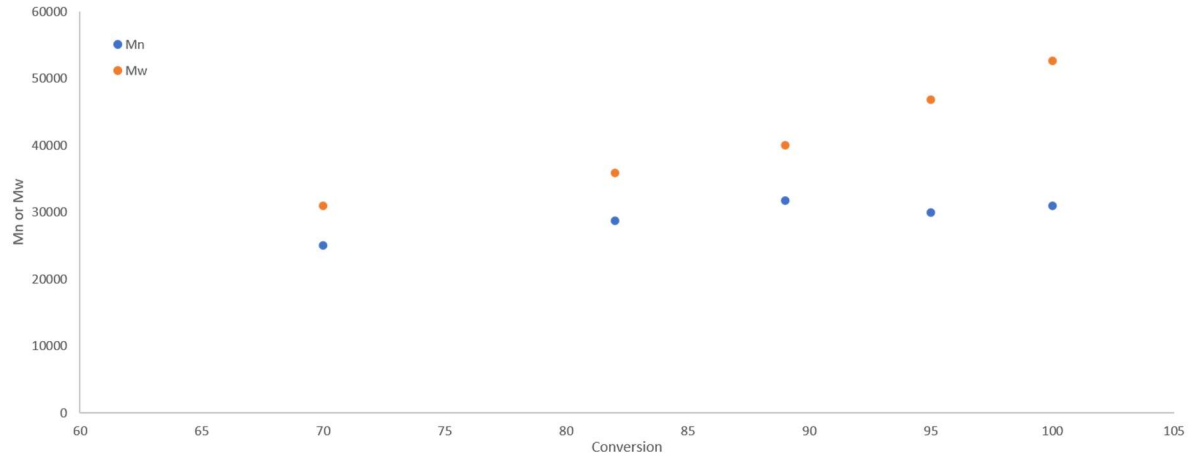

Figure 3.5 Plot of conversion vs M_n and M_w (1 mol% cat., 1 M, 70 °C, THF). No data below ca. 70% conversion as not possible to integrate the GPC trace.

Analysis of the reaction aliquots using ^{11}B and ^{31}P NMR spectroscopy showed a broadening of the polymer signals as conversion increases (Figure S3.35 and Figure S3.36). This is representative of higher molar mass material being formed later in the reaction, supporting the GPC analysis.

3.3.2.2 Effect of additional monomer

The addition of one further equiv. of $PhPH_2{\cdot}BH_3$ to a polymerisation reaction mixture (1 mol% cat., 1 M, 70 °C, THF) after initial full monomer consumption had occurred resulted in complete consumption of the second monomer, albeit at a slower rate than the first equiv.

(Figure S3.40). This indicated that the catalytic species remaining at the end of the dehydropolymerisation was still active for catalysis, albeit it with a decrease in activity. There was no significant change in the molar mass of the isolated material after the consumption of an additional equivalent of monomer, indicating that the polymerisation was not living (Figure S3.39).

3.3.2.3 Effect of reacting oligomeric material with $Ni(COD)_2$

We investigated whether there was any further dehydrocoupling that occurred when the oligomeric material that was isolated from the supernatant of the polymerisation was heated with additional $Ni(COD)_2$ (1 mol% cat., 1 M, 70 °C, 72 h, THF). The ^{31}P and ^{11}B NMR spectra of the material before and after heating were identical and GPC analysis showed no high molar mass material had been formed from the oligomers; however, it should be noted that if all of the material in the supernatant is comprised entirely of cyclic species this would affect the propensity for dehydrocoupling between oligomers to produce linear, high molar mass material.

3.3.2.4 Evidence for a homogeneous vs heterogeneous mechanism

Several tests to probe whether the active species in the reaction was homogeneous or heterogeneous have been carried out.[77,78] Adding PPh_3 to the reaction mixture did not inhibit the polymerisation (Figure S3.41). If the active species was heterogeneous, the addition of PPh_3 should completely poison the system as only a fraction of the metal atoms will be on the surface. Another common test into whether a catalyst is heterogenous of homogeneous involves mercury poisoning. Upon addition of excess mercury (60 equiv. per metal atom) to the $Ni(COD)_2$ system no suppression in activity was observed (Figure S3.42). This was indicative of a homogenous system as mercury would be expected to form an amalgam with a heterogeneous nickel catalyst and inhibit the activity.[79] Filtration of the reaction mixture through a 200 nm PTFE membrane also led to no significant decrease in catalyst activity (Figure S3.43), although it should be noted that the relative size of the filter vs the size of any nanoparticles can provide misleading results with this test. No evidence of nanoparticles was observed when TEM images of the reaction mixture were collected.

The UV-vis spectrum of the reaction mixture has a peak at ca. 310 nm, which is similar to what has been reported for the surface plasmon resonance of nickel nanoparticles.[80] While it is possible that large, but inactive, nanoparticles could be formed, these would be expected to

be observed in the TEM images. The peak at 310 nm is likely due to the presence of another species in the reaction mixture which absorbs at a similar wavelength.

When $PhPH_2{\cdot}BH_3$ was reacted with nickel nanoparticles (THF, 70 °C, 72 h) 30% conversion of the monomer was observed using ^{11}B NMR spectroscopy. This was directly comparable to the conversion of the control reaction of heating $PPhH_2{\cdot}BH_3$ with no catalyst (Figure S3.10). Furthermore, the addition of dimethylamine-borane, $Me_2NH{\cdot}BH_3$, a substrate reported to undergo dehydrogenation with Ni nanoparticles under mild conditions,[81] to the reaction mixture after consumption of $PhPH_2{\cdot}BH_3$ showed no evidence of conversion of $Me_2NH{\cdot}BH_3$, even upon heating to 70 °C for 20 h (Figure S3.45). The combination of the results from these experiments clearly points towards the active species in the catalytic reaction being homogeneous.

3.3.2.5 Postulated polymerisation mechanism

From the above experimental data we propose a chain-growth, homogeneous process for the dehydropolymerisation of $PhPH_2{\cdot}BH_3$ using $Ni(COD)_2$. The lack of any suppression of activity upon the addition of either PPh_3 or Hg strongly supports a homogeneous process. The observation of high molar mass material at moderate conversion (70%) is strong evidence for a chain-growth mechanism, and the increase in PDI beyond 70% conversion can be attributed to a very small degree of chain branching occurring in addition to linear growth (Figure S3.38). The absence of any increase in molar mass beyond 100% conversion, combined with the observation that isolated oligomeric material is not converted into polymer when heated with $Ni(COD)_2$, further suggests the operation of a chain-growth as opposed to step-growth polycondensation process.

Chain-growth processes often have an inverse relationship on molar mass and catalyst loading;[53] however, in our system the molar mass of the high molar mass fraction appears to be relatively insensitive to catalyst loading using GPC analysis (Table 3.1). This can be explained by considering the observation that when additional $PhPH_2{\cdot}BH_3$ is added to a polymerisation mixture which has reached full conversion, and the reaction heated until full consumption of the extra monomer is detected, there is no increase in the molar mass of the isolated material when compared to that of the material isolated after the consumption of the first monomer (Figure S3.39). This suggests that the chain termination and possibly chain transfer events determine the overall chain length, rather than the molar mass being

controlled by the catalyst loading. We suspect that the bimodal appearance of the GPC traces stems from termination events that are dependent on the presence of nickel as the molar mass distribution is significantly shifted towards the lower molar mass fraction at higher catalyst loadings (Figure S3.7). Furthermore, the GPC trace of the material isolated from the catalyst-free reaction is monomodal (Figure S3.15).

Attempts to isolate the active species through carrying out stoichiometric reactions have been unsuccessful. This is an area in which further work can be carried out.

3.3.3 Expansion of the substrate scope

In an attempt to demonstrate the versatility of $Ni(COD)_2$ for the dehydropolymerisation of phosphine-boranes, its activity towards the P-alkyl substituted derivative nHexPH$_2$·BH$_3$ was investigated (Scheme 3.2a). Using the optimised conditions for PhPH$_2$·BH$_3$ (1 mol% cat., 4 M, 70 °C, THF) conversion of nHexPH$_2$·BH$_3$ was significantly slower, 84% in 14 days as determined by ^{11}B NMR spectroscopy. After precipitation into H$_2$O:isopropanol (1:1) only a trace of high molar mass material was observed in the GPC chromatogram (Figure S3.46). Increasing the catalyst loading to 2.5% allowed for 90% conversion over 5 days and a greater quantity of high molar mass material was produced as determined by GPC analysis. There was, however, a very broad molar mass distribution which ranged from ca. 5,000 – 120,000 Da (Figure S3.47) which is suggestive of chain branching. The identity of the material was confirmed by a comparison of the ^{11}B and ^{31}P NMR shifts to literature values[66] and ESI-MS showed the anticipated monomer repeat unit (*m/z* = 130); however, the yield after precipitation was only 18%.

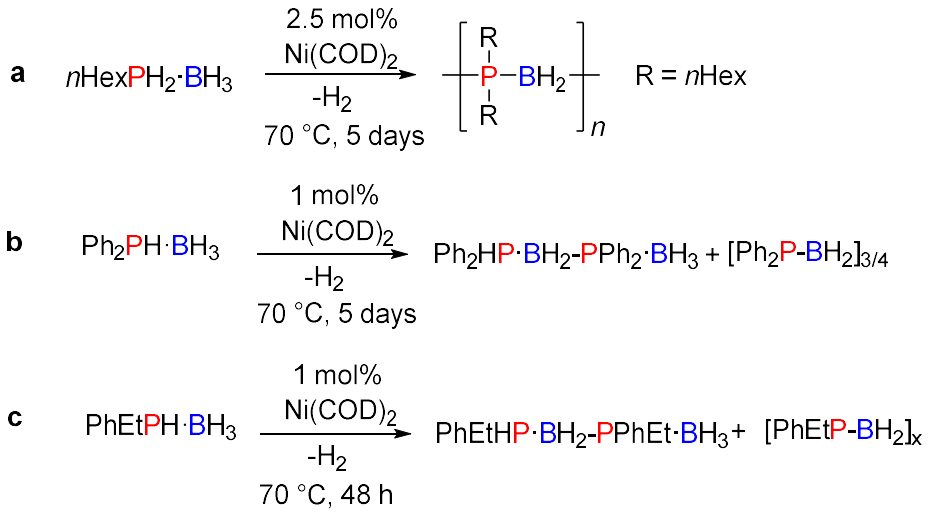

Scheme 3.2 Reactions between **a** nHexPH$_2$·BH$_3$; **b** Ph$_2$PH·BH$_3$; and **c** PhEtPH·BH$_3$ and catalytic $Ni(COD)_2$.

The activity of $Ni(COD)_2$ towards the P-disubstituted phosphine-boranes $PhEtH{\cdot}BH_3$ and $Ph_2PH{\cdot}BH_3$ were also investigated using the optimised conditions for $PhPH_2{\cdot}BH_3$ (1 mol% cat., 4 M, 70 °C, THF) (Scheme 3.2b and c). These substrates were chosen as thus far metal-catalysed dehydropolymerisation of P-disubstituted phosphine-borane monomers has been unsuccessful; however, high molar mass material $[RPhP–BH_2]_n$ (R = Ph or Et) has recently been reported using CAACs as stoichiometric hydrogen acceptors.[73] We therefore attempted to access these novel P-disubstituted polymers using catalytic quantities of $Ni(COD)_2$.

Full consumption of $Ph_2PH{\cdot}BH_3$ was achieved after 5 days as determined using ^{11}B NMR spectroscopy. Formation of the linear dimer $Ph_2PH{\cdot}BH_2–PPh_2{\cdot}BH_3$ (69%) (δ_B = -32.9 ppm (br) and -36.7 ppm (br); δ_P = -4.5 ppm (d) and -17.7 ppm) was confirmed by a comparison of the ^{11}B and ^{31}P NMR shifts with literature values. From integration of the NMR data a second species is detected (31%) which has ^{11}B and ^{31}P chemical shifts (δ_B = -32.9 ppm; δ_P = -17.7 ppm) coincidental with either small cyclics $[Ph_2P–BH_2]_{3/4}$ or $[Ph_2P–BH_2]_n$.[64] ESI-MS confirms the presence of $Ph_2PH{\cdot}BH_2–PPh_2{\cdot}BH_3$, $[Ph_2P–BH_2]_3$ and $[Ph_2P–BH_2]_4$ with no evidence of any higher molar mass material.

With $PhEtPH{\cdot}BH_3$ full consumption of the monomer was detected after 48 h by ^{11}B NMR spectroscopy. Two peaks were observed in both the ^{11}B and ^{31}P NMR spectra (δ_B = -35.2 ppm (br) and -39.2 ppm (m); δ_P = -2.0 ppm (d) and -21.8 ppm (br)) (Figure S3.56 and Figure S3.57). A combination of the NMR data and ESI-MS analysis (Figure S3.58a) led us to identify the major product as the linear dimer $PhEtPH{\cdot}BH_2–PPhEt{\cdot}BH_3$ (61%). As with the case of the diphenyl derivative, integration of the NMR spectra indicated that a further species is present (δ_B = -35.2 ppm; δ_P = -21.8 ppm). The observation of monomer repeat units (m/z = 150, n = 9) in the ESI-MS (Figure S3.58b) leads us to identify this additional species as oligomeric material, $[PhEtP–BH_2]_x$.

The GPC chromatograms of the material formed from $Ph_2PH{\cdot}BH_3$ and $PhEtPH{\cdot}BH_3$ both display a series of peaks with retention times that correspond to oligomeric or polymeric material (M_n = 1,300 – 11,300 Da for $Ph_2PH{\cdot}BH_3$ and M_n = 6,700 – 26,300 Da for $PhEtPH{\cdot}BH_3$) with low dispersity ($Đ$ = 1.02-1.06) (Figure S3.55 and Figure S3.59); however, these peaks represent only a small proportion of the isolated material. This observation, combined with the lack of any evidence for a degree of polymerisation greater than either n = 4 or 9, respectively, in the

ESI-MS spectra, indicates that further work needs to be undertaken in order to determine whether the peaks truly correspond to polymeric material.

3.4 Conclusions

In summary $Ni(COD)_2$ acts as a precatalyst for the dehydropolymerisation of $PhPH_2{\cdot}BH_3$ to produce high molar mass $[PhHP–BH_2]_n$ under relatively mild conditions. The six-membered ring $[PhHP–BH_2]_3$ (**3.1**) has been isolated from the polymerisation by-products and structurally characterised. It will be interesting to probe further reactivity of this species, an example being its propensity to undergo a ring-opening polymerisation reaction.

The mechanism of the $Ni(COD)_2$-catalysed dehydropolymerisation is postulated to involve a homogeneous chain-growth process, with evidence coming from molar mass vs conversion studies and poisoning experiments. The Ni precatalyst has also proved active for the dehydropolymerisation of the P-alkyl substituted phosphine-borane *n*$HexPH_2{\cdot}BH_3$. With the disubstituted derivatives $Ph_2PH{\cdot}BH_3$ and $PhEtPH{\cdot}BH_3$, the linear dimers $PPhRH{\cdot}BH_2–PPhR{\cdot}BH_3$ (R = Ph or Et) are the major products.

3.5 Supporting Information

3.5.1 General procedures, reagents and equipment

All manipulations were carried out either under an atmosphere of nitrogen gas using standard vacuum line and Schlenk techniques, or under an atmosphere of nitrogen within an M. Braun glovebox MB200-B maintained at < 0.1 ppm of H_2O and < 0.1 ppm of O_2. 2-*methyl*-THF was distilled over sodium-benzophenone ketyl prior to used and 1,4-dioxane was dried over molecular sieves (4 Å) and degassed with 3 freeze-pump thaw cycles prior to use. Tetrahydrofuran (THF) and hexane were dried via a Grubbs design solvent purification system.[82] Hexamethyldisiloxane (HMDSO) was purchased from Sigma Aldrich and used as received.

Deuterated solvents (benzene-d_6 and chloroform-*d*) were purchased from Sigma Aldrich and vacuum distilled from, sodium-benzophenone or CaH_2 respectively and stored over molecular sieves (4 Å). NMR spectra were recorded using Bruker 300 MHz, Bruker 360 MHz and Bruker 500 MHz NMR spectrometers. ^1H NMR spectra were calibrated using the residual protio signal of the solvent: (δ (ppm) $^1H(CDCl_3)$ = 7.24 and ^1H (C_6D_6) = 7.16). ^{13}C NMR spectra were calibrated using the residual protio signal of the solvent: (δ = $^{13}C(CDCl_3)$ = 77.2). ^{11}B and

^{31}P NMR spectra were calibrated against external standards (^{31}P: 85% H_3PO_4 (aq) (δ ^{31}P = 0.0); ^{11}B: $BF_3{\cdot}OEt_2$ (δ ^{11}B = 0.0)).

$PhPH_2{\cdot}BH_3$,[83] *n*$HexPH_2{\cdot}BH_3$,[66] $Ph_2PH{\cdot}BH_3$[84] and $PhEtPH{\cdot}BH_3$[85] were prepared according to literature procedures. $Ni(COD)_2$, PPh_3, Ni nanoparticles (< 100 nm) and $Me_2NH{\cdot}BH_3$ were purchased from Sigma Aldrich and used as received except $Me_2NH{\cdot}BH_3$ which was sublimed prior to use.

GPC was performed on a Malvern RI max Gel Permeation Chromatograph, equipped with an automatic sampler, a pump, an injector, and inline degasser. The columns (1 x T5000 and 1 x T3000) were contained within an oven (35 °C) and consisted of styrene/divinyl benzene gels. Sample elution was detected by means of a differential refractometer. THF (Fisher), containing 0.1 wt.% [*n*Bu_4N]Br, was used as the eluent at a flow rate of 1 mL min^{-1}. Samples were dissolved in the eluent (2 mg mL^{-1}) and filtered through a poly(tetrafluoroethylene) membrane of 200 nm pore size before analysis. The calibration was conducted using monodisperse polystyrene standards obtained from Aldrich. The lowest and highest molecular weight standards used were 1,200 Da and 4,200,000 Da respectively.

Electrospray ionisation mass spectrometry was performed using a MSQ Plus single quadrupole mass spectrometer (Thermo, MA). The instrument assembly includes a 515 HPLC pump (Waters, MA) with a flow rate set to 0.2 mL min^{-1}. A 50:50 solvent mixture was used comprising of Mili-Q™ water (Millipore, ON) and Optima™ Methanol (Fisher Chemical, NH). 200 uL of sample was injected using a manual injector (Rheodyne 7725i, IDEX, CA) in direct infusion mode. Mass spectrometer parameters include cone voltage set to 75 V, mass range set to 50-2000 m/z and scan time 1 second.

UV-Vis was carried out on an Agilent 8453 UV−visible spectrophotometer.

3.5.2 General procedure for $Ni(COD)_2$-catalysed dehydropolymerisation of $PhPH_2{\cdot}BH_3$

$PhPH_2{\cdot}BH_3$ (50 mg, 0.40 mmol) and $Ni(COD)_2$ (quantities shown in Table S3.1) were dissolved in solvent (volume and identity of solvent shown in Table S3.1) in a J. Young NMR tube and heated using an oil bath (temperature and time shown in Table S3.1). ^{31}P and ^{11}B NMR data was obtained on the reaction mixture prior to precipitation into cold (-40 °C) hexanes. The solution was centrifuged for 5 min at 4,000 RPM, the supernatant decanted, and the precipitate dried *in vacuo* for 48 h to give the isolated products as pale yellow solids.

Table S3.1 Conditions for optimisation of and exploration of polymerisation conditions.

Run	Cat. (mol%)	Cat. (mmol)	Cat. (mg)	Conc. (M)[a]	Solvent	Volume (µL)	Temp (°C)	Time (h)	Yield (%)[b]
1	1	0.004	1	1	THF	400	70	72	49
2	1	0.004	1	2	THF	200	70	72	55
3	1	0.004	1	4	THF	100	70	72	53
4	2.5	0.010	3	1	THF	400	70	72	41
5	5	0.020	6	1	THF	400	70	72	47
6	1	0.004	1	1	THF	400	50	195	33
7	1	0.004	1	1	THF	400	60	195	24
8	0	0	0	1	THF	400	70	72	2
9	0	0	0	1	THF	400	70	624	27
10	1	0.004	1	1	1,4-dioxane	400	70	110	37
11	1	0.004	1	1	1,4-dioxane	400	100	24	39
12	1	0.004	1	1	1,4-dioxane	400	100	72	49
13	1	0.004	1	1	2-*methyl*-THF	400	70	72	40

[a]Concentration of $PhPH_2BH_3$; [b]isolated yield.

3.5.2.1 Concentration dependence

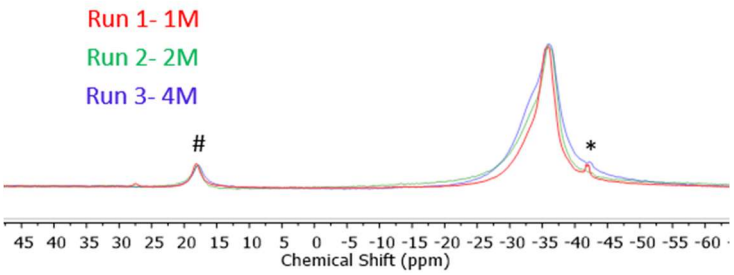

Figure S3.1 $^{11}B\{^1H\}$ NMR spectra (96 MHz, 298 K, THF) of the reaction mixture for runs 1-3 (Table S3.1) (*unreacted $PhPH_2{\cdot}BH_3$, #unidentified impurity).

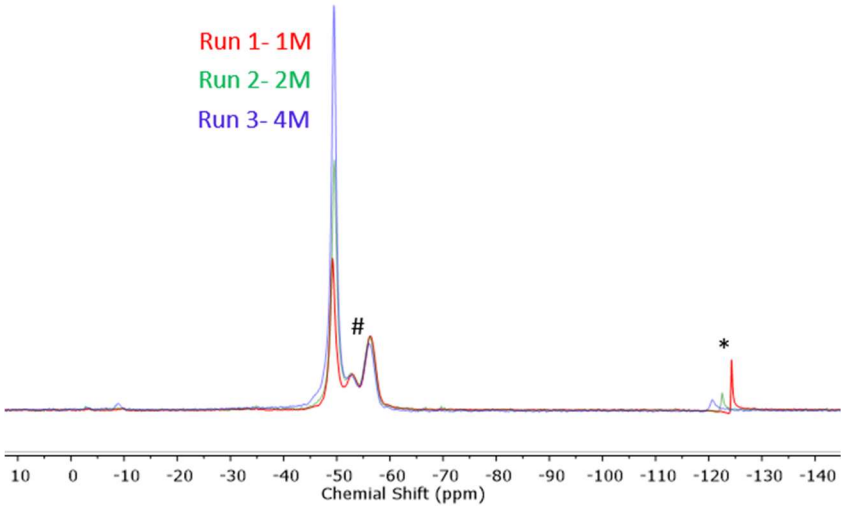

Figure S3.2 $^{31}P\{^1H\}$ NMR spectra (122 MHz, 298 K, THF) of the reaction mixture for runs 1-3 (Table S3.1) (*$PPhH_2$, #oligomeric material).

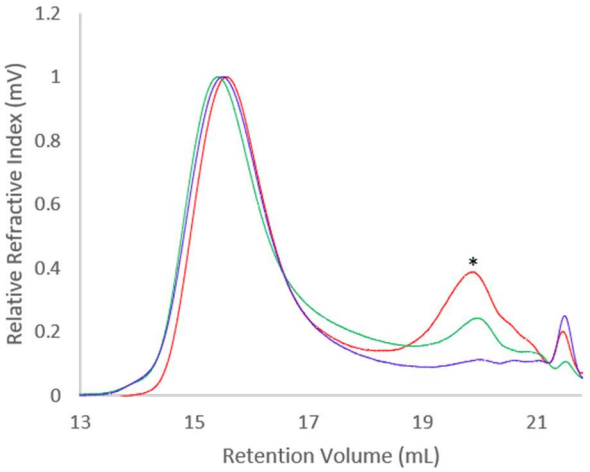

Run	M_n	M_w	PDI
1	32,900	53,500	1.63
2	26,900	56,900	2.11
3	28,400	58,200	2.05

Figure S3.3 GPC chromatogram of isolated $[PhHP–BH_2]_n$ from for runs 1-3 (Table S3.1). 2 mg mL^{-1} in THF with 0.1 w/w% nBu$_4$NBr in the THF eluent (*below calibration region).

3.5.2.2 Catalyst loading dependence

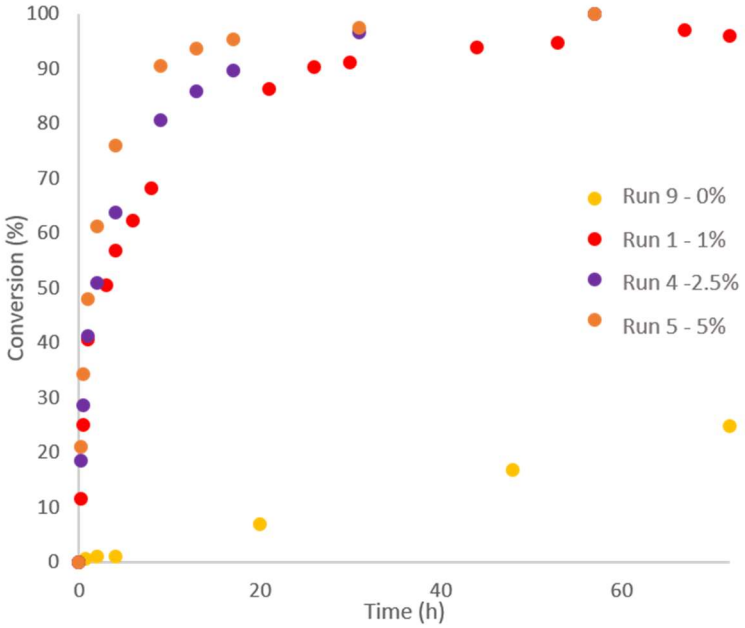

Figure S3.4 Plot of conversion vs time for runs 1, 4, 5 and 9 (Table S3.1). Conversion determined using relative integrals of ^{11}B NMR spectra.

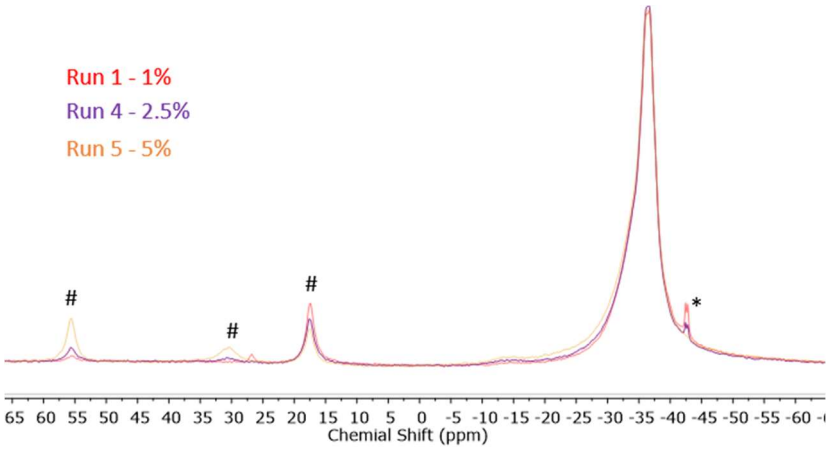

Figure S3.5 $^{11}B\{^1H\}$ NMR spectra (96 MHz, 298 K, THF) of the reaction mixture for runs 1, 4 and 5 (Table S3.1) (*unreacted $PhPH_2{\cdot}BH_3$, #unidentified impurity).

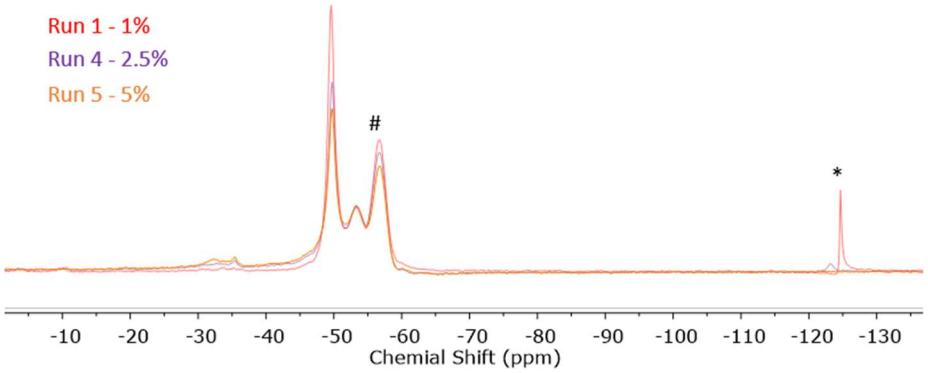

Figure S3.6 $^{31}P\{^1H\}$ NMR spectra (122 MHz, 298 K, THF) of the reaction mixture for runs 1, 4 and 5 (Table S3.1) (*$PPhH_2$, #oligomeric material).

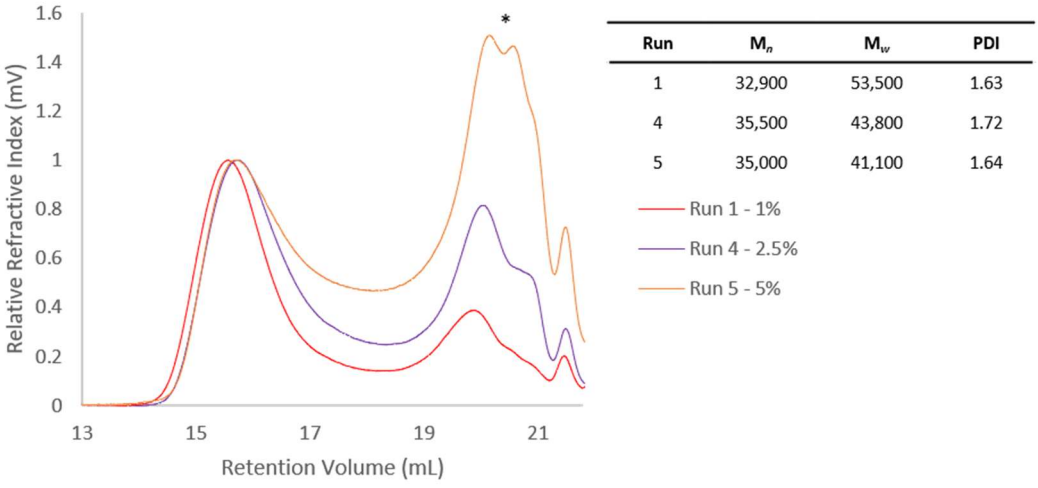

Run	M_n	M_w	PDI
1	32,900	53,500	1.63
4	35,500	43,800	1.72
5	35,000	41,100	1.64

Figure S3.7 GPC chromatogram of isolated $[PhHP–BH_2]_n$ from for runs 1, 4 and 5 (Table S3.1). 2 mg mL^{-1} in THF with 0.1 w/w% nBu$_4$NBr in the THF eluent (*below calibration region).

3.5.2.3 Temperature dependence

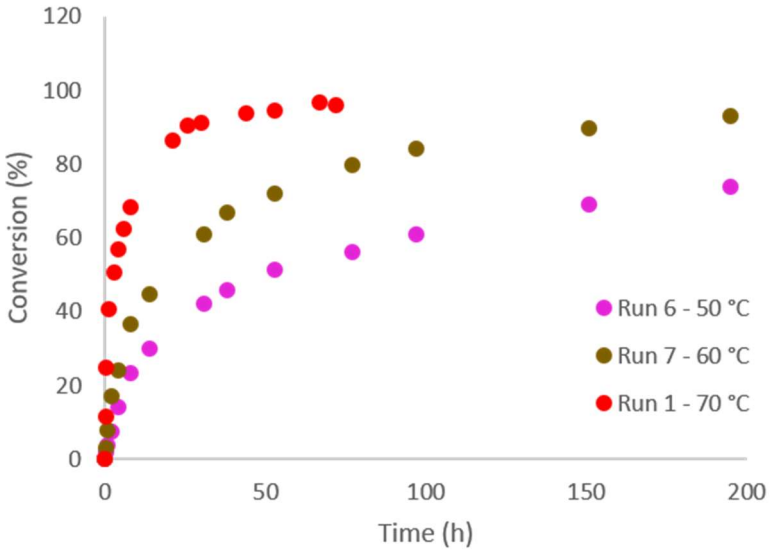

Figure S3.8 Plot of conversion vs time for runs 1, 6 and 7 (Table S3.1). Conversion determined using relative integrals of ^{11}B NMR spectra.

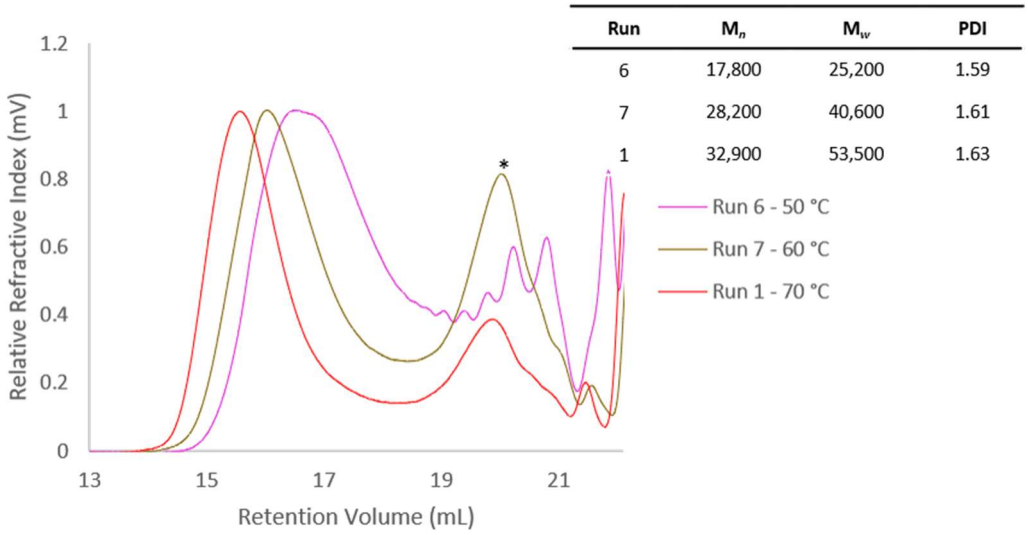

Run	M_n	M_w	PDI
6	17,800	25,200	1.59
7	28,200	40,600	1.61
1	32,900	53,500	1.63

Figure S3.9 GPC chromatogram of isolated [PhHP–BH_2]$_n$ from for runs 1, 6 and 7 (Table S3.1). 2 mg mL^{-1} in THF with 0.1 w/w% nBu$_4$NBr in the THF eluent (*below calibration region).

3.5.2.4 Control reaction with no catalyst

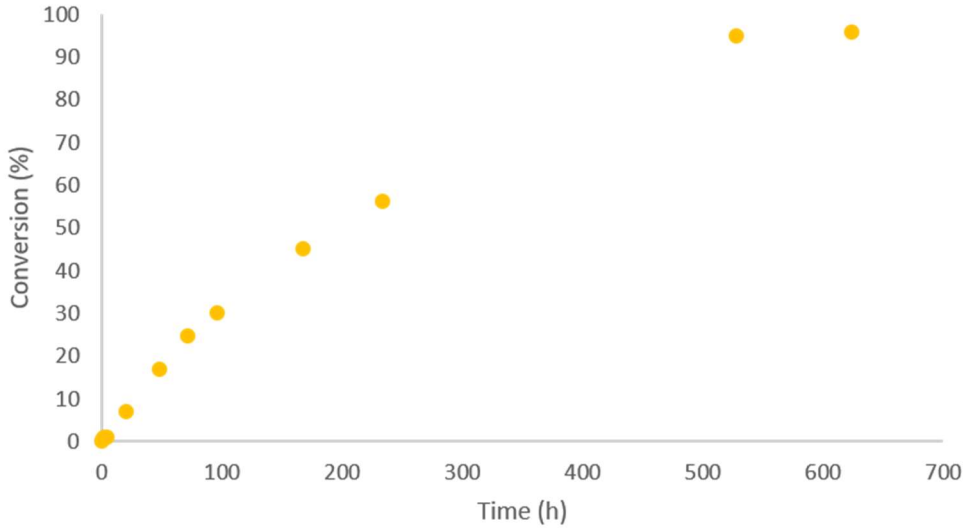

Figure S3.10 Plot of conversion vs time for run 9 (Table S3.1). Conversion determined using relative integrals of ^{11}B NMR spectra.

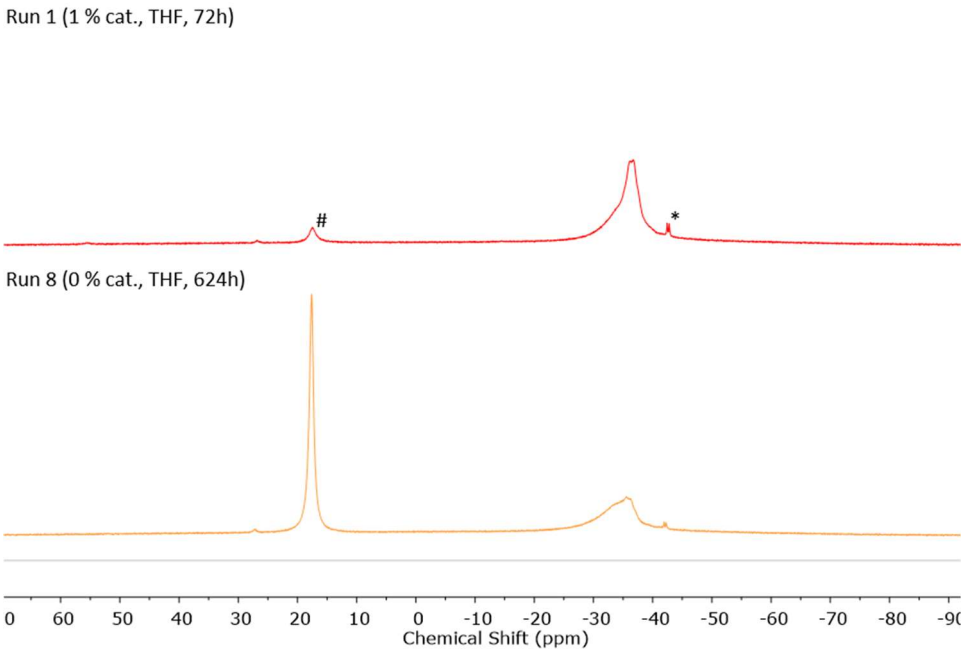

Figure S3.11 $^{11}B\{^{1}H\}$ NMR spectra (96 MHz, 298 K, THF) of the reaction mixture for runs 1, 8 and 9 (Table S3.1) (*unreacted $PhPH_2 \cdot BH_3$, #unidentified impurity).

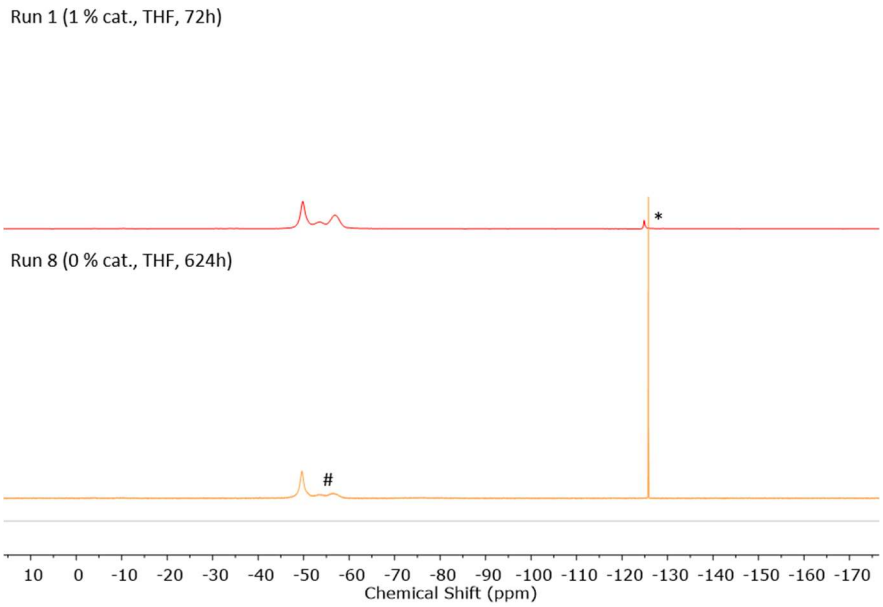

Figure S3.12 $^{31}P\{^{1}H\}$ NMR spectra (122 MHz, 298 K, THF) of the reaction mixture for runs 1, 8 and 9 (Table S3.1) (*$PPhH_2$, #oligomeric material).

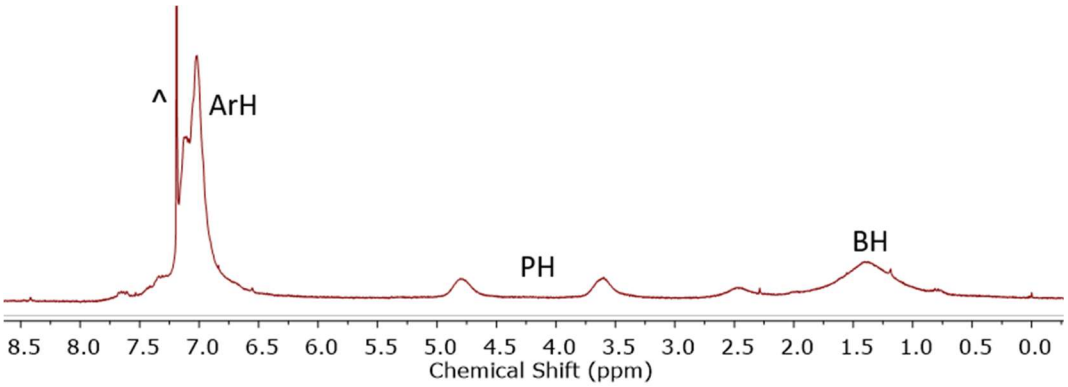

Figure S3.13 ^{1}H NMR spectrum (500 MHz, 298 K, $CDCl_3$) of $[PhHP–BH_2]_n$ (run 9) (^denotes residual partially protiated $CDCl_3$).

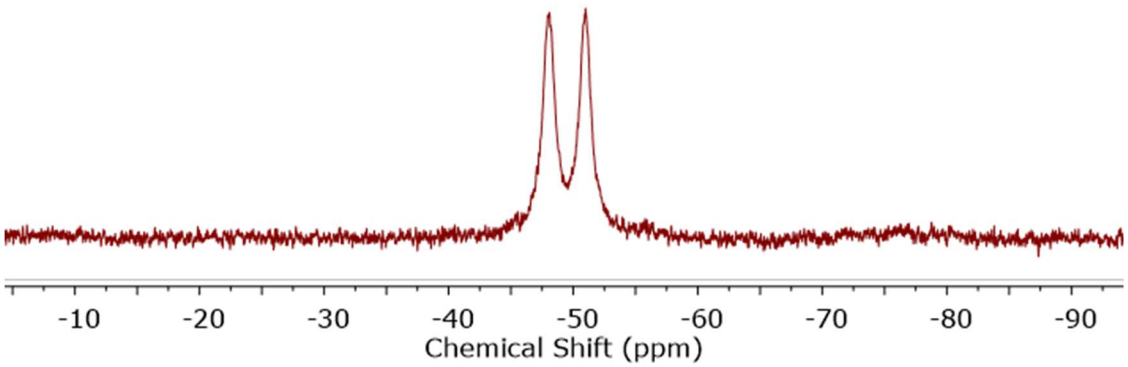

Figure S3.14 ^{31}P NMR spectrum (96 MHz, 298 K, $CDCl_3$) of $[PhHP–BH_2]_n$ (run 9).

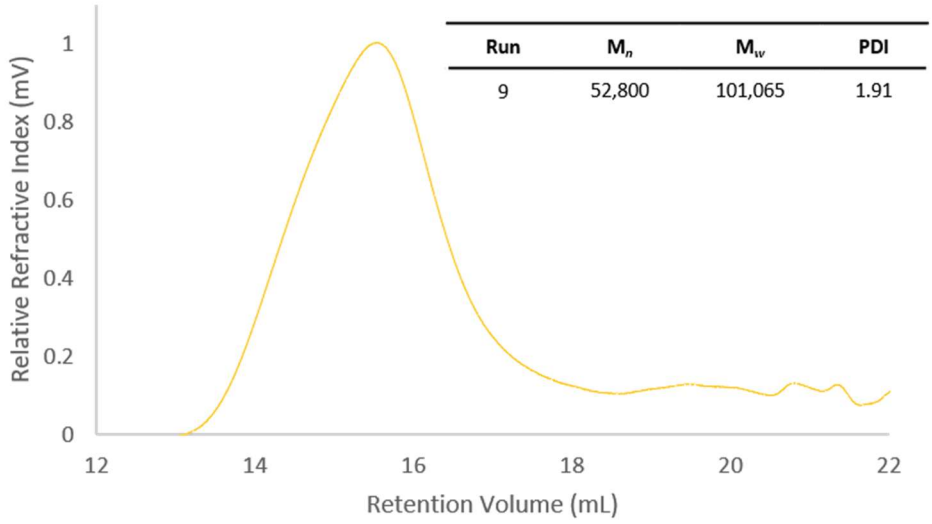

Figure S3.15 GPC chromatogram of isolated $[PhHP–BH_2]_n$ from for run 9 (Table S3.1). 2 mg mL^{-1} in THF with 0.1 w/w% nBu$_4$NBr in the THF eluent.

3.5.2.5 Solvent dependence

1,4-Dioxane

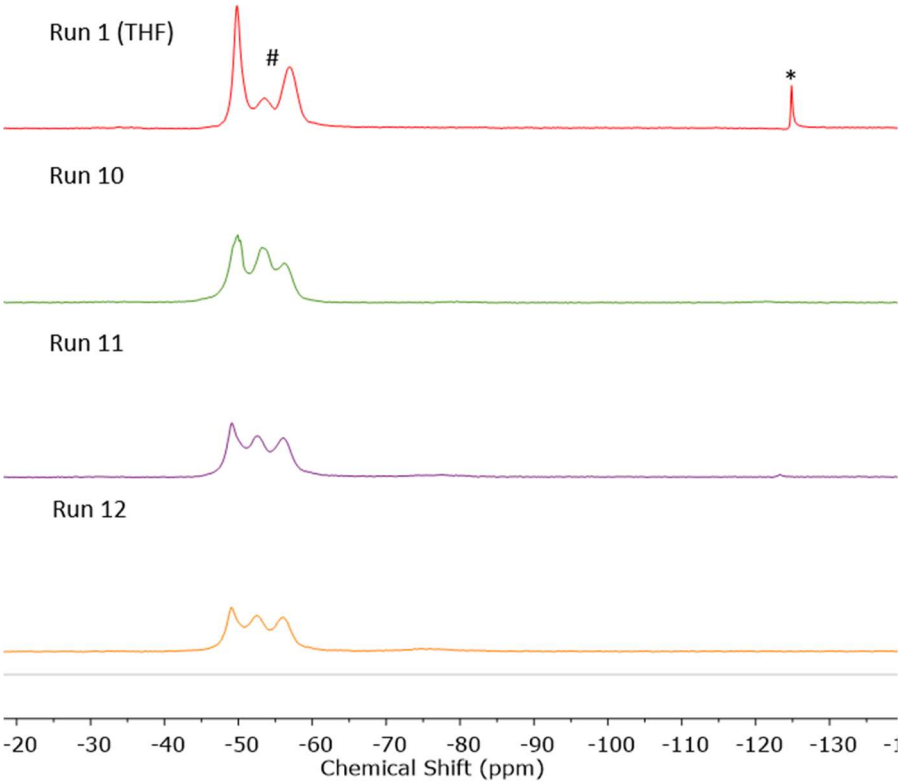

Figure S3.16 $^{31}P\{^1H\}$ NMR spectra (122 MHz, 298 K, 1,4-dioxane) of the reaction mixture for runs 10, 11 and 12 (Table S3.1). Run 1 included for a comparison with THF (*$PPhH_2$, #oligomeric material).

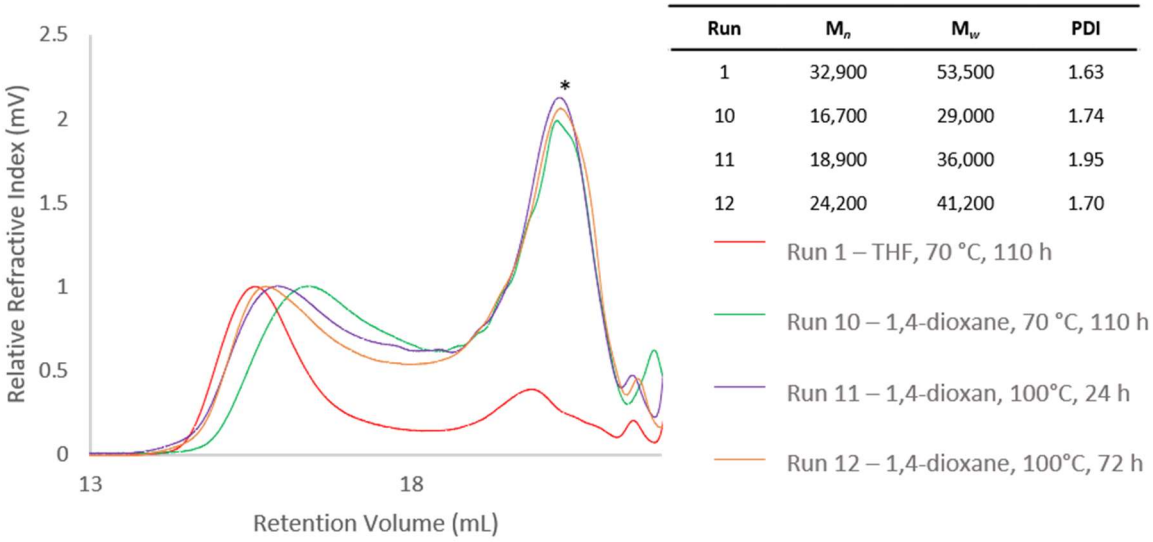

Run	M_n	M_w	PDI
1	32,900	53,500	1.63
10	16,700	29,000	1.74
11	18,900	36,000	1.95
12	24,200	41,200	1.70

Figure S3.17 GPC chromatogram of isolated [PhHP–BH_2]$_n$ from for runs 1, 10, 11 and 12 (Table S3.1). 2 mg mL^{-1} in THF with 0.1 w/w% *n*Bu_4NBr in the THF eluent (*below calibration region).

2-*methyl*-THF

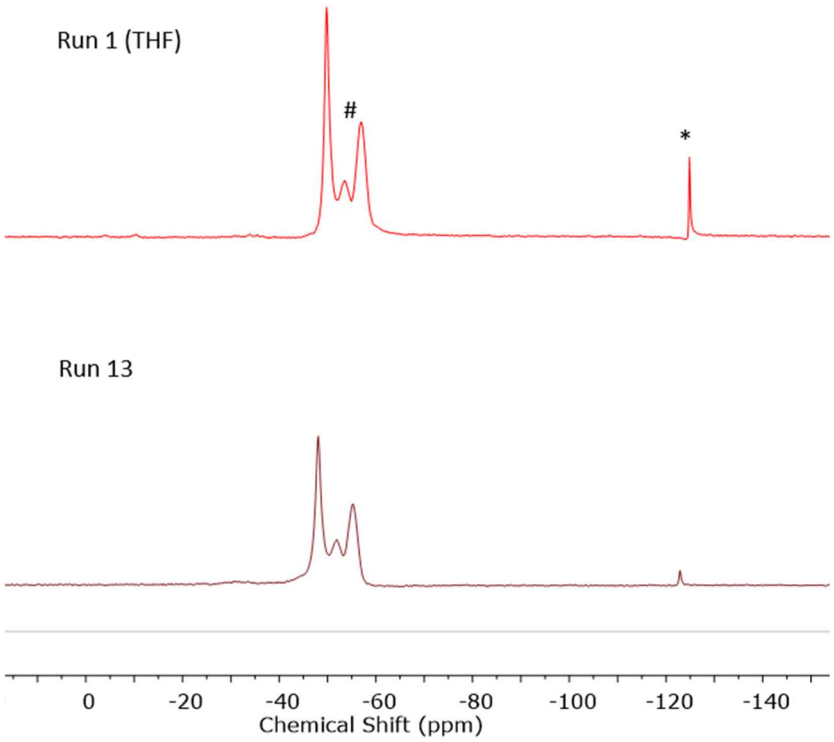

Figure S3.18 $^{31}P\{^1H\}$ NMR spectra (122 MHz, 298 K, 2-*methyl*-THF) of the reaction mixture for run 13 (Table S3.1). Run 1 included for a comparison with THF (*$PPhH_2$, #oligomeric material).

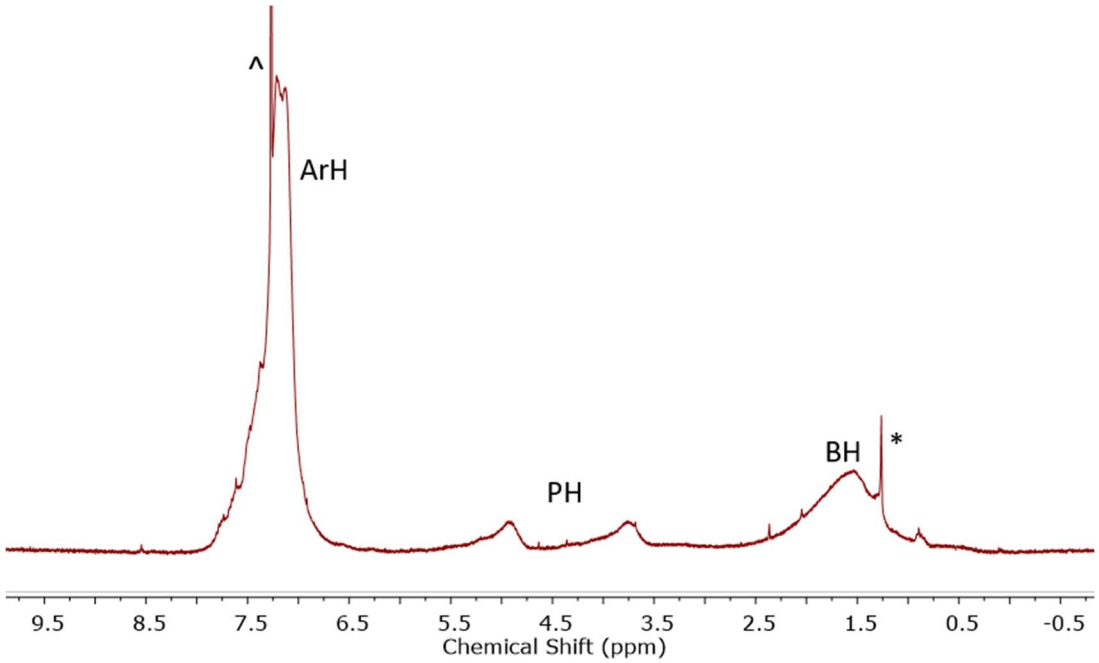

Figure S3.19 ^{1}H NMR spectrum (500 MHz, 298 K, $CDCl_3$) of $[PhHP–BH_2]_n$ (run 13) (^denotes residual partially protiated $CDCl_3$, * hexanes).

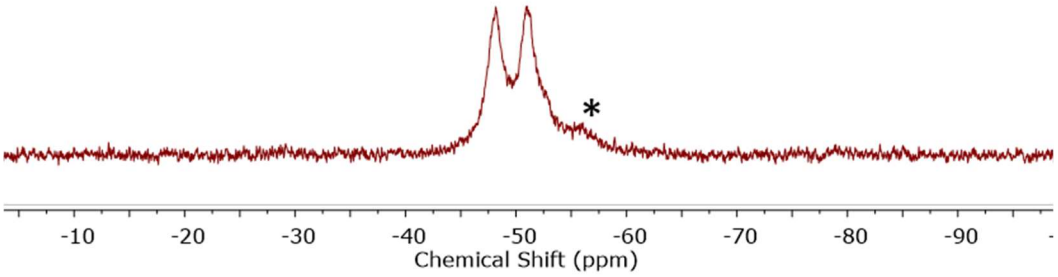

Figure S3.20 ^{31}P NMR spectrum (96 MHz, 298 K, $CDCl_3$) of $[PhHP–BH_2]_n$ (run 13). (*shoulder to $[PhHP–BH_2]_n$ potentially due to chain branching).

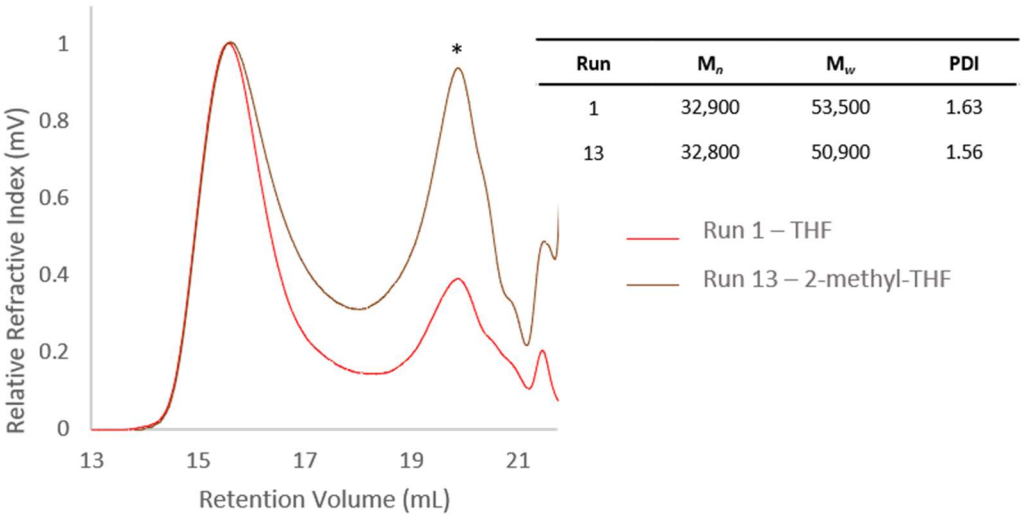

Run	M_n	M_w	PDI
1	32,900	53,500	1.63
13	32,800	50,900	1.56

Figure S3.21 GPC chromatogram of isolated $[PhHP–BH_2]_n$ from for runs 1 and 13 (Table S3.1). 2 mg mL^{-1} in THF with 0.1 w/w% nBu$_4$NBr in the THF eluent (*below calibration region).

3.5.3 Carrying out polymerisation in air

$PhPH_2{\cdot}BH_3$ (50 mg, 0.40 mmol) and $Ni(COD)_2$ (1 mg, 0.004 mmol) were dissolved in THF (400 µL) in a J. Young NMR tube. The reaction was opened to air for 15 min prior to resealing and heating to 70 °C for 38 h. ^{31}P and ^{11}B NMR data was obtained on the reaction mixture prior to precipitation into cold (-40 °C) hexanes (20 mL). The solution was centrifuged for 5 min at 4,000 RPM, the supernatant decanted, and the precipitate dried *in vacuo* for 48 h to give the isolated product as a pale yellow solid. Yield = 16 mg (33%)

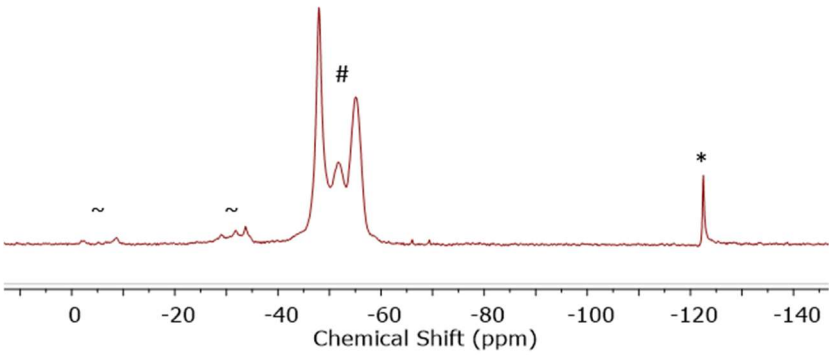

Figure S3.22 $^{31}P\{^1H\}$ NMR spectrum (122 MHz, 298 K, THF) of the reaction mixture for run 14 (Table 3.1) (*$PPhH_2$, #oligomeric material, ~unidentified impurity, presumably from some decomposition occurring in air).

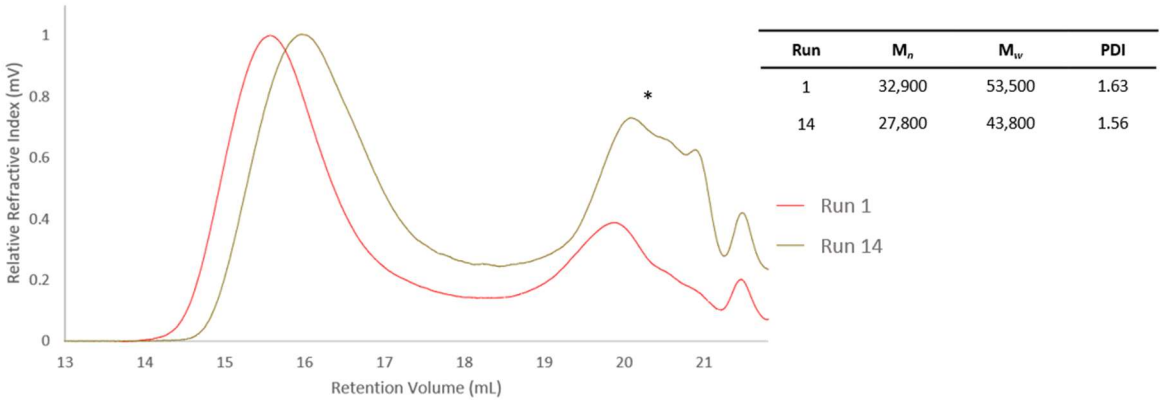

Run	M_n	M_w	PDI
1	32,900	53,500	1.63
14	27,800	43,800	1.56

Figure S3.23 GPC chromatogram of isolated $[PhHP–BH_2]_n$ from for runs 1 and 14 (Table 3.1). 2 mg mL^{-1} in THF with 0.1 w/w% nBu$_4$NBr in the THF eluent (*below calibration region).

3.5.4 Scaled up optimised conditions

$PhPH_2{\cdot}BH_3$ (200 mg, 1.61 mmol) and $Ni(COD)_2$ (4 mg, 0.02 mmol) were dissolved in THF (400 µL) in a J. Young Schlenk before heating at 70 °C for 72 h. The reaction mixture was precipitated into cold (-40 °C) hexanes (3 x 20 mL). The solution was centrifuged for 5 min at 4,000 RPM, the supernatant decanted, and the precipitate dried *in vacuo* for 48 h to give the isolated product as a pale yellow solid. NMR data matched that of previously reported $[PhHP–BH_2]_n$[64]. Yield = 103 mg (53%). M_n = 25,400 Da; $Đ$ = 2.00.

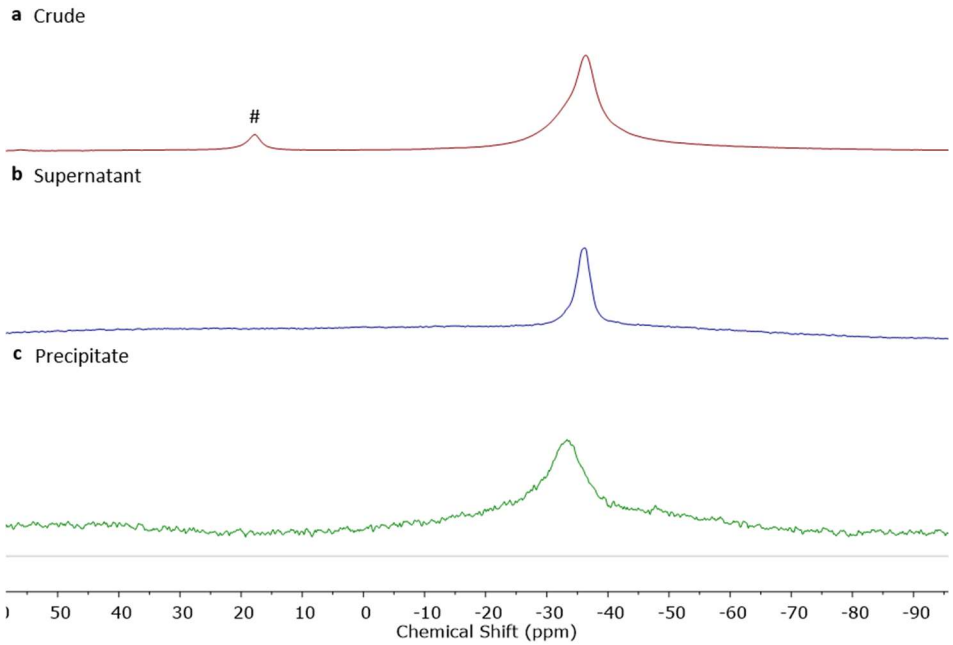

Figure S3.24 $^{11}B\{^{1}H\}$ NMR spectra (96 MHz, 298 K, THF) of the **a** polymerisation reaction mixture; **b** supernatant; and **c** precipitate for run 15 (Table 3.1) ($^{\#}$unidentified impurity).

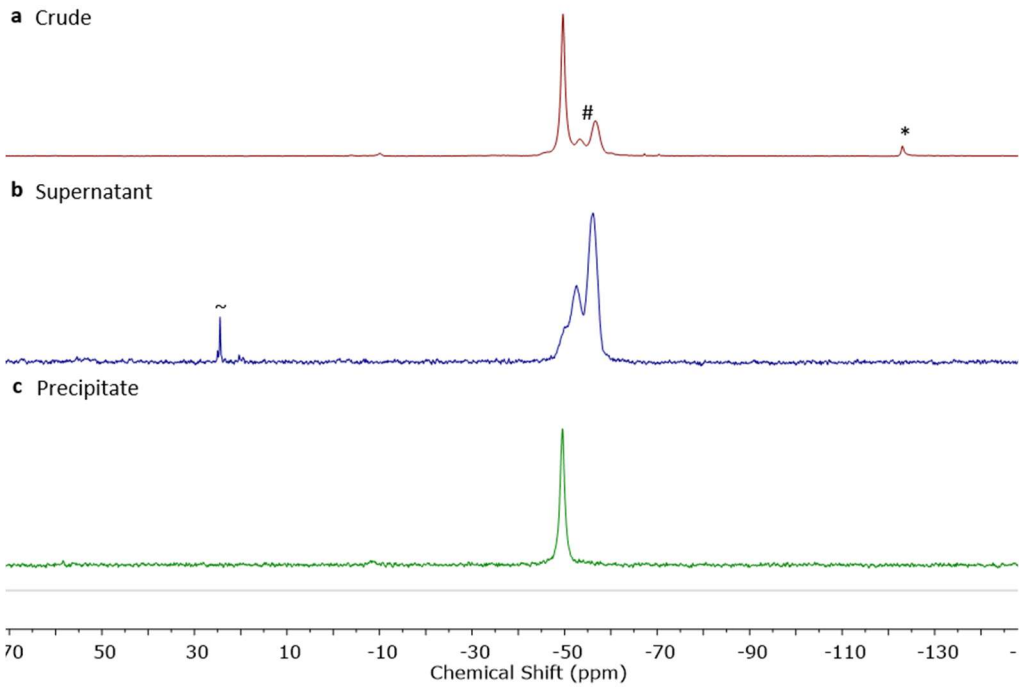

Figure S3.25 $^{31}P\{^{1}H\}$ NMR spectra (96 MHz, 298 K, THF) of the **a** polymerisation reaction mixture; **b** supernatant; and **c** precipitate for run 15 (Table 3.1) (*$PPhH_2$, $^{\#}$oligomeric material, ~$P(O)PhH_2$).

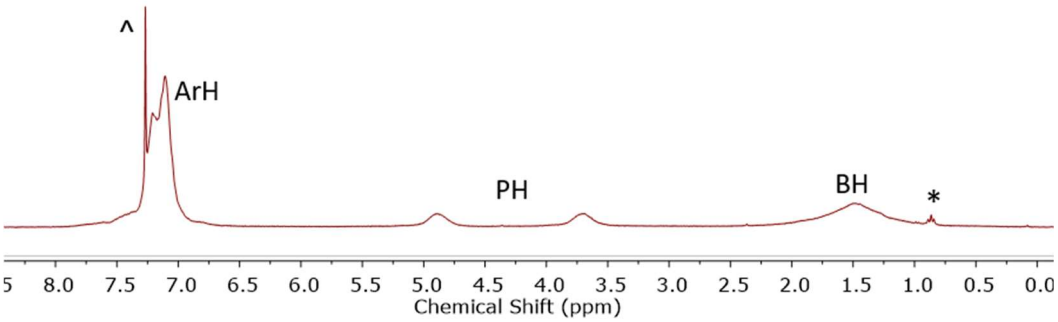

Figure S3.26 ^{1}H NMR spectrum (500 MHz, 298 K, $CDCl_3$) of $[PhHP–BH_2]_n$ (run 15) (^denotes residual partially protiated $CDCl_3$, * hexanes).

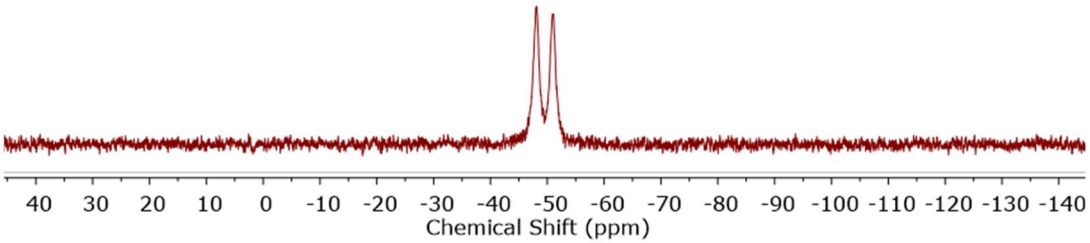

Figure S3.27 ^{31}P NMR spectrum (96 MHz, 298 K, $CDCl_3$) of $[PhHP–BH_2]_n$ (run 15).

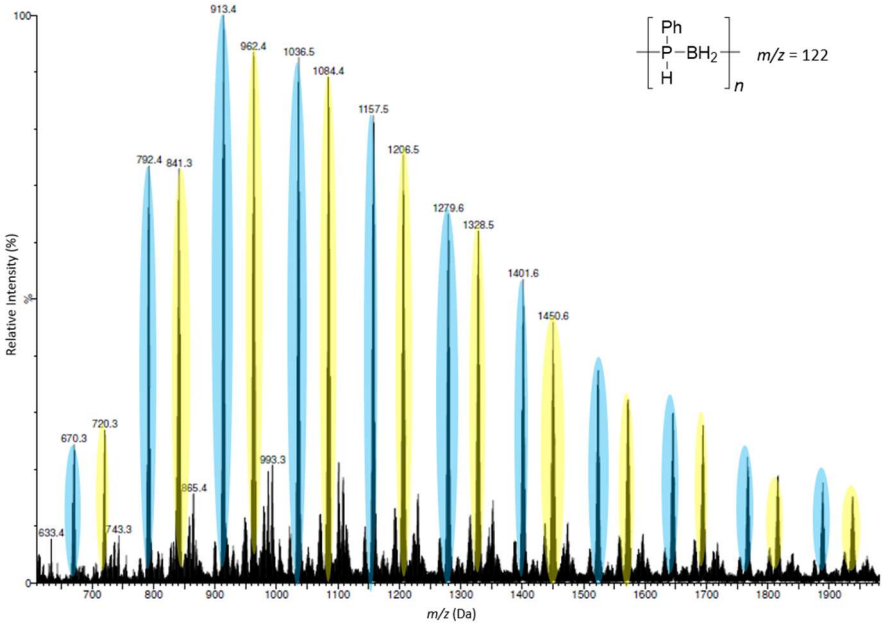

Figure S3.28 ESI(+)-MS spectrum of isolated $[PhHP–BH_2]_n$ (m/z = 122) from run 15 (Table 3.1) The species highlighted in yellow is a linear system with a $PPhH_2$ end group $(H\text{-}[PhHP–BH_2]_n\text{-}PPhH_2)^+$ and the species highlighted in blue has an unidentified end group.

3.5.5 Isolation of $[PhHP–BH_2]_3$ (3.1)

$PhPH_2{\cdot}BH_3$ (250 mg, 2.00 mmol) and $Ni(COD)_2$ (14 mg, 0.051 mmol) were dissolved in dioxane (8 mL) in a J. Young Schlenk. The reaction was heated to 100 °C for 24 h prior to precipitation into cold (-40 °C) hexanes (100 mL). The supernatant was decanted and the solvent removed *in vacuo* to leave a pale yellow oily solid. Single yellow crystals suitable for X-ray diffraction were grown from a THF solution layered with HMDSO at 22 °C. Yield = 17 mg (7%). EI-MS: expected 366.1370, actual 365.0989 ($[PhHP–BH_2]_3 – H^+$).

^{1}H NMR (500 MHz, 25 °C, $CDCl_3$): δ = 7.76 (m, 15H, Ar), 4.92 (dt, $^2J_{HP}$ = 348 Hz, $^3J_{HH}$ = 13.9 Hz 3H, PH), 2.40-0.95 (m, br, 6H, BH).

^{11}B NMR (96 MHz, 25 °C, $CDCl_3$): δ = -35.8 (br).

^{31}P NMR (122 MHz, 25 °C, $CDCl_3$): δ = -52.5 (d, $^2J_{PH}$ = 353 Hz).

^{13}C NMR (101 MHz, 25 °C, $CDCl_3$): δ = 132.8 (Ar^o), 130.2 (Ar^m), 128.7(Ar^p) (Ar^i not observed).

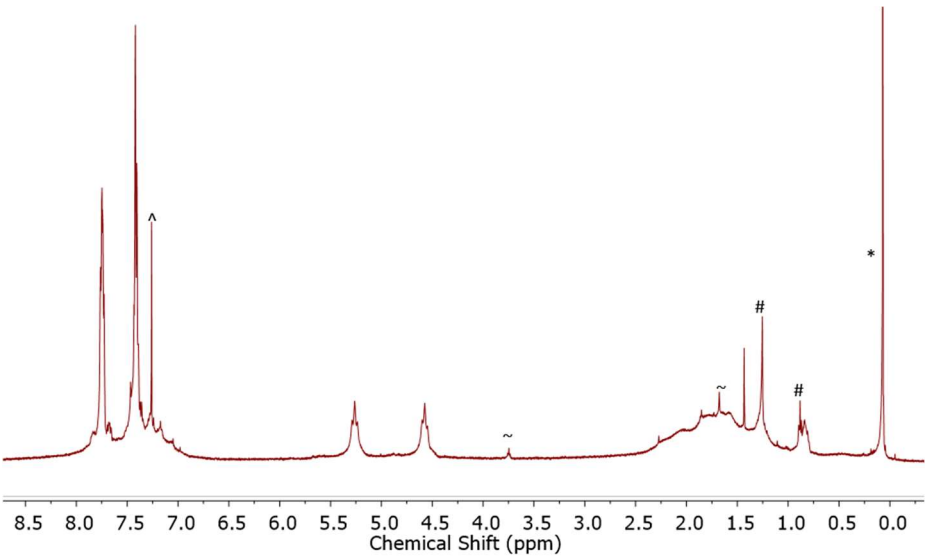

Figure S3.29 ^{1}H NMR spectrum (500 MHz, 298 K, $CDCl_3$) of **3.1** (^denotes residual partially protiated $CDCl_3$, ~THF, #hexanes, *HMDSO).

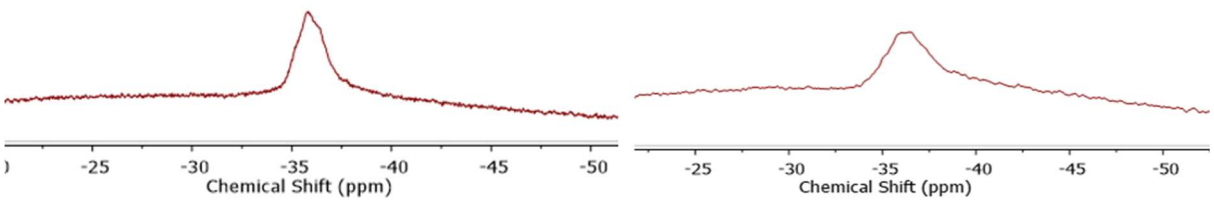

Figure S3.30 $^{11}B\{^1H\}$ (left) and ^{11}B (right) NMR spectra (96 MHz, 298 K, $CDCl_3$) of **3.1**.

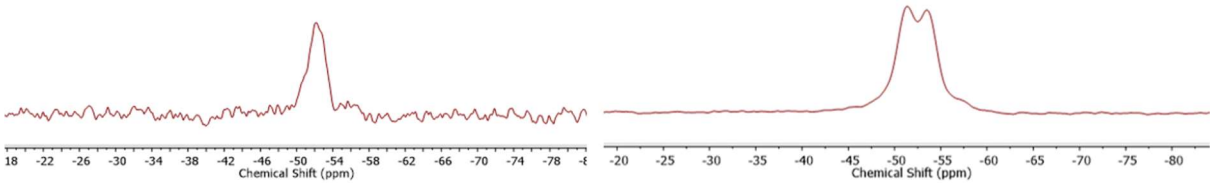

Figure S3.31 $^{31}P\{^{1}H\}$ (left) and ^{31}P (right) NMR spectra (122 MHz, 298 K, $CDCl_3$) of **3.1**.

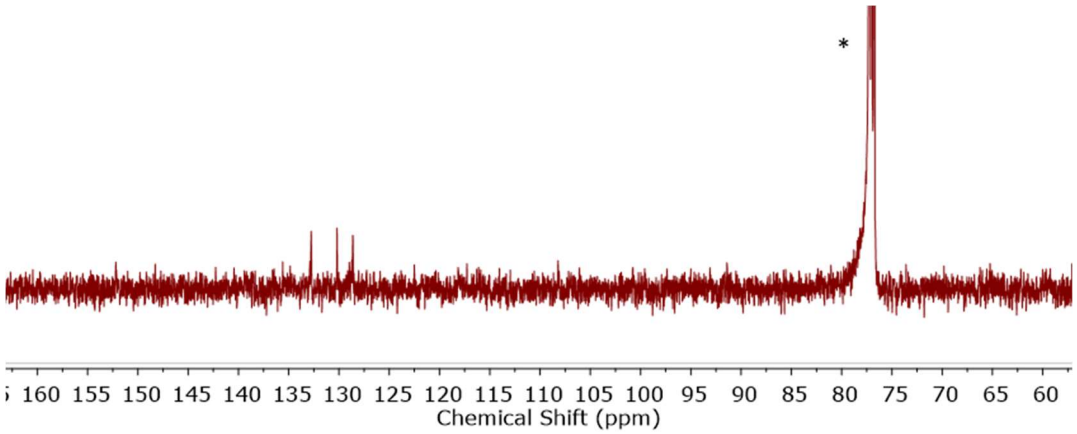

Figure S3.32 ^{13}C NMR spectra (101 MHz, 298 K, $CDCl_3$) of **3.1**.

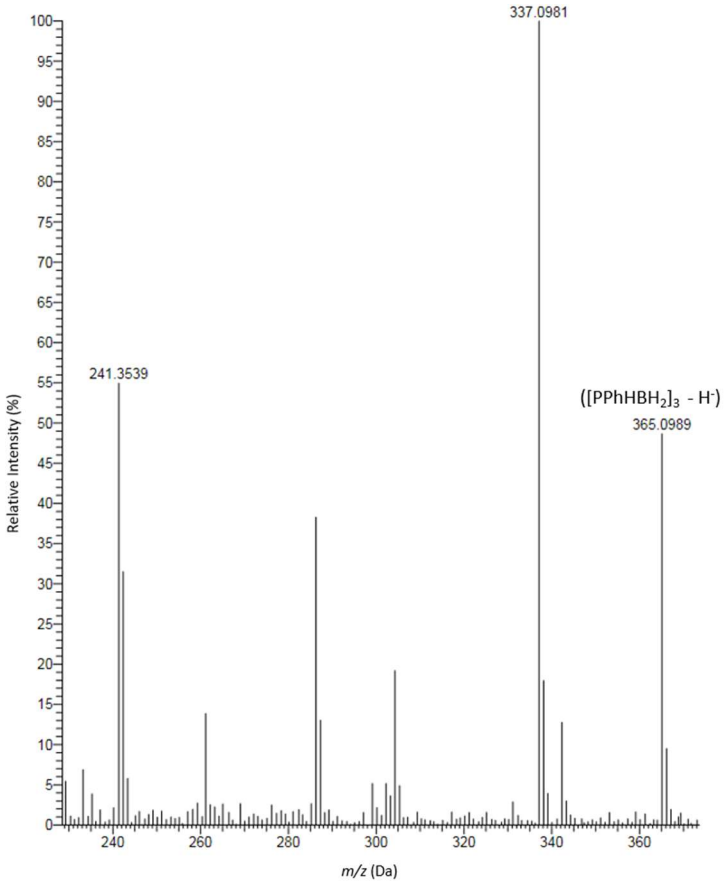

Figure S3.33 ESI(+)-MS spectrum of **3.1**.

3.5.6 Reaction of $[PhHP–BH_2]_3$ with $Ni(COD)_2$

$[PhHP–BH_2]_3$ (15 mg, 0.040 mmol) and $Ni(COD)_2$ (3 mg, 0.01 mmol) were dissolved in THF (400 µL) in a J. Young NMR tube before heating to 70 °C for 72 h. No conversion to new species was detected using ^{11}B or ^{31}P NMR spectroscopy.

3.5.7 Polymer growth kinetics

$PhPH_2{\cdot}BH_3$ (200 mg, 1.61 mmol) and $Ni(COD)_2$ (4 mg, 0.02 mmol) were dissolved in THF (1.6 mL) in a J. Young Schlenk before heating to 70 °C. Regular aliquots were taken from the reaction mixture over 144 h and filtered through a silica plug prior to GPC analysis. A separate reaction was set up in a J. Young NMR tube ($PhPH_2{\cdot}BH_3$ (50 mg, 0.40 mmol), $Ni(COD)_2$ (1 mg, 0.004 mmol, THF 400 µL) with a $B(OiPr)_3$ capillary to allow a conversion vs time plot to be made.

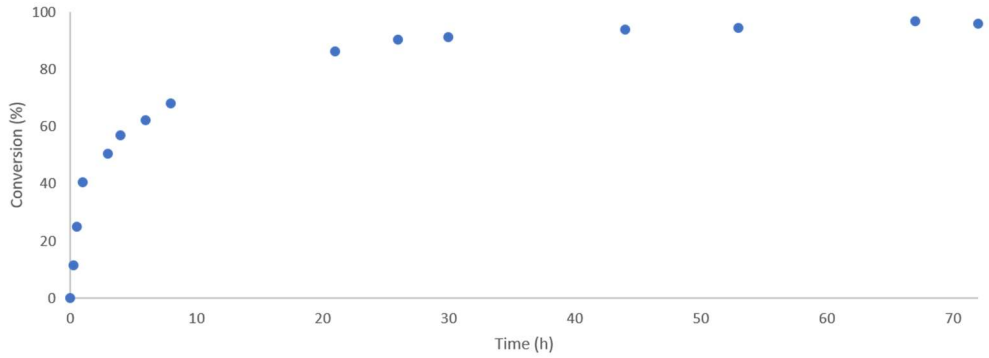

Figure S3.34 Plot of conversion vs time for polymerisation of $PhPH_2{\cdot}BH_3$ using $Ni(COD)_2$.

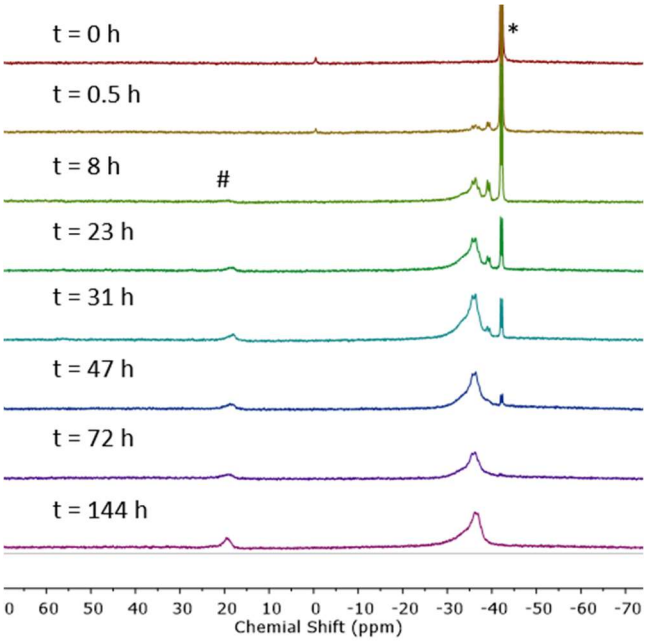

Figure S3.35 $^{11}B\{^1H\}$ NMR spectra (96 MHz, 298 K, $CDCl_3$) over time of reaction mixture for polymerisation of $PPhH_2{\cdot}BH_3$ using $Ni(COD)_2$ ($^*PhPH_2{\cdot}BH_3$, $^\#$unidentified impurity)..

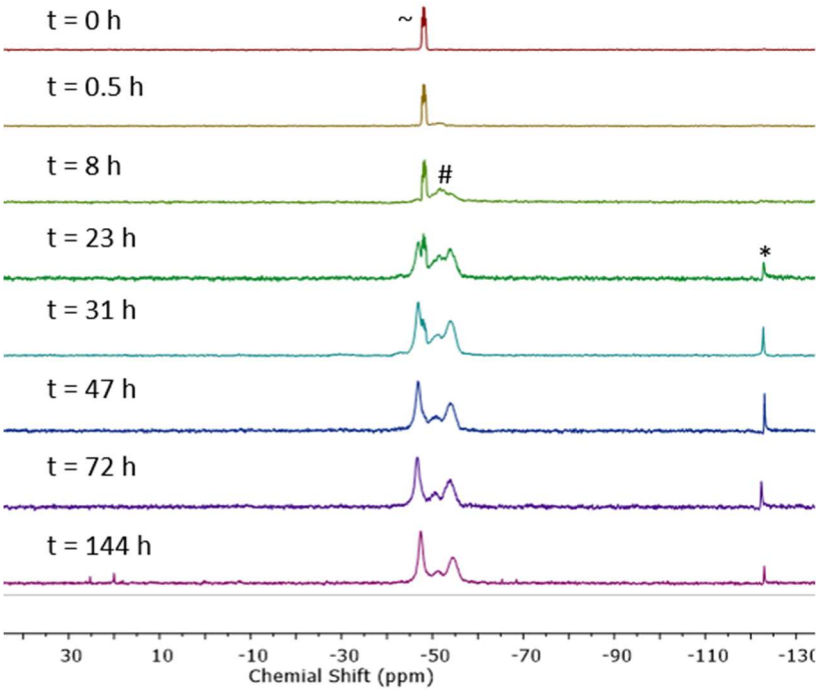

Figure S3.36 $^{31}P\{^{1}H\}$ NMR (122 MHz, 298 K, $CDCl_3$) over time of reaction mixture for polymerisation of $PhPH_2{\cdot}BH_3$ using $Ni(COD)_2$ ($^{\sim}PhPH_2{\cdot}BH_3$, $^{\#}$oligomeric material, $^{*}PPhH_2$).

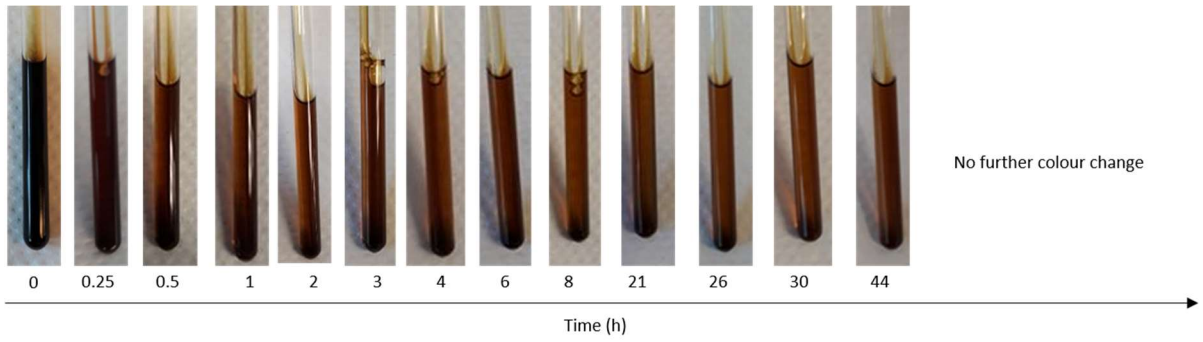

Figure S3.37 Colour over time of reaction mixture for polymerisation of $PhPH_2{\cdot}BH_3$ using $Ni(COD)_2$.

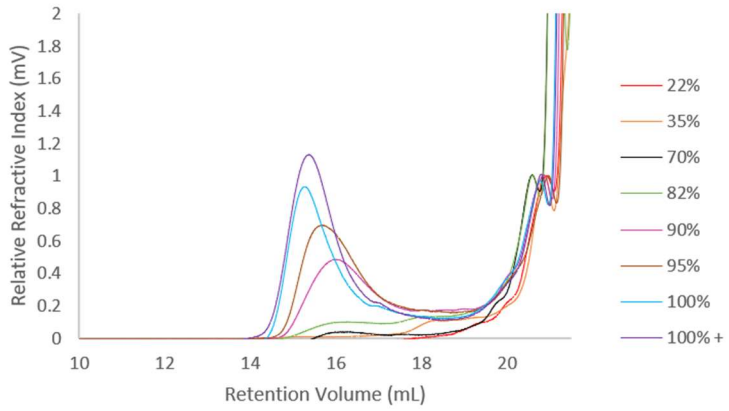

Conversion (%)	M_n	M_w	PDI
22	-	-	-
35	-	-	-
70	25,100	31,000	1.23
82	28,700	35,900	1.25
90	29,500	39,600	1.34
95	30,000	46,800	1.56
100	31,000	52,700	1.70
100+	30,800	54,800	1.78

Figure S3.38 GPC chromatograms of the reaction mixture for polymerisation of $PhPH_2{\cdot}BH_3$ using $Ni(COD)_2$ over time. 2 mg mL^{-1} in THF with 0.1 w/w% nBu$_4$NBr in the THF eluent.

3.5.8 Addition of more monomer after 100% conversion

$PhPH_2{\cdot}BH_3$ (50 mg, 0.40 mmol) and $Ni(COD)_2$ (1mg, 0.004 mmol) were dissolved in THF (400 µL) in a J. Young NMR tube before heating to 70 °C for 72 h. Half of the reaction mixture was precipitated into cold (-40 °C) hexanes (20 mL) and after centrifuging for 5 min at 4,000 RPM the supernatant was decanted and the precipitate dried *in vacuo* for 48 h and isolated as a pale yellow solid.

To the other half additional $PhPH_2{\cdot}BH_3$ (25 mg, 0.20 mmol) was added and the reaction heated to 70 °C for a further 72 h before precipitation into cold (-40 °C) hexanes (20 mL). The solution was centrifuged for 5 min at 4,000 RPM, the supernatant decanted, and the precipitate dried *in vacuo* for 48 h to give the isolated product as a pale yellow solid. GPC analysis was obtained on both precipitated samples.

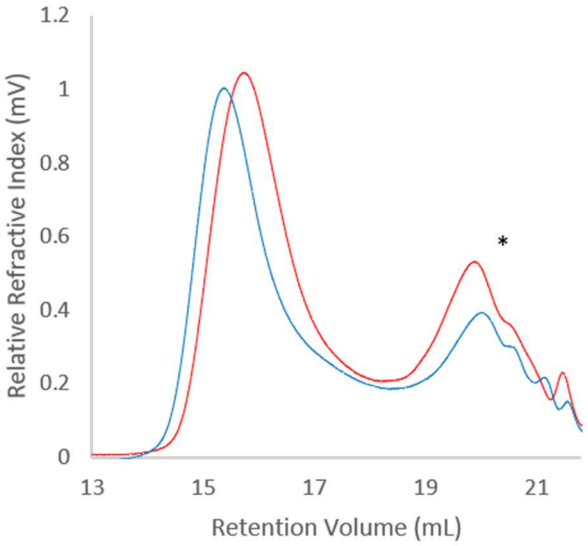

	M_n	M_w	PDI
First monomer	29,000	46,700	1.61
Additional monomer	30,000	55,900	1.86

First monomer

Additional monomer

Figure S3.39 GPC chromatograms of $[PhHP–BH_2]_n$ before and after addition of extra $PhPH_2{\cdot}BH_3$ after 100% conversion. 2 mg mL^{-1} in THF with 0.1 w/w% nBu$_4$NBr in the THF eluent (*below calibration region).

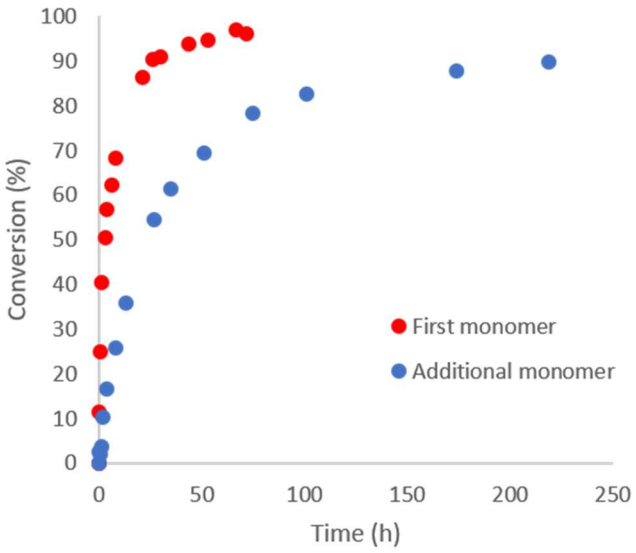

Figure S3.40 Plot of conversion vs time for first and second equiv. of $PhPH_2{\cdot}BH_3$. Conversion determined using relative integrals of ^{11}B NMR spectra.

3.5.9 Reaction of oligomeric material with $Ni(COD)_2$

$PhPH_2{\cdot}BH_3$ (125 mg, 1.01 mmol) and $Ni(COD)_2$ (7 mg, 0.02 mmol) were dissolved in THF (2 mL) in a J. Young Schlenk before heating to 70 °C for 72 h. The reaction mixture was filtered through a plug of silica prior to precipitation into cold (-40 °C) hexanes (100 mL). After centrifuging for 5 min at 4,000 RPM the supernatant was decanted and the solvent removed. The supernatant was dried *in vacuo* to leave a pale yellow oily solid. GPC analysis showed no high molar mass material.

Isolated oligomeric material (50 mg, 0.04 mmol) and $Ni(COD)_2$ (1 mg, 0.004 mmol) were dissolved in THF (400 µL) in a J. Young NMR tube and heated to 70 °C for 72 h. The reaction mixture was filtered through a plug of silica and dried *in vacuo* to leave a pale yellow oily solid. ^{11}B and ^{31}P NMR spectra were identical to the initially isolated oligomeric material and GPC analysis again showed the presence of no high molar mass material.

3.5.10 Homogenous vs heterogenous tests

3.5.10.1 PPh_3 poisoning

$PhPH_2{\cdot}BH_3$ (50 mg, 0.40 mmol) and $Ni(COD)_2$ (1mg, 0.004 mmol) were dissolved in THF (400 µL) in a J. Young NMR tube before heating to 70 °C for 15 min. PPh_3 (0.200 M in THF, 20 µL, 0.004 mmol) was then added and ^{11}B NMR spectroscopy was used to monitor the consumption of $PhPH_2{\cdot}BH_3$ over 57 h.

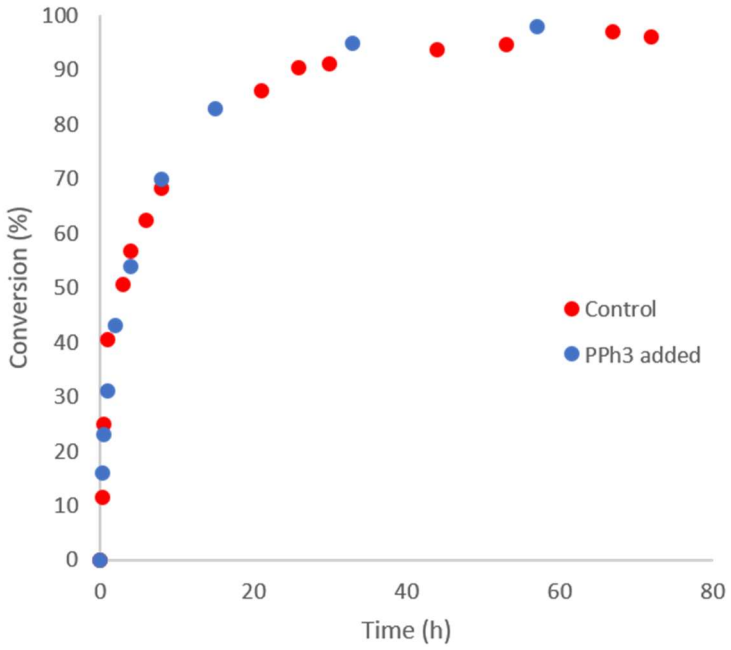

Figure S3.41 Plot of conversion vs time for PPh_3 poisoning experiment and control reaction. Conversion determined using relative integrals of ^{11}B NMR spectra.

3.5.10.2 Hg poisoning

$PhPH_2{\cdot}BH_3$ (50 mg, 0.40 mmol) and $Ni(COD)_2$ (1 mg, 0.004 mmol) were dissolved in THF (400 µL) in a J. Young NMR tube before heating to 70 °C for 15 min. Mercury (50 mg, 0.25 mmol) was then added and ^{11}B NMR spectroscopy was used to monitor the consumption of $PhPH_2{\cdot}BH_3$ over 31 h.

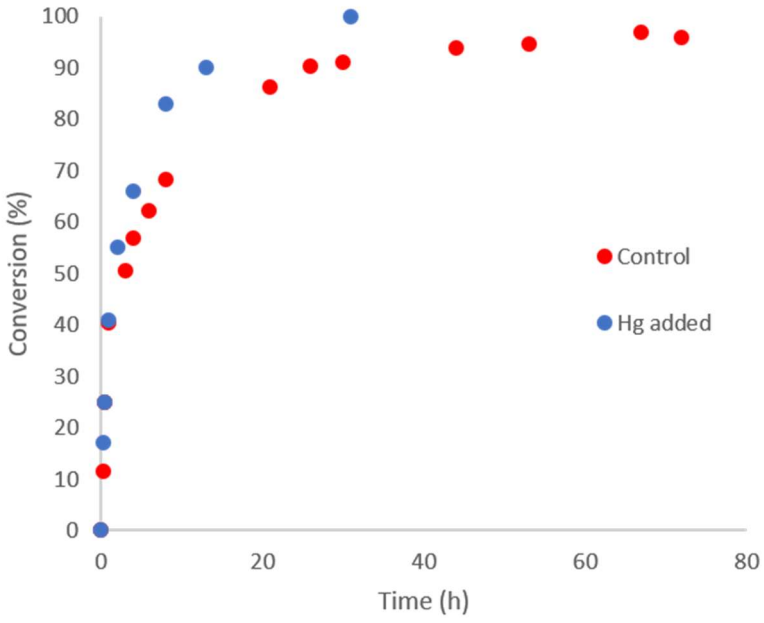

Figure S3.42 Plot of conversion vs time for Hg poisoning experiment and control reaction. Conversion determined using relative integrals of ^{11}B NMR spectra.

3.5.10.3 Filtration

Two sets of $PhPH_2{\cdot}BH_3$ (50 mg, 0.40 mmol) and $Ni(COD)_2$ (1 mg, 0.004 mmol) were dissolved in THF (400 µL) in separate J. Young NMR tubes. One was filtered through a 200 nm PTFE membrane filter prior to heating and the other was filtered after heating to 70 °C for 15 min. ^{11}B NMR spectroscopy was used to monitor the consumption of $PhPH_2{\cdot}BH_3$ over 57 h.

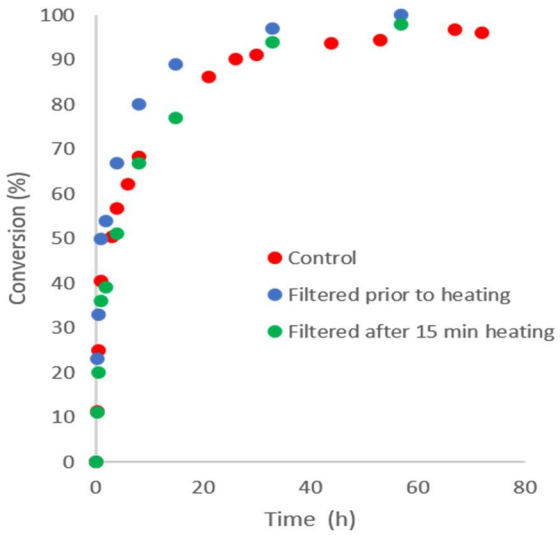

Figure S3.43 Plot of conversion vs time for filtration experiments and a control with no filtration. Conversion determined using relative integrals of ^{11}B NMR spectra.

3.5.10.4 UV-Vis

UV-Vis spectra were taken of a polymerisation reaction prior to work up and of isolated $[PhHP–BH_2]_n$. The crude reaction has two peaks and the peak at ca. 250 nm can be assigned as $[PhHP–BH_2]_n$.

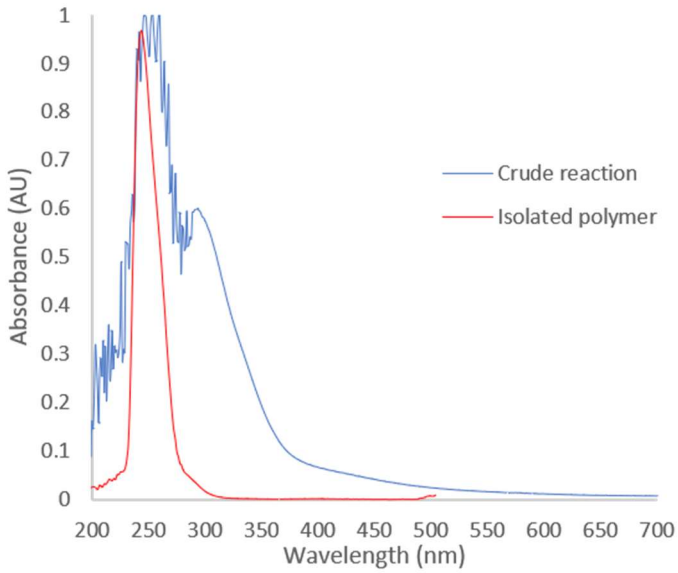

Figure S3.44 UV-Vis spectrum of a catalysis solution (1 mol% cat. 4 M, THF) 100x diluted.

3.5.10.5 Reaction of $PPhH_2{\cdot}BH_3$ with nickel nanoparticles

$PhPH_2{\cdot}BH_3$ (50 mg, 0.40 mmol) and nickel nanoparticles (< 100 nm) (1 mg) were dissolved in THF (400 µL) in a J. Young NMR tube and heated at 70 °C for 72 h. The reaction was filtered through a 200 nm PTFE membrane filter and the ^{11}B NMR spectrum recorded. 30% conversion of $PhPH_2{\cdot}BH_3$ was detected which is directly comparable to the conversion detected when the monomer is heated with no catalyst.

3.5.10.6 Addition of $Me_2NH{\cdot}BH_3$ to the crude reaction of the $Ni(COD)_2$-catalysed dehydropolymerisation of $PhPH_2{\cdot}BH_3$

$PhPH_2{\cdot}BH_3$ (50 mg, 0.40 mmol) and $Ni(COD)_2$ (1 mg, 0.004 mmol) were dissolved in THF (400 µL) in a J. Young NMR tube and heated at 70 °C for 72 h prior to addition of $MeNH_2{\cdot}BH_3$ (24 mg, 0.40 mmol). The reaction was heated to 70 °C for 20 h and no conversion of $MeNH_2{\cdot}BH_3$ was detected using ^{11}B NMR spectroscopy.

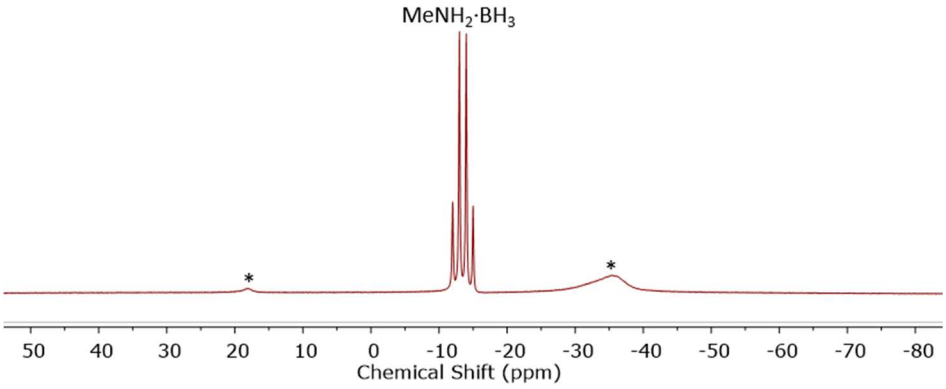

Figure S3.45 ^{11}B NMR spectrum (96 MHz, 298 K, THF) of the reaction mixture for the attempted dehydrogenation of $MeNH_2{\cdot}BH_2$ after 20h at 70 °C (*peaks present from the $[PhHP–BH_2]_n$ reaction mixture prior to addition of $MeNH_2{\cdot}BH_2$).

3.5.11 Substrate scope

3.5.11.1 *n*$HexPH_2{\cdot}BH_3$

n$HexPH_2{\cdot}BH_3$ (53 mg, 0.40 mmol) and $Ni(COD)_2$ (quantities shown in Table S3.2) were dissolved in THF (100 µL) in a J. Young NMR tube and heated using an oil bath to 70 °C (time shown in Table S3.2). The reaction mixtures were precipitated into cold (-40 °C) H_2O:isopropanol (1:1) (20 mL) prior to centrifuging at 4,000 RMP for 5 min to leave an oil layer on top of the solvent. The solvent was decanted and the product isolated as a brown oil which was dried for 48 h *in vacuo* (yields in Table S3.2). ^{11}B and ^{31}P NMR data match that of previously reported $[n\text{HexHP–BH}_2]_n$.[66]

Table S3.2 Conditions for polymerisation of *n*HexPH$_2$·BH$_3$.

Ni(COD)$_2$ (mol%)	Ni(COD)$_2$ (mmol)	Ni(COD)$_2$ (mg)	Conc. (M)	Temp (°C)	Time (days)	Conversion (%)[a]	Yield (%)[b]
1	0.004	1	1	70	14	84	41
2.5	0.010	3	1	70	5	90	18

[a]Conversion based on integration of crude ^{11}B NMR spectra; [b]yield is of material remaining after precipitation into cold H$_2$O:IPA (1:1).

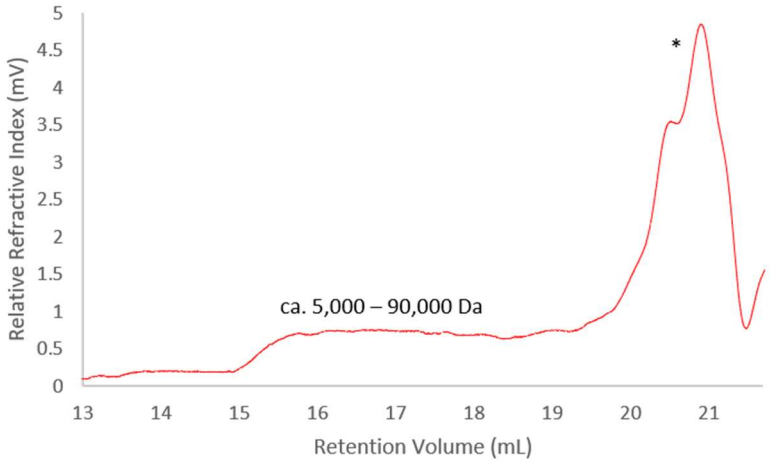

Figure S3.46 GPC chromatogram of isolated [*n*HexHP–BH$_2$]$_n$ from polymerisation of *n*HexPH$_2$·BH$_3$ with 1 mol% Ni(COD)$_2$ (Table S3.2). Not possible to integrate high molar mass material. 2 mg mL^{-1} in THF with 0.1 w/w% *n*Bu$_4$NBr in the THF eluent (*below calibration region).

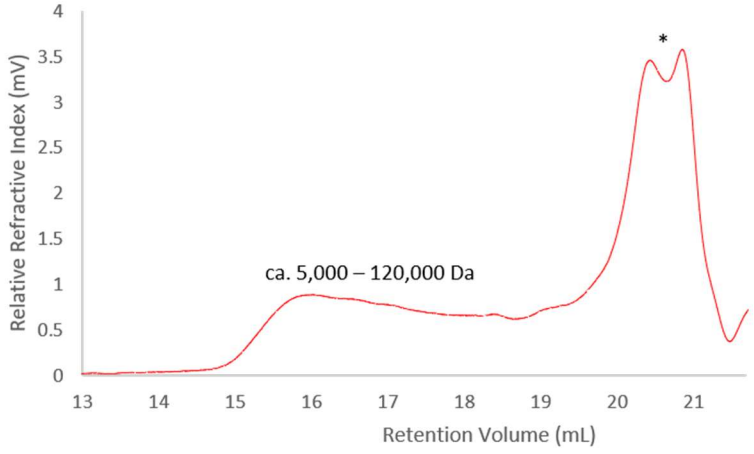

Figure S3.47 GPC chromatogram of isolated [*n*HexHP–BH$_2$]$_n$ from polymerisation of *n*HexPH$_2$·BH$_3$ with 2.5 mol% Ni(COD)$_2$ (Table S3.2). 2 mg mL^{-1} in THF with 0.1 w/w% *n*Bu$_4$NBr in the THF eluent (*below calibration region).

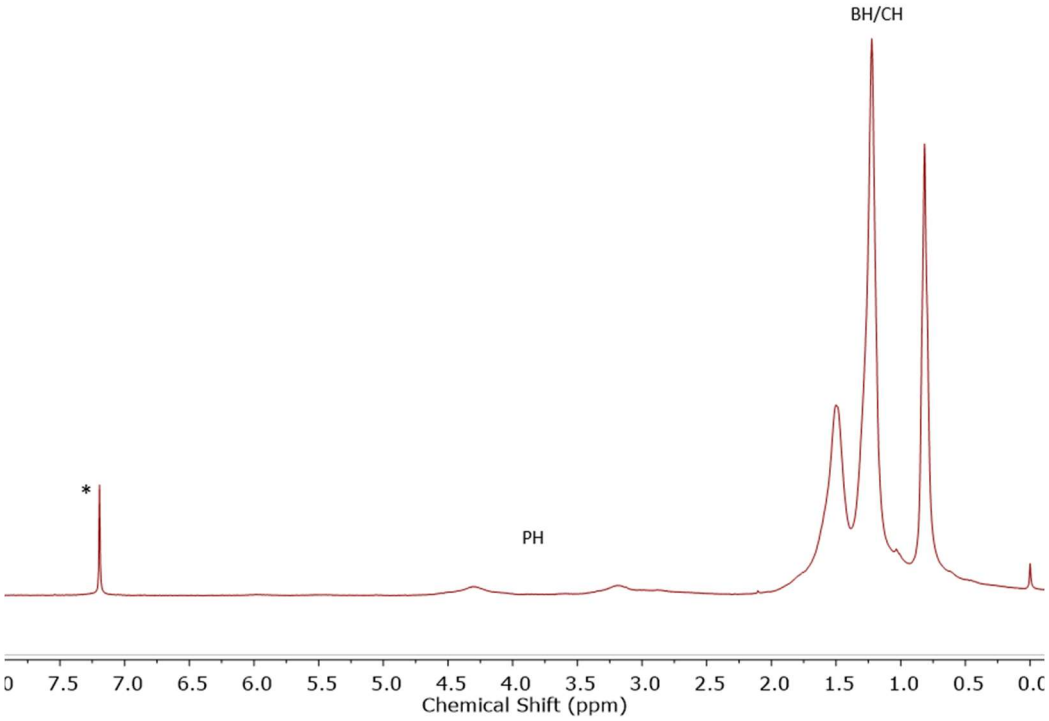

Figure S3.48 ^{1}H NMR spectrum (300 MHz, 298 K, $CDCl_3$) of isolated $[n\text{HexHP–BH}_2]_n$ from polymerisation of $n\text{HexPH}_2\text{BH}_3$ with 2.5 mol% $Ni(COD)_2$ (Table S3.2) (*denotes residual partially protiated $CDCl_3$).

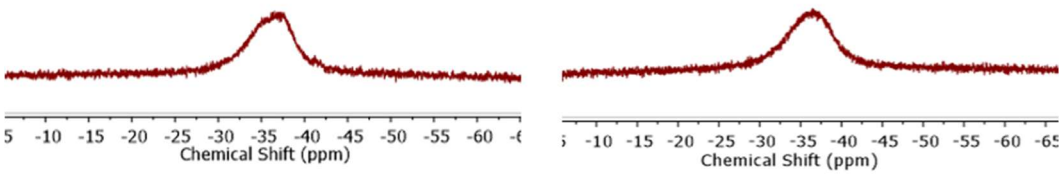

Figure S3.49 $^{11}B\{^{1}H\}$ (left) and ^{11}B (right) NMR spectra (96 MHz, 298 K, $CDCl_3$) of isolated $[n\text{HexHP–BH}_2]_n$ from polymerisation of $n\text{HexPH}_2\text{BH}_3$ with 2.5 mol% $Ni(COD)_2$ (Table S3.2).

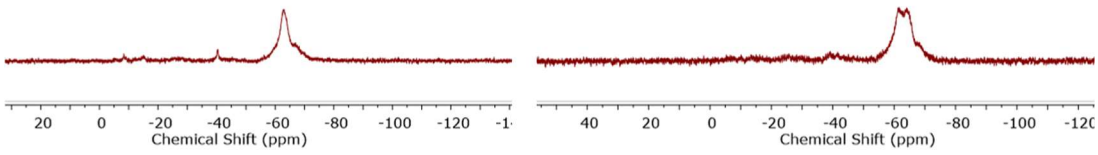

Figure S3.50 $^{31}P\{^{1}H\}$ (left) and ^{31}P (right) NMR spectra (122 MHz, 298 K, $CDCl_3$) of $[n\text{HexHP–BH}_2]_n$ from polymerisation of $n\text{HexPH}_2\text{BH}_3$ with 2.5 mol% $Ni(COD)_2$ (Table S3.2).

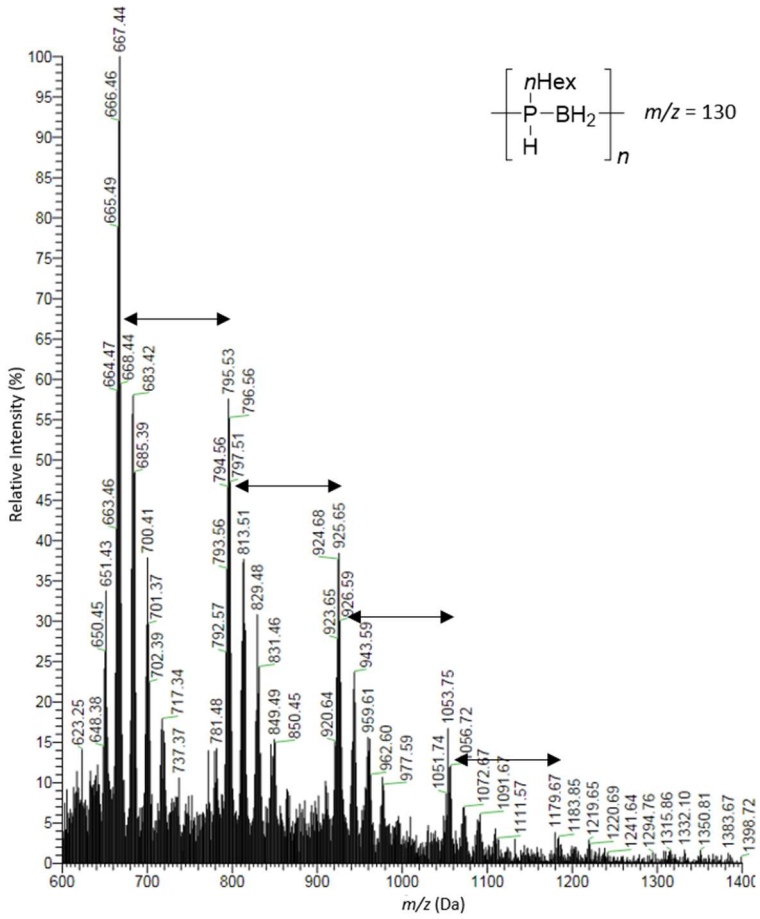

Figure S 3.51 ESI(+)-MS spectrum of isolated [*n*HexPHBH$_2$]$_n$ from polymerisation of *n*HexPH$_2$·BH$_3$ with 2.5 mol% Ni(COD)$_2$.

3.5.11.2 $Ph_2PH{\cdot}BH_3$

$Ph_2HP{\cdot}BH_3$ (73 mg, 0.37 mmol) and Ni(COD)$_2$ (1 mg, 0.004 mmol) were dissolved in THF (100 µL) in a J. Young NMR tube and heated using an oil bath to 70 °C for 5 days. The reaction mixture was precipitated into cold (-40 °C) hexanes (20 mL). The solution was centrifuged for 5 min at 4,000 RPM, the supernatant decanted, and the precipitate dried *in vacuo* for 48 h to give a pale yellow precipitate. ^{11}B and ^{31}P NMR data showed the presence of the same species in both the precipitate and supernatant indicating no separation had occurred.

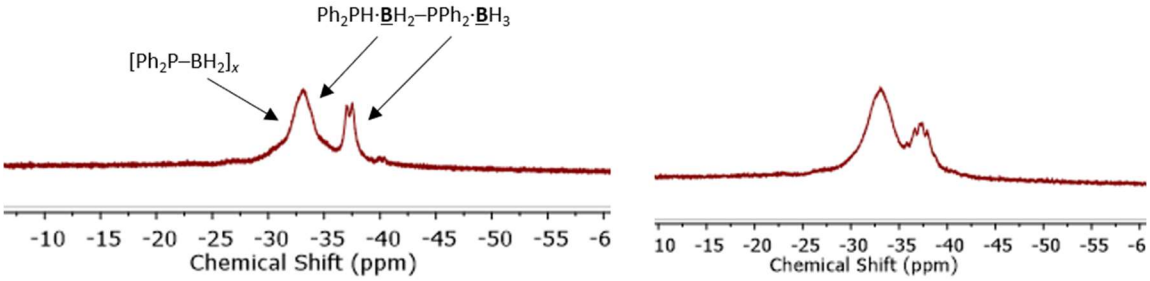

Figure S3.52 $^{11}B\{^1H\}$ (left) and ^{11}B (right) NMR spectra (96 MHz, 298 K, $CDCl_3$) of the precipitated material from the reaction of $Ph_2PH{\cdot}BH_3$ with 1 mol% Ni(COD)$_2$. Species identified based on literature values.[64]

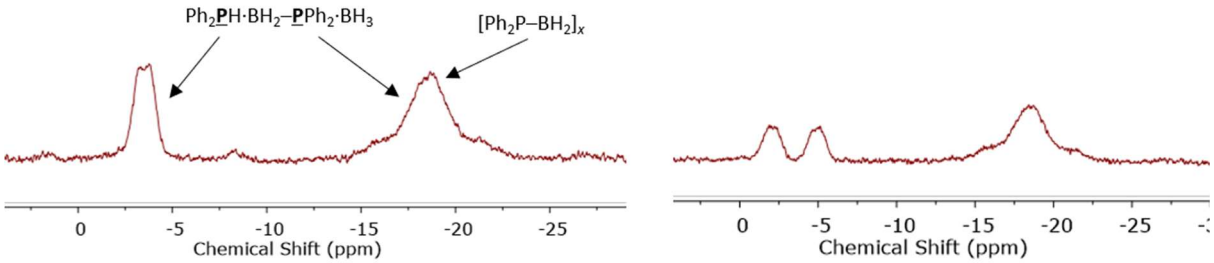

Figure S3.53 $^{31}P\{^{1}H\}$ (left) and ^{31}P (right) NMR spectra (122 MHz, 298 K, $CDCl_3$) of the precipitated material from the reaction of $Ph_2PH{\cdot}BH_3$ with 1 mol% $Ni(COD)_2$. Species identified based on literature values.[64]

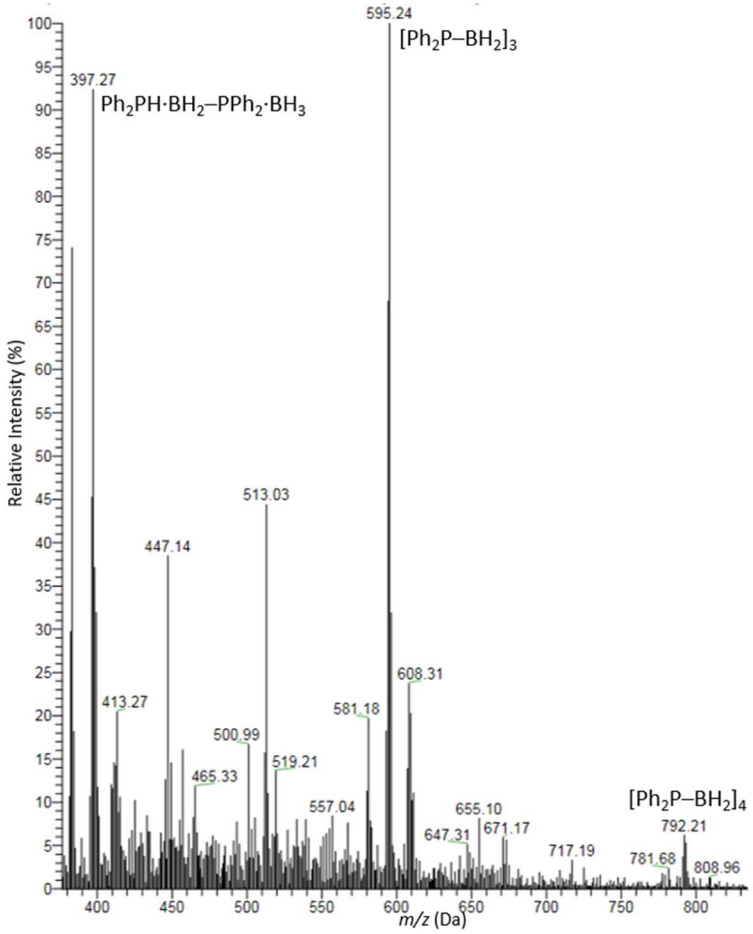

Figure S3.54 ESI(-)-MS spectrum of the precipitated material from the reaction of $Ph_2PH{\cdot}BH_3$ with 1 mol% $Ni(COD)_2$. No evidence of any higher molar mass material.

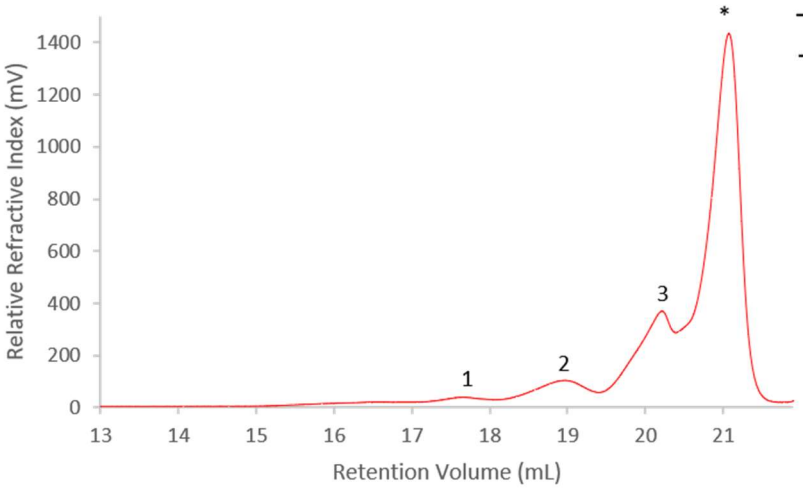

Peak	M_n	M_w	PDI
1	11,300	11,800	1.06
2	4,100	4,500	1.08
3	1,300	1,400	1.07

Figure S3.55 GPC chromatogram of the precipitated material from the reaction of $Ph_2PH{\cdot}BH_3$ with 1 mol% $Ni(COD)_2$. 2 mg mL^{-1} in THF with 0.1 w/w% nBu$_4$NBr in the THF eluent (*below calibration region).

3.5.11.3 PhEtPH·BH$_3$

PhEtPH·BH_3 (53 mg, 0.35 mmol) and $Ni(COD)_2$ (1mg, 0.004 mmol) were dissolved in THF (100 µL) in a J. Young NMR tube and heated using an oil bath to 70 °C for 48 h. The reaction mixture was precipitated into cold (-40 °C) hexanes (20 mL). The solution was centrifuged for 5 min at 4,000 RPM, the supernatant decanted, and the precipitate dried *in vacuo* for 48 h to give a pale yellow precipitate. ^{11}B and ^{31}P NMR data showed the presence of the same species in both the precipitate and supernatant indicating no separation had occurred.

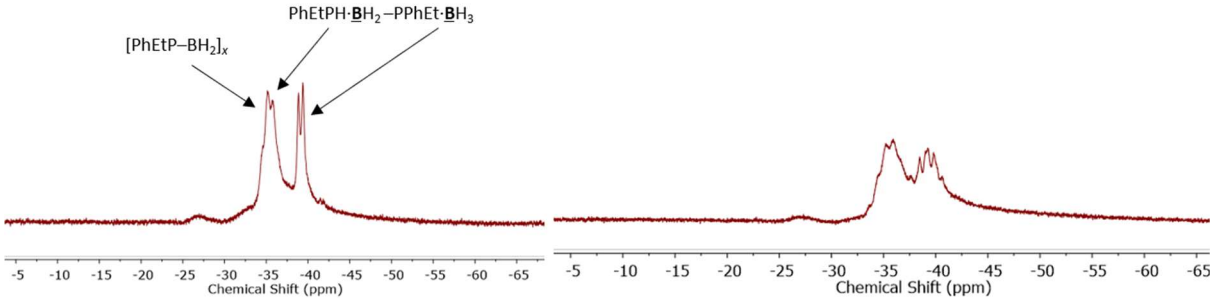

Figure S3.56 $^{11}B\{^1H\}$ (left) and ^{11}B (right) NMR spectra (96 MHz, 298 K, $CDCl_3$) of the precipitated material from the reaction of PhEtPH·BH_3 with 1 mol% $Ni(COD)_2$

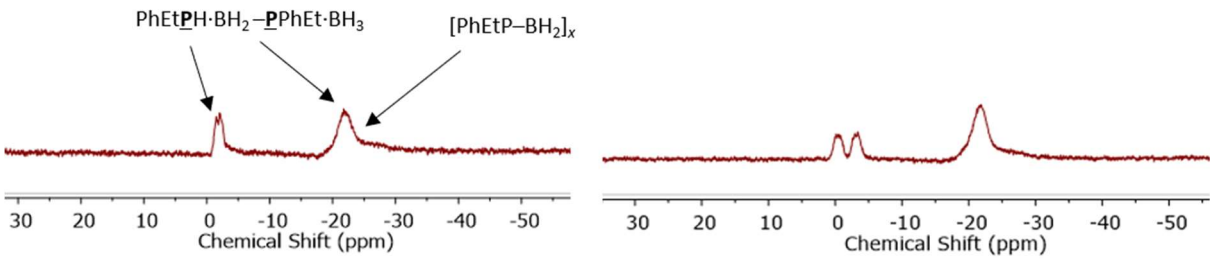

Figure S3.57 $^{31}P\{^1H\}$ (left) and ^{31}P (right) NMR spectra (122 MHz, 298 K, $CDCl_3$) of the precipitated material from the reaction of PhEtPH·BH_3 with 1 mol% $Ni(COD)_2$.

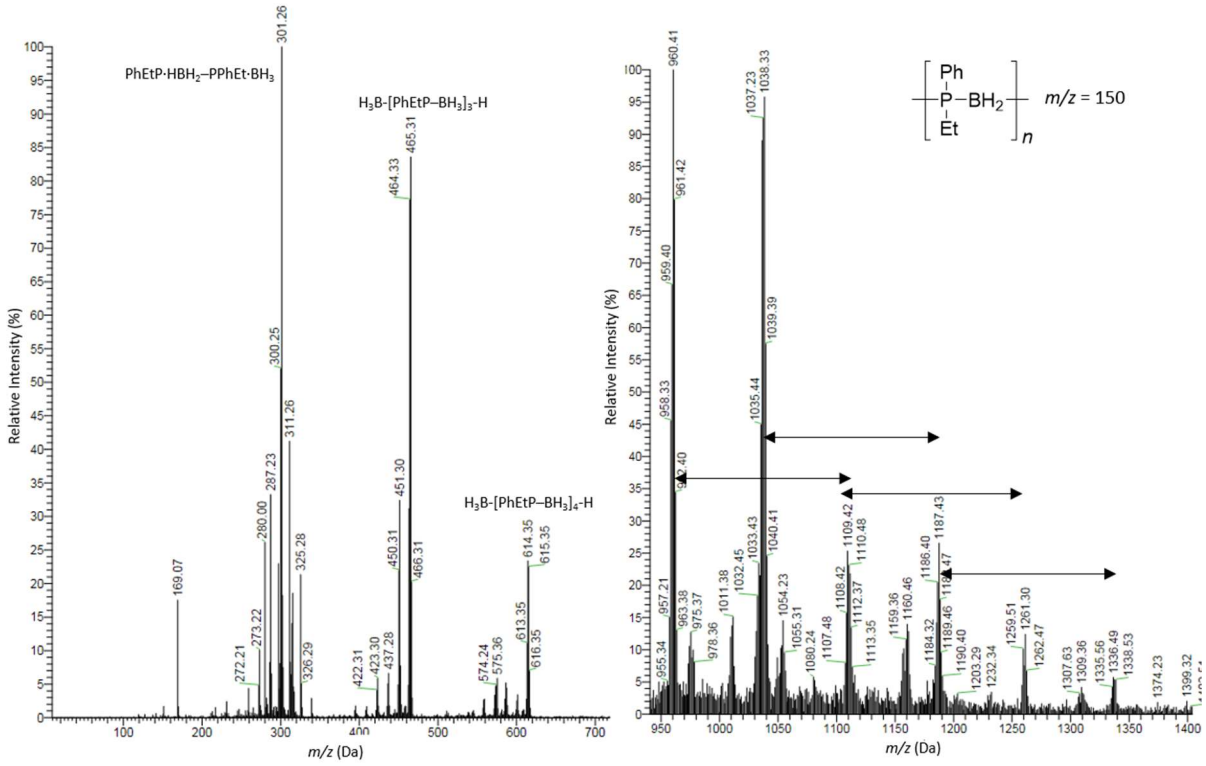

Figure S3.58 ESI(+)-MS (left) and ESI(-)-MS (right) spectra of the precipitated material from the reaction of $PhEtPH{\cdot}BH_3$ with 1 mol% $Ni(COD)_2$.

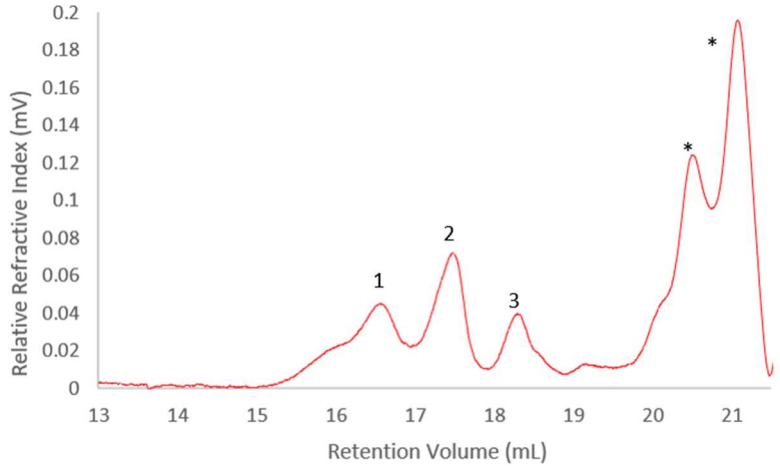

Peak	M_n	M_w	PDI
1	26300	27000	1.03
2	13900	14200	1.02
3	6700	6900	1.03

Figure S3.59 GPC chromatogram of the precipitated material from the reaction of $PhEtPH{\cdot}BH_3$ with 1 mol% $Ni(COD)_2$. 2 mg mL^{-1} in THF with 0.1 w/w% nBu$_4$NBr in the THF eluent (*below calibration region).

3.5.12 Supplementary tables

3.5.12.1 X-ray crystallography

X-ray data for **3.1** was carried out on a Bruker Apex II diffractometer using MoKα radiation (λ = 0.71073) Å at 100 K. The data collections were performed using a CCD area detector from a single crystal mounted on a glass fibre. Intensities were integrated[86] and absorption corrections based on equivalent reflections using SADABS[87] were applied. The structures were

solved by the dual-space algorithm SHELXT[88] and refined against all F^2 in ShelXL[89] using Olex2.[90] All the non-hydrogen atoms were refined anisotropically.

Table S3 Selected crystallographic data for **3.1**.

Compound number	**3.1**
Crystal colour	yellow
Empirical formula	C18H24B3P3
Formula weight	365.71
Temperature/K	100
Crystal system	monoclinic
Space group	P21/c
a/Å	5.4220(3)
b/Å	28.7837(16)
c/Å	12.9156(7)
α°	90
β°	94.110(4)
γ°	90
V/Å^3	2010.49(19)
Z	4
ρ_{calcd}g/cm^3	1.208
μ/mm^{-1}	0.293
F(000)	768
Radiation	MoKα (λ = 0.71073)
2Θ range for data collection/°	1.415 − 28.316
Reflection collected	34326
Independent reflections	34326
Goodness-of-fit on F^2	0.932
Final R indexes [I>=2σ (I)]	R_1 = 0.0492 wR_2 = 0.1109
R1; wR2 [all data]	R_1 = 0.0619 wR_2 = 0.1173
Largest diff. peak/hole / e Å^{-3}	0.387/-0.403

3.6 References

(1) Manners, I. Polymers and the Periodic Table: Recent Developments in Inorganic Polymer Science. *Angew. Chem. Int. Ed.* **1996**, *35*, 1602–1621.

(2) Priegert, A. M.; Rawe, B. W.; Serin, S. C.; Gates, D. P. Polymers and the p-Block Elements. *Chem. Soc. Rev.* **2016**, *45*, 922–953.

(3) Allcock, H. R. The Expanding Field of Polyphosphazene High Polymers. *Dalton Trans.* **2016**, *45*, 1856–1862.

(4) Neilson, R. H.; Wisian-Neilson, P. Poly(Alkyl/Arylphosphazenes) and Their Precursors. *Chem. Rev.* **1988**, *88*, 541–562.

(5) Montague, R. A.; Matyjaszewski, K. Synthesis of Poly[Bis(Trifluoroethoxy)Phosphazene] under Mild Conditions Using a Fluoride Initiator. *J. Am. Chem. Soc.* **1990**, *112*, 6721–6723.

(6) Honeyman, C. H.; Manners, I.; Morrissey, C. T.; Allcock, H. R. Ambient Temperature Synthesis of Poly(Dichlorophosphazene) with Molecular Weight Control. *J. Am. Chem. Soc.* **1995**, *117*, 7035–7036.

(7) De Jaeger, R.; Gleria, M. Poly(Organophosphazene)s and Related Compounds: Synthesis, Properties and Applications. *Prog. Polym. Sci.* **1998**, *23*, 179–276.

(8) Rothemund, S.; Teasdale, I. Preparation of Polyphosphazenes: A Tutorial Review. *Chem. Soc. Rev.* **2016**, *45*, 5200–5215.

(9) Wilfert, S.; Henke, H.; Schoefberger, W.; Brüggemann, O.; Teasdale, I. Chain-End-Functionalized Polyphosphazenes via a One-Pot Phosphine-Mediated Living Polymerization. *Macromol. Rapid Commun.* **2014**, *35*, 1135–1141.

(10) Presa-Soto, D.; Carriedo, G. A.; de la Campa, R.; Presa Soto, A. Formation and Reversible Morphological Transition of Bicontinuous Nanospheres and Toroidal Micelles by the Self-Assembly of a Crystalline-b-Coil Diblock Copolymer. *Angew. Chem. Int. Ed.* **2016**, *55*, 10102–10107.

(11) Allcock, H. R. Polyphosphazene Elastomers, Gels, and Other Soft Materials. *Soft Matter* **2012**, *8*, 7521–7532.

(12) Allcock, H. R.; Nelson, J. M.; Reeves, S. D.; Honeyman, C. H.; Manners, I. Ambient-Temperature Direct Synthesis of Poly(Organophosphazenes) via the “Living” Cationic Polymerization of Organo-Substituted Phosphoranimines. *Macromolecules* **1997**, *30*, 50–56.

(13) Allcock, H. R.; Kugel, R. L. Synthesis of High Polymeric Alkoxy-and Aryloxyphosphonitriles. *J. Am. Chem. Soc.* **1965**, *87*, 4216–4217.

(14) Allcock, H. R.; Kugel, R. L. Phosphonitrilic Compounds. VII. High Molecular Weight Poly(Diaminophosphazenes). *Inorg. Chem.* **1966**, *5*, 1716–1718.

(15) Allcock, H. R. Cross-Linking Reactions for the Conversion of Polyphosphazenes into Useful Materials. *Chem. Mater.* **1994**, *6*, 1476–1491.

(16) Mark, J. E. Some Interesting Things about Polysiloxanes. *Acc. Chem. Res.* **2004**, *37*, 946–953.

(17) Li, Y.; Kawakami, Y. Synthesis and Polymerization of an Optically Active Bifunctional Disiloxane. 1. Preparation of Optically Active and Highly Sstereoregular Poly[{(1S’)-1-(1-Naphthyl)-1-Phenyl-3,3-Dimethyldisiloxane-1,3-Diyl}ethylene] by Polyaddition via Hydrosilylation. *Macromolecules* **1998**, *31*, 5592–5597.

(18) Arson, S. J.; Semlyen, J. A. *Siloxane Polymers*; Englewood Cliffs, N.J. : Prentice Hall, 1993.

(19) West, R. The Polysilane High Polymers. *J. Organomet. Chem.* **1986**, *300*, 327–346.

(20) Miller, R. D.; Michl, J. Polysilane High Polymers. *Chem. Rev.* **1989**, *89*, 1359–1410.

(21) Aitken, C. T.; Harrod, J. F.; Samuel, E. Identification of Some Intermediates in the Titanocene-Catalyzed Dehydrogenative Coupling of Primary Organosilanes. *J. Am. Chem. Soc.* **1986**, *108*, 4059–4066.

(22) Tilley, T. D. The Coordination Polymerization of Silanes to Polysilanes by a "σ-Bond Metathesis" Mechanism. Implications for Linear Chain Growth. *Acc. Chem. Res.* **1993**, *26*, 22–29.

(23) Imori, T.; Lu, V.; Cai, H.; Tilley, T. D. Metal-Catalyzed Dehydropolymerization of Secondary Stannanes to High Molecular Weight Polystannanes. *J. Am. Chem. Soc.* **1995**, *117*, 9931–9940.

(24) Trummer, M.; Choffat, F.; Smith, P.; Caseri, W. Polystannanes: Synthesis, Properties, and Outlook. *Macromol. Rapid Commun.* **2012**, *33*, 448–460.

(25) Harrypersad, S.; Foucher, D. Alternating Polystannanes: Syntheses and Properties. *Chem. Commun.* **2015**, *51*, 7120–7123.

(26) Caseri, W. Polystannanes: Processible Molecular Metals with Defined Chemical Structures. *Chem. Soc. Rev.* **2016**, *45*, 5187–5199.

(27) Imori, T.; Tilley, T. D. High Molecular Mass Polystannanes via Dehydropolymerization of Di(n-Butyl)Stannane. *J. Chem. Soc. Chem. Commun.* **1993**, 1607–1609.

(28) Babcock, J. R.; Sita, J. R. Highly Branched, High Molecular Weight Polystannane from Dibutylstannane via a Novel Dehydropolymerization/Rearrangement Process. *J. Am. Chem. Soc.* **1996**, *118*, 12481–12482.

(29) Staubitz, A.; Soto, A. P.; Manners, I. Iridium-Catalyzed Dehydrocoupling of Primary Amine-Borane Adducts: A Route to High Molecular Weight Polyaminoboranes, Boron-Nitrogen Analogues of Polyolefins. *Angew. Chem. Int. Ed.* **2008**, *47*, 6212–6215.

(30) Dietrich, B. L.; Goldberg, K. I.; Heinekey, D. M.; Autrey, T.; Linehan, J. C. Iridium-Catalyzed Dehydrogenation of Substituted Amine Boranes: Kinetics, Thermodynamics, and Implications for Hydrogen Storage. *Inorg. Chem.* **2008**, *47*, 8583–8585.

(31) Colebatch, A. L.; Weller, A. S. Amine-Borane Dehydropolymerization: Challenges and Opportunities. *Chem. Eur. J.* **2019**, *25*, 1379–1390.

(32) Adams, G. M.; Colebatch, A. L.; Skornia, J. T.; McKay, A. I.; Johnson, H. C.; Lloyd-Jones, G. C.; Macgregor, S. A.; Beattie, N. A.; Weller, A. S. Dehydropolymerization of $H_3B{\cdot}NMeH_2$ To Form Polyaminoboranes Using [Rh(Xantphos-Alkyl)] Catalysts. *J. Am. Chem. Soc.* **2018**, *140*, 1481–1495.

(33) Winner, L.; Ewing, W. C.; Geetharani, K.; Dellermann, T.; Jouppi, B.; Kupfer, T.; Schäfer, M.; Braunschweig, H. Spontaneous Metal-Free Transfer Hydrogenation of Iminoboranes with Ammonia Borane and Amine Boranes. *Angew. Chem. Int. Ed.* **2018**, *57*, 12275–12279.

(34) Adams, G. M.; Ryan, D. E.; Beattie, N. A.; Mckay, A. I.; Lloyd-Jones, G. C.; Weller, A. S. Dehydropolymerization of $H_3B{\cdot}NMeH_2$ Using a $[Rh(DPEphos]^+$ Catalyst: The Promoting Effect of $NMeH_2$. *ACS Catal.* **2019**, *9*, 3657–3666.

(35) De Albuquerque Pinheiro, C. A.; Roiland, C.; Jehan, P.; Alcaraz, G. Solventless and Metal-Free Synthesis of High-Molecular-Mass Polyaminoboranes from Diisopropylaminoborane and Primary Amines. *Angew. Chem. Int. Ed.* **2018**, *57*, 1519–1522.

(36) Trose, M.; Reiß, M.; Reiß, F.; Anke, F.; Spannenberg, A.; Boye, S.; Lederer, A.; Arndt, P.; Beweries, T. Dehydropolymerisation of Methylamine Borane Using a Dinuclear 1,3-Allenediyl Bridged Zirconocene Complex. *Dalton Trans.* **2018**, *47*, 12858–12862.

(37) Jurca, T.; Dellermann, T.; Stubbs, N. E.; Resendiz-Lara, D. A.; Whittell, G. R.; Manners, I. Step-Growth Titanium-Catalysed Dehydropolymerisation of Amine-Boranes. *Chem. Sci.* **2018**, *9*, 3360–3366.

(38) Lichtenberg, C.; Adelhardt, M.; Gianetti, T. L.; Meyer, K.; De Bruin, B.; Grützmacher, H. Low-Valent Iron Mono-Diazadiene Compounds: Electronic Structure and Catalytic Application. *ACS Catal.* **2015**, *5*, 6230–6240.

(39) Staubitz, A.; Sloan, M. E.; Robertson, A. P. M.; Friedrich, A.; Schneider, S.; Gates, P. J.; Manners, I.; Schmedt auf der Günne, J. Catalytic Dehydrocoupling/Dehydrogenation of N-Methylamine-Borane and Ammonia-Borane: Synthesis and Characterization of High Molecular Weight Polyaminoboranes. *J. Am. Chem. Soc.* **2010**, *132*, 13332–13345.

(40) Vance, J. R.; Robertson, A. P. M.; Lee, K.; Manners, I. Photoactivated, Iron-Catalyzed Dehydrocoupling of Amine-Borane Adducts: Formation of Boron-Nitrogen Oligomers and Polymers. *Chem. Eur. J.* **2011**, *17*, 4099–4103.

(41) Robertson, A. P. M.; Suter, R.; Chabanne, L.; Whittell, G. R.; Manners, I. Heterogeneous Dehydrocoupling of Amine-Borane Adducts by Skeletal Nickel Catalysts. *Inorg. Chem.* **2011**, *50*, 12680–12691.

(42) Dallanegra, R.; Robertson, A. P. M. M.; Chaplin, A. B.; Manners, I.; Weller, A. S. Tuning the $[L_2Rh\cdots H_3B\cdot NR_3]^+$ interaction Using Phosphine Bite Angle. Demonstration by the Catalytic Formation of Polyaminoboranes. *Chem. Commun.* **2011**, *47*, 3763–3765.

(43) Baker, R. T.; Gordon, J. C.; Hamilton, C. W.; Henson, N. J.; Lin, P. H.; Maguire, S.; Murugesu, M.; Scott, B. L.; Smythe, N. C. Iron Complex-Catalyzed Ammonia-Borane Dehydrogenation. A Potential Route toward B-N-Containing Polymer Motifs Using Earth-Abundant Metal Catalysts. *J. Am. Chem. Soc.* **2012**, *134*, 5598–5609.

(44) Marziale, A. N.; Friedrich, A.; Klopsch, I.; Drees, M.; Celinski, V. R.; Schmedt auf der Günne, J.; Schneider, S. The Mechanism of Borane-Amine Dehydrocoupling with Bifunctional Ruthenium Catalysts. *J. Am. Chem. Soc.* **2013**, *135*, 13342–13355.

(45) Johnson, H. C.; Leitao, E. M.; Whittell, G. R.; Manners, I.; Lloyd-Jones, G. C.; Weller, A. S. Mechanistic Studies of the Dehydrocoupling and Dehydropolymerization of Amine-Boranes Using a $[Rh(Xantphos)]^+$ Catalyst. *J. Am. Chem. Soc.* **2014**, *136*, 9078–9093.

(46) Rossin, A.; Peruzzini, M. Ammonia-Borane and Amine-Borane Dehydrogenation Mediated by Complex Metal Hydrides. *Chem. Rev.* **2016**, *116*, 8848–8872.

(47) Han, D.; Anke, F.; Trose, M.; Beweries, T. Recent Advances in Transition Metal Catalysed Dehydropolymerisation of Amine Boranes and Phosphine Boranes. *Coord. Chem. Rev.* **2019**, *380*, 260–286.

(48) Bosdet, M. J. D.; Piers, W. E. B-N as a C-C Substitute in Aromatic Systems. *Can. J. Chem.* **2009**, 8–29.

(49) Staubitz, A.; Robertson, A. P. M.; Sloan, M. E.; Manners, I. Amine-and Phosphine-Borane Adducts: New Interest in Old Molecules. *Chem. Rev.* **2010**, *110*, 4023–4078.

(50) Liu, Z.; Marder, T. B. B-N versus C-C: How Similar Are They? *Angew. Chem. Int. Ed.* **2008**, *47*, 242–244.

(51) Dorn, H.; Rodezno, J. M.; Brunnhöfer, B.; Rivard, E.; Massey, J. A.; Manners, I. Synthesis, Characterization, and Properties of the Polyphosphinoboranes $[RPH\text{-}BH_2]_n$ (R = Ph, iBu, p-$nBuC_6H_4$, p-DodecylC_6H_4): Inorganic Polymers with a Phosphorus-Boron Backbone. *Macromolecules* **2003**, *36*, 291–297.

(52) Clark, T. J.; Rodezno, J. M. J. M.; Clendenning, S. B.; Aouba, S.; Brodersen, P. M.; Lough, A. J.; Ruda, H. E.; Manners, I. Rhodium-Catalyzed Dehydrocoupling of Fluorinated Phosphine–Borane Adducts: Synthesis, Characterization, and Properties of Cyclic and Polymeric Phosphinoboranes with Electron-Withdrawing Substituents at Phosphorus. *Chem. Eur. J.* **2005**, *5*, 4526–4534.

(53) Schäfer, A.; Jurca, T.; Turner, J.; Vance, J. R.; Lee, K.; Du, V. A.; Haddow, M. F.; Whittell, G. R.; Manners, I. Iron-Catalyzed Dehydropolymerization: A Convenient Route to Poly(Phosphinoboranes) with Molecular-Weight Control. *Angew. Chem. Int. Ed.* **2015**, *54*, 4836–4841.

(54) Jäkle, F. Advances in the Synthesis of Organoborane Polymers for Optical, Electronic, and Sensory Applications. *Chem. Rev.* **2010**, *110*, 3985–4022.

(55) Vidal, F.; Jäkle, F. Functional Polymeric Materials Based on Main-Group Elements. *Angew. Chem. Int. Ed.* **2019**, *58*, 5846–5870.

(56) Parshall, G. W. *The Chemistry of Boron and Its Compounds*; Wiley: New York, 1967.

(57) Mayer-Gall, T.; Knittel, D.; Gutmann, J. S.; Opwis, K. Permanent Flame Retardant Finishing of Textiles by Allyl-Functionalized Polyphosphazenes. *ACS Appl. Mater, Interfaces* **2015**, *7*, 9349–9363.

(58) Priegert, A. M.; Siu, P. W.; Hu, T. Q.; Gates, D. P. Flammability Properties of Paper Coated with Poly(Methylenephosphine), an Organophosphorus Polymer. *Fire Mater.* **2015**, *39*, 647–657.

(59) Joseph, P.; Tretsiakova-Mcnally, S. Reactive Modifications of Some Chain- and Step-Growth Polymers with Phosphorus-Containing Compounds: Effects on Flame Retardance—a Review. *Polym. Adv. Technol.* **2011**, *22*, 395–406.

(60) Burg, A. B.; Wagner, R. I. Chemistry of P-B Bonding: The Phosphinoborines and Their Polymers. *J. Am. Chem. Soc.* **1953**, *75*, 3872–3877.

(61) Burg, A. Phosphinoborine Polymer Rings and Chains from Tetramethylbiphosphine. *J. Inorg. Nucl. Chem.* **1959**, *2*, 258.

(62) Wagner, R. I.; Caserio, F. F. Linear Phosphinoborane Polymers. *J. Inorg. Nucl. Chem.* **1959**, *11*, 259.

(63) Dorn, H.; Singh, R. A.; Massey, J. A.; Lough, A. J.; Manners, I. Rhodium-Catalyzed Formation of Phosphorus-Boron Bonds: Synthesis of the First High Molecular Weight Poly(Phosphinoborane). *Angew. Chem. Int. Ed.* **1999**, *38*, 3321–3323.

(64) Dorn, H.; Singh, R. A.; Massey, J. A.; Nelson, J. M.; Jaska, C. A.; Lough, A. J.; Manners, I. Transition Metal-Catalyzed Formation of Phosphorus-Boron Bonds: A New Route to Phosphinoborane Rings, Chains, and Macromolecules. *J. Am. Chem. Soc.* **2000**, *122*, 6669–6678.

(65) Pandey, S.; Lönnecke, P.; Hey-Hawkins, E. Phosphorus-Boron-Based Polymers Obtained by Dehydrocoupling of Ferrocenylphosphine-Borane Adducts. *Eur. J. Inorg. Chem.* **2014**, 2456–2465.

(66) Cavaye, H.; Clegg, F.; Gould, P. J.; Ladyman, M. K.; Temple, T.; Dossi, E. Primary Alkylphosphine-Borane Polymers: Synthesis, Low Glass Transition Temperature, and a Predictive Capability Thereof. *Macromolecules* **2017**, *50*, 9239–9248.

(67) Turner, J. R.; Resendiz-lara, D. A.; Jurca, T.; Schäfer, A.; Vance, J. R.; Beckett, L.; Whittell, G. R.; Musgrave, R. A.; Sparkes, H. A.; Manners, I. Synthesis, Characterization, and Properties of Poly(Aryl)Phosphinoboranes Formed via Iron-Catalyzed Dehydropolymerization. *Macromol. Chem. Phys.* **2017**, *218*, 1700120.

(68) Arz, M. I.; Knights, A. W.; Manners, I. Synthesis and Post-Polymerization Functionalization of Halogen-Substituted Polyphosphinoboranes to Access Alkyne-Functionalized Derivatives. *Macromol. Rapid Commun.* **2019**, 1900468.

(69) Resendiz-Lara, D. A.; Annibale, V. T.; Knights, A. W.; Chitnis, S. S.; Manners, I. High Molar Mass Poly(Alkylphosphinoboranes) via Iron-Catalyzed Dehydropolymerization. *Manuscript in Preparation*.

(70) Paul, U. S. D.; Braunschweig, H.; Radius, U. Iridium-Catalysed Dehydrocoupling of Aryl Phosphine-Borane Adducts: Synthesis and Characterisation of High Molecular Weight Poly(Phosphinoboranes). *Chem. Commun.* **2016**, *52*, 8573–8576.

(71) Marquardt, C.; Jurca, T.; Schwan, K. C.; Stauber, A.; Virovets, A. V.; Whittell, G. R.; Manners, I.; Scheer, M. Metal-Free Addition/Head-to-Tail Polymerization of Transient Phosphinoboranes, RPH-BH_2: A Route to Poly(Alkylphosphinoboranes). *Angew. Chem. Int. Ed.* **2015**, *54*, 13782–13786.

(72) Stauber, A.; Jurca, T.; Marquardt, C.; Fleischmann, M.; Seidl, M.; Whittell, G. R.; Manners, I.; Scheer, M. A Convenient Route to Monoalkyl-Substituted Phosphanylboranes (HRP-BH_2-NMe_3): Prospective Precursors to Poly[(Alkylphosphino)-boranes]. *Eur. J. Inorg. Chem.* **2016**, 2684–2687.

(73) Oldroyd, N. L.; Manners, I.; Chitnis, S. S.; Annibale, V. T.; Arz, M. I.; Sparkes, H. A. Metal-Free Dehydropolymerisation of Phosphine- Boranes Using Cyclic (Alkyl)(Amino)Carbenes as Hydrogen Acceptors. *Nat. Commun.* **2019**, *10*, 1370–1379.

(74) Ananikov, V. P. Nickel: The " Spirited Horse " of Transition Metal Catalysis. **2015**, *5*, 1964–1971.

(75) Tasker, S. Z.; Standley, E. A.; Jamison, T. F. Recent Advances in Homogeneous Nickel Catalysis. *Nature* **2014**, *509*, 299–309.

(76) Bullen, G. J.; Mallinson, P. R. Molecular Structure of Cycloborataphosphonianes. Part 11. Crystal Structure of 1,1,3,3,5,5-Hexaphenylcyclotriborataphosphoniane $[(Ph_2P)BH_2]_3$. *J. C. S. Dalt.* **1973**, 1295–1300.

(77) Sonnenberg, J. F.; Morris, R. H. Distinguishing Homogeneous from Nanoparticle Asymmetric Iron Catalysis. *Catal. Sci. Technol.* **2014**, *4*, 3426–3438.

(78) Jaska, C. A.; Manners, I. Heterogeneous or Homogeneous Catalysis? Mechanistic Studies of the Rhodium-Catalyzed Dehydrocoupling of Amine-Borane and Phosphine-Borane Adducts. *J. Am. Chem. Soc.* **2004**, *126*, 9776–9785.

(79) Artero, V.; Fontecave, M. Solar Fuels Generation and Molecular Systems: Is It Homogeneous or Heterogeneous Catalysis? *Chem. Soc. Rev.* **2013**, *42*, 2338–2356.

(80) Johnson, N. A.; Southerland, M. R.; Youngs, W. J. Recent Developments in the Medicinal Applications of Silver-NHC Complexes and Imidazolium Salts. *Molecules* **2017**, *22*, 1–20.

(81) Demir, H.; Duman, S. Monodisperse Nickel Nanoparticles in the Solvent-Free Dehydrogenation of Dimethylamine Borane. *Int. J. Hydrogen Energy* **2015**, *40*, 10063–10071.

(82) Pangborn, A. B.; Giardello, M. A.; Grubbs, R. H.; Rosen, R. K.; Timmers, F. J. Safe and Convenient Procedure for Solvent Purification. *Organometallics* **1996**, *15*, 1518–1520.

(83) Hurtado, M.; Yanez, M.; Herrero, R.; Guerrero, A.; Juan, Z. D.; Jose-Luis, M. A.; Khater, B.; Guillemin, J. C. The Ever-Surprising Chemistry of Boron: Enhanced Acidity of Phosphine-Boranes. *Chem. Eur. J.* **2009**, *15*, 4622–4629.

(84) Nguyen, D. H.; Lauréano, H.; Jugé, S.; Kalck, P.; Daran, J. C.; Coppel, Y.; Urrutigoity, M.; Gouygou, M. First Dibenzophospholyl(Diphenylphosphino)Methane -Borane Hybrid P-(N_2-BH_3) Ligand: Synthesis and Rhodium(I) Complex. *Organometallics* **2009**, *28*, 6288–6292.

(85) Lebel, H.; Morin, S.; Paquet, V. Alkylation of Phosphine Boranes by Phase-Transfer Catalysis. *Org. Lett.* **2003**, *5*, 2347–2349.

(86) Bruker, SAINT+ v8.38A Integration Engine, Data Reduction Software, Bruker Analytical X-Ray Instruments Inc., Madison, WI, USA, 2015.

(87) Bruker, SADABS 2014/5, Bruker AXS Area Detector Scaling and Absorption Correction, Bruker Analytical X-Ray Instruments Inc., Madison, Wisconsin, USA, 2014/5.

(88) Sheldrick, G. M. SHELXT - Integrated Space-Group and Crystal-Structure Determination. *Acta Crystallogr. Sect. A Found. Crystallogr.* **2015**, *71*, 3–8.

(89) Sheldrick, G. M. Crystal Structure Refinement with SHELXL. *Acta Crystallogr. Sect. C Struct. Chem.* **2015**, *71*, 3–8.

(90) Dolomanov, O. V.; Bourhis, L. J.; Gildea, R. J.; Howard, J. A. K.; Puschmann, H. OLEX2: A Complete Structure Solution, Refinement and Analysis Program. *J. Appl. Crystallogr.* **2009**, *42*, 339–341.

Chapter 4
Stoichiometric and catalytic carbene-mediated depolymerisation of poly(N-methylaminoborane) $[MeHN–BH_2]_n$

4.1 Abstract

The reactions of the N-heterocyclic carbenes (NHCs) IDipp and I*t*Bu and the cyclic(alkyl)amino carbene (CAAC) CAAC^{Me} with a high molar mass polyaminoborane $[MeHN–BH_2]_n$ were investigated. Stoichiometric quantities of each carbene were found to cause rapid and complete depolymerisation with the major B–N containing product identified as the NHC-aminoborane adduct, IDipp–BH_2NMeH (**4.1**), cyclic borazane $[MeHN–BH_2]_3$, or borazine $[MeNBH]_3$ with IDipp, I*t*Bu, and CAAC^{Me}, respectively. With substoichiometric quantities of IDipp and I*t*Bu (down to 10 mol%) complete loss of high molar mass material was also detected indicating that the depolymerisation was catalytic. The main products of the reaction with substoichiometric IDipp were IDipp–BH_2NMeH (**4.1**) and $[MeHN–BH_2]_3$, and with substoichiometric I*t*Bu, $[MeHN–BH_2]_3$ and $[MeNBH]_3$. The product ratios were dependent on the quantity of NHC used. In contrast, under analogous substoichiometric conditions with CAAC^{Me}, high molar mass material was found to remain alongside the formation of $[MeNBH]_3$. Further reactivity studies were performed with the cyclic borazane $[MeHN–BH_2]_3$ and the adduct $MeNH_2{\cdot}BH_3$ to provide additional insight into the depolymerisation pathways. IDipp showed no reactivity towards $[MeHN–BH_2]_3$, whereas with 3 equiv. of I*t*Bu and CAAC^{Me}, the dehydrogenation product, $[MeNBH]_3$, was formed. With $MeNH_2{\cdot}BH_3$ 2 equiv. of carbene were used as the first acts to remove dihydrogen. The major species formed with the second equiv. of IDipp, I*t*Bu and CAAC^{Me} were IDipp–BH_2NMeH (**4.1**), $[MeNBH]_3$, and (CAAC^{Me}H)HB=NMeH (**4.2**) respectively. The latter species appears to arise from the insertion of the carbene into the B–H bond of $MeHN{=}BH_2$. The double E–H (E = B, N) bond activation product, (CAAC^{Me}H)HB=NMe(CAAC^{Me})H (**4.3**), was isolated from the reaction between 3 equiv. of CAAC^{Me} and $MeNH_2{\cdot}BH_3$. Possible mechanisms for the carbene-mediated depolymerisations are considered.

4.2 Introduction

Polyaminoboranes and polyphosphinoboranes are main group polymers with backbones consisting of alternating group 13 (B) and group 15 (N or P) elements.[1,2] The first high molar mass polyphosphinoboranes[3] and polyaminoboranes[4] were synthesised in 1999 and 2008, respectively, using transition-metal catalysts. Since these initial reports many further metal-catalysed, and more recently, metal-free routes for the polymerisations have been reported.[5–13]

Although polyaminoboranes and polyphosphinoboranes are formally isoelectronic with polyolefins the incorporation of main group elements into the polymer backbone evokes a variety of potential applications, including as hydrogen storage materials,[14] ceramic precursors,[15–17] piezoelectric materials,[18] flame retardants,[19] and electron beam resists in lithography.[20]

Whilst a significant amount of work has been carried out concerning the synthesis of polyaminoboranes and polyphosphinoboranes, there have been few reports on the reverse, depolymerisation, process. A consideration of the degradation of polymeric materials is of growing importance.[21,22] This is a particularly prominent issue with polyolefins, which, although being low-cost and exhibit long term durability the lack of facile degradation pathways leads to the generation of millions of tonnes of plastic waste.[23] In 2013 we published a preliminary study of the stability of poly(N-methylaminoborane), $[MeHN–BH_2]_n$, towards Lewis bases.[24] The addition of tri-cyclohexylphosphine (PCy_3) in THF resulted in no significant depolymerisation at temperatures up to 50 °C, whereas tri-*n*-butylphosphine $P(nBu)_3$ and 4-dimethylaminopyridine (DMAP) led to partial and almost complete depolymerisation, respectively, at 20 °C. These bases , however, did not form detectable adducts with the resulting B–N fragments. Further studies revealed the surprisingly facile depolymerisation of $[MeHN–BH_2]_n$ with the NHC IDipp (IDipp = 1,3-bis(2,6-diisopropylphenyl)-1,3-dihydro-2*H*-imidazol-2-ylidene) at 20 °C, with a stoichiometric reaction giving quantitative formation of an NHC-aminoborane adduct, IDipp–BH_2NMeH (Scheme 4.1a). More recently, in relevant work on a related system, Scheer *et al.* reported the depolymerisation of polyphosphinoboranes; however, even under much more forcing conditions complete depolymerisation was not achieved (Scheme 4.1b).[25]

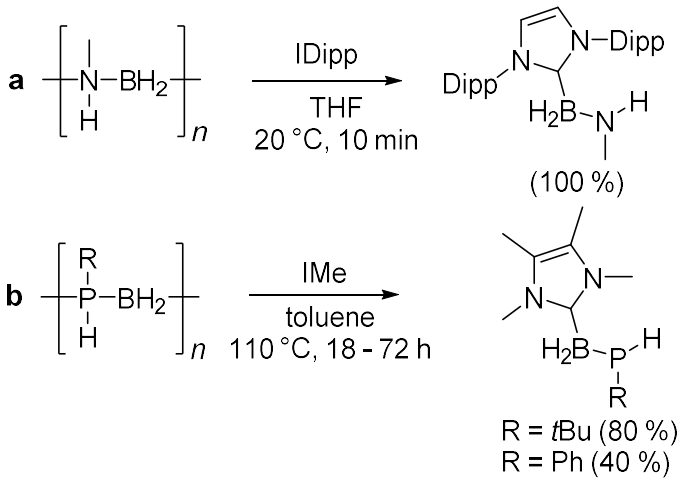

Scheme 4.1 Depolymerisation of **a** polyaminoboranes; and **b** polyphosphinoboranes using NHCs. Spectroscopic yields are shown.

Studies of the mechanism of the depolymerisation using NHCs were not reported in either case. In particular it was unclear whether the NHC has the capability to initiate depolymerisation at a site in the interior of the polymer chain, known as random degradation, or whether this can only occur at the chain ends in a process termed unzipping.[26]

This work represents an in depth study of the reaction of carbenes, NHCs, and CAACs, with poly(N-methylaminoborane) $[MeHN–BH_2]_n$. A range of isolable carbenes, IDipp, *It*Bu (I*t*Bu = 1,3-di-tert-butylimidazol-2-ylidene) and CAAC^{Me} (CAAC^{Me} = $:C(CH_2)(CMe_2)_2N$-2,6-*i*$Pr_2C_6H_3$) (Figure 4.1), with varying steric and electronic properties was utilised to gain complementary mechanistic insights into the depolymerisation process. The *tert*-butyl functionalised NHC, I*t*Bu, has greater steric bulk than the IDipp NHC whereas CAAC^{Me} has both greater electron donating and electron accepting properties than either of the NHCs.[27] The reactions of the carbenes with the molecular species $MeNH_2{\cdot}BH_3$ and cyclic borazane $[MeHN–BH_2]_3$ were also studied as these results, combined with those for the reactivity of $[MeHN–BH_2]_n$ with the different carbenes, were anticipated to provide more extensive insight into the mechanism(s) for the depolymerisation.

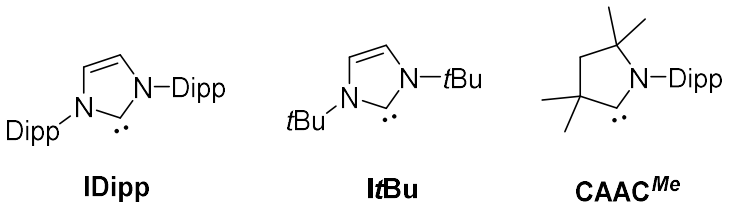

Figure 4.1 Carbenes explored in this work.

4.3 Results

4.3.1 Stoichiometric reactions between polyaminoborane $[MeHN–BH_2]_n$ and carbenes

For all of these studies poly(N-methylaminoborane) $[MeHN–BH_2]_n$ was synthesised via a previously reported iridium catalysed dehydrocoupling of N-methylamine-borane.[4] The polymer was isolated through precipitation into cold (-40 °C) hexanes. Characterisation by ^{11}B NMR spectroscopy in THF showed a single broad peak (δ_B = -4.9 ppm) (Figure S4.1) and GPC analysis on the polymer confirmed the high molar mass nature of the material (M_n = 26,100 Da; $Đ$ = 1.67) (Figure S4.2). The same sample of $[MeHN–BH_2]_n$ was used throughout this work.

As noted above, previous preliminary studies by our group have shown that a stoichiometric amount of IDipp facilitated rapid depolymerisation of poly(N-methylaminoborane) $[MeHN–BH_2]_n$ within 10 min at 20 °C in THF with quantitative conversion to a new boron-containing species (δ_B = -17.2 ppm (t)).[24] ^{11}B and ^{1}H NMR spectroscopy, together with electrospray ionisation mass spectrometry (ESI-MS), were used to identify the product as IDipp–BH_2NMeH (**4.1**), an NHC adduct of the transient methylaminoborane $MeHN=BH_2$, which is otherwise unstable above -10 °C.[28] The pure product was not isolated in this preliminary study although a similar adduct, IDipp–BCl_2NPh_2, formed by the reaction of IDipp with the isolable aminoborane $Ph_2N=BCl_2$, was characterised using single crystal X-ray diffraction. We have therefore reinvestigated the reaction between IDipp and $[MeHN–BH_2]_n$ with a view to the isolation and more complete characterisation of **4.1**. The stoichiometric reaction between these reagents in THF (22°C, 10 min), with $[MeHN–BH_2]_n$ added to a solution of IDipp, successfully led to the isolation of **4.1** and colourless crystals suitable for a single crystal X-ray diffraction study were grown from a 1:1 THF/pentane solution at -40 °C (Figure 4.2). The molecular structure in the solid state confirmed the nature of the product (Scheme 4.2a) and shows a tetracoordinate boron centre (B1) and a trigonal nitrogen atom (N1) distorted from planarity (Σ_{angles} = 337°). The B1–C1 bond length was found to be 1.631(3) Å, which is longer than the corresponding value in the NHC borane adduct IDipp–BH_3 (1.585(4) Å),[29] but comparable to values for other NHC–aminoborane adducts, IDipp–BH_2NHDipp and IDipp–BCl_2NPh_2 (B–C bond lengths 1.627(4) and 1.653(4) Å respectively).[24,30] The B–N bond length of 1.525(3) Å is shorter than the corresponding value of 1.602(7) Å in $MeNH_2{\cdot}BH_3$[31] and lies between those reported for

average single and double B–N bonds (1.58 Å and 1.40 Å respectively).[32] The ^{1}H, ^{11}B and ^{13}C NMR data for the adduct matched that described in the initial report of **4.1**.[24]

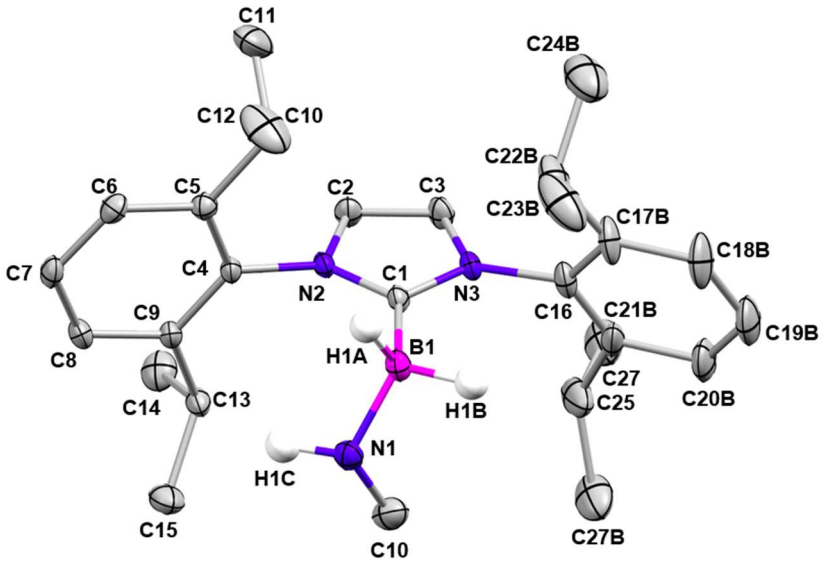

Figure 4.2 Thermal ellipsoid plot of IDipp–BH_2NMeH (**4.1**). Ellipsoids are shown at the 30% probability level. H atoms other than those on B1 and N1 have been omitted for clarity.

It should be noted that when the reverse addition was carried out, namely adding stoichiometric IDipp to a solution of $[MeHN–BH_2]_n$, ca. 20% of cyclic borazane $[MeHN–BH_2]_3$ (δ_B = -5.6 ppm (t))[33] was formed together with **4.1** (80%) (Figure S4.6). In the reactions of I*t*Bu and CAAC^{Me} with $[MeHN–BH_2]_n$ (described below) the products detected using ^{11}B NMR had no dependence on the order of addition. For consistency with the IDipp case, the text as written describes the reaction involving the addition of $[MeHN–BH_2]_n$ to carbene for both examples.

To probe the generality of the reaction, stoichiometric quantities of I*t*Bu and CAAC^{Me} were reacted with the same sample of poly(N-methylaminoborane) $[MeHN–BH_2]_n$ (M_n = 26,100 Da; $Đ$ = 1.67). In the reaction with I*t*Bu (THF, 22 °C, 30 min) proton coupled ^{11}B NMR spectroscopy evidenced full depolymerisation with cyclic borazane $[MeHN–BH_2]_3$ (δ_B = -5.6 ppm (t))[33] identified as the major product (88%) (Figure S4.3a and Scheme 4.2b(i)). Further analysis of the ^{11}B NMR spectrum revealed traces (ca. 7%, 2% and 3%) of three additional products (δ_B = 32.4 ppm (d), δ_B 27.4 ppm (d) and δ_B -15.6 ppm (t)) which were assigned as borazine $[MeNBH]_3$,[34] diaminoborane $(MeNH)_2BH$[24] and the analogous NHC-aminoborane adduct I*t*Bu–BH_2NMeH, respectively. The identity of I*t*Bu–BH_2NMeH was established based on the similarity of the ^{11}B NMR chemical shift to that of **4.1** (δ_B = -15.6 ppm

vs -17.2 ppm) and the similar coupling constant of the observed triplet ($^1J_{BH}$ = 92 Hz vs 90 Hz).[24] A peak of *m/z* = 222.1 was observed by electron ionisation mass spectroscopy (EI-MS) of the reaction solution further supported the formation of the adduct (Figure S4.4). Over 48 h the cyclic borazane [MeHN–BH_2]$_3$ was dehydrogenated to [MeNBH]$_3$ (Figure S4.3c) and ^{1}H NMR analysis of the reaction mixture evidenced a corresponding hydrogenation of I*t*Bu to (I*t*Bu)H_2[35] (Scheme 4.2b(ii)). In a separate experiment, monitoring a 1:1 reaction of CAAC^{Me} with [MeHN–BH_2]$_n$ (THF, 22 °C, 10 min) using ^{11}B and ^{1}H NMR spectroscopy showed complete conversion to [MeNBH]$_3$ (δ_B = 32.4 ppm (d))[34] and (CAAC^{Me})H_2[36] within 10 min together with a trace amount (ca. 5%) of CAAC^{Me}–BH_3 (δ_B = -33.4 ppm (q), $^1J_{BH}$ = 88 Hz)[37] (Scheme 4.2c).

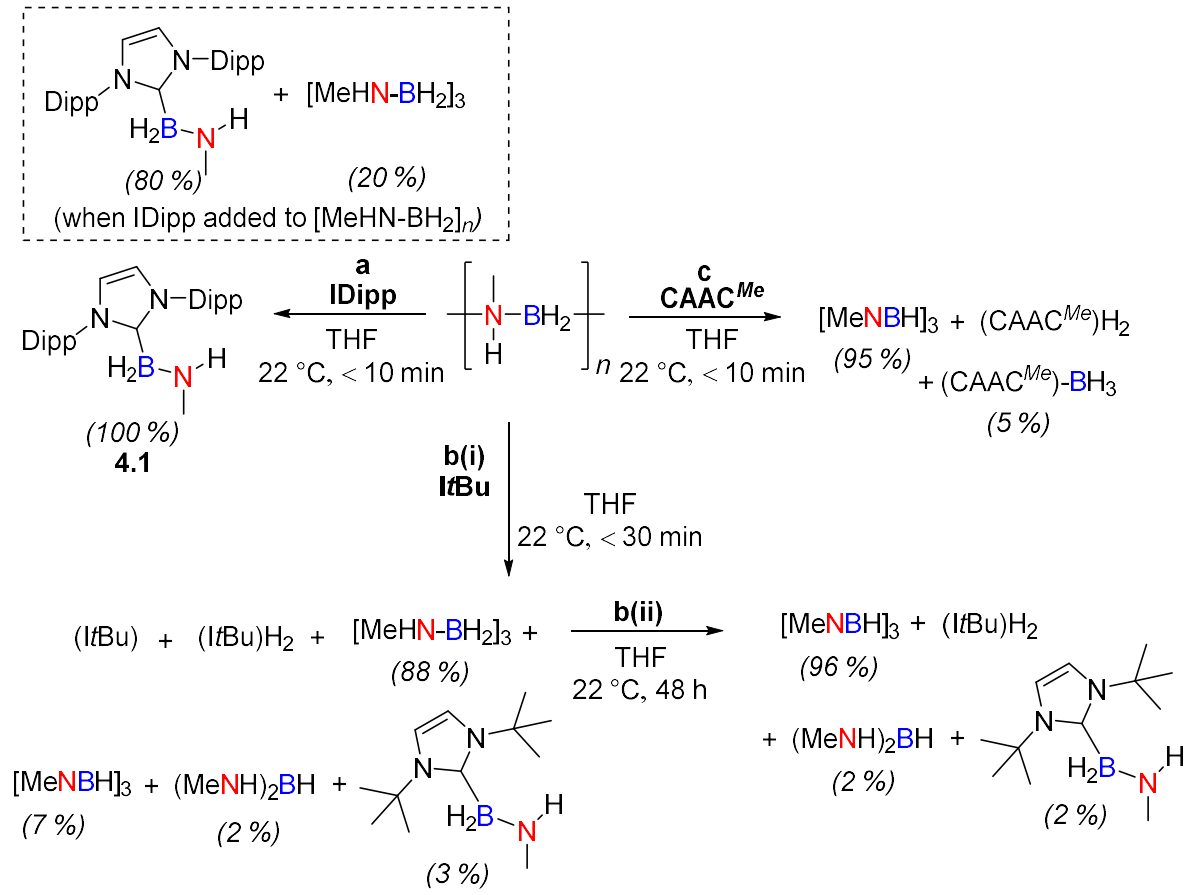

Scheme 4.2 Products of the stoichiometric reactions between [MeHN–BH_2]$_n$ and **a** IDipp[24]; **b** I*t*Bu; and **c** CAAC^{Me}. The polymer is added to a carbene solution unless otherwise stated. Spectroscopic yields of the boron containing species are given in brackets.

4.3.2 Substoichiometric reactions between polyaminoborane [MeHN–BH_2]$_n$ and carbenes

Substoichiometric quantities of IDipp, I*t*Bu and CAAC^{Me} were reacted with poly(N-methylaminoborane) [MeHN–BH_2]$_n$ (M_n = 26,100 Da; $Đ$ = 1.67) to probe whether the depolymerisation occurs with substoichiometric amounts of carbene. When

substoichiometric quantities of IDipp were used (10 – 50 mol%), under the same reaction conditions as for the stoichiometric case (22 °C, THF, polymer added to a carbene solution) the reaction again proceeded rapidly, reaching completion in under 10 min (Scheme 4.3a). The accompanying ^{11}B NMR spectra showed no trace of the characteristic broad peak (δ_B = -5.4 ppm) of $[MeHN–BH_2]_n$[4] and a more complex product distribution than in the stoichiometric reaction. IDipp–BH_2NMeH (**4.1**) (δ_B = -17.0 ppm (t)),[24] the exclusive product in the stoichiometric reaction, was identified as one of the depolymerisation products, along with cyclic borazane $[MeHN–BH_2]_3$ [δ_B = -5.6 ppm (t)),[33] and traces of borazine $[MeNBH]_3$ (δ_B = 32.4 ppm (d)),[34] diaminoborane $(MeNH)_2BH$ (δ_B = 27.4 ppm (d))[24] and $MeNH_2{\cdot}BH_3$ (δ_B = -19.0 ppm (q)).[38] It was noted that the ratio of $[MeHN–BH_2]_3$ to **4.1** formed decreased with the quantity of IDipp used (Figure S4.7). Analysis of the reaction mixtures corresponding to ≥ 10 mol% IDipp using gel permeation chromatography (GPC) showed no high molar mass material remained indicating that the addition of IDipp resulted in catalytic depolymerisation. When the quantity of IDipp added was reduced to 5 mol% a slightly broad peak remained in the ^{11}B NMR spectrum (δ_B = -5.7 ppm), with no change observed after 1 h, and GPC analysis showed the persistence of a small quantity of high molar mass material (M_n = 40,700 Da; $Đ$ = 1.10) (Figure S4.8). This showed that there is a limit (ca. 10 mol%) below which complete catalytic depolymerisation is not observed. Interestingly, in the case of 5 mol% of IDipp the M_n of the polymeric material which remained was higher than the M_n of the starting polymer.

As with the case of IDipp, when a substoichiometric quantity (10 mol%) of I*t*Bu was reacted with poly(N-methylaminoborane) $[MeHN–BH_2]_n$ (THF, 22 °C, 10 min) analysis by ^{11}B NMR spectroscopy showed complete consumption of the polymer. In this case the initial major species formed was cyclic borazane $[MeHN–BH_2]_3$ (δ_B = -5.6 ppm (t)).[33] Subsequently, analogous to the reaction of stoichiometric quantities of I*t*Bu with $[MeHN–BH_2]_n$, $[MeHN–BH_2]_3$ was dehydrogenated to borazine $[MeNBH]_3$ (δ_B = 32.4 ppm (d))[34] over 48 h; however, only the amount which corresponds to the quantity of I*t*Bu used was converted (Scheme 4.3b and Figure S4.9).

With substoichiometric quantities of CAAC^{Me} (5 – 90 mol%) (THF, 22 °C) a significant divergence in reactivity was observed, relative to that of IDipp and I*t*Bu (Scheme 4.3c). Although ^{11}B NMR spectroscopy indicated formation of borazine $[MeNBH]_3$ (δ_B = 32.4 ppm (d))[34] within 10 min, along with traces of CAAC^{Me}–BH_3 (δ_B = -33.0 ppm (q)),[37] a

broad peak (δ_B = -5.4 ppm), characteristic of the high molar mass starting polymer,[4] persisted. Notably there was no evidence of cyclic borazane $[MeHN–BH_2]_3$ in the ^{11}B NMR spectrum. GPC analysis confirmed that high molar mass material remained, with an increase in average molar mass when compared with the starting polymer (Scheme 4.3c and Figure S4.11). This is in stark contrast to the complete loss of high molar mass material in the analogous reactions involving 10 – 50 mol% of the NHCs. It is clear from the ^{11}B NMR spectra that a higher percentage of CAAC^{Me} results in a larger quantity of $[MeNBH]_3$ being formed (Figure S4.10). Furthermore, a comparison of the absolute integrals for the $[MeNBH]_3$ peaks when substoichiometric amounts of CAAC^{Me} were used, with the absolute integral of the $[MeNBH]_3$ peak when 100% of CAAC^{Me} was used, showed that the relative amount of $[MeNBH]_3$ formed linearly correlates with the percentage of CAAC^{Me} added (and (CAAC^{Me})H_2 formed) indicating that CAAC^{Me} facilitates quantitative dehydrogenation (Figure S4.10).[39]

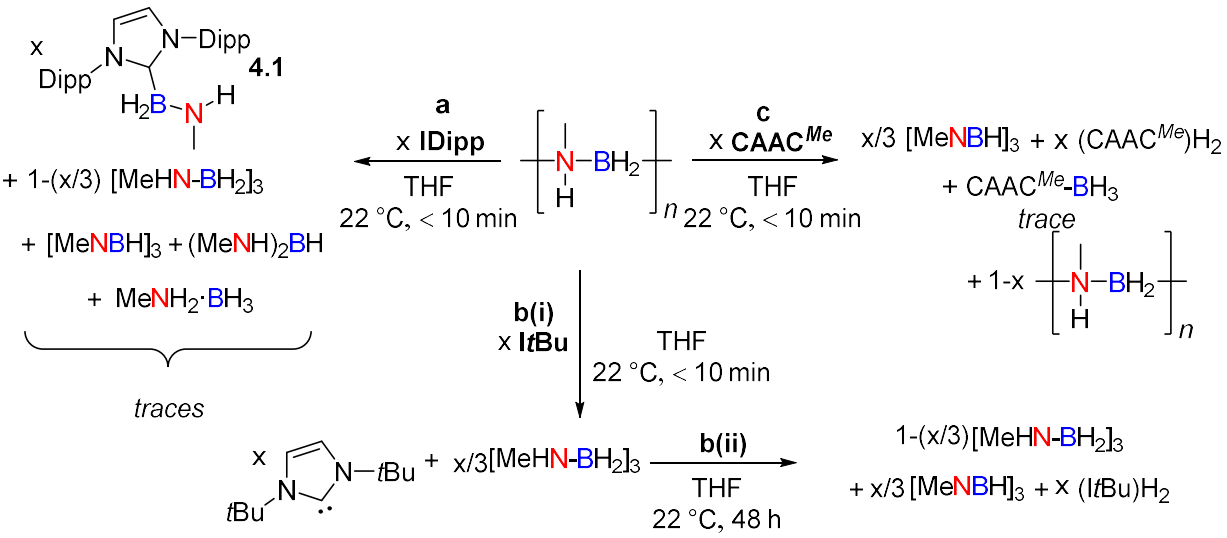

Scheme 4.3 Products of the reactions between poly(N-methylaminoborane) $[MeHN–BH_2]_n$ and substoichiometric amounts of **a** IDipp; **b** I*t*Bu; and **c** CAAC^{Me}. The polymer is added to a carbene solution in each reaction (x = mol% of carbene).

4.3.3 Further reactivity studies with poly(N-methylaminoborane) $[MeHN–BH_2]_n$ and cyclic borazane $[MeHN–BH_2]_3$

To aid with the proposal of a mechanism for the depolymerisation of poly(N-methylaminoborane) with carbenes a series of further reactions were performed.

4.3.3.1 Solution stability of poly(N-methylaminoborane) $[MeHN–BH_2]_n$

Monitoring a THF solution of poly(N-methylaminoborane) $[MeHN–BH_2]_n$ in the absence of any carbene over 16 h at 22 °C using ^{11}B NMR spectroscopy showed no conversion into any

other boron-containing species and GPC analysis showed no significant change in molar mass or dispersity.

4.3.3.2 Reaction between cyclic borazane [MeHN–BH$_2$]$_3$ and carbenes

In an attempt to establish the difference in the observed formation of the cyclic borazane [MeHN–BH$_2$]$_3$ or borazine [MeNBH]$_3$ with the carbenes the corresponding reactions of 3 equiv. of each carbene with an independently prepared sample of [MeHN–BH$_2$]$_3$ in THF were carried out. With IDipp ^{1}H and ^{11}B NMR spectroscopy showed that there was no dehydrogenation to [MeNBH]$_3$, even upon heating to 50 °C for 1 h (Scheme 4.4a). In contrast, when I*t*Bu and CAAC^{Me} were reacted directly with [MeHN–BH$_2$]$_3$ clean conversion to [MeNBH]$_3$ occurred in each case at 22 °C, over 24 h for I*t*Bu (Scheme 4.4b) and more rapidly over 1 h for CAAC^{Me} (Scheme 4.4c). It should be noted than when one equiv. of either I*t*Bu or CAAC^{Me} is reacted with [MeHN–BH$_2$]$_3$ one third is fully dehydrogenated to give [MeNBH]$_3$ and two thirds remained unreacted, and no intermediates were detected using ^{11}B NMR spectroscopy.

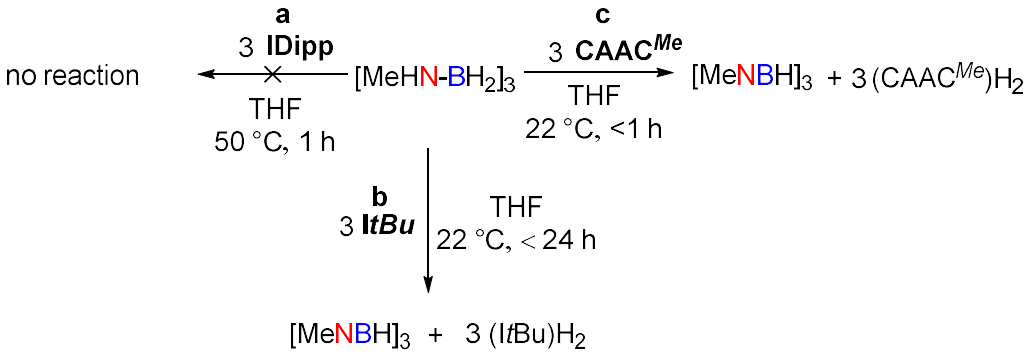

Scheme 4.4 Reaction of [MeHN–BH$_2$]$_3$ with **a** IDipp; **b** I*t*Bu; and **c** CAAC^{Me}.

4.3.3.3 Attempted detection of MeHN=BH$_2$ at low temperature

The rapid reaction between the carbenes and [MeHN–BH$_2$]$_n$ at 22 °C prevented the detection of any intermediates using ^{11}B or ^{1}H NMR spectroscopy. The monomer MeHN=BH$_2$ has previously been detected in solution at -10 °C.[28] To probe the possible formation of MeHN=BH$_2$ as an intermediate in the depolymerisations the reactions of [MeHN–BH$_2$]$_n$ with 10 mol% and 100 mol% of IDipp and with 100 mol% CAAC^{Me} were carried out in THF at low temperature (from -80 °C to 20 °C). No intermediates were observed using ^{11}B NMR spectroscopy and the carbenes were poorly soluble at low temperatures which created problems with stoichiometry (Figure S4.12 and Figure S4.13).

4.3.3.4 Carbene-mediated depolymerisation of $[MeHN–BH_2]_n$ in the presence of cyclohexene

There is precedent for the aminoborane monomer $MeHN=BH_2$ to be trapped by a hydroboration reaction with cyclohexene to give $MeHN=BCy_2$ (δ_B = ca. 45 ppm).[28,40] We carried out the depolymerisation of $[MeHN–BH_2]_n$ (THF, 22 °C, 10 min) with both stoichiometric and substoichiometric IDipp in the presence of excess cyclohexene with the goal of trapping any $MeHN=BH_2$ formed and thus confirming whether free monomer is released during the depolymerisation; however, the only products observed using ^{11}B NMR spectroscopy were identical to those formed in the depolymerisation reactions without the trapping reagent. This does not necessarily rule out the formation of free aminoborane as it may be that the rates of adduct and cyclic borazane formation are faster than the competing hydroboration reaction.[41]

4.3.3.5 Solution stability of $[MeHN–BH_2]_n$ in the presence of cyclohexene

Monitoring a THF solution at 22 °C of $[MeHN–BH_2]_n$ (M_n = 26,100 Da; $Đ$ = 1.67) in the presence of excess cyclohexene provided an interesting result. Very slowly (over three days) a new peak (δ_B = 45.3 ppm (br)),[28] identified as $MeHN=BCy_2$ was observed to form using ^{11}B NMR spectroscopy with no obvious sharpening of the peak of $[MeHN–BH_2]_n$ (δ_B = -5.5 ppm (br)) (Figure S4.14). Additional peaks corresponding to $[MeNBH]_3$ (δ_B = 32.4 ppm (d))[34] and $MeNH_2{\cdot}BH_3$ (δ_B = -19.0 ppm (q))[38] were also detected. This result is significant as the observed rate of the loss of $MeHN=BH_2$ from $[MeHN–BH_2]_n$ was considerably slower than the rate of depolymerisation with carbenes.

The persistence of the broad peak (δ_B = -5.5 ppm (br)), characteristic of polymeric material, upon addition of excess cyclohexene to poly(N-methylaminoborane), is suggestive that the aminoborane units are lost from the end of the polymer chain, rather than randomly in the center, as this would result in a significant reduction in molecular weight.[26] This was confirmed by GPC chromatography which clearly showed high molar mass material remaining (M_n = 44,400 Da; $Đ$ = 1.56) and, in a similar manner to the depolymerisation with $CAAC^{Me}$, the molar mass is increased relative to the starting polymer (Figure S4.15).

4.3.3.6 Reactivity of IDipp–BH_2NMeH (4.1) with excess cyclohexene

In an attempt to probe the reversibility of the C–B bond in **4.1** a THF solution of the adduct was exposed to excess cyclohexene in solution at 22 °C. If any cleavage of the B–C bond was to occur $MeHN=BCy_2$ would be expected to be detected as the cyclohexene would be

hydroborated by the free aminoborane monomer; however, using ^{11}B NMR spectroscopy there is no evidence of any reaction over 72 h (Scheme 4.5).

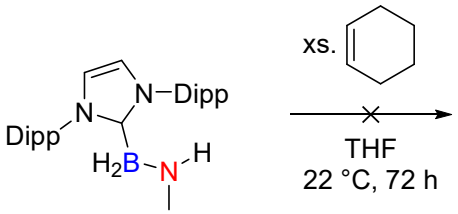

4.1

Scheme 4.5 Reaction of **4.1** with excess cyclohexene in THF.

4.3.4 Reactivity of $MeNH_2{\cdot}BH_3$ with carbenes

Following the investigations of the reactivity of carbenes with poly(N-methylaminoborane) $[MeHN–BH_2]_n$ and cyclic borazane $[MeHN–BH_2]_3$ we were interested to probe the reactivity with the parent amine-borane, $MeNH_2{\cdot}BH_3$. The reactivity of $MeNH_2{\cdot}BH_3$ with one and two equiv. of IDipp has previously been reported by Rivard *et al.* and by our group, respectively. In 2013 Rivard reported that $MeNH_2{\cdot}BH_3$ reacts with one equiv. of IDipp to give $(IDipp)H_2$ and another IDipp-containing species, identified as the carbene-bound B–N–B species, $IDipp–BH_2NHMe–BH_3$,[42] which can be formally regarded as a donor-acceptor adduct of an aminoborane. As Rivard *et al.* carried out the reaction in toluene we repeated it in THF to ensure consistency with the reactions we carried out with $[MeHN–BH_2]_n$ and $[MeHN–BH_2]_3$. The same boron-containing product was formed as determined by ^{11}B NMR spectroscopy (Scheme 4.6a). We previously reported that with two equiv. of IDipp the products are one equiv. each of $(IDipp)H_2$ and $IDipp–BH_2NMeH$ (**4.1**), the same adduct that is formed by the depolymerisation of $[MeHN–BH_2]_n$ using stoichiometric IDipp (Scheme 4.6b).[24]

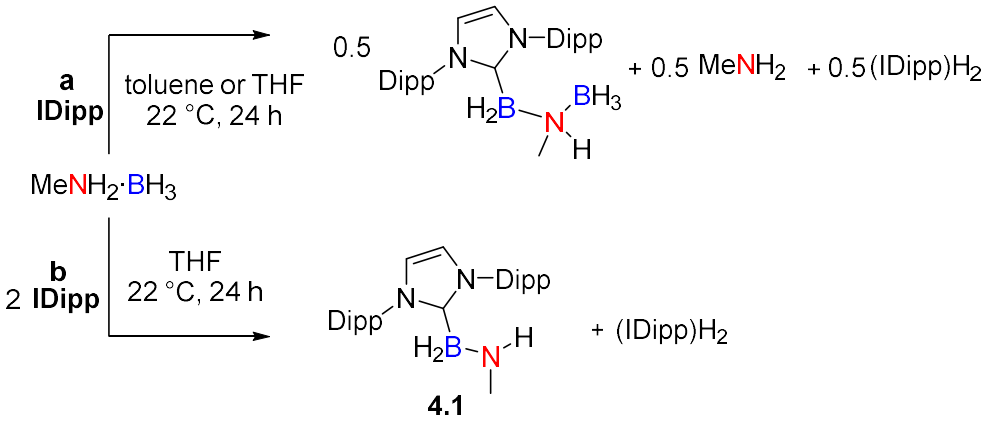

4.1

Scheme 4.6 Reaction of $MeNH_2{\cdot}BH_3$ with **a** 1 equiv.;[42] and **b** 2 equiv.[24] of IDipp.

We were interested in exploring whether when I*t*Bu was reacted with $MeNH_2{\cdot}BH_3$ the major product is cyclic borazane $[MeHN–BH_2]_3$, as is the case in the depolymerisation of $[MeHN–BH_2]_n$; I*t*Bu–BH_2NMeH, as is the case in the analogous reaction of IDipp with $MeNH_2{\cdot}BH_3$; or a different B–N containing species. The reaction of one equiv. of I*t*Bu with $MeNH_2{\cdot}BH_3$ in THF (2h, 22 °C), gave several ^{11}B containing products identified using a combination of ^{11}B NMR spectroscopy and EI-MS (Figure S4.16 and Figure S4.17). Although the major product (70%) was assigned as $[MeHN–BH_2]_3$ (δ_B = -5.6 ppm (t))[33] a broad peak (δ_B = -16 ppm to -20 ppm) (28%) was also observed for which product assignment was more difficult. The proton coupled ^{11}B NMR spectrum showed some splitting of this peak into a quartet with a chemical shift that coincides with that of $MeNH_2{\cdot}BH_3$ (δ_B = -18.9 ppm (t))[38] implying some of the starting amine-borane remains in the reaction mixture (Scheme 4.7a). No further conversion was observed after 24 h at 22 °C. With two equiv. of I*t*Bu, after 2 h at 22 °C in THF, ^{11}B NMR spectroscopy again showed the presence of several ^{11}B containing products, which after 48 h showed negligible change other than dehydrogenation of $[MeHN–BH_2]_3$ (δ_B = -5.6 ppm (t))[33] to $[MeNBH]_3$ (δ_B = 32.4 ppm (d))[34] (66%) (Figure S4.18). There was a small quantity of the adduct I*t*Bu–BH_2NMeH (δ_B = -15.4 ppm (t), *m/z* = 222.1) (9%) present along with the same broad peak (δ_B = -16 ppm to -20 ppm) (10%) that was observed in the previous reaction with one equiv. of I*t*Bu; however, the distinctive quartet which we assigned to $MeNH_2{\cdot}BH_3$ was no longer present. The consumption of $MeNH_2{\cdot}BH_3$ can be accounted for as it is anticipated it will have reacted with the additional equiv. of I*t*Bu. We postulate that the broad peak (δ_B = -16 ppm to -20 ppm) can be assigned to I*t*Bu–BH_2NHMe–BH_3 based on the similarity in ^{11}B chemical shift and peak width to that of IDipp–BH_2NHMe–BH_3[42] and a peak observed at *m/z* = 237.2 using EI-MS (Figure S4.19). Additionally, there was a broad peak (10%) (δ_B = -5.4 ppm (br)) which we attribute to a small quantity of oligomeric material $[MeHN–BH_2]_x$ (Scheme 4.7b). It is entirely possible that in the reaction with one equiv. of I*t*Bu that there is some oligomeric material formed; however, it is overlapping with the more significant cyclic borazane peak. The formation of any high molar mass material has been ruled out by the absence of a peak in the GPC chromatogram. The more complicated reaction mixture formed when using I*t*Bu, as opposed to IDipp, can be explained by the greater steric bulk of the *t*Bu substituted NHC disfavouring adduct formation, which is the sole product with IDipp. If the relative rates of dehydrogenation, adduct formation, borazane formation, oligomerisation and

carbene-bound B–N–B complex formation are competitive with each other the observed mixture of products would result.

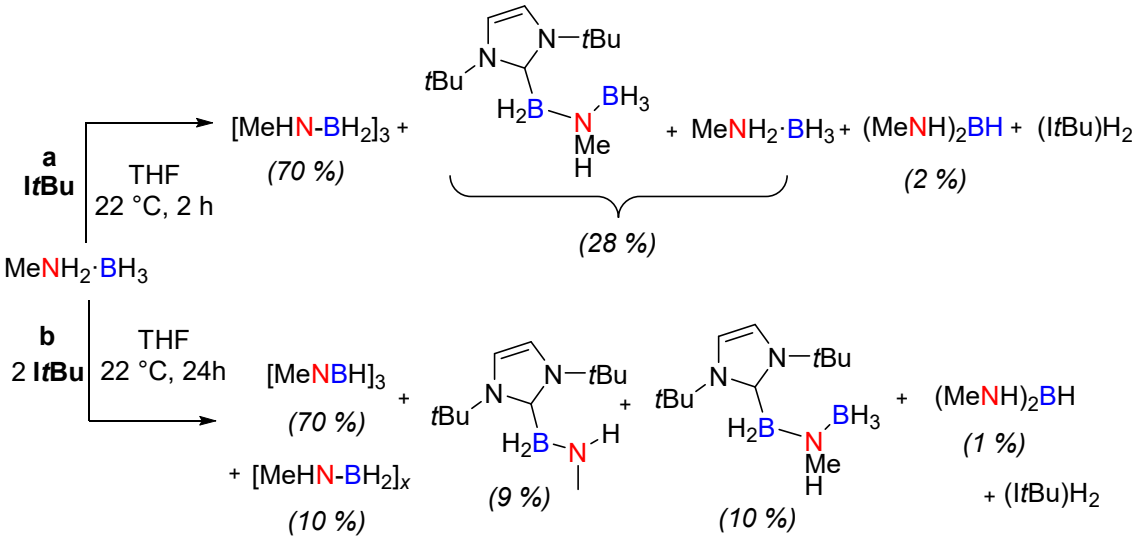

Scheme 4.7 Products of the reaction of $MeNH_2{\cdot}BH_3$ with **a** 1 equiv.; and **b** 2 equiv. of I*t*Bu.

When one equiv. of CAAC^{Me} was reacted with $MeNH_2{\cdot}BH_3$ (THF, 22 °C, 10 min) ^{1}H NMR spectroscopy showed full consumption of CAAC^{Me} accompanied by the formation of (CAAC^{Me})H_2[13] and two unsymmetrical CAAC^{Me} containing species, determined by two sets of two additional septets which correspond to the C*H*$(CH_3)_2$ protons of the Dipp groups. ^{11}B NMR spectroscopy showed that only half of the amine-borane was converted to a new boron-containing species (δ_B = 42.4 ppm (br)) with the other half remaining unreacted. The addition of a second equiv. of CAAC resulted in full consumption of $MeNH_2{\cdot}BH_3$ and full conversion to the two new boron containing species, which were subsequently identified as the *cis* and *trans* isomers of (CAAC^{Me}H)HB=NMeH (**4.2**). The formation of (CAAC^{Me})H_2 was indicative that dehydrogenation had occurred. B–H activation, rather than N–H activation, was determined as the NCH_3 peak in the ^{1}H NMR spectrum splits into a doublet and the ^{11}B chemical shift was comparable to that of MeHN=BMeH (δ_B = 41.9 ppm).[43]

When a third equiv. of CAAC^{Me} was added ^{1}H NMR spectroscopy confirmed full consumption of **4.2**, although heating to 70 °C for 1 h was required. Fractional crystallisation from a saturated hexanes solution at -40 °C facilitated the separation of two new products from the reaction mixture. X-ray crystallography was used to identify one of the products as *trans*-(CAAC^{Me}H)HB=NMe(CAAC^{Me}H) (*trans*-**4.3**) (Figure 4.3). Analysis of the crystal structure of *trans*-**4.3** showed a B–N bond length of 1.387(3) Å which is comparable to that reported for an average B–N double bond (1.40 Å).[32] B1 and N1 both exhibit trigonal planar geometries

(Σ_{angles} = 358° and 359° respectively). **4.3** can be formally described as the double E–H (E = B, N) bond activation product of the aminoborane monomer, MeHN=BH_2. The ^{1}H NMR spectrum of this species (Figure S4.22) is consistent with this structure as there were four septets (δ_H = 4.26 ppm, 3.81 ppm, 3.16 ppm and 2.87 ppm) which can be explained by the presence of two unsymmetrical CAAC^{Me} moieties in the molecule. Two singlets (δ_H = 4.98 ppm and 3.53 ppm) can be assigned to protons on the carbene centres following both B–H and N–H activation. The double E–H activation was further supported by the NCH_3 peak (δ_H = 1.79 ppm) being a singlet and the ^{11}B chemical shift being almost identical to that of the single activation product (δ_B = 44.3 ppm vs 42.4 ppm). It was possible to convert the other new product into *trans*-**4.3** through further heating at 80 °C which lead us, when combined with the ^{1}H NMR data, to assign the second product as *cis*-**4.3**.

Based on the above results we postulate that one equiv. of CAAC^{Me} acts to dehydrogenate $MeNH_2{\cdot}BH_3$. A second equiv. then forms the adduct, CAAC^{Me}–BH_2NMeH, analogous to the case with IDipp; however, this species is not observed as an intermediate as B–H activation occurs rapidly to give **4.2**. At this point the major product is the *trans* isomer, presumably due to the lower degree of steric hindrance than in *cis*-**4.2** (Scheme 4.8a). N–H activation occurs following the addition of a third equiv. of CAAC^{Me} giving **4.3**; however, due to the large steric profiles of both **4.2** and CAAC^{Me} heating was required for the second E–H bond activation to proceed at an appreciable rate. In this case the major product was the higher energy *cis* isomer which can be accounted for by presuming that conversion of *cis*-**4.2** into *trans*-**4.2** has a higher energy barrier than the N–H activation (Scheme 4.8b).

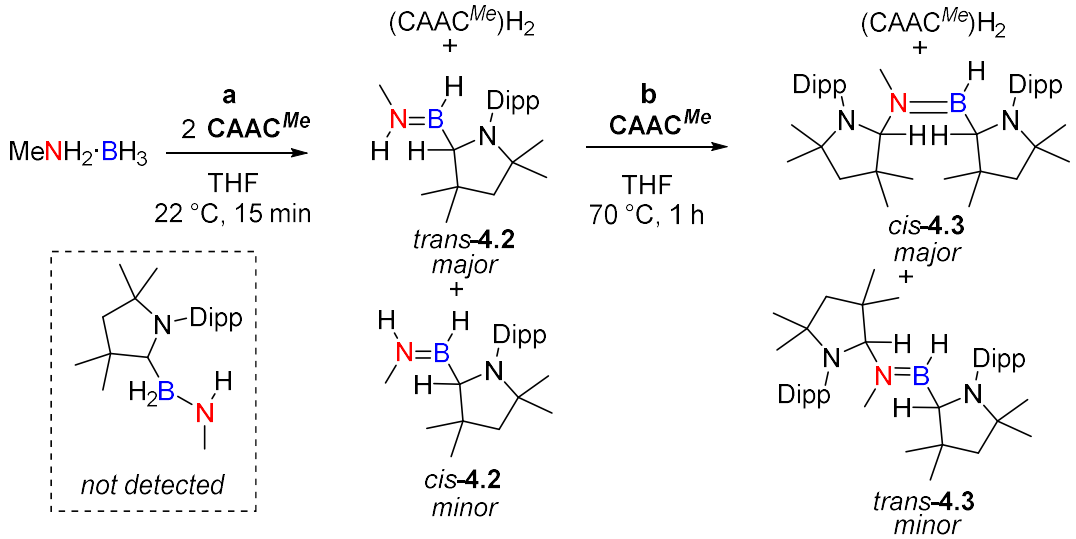

Scheme 4.8 Reaction of $MeNH_2{\cdot}BH_3$ with **a** 2 equiv.; and **b** 3 equiv. of CAAC^{Me}.

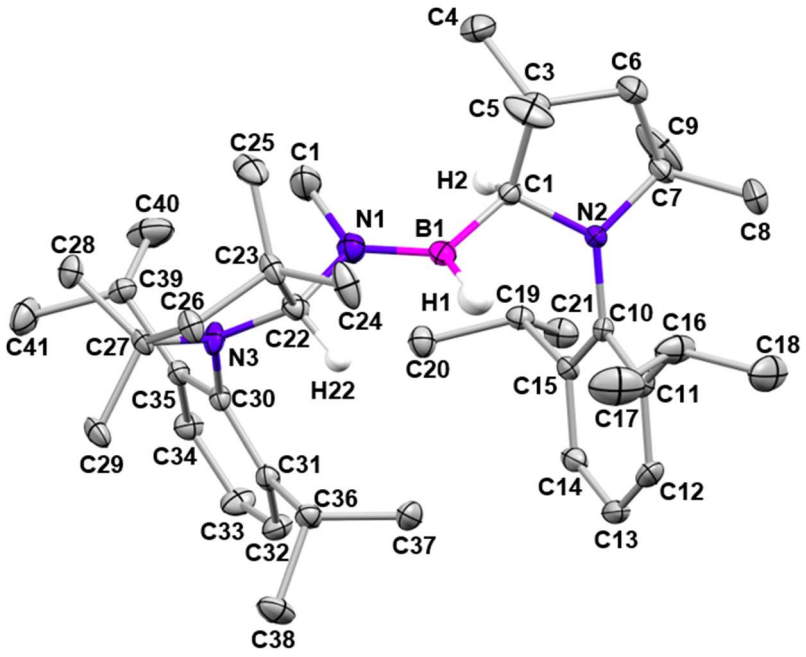

Figure 4.3 Thermal ellipsoid plot of *trans*-**4.3**. Ellipsoids are shown at the 30% probability level. H atoms other than those on C1, C22 and B1 have been omitted for clarity.

4.4 Discussion

Our studies of the reactions of the carbenes IDipp, I*t*Bu and CAAC^{Me} with poly(N-methylaminoborane) [MeHN–BH_2]$_n$, and also the polymer "model" analogues, cyclic borazane [MeHN–BH_2]$_3$ and the adduct $MeNH_2{\cdot}BH_3$ provide valuable insight into the polyaminoboranes depolymerisation in the presence of donor ligands. The results indicate that the mechanistic pathways vary with the nature of the carbene nucleophile. Although complete details cannot be definitively elucidated at this point, reasonable proposals for the various steps can be made.

In previous work ESI-MS analysis of [MeHN–BH_2]$_n$ synthesised using the same iridium catalyst as used in this study revealed that the polymer exists as linear chains possessing either borane (BH_3) or amine ($NMeH_2$) end groups.[44] When the solution stability of [MeHN–BH_2]$_n$ in the presence of cyclohexene as an aminoborane monomer trap was investigated (THF, 22 °C), MeHN=BCy_2 was observed to slowly form (ca. 30% over 30 days) together with small amounts of [MeNBH]$_3$ and $MeNH_2{\cdot}BH_3$ (Section 4.3.3.5). GPC analysis suggested that the aminoborane units were lost for the end of the polymer chain, rather than arising from cleavage of the interior of the polymer chain, as high molar mass material was found to remain. We postulate that a slow, reversible, dissociation of the polymer end groups (BH_3 or $NMeH_2$) facilitates loss

of an aminoborane monomer from the polymer chain terminus. It appears that the resulting monomer is either trapped with cyclohexene or undergoes a bimolecular disproportion reaction through H_2 transfer to give $[MeNBH]_3$ (presumably via the transient iminoborane MeN≡BH) and $MeNH_2{\cdot}BH_3$ (Figure 4.4). The latter process would be reminiscent of the well-characterised H_2-transfer reactions between aminoboranes and amine-boranes.[45] As the reaction of $[MeHN–BH_2]_n$ with cyclohexene was significantly slower than the rate observed with carbenes this provides evidence that these C-donors are inducing cleavage of the polyaminoboranes chain, rather than simply reacting with aminoborane species that have been spontaneously lost from the polymer in solution.

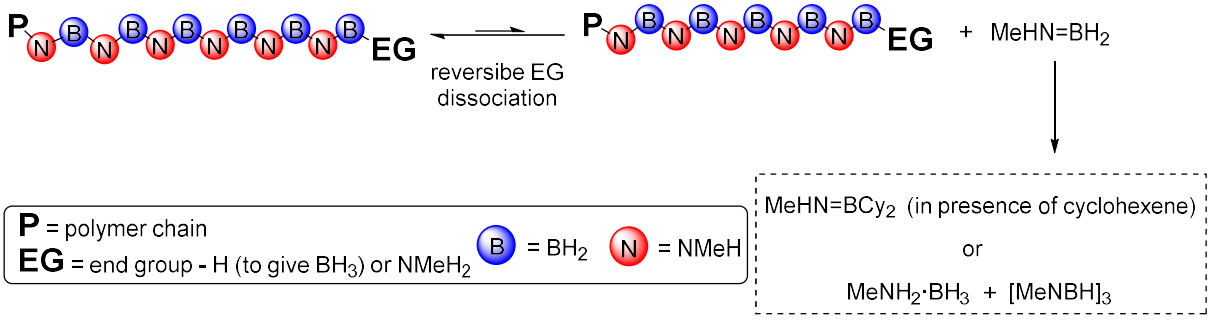

Figure 4.4 Proposed mechanism for the spontaneous depolymerisation of $[MeHN–BH_2]_n$ in THF.

4.4.1 Depolymerisation of $[MeHN–BH_2]_n$ mediated by NHCs and weaker donors

When a stoichiometric quantity of either IDipp or I*t*Bu was reacted with $[MeHN–BH_2]_n$, complete conversion to new molecular BN species were observed. With IDipp the major product was IDipp–BH_2NMeH (**4.1**), whereas with I*t*Bu the major product was borazine $[MeNBH]_3$ (Scheme 4.2). Full depolymerisation occurred upon the addition of substoichiometric quantities of both IDipp and I*t*Bu (Scheme 4.3).

Interestingly, the experimental results indicated that MeHN=BH_2 monomer is not released. For example, no MeHN=BCy_2 was intercepted when the depolymerisations were carried out in the presence of excess cyclohexene, a proven trap for this species.[40] In addition, no MeHN=BH_2 was detected using ^{11}B NMR spectroscopy when the depolymerisations were carried out at low temperatures.

We postulate that the NHCs initially interact randomly with the polymer to cleave the chain (Figure 4.5, Step 1). This has the effect of splitting the polymer into two chains, one with an NHC coordinated to boron and another which has an amine end group with a lone pair. Next, loss of NHC–BH_2NMeH occurs from newly generated polymer chain end to which it is

coordinated, (Figure 4.5, Step 2a), a reaction that may be mediated by further attack by the NHC at the penultimate BH_2 group. The other new polymer chain end with the amine terminus undergoes a back-biting reaction to release cyclic borazane $[MeHN–BH_2]_3$ (Figure 4.5, Step 2b). The polymer chains with terminal amine groups would be expected to spontaneously depolymerise as each loss of $[MeHN–BH_2]_3$ reveals another terminal amine with a lone pair, providing a possible explanation for the observed catalytic depolymerisation in the case of both NHCs.

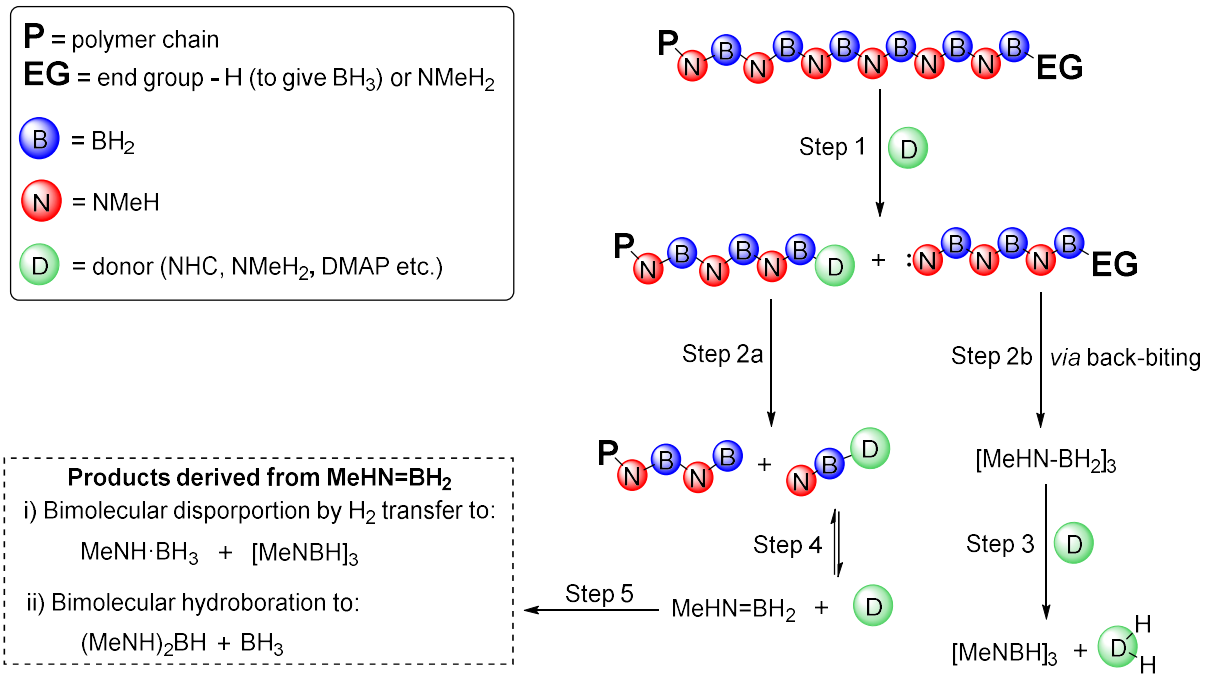

Figure 4.5 Proposed mechanism for depolymerisation of $[MeHN–BH_2]_n$ mediated by NHCs and weak donors.

The difference in product distribution in the cases of IDipp and I*t*Bu can be explained by considering the steric profile of the NHCs. IDipp, being less bulky, will likely attack the polymer main chain at a faster rate than I*t*Bu. If attack of IDipp on polymer BH_2 units is faster than the back-biting reaction (Figure 4.5, Step 2b), **4.1** will be the major product. Conversely, if attack of I*t*Bu on polymer BH_2 units is slower that the back-biting reaction, $[MeHN–BH_2]_3$ will be the major depolymerisation product. We showed in an independent reaction that I*t*Bu dehydrogenated $[MeHN–BH_2]_3$ to give $[MeNBH]_3$ at a comparable rate to that observed in the depolymerisation reaction, and we propose that this is the reason why borazine, rather than cyclic borazane, is observed as the final product in the I*t*Bu-mediated depolymerisation (Figure 4.5, Step 3).

It should be noted that this proposed mechanism can also be used to account for the different products observed when stoichiometric IDipp is added to $[MeHN–BH_2]_n$ compared to when the reverse addition is used (Scheme 4.2a). In the first case some back-biting reactions to produce $[MeHN–BH_2]_3$ occur prior to the full stoichiometric quantity of IDipp being added and being able to attack at the BH_2 of every monomer unit. In contrast, with I*t*Bu the slower attack on the chain means that the order of addition causes no detectable difference in the final products (Scheme 4.2b(i)) as in both cases back-biting occurs faster than attack of I*t*Bu on the polymer chain.

This proposed mechanism is supported by the observation that the depolymerisation can be mediated by other donor species besides NHCs. For example we previously reported that DMAP mediates the depolymerisation of $[MeHN–BH_2]_n$,[24] and a preliminary experiment showed that $NMeH_2$, a N-donor reminiscent of the nucleophilic site formed in the NHC-mediated chain cleavage step (Figure 4.5, Step 1), induces the depolymerisation of $[MeHN–BH_2]_n$ (Figure S4.29). Moreover, as DMAP and $NMeH_2$ are weaker donors than NHCs we anticipate that the adduct formed (Figure 4.5, Step 2a) will be in equilibrium with aminoborane monomer and the free donor (Figure 4.5, Step 4). This explains why with both DMAP and $NMeH_2$ no adduct is detected using NMR; instead the products are derived from $MeHN=BH_2$ (Figure 4.5, Step 5).[45,46]

4.4.2 Depolymerisation of $[MeHN–BH_2]_n$ mediated by CAAC^{Me}

In the reaction of $[MeHN–BH_2]_n$ with CAAC^{Me} there is no evidence for the formation of a donor-acceptor carbene adduct of the aminoborane monomer, or the related species (CAAC^{Me}H)HB=NMeH (**4.2**), in which the monomer has undergone B–H activation (Scheme 4.8). These are the species that would be expected to form if the depolymerisation proceeded by an initial donor-induced chain cleavage mechanism in similar manner to that proposed for the NHCs (Figure 4.5), and suggests that the reaction with CAAC^{Me} proceeds via a different pathway. Furthermore, in stark contrast to the NHCs, substoichiometric quantities of CAAC^{Me} did not facilitate complete depolymerisation and the depolymerisation was therefore not catalytic (Scheme 4.3).

The first step of the reaction of CAAC^{Me} with sp^3-hybridised BN polymer "models" $[MeHN–BH_2]_3$ and $MeNH_2{\cdot}BH_3$ involves dehydrogenation, and this is more facile than with the NHCs (Scheme 4.4 and Scheme 4.8). Analogous dehydrogenation of the linear polymer would

therefore be anticipated; however, it would be expected to be slower due to the presence of additional steric bulk. We postulate that the CAAC^{Me} initially dehydrogenates a MeHN–BH_2 unit in the polymer main chain (Figure 4.6, Step 1). The subsequent steps are highly speculative. Nevertheless, we tentatively predict the dehydrogenation causes cleavage of the polymer chain (Figure 4.6, Step 2). A back-biting reaction then occurs to release cyclic [MeHN–BH_2]$_2$[MeN=BH] (Figure 4.6, Step 3), which is rapidly dehydrogenated to borazine using an additional 2 molecules of CAAC^{Me} (Figure 4.6, Step 4).

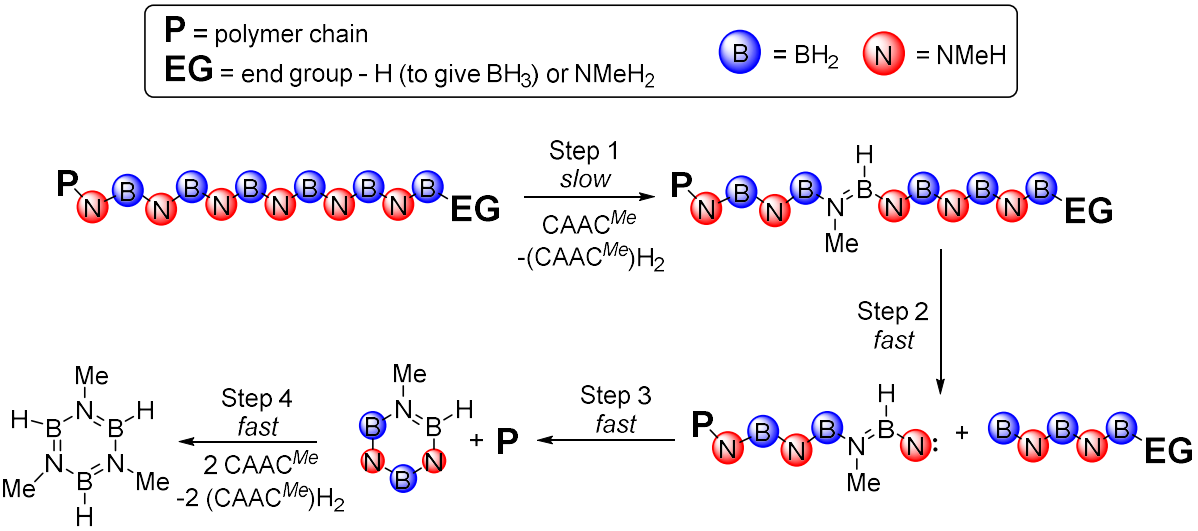

Figure 4.6 Proposed mechanism for depolymerisation of [MeHN–BH_2]$_n$ mediated by CAAC^{Me}.

If the initial dehydrogenation is slow and is followed by faster subsequent steps on fragments of species derived from the same polymer chain this mechanism explains why high molar mass polymer remains in the substoichiometric reactions of [MeHN–BH_2]$_n$ with CAAC^{Me}. An experiment which supports this concept is that when 1 equiv. of CAAC^{Me} is reacted with cyclic borazane [MeHN–BH_2]$_3$, a cyclic analogue of [MeHN–BH_2]$_n$, the products are 33.3% borazine [MeNBH]$_3$ and 66.7% unreacted cyclic borazane and the presumed partially dehydrogenated intermediate species [MeHN–BH_2]$_2$[MeNBH] and [MeHN–BH_2][MeNBH]$_2$ were not detected.

As already noted, surprisingly, when [MeHN–BH_2]$_n$ is reacted with substoichiometric CAAC^{Me} the molar mass of the remaining material actually increases (Table S4.2). A highly speculative explanation for this intriguing phenomenon is that it could stem from a polymer coiling effect. As the polyaminoborane is not highly soluble, shorter polymer chains are anticipated to be more effectively solvated. This would make access of a sterically encumbered reagent to the polymer backbone easier for the more swollen polymer coils formed by shorter chains, which would result in them being preferentially depolymerised.

4.5 Conclusions

We have studied the reactivity of both stoichiometric and catalytic quantities of IDipp, I*t*Bu and CAAC^{Me} with $[MeHN–BH_2]_n$ with the products having a clear dependence on the carbene used. The stoichiometric reaction of IDipp, I*t*Bu and CAAC^{Me} with $[MeHN–BH_2]_n$ all cause rapid, complete depolymerisation with the main B–N containing products being IDipp–BH_2NMeH (**4.1**), $[MeHN–BH_2]_3$ and $[MeNBH]_3$, respectively. With IDipp and I*t*Bu the depolymerisation was discovered to be catalytic under ambient conditions, providing both an energy and atom efficient method for controlled degradation of $[MeHN–BH_2]_n$. Conversely, with CAAC^{Me} high molar mass material remained even when 90 mol% of carbene was added. Cyclic borazane $[MeHN–BH_2]_3$ was used as polymer "model" analogue and was dehydrogenated to borazine $[MeNBH]_3$ with I*t*Bu and CAAC^{Me}, but was unreactive towards IDipp. The reaction of $MeNH_2{\cdot}BH_3$ with CAAC^{Me} allowed for the isolation of *trans*-(CAAC^{Me}H)HB=NMe(CAAC^{Me})H (*trans*-**4.3**), an aminoborane with both a B–H and N–H bond activated by CAAC^{Me}.

Depolymerisation mechanisms for each of the carbenes were proposed by considering the observed reactivity of the carbenes with $[MeHN–BH_2]_n$, $[MeHN–BH_2]_3$ and $MeNH_2{\cdot}BH_3$. We tentatively propose that the NHC-mediated depolymerisations proceed via a different mechanism to the case of CAAC^{Me}. With IDipp and I*t*Bu the NHC was predicted to attack at a central polymer BH_2 unit, causing chain cleavage to reveal a terminal amine moiety which facilitates a spontaneous back-biting reaction to release cyclic borazane. The difference in products with IDipp and I*t*Bu was explained by a consideration of the steric bulk around the carbene carbon centre. IDipp is less sterically encumbered, so should attack the polymer at a faster rate, and hence IDipp–BH_2NMeH rather than $[MeHN–BH_2]_3$ is the major depolymerisation product. CAAC^{Me} is postulated to initially dehydrogenate a $[MeHN–BH_2]$ unit in the polymer main chain, followed by faster polymer cleavage, back-biting and further dehydrogenation of fragments or species derived from the same polymer chain. This would explain why the depolymerisation with CAAC^{Me} is not catalytic.

4.6 Supporting Information

4.6.1 General procedures, reagents and equipment

All manipulations were carried out either under an atmosphere of nitrogen gas using standard vacuum line and Schlenk techniques, or under an atmosphere of nitrogen within an M. Braun glovebox MB150G-B maintained at < 0.1 ppm of H_2O and < 0.1 ppm of O_2. All solvents were dried via a Grubbs design solvent purification system.[47]

Benzene-d_6 was purchased from Sigma Aldrich, dried and vacuum distilled from sodium-benzophenone ketyl and stored over activated molecular sieves (4 Å). THF-d_8 and toluene-d_8 were purchased from Sigma and stored over activated molecular sieves (4 Å). NMR spectra were recorded using Oxford Jeol Eclipse 300 MHz, Bruker 500 MHz, Bruker 360 MHz and Bruker 300 MHz NMR spectrometers. ^{1}H NMR spectra were calibrated using the residual protio signal of the solvent (δ ^{1}H (C_6D_6) = 7.16) ^{13}C NMR spectra were calibrated using the solvent signal (δ ^{13}C(C_6D_6) = 128.0). ^{11}B NMR spectra were calibrated against external standards (^{11}B: $BF_3{\cdot}OEt_2$ (δ ^{11}B = 0.0). All chemical shifts are given in ppm (parts per million).

IDipp (IDipp = [(HCNDipp)$_2$C:], Dipp = 2,6-*i*Pr$_2$C$_6$H$_3$),[48] I*t*Bu (I*t*Bu = [(HCN*t*Bu)$_2$C]),[49] CAAC^{Me} (CAAC^{Me} = :C(CH$_2$)(CMe$_2$)$_2$N-2,6-*i*Pr$_2$C$_6$H$_3$),[50] [MeHN–BH_2]$_n$,[4] [MeHN–BH_2]$_3$,[34] $MeNH_2{\cdot}BH_3$[38] and IDipp–BH_2NMeH[24] were prepared according to literature procedures. $BH_3{\cdot}$THF (1 M in THF) was purchased from Acros Organics and trap-to-trap vacuum transferred prior to use. Cyclohexene was purchased from Sigma, dried over CaH_2 and distilled prior to use. All other regents were purchased from commercial sources and used as received.

GPC was performed on a Malvern RI max Gel Permeation Chromatograph, equipped with an automatic sampler, a pump, an injector, and inline degasser. The columns (1 x T5000 and 1 x T3000) were contained within an oven (35 °C) and consisted of styrene/divinyl benzene gels. Sample elution was detected by means of a differential refractometer. THF (Fisher), containing 0.1 wt.% [*n*Bu$_4$N]Br, was used as the eluent at a flow rate of 1 mL min^{-1}. Samples were dissolved in the eluent (2 mg mL^{-1}) and filtered through a poly(tetrafluoroethylene) membrane of 200 nm pore size before analysis. The calibration was conducted using monodisperse polystyrene standards obtained from Aldrich. The lowest and highest molecular weight standards used were 1,200 Da and 4,200,000 Da respectively.

Air-sensitive mass spectrometry experiments were conducted using a Finnigan Trace DSQ system with Direct Probe Controller (Thermo, MA). Samples were loaded in flared glass direct injection probe sample cups in a glovebox under an inert atmosphere then transferred in vials to a chamber flushed with N2 that was connected to the DSQ instrument. The sample cup was then inserted into the MS probe and then probe was inserted into the vacuum lock system of the probe inlet system then into the MS source of the DSQ. The sample was heated to 350 °C with the following temperature program (40 °C hold 1 min, ramp 60 °C min^{-1} to 350 °C hold 1 min). The DSQ MS was scanned continuously in EI mode from 100-1000 Da to analyse the thermally volatile analytes. The DSQ MS ion source temperature was set to 150 °C and electron energy set to 40 eV during analysis.

4.6.2 Synthesis of poly(N-methylaminoborane)

$[MeHN–BH_2]_n$ was synthesised via a previously reported iridium catalysed dehydrocoupling of N-methylamine-borane.[4] To a solution of $MeNH_2{\cdot}BH_3$ (1.00 g, 22.3 mmol) in THF (1.2 mL) was added IrH_2(POCOP) (POCOP = κ^3-1,3-$(OPtBu_2)_2C_6H_3$) (39 mg, 0.066 mmol, 0.3 mol%) in THF (1 mL) at 0 °C. The mixture was stirred at 22 °C for 1 h before precipitation from minimum THF (ca. 1 mL) into cold (-78 °C) hexanes (200 mL) three times. Yield = 669 mg (69.9 %). GPC: M_n = 26,100 Da; M_w =43,500 Da; $Đ$ = 1.67.

^{11}B and ^{1}H NMR data matches that previously reported in literature.[4]

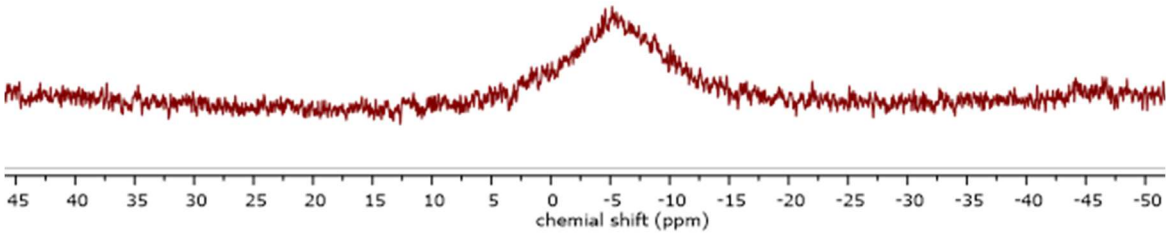

Figure S4.1 ^{11}B NMR spectra ($CDCl_3$, 96 MHz, 296 K) of $[MeHN–BH_2]_n$.

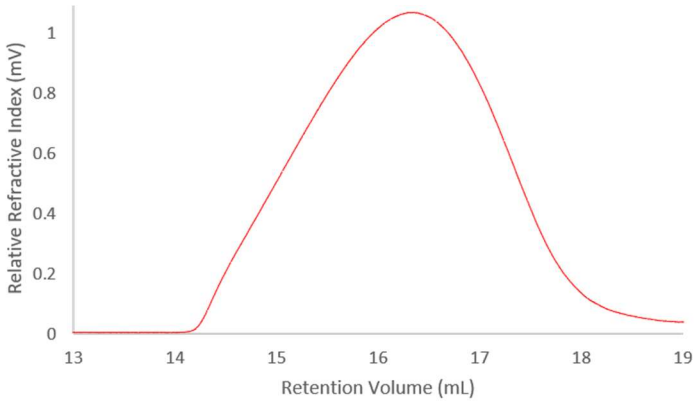

Figure S4.2 GPC chromatogram of $[MeHN–BH_2]_n$. 2 mg mL^{-1} in THF with 0.1 w/w% nBu$_4$NBr in the THF eluent.

4.6.3 Stoichiometric reactions between $[MeHN–BH_2]_n$ and IDipp, I*t*Bu and CAAC^{Me}

4.6.3.1 Synthesis of IDipp–BH_2NMeH (4.1)

To a solution of IDipp (906 mg, 2.37 mmol) in THF (3 mL) was added a solution of $[MeHN–BH_2]_n$ (100 mg, 2.37 mmol) in THF (1 mL) at 22 °C. The reaction was stirred for 5 min before the solution was concentrated to a volume of ca. 1 mL. The concentrated solution was layered with hexanes (1 mL) and single crystals of **4.1** suitable for X-ray diffraction studies were obtained from the solution at -40 °C. Yield = 641 mg (63.7 %).

^{1}H, ^{13}C and ^{11}B NMR data matches those previously reported in literature.[24]

4.6.3.2 Reaction of $[MeHN–BH_2]_n$ with I*t*Bu

To a solution of I*t*Bu (21 mg, 0.12 mmol) in THF (250 µL) was added a solution of $[MeHN–BH_2]_n$ (5 mg, 0.1 mmol) in THF (250 µL) at 22 °C. The reaction was monitored by ^{11}B NMR spectroscopy which after 30 min revealed depolymerisation to cyclic borazane $[MeHN–BH_2]_3$ (δ_B = -5.6 ppm (t), $^{1}J_{BH}$ = 107 Hz)[33] (88%), I*t*Bu–BH_2NMeH (δ_B = -15.6 ppm (t), $^{1}J_{HB}$ = 92 Hz) (3%) (assigned based on the similar chemical shift and coupling pattern to IDipp–BH_2NMeH[24] and the presence of a peak at *m/z* = 222.1 [*It*Bu-BH_2NMeH – H^-] in the EI mass spectrum), diaminoborane $(MeNH)_2BH$ (δ_B = 27.4 ppm (d), $^{1}J_{HB}$ = 130 Hz)[24] (2%) and borazine $[MeNBH]_3$ (δ_B = 32.4 ppm (d), $^{1}J_{BH}$ = 139 Hz)[34] (7%). After 48 h all $[MeHN–BH_2]_3$ is dehydrogenated to $[MeNBH]_3$ (determined using ^{11}B NMR spectroscopy) (Figure S4.3)and I*t*Bu is hydrogenated to (I*t*Bu)H_2[35] (determined using ^{1}H NMR spectroscopy).

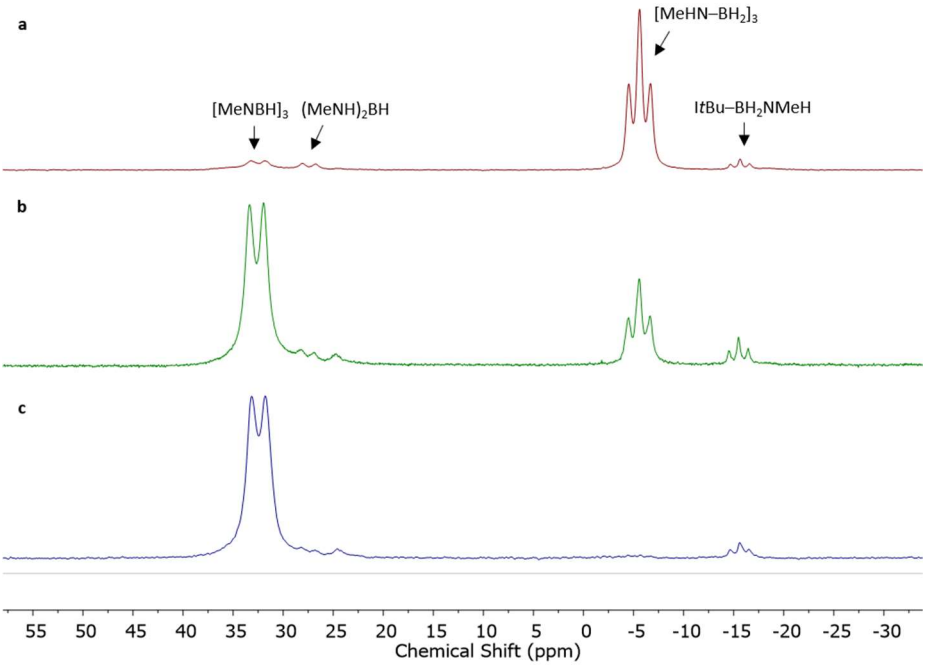

Figure S4.3 ^{11}B NMR spectra (THF, 96 MHz, 296 K) of the reaction mixture of $[MeHN–BH_2]_n$ and I*t*Bu after **a** 30 min; **b** 20 h; and **c** 48 h.

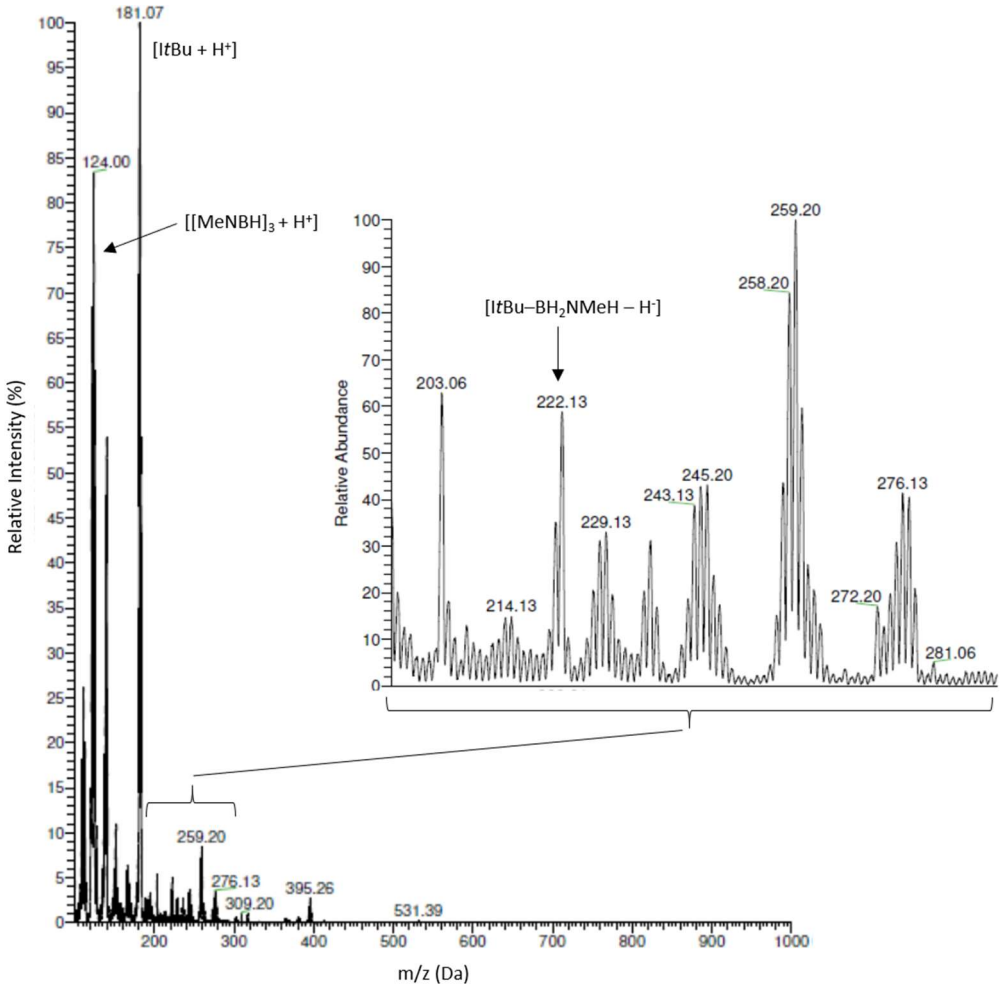

Figure S4.4 EI mass spectrum (+) of the reaction solution of I*t*Bu and $[MeHN–BH_2]_n$.

4.6.3.3 Reaction of $[MeHN–BH_2]_n$ with CAAC^{Me}

To a solution of CAAC^{Me} (34 mg, 0.12 mmol) in THF (250 µL) was added a solution of $[MeHN–BH_2]_n$ (5 mg, 0.1 mmol) in THF (250 µL) at 22 °C. The reaction was monitored by ^{11}B NMR spectrocopy which after 10 min revealed complete conversion to $[MeNBH]_3$ (δ_B = 32.4 ppm, $^1J_{BH}$ = 140 Hz)[34] and a trace amount of CAAC^{Me}–BH_3 (δ_B = -33.4 ppm (q), $^1J_{BH}$ = 88 Hz).

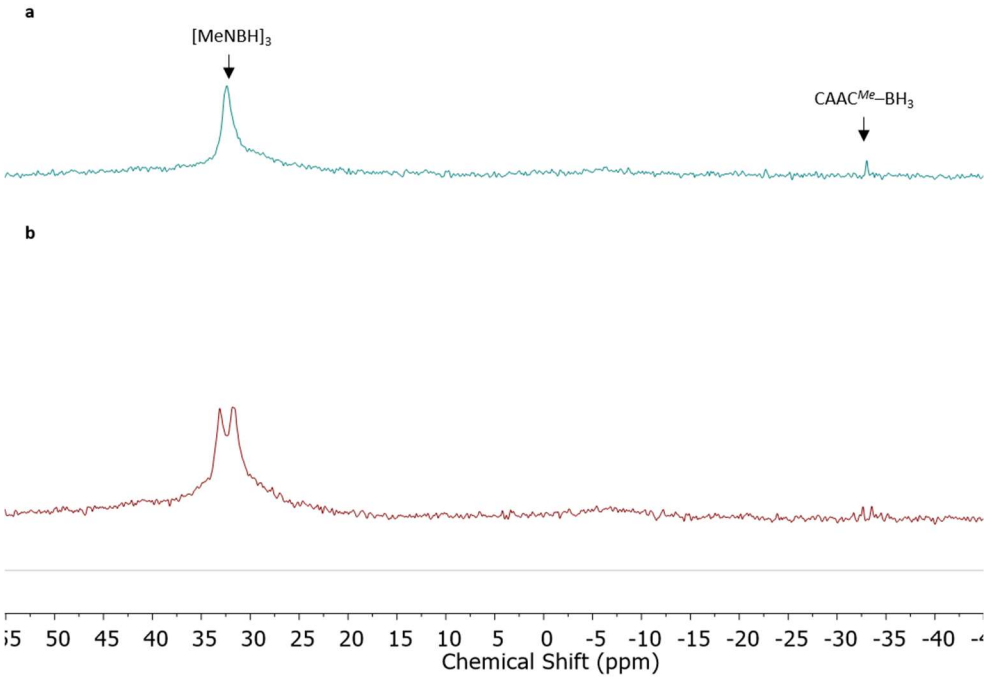

Figure S4.5 a $^{11}B\{^{1}H\}$; and **b** ^{11}B NMR spectra (THF, 96 MHz, 295 K) of the reaction mixture of $[MeHN–BH_2]_n$ and $CAAC^{Me}$.

4.6.3.2 Effect on the addition order of carbene to $[MeHN–BH_2]_n$ and vice versa

For each carbene, IDipp, I*t*Bu and $CAAC^{Me}$ (0.12 mmol in 250 µL THF), two reactions were set up. In the first the carbene solution was added to a solution of $[MeHN–BH_2]_n$ (5mg, 0.1 mmol) in THF (250 µL) and in the second the carbene solution was added to the polymer solution. After 10 min ^{11}B NMR spectra were recorded.

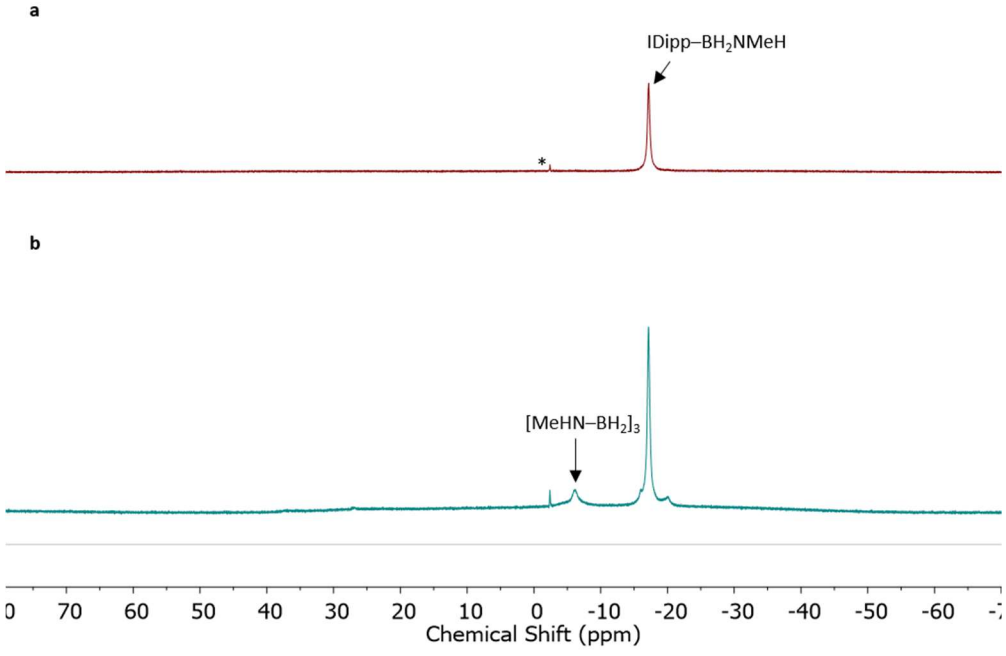

Figure S4.6 $^{11}B\{^{1}H\}$ NMR spectra (THF, 116 MHz, 298 K) of the reaction mixture of $[MeHN–BH_2]_n$ and IDipp after 10 min. **a** IDipp added to $[MeHN–BH_2]_n$; and **b** $[MeHN–BH_2]_n$ added to IDipp (*traces of $[BF_4]^-$ from the imidazolium salt).

4.6.4 Substoichiometric reactions between $[MeHN–BH_2]_n$ and IDipp, I*t*Bu and CAAC^{Me}

4.6.4.1 Reaction of $[MeHN–BH_2]_n$ with substoichiometric IDipp

IDipp (quantities shown in Table S4.1) was dissolved in THF (250 µL) and added to a solution of $[MeHN–BH_2]_n$ (10 mg, 0.23 mmol) in THF (250 µL). After 10 min ^{11}B NMR spectra were recorded and the samples were dried *in vacuo* prior to GPC analysis which showed no high molar mass material remained, other than when 5 mol% IDipp was used (Figure S4.8).

Table S4.1 Relative amounts of IDipp used in the substoichiometric reactions with $[MeHN–BH_2]_n$.

IDipp (mol%)	IDipp (mmol)	IDipp (mg)
5	0.011	5
10	0.023	9
25	0.058	23
50	0.11	45

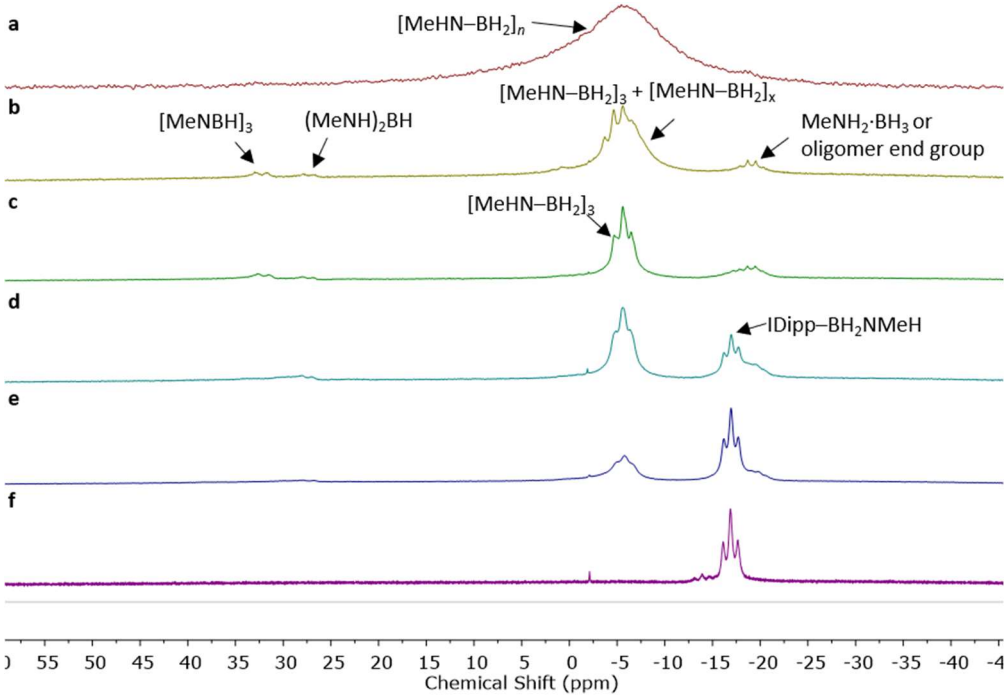

Figure S4.7 Stacked ^{11}B NMR (THF, 116 MHz, 298 K) for the reaction of $[MeHN–BH_2]_n$ and **a** 0 mol%; **b** 5 mol%; **c** 10 mol%; **d** 25 mol%; **e** 50 mol% and **f** 100 mol% of IDipp.

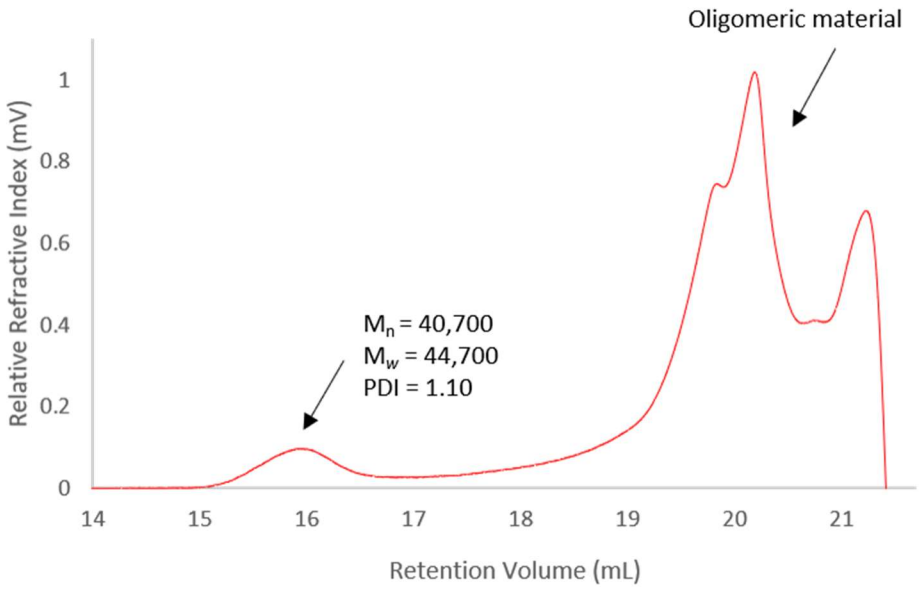

Figure S4.8 GPC chromatogram of the reaction of $[MeHN–BH_2]_n$ and 5 mol% of IDipp. 2 mg mL^{-1} in THF with 0.1 w/w% nBu$_4$NBr in the THF eluent.

4.6.4.2 Reaction of $[MeHN–BH_2]_n$ with substoichiometric ItBu

I*t*Bu (8 mg, 0.05 mmol) was dissolved in THF (250 µL) and added to a solution of $[MeHN–BH_2]_n$ (20 mg, 0.47 mmol) in THF (250 µL). After 10 min ^{11}B NMR spectroscopy showed full depolymerisation to $[MeHN–BH_2]_3$ (δ_B = -5.6 ppm (t), $^1J_{BH}$ = 109 Hz)[33] of which ca. 10% is converted to $[MeNBH]_3$ (δ_B = 32.7 ppm, $^1J_{BH}$ = 140 Hz)[34] over 48 h.

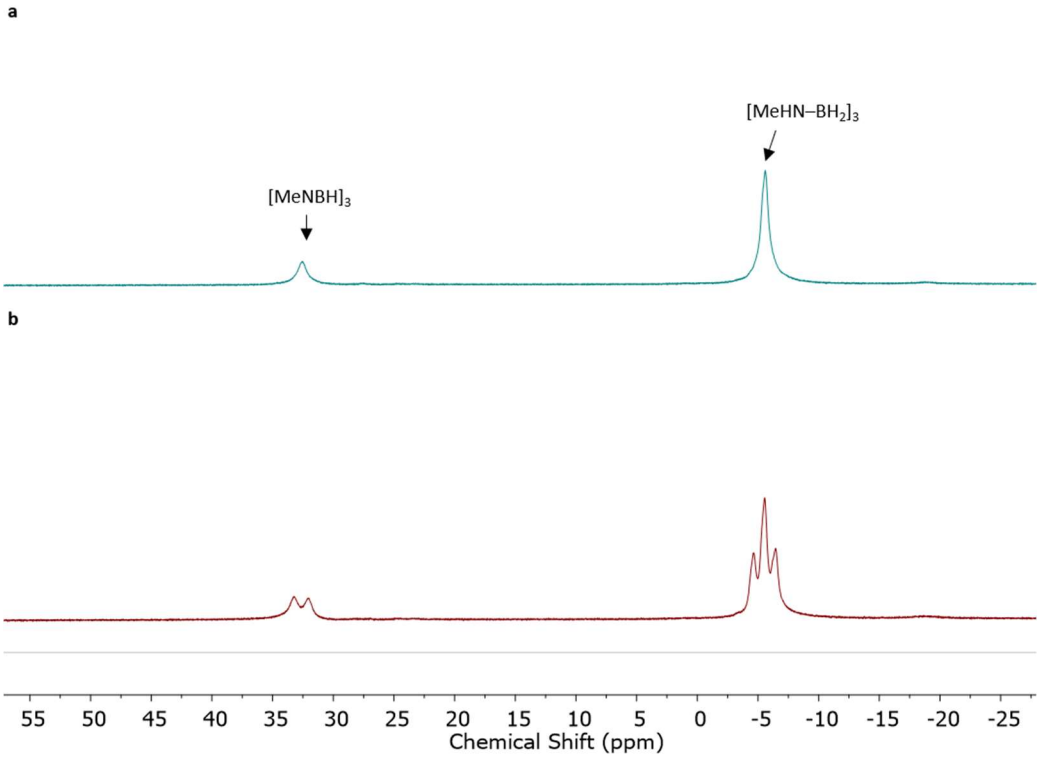

Figure S4.9 a $^{11}B\{^1H\}$; and **b** ^{11}B NMR spectra (THF, 116 MHz, 298 K) of the reaction mixture of $[MeHN–BH_2]_n$ and 10 mol% ItBu after 48 h.

4.6.4.3 Reaction of $[MeHN–BH_2]_n$ with substoichiometric $CAAC^{Me}$

$CAAC^{Me}$ (quantities shown in Table S4.2) was dissolved in THF (250 µL) and added to a solution of $[MeHN–BH_2]_n$ (10 mg, 0.23 mmol) in THF (250 µL). After 10 min ^{11}B NMR spectra were recorded and the samples were dried *in vacuo* prior to GPC analysis.

Table S4.2 Relative amounts of $CAAC^{Me}$ used in the substoichiometric reactions with $[MeHN–BH_2]_n$, conversion into borazine and M_n, M_w and PDI values of resulting material.

$CAAC^{Me}$ (mol%)	$CAAC^{Me}$ (mmol)	$CAAC^{Me}$ (mg)	Conversion into borazine (%)[a]	M_n (Da)	M_w (Da)	PDI
0	0	0	-	26,100	43,500	1.67
5	0.011	3	4	45,200	56,300	1.25
10	0.023	7	6	35,500	50,300	1.42
25	0.058	17	22	35,800	52,600	1.47
50	0.11	33	44	36,100	52,700	1.49
75	0.17	50	78	36,000	54,500	1.51
90	0.21	59	93	57,700	81,300	1.41
100	0.23	66	100	-	-	-

[a]Percentages relative to 100 mol% $CAAC^{Me}$ calculated using absolute integrals.

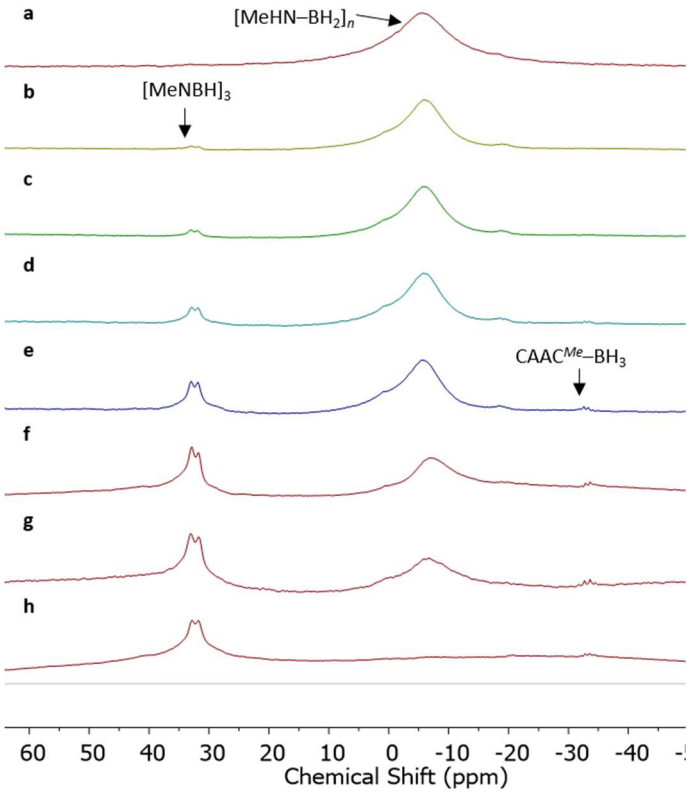

Figure S4.10 Stacked ^{11}B NMR NMR spectra (THF, 116 MHz, 298 K) for the reaction of $[MeHN–BH_2]_n$ and **a** 0 mol%; **b** 5 mol%; **c** 10 mol%; **d** 25 mol%; **e** 50 mol%; **f** 75 mol%; **g** 90 mol%; and **h** 100 mol**%** of $CAAC^{Me}$.

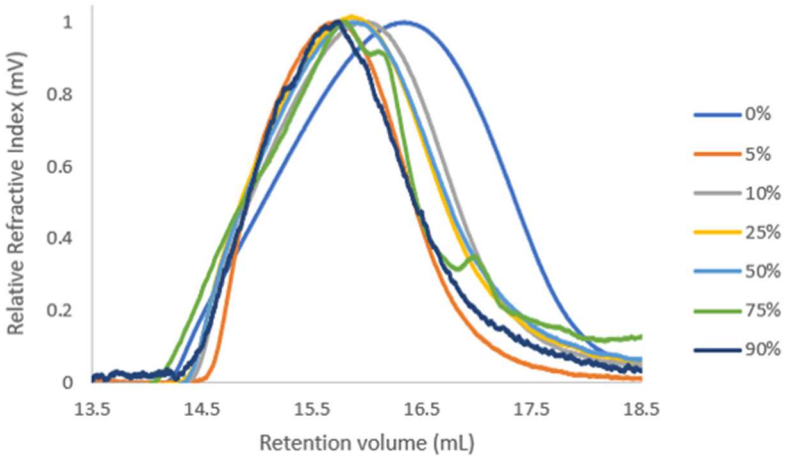

Figure S4.11 GPC chromatograms (high molar mass region) of reaction of $[MeHN–BH_2]_n$ with 0 mol%, 5 mol%, 10 mol%, 25 mol%, 50 mol%, 75 mol% and 90 mol% of CAAC^{Me}. Normalised to the polymer peak. 2 mg mL^{-1} in THF with 0.1 w/w% nBu$_4$NBr in the THF eluent.

4.6.5 Control reactions

4.6.5.1 Solution stability of $[MeHN–BH_2]_n$ in THF

$[MeHN–BH_2]_n$ (5 mg, 0.1 mmol) was dissolved in THF (0.5 mL) and monitored using ^{11}B NMR spectroscopy. After 16 h no conversion into other boron containing species was detected and GPC analysis showed no significant change in molar mass or polydispersity.

4.6.5.2 Reactions of $[MeHN–BH_2]_3$ with IDipp, I*t*Bu and CAAC^{Me}

IDipp (91 mg, 0.23 mmol), I*t*Bu (42 mg, 0.23 mmol) or CAAC^{Me} (67 mg, 0.23 mmol) was added to a solution of $[MeHN–BH_2]_3$ (10 mg, 0.078 mmol) in THF (0.5 mL) and the reaction monitored using ^{11}B NMR spectroscopy. With IDipp there was no conversion after 5 days at 22 °C or 1 h of heating at 50 °C. With I*t*Bu and CAAC^{Me} full conversion to $[MeNBH]_3$[34] was observed within 24 h and 1 h respectively.

4.6.5.3 Attempted observation of $MeHN=BH_2$ at low temperature

For each of the reaction which used low temperature NMR the following procedure was used. Carbene was dissolved in THF (250 µL) and transferred to an NMR tube. The solution was frozen using the glove box cold well cooled using liquid N_2. $[MeHN–BH_2]_n$ was dissolved in THF (250 µL) and cooled in the glove box freezer (-40 °C). The polymer solution was added to the frozen carbene solution in the glove box cold well. Once the whole sample had frozen the NMR tube was rapidly transferred from the glove box to a dry ice/acetone bath (-78 °C). The NMR machine was pre-cooled to -80 °C prior to the sample being transferred from the dry ice/acetone bath. ^{11}B{^{1}H} were recorded from -80 °C to 20 °C at intervals of 10 °C.

4.6.5.3.1 Reaction of $[MeHN–BH_2]_n$ with stoichiometric IDipp

IDipp (45 mg, 0.12 mmol) and $[MeHN–BH_2]_n$ (5 mg, 0.1 mmol) were used. At -40 °C there is evidence of the adduct IDipp–BH_2NMeH forming (δ_B = -16.9 ppm) and as the temperature is increased cyclic borazane $[MeHN–BH_2]_3$ (δ_B = -4.9 ppm) is detected. The results are comparable to the case where substoichiometric quantities of IDipp are reacted with $[MeHN–BH_2]_n$ at 22 °C. We anticipate that this is due to poor solubility of IDipp at low temperatures and this is supported by the observation of precipitate in the NMR tube at the end of the reaction. Most importantly there is no evidence of a peak at ca. δ_B = 45 ppm which would correspond to the aminoborane monomer $MeHN=BH_2$.[28]

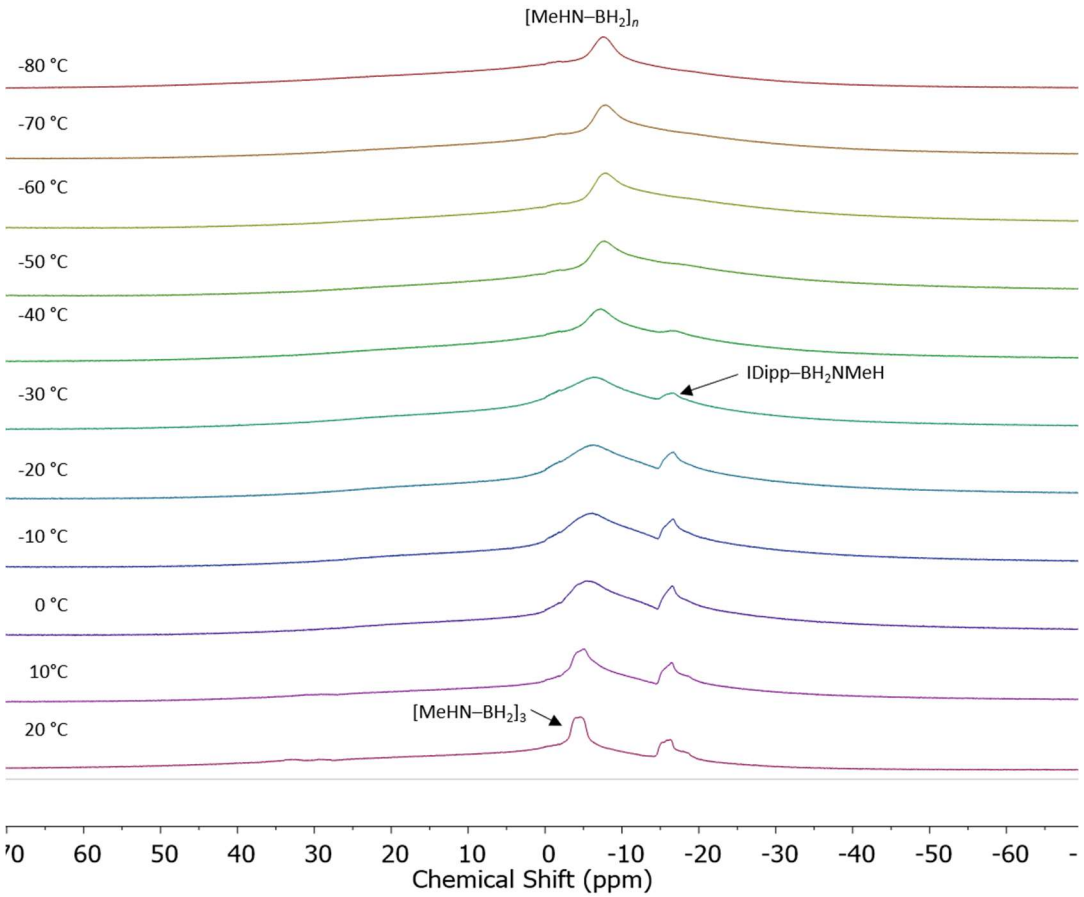

Figure S4.12 Stacked ^{11}B NMR NMR spectra (THF, 116 MHz) for the stoichiometric reaction of $[MeHN–BH_2]_n$ and Dipp from -80 °C to 20 °C.

4.6.5.3.2 Reaction of $[MeHN–BH_2]_n$ with stoichiometric CAAC^{Me}

CAAC^{Me} (33 mg, 0.12 mmol) and $[MeHN–BH_2]_n$ (5 mg, 0.1 mmol) were used. At -60 °C there is evidence of $[MeNBH]_3$ forming (δ_B = 34 ppm). As when the reaction is carried out with IDipp as the temperature is increased the ^{11}B NMR spectra are comparable to those obtained when substoichiometric quantities of CAAC^{Me} are used and precipitate is observed to form in the NMR tube. This indicates that CAAC^{Me} is poorly soluble at low temperature. There is no

evidence of a peak at ca. δ_B = 45 ppm which would correspond to the aminoborane monomer MeHN=BH_2.[28]

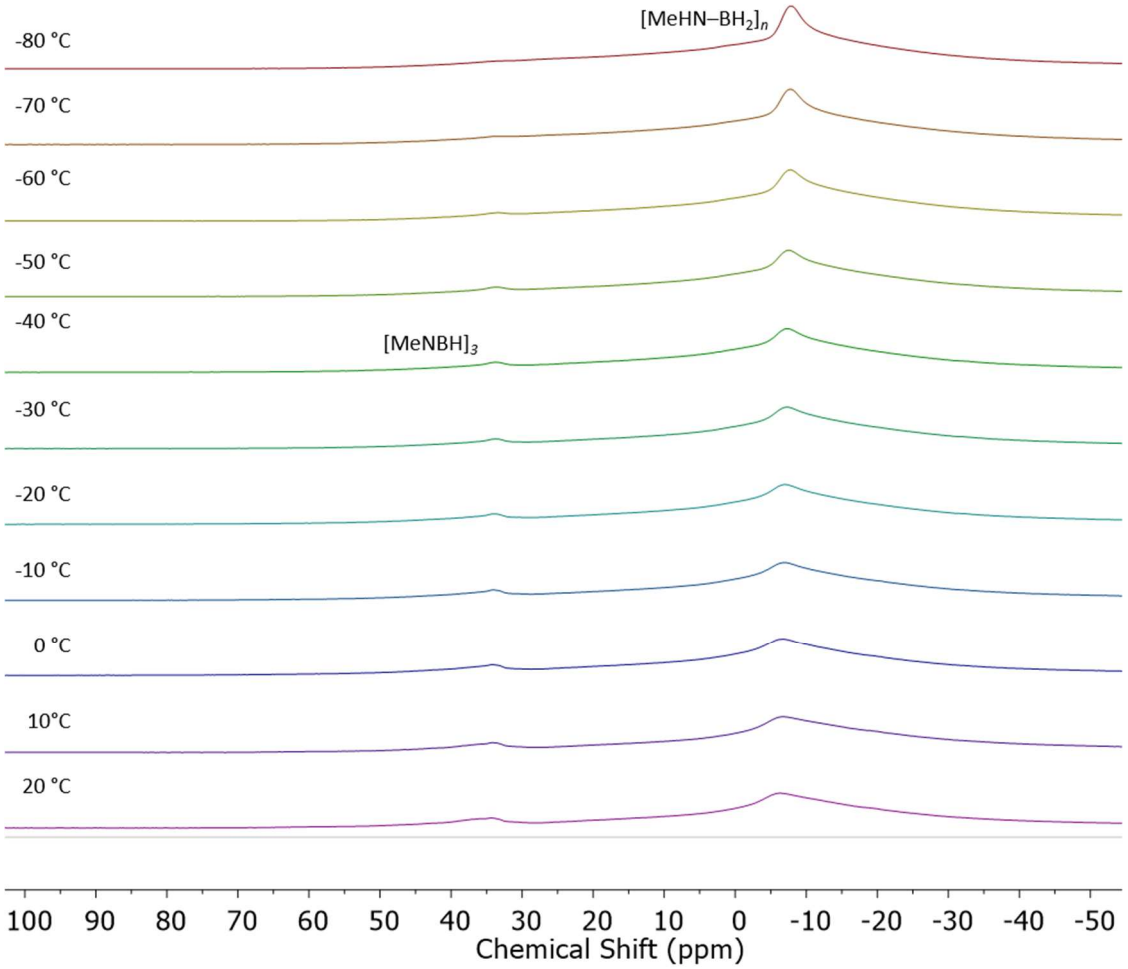

Figure S4.13 Stacked ^{11}B NMR NMR spectra (THF, 116 MHz) for the stoichiometric reaction of $[MeHN–BH_2]_n$ and $CAAC^{Me}$ from -80 °C to 20 °C.

4.6.5.3.3 Reaction of $[MeHN–BH_2]_n$ with 10 mol% IDipp

IDipp (5 mg, 0.01 mmol) and $[MeHN–BH_2]_n$ (5 mg, 0.1 mmol) were used. This reaction was carried out as the depolymerisation with IDipp had been shown to be catalytic. Using a substoichiometic, rather than stoichiometric, quantity of IDipp would potentially give us the best chance of detecting MeHN=BH_2 if it is released as only a small percentage could be trapped with IDipp. As with the stoichiometric reaction there is no evidence of a peak at ca. δ_B = 45 ppm which would correspond to the aminoborane monomer MeHN=BH_2.[28]

4.6.5.4 Cyclohexene trapping reactions

4.6.5.4.1 Depolymerisation of $[MeHN–BH_2]_n$ with stoichiometric IDipp in the presence of cyclohexene

To a solution of $[MeHN–BH_2]_n$ (5mg, 0.1 mmol) in THF (250 µL) was added cyclohexene (118 µL, 1.17 mmol). This solution was added to a solution of IDipp (45 mg, 0.12 mmol) in THF (250 µL). After 10 min ^{11}B NMR spectroscopy confirmed full conversion to $IDipp–BH_2NMeH$ (δ_B = 17.2 ppm (t)) with no evidence of any $MeHN=BCy_2$ (δ_B = ca. 45 ppm).[40]

4.6.5.4.2 Depolymerisation of $[MeHN–BH_2]_n$ with substoichiometric IDipp in the presence of cyclohexene

To a solution of $[MeHN–BH_2]_n$ (5mg, 0.1 mmol) in THF (250 µL) was added cyclohexene (118 µL, 1.17 mmol). This solution was added to a solution of IDipp (9 mg, 0.03 mmol) in THF (250 µL). After 10 min ^{11}B NMR spectroscopy confirmed full consumption of $[MeHN–BH_2]$ with no evidence of any $MeHN=BCy_2$ (δ_B = ca. 45 ppm).[40]

4.6.5.4.3 Control reaction of $[MeHN–BH_2]_n$ with cyclohexene

To a solution of $[MeHN–BH_2]_n$ (5mg, 0.1 mmol) in THF (0.5 mL) was added cyclohexene (118 µL, 1.17 mmol). ^{11}B NMR spectroscopy was used to monitor any change in the species present over time (Figure S4.14). GPC analysis of the sample after 30 days showed persistence of high molar mass material (Figure S4.15).

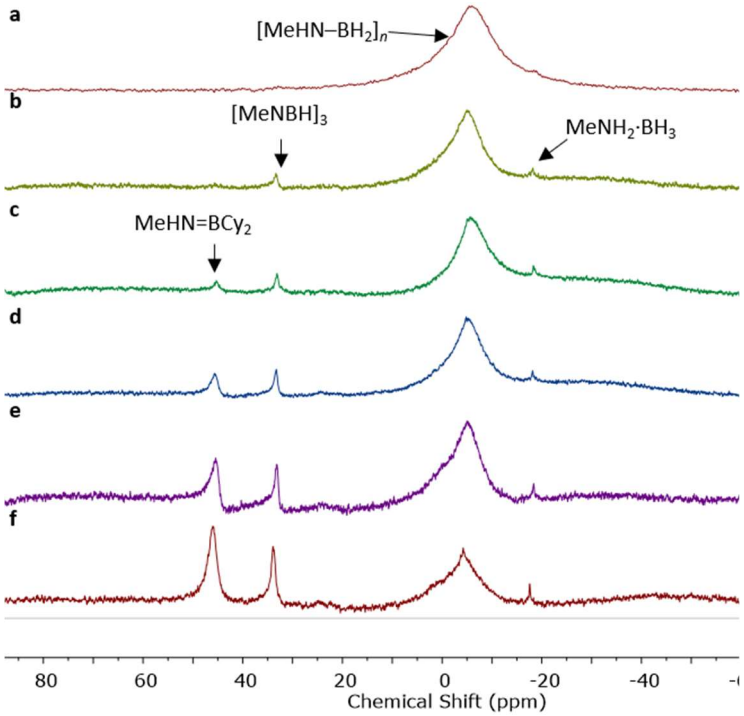

Figure S4.14 $^{11}B\{^1H\}$ NMR spectra (THF, 116 MHz, 298 K) of the reaction of $[MeHN–BH_2]_n$ with excess cyclohexene after **a** 0 days; **b** 1 days; **c** 3 days; **d** 8 days; **e** 14 days; and **f** 30 days.

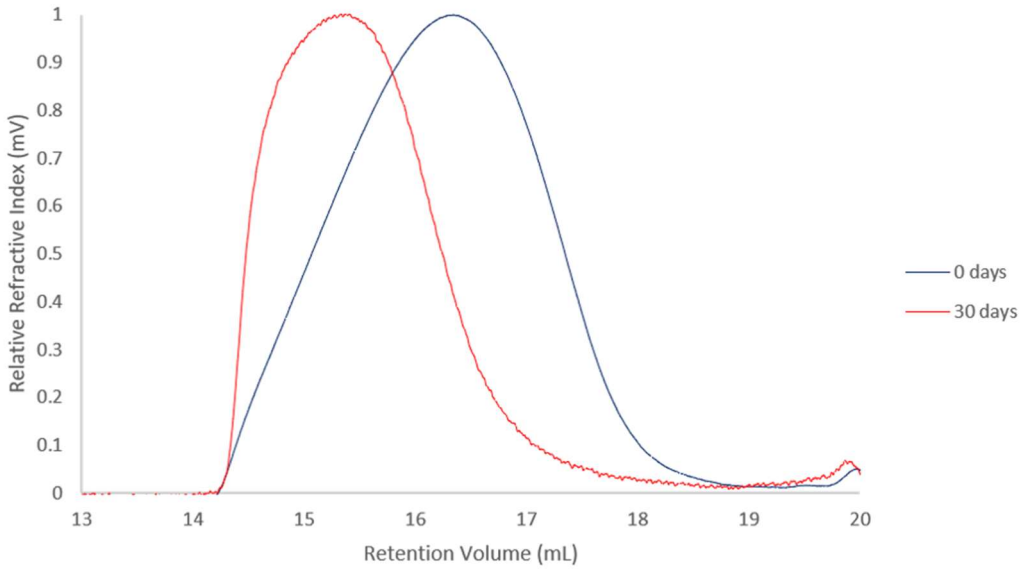

Figure S4.15 GPC chromatograms of reaction of $[MeHN–BH_2]_n$ with cyclohexene after 0 days and 30 days. 2 mg mL^{-1} in THF with 0.1 w/w% nBu$_4$NBr in the THF eluent.

4.6.5.4.4 Reaction of IDipp–BH_2NMeH with cyclohexene

IDipp–BH_2NMeH (10 mg, 0.023 mmol) was dissolved in THF (400 µL) in a J. Young NMR tube. Cyclohexene (230 µL, 2.32 mmol) was added and the reaction was monitored at 22 °C using ^{11}B NMR spectroscopy. No conversion was detected over 72 h.

4.6.6 Reactions of $MeNH_2{\cdot}BH_3$ with IDipp, I*t*Bu and CAAC^{Me}

4.6.6.1 $MeNH_2{\cdot}BH_3$ with one equivalent of IDipp

A THF solution (0.5 mL) of IDipp (43 mg, 0.11 mmol) was added to $MeNH_2{\cdot}BH_3$ (5 mg, 0.1 mmol). After 24 h ^{11}B NMR spectroscopy showed two peaks (δ_B = -16.6 ppm (br) and -15.6 ppm (br)) which are comparable with the previously reported compound IDipp-BH_2NHMeBH_3.[42]

4.6.6.2 $MeNH_2{\cdot}BH_3$ with one equivalent of I*t*Bu

A solution of I*t*Bu (40 mg, 0.22 mmol) in THF (0.3 mL) was added to a solution of $MeNH_2{\cdot}BH_3$ (10 mg, 0.22 mmol) in THF (0.3 mL). After 2 h ^{11}B NMR spectroscopy showed conversion to a mixture of ^{11}B containing species: $[MeHN–BH_2]_3$ (δ_B = -5.6 ppm (t), $^1J_{BH}$ = 110 Hz)[33] (70%), $(MeNH)_2BH$ (δ_B = 27.4 ppm (d), $^1J_{HB}$ = 156 Hz)[24] (2%), I*t*Bu–BH_2NMeHBH_3 (δ_B = -16 ppm to -20 ppm (br)) (assignment based on similarity of chemical shifts to IDipp–BH_2NMeH-BH_3[42] and the presence of a peak at *m/z* = 237.2 [*It*Bu-BH_2NMeHBH_3] in the EI mass spectrum) and $MeNH_2{\cdot}BH_3$ (δ_B = -18.9 ppm (q), $^1J_{BH}$ = 94 Hz).[38]

Monitoring the reaction for a further 24 h showed no change in the product distribution.

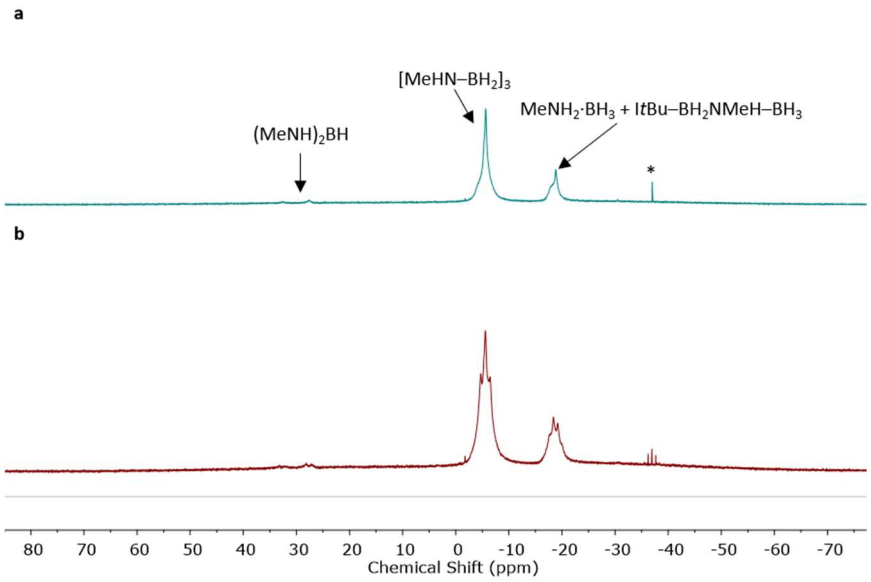

Figure S4.16 a $^{11}B\{^{1}H\}$ and **b** ^{11}B NMR spectra (THF, 116 MHz, 298 K) of the reaction mixture of $MeNH_2{\cdot}BH_3$ and one equiv. of ItBu after 2 h (*traces of $[BH_4]^-$ from the imidazolium salt).

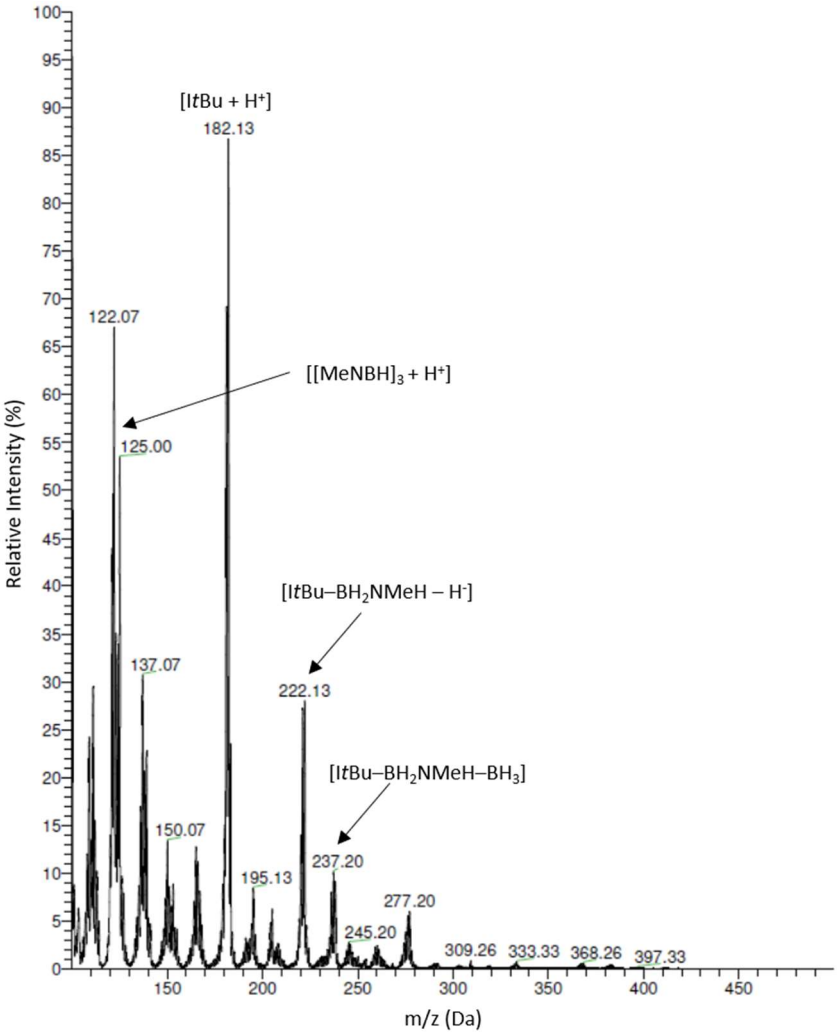

Figure S4.17 EI(+) mass spectrum of the reaction solution of I*t*Bu and $MeNH_2{\cdot}BH_3$.

4.6.6.3 $MeNH_2{\cdot}BH_3$ with two equivalents of I*t*Bu

A solution of I*t*Bu (80 mg, 0.45 mmol) in THF (0.3 mL) was added to a solution of $MeNH_2{\cdot}BH_3$ (10 mg, 0.22 mmol) in THF (0.3 mL). After 2 h ^{11}B NMR spectroscopy showed conversion to a mixture of ^{11}B containing species including $[MeHN–BH_2]_3$ (δ_B = -5.6 ppm (t), $^1J_{BH}$ = 105 Hz)[33] as the major species. Over 48 h $[MeHN–BH_2]_3$ is dehydrogenated to $[MeNBH]_3$[34] (δ_B = 32.4 ppm (t), $^1J_{BH}$ = 137 Hz) (66%) with negligible change in the other ^{11}B containing species: $(MeNH)_2BH$ (δ_B = 27.4 ppm (d)) (trace),[24] $[MeHN–BH_2]_x$ [δ_B -5.4 ppm (br)] (10%), I*t*Bu–BH_2NMeH (δ_B = -15.6 ppm(t), $^1J_{HB}$ = 92 Hz) (9%) (assigned base on the similar chemical shift and coupling to IDipp–BH_2NMeH[24] and the presence of a peak at *m/z* = 222.1 [*It*Bu-BH_2NMeH – H^-] in the EI mass spectrum) and I*t*Bu–BH_2NMeHBH_3 (δ_B = -16 ppm to -20 ppm (br)) (10%) (assignment based on similarity of chemical shifts to IDipp–BH_2NMeH–BH_3[42] and the presence of a peak at *m/z* = 237.3 [*It*Bu–BH_2NMeH–BH_3] in the EI mass spectrum). There is one unidentified product (δ_B = 24.4 ppm (s)) (5%).

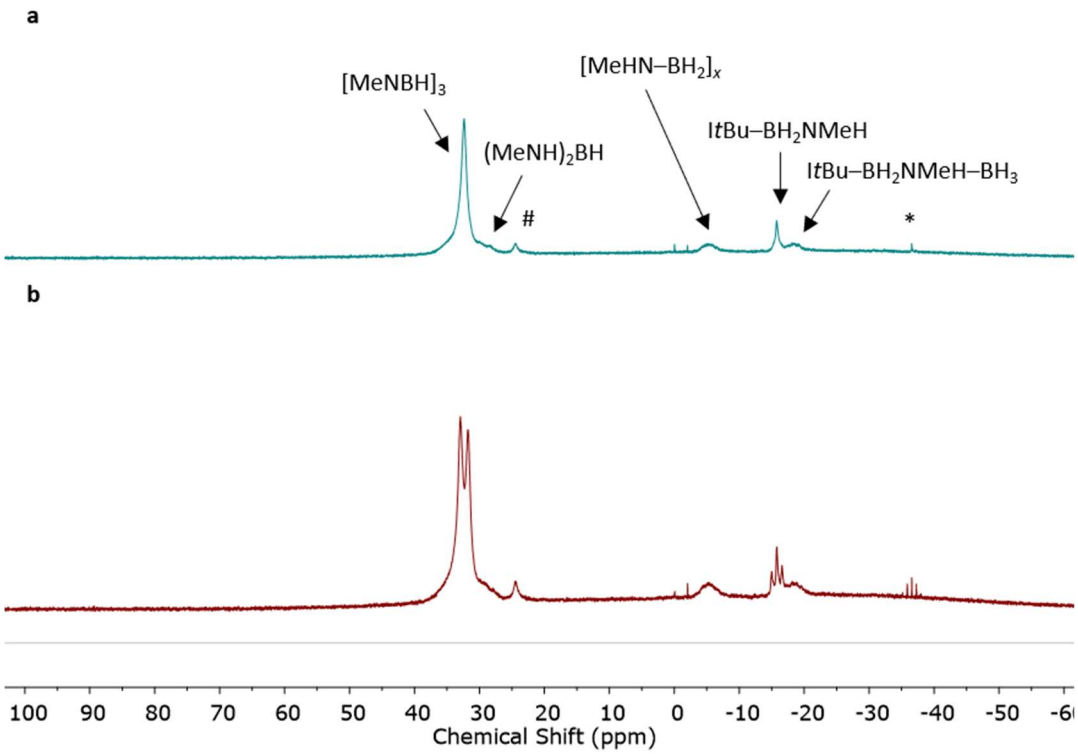

Figure S4.18 a $^{11}B\{^1H\}$; and **b** ^{11}B NMR spectra (THF, 116 MHz, 298 K) of the reaction mixture of $MeNH_2{\cdot}BH_3$ and two equiv. of ItBu after 48 h (*traces of $[BH_4]^-$ from carbene salt, #unidentified product).

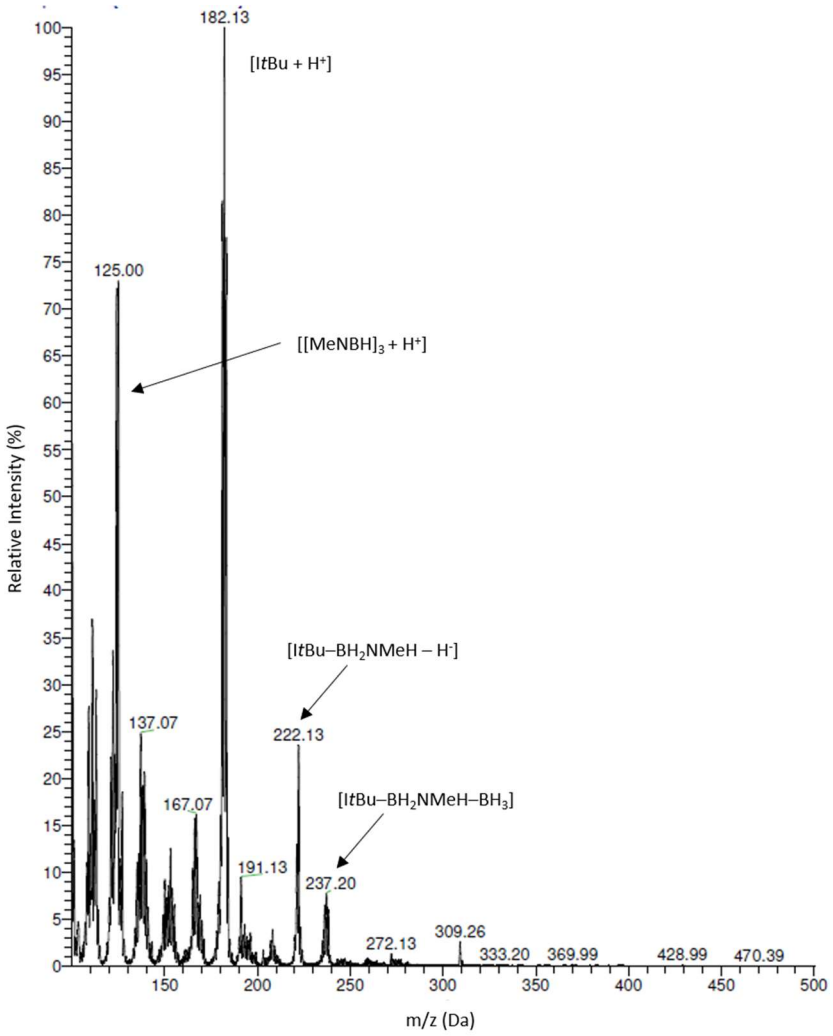

Figure S4.19 EI (+) mass spectrum of the reaction solution of 2 equiv. of I*t*Bu and $MeNH_2{\cdot}BH_3$.

4.6.6.4 $MeNH_2{\cdot}BH_3$ with two equivalents of CAAC^{Me}

CAAC^{Me} (500 mg, 1.75 mmol) was dissolved in THF (3mL) and slowly added to a solution of $MeNH_2{\cdot}BH_3$ (39 mg, 0.87 mmol) in THF (1 mL). The reaction was stirred at 22 °C for 15 min. ^{11}B NMR spectroscopy showed full conversion to a new boron containing species, along with ca. 15% of CAAC^{Me}–BH_3.[37] ^{1}H NMR spectroscopy showed the formation of (CAAC^{Me})H_2 and two unsymmetrical CAAC^{Me} containing products in a 90:10 ratio. The solvent was removed *in vacuo* to leave an oil which was redissolved in hexanes and at -40 °C and CAAC^{Me}–BH_3 crystallised out of the solution. Further separation of the new boron containing products proved unsuccessful due to the oily nature of the product. Based on the products of the reaction of $MeNH_2{\cdot}BH_3$ with three equiv. of CAAC^{Me} the new products have been assigned as the *cis* and *trans* isomers of (CAAC^{Me}H)HB=NMeH (**4.2**). The energy of both the cis and trans isomers were calculated using DFT and the trans isomer calculated to be 7.49 kJ mol^{-1} lower in energy, hence this has been assigned to the major isomer.

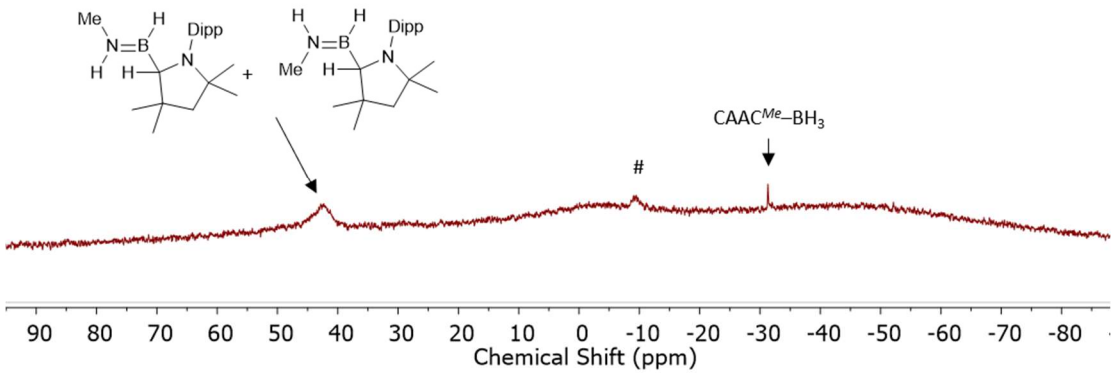

Figure S4.20 $^{11}B\{^{1}H\}$ NMR spectra (THF, 116 MHz, 298 K) of the reaction mixture of $MeNH_2{\cdot}BH_3$ and two equiv. of $CAAC^{Me}$ after 15 min ($^{\#}$unidentified product).

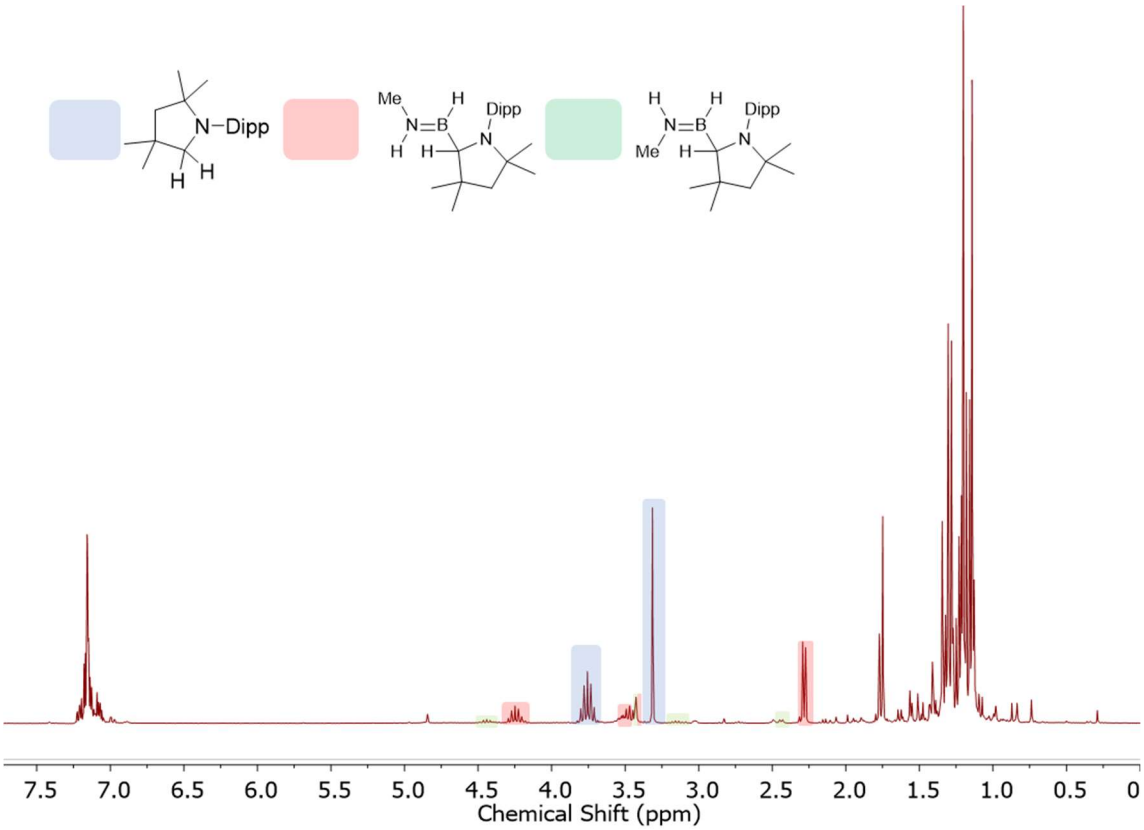

Figure S4.21 ^{1}H NMR spectra (C_6D_6, 300 MHz, 298 K) of the reaction of $MeNH_2{\cdot}BH_3$ and two equiv. of $CAAC^{Me}$ after CAAC–BH_3 was removed by recrystallisation from hexanes. The septets corresponding to the ($CH(CH_3)_2$) groups in ($CAAC^{Me}$)H_2 and each of the isomers have been highlighted along with the carbene C–H protons and the NMe_3 groups in the isomers.

4.6.6.5 Synthesis of the *cis*- and *trans*-($CAAC^{Me}$H)HB=NMe($CAAC^{Me}$H) (4.3)

$CAAC^{Me}$ (500 mg, 1.75 mmol) was dissolved in THF (3 mL) and slowly added to a solution of $MeNH_2{\cdot}BH_3$ (26 mg, 0.58 mmol) in THF (3mL). The reaction was heated to 70 °C for 1 h and full consumption of $CAAC^{Me}$ was observed using ^{1}H NMR spectroscopy. The solvent was removed *in vacuo* to leave an oily solid. This was redissolved in minimum hexanes and separation of the products was achieved through fractional precipitation at -40 °C. Due to the

separation method the yields are low and further purification was not possible. Single crystals of *trans*-**4.3** suitable for X-ray crystallisation were obtained from a saturated hexanes solution at -40 °C. DFT calculations on both the *cis* and *trans* isomers calculate the *trans* isomer to be 11.0 kJ mol^{-1} lower in energy. Yield (*trans*-**4.3** + *cis*-**4.3** = 28 mg + 40 mg = 19%. EI-MS (*trans*-**4.3**): expected 613.55, actual 613.66.

Trans-**4.3**

^{1}H NMR (C_6D_6, 500 MHz, 298 K): δ = 7.13-6.87 (m, 6H, ArH), 4.98 (s, 2H, NCH), 4.41 (br, 1H, BH), 4.26 (sept, $^{3}J_{HH}$ = 6.8 Hz, 1H, C*H*$(CH_3)_2$), 3.81 (sept, $^{3}J_{HH}$ = 6.8 Hz, 1H, C*H*$(CH_3)_2$), 3.53 (m, 1H, BCH), 3.16 (sept, $^{3}J_{HH}$ = 6.8 Hz, 1H, C*H*$(CH_3)_2$), 2.87 (sept, $^{3}J_{HH}$ = 6.8 Hz, 1H, C*H*$(CH_3)_2$), 2.83 (s, 3H, NCH_3), 1.79 (m, 2H, CH_2), 1.79 (s, 2H CH_2), 1.47 (s, 3H, $C(CH_2)(CH_3)_2$), 1.46 (s, 3H, $C(CH_2)(CH_3)_2$), 1.36 (d, $^{3}J_{HH}$ = 6.8 Hz 3H, $CH(CH_3)_2$), 1.29 (d, $^{3}J_{HH}$ = 6.8 Hz 3H, $CH(CH_3)_2$), 1.28 (s, 3H, $C(CH_2)(CH_3)_2$), 1. (s, 3H, $C(CH_2)(CH_3)_2$), 1.20 (d, $^{3}J_{HH}$ = 6.8 Hz 3H, $CH(CH_3)_2$), 1.18 (d, $^{3}J_{HH}$ = 6.8 Hz 3H, $CH(CH_3)_2$), 1. (d, $^{3}J_{HH}$ = 6.8 Hz 3H, $CH(CH_3)_2$), 1.11 (d, $^{3}J_{HH}$ = 6.8 Hz 3H, $CH(CH_3)_2$), 1.10 (s, 3H, $C(CH_2)(CH_3)_2$), 0.84 (s, 3H, $C(CH_2)(CH_3)_2$), 0.73 20 (d, $^{3}J_{HH}$ = 6.8 Hz 3H, $CH(CH_3)_2$), 0.35 20 (d, $^{3}J_{HH}$ = 6.8 Hz 3H, $CH(CH_3)_2$)

^{13}C (C_6D_6, 91 MHz, 298 K): δ = 152.62 (Ar), 151.1 (Ar), 149.6 (Ar), 148.8 (Ar), 140.6(Ar), 140.5 (Ar), 126.7 (Ar), 126.3 (Ar), 15.8 (Ar), 124.7 (ArH, 124.4 (Ar), 124.2 (Ar), 96.0 (NCH), 65.2 (BCH), 62.9 ($C(CH_3)_2(CH_2)$), 61.3 ($C(CH_3)_2(CH_2)$),)), 59.7 (CH_2), 56.6 (CH_2) 43.1 ($C(CH_3)_2(CH_2)$), 42.4 ($C(CH_3)_2(CH_2)$**,** 32.6 ($C(CH_2)(CH_3)_2$), 32.2 (NCH_3), 30.8 ($C(CH_2)(CH_3)_2$), 30.5 ($CH(CH_3)_2$), 30.0 ($C(CH_2)(CH_3)_2$), 29.8 ($CH(CH_3)_2$), 29.6 ($C(CH_2)(CH_3)_2$) ,29.2 ($C(CH_2)(CH_3)_2$) 28.9 ($CH(CH_3)_2$), 27.9 ($CH(CH_3)_2$), 27.8 ($CH(CH_3)_2$), 27.2 ($CH(CH_3)_2$),26.8 ($C(CH_2)(CH_3)_2$), 25.9 ($C(CH_2)(CH_3)_2$), 25.5 ($C(CH_2)(CH_3)_2$), 25.4 ($CH(CH_3)_2$),25.0 ($CH(CH_3)_2$), 24.9 ($CH(CH_3)_2$), 24.8 ($CH(CH_3)_2$), 24.7 ($CH(CH_3)_2$), 24.5 ($CH(CH_3)_2$).

^{11}B NMR (C_6D_6, 116 MHz, 298 K): δ = 44.3 (br)

Cis-**4.3**

^{1}H NMR (C_6D_6, 500 MHz, 298 K): δ = 7.25-7.05 (m, 6H, ArH), 4.98 (s, 2H, NCH), 4.43 (br, 1H BH), 4.28 (sept, $^{3}J_{HH}$ = 6.8 Hz, 1H, C*H*$(CH_3)_2$), 3.88 (sept, $^{3}J_{HH}$ = 6.8 Hz, 1H, C*H*$(CH_3)_2$), 3.59 (m, 1H, BCH), 3.55 (sept, $^{3}J_{HH}$ = 6.8 Hz, 1H, C*H*$(CH_3)_2$), 3.00 (sept, $^{3}J_{HH}$ = 6.8 Hz, 1H, C*H*$(CH_3)_2$), 2.86 (s, 3H, NCH_3), 1.74 (m, 2H, CH_2), 1.71 (m, 2H, CH_2), 1.46 (s, 3H, $C(CH_2)(CH_3)_2$), 1.45 (d, $^{3}J_{HH}$ = 6.8 Hz 3H, $CH(CH_3)_2$), 1.42 (d, $^{3}J_{HH}$ = 6.8 Hz 3H, $CH(CH_3)_2$), 1.24 (s, 3H, $C(CH_2)(CH_3)_2$), 1.36 (d, $^{3}J_{HH}$ = 6.8 Hz 3H, $CH(CH_3)_2$), 1.35 (d, $^{3}J_{HH}$ = 6.8 Hz 3H, $CH(CH_3)_2$), 1.34 (d, $^{3}J_{HH}$ = 6.8 Hz 3H,

CH(C<u>*H*</u>$_3$)$_2$), 1.30 (d, $^3J_{HH}$ = 6.8 Hz 3H, CH(C<u>*H*</u>$_3$)$_2$), 1.16 (d, $^3J_{HH}$ = 6.8 Hz 3H, CH(C<u>*H*</u>$_3$)$_2$), 1.15 (d, $^3J_{HH}$ = 6.8 Hz 3H, CH(C<u>*H*</u>$_3$)$_2$), 1.13 (s, 3H, C(CH$_2$)(C<u>*H*</u>$_3$)$_2$), 0.99 (s, 3H, C(CH$_2$)(C<u>*H*</u>$_3$)$_2$), 0.95 (s, 3H, C(CH$_2$)(C<u>*H*</u>$_3$)$_2$), 0.93 (s, 3H, C(CH$_2$)(C<u>*H*</u>$_3$)$_2$), 0.86 (s, 3H, C(CH$_2$)(C<u>*H*</u>$_3$)$_2$), 0.78 (s, 3H, C(CH$_2$)(C<u>*H*</u>$_3$)$_2$) Attempts to detect a cross peak of the B–H with NCH$_3$ using NOESY were made, although this proved unsuccessful, most likely due to fast relaxation of the B–H proton.

^{13}C (C$_6$D$_6$, 91 MHz, 298 K) δ = 153.1 (Ar), 152.0 (Ar), 150.4 (Ar), 148.9 (Ar), 141.1(Ar), 140.4 (ArH), 126.7 (Ar), 126.2 (Ar), 125.9 (Ar), 124.6 (Ar), 124.3 (Ar), 124.2 (Ar), 97.5 (NCH), 65.7 (BCH), 63.3 (<u>*C*</u>(CH$_3$)$_2$(CH$_2$)), 61.1 (<u>*C*</u>(CH$_3$)$_2$(CH$_2$)), 59.9 (CH$_2$) 56.7 (CH$_2$) 42.5 (<u>*C*</u>(CH$_3$)$_2$(CH$_2$)), 41.9 (<u>*C*</u>(CH$_3$)$_2$(CH$_2$)), 32.7 (C(CH$_2$)(<u>*C*</u>H$_3$)$_2$ 32.3 (NCH$_3$) 31.0 (C(CH$_2$)(<u>*C*</u>H$_3$)$_2$), 30.8 (C(CH$_2$)(<u>*C*</u>H$_3$)$_2$ 30.0 (C(CH$_2$)(<u>*C*</u>H$_3$)$_2$), 29.7 (<u>*C*</u>H(CH$_3$)$_2$), 29.4 (C(CH$_2$)(<u>*C*</u>H$_3$)$_2$) ,29.4 (<u>*C*</u>H(CH$_3$)$_2$), 28.3 (C(CH$_2$)(<u>*C*</u>H$_3$)$_2$), 27.9 (<u>*C*</u>H(CH$_3$)$_2$), 27.6 (<u>*C*</u>H(CH$_3$)$_2$), 27.6 (CH(<u>*C*</u>H$_3$)$_2$), 27.5 (C(CH$_2$)(<u>*C*</u>H$_3$)$_2$) 26.6 (CH(<u>*C*</u>H$_3$)$_2$),26.6 (<u>*C*</u>H(CH$_3$)$_2$), 25.9 (C(CH$_2$)(<u>*C*</u>H$_3$)$_2$) 25.9 (<u>*C*</u>H(CH$_3$)$_2$), 25.5 (<u>*C*</u>H(CH$_3$)$_2$), 24.7 (<u>*C*</u>H(CH$_3$)$_2$), 24.5 (C(CH$_2$)(<u>*C*</u>H$_3$)$_2$) 24.5 (<u>*C*</u>H(CH$_3$)$_2$)

^{11}B NMR (C$_6$D$_6$, 116 MHz, 298 K): δ = 45.8 (br)

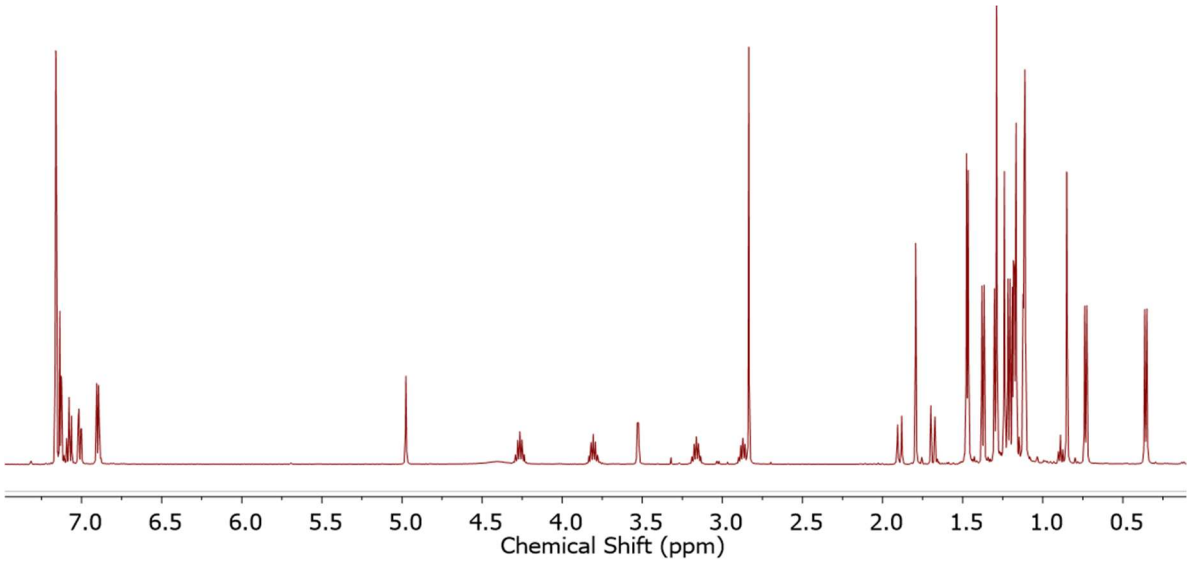

Figure S4.22 ^{1}H NMR spectra (C$_6$D$_6$, 500 MHz, 298 K) of *trans*-**4.3**.

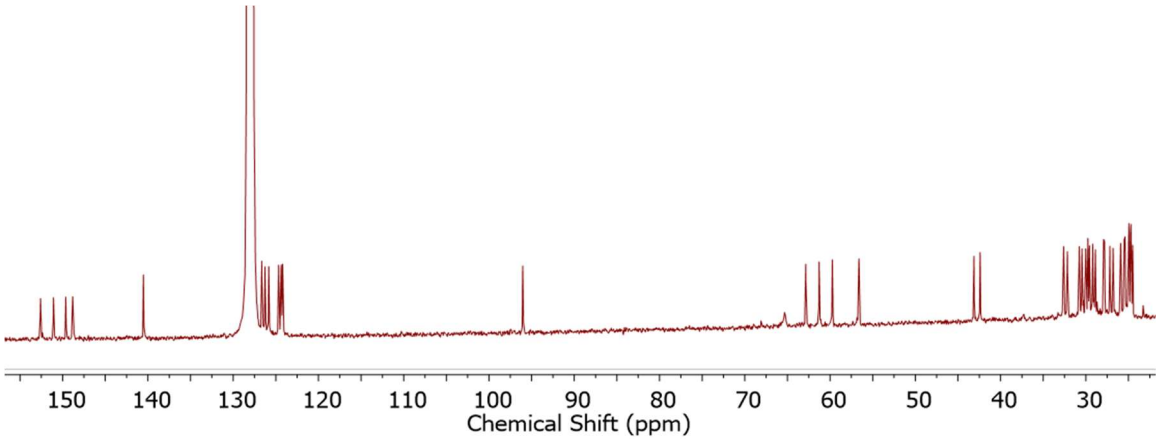

Figure S4.23 ^{13}C NMR spectra (C_6D_6, 91 MHz, 298 K) of *trans*-**4.3**.

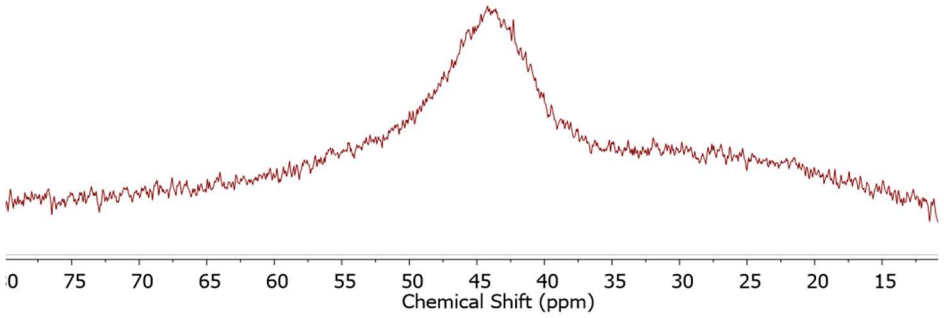

Figure S4.24 ^{11}B NMR (C_6D_6, 116 MHz, 298 K) of *trans*-**4.3**.

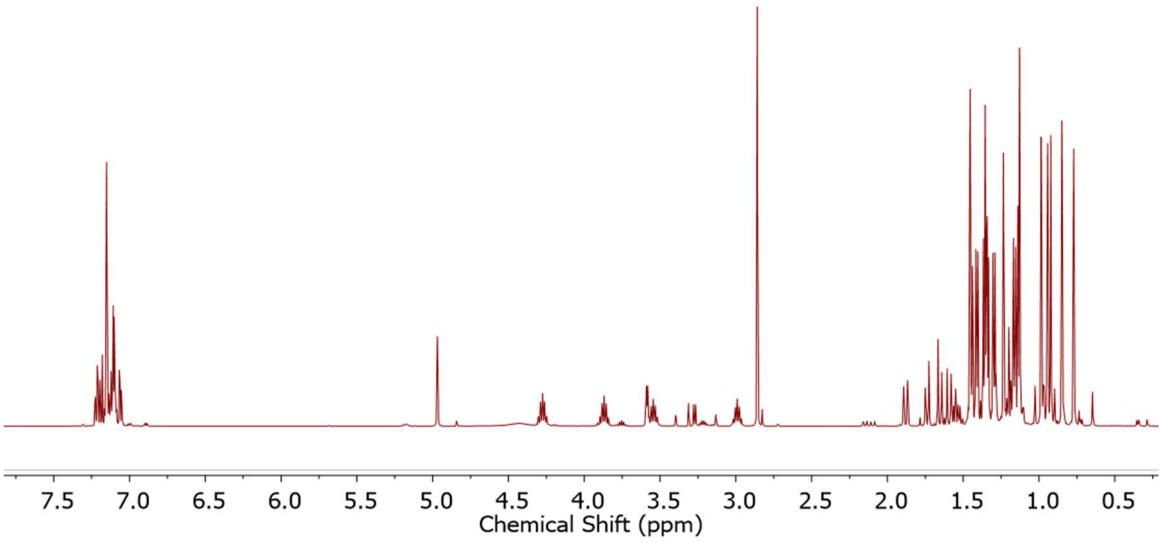

Figure S4.25 ^{1}H NMR spectra (C_6D_6, 500 MHz, 298 K) of *cis*-**4.3**.Trace quantities of *trans*-**4.3**.and (CAAC^{Me})H_2 remain as the small quantity of material isolated prevents further purification.

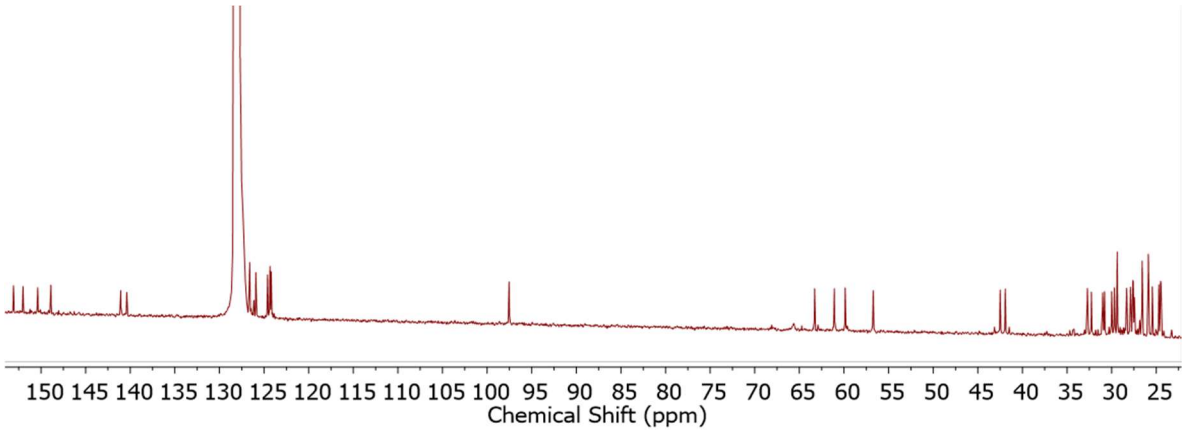

Figure S4.26 ^{13}C NMR spectra (C_6D_6, 91 MHz, 298 K) of *cis*-**4.3**

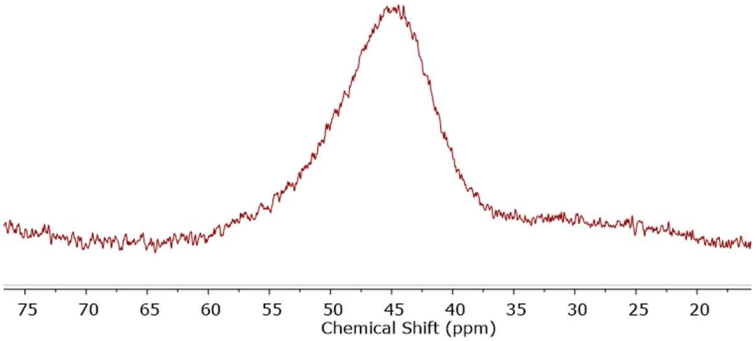

Figure S4.27 ^{11}B NMR (C_6D_6, 116 MHz, 298 K) of *cis*-**4.3**

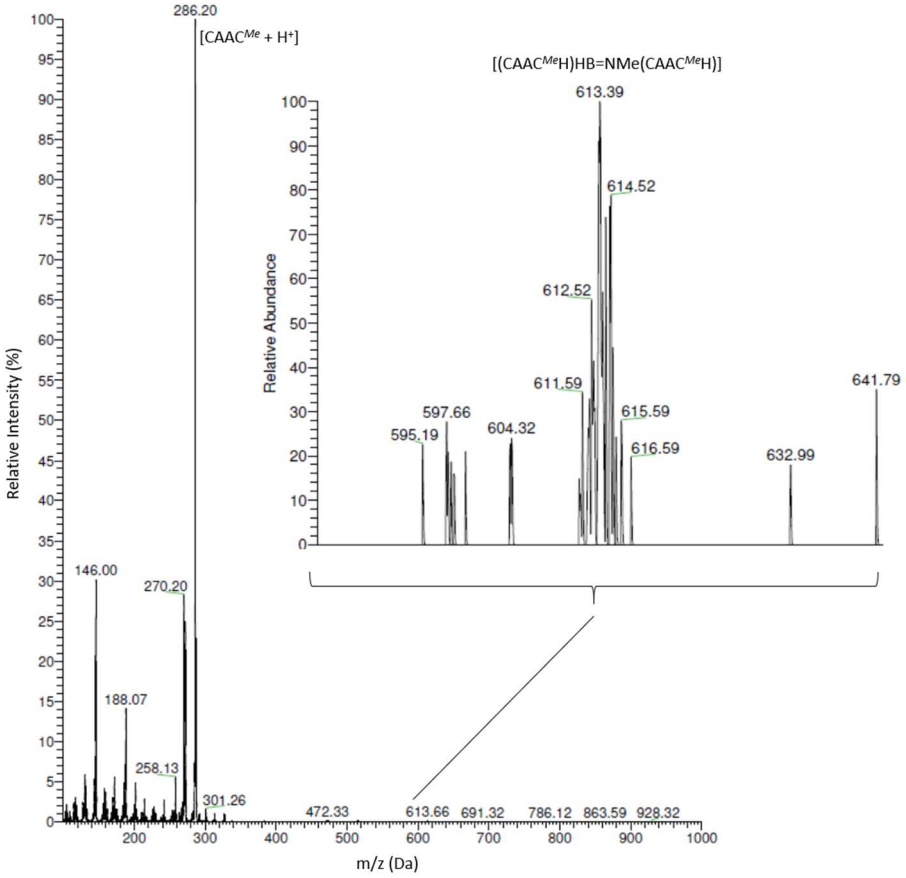

Figure S4.28 EI mass spectrum (+) of *trans*-**4.3**

4.6.7 Reaction of $[MeHN–BH_2]_n$ with stoichiometric $NMeH_2$

To a solution of $[MeHN–BH_2]_n$ (10 mg, 0.23 mmol) in THF (400 µL) was added $NMeH_2$ (117 µL, 0.233 mmol, 2 M in THF) at 22 °C. The reaction was monitored by ^{11}B NMR spectroscopy which over 24 h revealed depolymerisation to $(MeNH)_2BH$ (δ_B = 27.4 ppm (d)][24] (40 %), $[MeHN–BH_2]_{(3\ or\ x)}$ (39%), $MeNH_2{\cdot}BH_3$ [δ_B -19.0 ppm (q))[38] (6%) and an unidentified species (δ_B = 1.40 ppm).

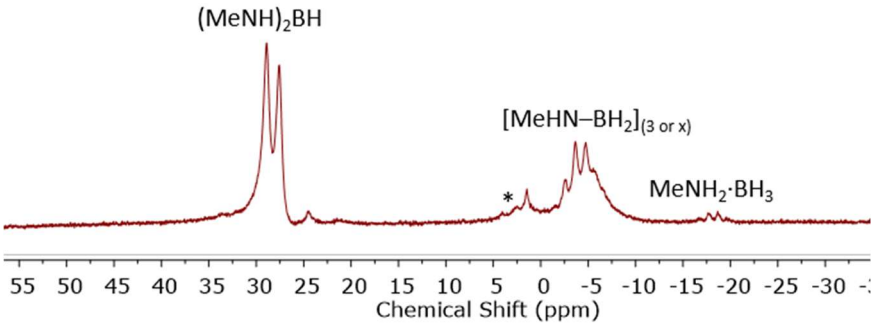

Figure S4.29 ^{11}B NMR spectra (THF, 96 MHz, 296 K) of the reaction mixture of $[MeHN–BH_2]_n$ and $MeNH_2$ after 24 h (*unidentified product)

4.6.8 Supplementary tables

4.6.5.2 X-ray crystallography

X-ray data for **4.1** was carried out on a Bruker Microstar rotating anode diffractometer using Cu Kα radiation (λ = 1.54178) at 100 K. The data for *trans*-**4.3** was carried out on a Bruker Apex II diffractometer using MoKα radiation (λ = 0.71073) Å at 150 K and 90 K respectively. The data collections were performed using a CCD area detector from a single crystal mounted on a glass fibre. Intensities were integrated[51] and absorption corrections based on equivalent reflections using SADABS[52] were applied. The structures were solved by the dual-space algorithm SHELXT[53] and refined against all F^2 in ShelXL[54] using Olex2.[55] All the non-hydrogen atoms were refined anisotropically.

Hydrogen atoms bound to N1 and B1 in **4.1** were located directly from the electron density map, while all other hydrogen atoms were calculated geometrically and refined using a riding model. Although the refinement of **4.1** was not ideal as there is most likely further disorder which cannot be sensibly modelled, the refinement does confirm the anticipated structure.

The H atom bound to B1 in *trans*-**4.3** was located directly from the electron density map, while other H-atoms were calculated geometrically and refined with the riding model. Disordered portions of CAAC-derived moieties in the structure of *trans*-**4.3** have the sum of the occupancies equal to 1.

Table S4.3 Selected crystallographic data for **4.1** and *trans*-**4.3**.

Compound	**4.1**	*trans*-**4.3**
Crystal colour	colourless	colourless
Empirical formula	$C_{28}H_{42}BN_3$	$C_{41}H_{68}BN_3$
Formula weight	431.45	613.79
Temperature/K	100(2)	150(2)
Crystal system	monoclinic	triclinic
Space group	*C*2/c	*P*-1
a/Å	32.148(2)	10.207(2)
b/Å	7.1932(5)	12.142(3)
c/Å	24.0752(16)	16.578(4)
α/°	90	84.428(15)
β/°	91.149(3)	78.013(14)
γ/°	90	71.931(12)
Volume/Å^3	5566.3(7)	1909.4(8)
Z	8	2
ρ_{calc}g/cm^3	1.030	1.068
μ/mm^{-1}	0.446	0.061
F(000)	1888.0	680
Radiation	CuKα (λ = 1.54178)	MoKα (λ = 0.71073)
2Θ range for data collection/°	5.498 - 133.418	1.765 − 27.881
Reflections collected	15989	30873
Independent reflections	4832	30873
Goodness-of-fit on F^2	1.359	1.033
Final R indexes [I>=2σ (I)]	R_1 = 0.1084 wR_2 = 0.2912	R_1 = 0.0725 wR_2 = 0.1925
Final R indexes [all data]	R_1 = 0.1142 wR_2 = 0.3043	R_1 = 0.1159 wR_2 = 0.2178
Largest diff. peak/hole / e Å^{-3}	0.90/-0.45	0.720/ -0.510

4.6.9 Supplementary data

4.6.5.2 Cartesian coordinates and SCF energies of the calculated structures

All calculations were performed using the Gaussian 09 suite.[56] Energy values were calculated in the gas phase using the hybrid exchange-correlation functional PBE0[57,58] in combination with the split-valence double-ζ basis set 6-31+G(d,p).[59–64] All stationary points were confirmed as a minimum by the lack of imaginary frequencies.

***Cis*-4.2; E_H = -955.75816717**

B	-2.60653	-0.14278	-0.80824
H	-3.30412	0.80627	-0.87944
N	-0.66362	-0.01478	0.25811
C	0.01101	-1.31978	0.20569
H	0.18156	-1.59238	-0.81486
H	0.94746	-1.25809	0.71965
H	-0.60492	-2.05877	0.6741
C	-3.07514	-1.56498	-1.50125
C	-4.15932	-2.2325	-0.66757
H	-2.16804	-2.21805	-1.55665
C	-5.35413	-2.49227	-1.57367
C	-5.05804	-1.86744	-2.92952
H	-5.52791	-3.59256	-1.68225
H	-6.28458	-2.05429	-1.13334

N	-3.63824	-1.32018	-2.89407
C	-3.99121	-1.45501	-4.31467
C	-3.59726	-2.58823	-5.02678
C	-4.72006	-0.45013	-4.95071
C	-3.93155	-2.71614	-6.37478
C	-5.05537	-0.57838	-6.29887
C	-4.66114	-1.71108	-7.01098
H	-3.62052	-3.60904	-6.93629
H	-5.6304	0.2139	-6.79998
H	-4.92465	-1.81218	-8.07383
C	-6.06027	-0.73741	-3.22981
H	-5.53992	0.19603	-3.28297
H	-6.54478	-0.92939	-4.16431
H	-6.79247	-0.69372	-2.45078
C	-5.20622	-2.91379	-4.04969
H	-5.36182	-2.41632	-4.98414
H	-4.31667	-3.50589	-4.10462
H	-6.04313	-3.54619	-3.8386
C	-3.64227	-3.55073	-0.06214
H	-3.29744	-3.37406	0.93525
H	-4.43459	-4.26961	-0.04351
H	-2.83555	-3.92442	-0.6575
C	-4.56621	-1.3236	0.50713
H	-3.77143	-1.28825	1.22266
H	-4.76259	-0.33676	0.14315
H	-5.44733	-1.71428	0.97179
C	-5.15524	0.80072	-4.16483
H	-4.72338	0.77521	-3.18618
C	-6.6906	0.8251	-4.04792
H	-6.97033	0.78848	-3.01578
H	-7.06756	1.72466	-4.48792
H	-7.10068	-0.02089	-4.55882
C	-4.6766	2.06388	-4.90437
H	-4.73027	2.90499	-4.24517
H	-3.66542	1.92704	-5.22637
H	-5.30156	2.23726	-5.75541
C	-2.79164	-3.69695	-4.32442
H	-1.86259	-3.29654	-3.97594
C	-2.51708	-4.84038	-5.31879
H	-1.95711	-4.46405	-6.14929
H	-1.95721	-5.61067	-4.83083
H	-3.44613	-5.24088	-5.66716
C	-3.59773	-4.23854	-3.12922
H	-3.03517	-5.0043	-2.63724
H	-3.79421	-3.44269	-2.44154
H	-4.52389	-4.64495	-3.47846
H	-0.30313	0.80397	0.70499

***Trans*-4.2; E_H = -955.76102151**

B	-2.60653	-0.14278	-0.80824
H	-2.66291	0.09597	-1.96246
N	-0.66362	-0.01478	0.25811
C	0.38905	0.38341	-0.68753
H	0.14899	1.33793	-1.10726
H	1.32549	0.4451	-0.17357
H	0.45887	-0.34296	-1.4701
C	-3.97174	-0.57176	0.01314
C	-4.85409	0.64479	0.25293
H	-3.64369	-1.01389	0.98746
C	-6.2358	0.33946	-0.30715
C	-6.16916	-1.00991	-1.00798
H	-6.99234	0.31247	0.51721
H	-6.55628	1.13846	-1.02154
N	-4.77832	-1.58643	-0.78487
C	-5.63554	-2.71778	-1.16711
C	-6.19361	-3.53384	-0.1827
C	-5.89112	-2.97539	-2.51391
C	-7.00651	-4.60765	-0.54512
C	-6.70504	-4.04889	-2.87657
C	-7.26263	-4.86509	-1.89246
H	-7.44591	-5.2513	0.23073
H	-6.90671	-4.25152	-3.93853
H	-7.90365	-5.71177	-2.17798
C	-6.44592	-0.84645	-2.51406
H	-5.57117	-1.11503	-3.06866
H	-7.2579	-1.48255	-2.79859
H	-6.70098	0.17182	-2.72137
C	-7.24438	-1.96107	-0.45049
H	-7.43846	-2.73623	-1.16209
H	-6.89724	-2.39504	0.46387
H	-8.14452	-1.41281	-0.26592
C	-4.93816	0.96478	1.75697
H	-4.21848	1.71765	2.00222
H	-5.91986	1.31981	1.99175
H	-4.73457	0.0792	2.32195
C	-4.2572	1.88335	-0.44083
H	-3.37014	2.18784	0.07424
H	-4.01583	1.64242	-1.45503
H	-4.97092	2.68035	-0.42374
C	-5.27543	-2.0746	-3.6007
H	-4.6032	-1.37673	-3.14683
C	-6.39609	-1.30894	-4.32836
H	-6.2554	-0.25691	-4.19291
H	-6.36693	-1.54117	-5.37245
H	-7.34457	-1.59675	-3.92531
C	-4.50658	-2.94387	-4.61304
H	-3.86211	-2.32282	-5.19943
H	-3.92151	-3.66974	-4.08797

H	-5.20193	-3.44303	-5.25509
C	-5.9103	-3.2497	1.30411
H	-4.85975	-3.33312	1.4893
C	-6.66761	-4.26934	2.17498
H	-6.3402	-5.25864	1.93211
H	-6.47066	-4.072	3.20802
H	-7.71817	-4.18582	1.98989
C	-6.38167	-1.82586	1.65352
H	-6.17878	-1.62604	2.68493
H	-5.86027	-1.11786	1.04378
H	-7.43345	-1.74439	1.47462
H	-0.52584	-0.19943	1.23121

***Cis*-4.3 E_H = -1790.30222930**

B	-2.60653	-0.14278	-0.80824
H	-2.66291	0.09597	-1.96246
N	-0.66362	-0.01478	0.25811
C	0.38905	0.38341	-0.68753
H	0.14899	1.33793	-1.10726
H	1.32549	0.4451	-0.17357
H	0.45887	-0.34296	-1.4701
C	-0.33383	-1.32613	0.83475
C	-1.01232	-1.50106	2.18605
H	-0.69482	-2.10223	0.11382
C	1.24938	-1.73736	2.53696
C	0.06873	-1.7707	3.22298
H	-0.123	-2.74037	3.74714
H	0.06796	-0.9688	4.00359
N	1.16815	-1.45406	1.04391
C	2.49372	-2.06694	0.87616
C	3.64499	-1.30475	1.07642
C	2.60057	-3.41047	0.5169
C	4.90279	-1.88586	0.91677
C	3.85868	-3.99217	0.35813
C	5.00971	-3.23009	0.55786
H	5.81027	-1.28499	1.07399
H	3.94262	-5.05161	0.07527
H	6.00155	-3.68807	0.4321
C	3.52654	0.17885	1.47201
H	3.15916	0.25251	2.47426
C	1.32992	-4.25206	0.29604
H	0.79072	-4.33225	1.21676
C	4.9116	0.84611	1.38264
H	4.81587	1.89399	1.57673
H	5.56613	0.40761	2.10666
H	5.31515	0.70034	0.40243
C	2.55179	0.8892	0.51447
H	2.36487	0.26342	-0.33309
H	1.63109	1.08492	1.02329
H	2.98216	1.8128	0.18791
C	0.44113	-3.57187	-0.76178
H	-0.52847	-3.38814	-0.34823
H	0.88464	-2.64395	-1.05701
H	0.34967	-4.21093	-1.6151
C	1.72411	-5.65843	-0.19215
H	2.31619	-6.14275	0.55603
H	0.84033	-6.23325	-0.37494
H	2.2897	-5.57645	-1.09675
C	2.18455	-0.72882	3.2297
H	3.20115	-1.03415	3.09474
H	2.04354	0.24122	2.80071
H	1.95874	-0.69281	4.27498
C	1.83387	-3.14048	2.78435
H	1.26627	-3.86468	2.23822
H	2.85241	-3.16529	2.45747
H	1.78904	-3.36638	3.82928
C	-1.80932	-0.23654	2.55669
H	-2.81743	-0.33663	2.21234
H	-1.80615	-0.11166	3.61938
H	-1.35813	0.61727	2.09589
C	-2.01461	-2.6692	2.13655
H	-2.76854	-2.52409	2.88183
H	-2.47139	-2.70651	1.16967
H	-1.50031	-3.58863	2.32377
C	-3.97174	-0.57176	0.01314
C	-4.85409	0.64479	0.25293
H	-3.64369	-1.01389	0.98746
C	-6.2358	0.33946	-0.30715
C	-6.16916	-1.00991	-1.00798
H	-6.99234	0.31247	0.51721
H	-6.55628	1.13846	-1.02154
N	-4.77832	-1.58643	-0.78487
C	-5.63554	-2.71778	-1.16711
C	-6.19361	-3.53384	-0.1827
C	-5.89112	-2.97539	-2.51391
C	-7.00651	-4.60765	-0.54512
C	-6.70504	-4.04889	-2.87657
C	-7.26263	-4.86509	-1.89246
H	-7.44591	-5.2513	0.23073
H	-6.90671	-4.25152	-3.93853
H	-7.90365	-5.71177	-2.17798
C	-6.44592	-0.84645	-2.51406
H	-5.57117	-1.11503	-3.06866
H	-7.2579	-1.48255	-2.79859
H	-6.70098	0.17182	-2.72137
C	-7.24438	-1.96107	-0.45049
H	-7.43846	-2.73623	-1.16209
H	-6.89724	-2.39504	0.46387
H	-8.14452	-1.41281	-0.26592
C	-4.93816	0.96478	1.75697
H	-4.21848	1.71765	2.00222

H	-5.91986	1.31981	1.99175
H	-4.73457	0.0792	2.32195
C	-4.2572	1.88335	-0.44083
H	-3.37014	2.18784	0.07424
H	-4.01583	1.64242	-1.45503
H	-4.97092	2.68035	-0.42374
C	-5.27543	-2.0746	-3.6007
H	-4.6032	-1.37673	-3.14683
C	-6.39609	-1.30894	-4.32836
H	-6.2554	-0.25691	-4.19291
H	-6.36693	-1.54117	-5.37245
H	-7.34457	-1.59675	-3.92531
C	-4.50658	-2.94387	-4.61304
H	-3.86211	-2.32282	-5.19943
H	-3.92151	-3.66974	-4.08797
H	-5.20193	-3.44303	-5.25509
C	-5.9103	-3.2497	1.30411
H	-4.85975	-3.33312	1.4893
C	-6.66761	-4.26934	2.17498
H	-6.3402	-5.25864	1.93211
H	-6.47066	-4.072	3.20802
H	-7.71817	-4.18582	1.98989
C	-6.38167	-1.82586	1.65352
H	-6.17878	-1.62604	2.68493
H	-5.86027	-1.11786	1.04378

***Trans*-4.3 E_H = -1790.30641009**

B	-2.30853	-0.35945	-0.00574
H	-2.76679	0.62424	0.45768
N	-0.74416	-0.58104	0.
C	-0.42977	-1.87163	-0.62963
H	-0.78643	-1.87261	-1.63843
H	0.62965	-2.0217	-0.62574
H	-0.90368	-2.66	-0.08301
C	-0.25416	-0.5797	1.38593
C	-0.88731	0.55761	2.17498
H	-0.53217	-1.56693	1.83366
C	1.39144	0.85959	2.27679
C	0.23317	1.43061	2.72178
H	0.16442	1.50565	3.83596
H	0.14982	2.47026	2.3161
N	1.25538	-0.38909	1.41751
C	2.64112	-0.74656	1.75347
C	3.69777	-0.21242	1.01546
C	2.89965	-1.61964	2.81008
C	5.01259	-0.55186	1.33364
C	4.21486	-1.95851	3.12912
C	5.27129	-1.42491	2.39104
H	5.84547	-0.13138	0.75159
H	4.41842	-2.6466	3.96253
H	6.30806	-1.69236	2.64176
C	3.41181	0.75065	-0.15173
H	3.05322	1.68204	0.23404
C	1.73348	-2.20917	3.62501
H	1.22113	-1.42097	4.13603
C	4.70745	0.98996	-0.94899
H	4.49223	1.59196	-1.807
H	5.41961	1.49376	-0.32937
H	5.11075	0.05046	-1.26454
C	2.3463	0.13388	-1.07688
H	2.22161	-0.90136	-0.83681
H	1.41663	0.64596	-0.94126
H	2.66035	0.22851	-2.09537
C	0.75538	-2.92674	2.67631
H	-0.22284	-2.50814	2.78927
H	1.08245	-2.8013	1.66528
H	0.72696	-3.96933	2.91524
C	2.2828	-3.21554	4.65314
H	2.93868	-2.71061	5.3312
H	1.47002	-3.64788	5.19846
H	2.82138	-3.98738	4.14412
C	2.21188	1.93606	1.54217
H	3.25518	1.72347	1.64816
H	1.9516	1.93642	0.50431
H	1.99893	2.89623	1.96362
C	2.14025	0.532	3.582
H	1.65358	-0.28179	4.07778
H	3.1497	0.2591	3.3552
H	2.13775	1.39107	4.21988
C	-1.82169	1.38483	1.27262
H	-2.81608	0.99486	1.33611
H	-1.81746	2.40514	1.59488
H	-1.48076	1.32923	0.25992
C	-1.74613	0.00022	3.32534
H	-2.50075	0.71304	3.58483
H	-2.20964	-0.91268	3.01443
H	-1.1247	-0.18699	4.17604
C	-3.30143	-1.50353	-0.65974
C	-4.62788	-1.547	0.08505
H	-2.77273	-2.48601	-0.57262
C	-5.74341	-1.35819	-0.93279
C	-5.10185	-1.06707	-2.28188
H	-6.37473	-2.28036	-0.9934
H	-6.41651	-0.51834	-0.62776
N	-3.59317	-1.18589	-2.11951
C	-3.86175	-1.30201	-3.5601
C	-3.95417	-2.56147	-4.15312
C	-4.0243	-0.1531	-4.33414
C	-4.20843	-2.67191	-5.52001
C	-4.27961	-0.26341	-5.70128
C	-4.37156	-1.52254	-6.29431

H	-4.28067	-3.66459	-5.98762
H	-4.40814	0.64262	-6.31125
H	-4.57208	-1.60986	-7.37202
C	-5.47921	0.34687	-2.76143
H	-4.59898	0.95312	-2.81196
H	-5.92712	0.28686	-3.73131
H	-6.17373	0.78306	-2.07419
C	-5.61062	-2.05711	-3.34611
H	-5.46093	-1.64132	-4.32059
H	-5.07083	-2.97734	-3.2642
H	-6.65359	-2.24055	-3.19296
C	-4.7904	-2.88842	0.82382
H	-4.47894	-2.77531	1.84122
H	-5.81706	-3.18862	0.79638
H	-4.18811	-3.63337	0.34716
C	-4.68042	-0.43486	1.14899
H	-4.00729	-0.67188	1.94625
H	-4.3948	0.49631	0.706
H	-5.67567	-0.35628	1.53396
C	-3.92256	1.23722	-3.67974
H	-3.62075	1.12968	-2.65884
C	-5.29466	1.93398	-3.73872
H	-5.63858	2.1292	-2.74448
H	-5.20334	2.85699	-4.27221
H	-5.99542	1.29985	-4.24045
C	-2.88313	2.08558	-4.4357
H	-2.61068	2.93092	-3.83899
H	-2.01421	1.49301	-4.63252
H	-3.30229	2.42224	-5.36082
C	-3.77357	-3.82967	-3.29833
H	-2.79216	-3.8357	-2.87205
C	-3.95614	-5.07609	-4.18416
H	-3.22716	-5.06693	-4.96736
H	-3.83052	-5.95724	-3.59027
H	-4.93759	-5.07013	-4.61032
C	-4.82288	-3.84276	-2.17122
H	-4.69316	-4.72059	-1.57332
H	-4.70028	-2.97336	-1.55966
H	-5.80427	-3.84343	-2.59778

References

(1) Jäkle, F.; Vidal, F. Functional Polymeric Materials Based on Main Group Elements. *Angew. Chem. Int. Ed.* **2018**, *58*, 5846 –5870.

(2) Priegert, A. M.; Rawe, B. W.; Serin, S. C.; Gates, D. P. Polymers and the p-Block Elements. *Chem. Soc. Rev.* **2016**, *45*, 922–953.

(3) Dorn, H.; Singh, R. A.; Massey, J. A.; Lough, A. J.; Manners, I. Rhodium-Catalyzed Formation of Phosphorus-Boron Bonds: Synthesis of the First High Molecular Weight Poly(Phosphinoborane). *Angew. Chem. Int. Ed.* **1999**, *38*, 3321–3323.

(4) Staubitz, A.; Soto, A. P.; Manners, I. Iridium-Catalyzed Dehydrocoupling of Primary Amine-Borane Adducts: A Route to High Molecular Weight Polyaminoboranes, Boron-Nitrogen Analogues of Polyolefins. *Angew. Chem. Int. Ed.* **2008**, *47*, 6212–6215.

(5) Staubitz, A.; Hoffmann, J.; Gliese, P. Boron-Containing Polymers: Group 13 – Group 15 Element Bonds Replacing Carbon – Carbon Bonds in Main Group Polyolefin Analogs. In *Smart Inorganic Polymers: Synthesis, Properties, and Emerging Applications in Materials and Life Sciences*; 2019; pp 17–39.

(6) Glüer, A.; Förster, M.; Celinski, V. R.; Schmedt Auf Der Günne, J.; Holthausen, M. C.; Schneider, S. Highly Active Iron Catalyst for Ammonia Borane Dehydrocoupling at Room Temperature. *ACS Catal.* **2015**, *5*, 7214–7217.

(7) Adams, G. M.; Ryan, D. E.; Beattie, N. A.; Mckay, A. I.; Lloyd-Jones, G. C.; Weller, A. S. Dehydropolymerization of $H_3B{\cdot}NMeH_2$ Using a $[Rh(DPEphos)]^+$ Catalyst: The Promoting Effect of $NMeH_2$. *ACS Catal.* **2019**, *9*, 3657–3666.

(8) Anke, F.; Han, D.; Klahn, M.; Spannenberg, A.; Beweries, T. Formation of High-Molecular Weight Polyaminoborane by Fe Hydride Catalysed Dehydrocoupling of Methylamine Borane. *Dalton Trans.* **2017**, *46*, 6843–6847.

(9) De Albuquerque Pinheiro, C. A.; Roiland, C.; Jehan, P.; Alcaraz, G. Solventless and Metal-Free Synthesis of High-Molecular-Mass Polyaminoboranes from Diisopropylaminoborane and Primary Amines. *Angew. Chem. Int. Ed.* **2018**, *57*, 1519–1522.

(10) Cavaye, H.; Clegg, F.; Gould, P. J.; Ladyman, M. K.; Temple, T.; Dossi, E. Primary Alkylphosphine-Borane Polymers: Synthesis, Low Glass Transition Temperature, and a Predictive Capability Thereof. *Macromolecules* **2017**, *50*, 9239–9248.

(11) Marquardt, C.; Jurca, T.; Schwan, K. C.; Stauber, A.; Virovets, A. V.; Whittell, G. R.; Manners, I.; Scheer, M. Metal-Free Addition/Head-to-Tail Polymerization of Transient Phosphinoboranes, $RPH{-}BH_2$: A Route to Poly(Alkylphosphinoboranes). *Angew. Chem. Int. Ed.* **2015**, *54*, 13782–13786.

(12) Schäfer, A.; Jurca, T.; Turner, J.; Vance, J. R.; Lee, K.; Du, V. A.; Haddow, M. F.; Whittell, G. R.; Manners, I. Iron-Catalyzed Dehydropolymerization: A Convenient Route to Poly(Phosphinoboranes) with Molecular-Weight Control. *Angew. Chem. Int. Ed.* **2015**, *54*, 4836–4841.

(13) Oldroyd, N. L.; Manners, I.; Chitnis, S. S.; Annibale, V. T.; Arz, M. I.; Sparkes, H. A. Metal-Free Dehydropolymerisation of Phosphine-Boranes Using Cyclic (Alkyl)(Amino)Carbenes as Hydrogen Acceptors. *Nat. Commun.* **2019**, *10*, 1370–1379.

(14) Hamilton, C. W.; Baker, R. T.; Staubitz, A.; Manners, I. B-N Compounds for Chemical Hydrogen Storage. *Chem. Soc. Rev.* **2009**, *38*, 279–293.

(15) Staubitz, A.; Robertson, A. P. M.; Sloan, M. E.; Manners, I. Amine- and Phosphine-Borane Adducts: New Interest in Old Molecules. *Chem. Rev.* **2010**, *110*, 4023–4078.

(16) Du, V. A.; Jurca, T.; Whittell, G. R.; Manners, I. Aluminum Borate Nanowires from the Pyrolysis of Polyaminoborane Precursors. *Dalton Trans.* **2016**, *45*, 1055–1062.

(17) Wang, X.; Hooper, T. N.; Kumar, A.; Priest, I. K.; Sheng, Y.; Samuels, T. O. M.; Wang, S.; Robertson, A. W.; Pacios, M.; Bhaskaran, H.; et al. Oligomeric Aminoborane Precursors for the Chemical Vapour Deposition Growth of Few-Layer Hexagonal Boron Nitride. *Cryst. Eng. Comm.* **2017**, *19*, 285–294.

(18) Nakhmanson, S. M.; Nardelli, M. B.; Bernholc, J. Ab Initio Studies of Polarization and Piezoelectricity in Vinylidene Fluoride and BN-Based Polymers. *Phys. Rev. Lett.* **2004**, *92*, 1–4.

(19) Priegert, A. M.; Siu, P. W.; Hu, T. Q.; Gates, D. P. Flammability Properties of Paper Coated with Poly(Methylenephosphine), an Organophosphorus Polymer. *Fire Mater.* **2015**, *39*, 647–657.

(20) Clark, T. J.; Rodezno, J. M. J. M.; Clendenning, S. B.; Aouba, S.; Brodersen, P. M.; Lough, A. J.; Ruda, H. E.; Manners, I. Rhodium-Catalyzed Dehydrocoupling of Fluorinated Phosphine–Borane Adducts: Synthesis, Characterization, and Properties of Cyclic and Polymeric Phosphinoboranes with Electron-Withdrawing Substituents at Phosphorus. *Chem. Eur. J.* **2005**, *5*, 4526–4534.

(21) Christensen, P. R.; Scheuermann, A. M.; Loeffler, K. E.; Helms, B. A. Closed-Loop Recycling of Plastics Enabled by Dynamic Covalent Diketoenamine Bonds. *Nat. Chem.* **2019**, *11*, 442–448.

(22) Zhu, J. B.; Watson, E. M.; Tang, J.; Chen, E. Y. X. A Synthetic Polymer System with Repeatable Chemical Recyclability. *Science* **2018**, *360* (6387), 398–403.

(23) Lu, X.-B.; Liu, Y.; Zhou, H. Learning Nature: Recycable Monomers and Polymers. *Chem. Eur. J.* **2018**, 11255 – 11266.

(24) Stubbs, N. E.; Jurca, T.; Leitao, E. M.; Woodall, C. H.; Manners, I. Polyaminoborane Main Chain Scission Using N-Heterocyclic Carbenes; Formation of Donor-Stabilised Monomeric Aminoboranes. *Chem. Commun.* **2013**, *49*, 9098–9100.

(25) Marquardt, C.; Hegen, O.; Vogel, A.; Stauber, A.; Bodensteiner, M.; Stauber, A.; Bodensteiner, M.; Timoshkin, A. Y.; Scheer, M. Depolymerization of Poly(Phosphinoboranes): From Polymers to Lewis Base Stabilized Monomers. *Chem. Eur. J.* **2018**, *24*, 360–363.

(26) Wiley, J.; Sons. Depolymerization. *Encyclopedia of Polymer Science and Technology*; 2007; pp 1–26.

(27) Melaimi, M.; Jazzar, R.; Soleilhavoup, M.; Bertrand, G. Cyclic (Alkyl)(Amino)Carbenes (CAACs): Recent Developments. *Angew. Chem. Int. Ed.* **2017**, *56*, 10046–10068.

(28) Metters, O. J.; Chapman, A. M.; Robertson, A. P. M.; Woodall, C. H.; Gates, P. J.; Wass, D. F.; Manners, I. Generation of Aminoborane Monomers RR'N=BH2 from Amine-Boronium Cations $[RR'NH\text{-}BH_2L]^+$: Metal Catalyst-Free Formation of Polyaminoboranes at Ambient Temperature. *Chem. Commun.* **2014**, *50*, 12146–12149.

(29) Wang, Y.; Quillian, B.; Wei, P.; Wannere, C. S.; Xie, Y.; King, R. B.; Schaefer, H. F.; Schleyer, P. V. R.; Robinson, G. H. A Stable Neutral Diborene Containing a B=B Double Bond. *J. Am. Chem. Soc.* **2007**, *129*, 12412–12413.

(30) Al-Rafia, S. M. I.; McDonald, R.; Ferguson, M. J.; Rivard, E. Preparation of Stable Low-Oxidation-State Group 14 Element Amidohydrides and Hydride-Mediated Ring-Expansion Chemistry of N-Heterocyclic Carbenes. *Chem. Eur. J.* **2012**, *18*, 13810–13820.

(31) Aldridge, S.; Downs, A. J.; Tang, C. Y.; Parsons, S.; Clarke, M. C.; Johnstone, R. D. L.; Robertson, H. E.; Rankin, D. W. H.; Wann, D. a. Structures and Aggregation of the Methylamine-Borane Molecules, $Me_nH_{3-n}N{\cdot}BH_3$ (n = 1-3), Studied by X-Ray Diffraction, Gas-Phase Electron Diffraction, and Quantum Chemical Calculations. *J. Am. Chem. Soc.* **2009**, *131*, 2231–2243.

(32) Paetzold, P. New Perspectives in Boron-Nitrogen Chemistry. *Pure Appl. Chem.* **1991**, *63*, 345–350.

(33) Narula, C. K.; Janik, J. F.; Duesler, E. N.; Paine, R. T.; Schaeffer, R. Convenient Synthesis, Separation, and X-Ray Crystal Structure Determinations of 1(e),3(e),5(e)-Trimethylcycloborazane and 1(e),3(e),5(a)-Trimethylcycloborazane. *Inorg. Chem.* **1986**, *25*, 3346–3349.

(34) Framery, E.; Vaultier, M. Efficient Synthesis and NMR Data of N- or B-Substituted Borazines. *Heteroat. Chem.* **2000**, *11*, 218–225.

(35) Runyon, J. W.; Steinhof, O.; Dias, H. V. R.; Calabrese, J. C.; Marshall, W. J.; Arduengo, A. J. Carbene-Based Lewis Pairs for Hydrogen Activation. *Aust. J. Chem.* **2011**, *64*, 1165–1172.

(36) Frey, G. D.; Lavallo, V.; Donnadieu, B.; Schoeller, W. W.; Bertrand, G. Facile Splitting of Hydrogen and Ammonia by Nucleophilic Activation at a Single Carbon Center. *Science* **2007**, *316*, 439–442.

(37) $CAAC^{Me}$–BH_3 was identified by comparing the ^{11}B chemical shift to that of the product of an independant reaction between $CAAC^{Me}$ and BH_3·THF.

(38) Jaska, C. A.; Temple, K.; Lough, A. J.; Manners, I. Transition Metal-Catalyzed Formation of Boron-Nitrogen Bonds: Catalytic Dehydrocoupling of Amine-Borane Adducts to Form Aminoboranes and Borazines. *J. Am. Chem. Soc.* **2003**, *125*, 9424–9434.

(39) It was not possible to integrate the $[MeNBH]_3$ peak directly against the polymer peak as polymers do not give accurate NMR integrals. Additionally, there is a degree in error in the absolute values which most likely results from weighing errors.

(40) Robertson, A. P. M.; Leitao, E. M.; Jurca, T.; Haddow, M. F.; Helten, H.; Lloyd-Jones, G. C.; Manners, I. Mechanisms of the Thermal and Catalytic Redistributions, Oligomerizations, and Polymerizations of Linear Diborazanes. *J. Am. Chem. Soc.* **2013**, *135*, 12670–12683.

(41) Colebatch, A. L.; Weller, A. S. Amine-Borane Dehydropolymerization: Challenges and Opportunities. *Chem. Eur. J.* **2019**, *25*, 1379–1390.

(42) Sabourin, K. J.; Malcolm, A. C.; Mcdonald, R.; Ferguson, M. J.; Rivard, E. Metal-Free Dehydrogenation of Amine–boranes by an N-Heterocyclic Carbene. *Dalton Trans.* **2013**, *42*, 4625–4632.

(43) Stubbs, N. E.; Schäfer, A.; Robertson, A. P. M. M.; Leitao, E. M.; Jurca, T.; Sparkes, H. A.; Woodall, C. H.; Haddow, M. F.; Manners, I. B-Methylated Amine-Boranes: Substituent Redistribution, Catalytic Dehydrogenation, and Facile Metal-Free Hydrogen Transfer Reactions. *Inorg. Chem.* **2015**, *54* (22), 10878–10889.

(44) Staubitz, A.; Sloan, M. E.; Robertson, A. P. M.; Friedrich, A.; Schneider, S.; Gates, P. J.; Manners, I.; Schmedt auf der Günne, J. Catalytic Dehydrocoupling/Dehydrogenation of N-Methylamine-Borane and Ammonia-Borane: Synthesis and Characterization of High Molecular Weight Polyaminoboranes. *J. Am. Chem. Soc.* **2010**, *132*, 13332–13345.

(45) Leitao, E. M.; Stubbs, N. E.; Robertson, A. P. M.; Helten, H.; Cox, R. J.; Lloyd-Jones, G. C.; Manners, I. Mechanism of Metal-Free Hydrogen Transfer between Amine-Boranes and Aminoboranes. *J. Am. Chem. Soc.* **2012**, *134*, 16805–16816.

(46) Metters, O. J.; Arz, M. I.; Musgrave, R. A.; Sparkes, H. A.; Duncan, F. Metal-Free Synthesis, Decomposition and Trapping of the Primary Aminoborane. *Manuscript in Preparation*.

(47) Pangborn, A. B.; Giardello, M. A.; Grubbs, R. H.; Rosen, R. K.; Timmers, F. J. Safe and Convenient Procedure for Solvent Purification. *Organometallics* **1996**, *15*, 1518–1520.

(48) Jafarpour, L.; Stevens, E. D.; Nolan, S. P. A Sterically Demanding Nucleophilic Carbene: 1,3-Bis(2,6-Diisopropylphenyl)Imidazol-2-Ylidene). Thermochemistry and Catalytic Application in Olefin Metathesis. *J. Organomet. Chem.* **2000**, *606*, 49–54.

(49) Scott, N. M.; Dorta, R.; Stevens, E. D.; Correa, A.; Cavallo, L.; Nolan, S. P. Interaction of a Bulky N-Heterocyclic Carbene Ligand with Rh(I) and Ir(I). Double C-H Activation and Isolation of Bare 14-Electron Rh(III) and Ir(III) Complexes. *J. Am. Chem. Soc.* **2005**, *127*, 3516–3526.

(50) Jazzar, R.; Dewhurst, R. D.; Bourg, J. B.; Donnadieu, B.; Canac, Y.; Bertrand, G. Intramolecular "Hydroiminiumation" of Alkenes: Application to the Synthesis of Conjugate Acids of Cyclic Alkyl Amino Carbenes (CAACs). *Angew. Chem. Int. Ed.* **2007**, *46*, 2899–2902.

(51) Bruker, SAINT+ v8.38A Integration Engine, Data Reduction Software, Bruker Analytical X-Ray Instruments Inc., Madison, WI, USA, 2015.

(52) Bruker, SADABS 2014/5, Bruker AXS Area Detector Scaling and Absorption Correction, Bruker Analytical X-Ray Instruments Inc., Madison, Wisconsin, USA, 2014/5.

(53) Sheldrick, G. M. SHELXT - Integrated Space-Group and Crystal-Structure Determination. *Acta Crystallogr. Sect. A Found. Crystallogr.* **2015**, *71*, 3–8.

(54) Sheldrick, G. M. Crystal Structure Refinement with SHELXL. *Acta Crystallogr. Sect. C Struct. Chem.* **2015**, *71*, 3–8.

(55) Dolomanov, O. V.; Bourhis, L. J.; Gildea, R. J.; Howard, J. A. K.; Puschmann, H. OLEX2: A Complete Structure Solution, Refinement and Analysis Program. *J. Appl. Crystallogr.* **2009**, *42*, 339–341.

(56) Frisch, M. J., Trucks, G. W., Schlegel, H. B., Scuseria, G. E., Robb, M. A., Cheeseman, J. R., Scalmani, G., Barone, V., Mennucci, B., Petersson, G. A., Nakatsuji, H., Caricato, M., Li, X., Hratchian, H. P., Izmaylov, A. F., Bloino, J., Zheng, G., Sonnenb.

(57) Adamo, C.; Barone, B. Toward Reliable Density Functional Methods without Adjustable Parameters: The PBE0 Model. *J. Chem. Phys.* **1999**, *110*, 6158–6170.

(58) Perdew, J. P.; Ernzerhof, M.; Burke, K. Rationale for Mixing Exact Exchange with Density Functional Approximations. *J. Chem. Phys.* **1996**, *105*, 9982–9985.

(59) Ditchfield, R.; Hehre, W. J.; Pople, J. A. Self-Consistent Molecular-Orbital Methods. IX. An Extended Gaussian-Type Basis for Molecular-Orbital Studies of Organic Molecules. *J. Chem. Phys.* **1971**, *54*, 724–728.

(60) Hehre, W. J.; Ditchfield, R.; Pople, J. A. Self-Consistent Molecular Orbital Methods. XII. Further Extensions of Gaussian-Type Basis Sets for Use in Molecular Orbital Studies of Organic Molecules. *J. Chem. Phys.* **1972**, *56*), 2257–2261.

(61) Hariharan, P. C.; Pople, J. A. Accuracy of AH n Equilibrium Geometries by Single Determinant Molecular Orbital Theory. *Mol. Phys.* **1974**, *27*, 209–214.

(62) Hariharan, P. C.; Pople, J. A. The Influence of Polarization Functions on Molecular Orbital Hydrogenation Energies. *Theor. Chem. Acc.* **1973**, *28*, 213–222.

(63) Gordon, M. S. The Isomers of Silacyclopropane. *Chem. Phys. Lett.* **1980**, *76*, 163–168.

(64) Francl, M. M.; Pietro, W. J.; Hehre, W. J.; Binkley, J. S.; Gordon, M. S.; DeFrees, J. A.; Pople, J. A. Self-consistent Molecular Orbital Methods. XXIII. A Polarization-type Basis Set for Second-row Elements. *J. Chem. Phys.* **1982**, *77*, 3654–3665.

Chapter 5
Extension of the substrate scope of the CAAC-mediated dehydropolymerisation of phosphine-boranes and studies of the reactivity of IDipp–BH_2NMeH

5.1 Introductory comments

This chapter consists of two quite different but short projects which extend the work reported in Chapters 2 and 4. Firstly, the extension of the substrate scope of the CAAC-mediated dehydropolymerisation of phosphine-boranes to $PEt_2H{\cdot}BH_3$, $MePhPH{\cdot}BH_3$ and $n Hex_2PH{\cdot}BH_3$ will be discussed together with efforts to synthesise the copolymers $[Ph_2P–BH_2]_n$-*r*-$[PhHP–BH_2]_m$. This will be followed by a section which describes reactivity of the carbene-aminoborane adduct IDipp–BH_2NMeH both thermally and upon the addition of Lewis bases.

5.2 Abstract

Cyclic (alkyl)(amino)carbenes (CAACs) have been reported to successfully dehydrogenate a series of phosphine-boranes, which subsequently undergo a head-to-tail polymerisation. Using this method the first examples of P-disubstituted polyphosphinoboranes were reported $[RR'P–BH_2]_n$ (R = R' = Ph; R = Ph, R' = Et), albeit with low isolated yields and only small quantities of high molar mass material. Herein we report the results of an extension of this methodology to three additional phosphine-boranes: *rac*-$Ph(Me)PH{\cdot}BH_3$, $Et_2PH{\cdot}BH_3$ and $n Hex_2PH{\cdot}BH_3$. With *rac*-$Ph(Me)PH{\cdot}BH_3$ and $n Hex_2PH{\cdot}BH_3$ a small quantity of high molar mass material is formed; however, no improvement on previously reported substrates is observed. The dehydrogenation of $Et_2PH{\cdot}BH_3$ results in insoluble, semi-crystalline $[Et_2P–BH_2]_n$. Attempts were made to prepare the copolymer $[Ph_2P–BH_2]_n$-*r*-$[PhHP–BH_2]_m$ from $PhPH_2{\cdot}BH_3$ and $Ph_2PH{\cdot}BH_3$; however, concomitant formation of the homopolymers $[Ph_2P–BH_2]_n$ and $[PhHP–BH_2]_n$ was detected.

The carbene-aminoborane adduct IDipp–BH_2NMeH was found to thermally either undergo a 5- to 6-membered ring-expansion reaction with boron being inserted into the C–N bond of

the N-heterocyclic carbene (NHC) giving [(HCNDipp)$_2$CH$_2$BNHMe] (**5.2**) or converting into IDipp–BH$_2$·NMeBH·NMeH (**5.3**). The product distribution has a dependence on reaction temperature, concentration and solvent polarity.

Attempts were made to regenerate [MeHN–BH$_2$]$_n$ from IDipp–BH$_2$NMeH by releasing the monomer MeHN=BH$_2$ using the Lewis acids Cl$_2$B=NPh$_2$, BCl$_3$ or B(C$_6$F$_5$)$_3$ to abstract the carbene. This, however, proved to be unsuccessful and was not a feasible strategy for regenerating [MeHN–BH$_2$]$_n$.

5.3 Extension of the substrate scope of the CAAC-mediated dehydropolymerisation of phosphine-boranes

5.3.1 Introduction

The polymerisation of P-disubstituted phosphine-boranes using a CAAC-mediated dehydrogenation route was discussed in Chapter 2.[1] Although this method allowed access to the first examples of high molar mass P-disubstituted polyphosphinoboranes [PhEtP–BH$_2$]$_n$ and [Ph$_2$P–BH$_2$]$_n$, there were a number of drawbacks. The isolated yields were low as a significant amount of oligomeric material was formed which was removed through precipitation into hexanes, and in each case GPC analysis showed a bimodal distribution with only a minor high molar mass peak (Figure 5.1). Furthermore, with the diphenyl substrate, Ph$_2$PH·BH$_3$, the linear dimer Ph$_2$PH·BH$_2$–PPh$_2$·BH$_3$ was also formed and proved difficult to separate from the polymer (Scheme 5.1).

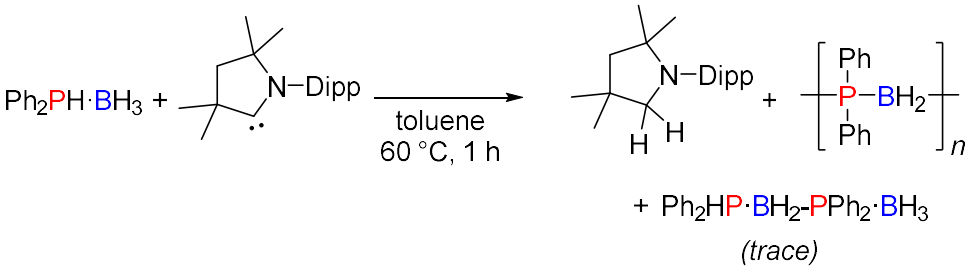

Scheme 5.1 Reaction of Ph$_2$PH·BH$_3$ with CAAC^{Me}.

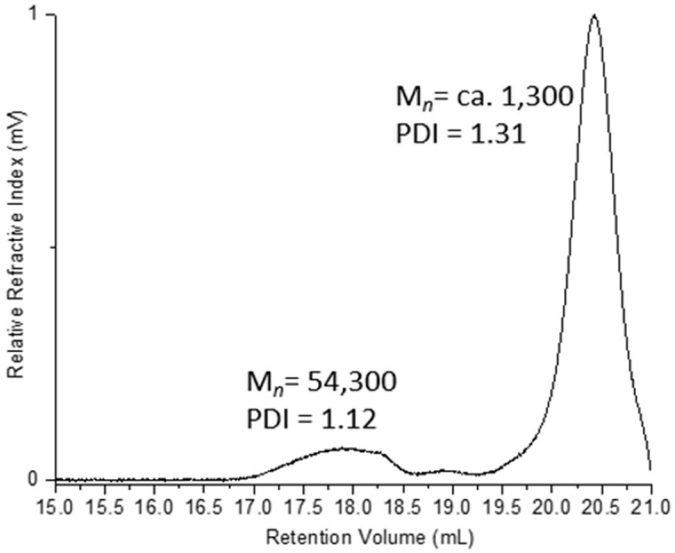

Figure 5.1 GPC trace of the products of the reaction between $Ph_2PH{\cdot}BH_3$ and $CAAC^{Me}$ after work up to exemplify the minor high molar mass component. $(CAAC^{Me})H_2$ is removed through precipitation of the reaction mixture into cold (-40 °C) hexanes.[1]

We were interested in identifying a P-disubstituted phosphine-borane monomer which can undergo dehydropolymerisation to produce a greater quantity of high molar mass material than the previous substrates ($PhEtPH{\cdot}BH_3$ and $Ph_2PH{\cdot}BH_3$).

Copolymerisations have previously been reported in polyaminoborane chemistry. The homopolymer $[H_2N–BH_2]_n$ is insoluble; however, when $H_3N{\cdot}BH_3$ is copolymerised with $MeNH_2{\cdot}BH_3$ the soluble, high molar mass copolymer $[H_2N–BH_2]_n$-*r*-$[MeHN–BH_2]_m$ can be synthesised (Scheme 5.2a).[2] A second example is the synthesis of the copolymers $[RHN–BH_2]_n$-*r*-$[R'HN–BH_2]_m$ (R = allyl; R' = $(CH_2)(C_6H_5X)$; X = Br, H) which are fully soluble in THF. The homo-depolymerisations of $RH_2N{\cdot}BH_3$ (R = allyl) or $R'H_2N{\cdot}BH_3$ (R' = $(CH_2)(C_6H_5X)$; X = Br, H) resulted in a highly soluble viscous oil, or solid polymers with insoluble fractions, respectively.[3]

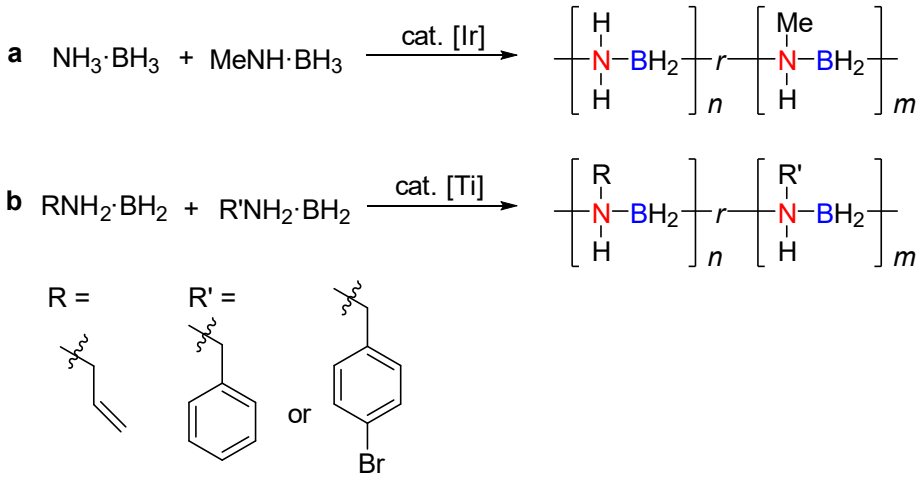

Scheme 5.2 Previously reported copolymerisations of amine-boranes[2,3]

We targeted the synthesis of copolymers comprising both $Ph_2P–BH_2$ and $PhHP–BH_2$ repeat units. We envisioned that incorporating P-monosubstituted units may allow for the synthesis of more high molar mass material by creating a spacer between the more sterically encumbered P-disubstituted units. Although, if successful, this strategy would not result in a fully P-disubstituted polymer, it would be interesting to investigate the material properties of a high molar mass, partially P-disubstituted polyphosphinoborane.

5.3.2 Results and discussion

5.3.2.1 Polymerisation of *rac*-Ph(Me)PH·BH_3 using CAAC^{Me}

The methylated adduct *rac*-Ph(Me)PH·BH_3 was selected as a candidate for the CAAC-mediated polymerisation because a potential reason for the low yield of high molar material formed with the ethyl analogue, *rac*-Ph(Et)PH·BH_3, could be the presence of additional steric bulk due to the Et substituent disfavouring the formation of high molar mass material. Replacing the Et substituent with a Me substituent would decrease the steric encumbrance of the monomer and allow for the study of the effect of steric bulk on the yield of high molar mass material.

CAAC^{Me} and *rac*-Ph(Me)PH·BH_3 (1:1) were dissolved in toluene at 22 °C and immediate conversion to two new species was observed using ^{31}P NMR spectroscopy (δ_P = 6.8 ppm (s) and 10.0 ppm (s) (Figure S5.1). These species are assigned as the diastereomeric products of the insertion of the P–H bond into the carbene centre, CAAC^{Me}(H)PhMePBH_3. Heating the solution (4 M, 100 °C, 24 h) effected complete conversion to (CAAC^{Me})H_2 and a new phosphorus containing species (δ_P = -34.1 ppm (s)). Removal of (CAAC^{Me})H_2 through precipitation into hexanes and ESI-MS analysis of the isolated product confirmed the presence of the repeat unit Δ(*m*/z) = 136 (molecular weight of PhMeP–BH_2 = 136.1) (Figure S5.5); however, as for the case of $[Ph_2P–BH_2]_n$ and $[PhEtP–BH_2]_n$, GPC analysis showed a bimodal distribution with only small fraction (ca. 18 %) of high molar mass material (M_n = 38,400 Da; *Đ* = 1.31) (Figure S5.6).

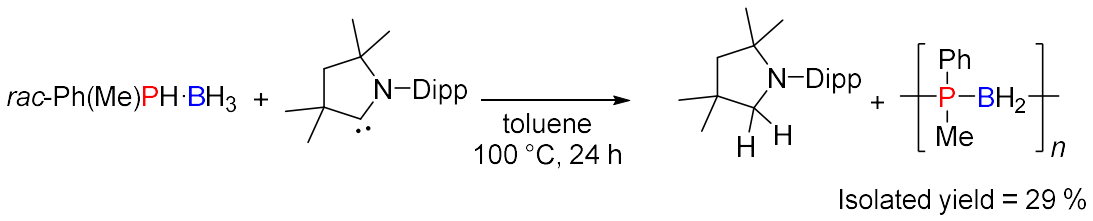

Scheme 5.3 CAAC^{Me} mediated dehydropolymerisation of *rac*-Ph(Me)PH·BH_3.

5.3.2.2 Polymerisation of $Et_2PH{\cdot}BH_3$ using $CAAC^{Me}$

Thus far there have been no reported examples of P-disubstituted polyphosphinoboranes with two alkyl substituents on phosphorus. $Et_2PH{\cdot}BH_3$ was chosen as a substrate to explore as it would produce a monomer with low steric bulk whilst avoiding the use of gaseous dimethylphosphine. $Et_2PH{\cdot}BH_3$ was targeted over $MeEtPH{\cdot}BH_3$ due to the commercial availability of Et_2PH.

The P–H activation compound, $CAAC^{Me}(H)Et_2PBH_3$ (**5.1**), was synthesised either through a direct reaction of $CAAC^{Me}$ with $Et_2PH{\cdot}BH_3$ (Scheme 5.4a), or through a stepwise approach involving activation of PEt_2H at the carbene centre followed by addition of $BH_3{\cdot}SMe_2$ (Scheme 5.4b).

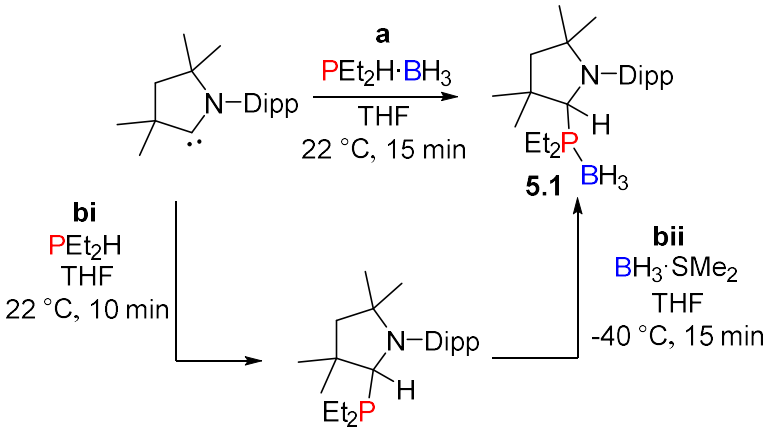

Scheme 5.4 Synthesis of **5.1** through **a** direct P–H activation of $Et_2PH{\cdot}BH_3$; and **b** a stepwise approach.

Single crystals suitable for X-ray diffraction were grown from a saturated hexanes solution at -40 °C which allowed the identity of the product to be confirmed as $CAAC^{Me}(H)Et_2PBH_3$ (Figure 5.2). ^{11}B and ^{31}P NMR spectra (Figure S5.9 and Figure S5.10) both showed single peaks (δ_B = -40.3 ppm (m) and δ_P = 26.1 ppm (d)) with chemical shifts comparable to those of $CAAC^{Me}(H)PhEtPBH_3$.[1]

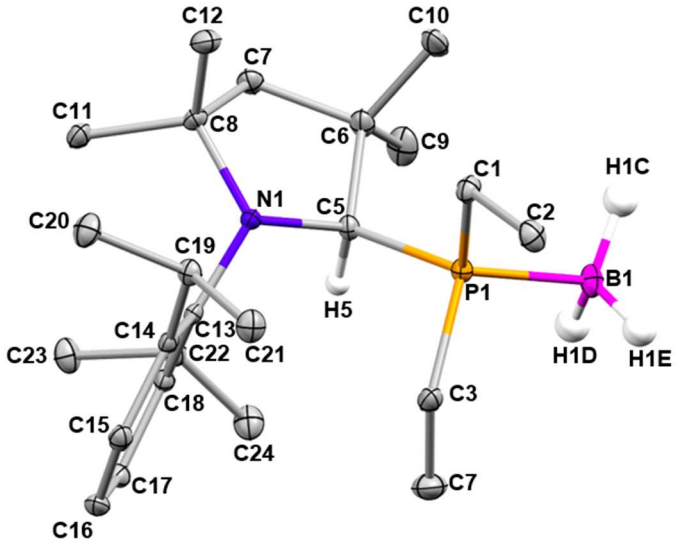

Figure 5.2 Thermal ellipsoid plot of CAAC^{Me}(H)Et$_2$PBH$_3$ (**5.1**). Ellipsoids are shown at the 30% probability level. H atoms other than those on C5 and B1 have been omitted for clarity.

We found that **5.1** was significantly more thermally stable than CAAC^{Me}(H)PRR'BH$_3$ (R = H, R' = Ph; R = R' = Ph; R = Ph, R' = Et and R = Ph, R' = Me) and must be heated to 140 °C for hydride transfer from B to C to occur at an appreciable rate (Scheme 5.5). Over 24 h in *o*-xylenes, full conversion of **5.1** was observed together with formation of a white precipitate which was insoluble in common solvents. Both the ^{11}B and ^{31}P NMR spectra of the soluble part of the reaction mixture showed two peaks, one major and one minor, with similar chemical shifts (δ_B = ca. -35 ppm and δ_P = ca. -29 ppm) (Figure S5.14a and Figure S5.15a). The ^{31}P NMR peaks were broad and no coupling was detected; however, the ^{11}B spectra showed a distinctive coupling pattern of the major peaks. The decoupled ^{11}B NMR spectrum showed a triplet and the coupled spectrum showed further splitting of each peak into a triplet of triplets, indicative of a ~PEt$_2$–BH$_2$–PEt$_2$~ system where the boron couples to two B–H hydrogens and to two adjacent phosphorus atoms. ESI-MS analysis on the soluble portion of the reaction mixture confirmed the presence of the repeat unit Δ(*m*/z) = 102 (molecular weight of Et$_2$P–BH$_2$ = 102.1) (Figure S5.16). The combination of the NMR and ESI-MS data led us to assign the soluble product as oligomeric [Et$_2$P–BH$_2$]$_x$ with the minor peaks in the ^{11}B and ^{31}P NMR spectra tentatively assigned as end groups.

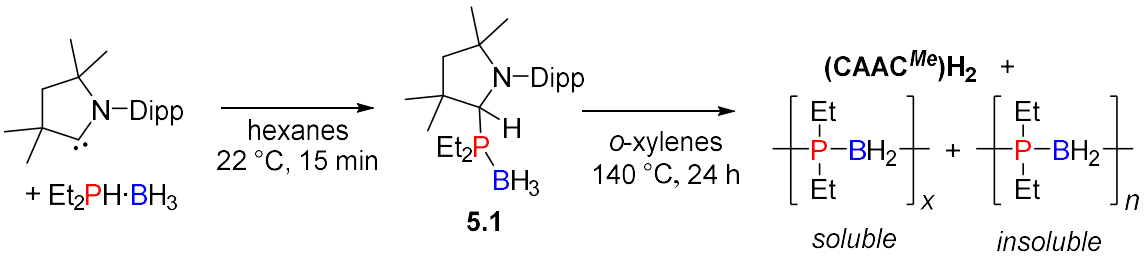

Scheme 5.5 CAAC-mediated dehydropolymerisation of $Et_2PH{\cdot}BH_3$.

Solid state ^{1}H, ^{13}C, ^{11}B and ^{31}P CP-MAS NMR spectroscopy was carried out on the insoluble material. The ^{11}B and ^{31}P spectra showed peaks with very similar chemical shifts to the soluble material which suggested that the soluble and insoluble material were structurally related (Figure S5.14b and Figure S5.15b). From this we postulated that the insoluble material is polymeric $[Et_2P–BH_2]_n$. The solid state ^{13}C NMR spectrum showed two sets of two peaks (δ_c = 19.8 and 17.7 ppm; 9.5 and 8.9 ppm) which correspond to the CH_2 and CH_3 protons of the ethyl substituents respectively. We tentatively attribute the presence of two sets of peaks to be due to the formation of both cyclic and linear species (Figure S5.13).

The thermal behaviour of the insoluble material was investigated using differential scanning calorimetry (DSC) and thermogravimetric analysis (TGA). It should be noted that when the glass transition temperature (T_g) values of a series of polyphosphinoboranes are compared to the T_g values of the analogous polyolefins the polyolefins present higher transition temperatures (Table 5.1). This has been postulated to be due to the polyphosphinoboranes having a higher degree of torsional flexibility in the main chain as the P–B bond length (1.9 – 2.0 Å) is greater than the C–C bond length (ca. 1.54 Å), reducing steric interaction between substituents and generating free volume which facilitates the polymer motion.[4] Based purely on this data the T_g value of $[Et_2P–BH_2]_n$ would be predicted to be lower than -73 °C; however, surprisingly, the T_g must be above room temperature as the material is a fine powder at 22 °C.

Table 5.1 T_g values for a series of analogous polyolefins and polyphosphinoboranes.

Polyolefin	T_g (°C)	Polyphosphinoborane	T_g (°C)
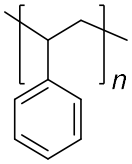	107	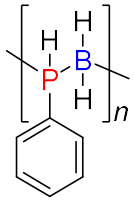	38
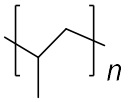	-6	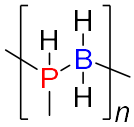	-24
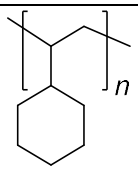	120	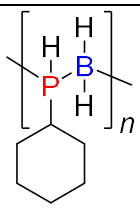	-2
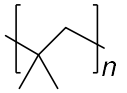	-73*	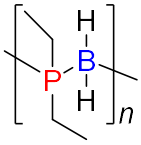	ca. 130 -140

*No reported data for $[Et_2C–CH_2]_n$.

The TGA analysis of our material showed the decomposition temperature $T_{5\%}$ to be 160 °C (Figure S5.17) and DSC showed an apparent glass transition (T_g) of 141 °C (Figure S5.18). We were initially concerned that the transition we were observing was not a T_g and was in some way related to *o*-xylene being trapped within the polymer chain, of which there is some evidence in the CP-MAS ^{1}H NMR (Figure S5.12), as the boiling point of *o*-xylene is 144 °C. To probe this issue further the polymerisation was carried out under identical conditions; however, mesitylene was used rather than *o*-xylene as the solvent. If trapped solvent was responsible for the transition observed in the DSC trace it would be expected to shift to a higher temperature (ca. 165 °C in the mesitylene) due to the higher boiling point. The DSC thermogram conversely showed a shift to a lower temperature (132 °C) (Figure S5.19), leading us to believe that the transition observed is a property of the polymer formed and not trapped solvent. Mesitylene, with the higher boiling point, was harder to fully remove from the isolated polymer, so more remained and has a greater plasticising effect, explaining why the T_g is shifted to a slightly lower temperature when mesitylene was used as the solvent.

In an attempt to explain why the T_g value of $[Et_2P–BH_2]_n$ appeared anonymously high we carried out powder XRD analysis on the sample. Both crystalline and amorphous regions were observed in the diffraction pattern, indicating that the material was semi-crystalline (Figure

S5.19). The polymer chains in the amorphous regions may also enter the crystallites, resulting in restricted conformational motion and explaining the high T_g value. As only the amorphous fraction of the material will display a glass transition this may also explain why the transition appears to be fairly weak.[5] We were confident that the transition observed in the DSC trace was a T_g as a opposed to a T_m based on the peak shape as T_g represents a second order transition. The T_m of the crystalline fraction may be higher than the decomposition temperature, and hence above the temperature range for the DSC measurement (-80 to 160 °C).

5.3.2.3 Polymerisation of *n*Hex$_2$PH·BH$_3$ using CAAC^{Me}

Following the synthesis of insoluble $[Et_2P–BH_2]_n$ the polymerisation was attempted using *n*Hex$_2$PH·BH$_3$ as an alternative substrate as it was anticipated that increasing the length of the alkyl chain would increase solubility (Scheme 5.6). Upon heating a solution of CAAC^{Me} and *n*Hex$_2$PH·BH$_3$ in *o*-xylene at 130 °C for 24 h, ^{11}B and ^{31}P NMR spectroscopy showed formation of new species (δ_B =-36.5 ppm (br) and δ_P = -28.5 (br) and -31.5 (br)) (Figure S5.22 and Figure S5.23) with chemical shifts similar to those assigned as $[Et_2P–BH_2]_n$. Attempts to separate the (CAAC^{Me})H$_2$ by product from the reaction mixture were unsuccessful. ESI-MS analysis of the crude reaction mixture confirmed the presence of the repeat unit Δ(*m*/z) = 214 (molecular weight of *n*Hex$_2$P–BH$_2$ = 214.2) (Figure S5.24) and GPC analysis showed the presence of a very small amount of high molar mass material (M_n = 89,600 Da; *Đ* = 1.06) (Figure S5.25). These results indicated that a small amount of soluble high molar mass $[n\text{Hex}_2\text{P–BH}_2]_n$ had been synthesised along with a significant quantity of oligomeric material.

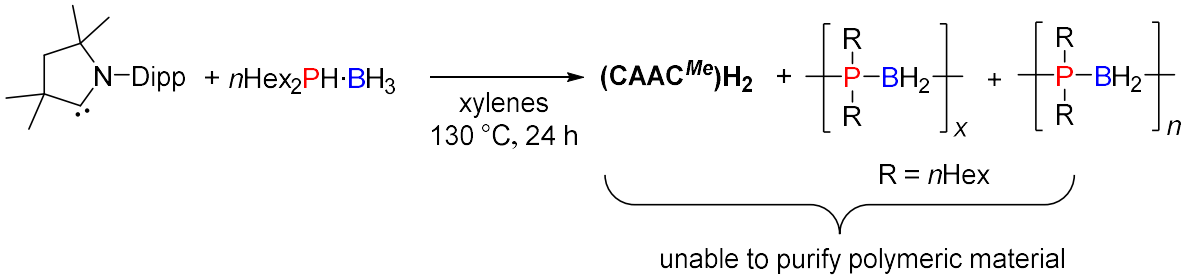

Scheme 5.6 CAAC-mediated dehydropolymerisation of *n*Hex$_2$PH·BH$_3$.

5.3.2.4 Attempted synthesis of the copolymers $[Ph_2P–BH_2]_n$-*r*-$[PhHP–BH_2]_m$ mediated by CAAC^{Me}

We hypothesised that copolymerisation of PhPH$_2$·BH$_3$ with Ph$_2$PH·BH$_3$ might yield a larger quantity of high molar mass material containing a substantial proportion of P-disubstituted units. A range of ratios spanning 95:5 to 5:95 was investigated and the ^{31}P NMR, GPC and

ESI-MS data of the isolated material were compared to that of the homopolymerisations of $PhPH_2{\cdot}BH_3$ and $Ph_2PH{\cdot}BH_3$.

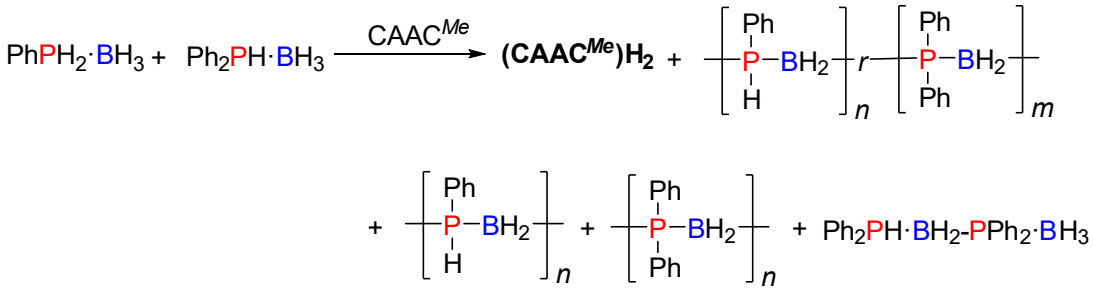

Scheme 5.7 Copolymerisation of $PhPH_2{\cdot}BH_3$ with $Ph_2PH{\cdot}BH_3$ using $CAAC^{Me}$.

Peaks corresponding to $PhHP–BH_2$ repeat units were observed in the ^{31}P NMR spectra of all the samples in which $PhPH_2{\cdot}BH_3$ was used. The linear dimer, $Ph_2PH{\cdot}BH_2–PPh_2{\cdot}BH_3$, was similarly observed in all the samples in which $Ph_2PH{\cdot}BH_3$ is used; however, the repeat unit $Ph_2P–BH_2$ was only convincingly observed when over 50 % of the disubstituted monomer is used (Figure 5.3). GPC analysis on each of the samples showed the presence of high molar mass material in each case (M_n = 17,000 – 35,000 Da; $Đ$ = 1.19 – 1.52); however, there were significant quantities of oligomeric material (Figure S5.28).

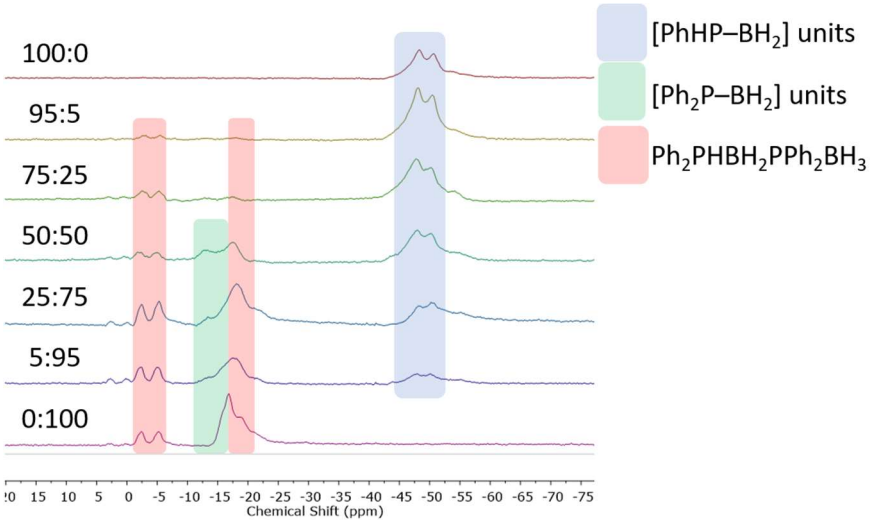

Figure 5.3 ^{31}P NMR spectra (122 MHz, 25 °C, $CDCl_3$) of the isolated material from the copolymerisations of $PhPH_2{\cdot}BH_3$ with $Ph_2PH{\cdot}BH_3$.

From the NMR and GPC data it was not possible to establish whether copolymerisation had occurred as it is possible that the $PhHP–BH_2$ and $Ph_2P–BH_2$ units observed in the ^{31}P NMR spectra were a result of the formation of homopolymers, $[PhHP–BH_2]_n$ and $[Ph_2P–BH_2]_n$. ESI-MS of the attempted copolymerisations showed a distribution of peaks that were not present in either of the homopolymer spectra (Figure 5.4). Furthermore it was possible to select a peak and locate peaks giving a *m/z* mass difference of $PhHP–BH_2$ (*m/z* = 122) and

$Ph_2P–BH_2$ (*m/z* = 198) (Figure 5.4). Although this provided evidence that the copolymer $[Ph_2P–BH_2]_n$-*r*-$[PhHP–BH_2]_m$ had been synthesised, distributions which can be assigned to the homopolymers were detected in the copolymerisation samples, suggesting that the isolated material contained a combination of $[Ph_2P–BH_2]_n$, $[PhHP–BH_2]_m$ and $[Ph_2P–BH_2]_n$-*r*-$[PhHP–BH_2]_m$.

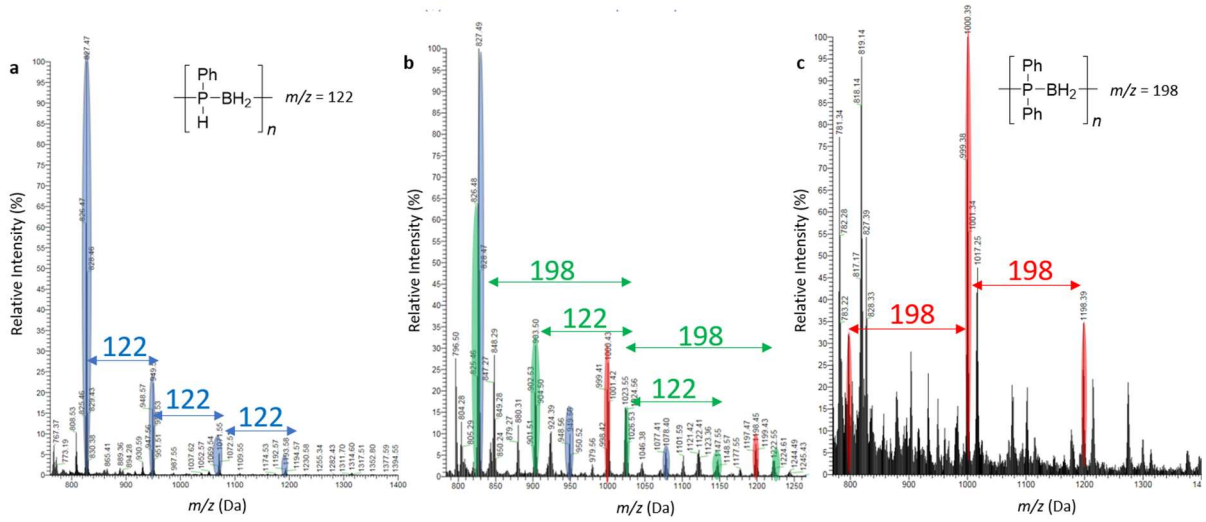

Figure 5.4 ESI(+)-MS spectrum in positive mode in THF:IPA (1:9) of the isolated material from the polymerisations of **a** $PhPH_2·BH_3$; **b** $PhPH_2·BH_3$ with $Ph_2PH·BH_3$ (50:50); and **c** $Ph_2PH·BH_3$.

5.3.3 Conclusions

We have attempted the CAAC-mediated dehydropolymerisation of three P-disubstituted phosphine-boranes, *rac*-$Ph(Me)PH·BH_3$, $Et_2PH·BH_3$ and *n*$Hex_2PH·BH_3$. With *rac*-$Ph(Me)PH·BH_3$ the dehydropolymerisation was successful; however, as with previously reported $[PhEtP–BH_2]_n$, the yield of isolated material was low and only a small quantity of high molar mass $[PhMeP–BH_2]_n$ was detected using GPC analysis. This showed that decreasing the sterics of the second phosphorus substituent, when the first is phenyl, did not facilitate the formation of larger quantities of high molar mass material. The dehydropolymerisation $Et_2PH·BH_3$ required more forcing conditions (140 °C) to proceed and resulted in the formation of an insoluble material which has been assigned as $[Et_2P–BH_2]_n$. This material has been identified as semi-crystalline using powder XRD which can be used to explain the unusually high T_g value. Owing to its insolubility, the molar mass of $[Et_2P–BH_2]_n$ could not be determined. Attempts to synthesise a soluble P-dialkyl substituted polyphosphinoborane through increasing the length of the alkyl chain were made using *n*$Hex_2PH·BH_3$ as the substrate. Although $CAAC^{Me}$-mediated dehydrogenation is successful only a trace of high molar mass material was produced and separation from the $(CAAC^{Me})H_2$ by product has not been successful.

The copolymerisation of $PhPH_2{\cdot}BH_3$ with $Ph_2PH{\cdot}BH_3$ was attempted and ESI-MS indicated that a mixture of $[Ph_2P–BH_2]_n$, $[PhHP–BH_2]_m$ and $[Ph_2P–BH_2]_n$-*r*-$[PhHP–BH_2]_m$ was formed. Neither a molar mass nor yield of the copolymer was reported as distinguishing it from the homopolymers using ^{31}P NMR spectroscopy or GPC analysis was not possible.

5.4 Studies of the reactivity of IDipp–BH_2NMeH

5.4.1 Introduction

In 2013 our group reported the synthesis of the NHC-aminoborane adduct, IDipp–BH_2NMeH, and more recently this compound has been structurally characterised (Chapter 4).[6] This adduct can be synthesised either through the stoichiometric reaction of IDipp (IDipp = 1,3-bis(2,6-diisopropylphenyl)-1,3-dihydro-2*H*-imidazol-2-ylidene) with poly(N-methylaminoborane), $[MeHN–BH_2]_n$, or the reaction of two equiv. of IDipp with $MeNH_2{\cdot}BH_3$. In the first case IDipp acts to both depolymerise $[MeHN–BH_2]_n$ and trap the aminoborane monomers which are released (Scheme 5.8a). With $MeNH_2{\cdot}BH_3$ one equivalent of IDipp acts to dehydrogenate the amine-borane and the second equivalent traps the aminoborane monomer (Scheme 5.8b). We were interested in further exploring the reactivity of the adduct.

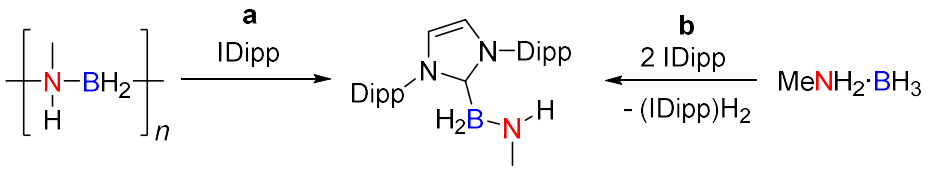

Scheme 5.8 Syntheses of IDipp–BH_2NMeH.[6]

It has been reported by Rivard *et al.* that the aminoborane adduct IDipp–BH_2NHDipp undergoes a 5- to 6-membered ring expansion reaction to give $[(HCNDipp)_2CH_2BNHDipp]$ upon heating through the insertion of the borane into the C–N bond of the NHC (Scheme 5.9).[7] We were interested to investigate whether the adduct, IDipp–BH_2NMeH, would undergo the same thermal transformation.

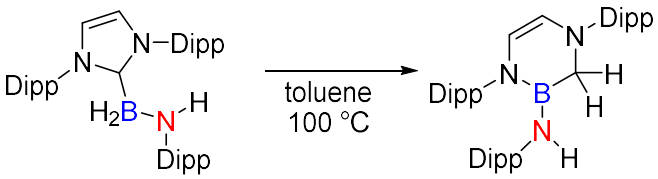

Scheme 5.9 Thermal ring expansion reaction of IDipp–BH_2NHDipp.[7]

Our group demonstrated that it was possible to abstract the NHC from the adduct IDipp–BH_2N*i*Pr_2 with one equiv. of the strong Lewis acids, tri-pentafluorophenylborane, $B(C_6F_5)_3$ or $Ph_2N{=}BCl_2$ (Scheme 5.10).[6,8] These displacement reactions are reported to be successful as strong Lewis acids form stronger B–C bonds with the carbene centre than *i*$Pr_2N{=}BH_2$.

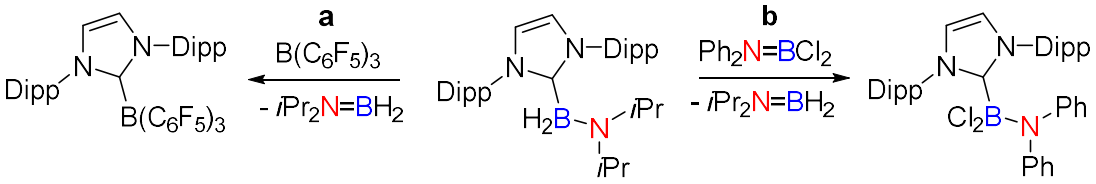

Scheme 5.10 Previously reported displacement of aminoboranes by Lewis acids.[6,8]

We postulated that it should be possible to carry out a displacement reaction with IDipp–BH_2NMeH and a Lewis acid, analogous to those reported above with IDipp–BH_2N*i*Pr_2, to release the aminoborane monomer, $MeHN{=}BH_2$, which may undergo a head-to-tail polymerisation to regenerate poly(N-methylaminoborane), $[MeHN–BH_2]_n$. A successful head-to-tail polymerisation of aminoborane monomers was reported in 2017 by Alcaraz *et al.* in which *i*$Pr_2N{=}BH_2$ is used as a BH_2 transfer agent to yield the desired aminoborane monomer for polymerisation.[9] If the proposed displacement and subsequent polymerisation are successful this would provide a method of recycling polyaminoboranes, an attractive target in the field of polymer science (Scheme 5.11). As we have discovered that substoichiometric quantities of NHC cause catalytic depolymerisation of $[MeHN–BH_2]_n$ (Chapter 4) it is important that the Lewis acid added forms a strong bond with the carbene centre.

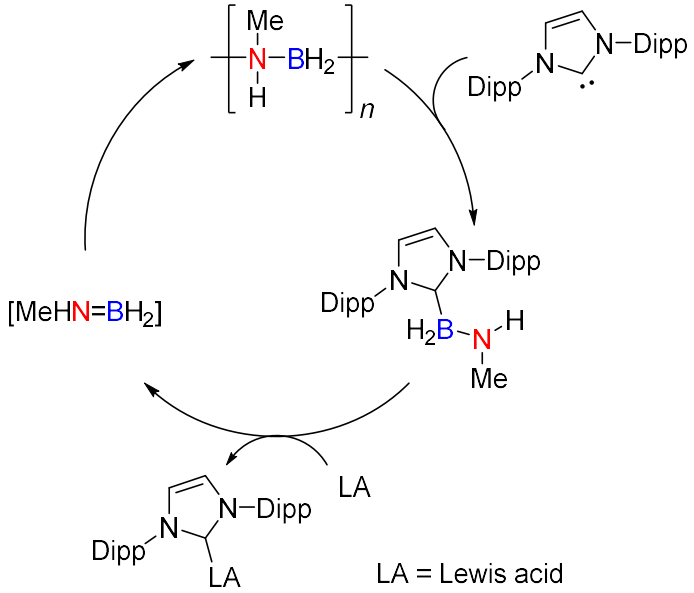

Scheme 5.11 Proposed recycling route of polyaminoboranes using Lewis acids to abstract the NHC from the adduct.

5.4.2 Results and discussion

5.4.2.1 Thermal reactivity of IDipp–BH_2NMeH

Upon heating a concentrated solution of IDipp–BH_2NMeH to 80 °C for 24 h, full conversion of the adduct was observed with two new major peaks being observed in the ^{11}B NMR spectrum at δ_B = 30.6 ppm (br), tentatively assigned as the product of a 5- to 6-member ring expansion (**5.2**) (Scheme 5.9),[7] and an unknown species at δ_B= -18.3 ppm (t) ($^3J_{BH}$ = 89 Hz) in a ca. 2:1 ratio. The ^1H NMR spectrum of the reaction mixture showed the presence of four IDipp containing species and a peak which corresponds to dihydrogen (Figure 5.5).

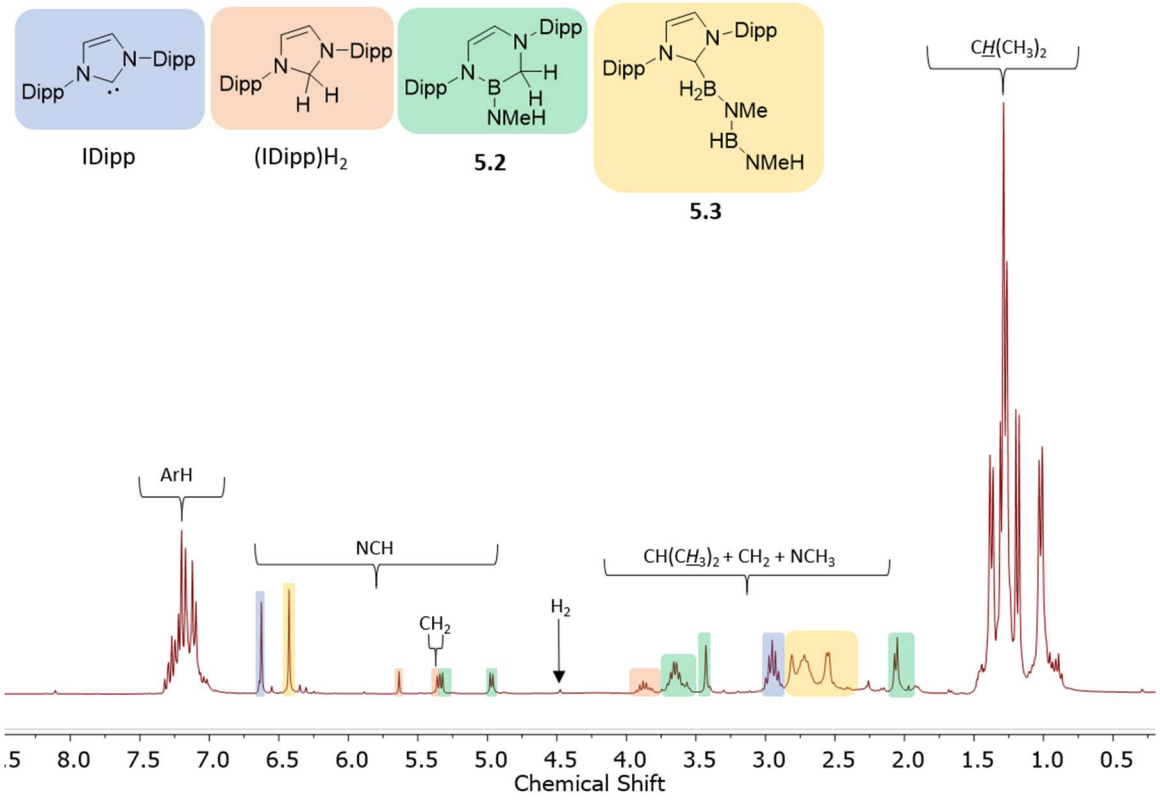

Figure 5.5 Representative ^1H NMR spectrum (C_6D_6, 500 MHz, 298 K) of the reaction mixture of the thermolysis of IDipp–BH_2NMeH (run 1).

IDipp[10] and (IDipp)H_2[11,12] were identified based on literature data and **5.2** was identified based on the similarity of the ^1H and ^{11}B NMR data to that of [(HCNDipp)$_2$$CH_2$BNHDipp].[7] Crystals grown from the reaction mixture at 22 °C allowed identification of the final product as IDipp–BH_2·NMeBH·NMeH (**5.3**) using X-ray crystallography (Figure 5.6). The C1–B1 and B1–N3 bond lengths in **5.3** are 1.626(2) Å and 1.532(2) Å, respectively, and were very similar to the analogous bonds in IDipp–BH_2NMeH (1.631(3) Å and 1.525(3) Å). The lengths of N3–B2 (1.408(2) Å) and B2–N4 (1.411(2) Å) were almost identical and close to the reported average double B–N length (1.40 Å).[13] B1 is tetrahedral whereas N3, B2 and N4 show trigonal planar

geometries (Σ_{angles} = 360 °). The ^{11}B chemical shift of B1 (δ_B = -18.3 ppm (t)) is comparable to that of the analogous boron in IDipp–BH_2NMeH [δ_B -17.0 ppm (t)] and the chemical shift of B2 (δ_B = 32.6 (br)) can be compared to that of [MeNBH]$_3$.[14] The observation of only one septet (albeit broad) and two doublets, which are assigned to the Dipp isopropyl groups, using ^{1}H NMR spectroscopy indicated that there is free rotation around the C1–B1 bond under ambient conditions (Figure S5.29).

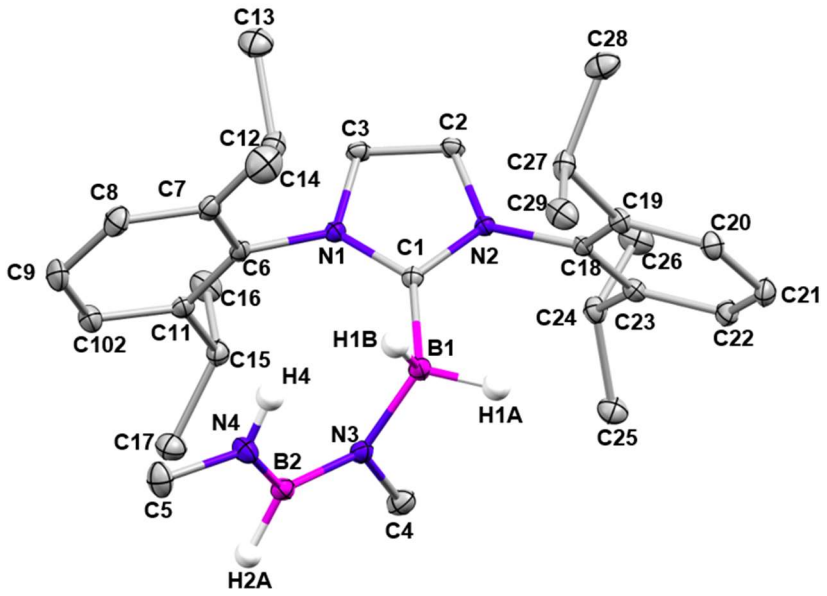

Figure 5.6 Thermal ellipsoid plot of IDipp–BH_2NMeBHNMeH (**5.3**). Ellipsoids are shown at the 30% probability level. H atoms other than those on B1, H2A and N4 have been omitted for clarity.

5.3 contains a trapped iminoborane unit (MeN≡BH), the inorganic analogue of propyne. Iminoboranes are challenging to isolate as the core B–N bond is highly polar which makes the species vulnerable to cyclooligomerisation.[15] In 2015 Rivard *et al*. reported the first stable molecular adduct containing HB≡NH using a donor acceptor approach in which the iminoborane is sandwiched between a Lewis-base and Lewis-acid.[16] In this work the iminoborane unit is trapped by an electron donating amide and electron accepting borenium moiety (Figure 5.7).

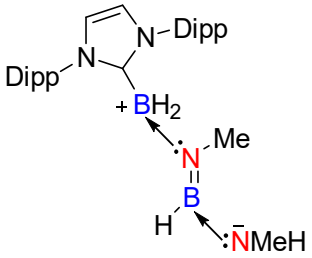

Figure 5.7 Illustration of the donor-acceptor stabilised iminoborane.

We postulated that IDipp–BH_2NMeH is in equilibrium with the free NHC and aminoborane monomer and, upon heating, one of two irreversible reactions can occur. Either a ring expansion reaction, analogous to that reported by Rivard *et al.*,[7] to give **5.2** (Scheme 5.12a) or a dehydrocoupling reaction between IDipp–BH_2NMeH and free aminoborane monomer to yield **5.3** (Scheme 5.12b).

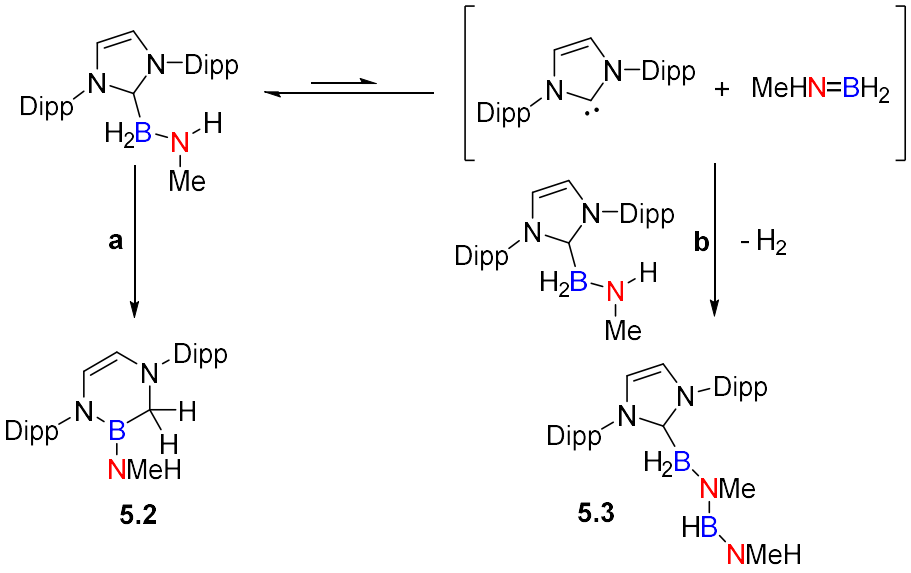

Scheme 5.12 Proposed routes to **a** [$(HCNDipp)_2CH_2BNMeH$]; and **b** IDipp–$BH_2NMeBHNMeH$.

Based on the above equilibrium altering the reaction conditions should affect the product distribution (Table 5.2). Increasing the concentration (run 1 vs run 2 vs run 3) was found to increase the quantity of the dehydrocoupling product. This was anticipated as this is a bimolecular reaction. Higher temperatures (run 4 vs run 2 vs run 5) favoured **5.2**, and we attribute this to the ring expansion being a unimolecular process with an expected negligible entropy of activation ($\Delta S^{\ddagger}$), whereas the $\Delta S^{\ddagger}$ for the bimolecular dehydrocoupling process should be large and negative and therefore less favoured at high temperatures. Increasing the solvent polarity from benzene to THF (run 2 vs run 6) increased the ratio of the dehydrocoupling product, which we attribute is due to stabilisation of the aminoborane monomer and consequent shift of the equilibrium to the free NHC and monomer rather than the adduct. When a further equivalent of IDipp was added to the 1:1 reaction mixture full conversion to the ring expansion product was observed using ^{1}H and ^{11}B NMR spectroscopy (run 7), further supporting the postulated equilibrium.

Table 5.2 Ratio of **5.2** and **5.3** formed under different conditions

Run	Conc. (M)	Temp. (°C)	Solvent	Ratio of **5.2**:**5.3**[a]
1	0.46	80	C_6D_6	38:62
2	0.09	80	C_6D_6	76:24
3	0.02	80	C_6D_6	86:14
4	0.09	100	C_6D_6	95:5
5	0.09	60	C_6D_6	39:61
6	0.09	80	THF-d_8	67:33
7[b]	0.09	80	C_6D_6	100:0

[a]Determined by integrating the CH_2 peak (δ_H = 3.43 ppm) of **5.2** and the NHC backbone peak (δ_H = 6.43 ppm) of **5.3** in the ^{1}H NMR spectra, [b]extra equivalent of IDipp added.

5.4.2.2 Attempts to regenerate [MeHN–BH_2]$_n$ from IDipp–BH_2NMeH by addition of Lewis acids

Following the successful displacement of *i*Pr_2N=BH_2 in IDipp–BH_2N*i*Pr_2 with Ph_2N=BCl_2[8] the analogous reaction with IDipp–BH_2NMeH was attempted. A stoichiometric quantity of IDipp–BH_2NMeH in toluene was added to a solution of Ph_2N=BCl_2 in toluene at 22 °C (Scheme 5.14). Within 10 min quantitative consumption of IDipp–BH_2NMeH and formation of multiple new species were detected using ^{11}B NMR spectroscopy (δ_B = 30.7 ppm (br) (ca. 49%), 8.0 ppm (s) (ca. 2%), 2.5 ppm (br) (trace) and -16.1 ppm (br) (ca. 49%)) (Figure S5.33). A small amount of white precipitate was also observed. The trace signal at δ_B = 2.5 ppm was tentatively assigned as the adduct IDipp–BCl_2NPh_2 (δ_B = 1.2 ppm (s)).[8] There was no evidence using ^{11}B NMR spectroscopy of [MeHN–BH_2]$_n$ (δ_B = -6 ppm (br))[17] being generated. ^{1}H NMR spectroscopy on the reaction mixture in $CDCl_3$ showed a peak at δ_H = 10.01 ppm, which was indicative of an imidazolium salt, [IDippH]$^+$X$^-$, being formed.

The reaction of IDipp–BH_2NMeH with one equiv. of BCl_3 was carried out so a comparison of the species formed could be made (Scheme 5.14). Full consumption of IDipp–BH_2NMeH was observed after 10 min and again multiple species were formed as detected by ^{11}B NMR spectroscopy (δ_B = 34.1 ppm (br) (ca. 20%), 7.8 ppm (s) (ca. 13%), 7.4 ppm (s) (ca. 54%), 3.1 ppm (br) (ca. 3%), -5.3 ppm (br) (trace) and -17.9 ppm (br) (ca. 9%)) (Figure S5.36). The peak with chemical shift δ_B = 3.1 ppm has tentatively been assigned as the adduct IDipp–BCl_3.[18] Similar to the analogous reaction with Ph_2N=BCl_2 a white precipitate was observed to form and ^{1}H NMR analysis in $CDCl_3$ shows a peak characteristic of an imidazolium proton (δ_H = 9.53 ppm).

We anticipate that the presence of a N–H bond and a B–Cl bond in the reaction mixtures results in the formation of B–N bonds with the release of HCl. The HCl most likely

subsequently reacts with IDipp, giving [IDippH]Cl, thus explaining the formation of the white precipitate and the presence of an imidazolium proton signal in the ^{1}H NMR spectrum (Scheme 5.13). This side reaction does not present a problem in the previously reported displacement reaction of IDipp–BH_2N*i*Pr_2 as, due to the disubstituted nitrogen, there are no N–H bonds available (Scheme 5.10b).

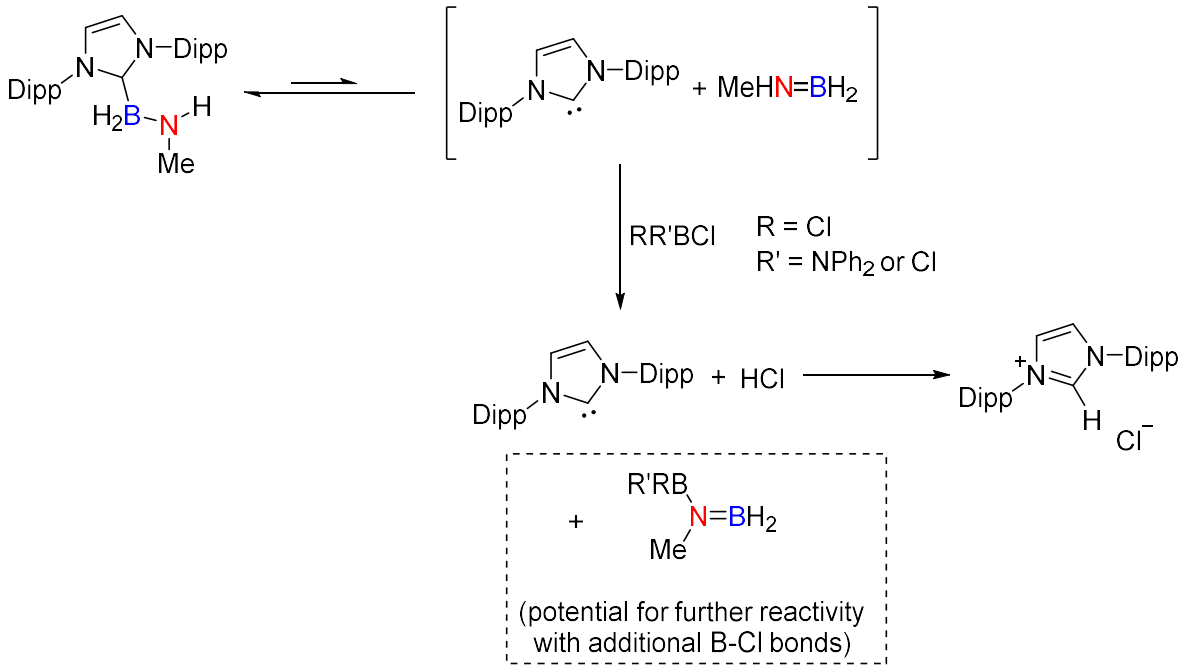

Scheme 5.13 Postulated route for the formation of [IDippH]Cl.

The observation of a broad peak (δ_B = -5.3 ppm (br) (trace)) in the ^{11}B NMR spectrum of the reaction between IDipp–BH_2NMeH and BCl_3 led us to further investigate the reaction mixtures as [MeHN–BH_2]$_n$ would be expected to display a similar boron signal. GPC analysis was carried out on the reaction mixtures with both $Ph_2N{=}BCl_2$ and BCl_3 and a small amount of high molar mass material (M_n = 26,100 Da; $Đ$ = 1.56 and M_n = 26,600 Da; $Đ$ = 1.81) was detected in each case (Figure S5.34 and Figure S5.37). ESI-MS showed the presence of material with the anticipated monomer repeat unit (*m/z* = 43.1) (Figure S5.35 and Figure S5.38). The weak signal in the GPC spectrum coupled with trace signals corresponding to [MeHN–BH_2]$_n$ in the ^{11}B NMR spectra leads us to determine that only trace quantities of polymer are being regenerated from the adduct (Scheme 5.14). As regeneration of the polymer was the goal of these experiments, no further investigations were carried out to probe the identity of the unidentified reaction products.

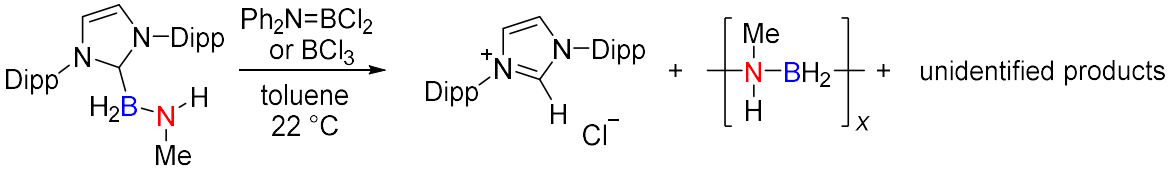

Scheme 5.14 Reaction of IDipp–BH_2NMeH with $Ph_2N{=}BCl_2$ or BCl_3.

In an attempt to avoid the unwanted side reactions postulated to be occurring as a result of the B–Cl bonds in the Lewis acid we reacted IDipp–BH_2NMeH with one equiv. of $B(C_6F_5)_3$.[19] $B(C_6F_5)_3$ was selected due to its previous success in abstracting the NHC from IDipp–BH_2N*i*Pr_2.[6] Within 1 h full consumption of IDipp–BH_2NMeH was observed and three new species were detected using ^{11}B NMR spectroscopy (δ_B = -5.0 ppm (s) (35%), -17.1 ppm (br) (19%) and -24.8 ppm (d, $^1J_{HB}$ = 83.7 Hz) (47%)) (Figure S5.39). There was no evidence of the broad peak (δ_B = ca. -6 ppm) characteristic of the formation of [MeHN–BH_2]$_n$ or a singlet corresponding to IDipp–$B(C_6F_5)_3$ (δ_B = -15.6 ppm).[20] The doublet with an ^{11}B chemical shift of -24.8 ppm has been assigned as the tris(pentafluorophenyl)borane hydride anion, $H[B(C_6F_5)_3]^-$.[20] We postulate that $B(C_6F_5)_3$ abstracts a hydride at boron from IDipp–BH_2NMeH, rather than abstracting the NHC; however, the structure of the compound formed has not been determined. We predict that the extra steric encumbrance arising from the presence of the two isopropyl groups at nitrogen in IDipp–BH_2N*i*Pr_2 prevent $B(C_6F_5)_3$ accessing and abstracting a hydride and thus the successful displacement reaction occurs (Scheme 5.10a).

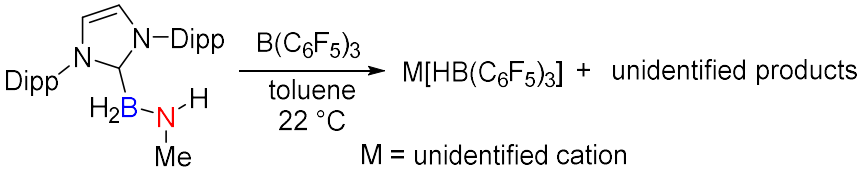

Scheme 5.15 Reaction of IDipp–BH_2NMeH with $B(C_6F_5)_3$.

5.4.3 Conclusions

We have studied both the thermal reactivity of IDipp–BH_2NMeH and the reactivity with a number of Lewis acids. Upon heating IDipp–BH_2NMeH two new boron containing products have been observed to form, the first of which has been identified as the product of a 5- to 6-membered ring expansion reaction, **5.2**. The second product has been isolated and characterised using X-ray crystallography to reveal the structure as IDipp–BH_2·NMeBH·NMeH (**5.3**). We postulate that this species is the product of a dehydrocoupling reaction between IDipp–BH_2NMeH and an aminoborane monomer MeHN=BH_2, present in solution due to the

adduct being in equilibrium with the free NHC and monomer. The relative distribution of **5.2** and **5.3** can be tuned by varying concentration, temperature or solvent polarity.

Reactions of IDipp–BH_2NMeH with the Lewis bases $Ph_2N{=}BCl_2$, BCl_3 and $B(C_6F_5)_3$ were investigated with the goal of abstracting the NHC and releasing [MeHN–BH_2] to facilitate a head-to-tail polymerisation. Although [MeHN–BH_2]$_n$ was detected using a combination of GPC and ESI-MS analysis in the reactions with $Ph_2N{=}BCl_2$ and BCl_3 the polymer was only formed in trace amounts based on the ^{11}B NMR spectra. The observation of a white precipitate forming in each case led us to postulate that HCl is being released from the reaction of an N–H bond with a B–Cl bond and forming the imidazolium sat [IDippH]Cl. In the reaction with $B(C_6F_5)_3$ the formation of the anion $[HB(C_6F_5)_3]^-$ was detected using ^{11}B NMR spectroscopy. We anticipate that $B(C_6F_5)_3$ is abstracting a hydride from the B–H bond of the adduct. As our goal was to reform the polymer from the adduct further investigations to determine the identity of all the products formed with $Ph_2N{=}BCl_2$, BCl_3 and $B(C_6F_5)_3$ have not been carried out.

Although the idea of releasing MeHN=BH_2 from the adduct, with the goal of regenerating the polymer, would represent a significant development in polyaminoborane chemistry it has to be noted that this is not a particularly plausible route. If a Lewis acid was found to successfully abstract the NHC and not react with the adduct in any other way, a challenge in itself, it is to be expected that higher concentration of the reaction solution would favour high molar mass material. As a large quantity of IDipp–BH_2NMeH can theoretically release only a small amount of MeHN=BH_2, for example 100 mg of adduct would release only 10 mg of monomer, solubility becomes an issue when attempting to obtain a high concentration of monomer.

5.5 Supporting information

5.5.1 General procedures, reagents and equipment

All manipulations were carried out either under an atmosphere of nitrogen gas using standard vacuum line and Schlenk techniques, or under an atmosphere of nitrogen within an M. Braun glovebox MB150G-B maintained at < 0.1 ppm of H_2O and < 0.1 ppm of O_2. All solvents were dried via a Grubbs design solvent purification system[21] except *o*-xylenes and mesitylene which were dried over activated molecular sieves (4Å) and degassed prior to use. Deuterated solvents were purchased from Sigma Aldrich.

Benzene-d_6, toluene-d_8 and THF-d_8 were dried and vacuum distilled from sodium-benzophenone ketyl and chloroform-*d* was dried, and vacuum distilled from CaH_2 prior to storing over activated molecular sieves (4 Å). NMR spectra were recorded using Bruker 300 MHz, Bruker 360 MHz and Bruker 500 MHz and Bruker 300 MHz NMR spectrometers. ^{1}H NMR spectra were calibrated using the residual protio signal of the solvent (δ ^{1}H (C_6D_6) = 7.16 ppm, ^{1}H(toluene-d_8) = 2.08, ^{1}H(THF-d_8) = 3.58, 1.72 and ^{1}H($CDCl_3$) = 7.26). ^{13}C NMR spectra were calibrated using the solvent signal (δ ^{13}C(C_6D_6) = 128.0 ppm). ^{11}B NMR spectra were calibrated against external standards (^{11}B: $BF_3{\cdot}OEt_2$ (δ ^{11}B = 0.0 ppm). All chemical shifts are given in ppm (parts per million).

$CAAC^{Me}$,[22] rac-Ph(Me)PH·BH_3,[23] $PCl_2(NEt_2)$[24] BH_2NMeH,[6] IDipp[10] and $Ph_2N{=}BH_2$[6] were prepared according to literature procedures. $B(C_6F_5)_3$ was purchased from Sigma Aldrich and purified using sublimation prior to use. All other chemicals were purchased from Sigma Aldrich and used as received.

GPC was performed on a Malvern RI max Gel Permeation Chromatograph, equipped with an automatic sampler, a pump, an injector, and inline degasser. The columns (1 x T5000 and 1 x T3000) were contained within an oven (35 °C) and consisted of styrene/divinyl benzene gels. Sample elution was detected by means of a differential refractometer. THF (Fisher), containing 0.1 wt.% [nBu$_4$N]Br, was used as the eluent at a flow rate of 1 mL min^{-1}. Samples were dissolved in the eluent (2 mg mL^{-1}) and filtered through a poly(tetrafluoroethylene) membrane of 200 nm pore size before analysis. The calibration was conducted using monodisperse polystyrene standards obtained from Aldrich. The lowest and highest molecular weight standards used were 1,200 Da and 4,200,000 Da respectively.

Solid state NMR was run on a Bruker Avance III 400 MHz spectrometer. ^{1}H spectra were referenced to adamantane (δ = 1.85 ppm), ^{13}C spectra were referenced to glycine (δ = 176.5 ppm), ^{11}B spectra were referenced to $NaBH_4$ (δ = -42.1 ppm) and ^{31}P spectra were referenced to $[NH_4][H_2PO_4]$ (δ = 0.9 ppm).

Electrospray ionisation mass spectrometry (ESI-MS) was performed using a MSQ Plus single quadrupole mass spectrometer (Thermo, MA). The instrument assembly includes a 515 HPLC pump (Waters, MA) with a flow rate set to 0.2 mL min^{-1}. A 50:50 solvent mixture was used comprising of Mili-Q™ water (Millipore, ON) and Optima™ Methanol (Fisher Chemical, NH). 200 uL of sample was injected using a manual injector (Rheodyne 7725i, IDEX, CA) in direct

infusion mode. Mass spectrometer parameters include cone voltage set to 75 V, mass range set to 50-2000 m/z and scan time 1 second.

Powder XRD diffraction patterns were collected using a Bruker D8-Advance X-ray diffractometer equipped with a LynxEye silicon strip detector using copper $K\alpha_1$ and $K\alpha_1$ radiation and a nickel filter (40 kV, 40 mA).

Differential scanning calorimetry (DSC) thermograms were measured using a DSC25 device with a heating/cooling rate of 10 °C min^{-1} and thermal gravimetric analysis (TGA) was carried out using an SDT Q600 device with a heating rate of 5 °C min^{-1} under a nitrogen atmosphere.

Air-sensitive mass spectrometry experiments were conducted using a Finnigan Trace DSQ system with Direct Probe Controller (Thermo, MA). Samples were loaded in flared glass direct injection probe sample cups in a glovebox under an inert atmosphere then transferred in vials to a chamber flushed with N_2 that was connected to the DSQ instrument. The sample cup was then inserted into the MS probe and then probe was inserted into the vacuum lock system of the probe inlet system then into the MS source of the DSQ. The sample was heated to 350 °C with the following temperature program (40 °C hold 1 min, ramp 60 °C min^{-1} to 350 °C hold 1 min). The DSQ MS was scanned continuously in EI mode from 100-1000 Da to analyse the thermally volatile analytes. The DSQ MS ion source temperature was set to 150 °C and electron energy set to 40eV during analysis.

5.5.2 Polymerisation of *rac*-Ph(Me)PH·BH_3 using $CAAC^{Me}$

$CAAC^{Me}$ (736 mg, 2.58 mmol) and *rac*-Ph(Me)PH·BH_3 (356 mg, 2.58 mmol) were dissolved in toluene (650 µL) in a sealed J. Young Schlenk and heated to 100 °C for 24h. The reaction mixture was added dropwise into 20 mL of rapidly stirred cold hexanes at -40 °C yielding a precipitate and the supernatant was decanted. The precipitation was repeated twice more prior to drying in vacuo to leave an off-white powder. GPC analysis showed a bimodal distribution with ca. 18% corresponding to high molar mass material. Yield (precipitated material) = 100 mg (29 %).

^{1}H NMR (300 MHz, 298 K, $CDCl_3$): δ = 7.83- 6.94 (m, br, Ar), 1.80 – 0.61 (m, br, BH_2, CH_3).

^{11}B NMR (96 MHz, 298 K, $CDCl_3$): δ = -29.1 (br).

^{31}P NMR (122 MHz, 298 K, $CDCl_3$): δ = -34.1 (br).

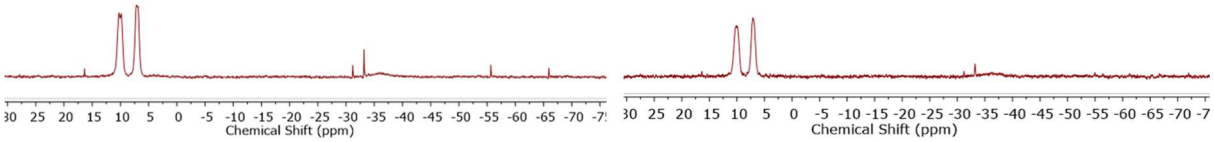

Figure S5.1 $^{31}P\{^{1}H\}$ (left) and ^{31}P (right) NMR spectra (122 MHz, 298 K, toluene) of the reaction mixture of PhMePH·BH_3 and $CAAC^{Me}$ prior to heating showing formation of $CAAC^{Me}$(H)PhMePBH_3.

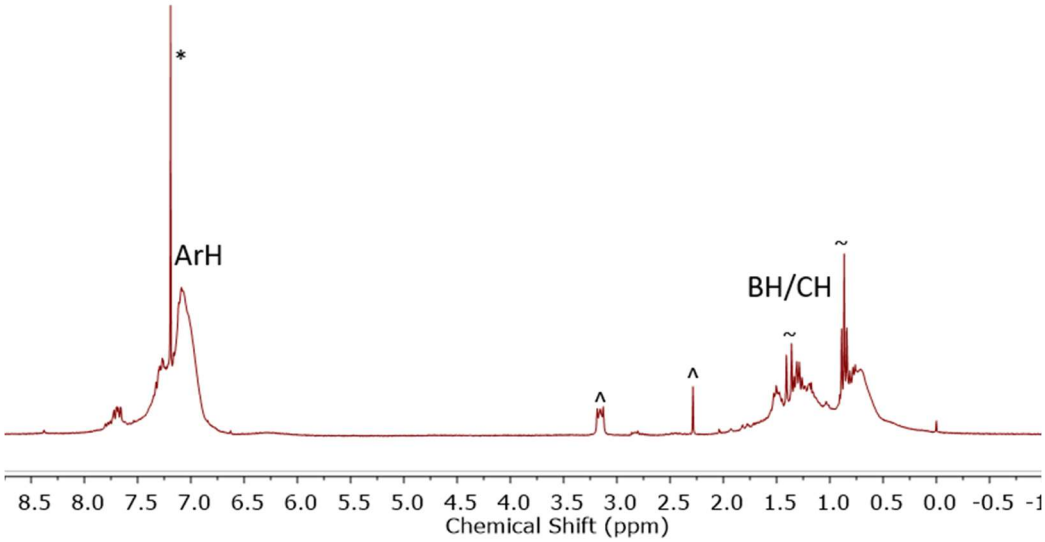

Figure S5.2 ^{1}H NMR spectrum (300 MHz, 298 K, $CDCl_3$) of isolated $[PhMeP–BH_2]_n$ formed from PhMePH·BH_3 and $CAAC^{Me}$ (*denotes residual partially protiated $CDCl_3$, ~denotes trace hexanes, #unidentified impurity).

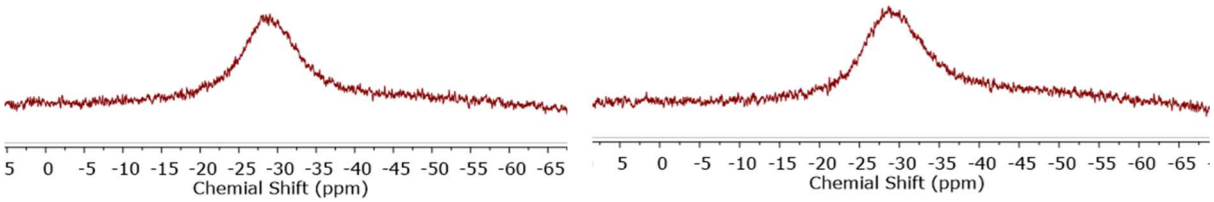

Figure S5.3 $^{11}B\{^{1}H\}$ (left) and ^{11}B (right) NMR spectra (96 MHz, 298 K, $CDCl_3$) of isolated $[PhEtP–BH_2]_n$ formed from PhMePH·BH_3 and $CAAC^{Me}$..

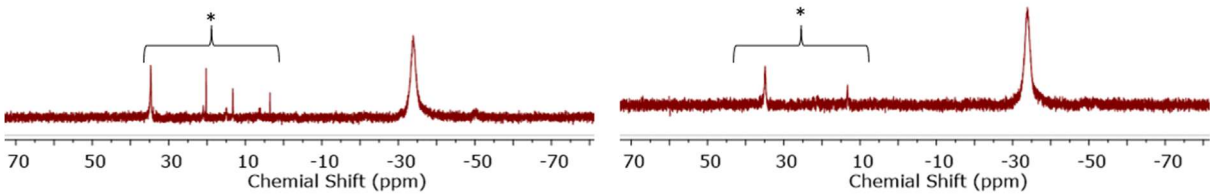

Figure S5.4 $^{31}P\{^{1}H\}$ (left) and ^{31}P (right) NMR spectra (122 MHz, 298 K, $CDCl_3$) of isolated $[PhEtP–BH_2]_n$ formed from PhMePH·BH_3 and $CAAC^{Me}$ (*denotes unidentified impurities)..

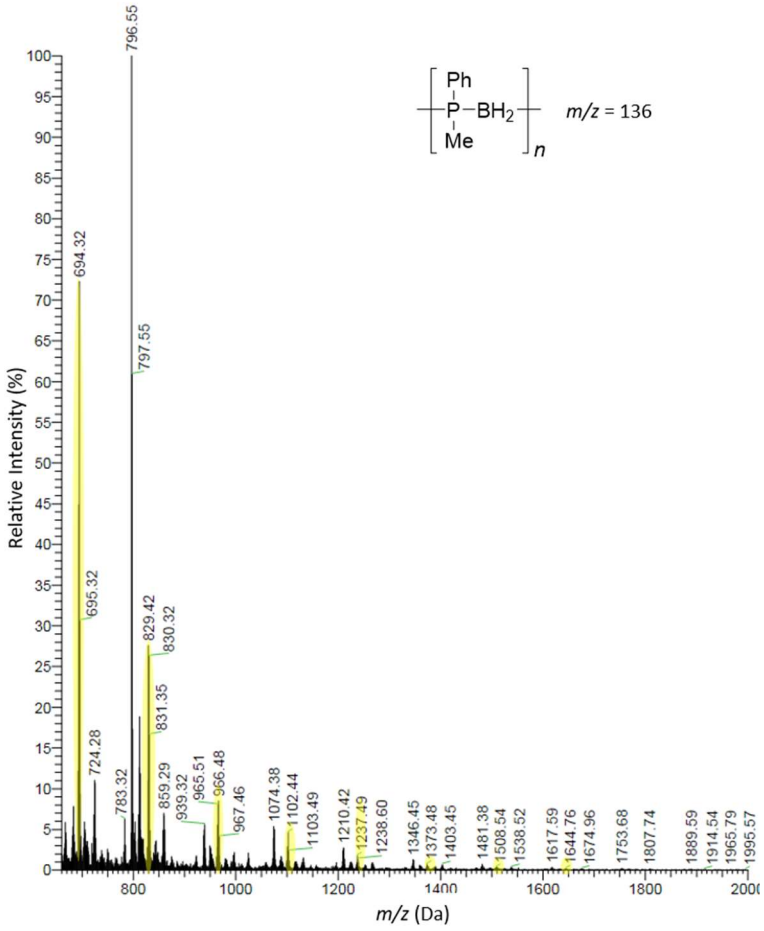

Figure S5.5 ESI(+)-MS spectrum in positive mode in THF:IPA (1:9) of isolated $[PhMeP–BH_2]_n$ formed from $PhMePH·BH_3$ and $CAAC^{Me}$. The predominant species, highlighted in yellow, is a linear system with a $CAAC^{Me}$ end group $(H\text{-}[PhMeP–BH_2]_n\text{-}CAAC^{Me})^+$.

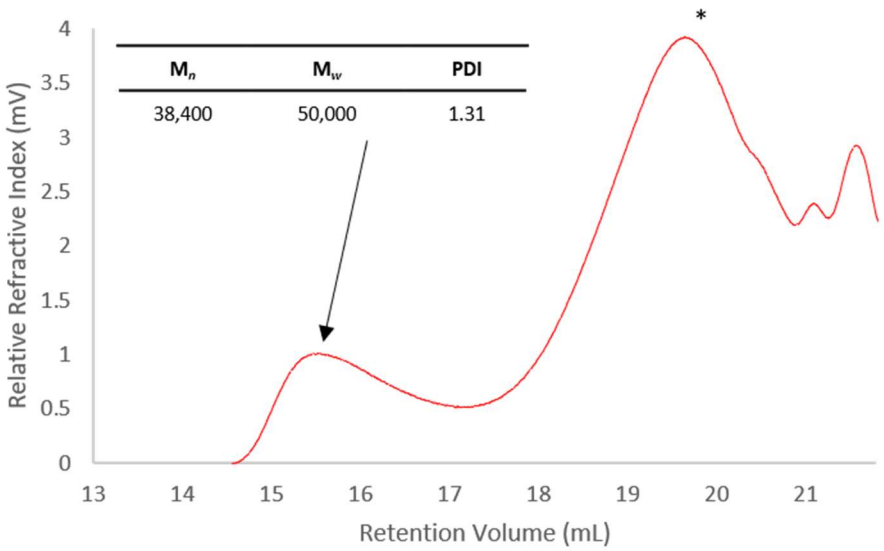

Figure S5.6 GPC chromatogram of isolated $[PhMeP–BH_2]_n$ formed from $PhMePH·BH_3$ and $CAAC^{Me}$. 2 mg mL^{-1} in THF with 0.1 w/w% nBu$_4$NBr in the THF eluent. The highest molar mass peak accounts for ca. 18% of the precipitated material.

5.5.3 Polymerisation of $Et_2PH{\cdot}BH_3$ using $CAAC^{Me}$

5.5.3.1 Synthesis of $PEt_2H{\cdot}BH_3$

$BH_3{\cdot}THF$ (1M in THF, 13.3 mL, 0.0133 mmol) was added slowly to PEt_2H (10 wt.% in hexanes, 1.0 g, 0.011 mmol) at -78 °C. The reaction was slowly warmed to 22 °C and stirred for 1 h. The solvent was removed *in vacuo* to leave a colourless oil which was filtered through a PTFE membrane (pore size 450 nm). Yield = 810 mg (70%).

^{11}B, ^{31}P and ^{1}H NMR data matches that previously reported.[25]

5.5.3.2 Synthesis of $CAAC^{Me}(H)Et_2PBH_3$ (5.1)

Method A

$CAAC^{Me}$ (1.00 g, 3.50 mmol) was dissolved in hexanes (5 mL) and added to $PEt_2H{\cdot}BH_3$ (364 mg, 3.50 mmol) in hexanes (5 mL). The reaction was stirred for 15 min and the solvent removed *in vacuo*. No work up was carried out prior to polymerisation. NMR data matches that of Method B.

Method B

$CAAC^{Me}$ (400 mg, 1.40 mmol) was dissolved in THF (2 mL) and PEt_2H (133 mg, 1.47 mmol) added dropwise. The reaction mixture was stirred for 10 min prior to volatiles being removed *in vacuo* to give $CAAC(H)PEt_2$. $CAAC(H)PEt_2$ (192 mg, 0.511 mmol) was dissolved in THF (1 mL) and cooled to -40°C. $BH_3{\cdot}SMe_2$ (2M in toluene, 0.27 mL, 0.54 mmol) was added and the reaction stirred for 15 min prior to the solvent being removed *in vacuo*. The product was recrystallised from hexanes at -40 °C. Yield = 42 mg (39%).

^{1}H NMR ($CDCl_3$, 500 MHz, 298 K): δ = 7.19-7.16 (m, 1H, $Dipp^p$), 7.09-7.07 (m, 2H $Dipp^m$), 4.05 (s, 1H, NCH), 3.93 (sept, 1H, $^{3}J_{HH}$ = 6.8, C*H*$(CH_3)_2$) , 3.05 (sept, 1H, *J* = 6.8, C*H*$(CH_3)_2$), 2.06 (m, 2H, CH_2), 1.72 (m, 1H, P*CH*$_2CH_3$), 1.63 (m, 1H, P*CH*$_2CH_3$), 1.62 (s, 3H, NC(HP)C(C*H*$_3)_2$), 1.57 (s, 3H, NC$(CH_3)_2$), 1.41 (s, 3H, C(H)(P)C(C*H*$_3)_2$), 1.38 (d, 3H, $^{3}J_{HH}$ = 6.8, CH(C*H*$_3)_2$), 1.25 (d, 3H, $^{3}J_{HH}$ = 6.8, CH(C*H*$_3)_2$), 1.23 (d, 3H, $^{3}J_{HH}$ = 6.8, CH(C*H*$_3)_2$), 1.18 (d, 3H, $^{3}J_{HH}$ = 6.8, CH(C*H*$_3)_2$), 1.00 (m, 3H, PCH_2C*H*$_3$), 0.79 (m, 3H, PCH_2C*H*$_3$), 0.89 (s, 3H, NC$(CH_3)_2$)0.56 (m, 3H, BH_3)

^{13}C NMR ($CDCl_3$, 126 MHz, 298 K): δ = 150.3 (Ar), 147.4 (Ar), 144.3 (Ar), 126.8 (Ar), 125.9 (Ar), 124.5 (Ar), 73.4 (NCP), 64.3 (N*C*$(CH_3)_2$), 60.2 (CH_2), 43.3 (NC(HP)*C*$(CH_3)_2$), 32.8 (NC(HP)C(*C*$H_3)_2$), 32.4 (NC(HP)C(*C*$H_3)_2$), 28.8 (NC(*C*$H_3)_2$), 28.6 (NC(*C*$H_3)_2$), 28.5 (*C*H$(CH_3)_2$), 27.5 (*C*H$(CH_3)_2$), 26.8 (CH(*C*$H_3)_2$), 25.6 (CH(*C*$H_3)_2$), 24.8 (CH(*C*$H_3)_2$), 24.5 (CH(*C*$H_3)_2$), 16.0 (CH_3*C*H_2), 13.7 (CH_3*C*H_2), 7.4 (*C*H_3CH_2), 7.0 (*C*H_3CH_2)

$^{11}B\{^{1}H\}$ NMR ($CDCl_3$, 96 MHz, 295 K): δ = -40.3 (d, $^{1}J_{BP}$ = 44 Hz)

^{11}B NMR ($CDCl_3$, 96 MHz, 295 K): δ = -40.3 (m)

$^{31}P\{^{1}H\}$ ($CDCl_3$, 122 MHz, 298 K): δ = 26.1 (d, $^{1}J_{BP}$ = 50 Hz)

^{31}P ($CDCl_3$, 122 MHz, 298 K): δ = 26.1 (m)

Elemental analysis for $C_{24}H_{45}BNP$: (calcd/expt): C(74.02/74.00), H(11.65/11.95), N(3.60/3.54).

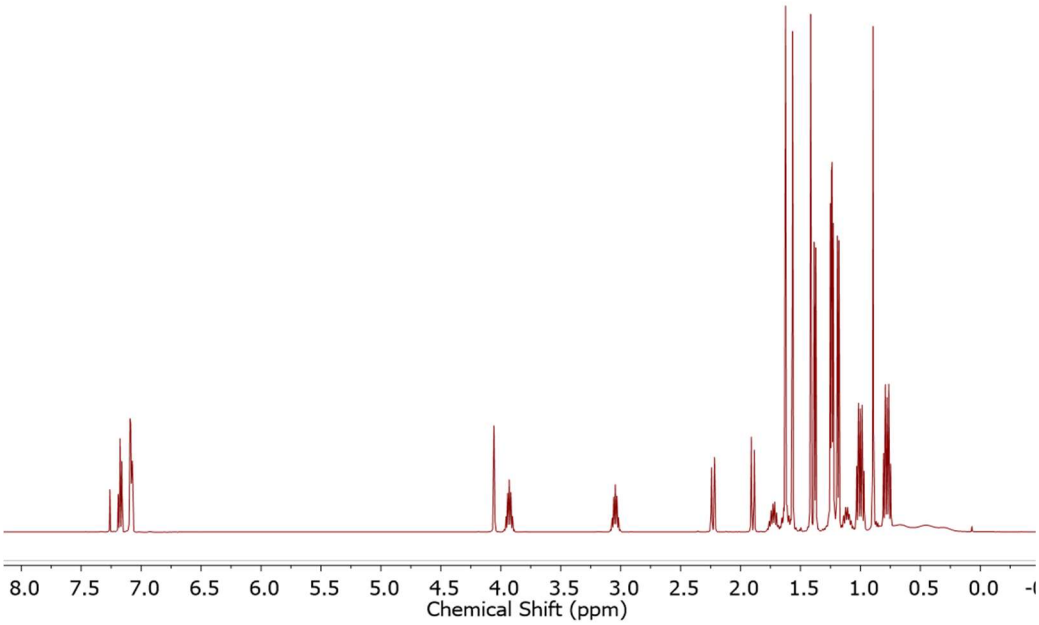

Figure S5.7 ^{1}H NMR spectrum ($CDCl_3$, 500 MHz, 298 K) of **5.1**.

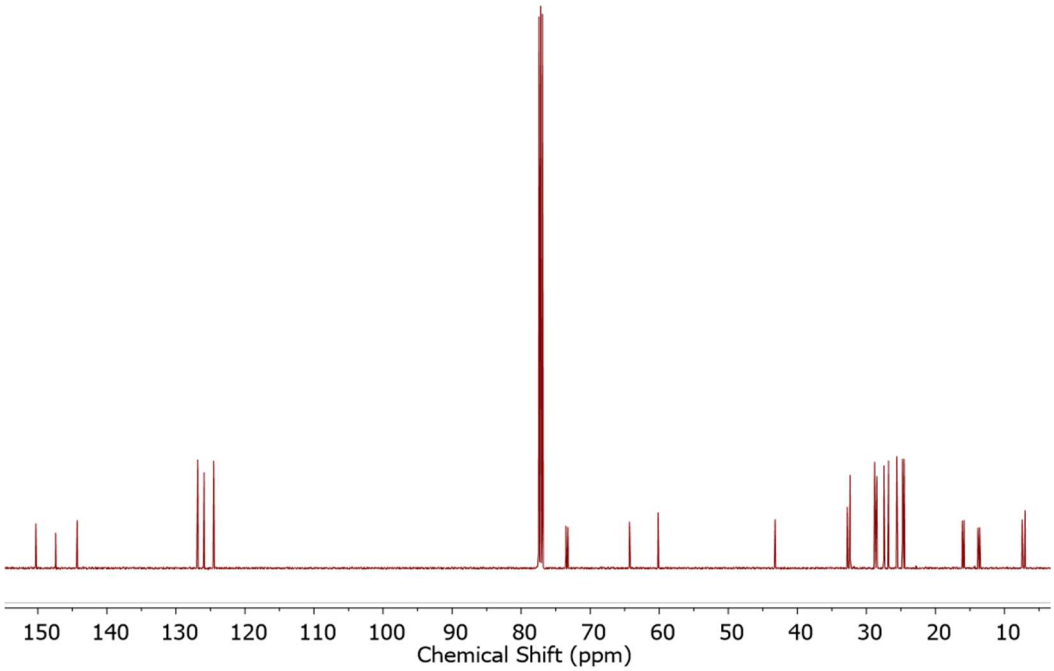

Figure S5.8 ^{1}H NMR spectrum ($CDCl_3$, 126 MHz, 298 K) of **5.1**.

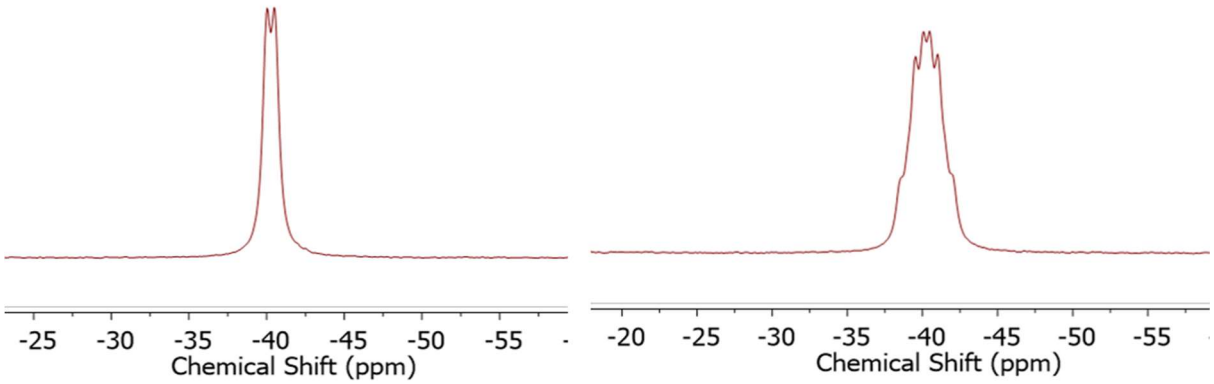

Figure S5.9 $^{11}B\{^{1}H\}$ (left) and ^{11}B (right) NMR spectra ($CDCl_3$, 96 MHz, 295 K) of **5.1**.

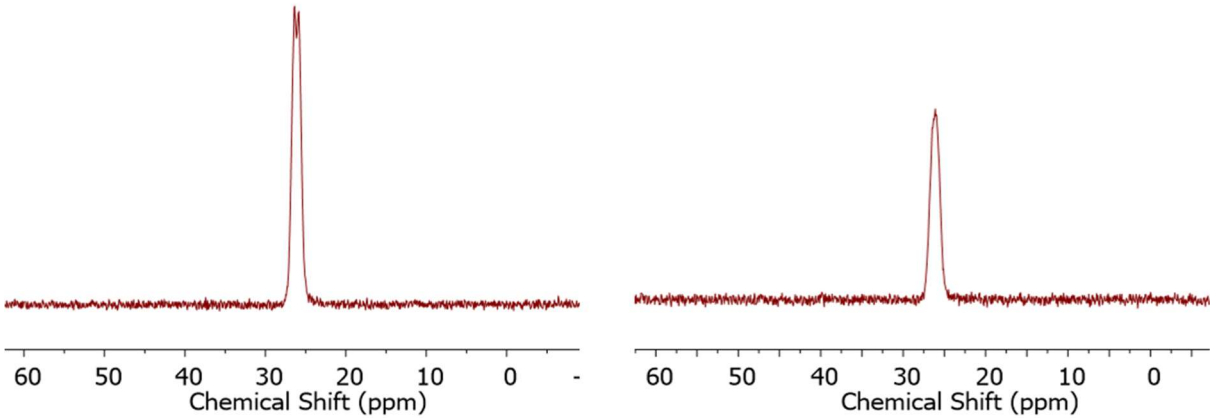

Figure S5.10 $^{31}P\{^{1}H\}$ (left) and ^{31}P (right) NMR spectra ($CDCl_3$, 122 MHz, 298 K) of **5.1**.

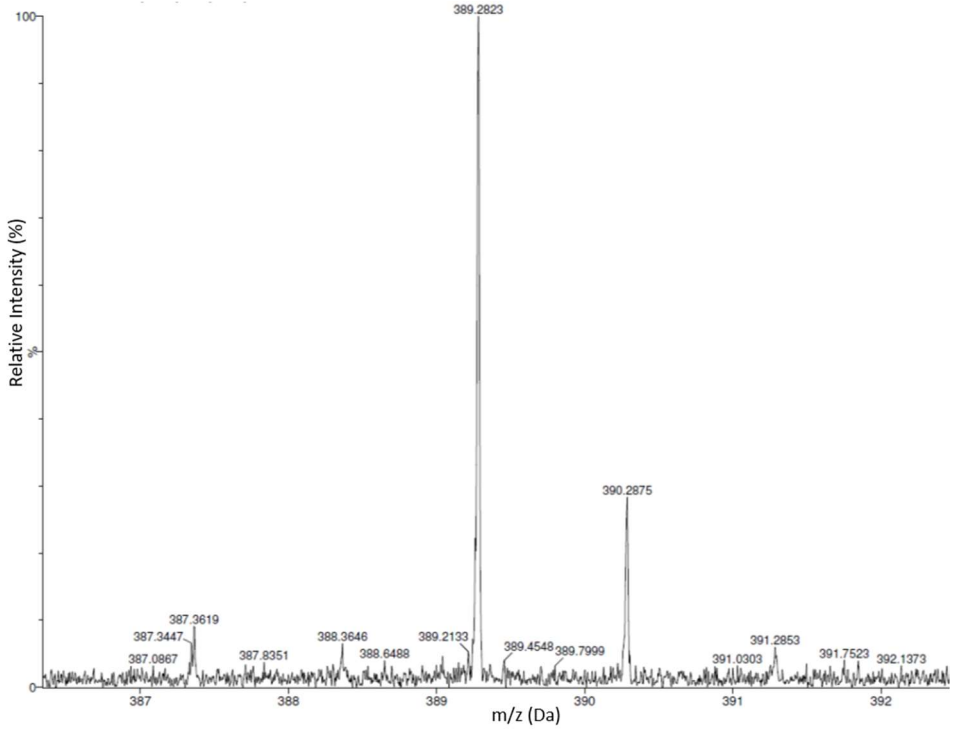

Figure S 5.11 ESI(+)-MS spectrum of **5.1** in DCM (sample injection performed under ambient conditions in air).

5.5.3.3 Synthesis of $[Et_2P–BH_2]_n$

The material synthesised in 5.5.3.2 (Method A) was dissolved in *o*-xylenes (1.7 mL) and heated to 140 °C for 24 h. Full consumption of $CAAC^{Me}(H)Et_2PBH_3$ was detected using ^{11}B NMR spectroscopy and a white precipitate can be observed to form. The reaction mixture was centrifuged, and the xylene soluble fraction decanted off. The white precipitate (insoluble in THF, toluene and hexanes) was washed with a combination of these solvents to leave a white powder. Yield = 101 mg (28%).

^{1}H NMR (CP-MAS): δ = 1.33 (br)

^{13}C NMR (CP-MAS): δ = 19.8, 17.7, 9.5, 8.9

$^{11}B\{^{1}H\}$ NMR (CP-MAS): δ = -37.7

$^{31}P\{^{1}H\}$ NMR (CP-MAS): δ = -22.3

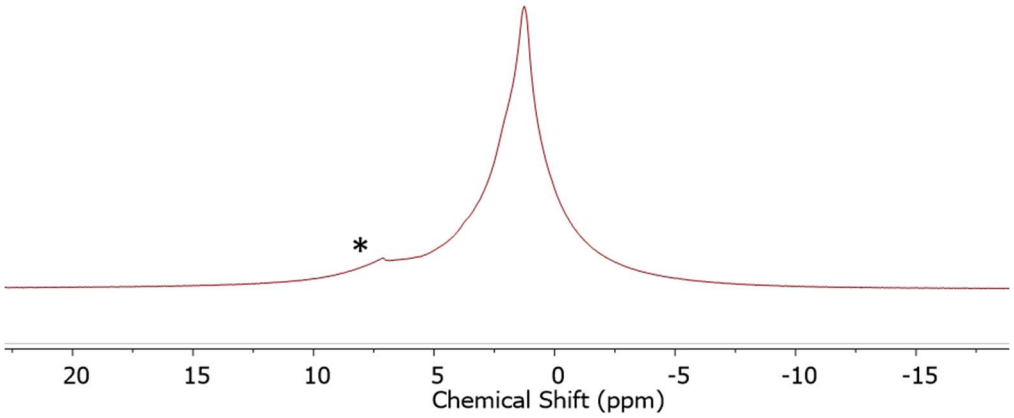

Figure S5.12 ^{1}H NMR (CP-MAS) of $[Et_2P–BH_2]_n$ (*postulated to be residual *o*-xylene trapped within the polymer chains).

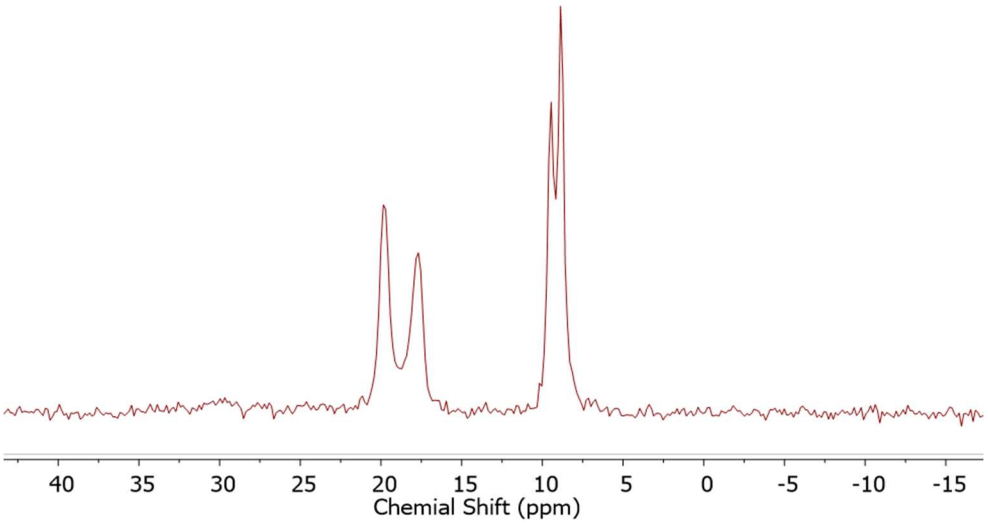

Figure S5.13 ^{13}C NMR (CP-MAS) of $[Et_2P–BH_2]_n$.

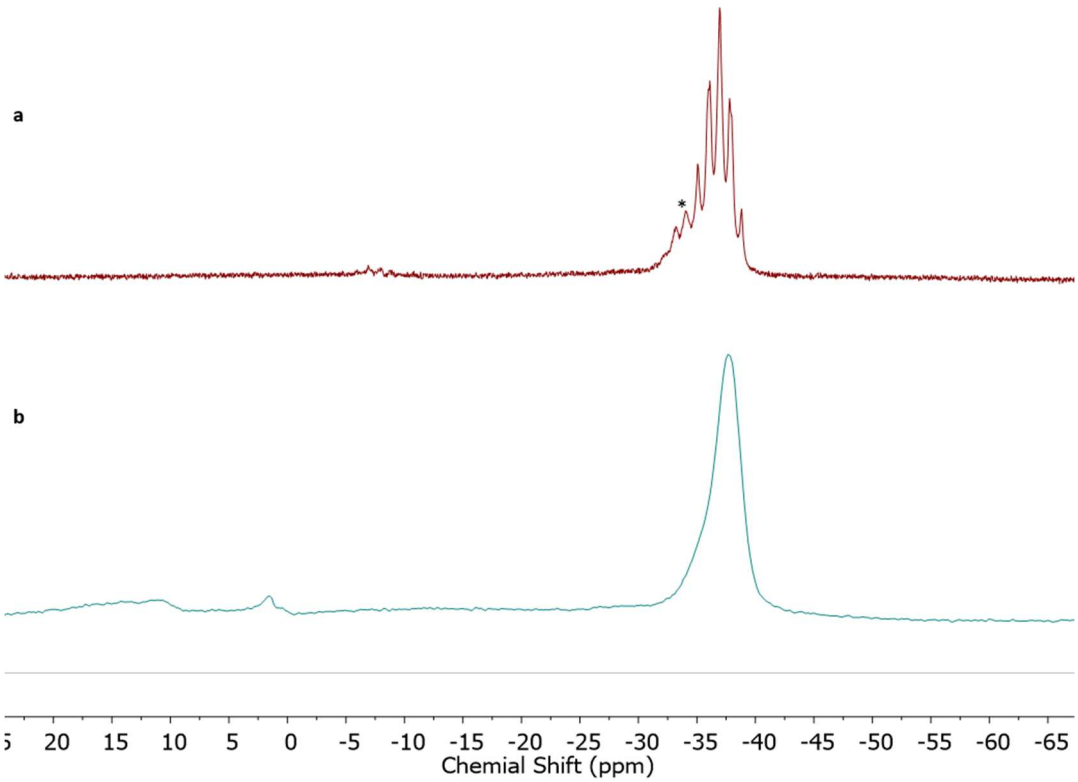

Figure S5.14 a ^{11}B NMR (*o*-xylene, 96 MHz, 298 K) and **b** ^{11}B NMR (CP-MAS) of $[Et_2P–BH_2]_n$ (*denotes possible end group).

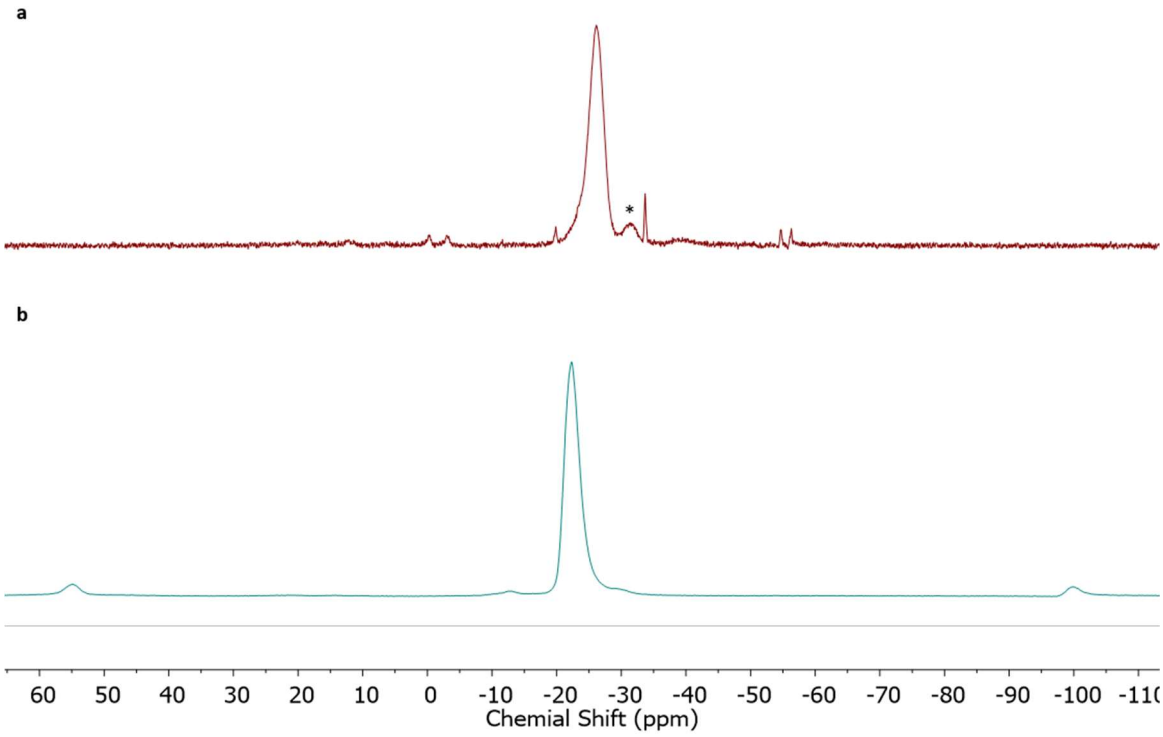

Figure S5.15 a ^{31}P NMR (*o*-xylene, 122 MHz, 298 K) and **b** ^{31}P NMR (CP-MAS) of $[Et_2P–BH_2]_n$ (*denotes possible end group).

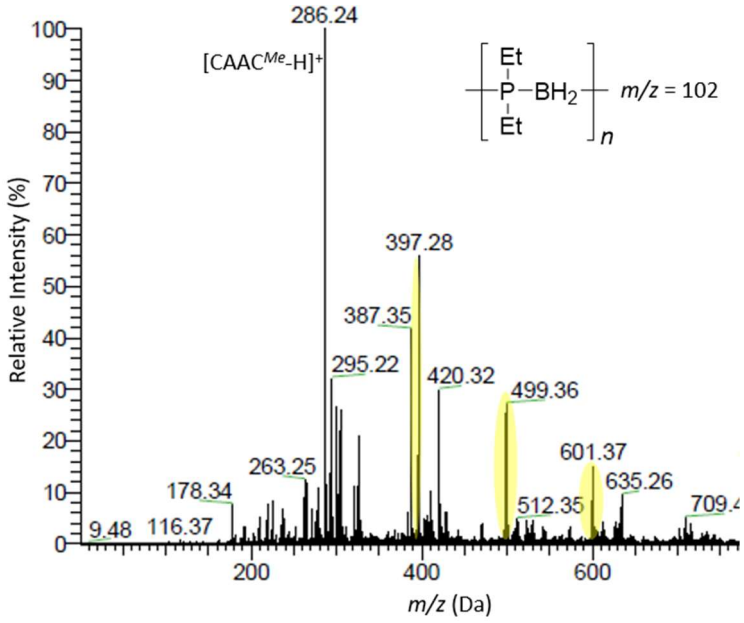

Figure S5.16 ESI(+)-MS spectrum in positive mode in THF:IPA (1:9) of isolated $[Et_2P–BH_2]_n$ formed from $Et_2PH·BH_3$ and $CAAC^{Me}$

5.5.3.4 Thermal analysis of $[Et_2P–BH_2]_n$

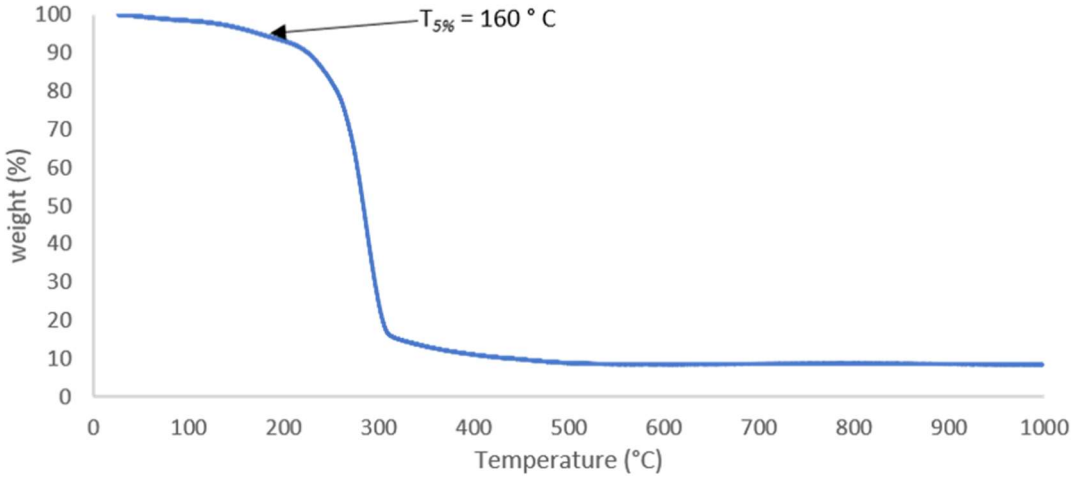

Figure S5.17 TGA thermogram of $[Et_2P–BH_2]_n$ (heating rate: 5 °C min^{-1}).

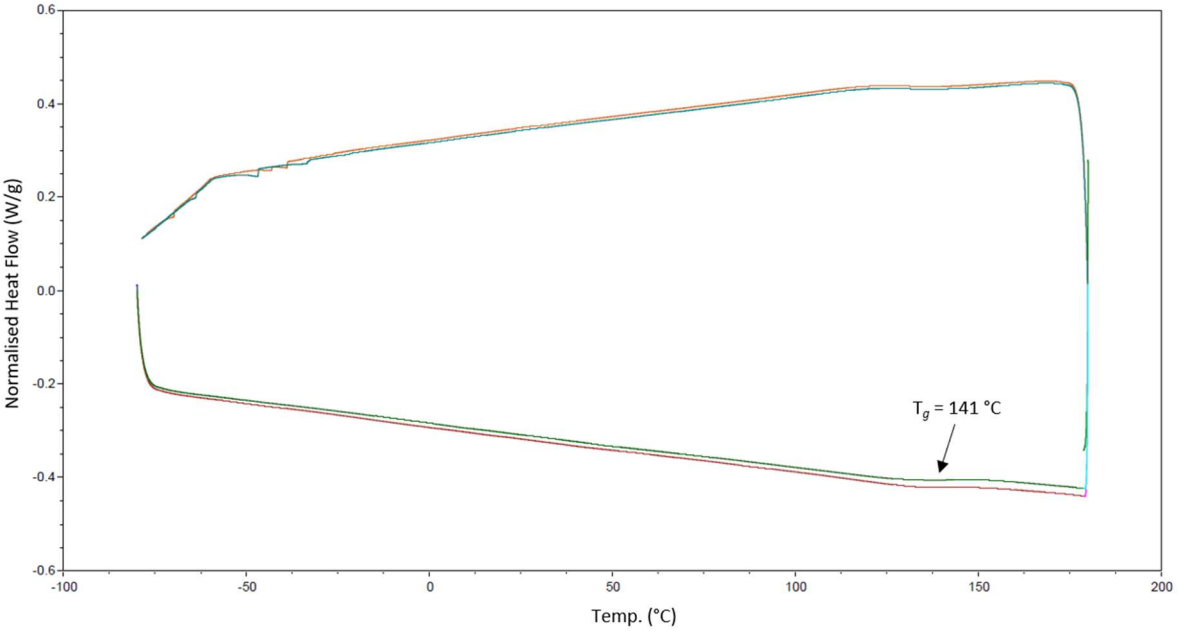

Figure S5.18 DSC thermogram for $[Et_2P–BH_2]_n$ synthesised in *o*-xylene (heating rate: 10 °C min^{-1} and first cycle excluded).

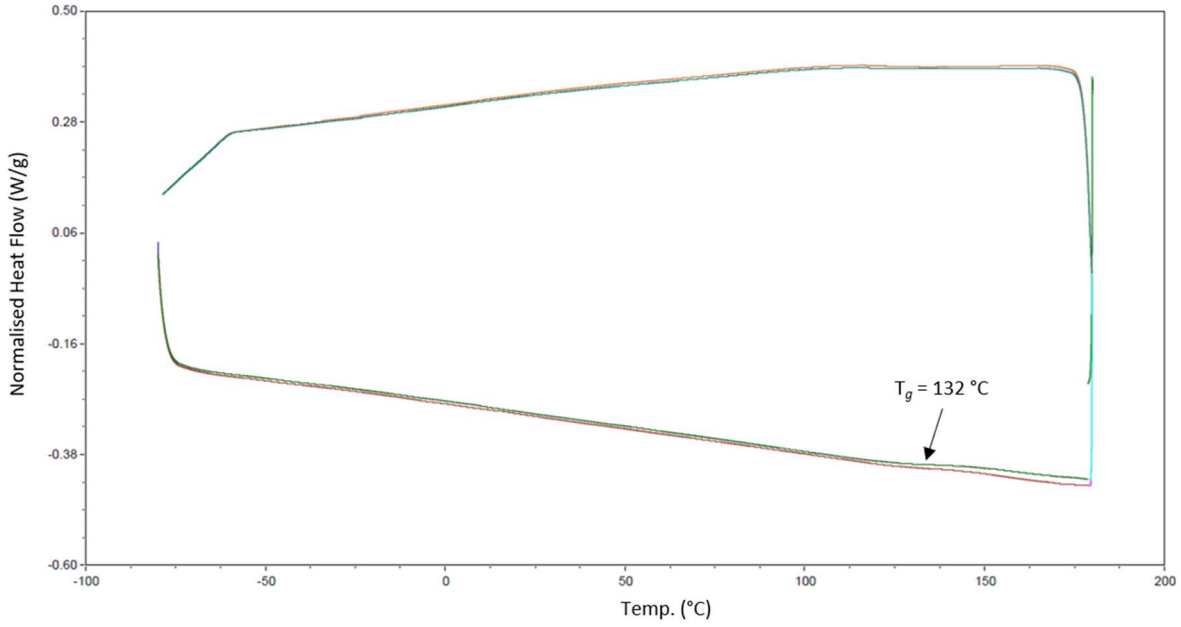

Figure S5.19 DSC thermogram for $[Et_2P–BH_2]_n$ synthesised in mesitylene (heating rate: 10 °C min^{-1} and first cycle excluded).

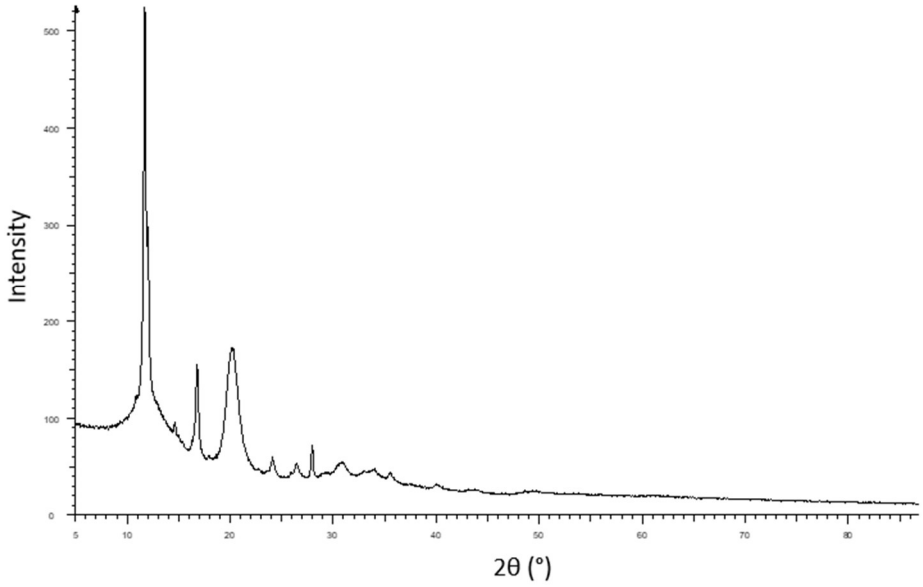

Figure S5.20 Powder XRD spectrum of $[Et_2P–BH_2]_n$ synthesised in *o*-xylene..

5.5.4 Polymerisation of *n*Hex$_2$PH·BH$_3$ using CAAC^{Me}

5.5.4.1 Synthesis of *n*Hex$_2$PH·BH$_3$

This procedure is adapted from that of a synthesis reported for *n*HexPH$_2$·BH$_3$.[26]

*n*HexLi (2.6 M in hexanes, 34.0 mL, 0.0689 mol) dissolved in Et_2O (60 mL) was added to a solution of $(Et_2N)PCl_2$ (5.33 g, 0.0306 mol) in Et_2O (40 mL) at -78 °C over 15 min. The reaction was stirred for a further 15 min at -78 °C and for 2 h at 22 °C before cooling back to -78 °C. HCl (2M in Et_2O, 28.0 mL, 0.0643 mol) was added over 15 min prior to stirring for 1 h at -78 °C and 18 h at 22 °C. The reaction was filtered to leave a white solid which was washed with Et_2O (120 mL). The solvent was removed *in vacuo* to leave a colourless oil. ^{31}P NMR spectroscopy was used to confirm synthesis of *n*Hex$_2$PCl. Yield = 6.50 g (90 %)

*n*Hex$_2$PCl (6.50 g, 0.0275 mol) was redissolved in Et_2O (40 mL) and added to slurry of $LiBH_4$ (628 mg, 0.0288 mmol) in Et_2O (60 mL) at 0 °C over 20 min. The reaction was stirred at 22 °C for 18 h prior to removing the solvent *in vacuo*, extracting into hexanes (50 mL) and filtering. The product was isolated as a colourless oil after removing the solvent *in vacuo*. Yield = 4.78 g (80 %).

^{31}P and ^{1}H NMR data matches that previously reported.[27]

5.5.4.2 Synthesis of [*n*Hex$_2$P–BH$_2$]$_n$

CAAC^{Me} (300 mg, 1.05 mmol) and *n*Hex$_2$PH·BH$_3$ (227 mg, 1.05 mmol) were dissolved in *o*-xylenes (500 µL) in a sealed J. Young Schlenk and heated to 130 °C for 24 h. ^{11}B and ^{31}P NMR spectroscopy showed full conversion to a new phosphorus and boron species. The solvent was removed *in vacuo* to leave a viscous oil. Further purification to separate the (CAAC^{Me})H$_2$ by product from the P–B containing product has not been successful.

^{1}H NMR (300 MHz, 298 K, $CDCl_3$): δ = 1.58 – 0.76 (m, br, BH_2, CH_2, CH_3).

^{11}B NMR (96 MHz, 298 K, $CDCl_3$): δ = -36.5 (br).

^{31}P NMR (122 MHz, 298 K, $CDCl_3$): δ = -28.5 (br), -31.5 (br).

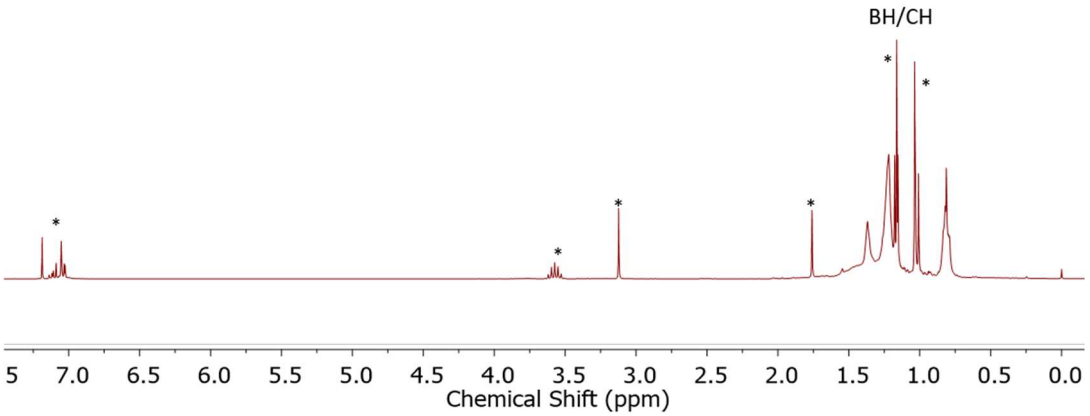

Figure S5.21 ^{1}H NMR spectrum (300 MHz, 298 K, $CDCl_3$) of the crude reaction of CAAC^{Me} and *n*Hex$_2$PH·BH$_3$ (~denotes residual partially protiated $CDCl_3$,*denotes (CAAC^{Me})H$_2$).

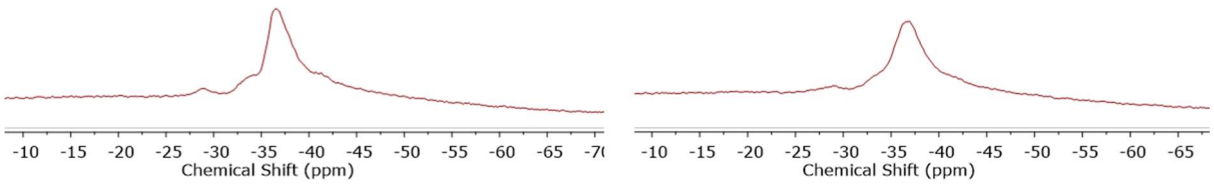

Figure S5.22 ^{11}B{^{1}H} (left) and ^{11}B (right) NMR spectra (96 MHz, 298 K, $CDCl_3$) of the crude reaction of CAAC^{Me} and *n*Hex$_2$PH·BH$_3$.

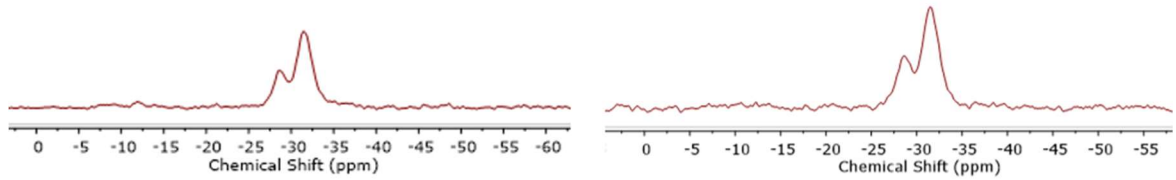

Figure S5.23 ^{31}P{^{1}H} (left) and ^{31}P (right) NMR spectra (122 MHz, 298 K, $CDCl_3$) of the crude reaction of CAAC^{Me} and *n*Hex$_2$PH·BH$_3$. The observation of two peaks is explained by the presence of oligomeric and polymeric material.

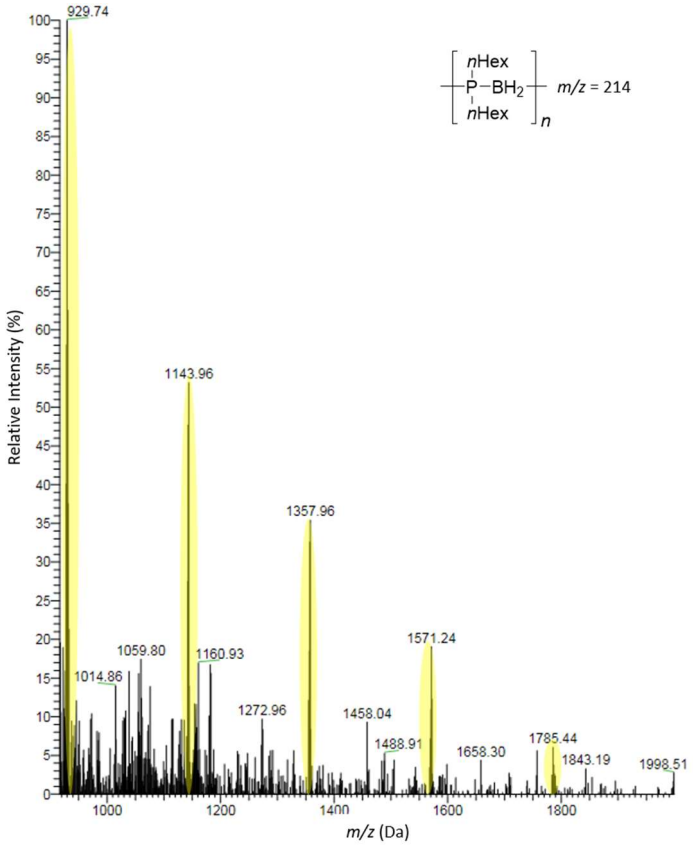

Figure S5.24 ESI(+)-MS spectrum in positive mode in THF:IPA (1:9) of the material from the crude reaction of CAAC^{Me} and *n*Hex$_2$PH·BH$_3$.The predominant species, highlighted in yellow, is a linear system with a CAAC^{Me} end group (H-[*n*Hex$_2$P–BH$_2$]$_n$-CAAC^{Me})$^+$.

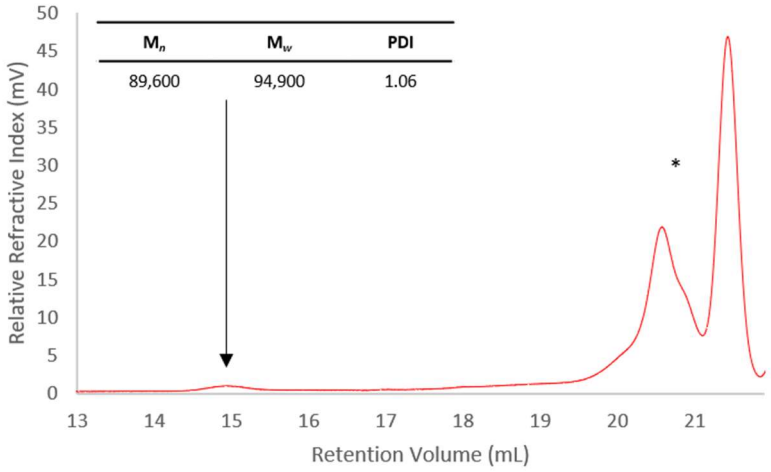

Figure S5.25 GPC chromatogram of the material from the crude reaction of CAAC^{Me} and *n*Hex$_2$PH·BH$_3$. 2 mg mL^{-1} in THF with 0.1 w/w% *n*Bu$_4$NBr in the THF eluent (*oligomeric material and (CAAC^{Me})H$_2$).

5.5.5 Attempted synthesis of copolymers [Ph$_2$P–BH$_2$]$_n$-r-[PhHP–BH$_2$]$_m$ using CAAC^{Me}

CAAC^{Me} (115 mg, 0.403 mmol) and PhPH$_2$·BH$_3$/Ph$_2$PH·BH$_3$ (quantities shown in Table S5.1) were dissolved in toluene (200 µL) in a J. Young Schlenk and heated to 60 °C for 3h. NMR, ESI-

MS and GPC analysis were carried out after precipitation of the reaction mixture into cold (-40 °C) hexanes.

Table S5.1 Copolymerisation of $PhPH_2{\cdot}BH_3$ with $Ph_2PH{\cdot}BH_3$.

Run	$PhPH_2{\cdot}BH_3$: $Ph_2PH{\cdot}BH_3$	$PhPH_2{\cdot}BH_3$		$Ph_2PH{\cdot}BH_3$	
		mg	mmol	mg	mmol
1	100:0	50	0.40	0	0
2	95:5	45	0.36	8	0.04
3	75:25	37	0.30	20	0.10
4	50:50	25	0.20	40	0.20
5	25:75	12	0.10	60	0.30
6	5:95	5	0.04	72	0.36
7	0:100	0	0	80	0.40

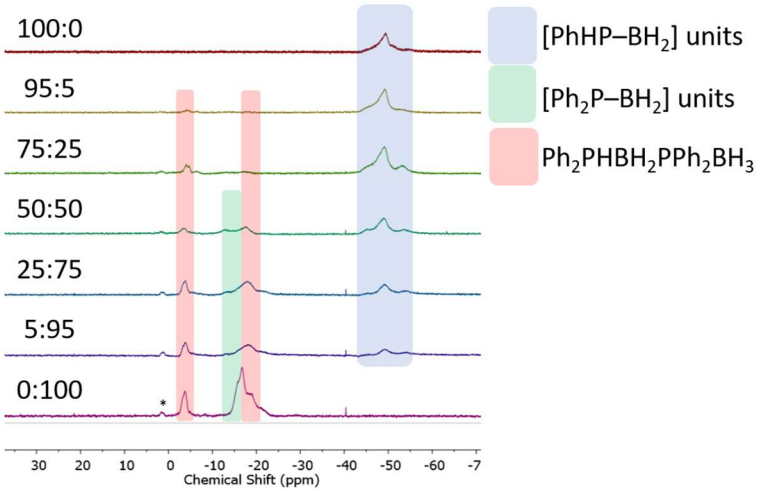

Figure S5.26 $^{31}P\{^{1}H\}$ NMR spectra (122 MHz, 298 K, $CDCl_3$) of the isolated material from the copolymerisations of $PhPH_2{\cdot}BH_3$ with $Ph_2PH{\cdot}BH_3$ (*unreacted $Ph_2PH{\cdot}BH_3$).

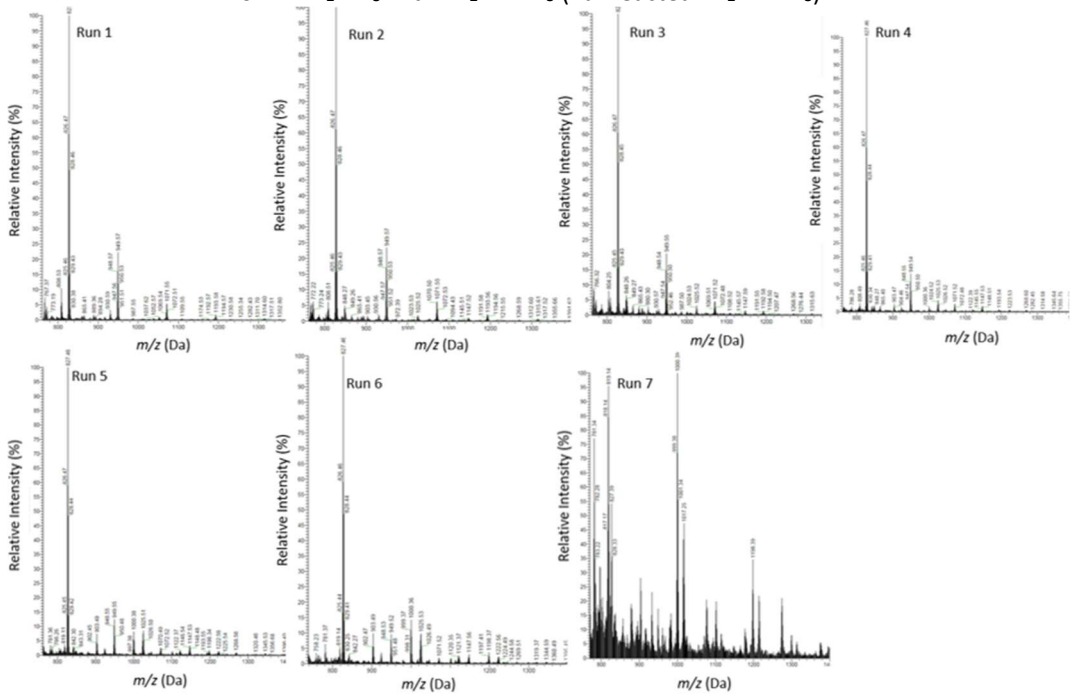

Figure S5.27 ESI(+)-MS spectrum in positive mode in THF:IPA (1:9) of the isolated material from the copolymerisations of $PhPH_2{\cdot}BH_3$ with $Ph_2PH{\cdot}BH_3$

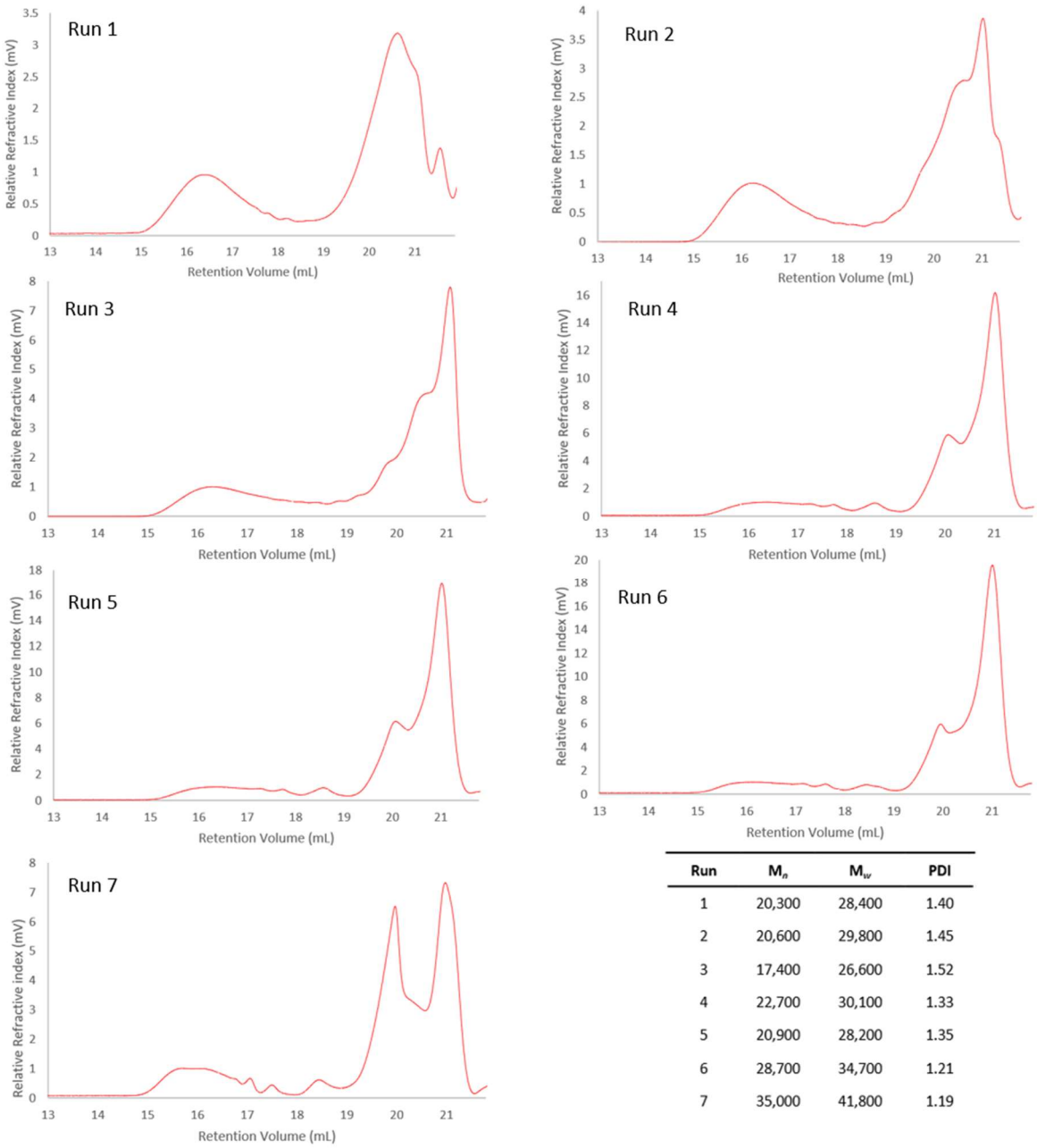

Run	M_n	M_w	PDI
1	20,300	28,400	1.40
2	20,600	29,800	1.45
3	17,400	26,600	1.52
4	22,700	30,100	1.33
5	20,900	28,200	1.35
6	28,700	34,700	1.21
7	35,000	41,800	1.19

Figure S5.28 GPC chromatograms of the isolated material from the copolymerisations of $PhPH_2{\cdot}BH_3$ with $Ph_2PH{\cdot}BH_3$**.** 2 mg mL^{-1} in THF with 0.1 w/w% $n$$Bu_4NBr$ in the THF eluent.

5.5.6 Thermolysis of Dipp–BH_2NMeH

5.5.6.1 Synthesis of ring expansion product (5.2)

IDipp–BH_2NMeH (280 mg, 0.633 mmol) was dissolved in toluene (10 mL) and heated at 80 °C for 24 h. The solvent was removed *in vacuo* to leave a yellow oil. Purification and crystallisation attempts were unsuccessful.

^{1}H and ^{11}B NMR data were comparable to that of [(HCNDipp)$_2$CH$_2$BNHDipp].[7]

5.5.6.2 Synthesis of IDipp–BH_2·NMeBH·NMeH (5.3)

IDipp–BH_2NMeH (100 mg, 0.230 mmol) was dissolved in C_6D_6 (500 µL) and heated to 80 °C for 24 h. ^{1}H NMR spectroscopy of the reaction mixture showed the presence of several NHC containing species (Figure 5.5). Single crystals of IDipp–BH_2·NMeBH·NMeH suitable for X-ray diffraction were grown from the reaction mixture over 1 week at 22 °C and sent for analysis. Remaining crystals were purified by washing with hexanes. Yield = 4 mg (8%). EI-MS: expected 471.39, actual 471.39.

^{1}H NMR (C_6D_6, 500 MHz, 298 K): δ = 7.26-7.22 (m, 2H, Dipp^p), 7.12-7.10 (m, 4H, Dipp^m), 6.37 (s, 2H, NCH), 4.30 (br, 1H, NH), 2.85 (s, 3H, $NB_2(CH_3)$), 2.74 (m, 4H, C<u>*H*</u>$(CH_3)_2$), 2.59 (d, $^3J_{HH}$ = 5.7 Hz, 3H, NH(C<u>*H*</u>$_3$)), 1.39 (d, $^3J_{HH}$ = 5.8 Hz, 12 H, CH(C<u>*H*</u>$_3)_2$), (d, $^3J_{HH}$ = 5.8 Hz, 12 H, CH(C<u>*H*</u>$_3)_2$). B–H signals not detected.

^{13}C (C_6D_6, 91 MHz, 298 K): δ = 175.9 (CB), 145.8 (Ar), 134.9 (Ar), 130.1 (Ar), 123.9 (Ar), 122.5 (NCH), 44.6 (NCH_3), 32.2 ($NHCH_3$), 28.9 (<u>*C*</u>H$(CH_3)_2$), 25.8 (CH(<u>*C*</u>H$_3)_2$), 22.7 (CH(<u>*C*</u>H$_3)_2$). The carbene carbon was assigned using ^{1}H,^{13}C-HMBC.

^{11}B NMR (C_6D_6, 116 MHz, 298 K): δ = 32.6 (br, B), -18.3 (t, $^1J_{BH}$ = 89 Hz, BH_2).

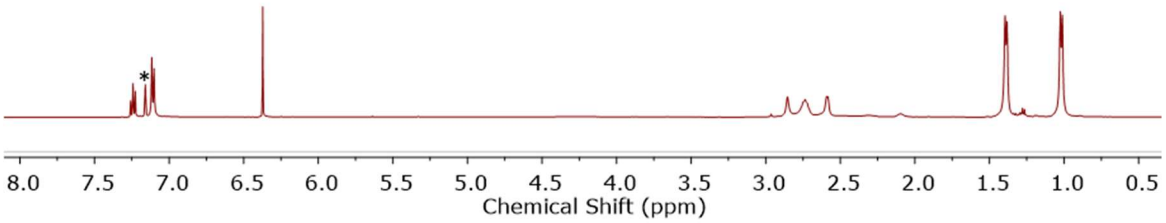

Figure S5.29 ^{1}H NMR spectra (C_6D_6, 500 MHz, 298 K) of **5.3** (*denotes residual partially protiated C_6D_6).

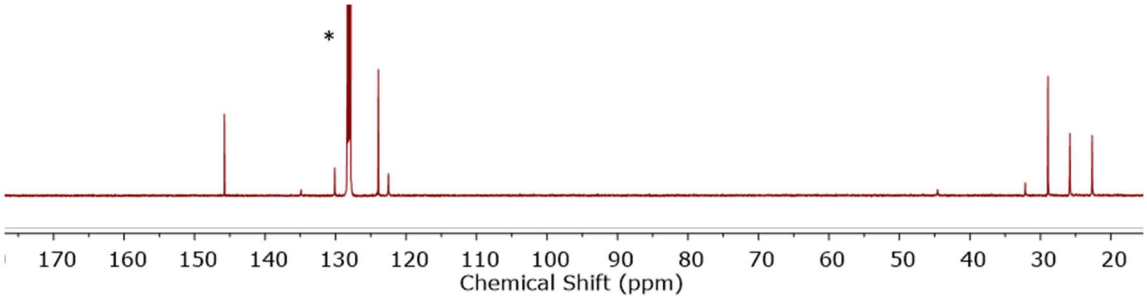

Figure S5.30 ^{13}C NMR spectra (C_6D_6, 91 MHz, 298 K) of **5.3**.

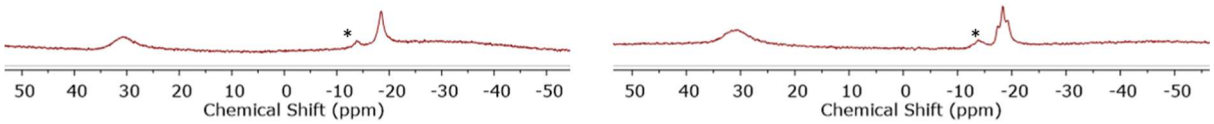

Figure S5.31 $^{11}B\{^{1}H\}$ (left) and ^{11}B (right) NMR spectra (THF, 116 MHz, 298 K) of **5.3** (*unidentified impurity).

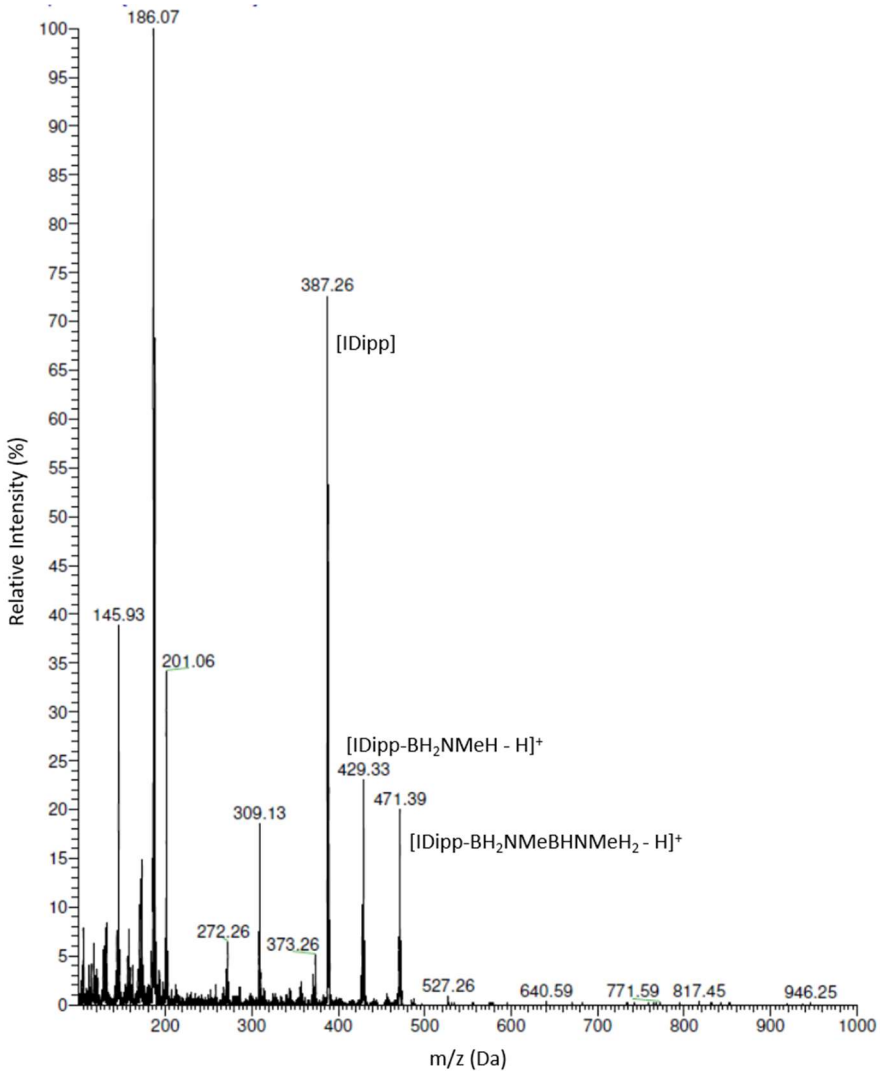

Figure S5.32 EI (+) mass spectrum of **5.3**.

5.5.7 Addition of Lewis acids to IDipp–BH_2NMeH

5.5.7.1 Attempted regeneration of $[MeHN–BH_2]_n$ from IDipp–BH_2NMeH with $Ph_2N=BCl_2$

To a solution of $Ph_2N=BCl_2$ (11 mg, 0.046 mmol) in toluene (250 µL) was added a solution of IDipp–BH_2NMeH (20 mg, 0.046 mmol) in toluene (250 µL) at 22 °C in a J. Young NMR tube. A small amount of white precipitated was immediately observed. The reaction mixture was analysed by ^{11}B NMR spectroscopy after 10 min and quantitative consumption of the triplet which corresponds to IDipp–BH_2NMeH [δ_B = -16.2 ppm][8] was detected. A small peak at δ_B = 2.5 ppm was tentatively assigned as IDipp–BCl_2NPh_2 (δ_B = 1.2 ppm (s))[8] and peaks at

(δ = 30.7 ppm (br) (ca. 49%), 8.0 ppm (s) (ca. 2%) and -16.1 ppm (br) (ca. 49%)) are currently unassigned. Analysis of the crude material by ESI-MS revealed peaks with a difference of *m/*z = 43 and GPC analysis shows a small quantity of high molar mass material.

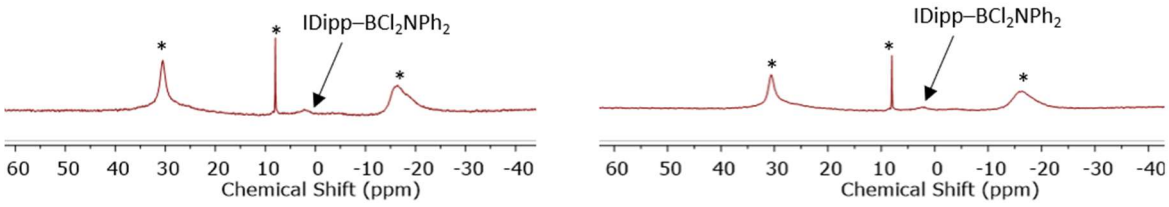

Figure S5.33 $^{11}B\{^{1}H\}$ (left) and ^{11}B (right) NMR spectra (96 MHz, 293 K, toluene) of the reaction solution of $Ph_2N{=}BCl_2$ and IDipp–BH_2NMeH (*unassigned products).

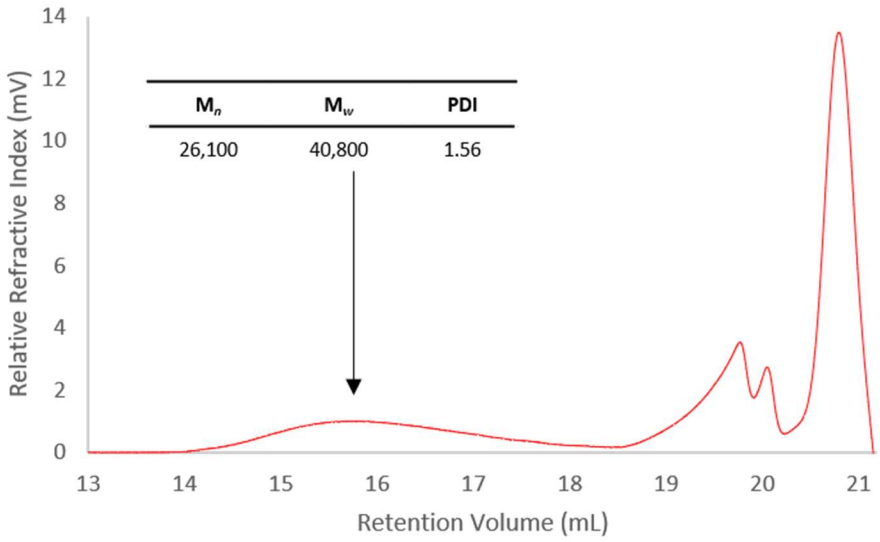

Figure S5.34 GPC chromatogram of the products of the reaction between $Ph_2N{=}BCl_2$ and IDipp–BH_2NMeH. 2 mg mL^{-1} in THF with 0.1 w/w% *n*Bu_4NBr in the THF eluent.

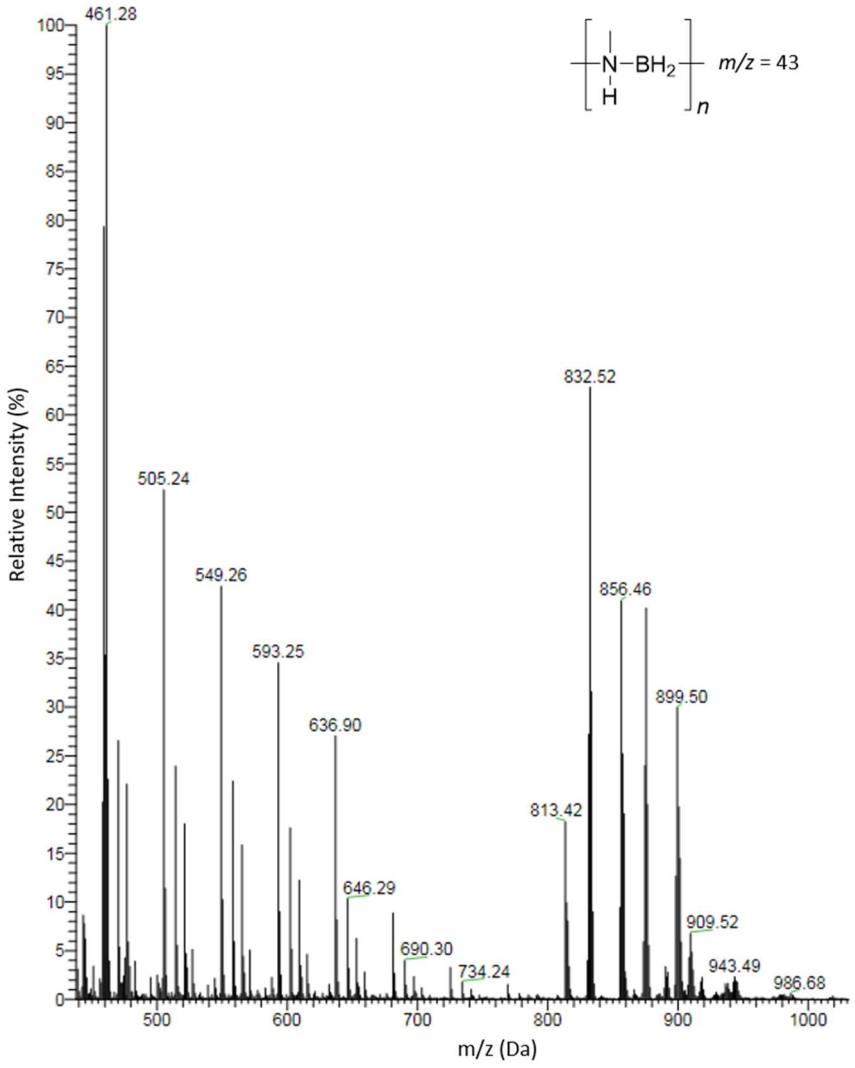

Figure S5.35 ESI(+)-MS spectrum the products of the reaction between $Ph_2N{=}BCl_2$ and IDipp–BH_2NMeH. in DCM:IPA (1:9).

5.5.7.2 Attempted regeneration of $[MeHN–BH_2]_n$ from IDipp–BH_2NMeH with BCl_3

To a solution of IDipp–BH_2NMeH (20 mg, 0.046 mmol) in toluene (500 µL) in a J. Young NMR tube was added a solution of BCl_3 (1M in hexanes, 46 µL, 0.046 mmol) at 22 °C. A small amount of white precipitated was immediately observed. The reaction mixture was analysed by ^{11}B NMR spectroscopy after 10 min and quantitative consumption of the triplet which corresponds to IDipp–BH_2NMeH (δ_B = -16.2 ppm)[8] was detected. Peaks at (δ_B = 3.1 ppm) (ca. 3%) and (δ_B = -5.3 ppm (br)) (trace) were tentatively assigned as IDipp–BCl_3[18] and $[MeHN–BH_2]_n$[17] respectively. Peaks at (δ_B = 34.1 ppm (br) (ca. 20%), 7.8 ppm (s) (ca. 13%), 7.4 (s) ppm (ca. 54%) and -17.9 ppm (br) (ca. 9%)) are currently unassigned. Analysis of the crude material by ESI-MS revealed peaks with a difference of *m/z* = 43 and GPC analysis shows a small quantity of high molar mass material.

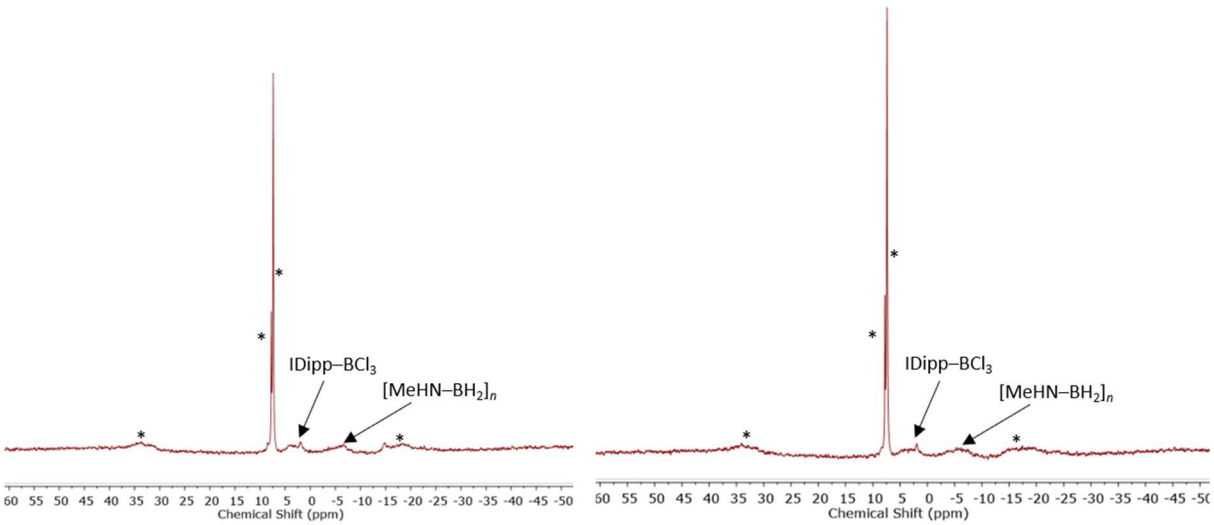

Figure S5.36 $^{11}B\{^{1}H\}$ (left) and ^{11}B (right) NMR spectra (96 MHz, 293 K, toluene) of the reaction solution of $Ph_2N{=}BCl_2$ and IDipp–BH_2NMeH (*unassigned products).

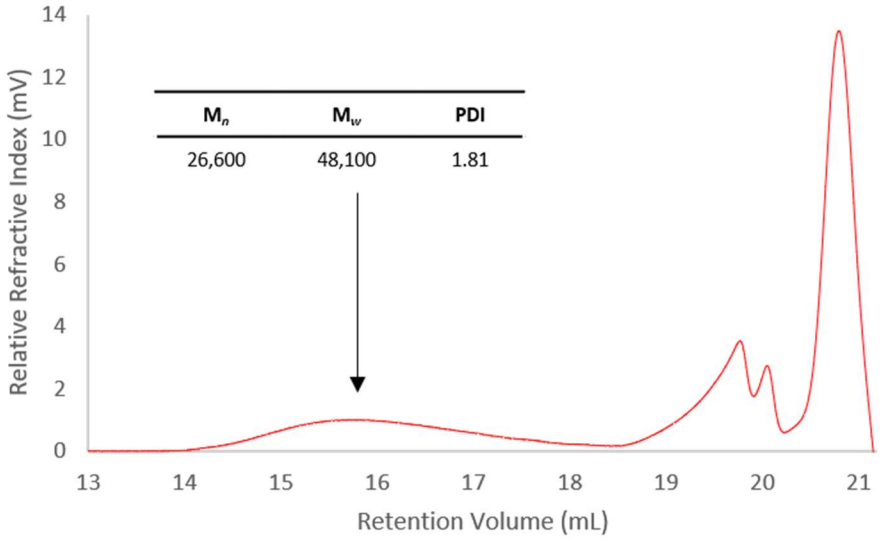

Figure S5.37 GPC chromatogram of the products of the reaction between BCl_3 and IDipp–BH_2NMeH. 2 mg mL^{-1} in THF with 0.1 w/w% nBu$_4$NBr in the THF eluent.

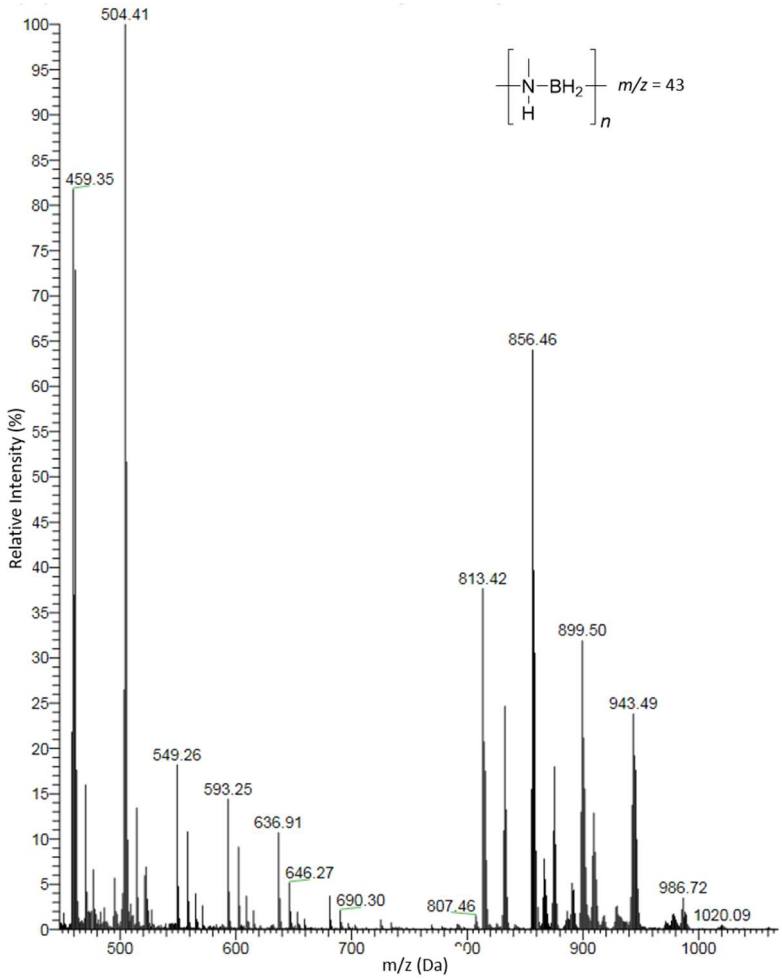

Figure S5.38 ESI-MS ESI(+)-MS spectrum the products of the reaction between BCl_3 and IDipp–BH_2NMeH in DCM:IPA (1:9).

5.5.7.3 Attempted regeneration of $[MeHN–BH_2]_n$ from IDipp–BH_2NMeH with $B(C_6F_5)_3$

To a solution of $B(C_6F_5)_3$ (128 mg, 0.250 mmol) in toluene (250 µL) was added a solution of IDipp–BH_2NMeH (108 mg, 0.250 mmol) in toluene (250 µL) at 22 °C in a J. Young NMR tube. The reaction mixture was analysed by ^{11}B NMR spectroscopy after 1 h and quantitative consumption of the triplet which corresponds to IDipp–BH_2NMeH (δ_B = -16.2 ppm)[8] was detected. A peak at (δ_B = -24.8 ppm (d, $^1J_{HB}$ = 83.7 Hz)) was assigned as $[HB(C_6F_5)_3]^{-}$[20] along with two unassigned species (δ_B = -5.0 ppm (s) (35%) and -17.1 ppm (br) (19%)).

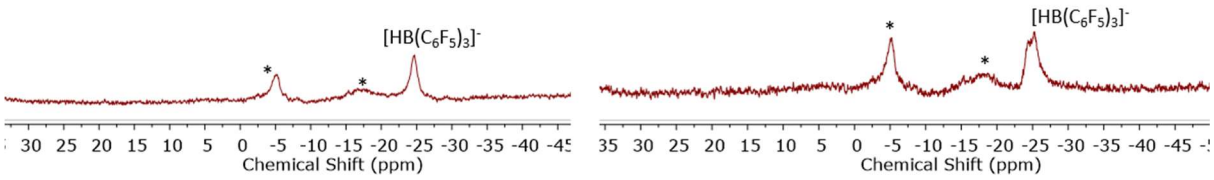

Figure S5.39 $^{11}B\{^1H\}$ (left) and ^{11}B (right) NMR spectra (96 MHz, 293 K, toluene) of the reaction solution of $Ph_2N{=}BCl_2$ and IDipp–BH_2NMeH (*unassigned products).

5.5.8 Supplementary Tables

5.5.8.1 X-ray crystallography

X-ray diffraction experiments of $CAAC^{Me}(H)(PEt_2BH_3)$ was carried out at 100 K on a Bruker APEX II diffractometer using Mo-K_α radiation (λ = 0.71073 Å). The data collections were performed using a CCD area detector from a single crystal mounted on a glass fibre. Intensities were integrated[28] and absorption corrections based on equivalent reflections using SADABS[29] were applied. The structures were solved by the dual-space algorithm SHELXT[30] and refined against all F^2 in ShelXL[31] using Olex2.[32] All the non-hydrogen atoms were refined anisotropically.

Table S5.2 Selected crystallographic data for **5.1** and **5.3**.

Compound	**5.1**	**5.3**
Crystal colour	colourless	yellow
Empirical formula	$C_{24}H_{45}BNP$	$C_{29}H_{46}B_2N_4$
Formula weight	389.39	472.32
Temperature/K	100(2)	90(2)
Crystal system	monoclinic	monoclinic
Space group	C12/c1	$P2_1/n$
a/Å	24.9103(6)	11.9760(18)
b/Å	24.7873(6)	13.819(2)
c/Å	15.8667(4)	18.396(3)
α/°	90	90
β/°	91.6820(10)	103.896(4)
γ/°	90	90
Volume/Å^3	9792.8(4)	2955.2(8)
Z	16	4
ρ_{calc}g/cm^3	1.056	1.062
μ/mm^{-1}	0.121	0.061
F(000)	3456	1032
Radiation	MoKα (λ = 0.71073)	MoKα (λ = 0.71073)
2Θ range for data collection/°	1.159 – 27.190	1.846 – 24.996
Reflections collected	82748	27173
Independent reflections	82748	27173
Goodness-of-fit on F^2	1.037	1.025
Final R indexes [I>=2σ (I)]	R_1 = 0.0437 wR_2 = 0.1012	R_1 = 0.0367 wR_2 = 0.0892
Final R indexes [all data]	R_1 = 0.0616 wR_2 = 0.1102	R_1 = 0.0436 wR_2 = 0.0945
Largest diff. peak/hole / e Å^{-3}	0.485/-0.306	0.200/ -0.195

5.6 References

(1) Oldroyd, N. L.; Manners, I.; Chitnis, S. S.; Annibale, V. T.; Arz, M. I.; Sparkes, H. A. Metal-Free Dehydropolymerisation of Phosphine-Boranes Using Cyclic (Alkyl)(Amino)Carbenes as Hydrogen Acceptors. *Nat. Commun.* **2019**, *10*, 1370–1379.

(2) Staubitz, A.; Sloan, M. E.; Robertson, A. P. M.; Friedrich, A.; Schneider, S.; Gates, P. J.; Manners, I.; Schmedt auf der Günne, J. Catalytic Dehydrocoupling/Dehydrogenation of N-Methylamine-Borane and Ammonia-Borane: Synthesis and Characterization of High Molecular Weight Polyaminoboranes. *J. Am. Chem. Soc.* **2010**, *132*, 13332–13345.

(3) Lapierre, E. A.; Patrick, B. O.; Manners, I. Trivalent Titanocene Alkyls and Hydrides as Well-Defined, Highly Active, and Broad Scope Pre-Catalysts for Dehydropolymerization of Amine-Boranes. *J. Am. Chem. Soc.* **2019**, *141*, 20009–200015.

(4) Dorn, H.; Rodezno, J. M.; Brunnhöfer, B.; Rivard, E.; Massey, J. A.; Manners, I. Synthesis, Characterization, and Properties of the Polyphosphinoboranes $[RPH\text{-}BH_2]_n$ (R = Ph, iBu, p-nBuC_6H_4, p-DodecylC_6H_4): Inorganic Polymers with a Phosphorus-Boron Backbone. *Macromolecules* **2003**, *36*, 291–297.

(5) Safranski, D. L. *Introduction to Shape-Memory Polymers*; Elsevier Inc.: Atlanta, 2017.

(6) Stubbs, N. E.; Jurca, T.; Leitao, E. M.; Woodall, C. H.; Manners, I. Polyaminoborane Main Chain Scission Using N-Heterocyclic Carbenes; Formation of Donor-Stabilised Monomeric Aminoboranes. *Chem. Commun.* **2013**, *49*, 9098–9100.

(7) Al-Rafia, S. M. I.; McDonald, R.; Ferguson, M. J.; Rivard, E. Preparation of Stable Low-Oxidation-State Group 14 Element Amidohydrides and Hydride-Mediated Ring-Expansion Chemistry of N-Heterocyclic Carbenes. *Chem. Eur. J.* **2012**, *18*, 13810–13820.

(8) Stubbs, N. E. Metal-Catalysed and Metal-Free Dehydrogenation of Amine-Boranes. *PhD Thesis* **2015**.

(9) De Albuquerque Pinheiro, C. A.; Roiland, C.; Jehan, P.; Alcaraz, G.; Jéhan, P.; Alcaraz, G. Solventless and Metal-Free Synthesis of High Molecular Mass Polyaminoboranes from Diisopropylaminoborane and Primary Amines. *Angew. Chem. Int. Ed.* **2017**, *57*, 1519–1522.

(10) Jafarpour, L.; Stevens, E. D.; Nolan, S. P. A Sterically Demanding Nucleophilic Carbene: 1,3-Bis(2,6-Diisopropylphenyl)Imidazol-2-Ylidene). Thermochemistry and Catalytic Application in Olefin Metathesis. *J. Organomet. Chem.* **2000**, *606*, 49–54.

(11) Al-Rafia, S. M. I.; Malcolm, A. C.; Liew, S. K.; Ferguson, M. J.; Rivard, E. Stabilization of the Heavy Methylene Analogues, GeH_2 and SnH_2, within the Coordination Sphere of a Transition Metal. *J. Am. Chem. Soc.* **2011**, *133*, 777–779.

(12) The small quantities of (IDipp)H_2 formed are thought to come from IDipp dehydrogenating trace amounts of $MeNH_2BH_3$ present in the adduct starting material.

(13) Paetzold, P. New Perspectives in Boron-Nitrogen Chemistry. *Pure Appl. Chem.* **1991**, *63*, 345–350.

(14) Framery, E.; Vaultier, M. Efficient Synthesis and NMR Data of N- or B-Substituted Borazines. *Heteroat. Chem.* **2000**, *11*, 218–225.

(15) Paetzold, P. Iminiboranes. *Anvances Inorg. Chem.* **1987**, *31*, 123–170.

(16) Swarnakar, A. K.; Hering-Junghans, C.; Nagata, K.; Ferguson, M. J.; McDonald, R.; Tokitoh, N.; Rivard, E. Encapsulating Inorganic Acetylene, HBNH, Using Flanking Coordinative Interactions. *Angew. Chem. Int. Ed.* **2015**, *54*, 10666–10669.

(17) Dietrich, B. L.; Goldberg, K. I.; Heinekey, D. M.; Autrey, T.; Linehan, J. C. Iridium-Catalyzed Dehydrogenation of Substituted Amine Boranes: Kinetics, Thermodynamics, and Implications for Hydrogen Storage. *Inorg. Chem.* **2008**, *47*, 8583–8585.

(18) Rana, R. Synthesis of N-Heterocyclic Carbene Adduct with BCl_3 and Its Reactivity with Amines And Zn (II) Complexes Bearing N , O-Chelate Ligands: Synthesis and Characterization. *Masters Thesis* **2016**.

(19) This reaction has previously been reported (Stubbs, N. PhD Thesis, 2015); however, we believe the assignment of borazane $[MeHN–BH_2]_3$ as a product is incorrect as no splitting into the anticipated triplet is observed using ^{11}B NMR spectroscopy.

(20) Chase, P. A.; Stephan, D. W. Hydrogen and Amine Activation by a Frustrated Lewis Pair of a Bulky N-Heterocyclic Carbene and $B(C_6F_5)_3$. *Angew. Chem. Int. Ed.* **2008**, *47*, 7433–7437.

(21) Pangborn, A. B.; Giardello, M. A.; Grubbs, R. H.; Rosen, R. K.; Timmers, F. J. Safe and Convenient Procedure for Solvent Purification. *Organometallics* **1996**, *15*, 1518–1520.

(22) Jazzar, R.; Dewhurst, R. D.; Bourg, J. B.; Donnadieu, B.; Canac, Y.; Bertrand, G. Intramolecular "Hydroiminiumation" of Alkenes: Application to the Synthesis of Conjugate Acids of Cyclic Alkyl Amino Carbenes (CAACs). *Angew. Chem. Int. Ed.* **2007**, *46*, 2899–2902.

(23) Lebel, H.; Morin, S.; Paquet, V. Alkylation of Phosphine Boranes by Phase-Transfer Catalysis. *Org. Lett.* **2003**, *5*, 2347–2349.

(24) Gregory, M.; Catimel, B.; Yin, M. X.; Condron, M.; Burgess, A. W.; Holmes, A. B. Synthesis of a Tethered Myo-Inositol (1,3,4,5,6)Pentakisphosphate (IP5) Derivative as a Probe for Biological Studies. *Synlett* **2016**, *27*, 121–125.

(25) Busacca, C. A.; Qu, B.; Farber, E.; Haddad, N.; Gr, N.; Saha, A. K.; Eriksson, M. C.; Wu, J.; Fandrick, K. R.; Han, S.; et al. Hydrophosphination of Propargylic Alcohols and Amines with Phosphine Boranes. *Org. Lett.* **2013**, *2*, 4–7.

(26) Cavaye, H.; Clegg, F.; Gould, P. J.; Ladyman, M. K.; Temple, T.; Dossi, E. Primary Alkylphosphine-Borane Polymers: Synthesis, Low Glass Transition Temperature, and a Predictive Capability Thereof. *Macromolecules* **2017**, *50*, 9239–9248.

(27) Stankevič, M.; Pietrusiewicz, K. M. An Expedient Reduction of Sec-Phosphine Oxides to Sec-Phosphine-Boranes by $BH_3{\cdot}SMe_2$. *Synlett* **2003**, *7*, 1012–1016.

(28) Bruker, SAINT+ v8.38A Integration Engine, Data Reduction Software, Bruker Analytical X-Ray Instruments Inc., Madison, WI, USA, 2015.

(29) Bruker, SADABS 2014/5, Bruker AXS Area Detector Scaling and Absorption Correction, Bruker Analytical X-Ray Instruments Inc., Madison, Wisconsin, USA, 2014/5.

(30) Sheldrick, G. M. SHELXT - Integrated Space-Group and Crystal-Structure Determination. *Acta Crystallogr. Sect. A Found. Crystallogr.* **2015**, *71*, 3–8.

(31) Sheldrick, G. M. Crystal Structure Refinement with SHELXL. *Acta Crystallogr. Sect. C Struct. Chem.* **2015**, *71*, 3–8.

(32) Dolomanov, O. V.; Bourhis, L. J.; Gildea, R. J.; Howard, J. A. K.; Puschmann, H. OLEX2: A Complete Structure Solution, Refinement and Analysis Program. *J. Appl. Crystallogr.* **2009**, *42*, 339–341.

Chapter 6
Outlook

Following on from the results reported in this thesis it is proposed that further work could be productively undertaken in the following areas:

6.1 Investigating other metal-free routes for the dehydropolymerisation of phosphine-boranes

Chapters 2 and 5 discuss the synthesis of polyphosphinoboranes using cyclic alkyl(amino)carbenes (CAACs) as stoichiometric hydrogen acceptors. Although this method allows access to a range of polymers, including the first examples of high molar mass P-disubstituted polyphosphinoboranes, $[Ph_2P–BH_2]_n$ and $[PhEtP–BH_2]_n$, the polymerisation method is far from ideal as the requirement of stoichiometric quantities of CAAC results in poor atom economy and a low yield of high molar mass material. The high molar mass of the CAACs also limits the concentration at which the polymerisation reaction can be carried out whilst maintaining a homogeneous solution.

Thus far, there have been no examples reported of reversible H_2 activation at a carbene centre, presumably due to the strength of the resulting C–H bonds. We anticipate that future work could focus on developing alternative main group compounds which are able to both dehydrogenate phosphine-boranes and release dihydrogen to regenerate the active species facilitating a catalytic process. Focussing on the development of a main group catalysts will hopefully provide the opportunity to further extend the substrate scope of P-disubstituted polyphosphinoboranes, species which have thus far not been accessed using transition-metal catalysts. It is worth considering main group compounds which have demonstrated an ability to catalytically dehydrogenate amine-boranes. Some examples of which are frustrated Lewis pair (FLP) systems reported by Aldridge *et al*. and Bourissou *et al.* (Figure 6.1).[1,2]

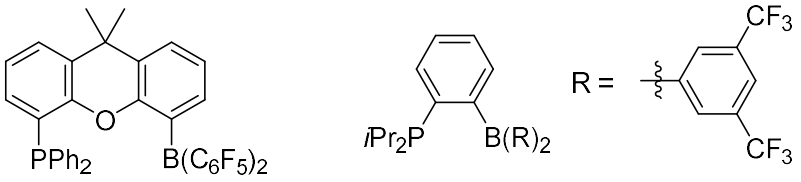

Aldridge, 2016 *Bourissou, 2018*

Figure 6.1 Main group FLP systems which have been successful for catalytic dehydrogenation of amine-boranes.[1,2]

The low yield of high molar mass material was postulated to either result from cyclic oligomers forming as a result of back-biting or chain termination involving chain-end capping with Lewis acids and bases. As CAAC end groups were detected using ESI-MS it is anticipated that if the dehydropolymerisation could be performed using a catalytic, rather than a stoichiometric quantity of a hydrogen acceptor, the instances of premature chain-end capping would be significantly reduced. The development of a catalyst would also significantly improve the atom economy of the dehydropolymerisation. Additionally, increasing the concentration of the polymerisation reaction mixture would likely favour linear chain propagation; however, it should be considered that a high concentration might also favour bimolecular chain termination or chain transfer events.

6.2 Material properties and applications of P-disubstituted polyphosphinoboranes

A recent publication by our group reported a post-polymerisation modification of P-monosubstituted polyphosphinoboranes via the insertion of olefins into the P–H bonds, with material properties which could be tuned by varying the degree of hydrophosphination and alkene used.[3] The CAAC-mediated dehydropolymerisation route discussed in Chapters 2 and 5 allows access to P-disubstituted materials via the direct dehydrogenation of phosphine-borane monomers. This method enables the properties of the polymers to be tuned by altering the substituents of the monomer and does not rely on the initial synthesis of a P-monosubstituted polyphosphinoborane.

The development of a catalyst for the dehydropolymerisation of P-disubstituted phosphine-boranes would allow for the synthesis of high molar mass polymer to be much more atom efficient and should facilitate scale up. Subsequently this will enable the material properties, such as thermal and oxidative stability, ceramic yields, and glass transition temperatures of P-disubstituted polyphosphinoboranes to be investigated. It is anticipated

that P-disubstituted polyphosphinoboranes will exhibit different properties to those of P-monosubstituted polyphosphinoboranes. In particular it is predicted that the P-disubstituted derivatives will display an increase in long-term stability as a result of the removal of a reactive P–H bond. The synthesis of a larger quantity of $[Et_2P–BH_2]_n$ is an especially attractive target due to its semi-crystalline properties. Crystalline polyphosphinoboranes would have advantages over their amorphous congeners such as greater mechanical strength and Young's modulus and would allow easy processing into melt-spun fibres.

6.3 Detailed mechanistic studies into the dehydropolymerisation of phosphine-boranes using $Ni(COD)_2$ precatalyst

Chapter 3 described the dehydropolymerisation of $PPhH_2{\cdot}BH_3$ using $Ni(COD)_2$ (COD = 1,5-cyclooctadiene) as a precatalyst. Although we have proposed that the reaction operates via a homogeneous chain-growth mechanism a detailed study into the mechanism of the catalysis should be undertaken as a greater understanding could be used to aid future catalyst design. A combination of computational studies, isotopic labelling studies and isolation of reactive intermediates should be carried out.

It was reported by Weller *et al.* that the COD ligands of the catalyst $[Rh(COD)_2][BAr^F{}_4]$ ($BAr^F{}_4$ = $[B(3,5\text{-}(CF_3)_2C_6H_3)_4]^-$) are displaced by tBu$_2$PH in the reaction with the secondary phosphine-borane, tBu$_2$PH·BH$_3$, presumably as a result of the cleavage of the P–B bond of the phosphine-borane at the Rh centre.[4] Attempts should be made to try and isolate the active species in the $Ni(COD)_2$ catalysed dehydropolymerisation and this could be done through carrying out stoichiometric reactions of $Ni(COD)_2$ with both phosphines and phosphine-boranes. It is anticipated that using the disubstituted derivatives Ph_2PH and $Ph_2PH{\cdot}BH_3$ may assist with crystallisation.

6.4 Reactivity of the cyclic trimer $[PhHP–BH_2]_3$

The isolation of the 6-membered ring $[PhHP–BH_2]_3$ is reported in Chapter 3. This species is a side product of the $Ni(COD)_2$ catalysed polymerisation of $PhPH_2{\cdot}BH_3$; however, it is also an interesting compound in its own right.

It will be interesting to investigate whether it is possible to functionalise the P–H bonds of $[PhHP–BH_2]_3$ using hydrophosphination reactions as has been reported by Gaumont *et al.* for

phosphine-boranes, and more recently by Manners *et al.* for polyphosphinoboranes (Scheme 6.1a).[3,5]

The presence of both P–H and B–H bonds opens the possibility for dehydrogenation of the rings to occur to give a compound which would be isoelectronic to borazine (Scheme 6.1b). Power *et al*. reported P–B borazine analogues in the 1980s using bulky substituents to favour B–P π-bonding.[6,7] It is anticipated that it may be possible for a dehydrocoupling reaction between rings to occur to give two 6-membered rings joined by a P–B bond (Scheme 6.1c). A novel structure that could be targeted would be a hexagonal cage structure in which dehydrocoupling occurs between all B–P units on two of the 6-memebered rings (Scheme 6.1d). A similar structure was reported by Schmidt *et al.* for amidoalane systems.[9]

It is feasible that the 6-membered cyclic oligomer $[PhHP–BH_2]_3$ may undergo a ring-opening polymerisation (ROP) reaction either thermally or through the use of an initiator (Scheme 6.1e). ROP has provided an important route to high molar mass main group polymers; however, in most cases the rings are strained and sterically demanding substituents are present in the cyclic monomers.[10–12]

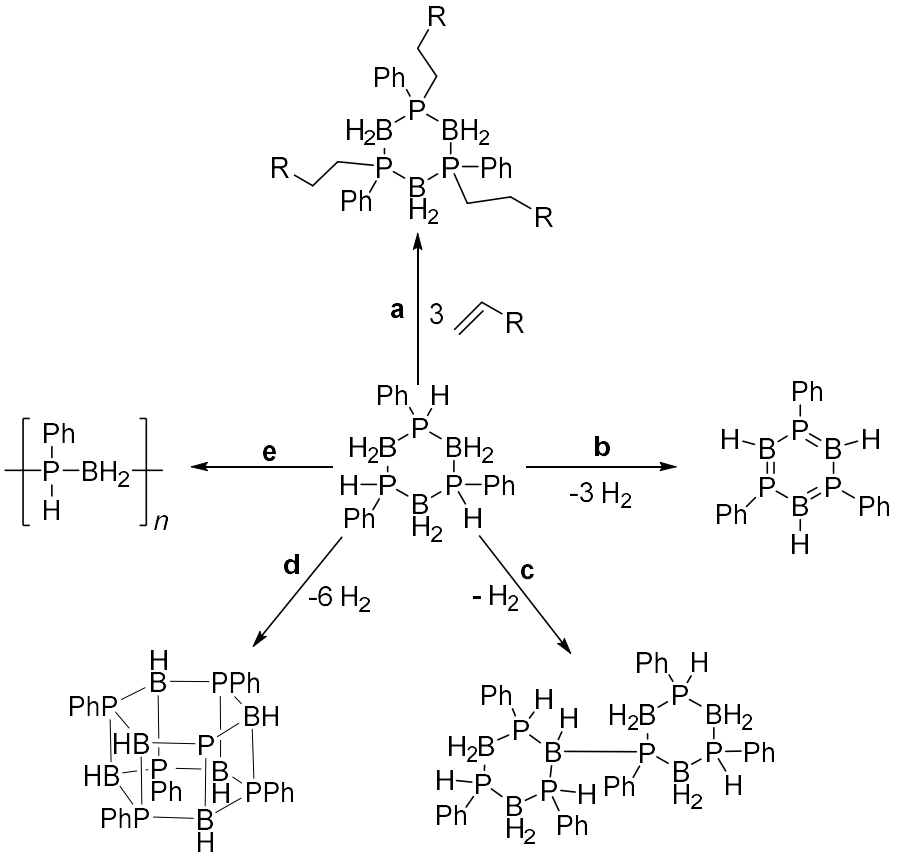

Scheme 6.1 Potential further reactivity of $[PhHP–BH_2]_3$: **a** functionalisation of P–H bonds; **b** dehydrogenation; **c** dehydrocoupling; and **d** ring-opening polymerisation.

6.5 Reactivity of ammonia-borane with CAACs

In Chapter 4 the synthesis of *cis*- and *trans*-(CAAC^{Me}H)HB=NMe(CAAC^{Me}H) is reported through the reaction of $MeNH_2{\cdot}BH_3$ with three equiv. of CAAC^{Me}. One equiv. of CAAC^{Me} is believed to dehydrogenate the amine-borane and the further two equivalents insert into the B–H and N–H bonds. A preliminary investigation into the reaction of $Me_2NH{\cdot}BH_3$ with two equiv. of CAAC^{Me} appears to give (CAAC^{Me}H)HB=NMe$_2$, a result similar to that of $MeNH_2{\cdot}BH_3$; however, with the N-disubstituted amine-borane no N–H bond is available for N–H activation by CAAC^{Me} post dehydrogenation.

Probing the product/products of the reaction between ammonia-borane, $NH_3{\cdot}BH_3$ and CAAC^{Me} would be a relevant study. If (CAAC^{Me}H)HB=NH(CAAC^{Me}H) could be prepared successfully from the reaction of $NH_3{\cdot}BH_3$ with 3 equiv. of CAAC^{Me}, analogous to reaction involving $MeNH_2{\cdot}BH_3$, it would be interesting to investigate whether the addition of further equivalents of CAAC^{Me} activate the remaining N–H or B–H bonds, or if this species could be dehydrogenated to give an iminoborane, the BN analogue of an alkyne (Scheme 6.2). Iminoboranes are difficult to isolate due to their propensity to undergo cyclooligomerisation; however, it is anticipated that in this case the steric bulk introduced by CAAC^{Me} may be sufficient to stabilise the iminoborane.[13–15] It may also be possible to tune the steric bulk by altering the CAAC substituents.

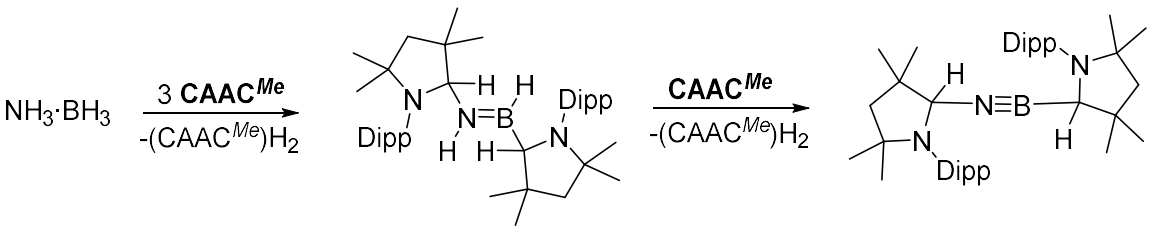

Scheme 6.2 Proposed synthesis of an iminoborane from $NH_3{\cdot}BH_3$ and CAAC^{Me}.

6.6 Thermolysis of IDipp–BH_2NH_2 adduct

In Chapter 5 the synthesis of IDipp–$BH_2{\cdot}$NMeBH·NMeH was discussed. This species can be described as an iminoborane unit trapped by an electron donating amide and electron accepting borenium moiety and is synthesised through the thermolysis of the adduct IDipp–BH_2NMeH. Previous work in our group showed the adduct IDipp–BH_2NH_2 was accessible by reacting IDipp with $[H_2N–BH_2]_n$.[16]

Rivard *et al*. have reported examples of stable molecular adducts containing HB≡NH using a donor acceptor approach in which the iminoborane is sandwiched between a Lewis-base and Lewis-acid (Figure 6.2a and b).[13,17]

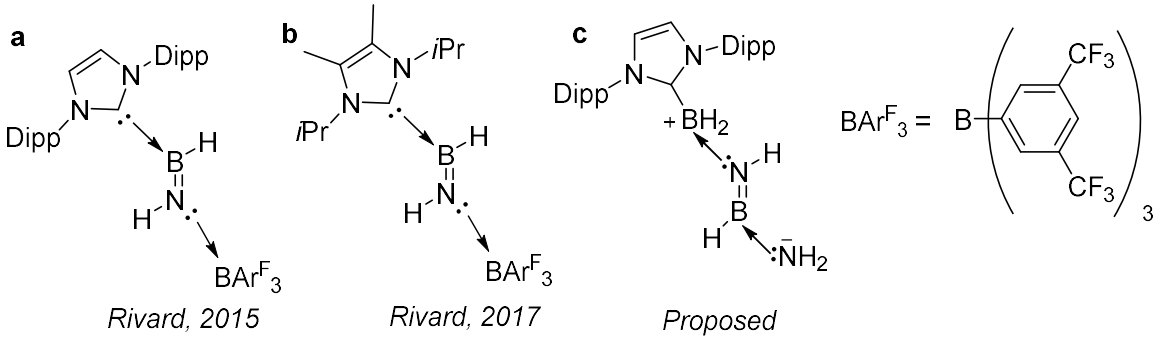

Figure 6.2 a and **b** Trapped iminoboranes reported by Rivard *et al*; and **c** proposed trapped iminoborane.

It was postulated that these species may provide a solution-phase route to boron nitride *via* dehydrogenation (Scheme 6.3); however, attempts to release H_2 using dehydrogenation catalysts were unsuccessful. This was attributed to the steric bulk of the capping groups.

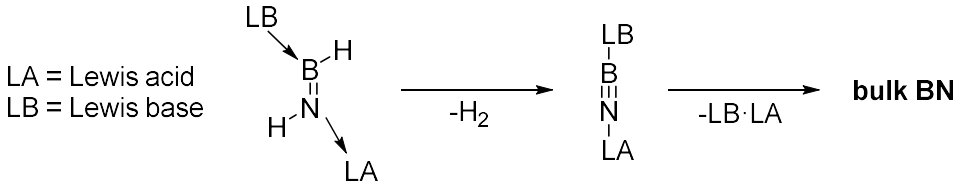

Scheme 6.3 Proposed route to bulk boron nitride.

It will be interesting to probe whether the thermolysis of IDipp–BH_2NH_2 gives IDipp–BH_2·NHBH·NH_2 (Figure 6.2c). This compound will have lower steric bulk around the trapped iminoborane than the compounds synthesised by Rivard, potentially allowing further dehydrogenation to take place.

6.7 References

(1) Mo, Z.; Rit, A.; Campos, J.; Kolychev, E. L.; Aldridge, S. Catalytic B-N Dehydrogenation Using Frustrated Lewis Pairs: Evidence for a Chain-Growth Coupling Mechanism. *J. Am. Chem. Soc.* **2016**, *138*, 3306–3309.

(2) Boudjelel, M.; Sosa Carrizo, E. D.; Mallet-Ladeira, S.; Massou, S.; Miqueu, K.; Bouhadir, G.; Bourissou, D. Catalytic Dehydrogenation of (Di)Amine-Boranes with a Geometrically Constrained Phosphine-Borane Lewis Pair. *ACS Catal.* **2018**, *8*, 4459–4464.

(3) Knights, A. W.; Chitnis, S. S.; Manners, I. Photolytic, Radical-Mediated Hydrophosphination: A Convenient Post-Polymerisation Modification Route to P-Di(Organosubstituted) Polyphosphinoboranes [RR'PBH_2]$_n$. *Chem. Sci.* **2019**, *10*, 7281–7289.

(4) Huertos, M. A.; Weller, A. S. Intermediates in the Rh-Catalysed Dehydrocoupling of Phosphine-Borane. *Chem. Commun.* **2012**, *48*, 7185–7187.

(5) Mimeau, D.; Delacroix, O.; Gaumont, A.-C. Regioselective Uncatalysed Hydrophosphination of Alkenes: A Facile Route to P-Alkylated Phosphine Derivatives. *Chem. Commun.* **2003**, 2928–2929.

(6) Rasika Dias, H. V.; Power, P. P. Boron-Phosphorus Analogues of Benzene and Cyclobutadiene. Synthesis and Characterization of the Boraphosphabenzenes $(RBPR')_3$ (R = Mes, Ph; R' = Ph, Mes, C_6H_{11},t-Bu) and the Diphosphadiboretane $(ThexylBPMes)_2$. *J. Am. Chem. Soc.* **1989**, *111*, 144–148.

(7) Dias, H. V. R.; Power, P. P. Synthesis and X-Ray Structure of $(2,4,6\text{-}Me_3C_6H_2BPC_6H_{11})_3$: A Boron-Phosphorus Analogue of Borazine. *Angew. Chem Int. Ed. English* **1987**, *26*, 1270–1271.

(8) Power, P. P. π Bonding and the Lone Pair Effect in Multiple Bonds between Heavier Main Group Elements. **1999**, *99*, 3643–3503.

(9) Reddy, N. D.; Roesky, H. W.; Noltemeyer, M.; Schmidt, H. G. Reactions of $AlH_3{\cdot}NMe_3$ with Nitriles: Structural Characterization and Substitution Reactions of Hexameric Aluminum Imides. *Inorg. Chem.* **2002**, *41*, 2374–2378.

(10) Arz, M. I.; Annibale, V. T.; Kelly, N. L.; Hanna, J.; Manners, I. Ring-Opening Polymerization of Cyclic Phosphonates: Access to Inorganic Polymers with a P(V)–O Main Chain. **2018**, *141*, 6–11.

(11) Dubois, P.; Coulembier, O.; Raquez, J.-M. *Handbook of Ring-Opening Polymerization*; Wiley, 2009.

(12) Allcock, H. R.; Kugel, R. L.; Valan, K. J. Phosphonitrilic Compounds. VI. High Molecular Weight Poly(Alkoxy- and Aryloxyphosphazenes). *Inorg. Chem.* **1966**, *5*, 1709–1715.

(13) Swarnakar, A. K.; Hering-Junghans, C.; Ferguson, M. J.; McDonald, R.; Rivard, E. Reactivity of a Coordinated Inorganic Acetylene Unit, HBNH, and the Azidoborane Cation $[HB(N_3)]^+$. *Chem. Sci.* **2017**, 8, 2337–2343.

(14) Bulak, E.; Herberich, G. E.; Manners, I.; Mayer, H.; Paetzold, P. Synthesis and Structure of [CpzNbH(TBuB=NtBu)], a Compound with Side-on Coordinated Iminoborane. *Angew. Chem. Int. Ed.* **1988**, *27*, 958–959.

(15) Paetzold, P. Iminoboranes. *Adv. Inorg. Chem.* **1987**, *31*, 123–170.

(16) Stubbs, N. E.; Jurca, T.; Leitao, E. M.; Woodall, C. H.; Manners, I. Polyaminoborane Main Chain Scission Using N-Heterocyclic Carbenes; Formation of Donor-Stabilised Monomeric Aminoboranes. *Chem. Commun.* **2013**, *49*, 9098–9100.

(17) Swarnakar, A. K.; Hering-Junghans, C.; Nagata, K.; Ferguson, M. J.; McDonald, R.; Tokitoh, N.; Rivard, E. Encapsulating Inorganic Acetylene, HBNH, Using Flanking Coordinative Interactions. *Angew. Chem. Int. Ed.* **2015**, *54*, 10666–10669.